Effect of Copper and Magnesium on the Precipitation Characteristics of Al-Li-Mg, Al-Li-Cu and Al-Li-Cu-Mg Alloys

by

Spyros Katsikis

The University of Nottingham

School of Mechanical, Materials and Manufacturing Engineering

Thesis submitted to the University of Nottingham for the degree of

Doctor of Philosophy

August 2001

CONTENTS

Abstract

The effects of copper and magnesium on the precipitation characteristics of Al-Li-Mg, Al-Li-Cu, and Al-Li-Cu-Mg alloys have been investigated during isochronal and isothermal ageing. In Al-Li-Mg alloys, increasing the magnesium concentration results in stimulation of δ′ precipitation by a shift of the α/δ′ solvus boundary to higher temperatures. It was shown that for each wt%Mg present in the alloy the α/δ′ solvus boundary shifts by 7.0°C. In Al-Li-Cu alloys the concentration of copper has no effect on the position of the α/δ′ solvus boundary. The significant stimulation of δ′ observed in Al-Li-Cu alloys was shown to be due to the formation of GP_{Cu} zones that act as heterogeneous nucleation centres. TEM analysis showed that this heterogeneous nucleation produced composite precipitates consisting of an inner plate of GP_{Cu} zone and an outer cylindrical shell of δ′. At high copper concentrations (Cu≥2.0%) and long ageing times at 150°C, significant retardation of δ′ precipitation takes place due to precipitation of the equilibrium T_1 and T_2 phases.

The mechanisms by which copper and magnesium affect the precipitation characteristics of Al-Li-Cu-Mg alloys are different than those operating in the ternary Al-Li-Mg alloys and Al-Li-Cu alloys. In 1.7Li1.2CuXMg alloys, increasing the magnesium concentration beyond 1.2% causes significant stimulation of δ′ precipitation through the formation of Li-Cu-Mg clusters (mechanism referred to as CLδ′) that are capable of rapidly developing into δ′. It is proposed that in 1.7Li1.2CuXMg alloys the initial 1.2%Mg added is consumed in the formation of GPB zones that have very little effect on δ′ precipitation. As the magnesium concentration increases to levels higher than 1.2%, the magnesium is free in the matrix to gather both copper and lithium thus forming Li-Cu-Mg clusters which are extremely effective at nucleating δ′.

In 1.7Li1.2MgXCu alloys the mechanisms by which stimulation of δ′ precipitation takes place are again by formation of Li-Cu-Mg clusters (CLδ′), and by nucleation on GPB zones (mechanism referred to as GPδ′). During ageing at 70 and 100°C, and for copper concentrations in the range 0-1.2%, the dominant precipitation mechanism is GPδ′. For higher copper concentrations (1.2<Cu≤3.0) the dominant process is CLδ′. Increasing the ageing conditions to 150°C causes precipitation of δ′ through classical nucleation and growth for low copper concentrations. For high copper concentrations, the precipitation of δ′ comes about through the GPδ′ mechanism. Using Kissinger's method, it was found that the activation energy for δ′ formation in Al-Li-Cu-Mg is equal to 62 kJ/mol, suggesting that the kinetics of the δ′ precipitation process are also controlled by the presence of excess vacancies quenched-in from

solution heat treatment. It is likely that the Li-Cu-Mg clusters that develop in the alloy also gather excess vacancies thus making the clusters vacancy-rich.

For all the alloy systems (Al-Li-Cu, Al-Li-Mg, and Al-Li-Cu-Mg alloys) and independently of the concentrations of copper and magnesium, the largest volume fraction of δ′ precipitates form during ageing at 100°C where there is an optimum combination of thermodynamics and kinetics.

Ageing the alloys at 150°C (standard heat treatment for lithium containing alloys) and subsequently exposing at 70°C (to simulate service conditions for an aerospace alloy) resulted in embrittlement due to precipitation of additional (fine) δ′. This embrittlement was shown to be closely related to the volume fraction of δ′ that precipitates during exposure. In Al-Li-Mg and Al-Li-Cu ternary alloys, increasing the concentration of magnesium and copper respectively, resulted in increased volume fractions of δ′ precipitated during exposure and hence increased degrees of embrittlement. For Al-Li-Cu-Mg alloys the maximum volume fraction of δ′ precipitated during exposure occurred in the 1.7Li1.2Cu1.2Mg alloy. It was shown that this alloy composition also showed the maximum degree of embrittlement.

INTRODUCTION

Competition between materials to decrease the structural weight of aircraft vehicles is intense. Reducing the density of the alloy used to construct the aircraft is the most effective factor for achieving this aim.

Lithium is the lightest metallic element (density 0.54 g/cm^3) and one of relatively few elements that shows high solid solubility in aluminium, this being approximately 4wt% (16at%) at 610 °C. This high solubility is significant because for each 1% addition of lithium, the density of an aluminium alloy is decreased by 3%. Not only does lithium cause a decrease in the density of aluminium alloys, but also it causes a marked increase in the elastic modulus of aluminium (6% increase for each 1% added).

The Al-Li alloys listed in **table 1 [1]** have the potential to save up to 10% of the weight of an aircraft by direct substitution of conventional aluminium alloys and up to 18% in weight if the increased specific stiffness (modulus/density) can be used. This means that Al-Li alloys can be potential alternatives to composite materials. The specific mechanical properties of composites are somewhat superior but Al-Li alloys have the great advantage that conventional structural design principles and fabrication processes can be used.

Figure 1 [2] summarises the influences of improvements in various properties, including density and stiffness, on the potential weight savings for aircraft structures.

It is obvious that reducing density is the most effective way of saving weight. Less effective are increasing strength and stiffness. Improvements in damage tolerance properties (fracture, fatigue and stress corrosion resistance) have the least capacity for saving weight.

Binary and more complex aluminium alloys containing lithium respond to age hardening and develop their strength principally from the precipitation of small spherical particles of $\delta'(Al_3Li)$, which have an ordered $L1_2$ structure.

Unfortunately, δ' precipitates also result in poor ductility and low fracture toughness when the alloys are aged to peak strength. This disadvantage can be controlled by underageing to below peak strength. However, in this lightly-aged condition, exposure to moderate elevated temperatures in service (e.g 70-100°C) results in an increase in strength and a reduction in toughness. This instability of mechanical properties is a significant problem to the aerospace industry. One of the objectives of the present research work is to investigate the ways of minimising this instability by microstructural control of the alloys.

Some initial work has been done about the problem of thermal instability and various metallurgical effects have been suggested. In 8090 (Al-Li-Cu-Mg) alloys, these reasons include the segregation of lithium atoms to grain boundaries, the precipitation of small $\delta'(Al_3Li)$ precipitates, and GP zone formation [3].

In 2090 alloys the thermal instability has been attributed to precipitation of $T_1(Al_2CuLi)$ phase or GP zones. In all of these studies the determination of the reasons that cause the thermal instability is made difficult by the fact that during

exposure a combination of phases are produced that are based on the Al-Li, Al-Cu-Mg, Al-Li-Cu, Al-Li-Mg and Al-Li-Cu-Mg systems [3].

The present work has focused on the influence of magnesium and copper on the behaviour of ternary Al-Li-Mg, Al-Li-Cu and quaternary Al-Li-Cu-Mg alloys. A low lithium concentration (1.7 wt%) has been used in order to reduce the volume fraction of δ′, the formation of which tends to mask any effects due to the copper and magnesium additions.

Table1: Families of Al-Li alloys intended to replace conventional aluminium alloys [1]

Conventional alloys to be replaced	**Al-Li based alloys**		
	Alcoa	Alcan	Cegedur-Pechiney
7075-T6 (5.6Zn2.5Mg1.6Cu0.23Cr) **High strength**	**2090** (*2.2Li2.7Cu0.12Zr*)	**8091** (*2.6Li1.9Cu0.9Mg0.12Zr*)	
2014-T6 (*4.4Cu0.5Mg0.9Si0.8Mn*) **Medium-high strength**	**8090** (*2.4Li1.3Cu0.9Mg0.10Zr*)	**8090**	**8090**
2024-T3 (*4.4Cu1.5Mg0.6Mn*) **Damage tolerant**	**8090** **2091** (*2.0Li2.1Cu1.5Mg 0.10Zr*)	**8090-T81**	**2091**
7075-T73 **Corrosion resistant**	**8092** (*2.4Li0.65Cu1.2Mg0.12Zr*)		
Minimum density general purpose	**8192** (*Composition not given*)		

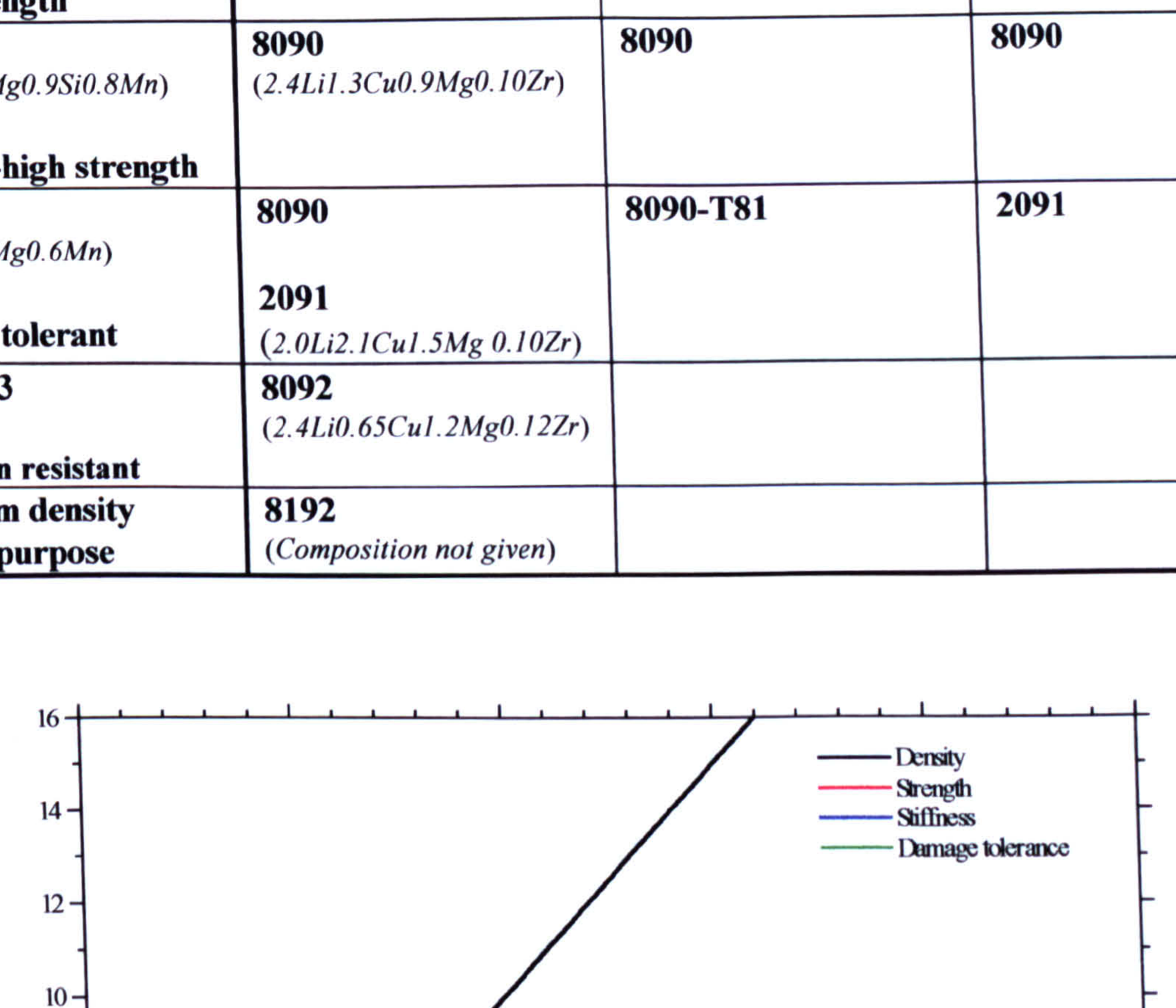

Figure1: Effects of property improvements on aircraft structural weight savings [2]

CHAPTER 1

Development of Al-Li based alloys – General characteristics

1.1 Retrospection of Al-Li based alloys

Although lithium was used as early as 1924 in small additions to improve the mechanical properties of Al-Zn-Cu alloys (Scleron alloys), it was two decades later (1945) when LeBaron discovered that lithium could be a major strengthening species in Al-Cu alloys containing small amounts of cadmium. Based on LeBaron's discovery, Alcoa developed in 1957 the Al-1.1Li-4.5Cu-0.5Mn-0.2Cd alloy (X2020) with application in the production of wing covers and horizontal stabilisers for RA-5C Vigilante aircraft. Unfortunately, mechanical tests indicated that the fracture toughness of this alloy was the lowest among all the commercially used aerospace alloys and its further usage was abandoned.

In the 1960s significant research in Al-Li alloys took place in the former Soviet Union. This led to the development of a 2020-series alloy (VAD-23) with nominal composition Al-1.1Li-5.3Cu0.6Mn-0.17Cd. A lower-strength ageing treatment was used on this alloy that resulted in improved fracture toughness. In the late 1960s a new alloy was announced by the Soviets with nominal composition Al-2.0Li-5.3Mg-0.5Mn designated as 01420. This alloy had very similar characteristics to modern Al-Li alloys as it had a considerably lower

density than other conventional aerospace aluminium alloys. Alloy 01420 found wide use on Soviet aircraft structures.

Extensive research and development of Al-Li based alloys with advanced engineering properties commenced in the mid-1970s to early 1980s by Alcan, Alcoa and Pechiney. The main reasons that motivated the development of this new generation of alloys was the potential threat of replacement of aluminium aerospace alloys by resin-matrix composites, and the acceptance that reducing density is the most effective way for saving structural weight of an aerospace vehicle. In the late 1980s the development work led to the design of Al-Li type alloys with additions of copper, zirconium, and/or magnesium in order to attain the optimum combination of mechanical properties. These commercial alloys are designated as weldalite 049, 2090, 2091, 8090, and CP276 with nominal compositions given in **table 1.1** [5].

Figure 1.1 presents an overview of the main factors that have marked the development of Al-Li based alloys [4].

1.2 Selection criteria of lithium as the alloying element for the development of low density aluminium based alloys.

As described previously, the most effective way of saving weight for aircraft structures is by reducing density. For aluminium alloys, additions of lithium and beryllium are two of the most effective elements for decreasing density (**figure 1.2**). Lithium, as the lightest metal, causes a significant decrease in the density.

Each 1% of lithium (maximum solubility 4wt% or 16at% at 610°C) reduces density by about 3% and increases the elastic modulus by about 6%. Furthermore, small amounts of lithium cause the precipitation strengthening of aluminium due to the formation of an homogeneous distribution of coherent $\delta'(Al_3Li)$ particles. Conversely, beryllium additions do not cause significant precipitation strengthening in aluminium [5]. The combination of density-decrease and precipitation hardening was the main reason for choosing lithium as the metallic element for the development of low density aluminium alloys. We have to mention that heavier elements, such as copper, are also present in more complicated Al-Li systems, which reduces the effectiveness of lithium on the alloy density. **Figure 1.2** shows the influence of some other alloying additions on the density of aluminium, and **figure 1.3** gives a comparison of densities for several Al-Li based alloys and conventional aluminium alloys [4].

An equation developed by Peel [6] gives the density of an alloy in terms of its composition in weight percent:

Density (g/cc)=2.71+0.024%Cu+0.018%Zn+0.022%Mn-0.079%Li-0.01%Mg-0.004%Si

1.3 Further solute additions to Al-Li based alloys

Improvement to mechanical properties such as ductility and toughness is achieved by the addition of further alloying elements. Copper and magnesium cause precipitation of the intermetallic phases $Al_2CuLi(T_1)$ and $Al_2CuMg(S)$

which impede the movement of dislocations more effectively than the coherent δ′(Al_3Li) precipitates. The last are sheared by dislocations causing heterogeneous planar slip and low fracture toughness. Moreover magnesium and copper can decrease the formation of precipitate free zones (PFZs) near the grain boundaries. Zirconium forms fine cubic Al_3Zr coherent dispersoids which assist in controlling recrystallization and grain size during casting and hot working. The phases precipitated in Al-Li based alloy systems after various heat treatments are presented in **figure 1.4 [4]**.

The various commercial Al-Li based alloys can be classified in terms of their response to heat treatment; these are the high strength (2090), medium strength (8090), and damage tolerant (2091 and 8090) grades of alloy. In table 1.1 are given the compositions of current Al-Li commercial alloys.

1.4 Production of Al-Li based alloys

The special properties of lithium, such as high reactivity (lithium is a highly reactive element forming oxides and nitrides very easily), low density, low melting point and its high price require special techniques to be used for the production of the commercial Al-Li alloys.

Ingot metallurgy is the most common route for the production of Al-Li alloys on an industrial scale. The high reactivity of lithium led to the use of the Vacuum Induction Melting Furnace (VIM) that is well established in the special metals industry. The VIM furnace allows melting and casting of superalloys and nonferrous alloys under vacuum or inert gas conditions. The low cost of

production, the large ingot sizes and the use of standard production equipment has made ingot metallurgy the main route for the production of Al-Li alloys. However, due to segregation problems the maximum concentration of lithium that can be produced by ingot metallurgy is 2.5%. This, together with the coarse grain structure, led to the development of Al-Li alloys by rapidly solidified powder metallurgy (RS-PM). This technology made possible the structure control and an increased concentration of lithium. However, considerable oxygen contamination resulted in the presence of oxide stringers in the hot worked alloys with deleterious effects on the mechanical properties **[7, 8]**.

In order to overcome the problems of ingot metallurgy (lithium segregation, coarse microstructure, formation of intermetallic particles) and RS-PM (oxygen contamination) the spray-casting process was developed. This process involves atomisation of an alloy melt into a spray of liquid droplets and impingement of these droplets onto a substrate. The significantly higher rates of solidification compared with those during conventional casting, causes refinement of the grain size (fine, equiaxed grains of size 30-50 μm) and intermetallic particles (~0.5 μm) **[9, 10, 11]**. This has the result of eliminating the anisotropic properties observed in die-cast ingots, thereby resulting in improved ductility and fracture toughness in the short-transverse direction **[10, 11]**, and the faster dissolution of particles during homogenisation or solution treatment **[10]**. However, the improved mechanical properties due to the more isotropic properties are limited by the precipitation of second phase particles on the grain boundaries during the ageing treatment **[10]**.

1.4.1 The role of alkali impurities

The presence of alkali impurities (notably sodium and potassium) in grain boundaries cause a decrease of ductility and fracture toughness in Al-Li alloys. In other aluminium systems these elements are incorporated into less deleterious solid compounds by other elements such as silicon.

Investigators observed on the fracture surface of partially or fully recrystallized Al-Li based alloys, the presence of intergranular brittle islands. The size and the number of these islands increase with increasing concentration of sodium and potasium above 3 ppm **[12]**.

Conventional methods of melting and casting result in the presence of alkali impurities in the range 3-10 ppm. The concentration of the alkali impurities can be decreased to below 1 ppm by vacuum melting and refining, and this improves the fracture toughness at room temperature.

The intergranular fracture which takes place in Al-Li based alloys can also be attributed to the presence of hydrogen, grain boundary precipitate-free zones, and the equilibrium grain boundary phase δ(AlLi).

The last two factors (PFZs and δ(AlLi)) are examined more extensively in later chapters.

1.5 Applications of current Al-Li based alloys

Al-Li based alloys were developed primarily for weight savings due to the decreased density and increased stiffness in comparison with conventional

aluminium alloys. However, in spite of the unique properties of Al-Li based alloys, their use is limited due to their high cost of production. It has been estimated that the cost of Al-Li alloys is three to five times higher than that of conventional aluminium alloys because of the use of specialised casting equipment and the high cost of lithium. For these reasons the use of Al-Li alloys is limited to applications where weight reduction is crucial [5].

Commercial applications

The commercial applications are associated with aircraft parts such as leading and trailing edges, access covers, seat tracks and wing skins.

Military applications

The Al-Li based alloys replace conventional alloys in the form of superplastic-formed sheet parts and conventionally formed 2090, 2091, 8090 sheets for structures, wing skins and plate parts.

Space applications

In space applications the weight savings is the first priority. Al-Li alloys are used for integrally stiffened primary structures and tankage. They are also used for sheet and stringer constructions of rocket shrouds, formings and adapters. The alloy 2090 is a candidate material for the cryogenic tankage of rocket booster systems.

Table 1.1: Compositions (wt%) of commercial Al-Li based alloys [5]

Composition					
Element	**2090(a)**	**2091(a)**	**8090(a)**	**Weldalite049**	**CP276(b)**
Silicon	0.10	0.20	0.20	-	-
Iron	0.12	0.30	0.30	-	-
Copper	2.4-3.0	1.8-2.5	1.0-1.6	5.4	2.7
Manganese	0.05	0.10	0.10	-	-
Magnesium	0.25	1.1-1.9	0.6-1.3	0.4	0.5
Chromium	0.05	0.10	0.10	-	-
Zinc	0.10	0.25	0.25	-	-
Lithium	1.9-2.6	1.7-2.3	2.2-2.7	1.3	2.2
Zirconium	0.08-0.15	0.04-0.16	0.04-0.16	0.14	0.12
Titanium	0.15	0.10	0.10	-	-
Other, each	0.05	0.05	0.05	(Ag: 0.4)	-
Other, total	0.15	0.15	0.15	-	-
Aluminium	Bal.	Bal.	Bal.	Bal.	Bal.

(a):Registered limits (b):Nominal

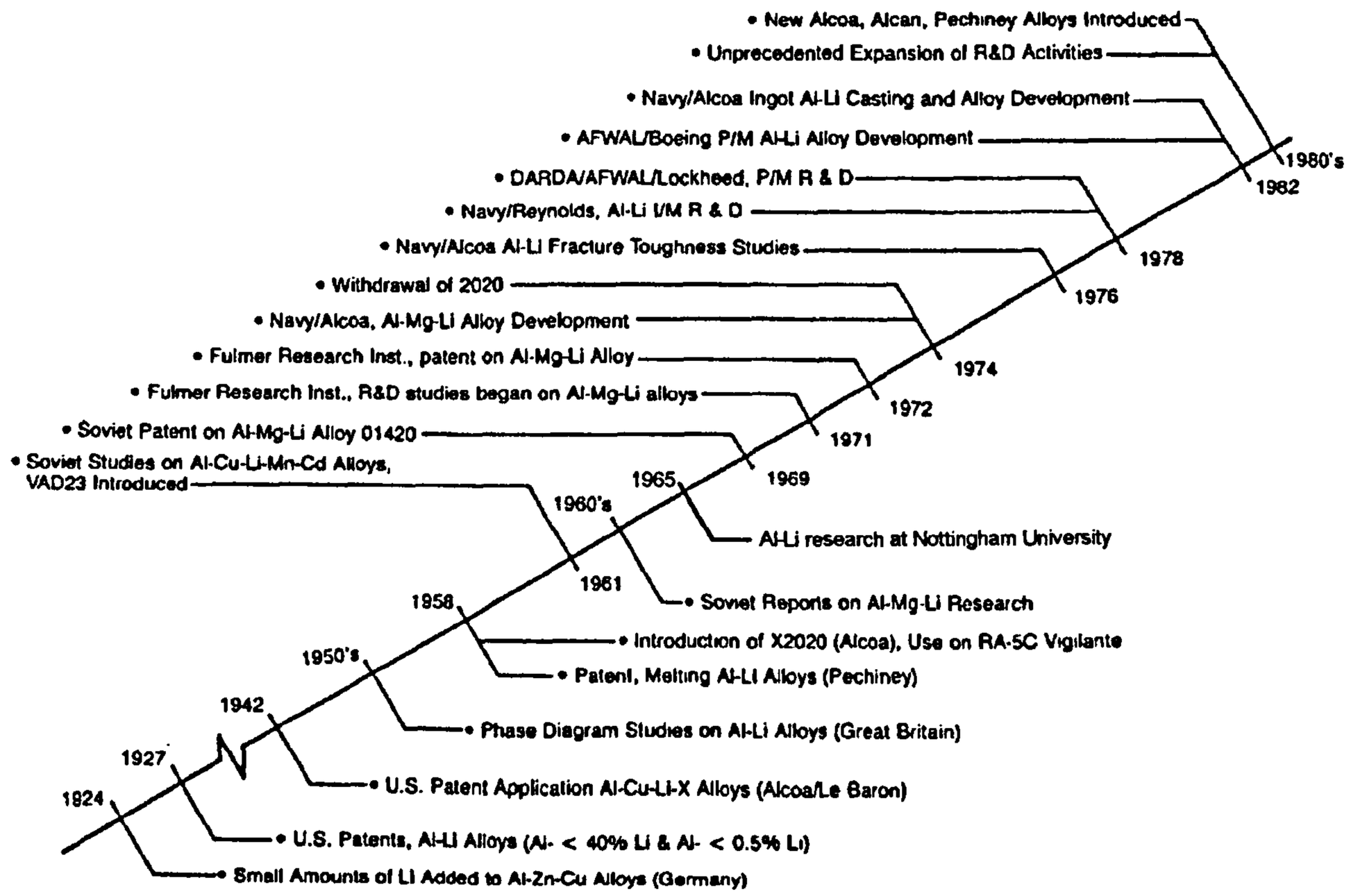

Figure 1.1: Overview of the main facts that marked the development of Al-Li alloys

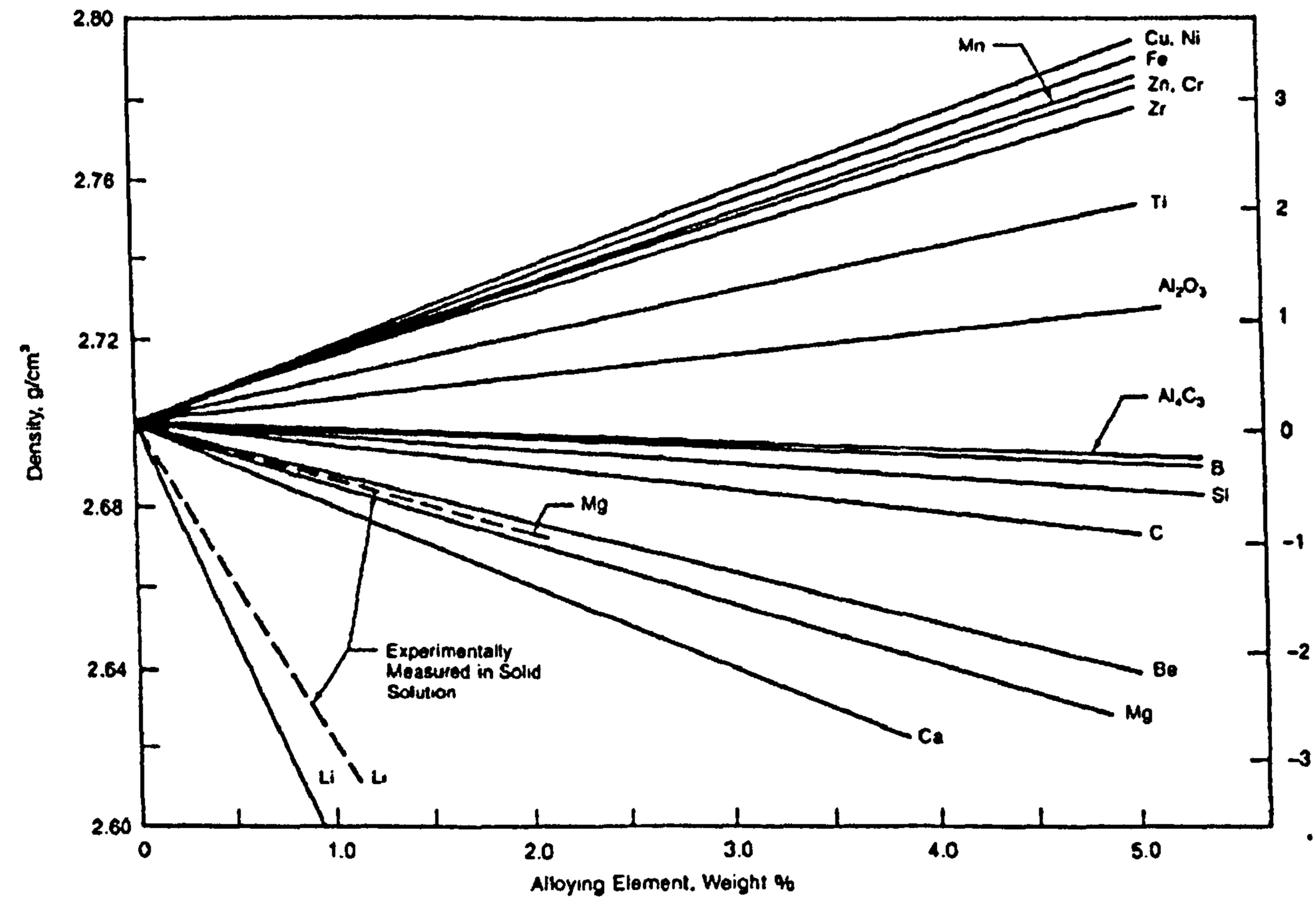

Figure 1.2: Influence of alloying elements on the density of aluminium

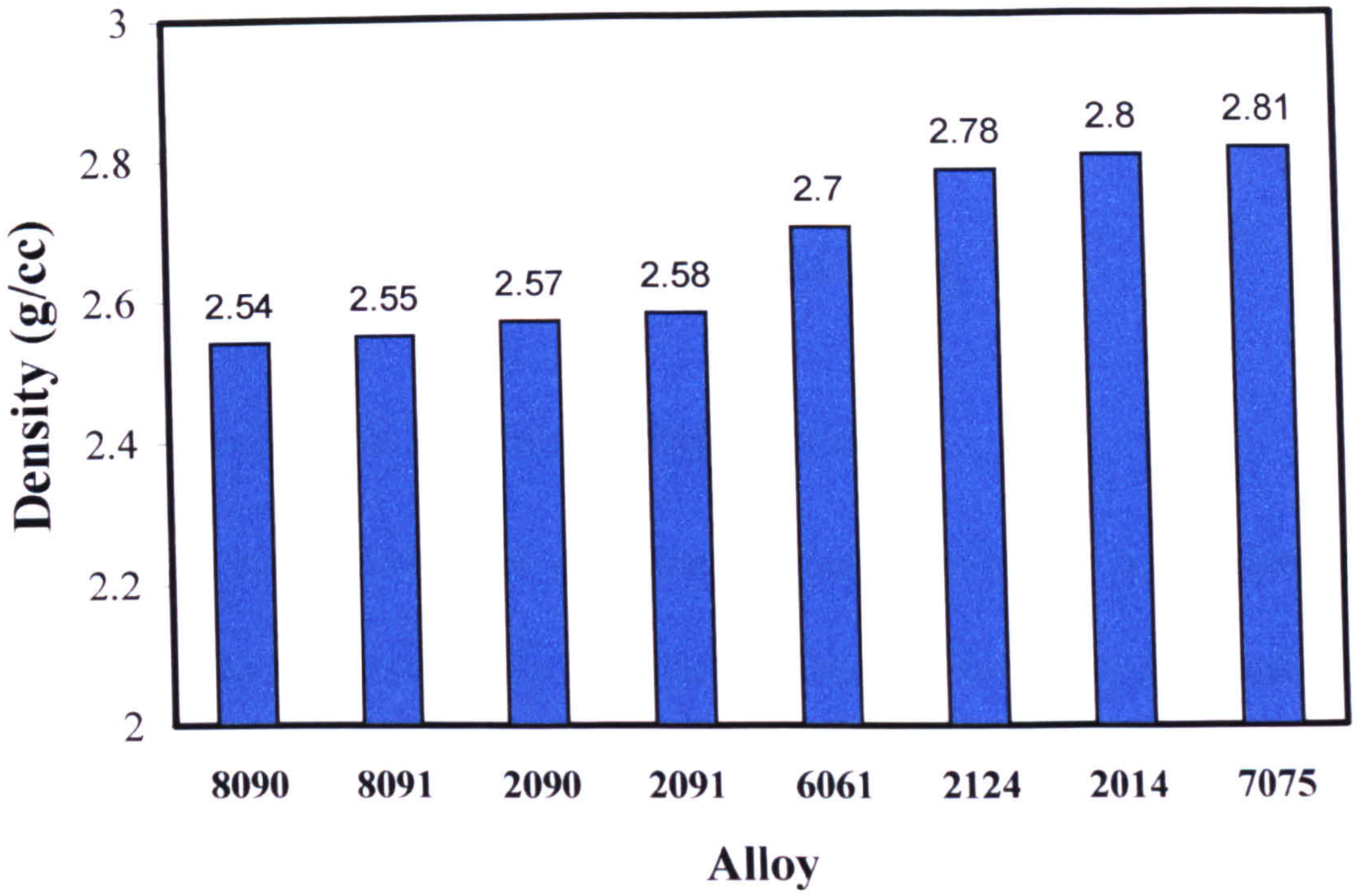

Figure 1.3: Comparison between the densities of Al-Li based alloys and conventional aluminium alloys.

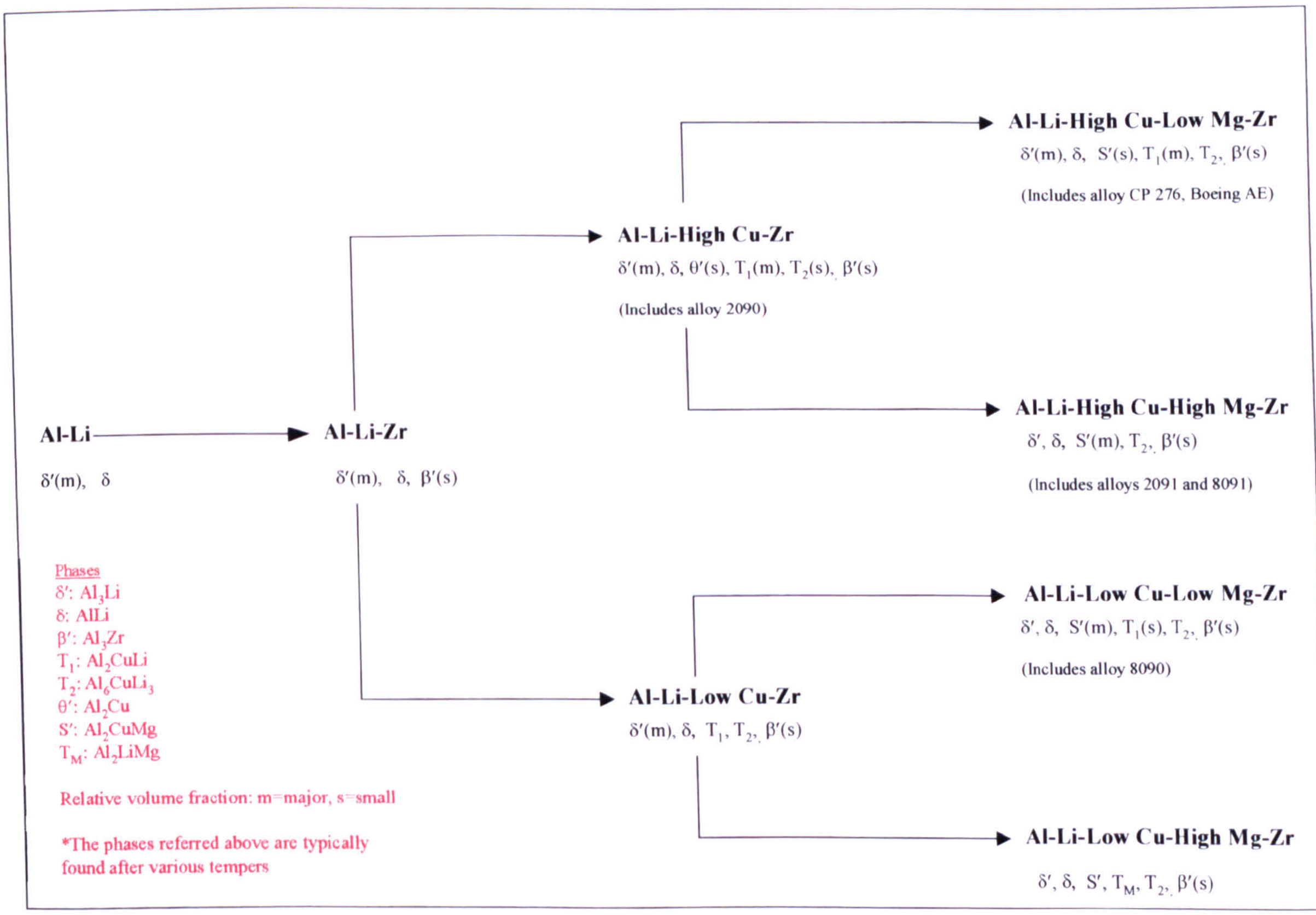

Figure 1.4: The phases precipitated in Al-Li based alloy systems after various heat treatments.

CHAPTER 2

Fundamental principles of age-hardening

2.1 Decomposition in age-hardening systems

The essential requirement for an alloy system to develop age-hardening is a decrease in the solid-solubility of one or more of the alloying elements with falling temperature. The age-hardening process involves the following steps:

1. Solution heat treatment (solutionizing). The alloy is heated to a relatively high temperature between the solvus and solidus temperatures and kept there until a uniform solid solution is produced e.g. point K in **figure 2.1.**
2. Rapid cooling or quenching. The sample is rapidly cooled from the solutionizing temperature to a low temperature, usually room temperature so that a supersaturated solid solution is obtained e.g. point L in **figure 2.1.**
3. Ageing. The solution heat-treated and quenched alloy undergoes controlled decomposition by ageing for reasonable times at one or sometimes two intermediate temperatures (e.g. point M in **figure 2.1**) so that a finely dispersed precipitate forms. The formation of a fine dispersion of precipitates is the aim of age-hardening. These precipitates impede the movement of dislocations during deformation resulting in strengthening of the alloy.

The decomposition process of the supersaturated solid solution during ageing usually involves more than one stage. In the supersaturated solid-solution condition a precipitation-hardenable alloy is unstable and tends to lower its free energy by the spontaneous decomposition of the supersaturated solid solution into metastable phases or the equilibrium phases. When a supersaturated solid solution is aged at a relatively low temperature e.g. room temperature, ordered solute-rich clusters of atoms called Guinier-Preston (GP) zones form instead of the equilibrium phase. GP zone formation requires diffusion of atoms over relatively small distances so that a very fine dispersion forms of extremely high density (10^{17}-10^{18} cm^{-3}).

The direct precipitation of the equilibrium phase would result in a much larger lowering of the free energy of the system, but such phases usually have incoherent interfaces with the matrix and therefore a large activation energy for nucleation. GP zones on the other hand, have a very low interfacial energy resulting in a much smaller relative activation energy barrier for nucleation compared with the equilibrium phase. In addition, GP zones minimize their strain energy by selecting a needle or disc-shape perpendicular to the elastically soft directions of the matrix causing further decrease of the energy barrier for nucleation.

As the ageing conditions (time and/or temperature) increase, the formation of GP zones is followed by the precipitation of transition or intermediate phases. The transition phases precede the formation of the equilibrium phase because, like GP zones, their nucleation energy barrier is lower than that of the

equilibrium phase. The transition phases have a crystal structure that is related to that of the matrix and therefore there is a high degree of coherence between matrix and precipitate that results in low levels of interfacial energy. A schematic of the products during the decomposition process of an age-hardened alloy system is given in **figure 2.2.**

2.2 Strengthening mechanisms in age-hardening systems

The strength of an age-hardenable alloy depends on the interaction of moving dislocations with the internal stresses around precipitates (GP zones) and the precipitates themselves. It has been estimated that the maximum impediment to the movement of dislocations occurs when the spacing between precipitates is equal to the limiting radius of curvature of dislocation lines, which is approximately 10 nm. GP zones can be easily sheared by moving dislocations and therefore are not very effective obstacles to the movement of dislocations. Thus, the moderate increase in yield strength that follows the formation of GP zones is attributed to their high number-density. As dislocations shear the GP zones the number of solute-solvent bonds increases tending to reverse the clustering process. For this, further work must be done by the applied stress (chemical hardening) that makes a contribution to the overall strengthening. Once GP zones are sheared, dislocations continue to pass through them resulting in intense localized planar slip which in turn leads to stress concentration at the grain boundaries and intergranular failure.

The formation of intermediate precipitates that are large in size and widely spaced results in significant work-hardening as the dislocations can easily bow out between them and form dislocation loops (Orowan theory). However, the yield strength remains low as these precipitates can be readily bypassed by the dislocations.

Peak strength in a precipitation-hardenable alloy is achieved by the formation of precipitates that resist shearing by dislocations and are also too closely spaced to be bypassed by dislocations.

Figure 2.3 presents the schematic of a hardness-ageing time curve of an age-hardened alloy at a particular ageing temperature.

2.3 Precipitate free zones

Precipitate free zones (PFZs) are defined as zones adjacent to grain boundaries that are depleted of precipitate. The PFZs are developed due to the following reasons:

- The formation of relatively large precipitates on the grain boundaries resulting in the local diffusion of solute from regions adjacent to the grain boundaries.
- Grain boundaries acting as sinks for vacancies. The vacancy concentration adjacent to the grain boundary is then reduced to such a low level that nucleation of precipitates cannot take place in these regions.

The PFZs are relatively weak regions compared with the remainder of the

precipitation-hardened matrix and therefore can undergo preferential deformation causing high stress concentrations at triple points that in turn leads to premature cracking.

Methods for the decrease of the width of PFZs involve solution heat treatment at higher temperatures, faster quenching rates and lower ageing temperatures.

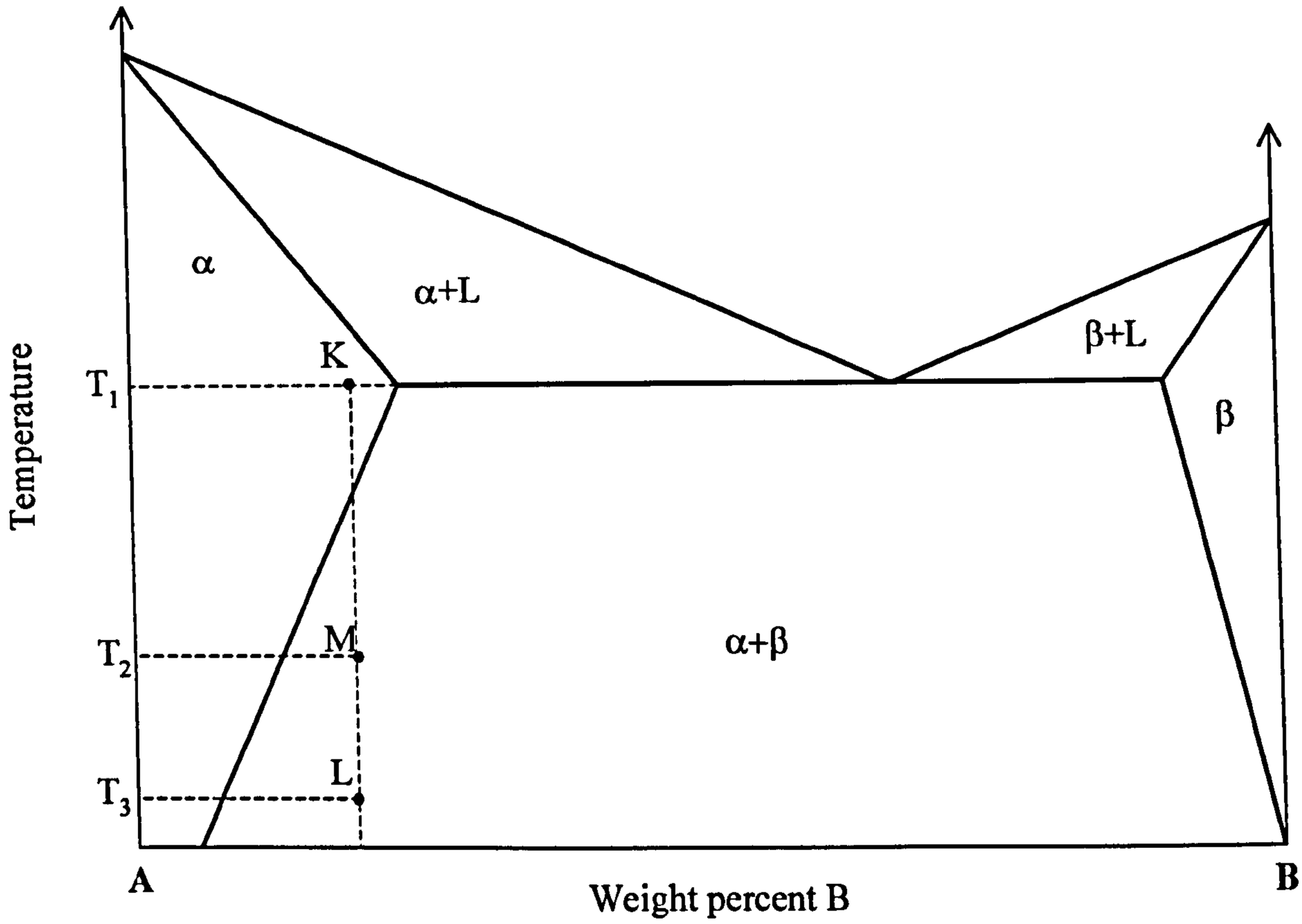

Figure 2.1: A-B binary phase diagram with terminal solid solution α. The solid solubility of B in A is decreasing with decreasing temperature.

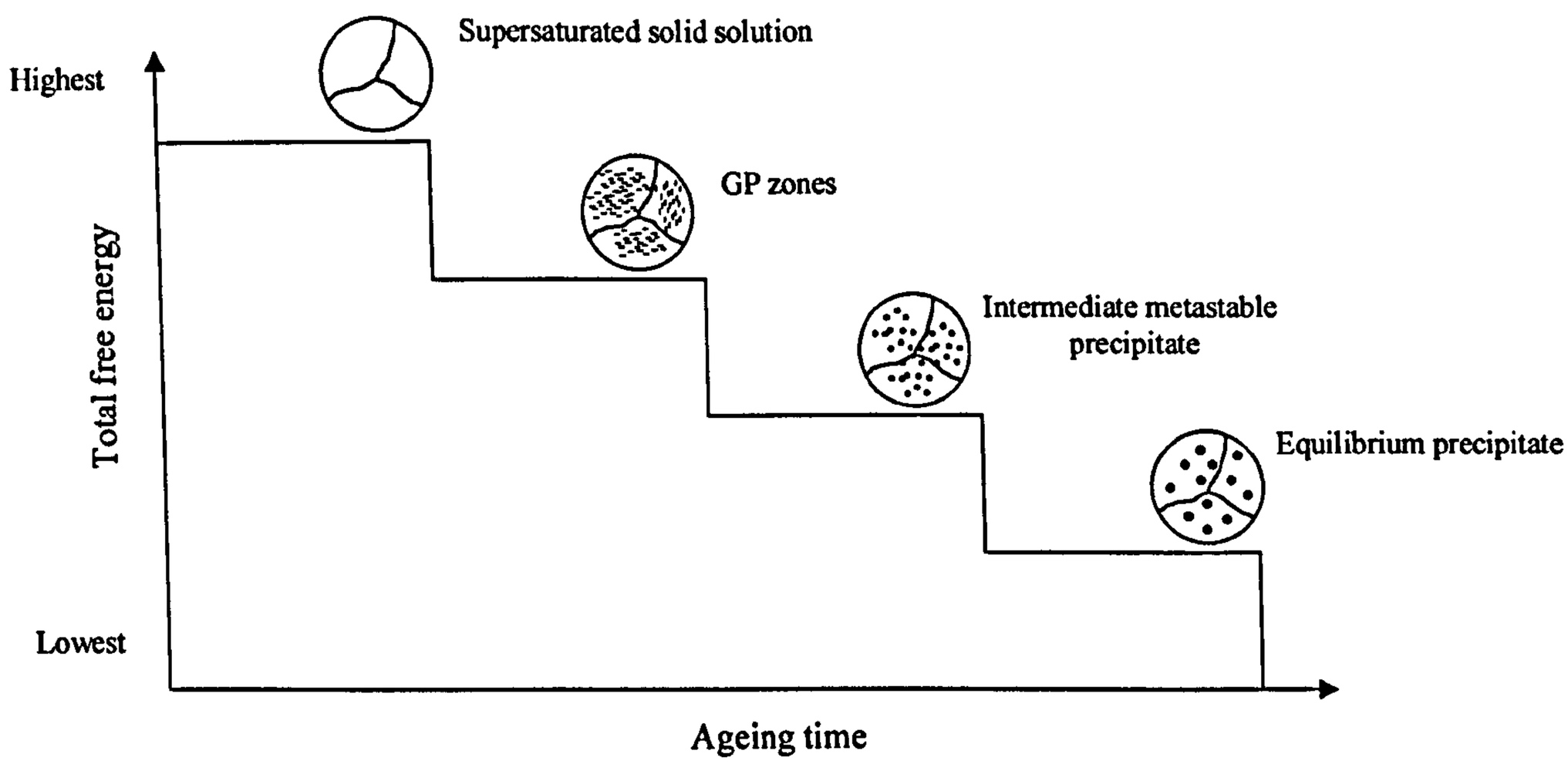

Figure 2.2: A schematic of the products formed during the decomposition process of an age-hardened alloy.

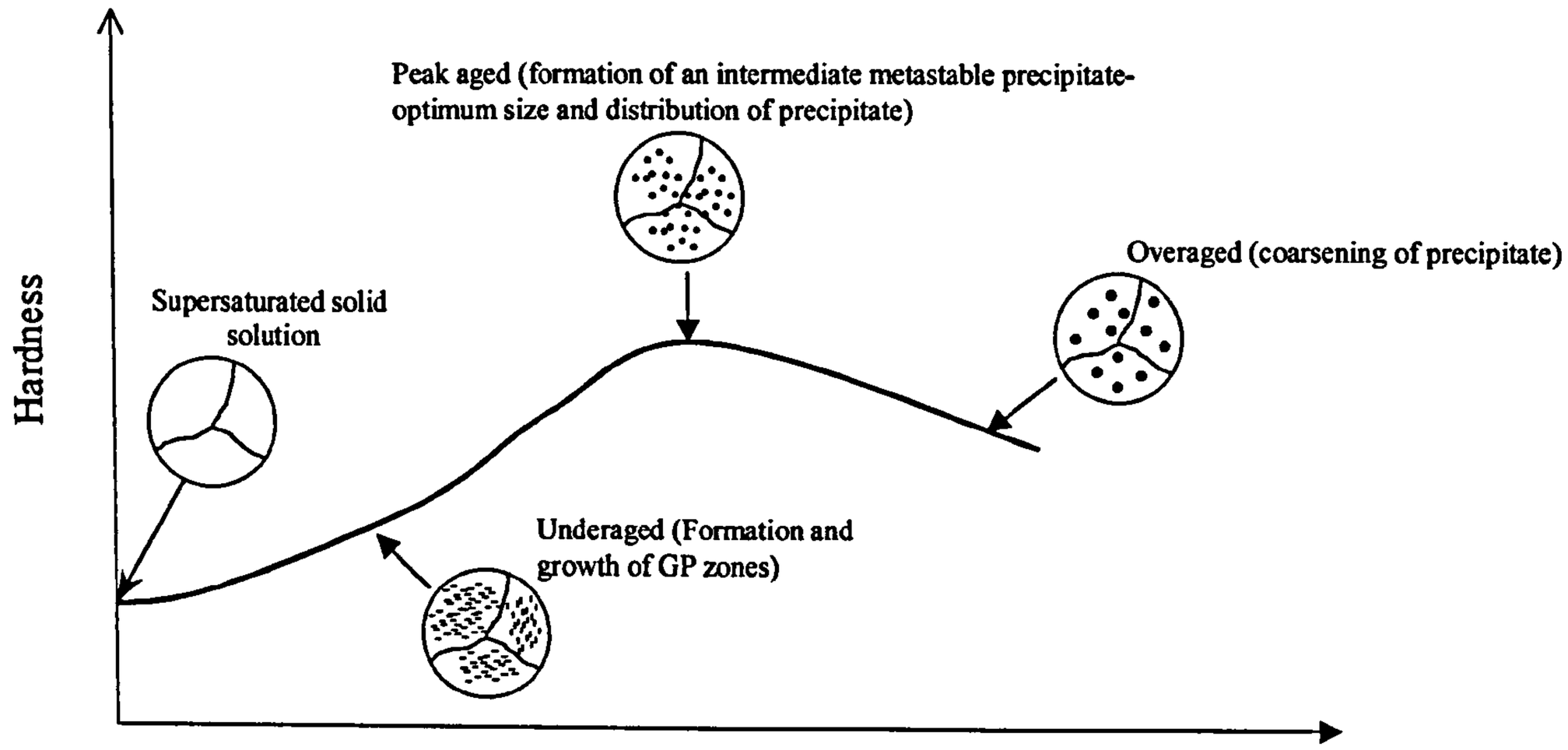

Figure 2.3: Schematic of a hardness-ageing time curve of a precipitation-hardened alloy system.

CHAPTER 3

Al-Li binary alloys

3.1 The Al-Li phase diagram

The most important phases that form in binary Al-Li alloys are the equilibrium δ (AlLi) and the metastable δ′ (Al_3Li) phases. The region of interest of the phase diagram, with regard to the present project, is that position extending up to 6.6wt% (25at%) Li where the δ′ phase is situated. The phase boundaries contained in this region are the α/δ equilibrium solvus line, the α/δ′ metastable solvus line and the (α+δ′/δ′) boundary.

Because the maximum limit of lithium solubility in aluminium at 610 °C is about 4.0wt% (16at%) it is not possible to extend the experimental α/δ′ solvus line to beyond this composition. However, this limit does not apply to theoretical calculations. The theoretical phase diagrams of Sigli and Sanchez **[13]** showing the α/δ′ solvus, the α+δ′ phase field and a low temperature miscibility gap (**figure 3.1**) and that of Khachaturyan et al **[14]** showing the α+δ′ phase field (**figure 3.2**) are the two most important studies of this kind. These theoretical phase diagrams show substantial differences. The Sigli-Sanchez phase diagram predicts a low temperature miscibility gap, metastable with respect to the δ′

phase, while the Khachaturyan phase diagram predicts that the whole α+δ′ phase field is effectively a miscibility gap and the δ′ forms by a spinodal ordering process.

According to Khachaturyan's phase diagram (**figure 3.2**) the metastable α+δ′ miscibility gap contains four sub-phase fields. A solid solution quenched into regions A or D is metastable and decomposes by homogeneous nucleation and growth. In regions B and D[1]C the system can decrease its free energy by a congruent ordering reaction. This means that lithium atoms move to the appropriate sublattice sites of the ordered $L1_2$ superlattice, without any change of local composition, i.e. without decomposition. The difference between subfield B and C is one of solid solution stability. In field B the disordered solid solution is metastable in terms of an ordered phase of the same composition and as a result ordering proceeds through nucleation of ordered domains. In subfield C the solid solution is completely unstable and follows continuous or spinodal ordering without nucleation. In both fields (B and C) the theoretical calculations predict a secondary process, spinodal decomposition which occurs in the congruently ordered solid solution. When the concentration of the lithium-depleted regions decreases beyond a certain value, spontaneous disordering occurs in these regions, resulting in $L1_2$ long-range ordered δ′ precipitates in a disordered solid solution matrix **[14]**.

A more accurate α/δ′ metastable solvus line was established by Noble and Bray **[16]**. By means of electrical resistivity measurements and differential scanning

calorimetry, the experimental α/δ′ metastable solvus boundary was defined in Al-Li alloys containing 2-13at% Li and was described by the equation:

$$\mathbf{lnC_e(at\%) = 4.176 - 9180/RT}$$

where C_e is the equilibrium concentration of lithium in solid solution at temperature T(K). The experimental α/δ′ metastable solvus line is in good agreement with that predicted by the theoretical phase diagram of Khachaturyan described in the last paragraph.

3.2 Characteristics of δ′(Al_3Li)

In the $L1_2$ unit cell of Al_3Li, the aluminium and lithium are positioned at specific locations. The eight corner sites are occupied by lithium, and the six face-centred positions are occupied by aluminium. The geometrical similarity between the lattice of the δ′ precipitates and the face-centred cubic matrix facilitates the observed cube/cube orientation dependence between precipitate and matrix. The lattice parameters of the precipitate are closely matched to those of the matrix resulting in a very small lattice mismatch. The values of misfit strains, which were obtained by TEM studies, scatter between -0.3% and -0.08%. X-Ray line profile analysis determined even smaller values. Similarly, the surface free energy of the δ′/α interface is very low, of the order of 10 mJ/m^2 and consequently the precipitates retain their spherical shape over an extremely wide size range, up to several hundred nanometers [**15**].

3.3 Precipitation of δ′

Noble and Thompson [17] reported on the structural ageing characteristics of aluminium alloys containing 2 and 4wt% lithium. Electron microscopy and electrical resistivity showed that the only phases present in quenched and aged alloys were δ and δ′. From their results we can summarise that:

- The age hardening in Al-Li alloys is a two stage process:

  $solid\ solution \rightarrow \delta'(Al_3Li) \rightarrow \delta(AlLi)$.

- Formation of δ′ at ageing temperatures below 60°C is accompanied by an anomalous increase in resistivity that was attributed to electron scattering from very small particles of δ′ (1-2 nm).

- The δ phase has a fcc or bcc structure and forms as plates on {111} planes.

- The precipitation density of δ′ is much higher than that of δ, and consequently hardening is caused by δ′ precipitation. Maximum strengthening in a 2wt% lithium alloy is associated with a δ′ of size 0.03 μm and number-density $2.6 \times 10^{15} cm^{-3}$.

- Ageing at temperatures above 200 °C resulted in rapid coarsening of the δ′; the coarsening obeyed the Lifshits-Wagner (LW) theory. The activation energy for the coarsening of δ′ was found to be 140±2 kJ/mol. Since the δ′ precipitates obey the LW coarsening theory, coarsening occurs by selective growth of the larger precipitates, the process being controlled by the diffusion of lithium to the δ′.

- In the higher-lithium alloys, which contain a very high volume fraction of δ′, coalescence of particles occurred (**figure 3.3**).
- At ageing temperatures just below the δ′ solvus, precipitation occurs completely on dislocations in both alloys (**figure 3.4**).

In more recent work, *Noble* and *Trowsdale* **[18]** studied the early stages of low-temperature ageing of an Al-3.7wt%Li alloy by differential scanning calorimetry, X-ray diffraction and transmission electron microscopy. According to their results, δ′ precipitation occurs in this alloy with an activation energy of 86kJ/mol, which is considerably lower than the activation energy for diffusion of lithium in aluminium (130kJ/mol). This indicates that δ′ precipitation is controlled by a slow reaction involving excess vacancies from the quench. Exothermic events in the DSC trace show the presence of δ′ precursor structures in the alloy which have been interpreted as congruent ordering followed by spinodal decomposition. The activation energy of these precursor structures was measured and found to be 54kJ/mol. This value is equal to the energy for the movement of quenched-in vacancies in the alloy. Consequently, the precursor events are controlled by the hold time at room temperature, the quench rate, and small amounts of cold work, since these processes govern the number of excess vacancies in the alloy.

The decomposition of an Al-1.85wt% Li alloy during isothermal ageing has also been studied by Schmitz and Haasen **[19]** using High Resolution Electron

Microscopy (HREM). The size distributions of the precipitates and the decomposition parameters such as mean radius, particle density and precipitated volume fraction were measured.

In the as quenched specimen, many small $L1_2$ ordered domains with a somewhat diffuse interface were observed. Apart from a few larger ordered particles, which appeared during the first minutes of ageing, this diffuse domain structure remains during 1-2 min. ageing at 190°C. Presumably the few larger particles are due to heterogeneous nucleation. After 4min. at 190°C a large number of nearly spherical δ' particles with a clear sharp interface were observed. With further ageing these spherical particles grew whereas the ordered domains, observed in the as quenched state, disappeared.

The decomposition sequence described above produced, for intermediate ageing times, a bimodal size distribution defined by one distribution peak at r=1nm belonging to the small ordered domains and a second distribution peak at larger radii belonging to the spherical precipitates with sharp interfaces. The distribution peak at small radii disappears in later stages of ageing.

Baumann and Williams [**20**] have made an important study of the influence of nucleation temperature and pre-ageing thermal history on $\delta'(Al_3Li)$ distributions in a binary Al-2.0wt%Li alloy. All samples were given an initial solution treatment of 20 minutes at 570°C. Following this, one of three different processing sequences was employed:

I) *Water-quench procedure (WQ)*: Samples were water quenched to room temperature from the solution treatment temperature and then transferred to a furnace at the ageing temperature.

II) *Direct -quench procedure (DQ)* : Samples were directly transferred from the solution treatment furnace to an oil bath at the ageing temperature.

III) *Step-quench procedure (SQ)*: Samples were transferred from the solution treatment furnace to a furnace at 350°C for 20min to anneal out excess vacancies and then transferred to an oil bath at the ageing temperature.

Two ageing temperatures were studied (200 and 220°C) and after heat treatment all the samples were examined by TEM. The results obtained by Baumann & Williams can be divided into δ′ nucleation and δ′ growth events:

δ′ nucleation

Under the conditions tested, the W.Q samples always showed a higher particle number density (N_V) and smaller average radius (R) of δ′ compared to the D.Q and S.Q procedures.

Examination of the W.Q samples prior to ageing revealed that δ′ had already precipitated as a very fine dispersion (1.5 nm diameter).

At an ageing temperature of 200 °C which corresponds to an undercooling ΔT of 60°C there was no significant difference between the D.Q. and the S.Q. samples. δ′ nucleation in both cases was coherent and homogeneous showing no preference for nucleation near dislocations.

When nucleation and growth occurred at 220°C (ΔT=40°C), the δ′ particles in the S.Q. samples were significantly fewer in number and larger in size than those in the D.Q. samples. The D.Q. samples (**figure 3.5a,b**) were characterised by a predominantly coherent, homogeneous, particle distribution. The S.Q. samples (**figure 3.5c,d**) were characterised by a coarser dispersion of δ′ particles which are almost all associated with dislocations.

Baumann and Williams concluded from these results that:

- Homogeneous nucleation occurs at relatively low undercooling in this alloy (ΔT=60°C)
- N_V increases rapidly with increasing undercooling.
- Heterogeneous nucleation occurs at very low degree of undercooling.

δ′ growth

The D.Q. sample showed a higher particle growth rate than the S.Q. sample over the growth period investigated. Particles nucleated at high levels of undercooling tended to retain their spherical morphology, whereas at lower undercooling they observed dendritic particle shapes when particles nucleated homogeneously and were widely spaced, or plate-like when they nucleated along the length of a dislocation.

For bulk diffusion-controlled growth of a spherical particle in an infinite matrix supersaturated with solute, it was shown that the particle radius *R* increased parabolically with time *t* according to the equation:

$$R=\lambda(Dt)^{1/2}$$

where the proportionality constant λ is a function of the degree of supersaturation and D the interdiffusion coefficient.

3.4 Coarsening of δ′

The first study of coarsening of δ′ in Al-Li alloys was undertaken by Noble and Thompson **[17]** and they showed that the coarsening process followed the Lifshits-Wagner theory. Many studies on coarsening behaviour of δ′ have followed, but the most comprehensive study has been done by Mahalingam et al **[21]**. These workers studied the coarsening process of the metastable δ′ phase in a series of binary Al-Li alloys containing between 2.4 and 4.5 wt% Li using TEM. The isothermal ageing times were varied from 12 h to 10 days at 200 and 225 °C.

During the isothermal ageing process the δ′ precipitates coarsen according to the Lifshits-Wagner theory, in agreement with the results of Noble and Thompson **[17]**. Their results were fitted to the relation: $\mathbf{R^3 - R_0^3 = kt}$ where **k** is the coarsening constant and R_0 the δ′ size at the start of coarsening. The authors suggest the following empirical equation which relates the lithium content, ageing time and ageing temperature T to the coarsening constant **k**:

$$\mathbf{lnkT=b/t + c}$$

$$\mathbf{b=-2545.73(wt\%Li) - 4749.06}$$

$$c=5.88(wt\%Li) - 36.87$$

3.5 δ′ precipitate free zones

The growth kinetics of δ′ precipitate free zones (PFZs) at the grain boundaries have been investigated by Jha, Sanders, and Dayananda [22]. Several Al-Li alloys were examined at a large range of ageing temperatures (168-225°C) and ageing times.

In recrystallised alloys the growth of PFZ's takes place by a solute depletion mechanism. The solute is consumed during the growth of equilibrium δ precipitates at grain boundaries. The δ phase begins to nucleate on the grain boundaries from the early stages of ageing. The number-density of δ particles increases with ageing time. The PFZ width increases with the ageing time and the thickness of δ particles also increases.

The growth of the PFZ is diffusion controlled and it grows parabolically with time according to the equation:

$$h=K_p t^{1/2}$$

where **h** is the half PFZ width and **t** the ageing time at a given temperature.

In unrecrystallized Al-Li-Zr alloys, the PFZ width depends upon the nature of the grain boundaries and the distribution of δ particles amongst the various grain boundaries. Small angle grain boundaries (misorientation<10°) and twist boundaries had narrow or no PFZs associated with them. The high angle grain boundaries have larger energy and therefore are potential sites for the nucleation

of the equilibrium δ particles. The growth rate of the PFZ is higher in unrecrystallised zirconium containing alloys than in recrystallised alloys of similar lithium content. A higher concentration of lithium also accelerates the rate of PFZ growth and this observation suggests a possible change in the interdiffusion coefficient as the lithium content increases.

3.6 Stability of δ′ at low service temperatures

When aged Al-Li alloys are exposed to temperatures of 70-130 ^{o}C during service, continued ageing can take place, i.e. further δ′ precipitation occurs. Noble et al [3] have made an extensive study on this effect and shown the following:

- Exposure for long periods of time at 70-130 °C causes further decomposition of aged alloys containing 1.7-3.05 wt% Li.
- Exposure at 70 °C causes the formation of extremely fine δ′ particles. The absence of quenched-in vacancies in aged alloys results in very slow kinetics of precipitation at 70°C, and consequently the δ′ precipitates had a size of only a few nanometers and a volume fraction of 0.028 after 1000 h exposure.
- As the exposure temperature is raised from 70 to 130 °C there is a gradual change in the decomposition process from the formation of small δ′ particles to the growth of existing δ′ particles present from the preage at 150°C.

3.7 Zirconium incorporated as a dispersoid-forming element

Zirconium is used to produce grain refinement of cast structures and to inhibit recrystallization in wrought structures. Typical additions range between 0.05 and 0.2wt%. The zirconium produces fine (20-30nm diameter) dispersions of coherent Al_3Zr (β') precipitates with a metastable cubic $L1_2$ structure. The dispersions are very stable due to the low zirconium solubility in aluminium, the small misfit and the low diffusion rate of zirconium in aluminium. The (β') particles also provide heterogeneous sites for δ′ nucleation. The reduction in both strain and surface energy terms associated with δ′-nucleation are held to be responsible for the effectiveness of the β' precipitates as nucleation sites with the δ′-coated β' precipitates behaving as a population of larger δ′-precipitates. In **figure 3.6** we can see the β'-cores within the composite δ′-β' precipitates [**23**].

3.8 Mechanical properties of binary Al-Li alloys

As we have already seen, the age hardening of Al-Li alloys involves the continuous precipitation of δ′ (Al_3Li) from a supersaturated solid solution. Noble et al [**24**] have examined how this precipitation of δ′ affects the mechanical properties of alloys containing up to 5.3 wt% lithium.

A linear relation was found between the proof stress of aged alloys and the lithium concentration up to 3.7 wt% Li, which is the maximum solid solubility of lithium in aluminium.

At lithium concentrations higher than 3.7 wt% the equilibrium δ phase appears in the microstructure. The δ precipitates are soft (160 HV) compared with intermetallics that appear in other aluminium alloys (400-700 HV). Consequently, the presence of δ does not have any important effect on the proof stress of the Al-Li alloys. However, the δ particles are brittle and this is the reason that the elongation falls to very low levels at a lithium concentration of 5.3 wt%.

When in solid solution, lithium atoms produce only a small degree of strengthening (6.5 MN m^{-2}/ at%). However, in the aged condition, volume fractions of δ′ exceeding 20% can be produced and this is accompanied by a considerable increase in strength. For an alloy containing 3.7 wt% Li the maximum proof stress and tensile strength are 370 and 450 MN/m^2 respectively. Alloys which have been aged to just before the peak hardness contain δ′ particles that are sheared by dislocations moving on {111} slip planes. Additional confirmation of particle shearing is provided by the presence of dislocations pairs and areas of intense localized slip, both of which must be produced by dislocations cutting through the δ′ particles. The dislocation-cutting process involves a number of mechanisms which can contribute to strengthening. Such mechanisms include strengthening from coherency strains around the precipitates, increased surface area of the sheared precipitates, differences in elastic modulus between matrix and precipitate, and creation of antiphase boundary as dislocations cut the ordered precipitates.

The two first mechanisms contribute very little to the observed strength. The main strength is attributed either to order hardening (development of antiphase boundary) or a combination of order plus modulus hardening (**figure 3.7**).

The strengthening increment due to modulus hardening is given by the equation:

$$\Delta\tau_g = \Delta G/4\pi^2(3\ \Delta G/G\ b)^{1/2}[0.8 - 0.143\ln(r/b)]^{3/2}\ r^{1/2}\ f^{1/2}$$

where ΔG is the difference in modulus between precipitate and matrix.

G is the shear modulus of the matrix

b is the magnitude of the Burgers vector of dislocations in the matrix.

r is the effective planar radius of particles.

f is the volume fraction of δ'.

The strengthening increment due to order hardening is given by the equation:

$$\Delta\tau_o = (\gamma/2b)\ [(4\gamma rf/\pi T)^{1/2} - f] \text{ for } \pi Tf/4\gamma < r < T/\gamma$$

$$\Delta\tau_o = (\gamma/2b)\ [(4f/\pi)^{1/2} - f] \text{ for } T/\gamma < r$$

where γ is the energy of the antiphase boundary and T the line tension of the dislocation.

This latter equation is derived from the fact that dislocations in ordered alloys glide in pairs. The leading one, D1, destroys the order in the precipitates along the glide plane and creates antiphase boundaries. The trailing dislocation, D2, which glides in the same plane, restores the order and eliminates the boundaries. **Figure 3.8** shows a schematic of the mechanism.

The shearing of the δ' precipitates causes not only high strength but also intense

planar slip. Because cross slip is difficult in Al-Li alloys, dislocations travel in pairs resulting in coarse heterogeneous slip. This kind of slip leads to stress concentration where the slip bands meet the grain boundaries and the result is brittle intergranular failure. The higher the volume fraction of δ′ the more intense is the planar slip and the higher the degree of intergranular brittleness in the alloy.

3.9 Mechanical properties after long term service exposure

Noble et al [3] have investigated the mechanical properties of binary Al-Li alloys containing 1.7, 2.5 and 3.05 wt% Li which have been aged for 24 h at 150°C and then exposed for a long period of time at 70, 100 and 130 °C. From these results it is clear that the changes in mechanical properties resulting from exposure of the 1.7 and 2.5 Li alloys are the result of additional δ′ precipitation. Exposure at 70°C causes a bimodal microstructure which consists of very fine exposure-δ′ forming between coarse δ′ particles from the pre-age. This fine precipitation causes only a very small change in the strength and the fracture energy. Larger changes in mechanical properties result from exposure at 100 and 130 °C and this can be attributed to either the formation of additional δ′ precipitation of relatively large size or growth of pre-existing δ′ particles from the pre-age, or a combination of the two effects.

For the 2.5 Li alloys 30% of the changes in mechanical properties resulting from

exposure at 100°C for 1000 h can be attributed to the growth of pre-existing δ′ particles. The remaining changes are due to the formation of an additional dispersion of δ′ between the coarse δ′ particles produced during the pre-age. For the 1.7 Li alloy the volume fraction of δ′ produced during the 150°C pre-age is very small and consequently the growth of these precipitates contributes very little to exposure embrittlement. As a result, the largest contribution to embrittlement at 100 and 130 °C is attributed to the formation of a fresh dispersion of δ′.

Noble et al **[25]** have also studied exposure embrittlement in recrystallised and unrecrystallised Al-Li binary alloys. Binary Al-Li alloys containing 2.6 wt% Li (recrystallised microstructure) and 3.2 wt%Li (unrecrystallised microstructure) after solution treatment and ageing for 24 h at 150°C were exposed for up to 1000h at 130°C. Exposure of both alloys yielded increments in the proof stress and tensile strength, and decrements in ductility and fracture energy. The strength increases and fracture energy decreases were marginally higher in the unrecrystallised alloy.

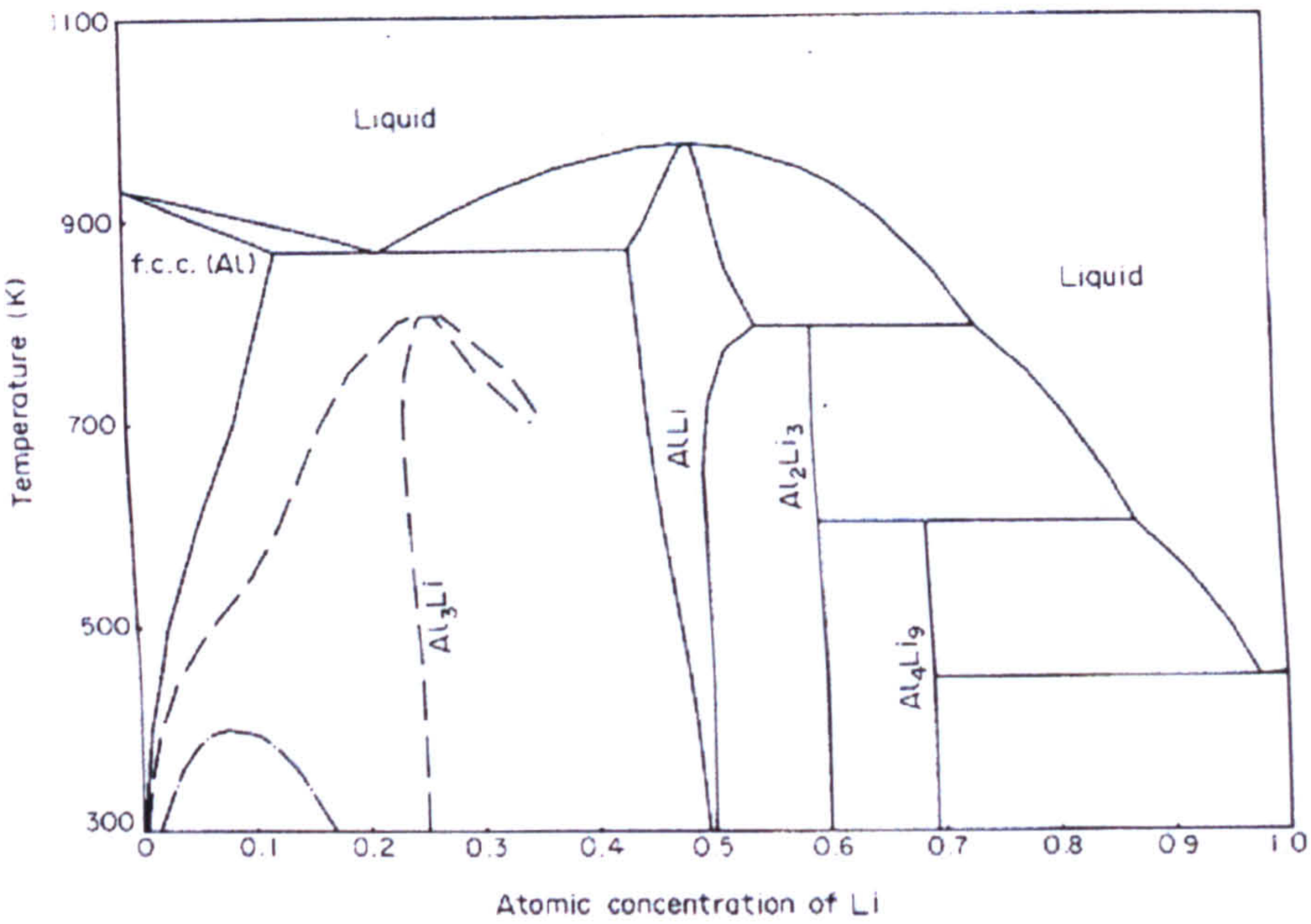

Figure 3.1: Theoretical phase diagram of Sigli and Sanchez showing the α/δ solvus, the α+δ′ phase field and the low temperature miscibility gap [13].

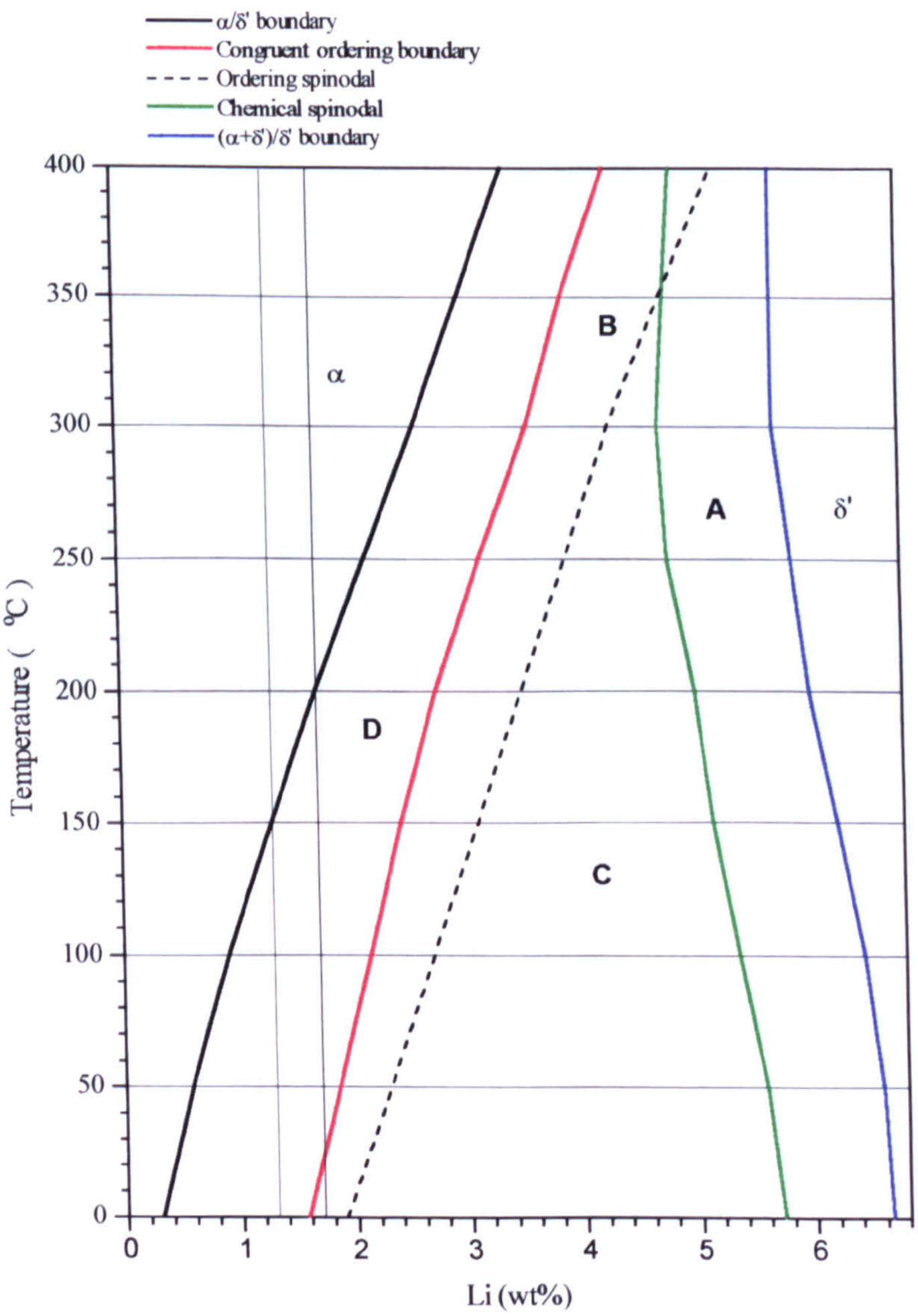

Figure 3.2: Theoretical phase diagram of Khachaturyan et al [14]. The α/δ′ boundary is as defined by Noble and Bray [16].

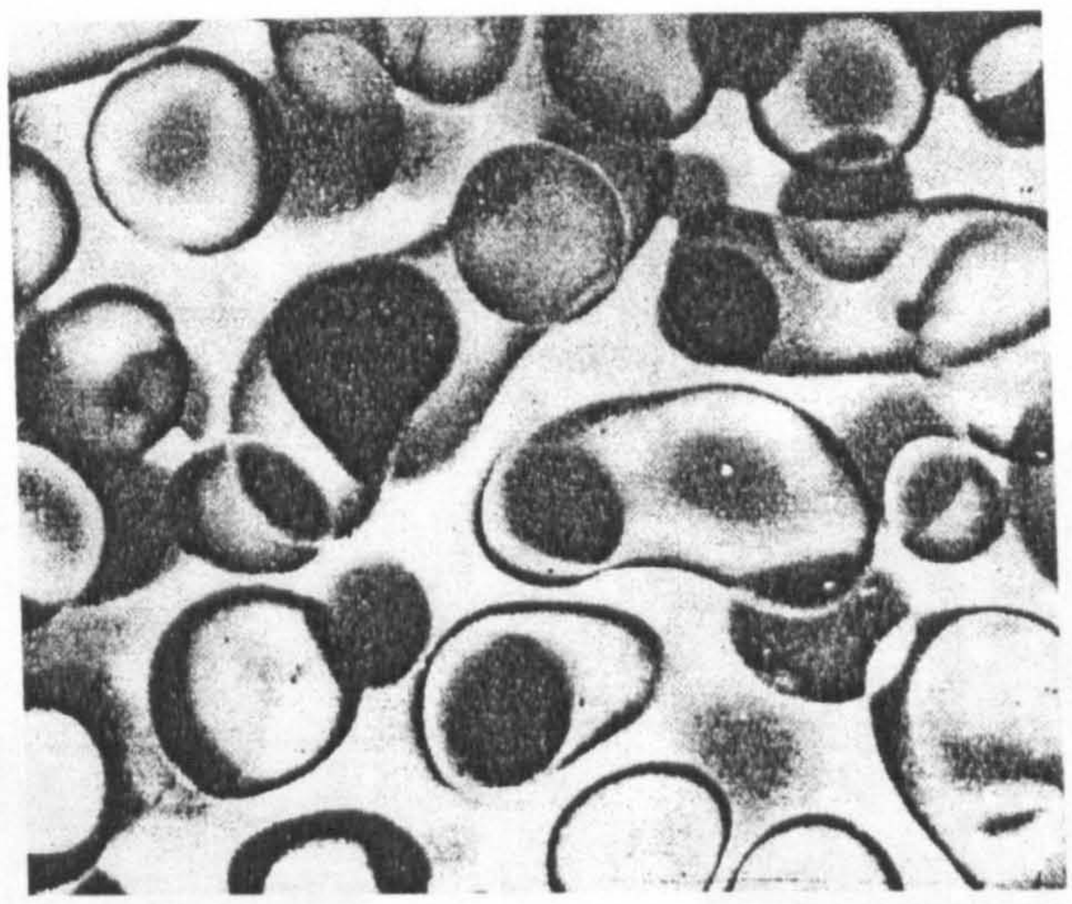

Figure 3.3: δ′ coalescence in an Al-4.0wt%Li after ageing for 80 h at 220°C [**17**].
Zone axis: <100>.

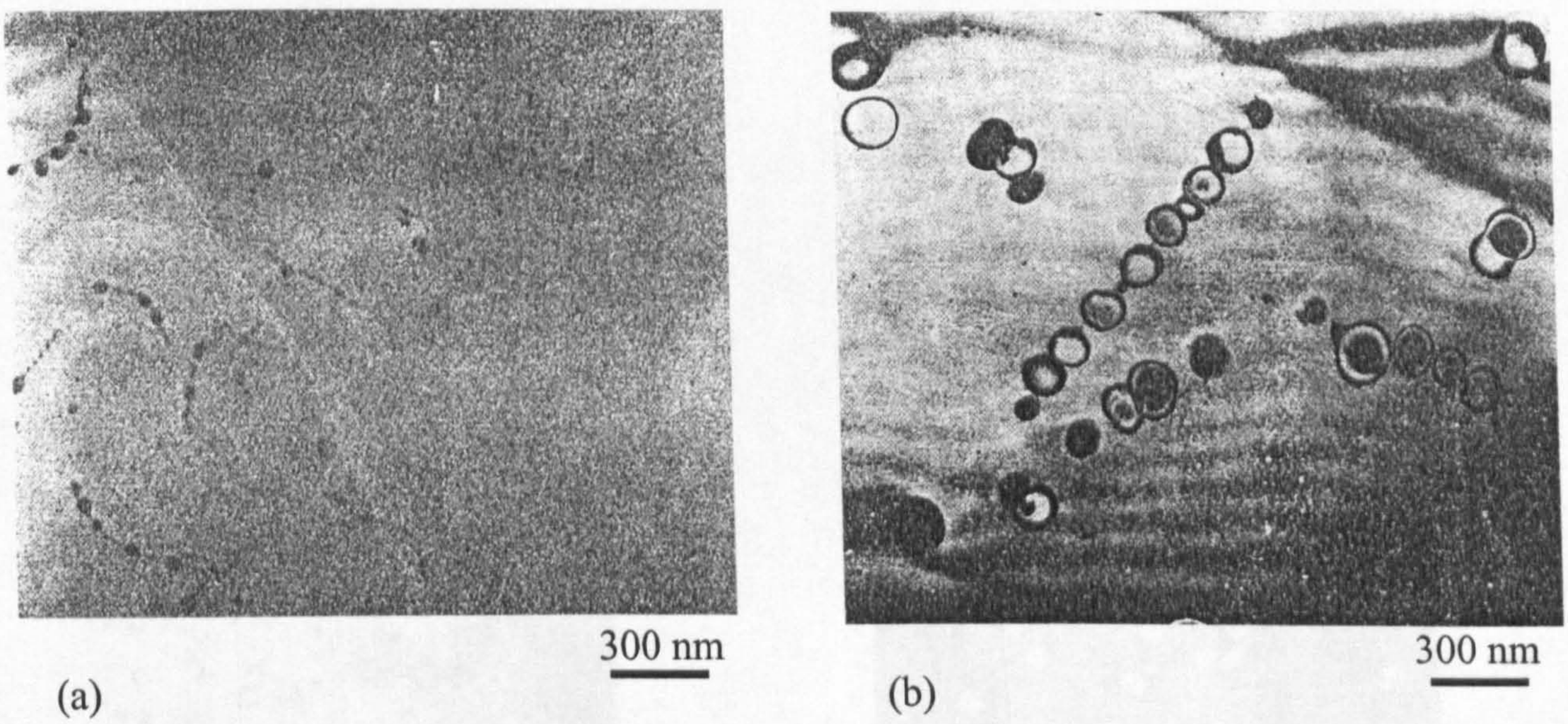

Figure 3.4: δ′ precipitated on dislocations in an Al-2.0wt%Li after ageing at 220°C [**17**].
(a) Age for 2 h. Zone axis: <110>.
(b) Age for 12 h. Zone axis: <310>.

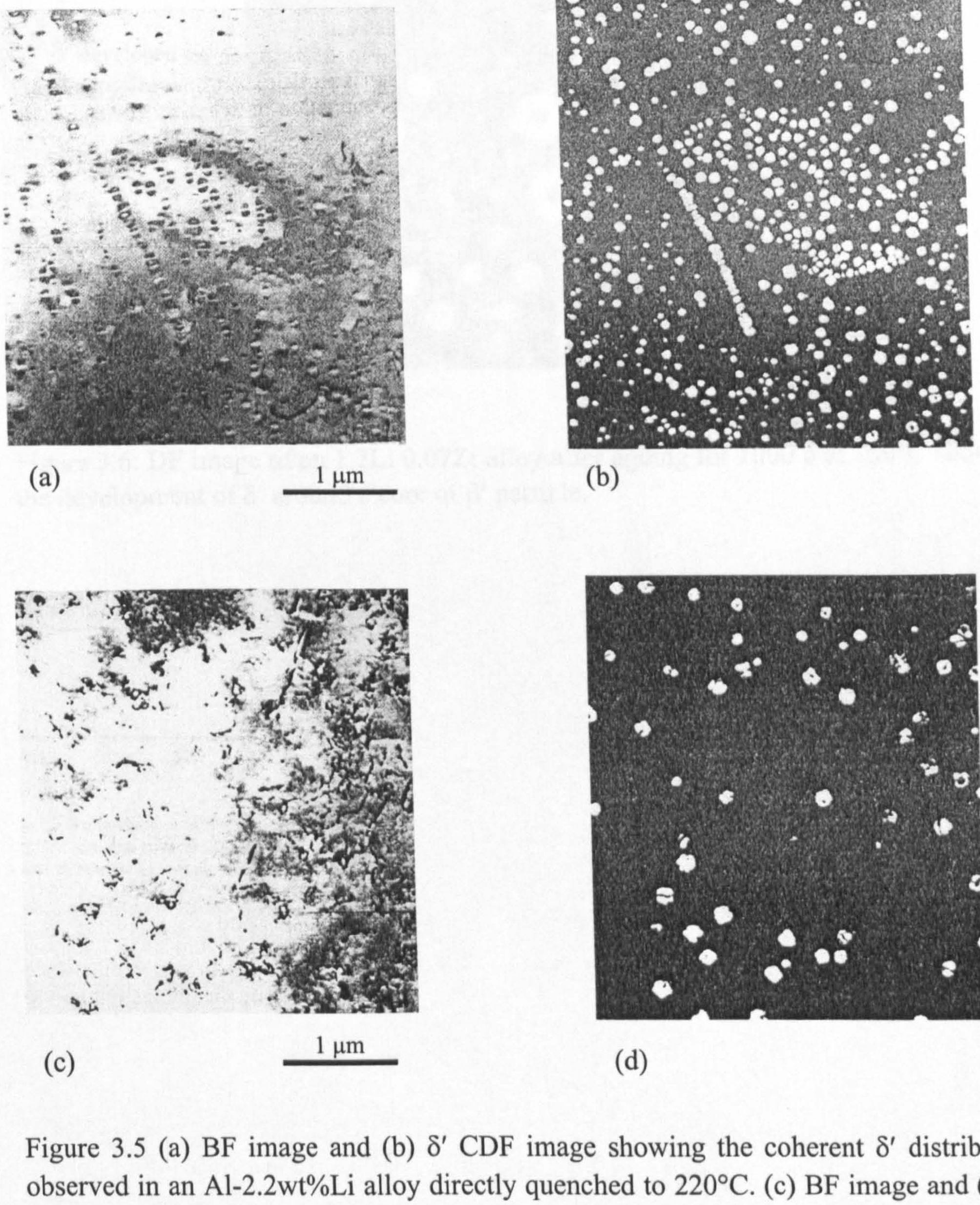

Figure 3.5 (a) BF image and (b) δ′ CDF image showing the coherent δ′ distribution observed in an Al-2.2wt%Li alloy directly quenched to 220°C. (c) BF image and (d) δ′ CDF image showing the δ′ precipitates associated with dislocations in the material step quenched to 220°C [**20**].

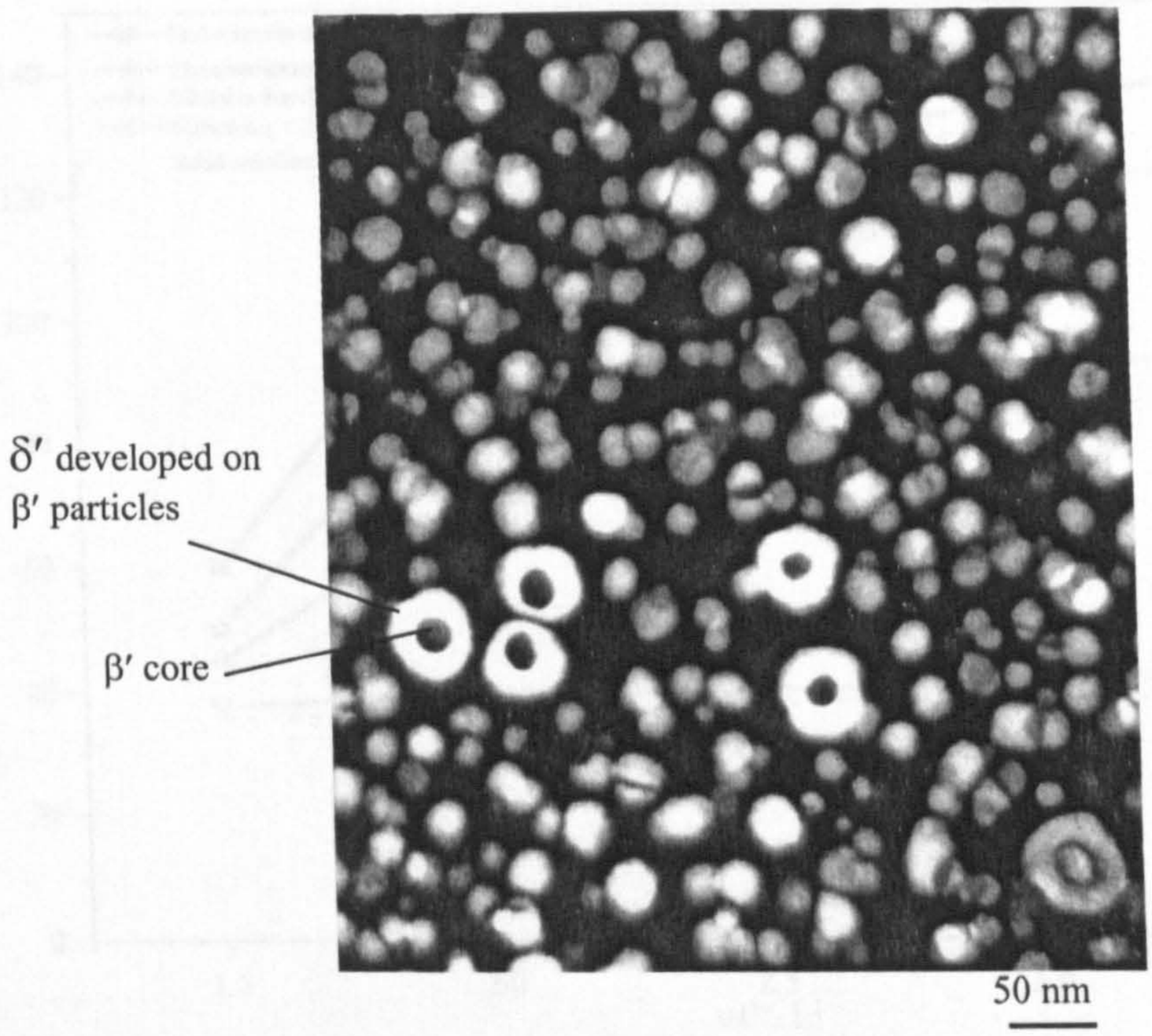

Figure 3.6: DF image of an 1.7Li 0.07Zr alloy after ageing for 1000 h at 150°C showing the development of δ′ around a core of β′ particle.

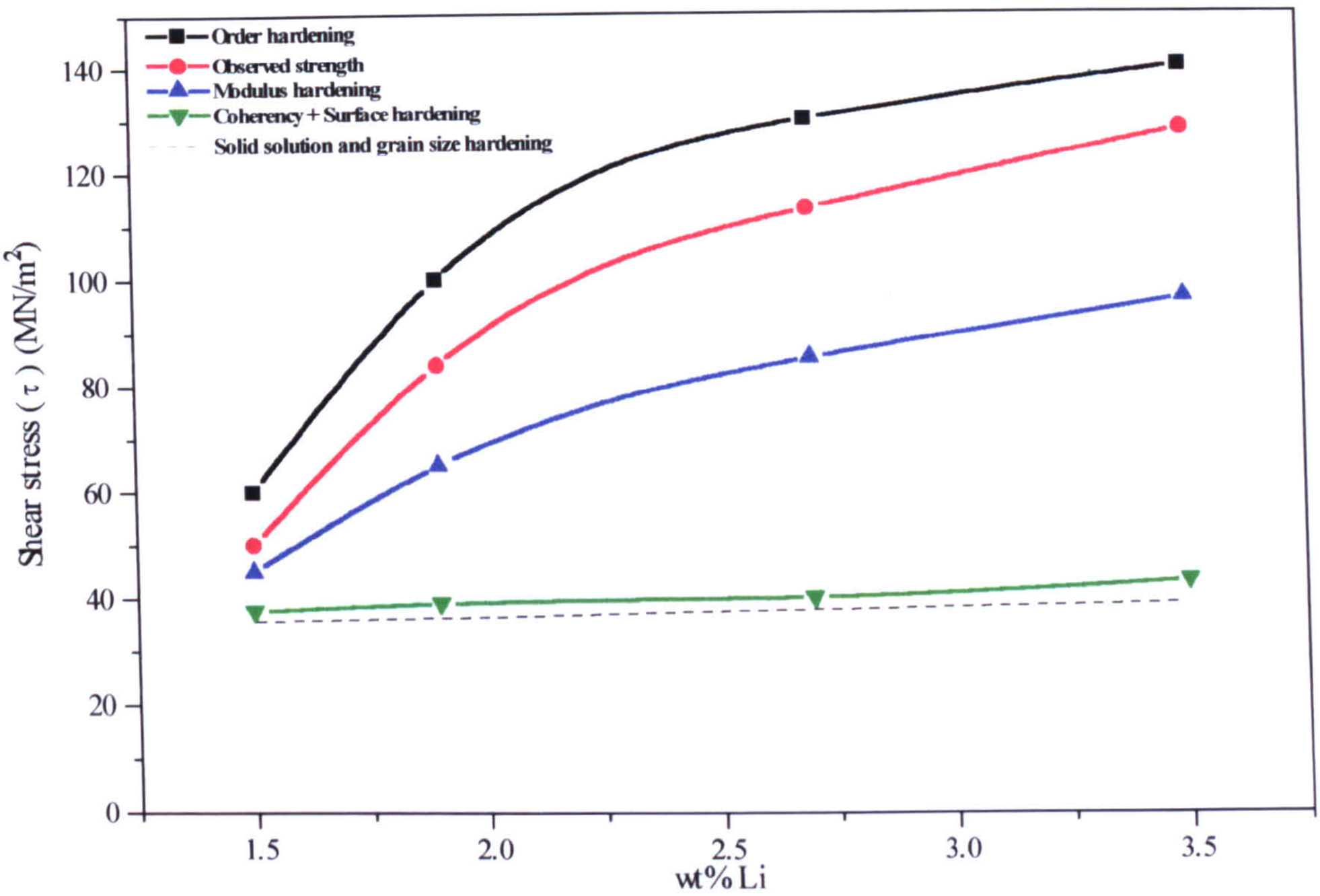

Figure 3.7: Contribution of various mechanisms to strength of Al-Li alloys.

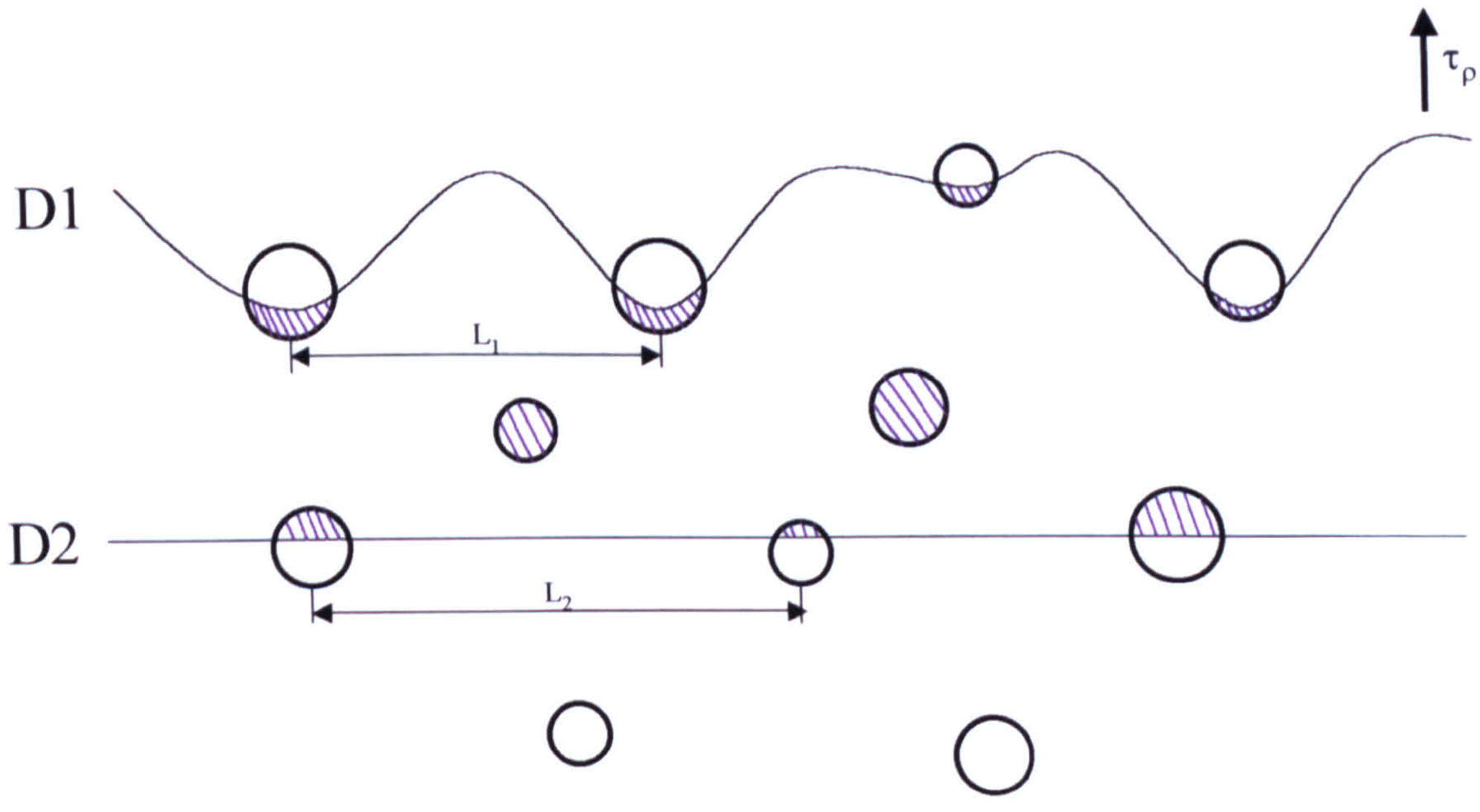

Figure 3.8: Schematic of paired dislocations D1 and D2. The image plane is their common {111}-slip plane. The antiphase boundaries are shown hatched.

CHAPTER 4

Al-Li-Mg alloys

4.1 The Al-Li-Mg phase diagram

Figure 4.1 [23, 26] shows an isothermal section of the Al-Li-Mg system at 200°C. This isothermal section shows the presence of α, α+δ (AlLi), α+T_M (Al_2LiMg) and α+γ ($Al_{12}Mg_{17}$) fields.

4.2 Precipitation characteristics

Magnesium has a high solid solubility in aluminium and this is relatively unaffected by the presence of lithium. Consequently, in practical alloy compositions supersaturation of magnesium remains low and no additional metastable phases form besides δ′. The only phase containing magnesium found in commercial Al-Li-Mg alloys is the equilibrium phase Al_2LiMg (T_M) which nucleates heterogeneously giving rise to coarse particle dispersions without benefit to mechanical properties [**23**].

Trowsdale et al [**27**] studied alloys containing Al4%Li0-2%Mg. TEM diffraction patterns indicated the presence of very fine δ′ at low ageing temperatures and short ageing times. Very small (30-40nm) particles of β' (Al_3Zr) were also present in as-quenched alloys containing >0.1% Zr. In all the alloys the

mechanical properties were controlled by the δ′ particles; no Al_2LiMg phase was detected.

4.3 Effect of magnesium on the α/δ′ solvus

Two groups of workers have looked at this question and both have concluded that magnesium additions raise the δ' solvus. Baumann and Williams [**28**] showed that magnesium reduced the solubility of lithium in aluminium resulting in an increase in the δ' solvus of 20°C/wt% Mg. Valentine and Sanders [**29**] measured an increase of 5°C/wt%.

4.4 Mechanical properties

Provided that alloy chemistry and heat treatment are controlled to inhibit the formation of Al_2LiMg on ageing, magnesium additions can produce significant improvement to the properties of binary Al-Li alloys. Magnesium contributes to strength by solution hardening, a reduction in lithium solubility which increases the volume fraction of δ′, and possibly by incorporation into δ′ itself.

Trowsdale et al [**27**] have shown that the mechanical properties of Al4%Li0-2%Mg alloys are critically dependent on grain structure and state of recrystallisation. Unrecrystallised ingot alloys had higher fracture energies than recrystallised alloys as a result of transgranular failure in the former and intergranular failure in the latter. The intergranular fracture in the recrystallised alloys is the result of the presence of large particles of δ at grain boundaries in

the solution treated condition and smaller particles of δ produced during ageing. δ precipitates were also produced during ageing in the unrecrystallised alloy but they did not lead to intergranular failure due to the highly elongated grain structure of the unrecrystallised alloy.

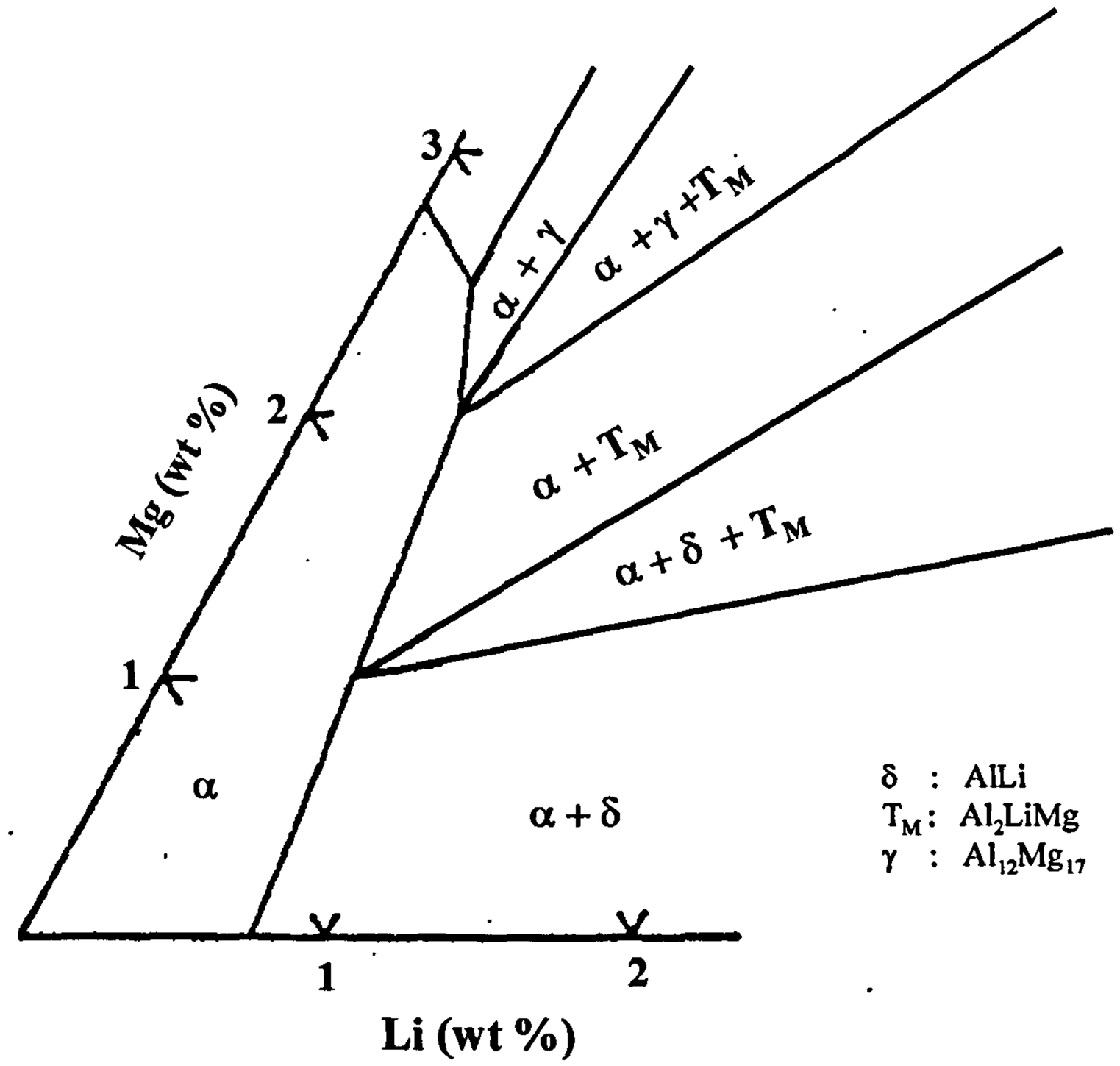

Figure 4.1: Isothermal section of Al-Li-Mg system at 200°C.

CHAPTER 5

Al-Li-Cu alloys

5.1 The Al-Li-Cu phase diagram

Figure 5.1 shows an isothermal section of the Al-Li-Cu system at 350°C **[31, 33]**. The isothermal section shows the $\alpha+\theta$, $\alpha+T_\beta$, $\alpha+T_1$, $\alpha+T_2$ and the phase $\alpha+\delta$ fields. The various phases are as follows : $\theta = Al_2Cu$, $T_B = Al_7Cu_4Li$, $T_1 = Al_2CuLi$, and $T_2 = Al_6CuLi_3$.

5.2 Precipitation characteristics

In a critical assessment published by Flower and Gregson **[23]** the microstructure of the ternary system Al-Li-Cu is reviewed. Investigations on Al-Li alloys containing > 3wt% Cu showed that the metastable percursors to θ (Al_2Cu) which occur in binary Al-Cu alloys also occur in the ternary system. The lithium additions in the solid solution range (4.5%Cu, 0.4-1.5%Li) modify the structure of the homogeneously nucleated GP zones and θ'' can be suppressed with a consequent enhancement of θ' precipitation in alloys containing up to 5%Cu and 2.5%Li.

The presence of lithium can also cause precipitation of the ternary phase T_1 (Al_2CuLi) and Thompson and Noble **[30]** have shown that this phase exhibits a very high electrical resistivity. Further studies by Noble and Tompson **[31]** have shown that the T_1 phase precipitates either at GP zones in alloys with high Cu/Li ratios (3.5%Cu, 1.5%Li) or at matrix dislocations in alloys of lower Cu/Li ratio (2.5%Cu, 2%Li).

The plate-shaped T_1 phase has a {111} habit plane and a hexagonal structure **[31]**. The orientation relationship to the aluminium matrix is:

$$(0001)T_1 \,//\, (111)_{Al}$$

$$[1010]_{T_1} \,//\, [110]_{Al}$$

T_2 (Al_6CuLi_3), is another ternary phase precipitated in the Al-Li-Cu system, and this has an icosahedral bcc structure. The T_2 phase forms predominantly above 190°C. It has been proposed **[23]** that T_2 has a metastable precursor T'_2 formed by incorporation of lithium into θ' phase. This proposal is under dispute. The T_2 phase, along with δ (AlLi), is often observed to precipitate at grain boundaries.

Suresh et al **[32]** have made an important study on three different Al-Li-Cu-Zr alloys (**table 5.1**). In alloy A, the major precipitates present in the matrix were T_1, θ', and β'. The T_1 phase was observed to be distributed both within the matrix and at low angle boundaries. It should be noted that no δ', T_2, or δ was observed in alloy A.

In alloy B, in the under aged and peak aged tempers the matrix phases precipitated were δ′, T_1, θ', and β'. The δ′ showed a trimodal distribution consisting of small spherical δ′ particles, δ′ coating the θ′ and δ′ which had ecapsulated the β′. Precipitation of T_2 phase was first detected after 2.25h of ageing at a temperature of 191°C and the volume fraction of this phase increased with ageing time. Gross over-ageing caused precipitation of T_2 on the low-angle grain boundaries and within the matrix.

Although the precipitation characteristics of alloy C follows the same trend as alloy B, the volume fraction of the various precipitates were notably affected by the high Li/Cu ratio in this alloy. Considerably more δ′ and T_2 precipitates are formed and copious precipitation of T_2 occurs at lower ageing times. The tri-modal δ′ distribution is still observed. However, the most important point is that the dominant δ′ morphology at peak age is spherical particles which is markedly different to that found in alloy B at the same ageing condition.

5.3 Effect of copper on the α/δ′ solvus

There is disagreement about the influence of copper on the δ′-solvus. Baumann and Williams [**28**] suggest that the copper does not modify the δ′ solvus, whereas Hardy and Silcock [**33**] indicated that copper decreases the lithium solid solubility in aluminium and consequently increases the δ′ solvus.

Mondolfo [**34**] shows a ternary isothermal section of the Al-Li-Cu system which

indicates that Cu does not influence the solid solubility of lithium.

5.4 Mechanical properties

Sanders and Starke [35] have reviewed the influence of the metastable and equilibrium phases on the mechanical properties of Al-Li-Cu alloys. When the T_1 phase is the only one present in the microstructure, it is usually looped and by-passed by dislocations. However, when δ' is present the T_1 phase may be sheared by dislocations. This results from the superdislocations, associated with δ', having a pileup force sufficient to shear the partially coherent T_1 precipitates.

By combining the effects of stretch, ageing time, and ageing temperature, the strength and toughness of Al-Li-Cu alloys can be considerably improved. By stretching, the number-density of phases such as T_1 and θ' is increased. By lowering the ageing temperature the supersaturation is increased and consequently there is an increased driving force for the nucleation of T_1. Furthermore, by lowering the ageing temperature the diffusion distances are reduced, thus refining both the matrix precipitates and the grain boundary phases. The formation of T_2 (Al_2CuLi_3) precipitates (which have a high lithium concentration) along the grain boundaries can lead to the development of δ' PFZs adjacent to these boundaries. These PFZs cause a reduction in ductility and fracture toughness.

According to Suresh et al [**32**] microstructures which contain δ′ (matrix) particles, lead to slip planarity. This then leads to strain localization at grain boundary δ/T_2 precipitates, promoting grain boundary failure and reduction in fracture toughness. These authors conclude that the overall fracture process in all lithium-containing alloys is dictated by competition between deformation within the matrix and grain boundary failure.

Table 5.1: Compositions of alloys (wt%) studied by Suresh et al [**32**]

alloy/element	**Li**	**Cu**	**Zr**	**Al**
A.	1.1	4.6	0.17	balance
B.	2.1	2.9	0.12	balance
C.	2.9	1.1	0.11	balance

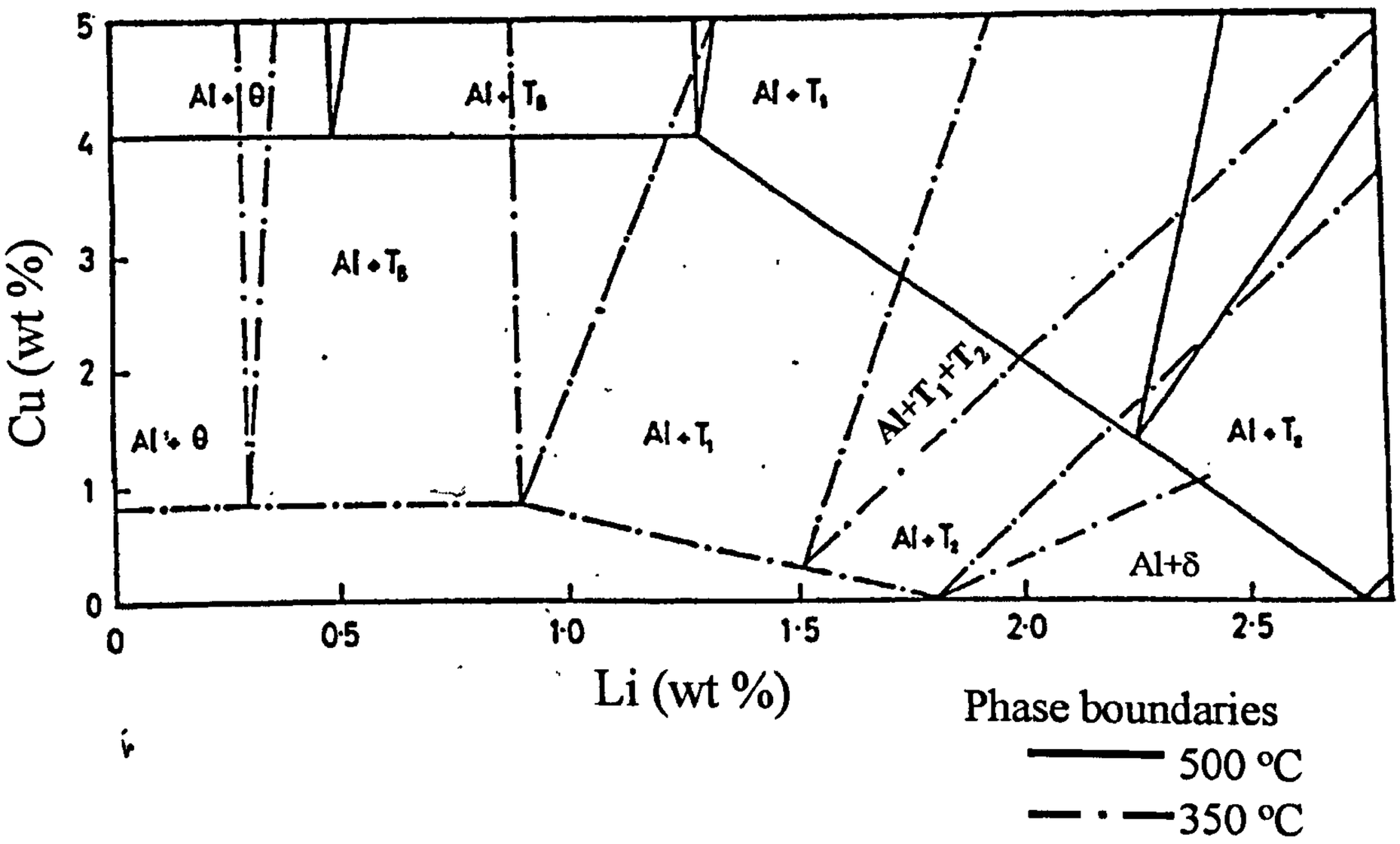

Figure 5.1: Isothermal section of Al-Li-Cu system at 350 and 500°C.

CHAPTER 6

Al-Li-Cu-Mg alloys

6.1 The Al-Li-Cu-Mg phase diagram

Figure 6.1 shows the isothermal section at 190°C of Al-Cu-Mg alloys containing 2-3 wt% Li. The diagram shows the presence of the δ′, S, T_1 and θ′ phases [**23**].

6.2 Precipitation characteristics

Starink and Gregson [**36**] have studied the thermodynamic and precipitation characteristics of 8090 (2.5Li-1.2Cu-0.7Mg) alloy using DSC and TEM.

According to these authors the hardening of 8090 alloys is the result of two precipitation sequences:

I. Li in Al-rich phase→δ′→δ

II. Cu, Mg in Al-rich phase→GPB zones→S'→ S

where GPB zones are Guinier -Preston zones containing both Cu and Mg, and S' is a slightly strained semi-coherent version of the incoherent S (Al_2CuMg) phase. The S and S' phases have the same morphology and orientation relationship and only slightly different lattice parameters. It must be mentioned that there have

been no TEM observations of GPB zones in lithium containing alloys, but the S′ and S phases are frequently observed **[23]**.

The most important precipitation reactions in Al-Li-Cu-Mg alloys of commercial importance involve δ′, T_1(low magnesium, low copper), S(high magnesium, high and low copper) and θ′ (low magnesium, high copper).

The addition of small amounts (0.5-1.0%) of magnesium to a high copper-containing alloy such as 2090 (Al-2.7Cu-2.2Li-0.12Zr) suppresses the formation of θ' and introduces the S' phase **[35]**. Because S' contains no lithium, δ′ precipitation is not significantly affected by the magnesium addition and T_1 remains the dominant secondary phase.

In low-lithium alloys, such as Al-1.6Li-3Cu-0.8Mg little or no δ′ forms and there appears to be equal amounts of T_1 and S' phases present.

In higher-lithium, lower copper alloys such as 8090 (Al-2.5Li-1.2Cu-0.7Mg), S' along with a small amount of T_1 forms together with δ′.

As the copper/lithium ratio is further increased, the precipitation of T_1 is fully suppressed and S' becomes the major secondary phase. A representative alloy, which shows this behaviour, is 2091 (Al-2Li-2.2Cu-1.5Mg).

The precipitation of T_1 is similar to that which takes place in Al-Li-Cu alloys. However this T_1 precipitation is affected by competition with S for both heterogeneous nucleation sites and available copper atoms.

The precipitation of S phase is of principal importance in commercial Al-Li-Cu-

Mg alloys. In these alloys nucleation of S usually takes place on dislocations. The density of dislocation nucleation sites can be increased by giving the alloy a pre-ageing stretch. Under these conditions widespread heterogeneous precipitation of S phase occurs. The high density of S particles that are produced disperses the slip when the alloy is deformed, thus improving the fracture toughness of the alloy.

A uniform distribution of S phase can also be produced by simultaneously increasing the copper and magnesium concentration and increasing the free vacancy concentration. The latter can be controlled by both solution treatment temperature and a low temperature pre-age before heat treatment at 190°C. During the first stages of precipitation the vacancies are strongly bound to lithium atoms. As the δ′ particles grow at low temperatures the vacancies are released and then can aid the precipitation of S phase. This model is supported by observations of the formation of dislocation loops and helices during the ageing of Al-Li-Cu and Al-Li-Cu-Mg alloys. The mechanism of how vacancies promote homogeneous precipitation of S is not clear. A widespread distribution of vacancy clusters (before their condensation into loops) probably provide sites for the precipitation of S laths. Another possibility is the vacancy clusters become enriched with copper and magnesium and then develop into S precipitates via GPB-type zones. In both cases, a high vacancy concentration is required for nucleation of S and to accelerate the diffusion required for precipitate growth.

In addition to δ′, T_1 and S phases a copper-rich icosahedral grain boundary phase can occur during ageing. It has the composition $Al_6Cu(Li,Mg)_3$ and has a similar structure to T_2 (Al_6CuLi_3) which precipitates in Al-Li-Cu alloys. Investigations have shown that precipitation of this phase is likely to take place only at high-angle boundaries and triple points. The density of such sites is low in highly textured unrecrystallised zirconium-containing alloys and therefore the icosahedral phase is more prominent in recrystallised alloys.

6.3 The effect of combined additions of copper and magnesium on the α/δ′ solvus

Very little work has been done on the effect of combined additions of copper and magnesium on the position of the δ′ solvus. Valentine and Sanders [**29**] studied the effect of increasing copper concentrations on the δ′ solvus of an Al-2.0Li-2.7Mg alloy. The single addition of 2.7% Mg addition increased the δ′ solvus by 14 °C which which is consistent with that described in section 4.4.3. Addition of copper to the Al-2.0Li-2.7Mg alloy in the range 0.3 to 3% produced no further change in the position of the δ’ solvus. This is an important result and indicates that the δ′ solvus in alloys of 8090 composition is approximately 5°C above that of an equivalent Al-Li binary alloy.

6.4 Mechanical properties

The main strengthening phase in Al-Li-Cu-Mg alloys is δ′. The role of S phase is to disperse slip and thus improve the fracture toughness. Crooks and Starke **[37]** have reported that when S' is present in Al-Li-Cu-Mg alloys, strain localisation is suppressed, indicating that the precipitate is not sheared by dislocations. Their observations were confirmed by Flower and Gregson **[38]** who showed that the S' precipitates do not have densely packed slip planes parallel to the aluminium matrix planes and consequently they are not penetrated by dislocations.

Gilmore and Starke **[39]** have studied the effects of magnesium on the mechanical properties of an Al-4.22Cu-1.31Li-0.16Zr alloy. According to these authors 0.5% Mg increased the peak yield strength by 30%. The increase in strength in the early stages of ageing is due to the precipitation of a high number-density of θ" particles and GP zones. As ageing proceeds, significant amounts of T_1 form preferentially near dislocations and subgrain boundaries.

Noble et al **[40]** have investigated the low temperature embrittlement of 8090 alloys. According to their results when 8090 is exposed at 70°C for 1000 h after prior ageing at 150°C, a 28% reduction in fracture energy and 6% increment in proof stress occurs. A possible reason for the embrittlement of 8090 during exposure at 70°C is the formation of a mixture of fine δ′ and GPB zones, but further work is needed to investigate this possibility.

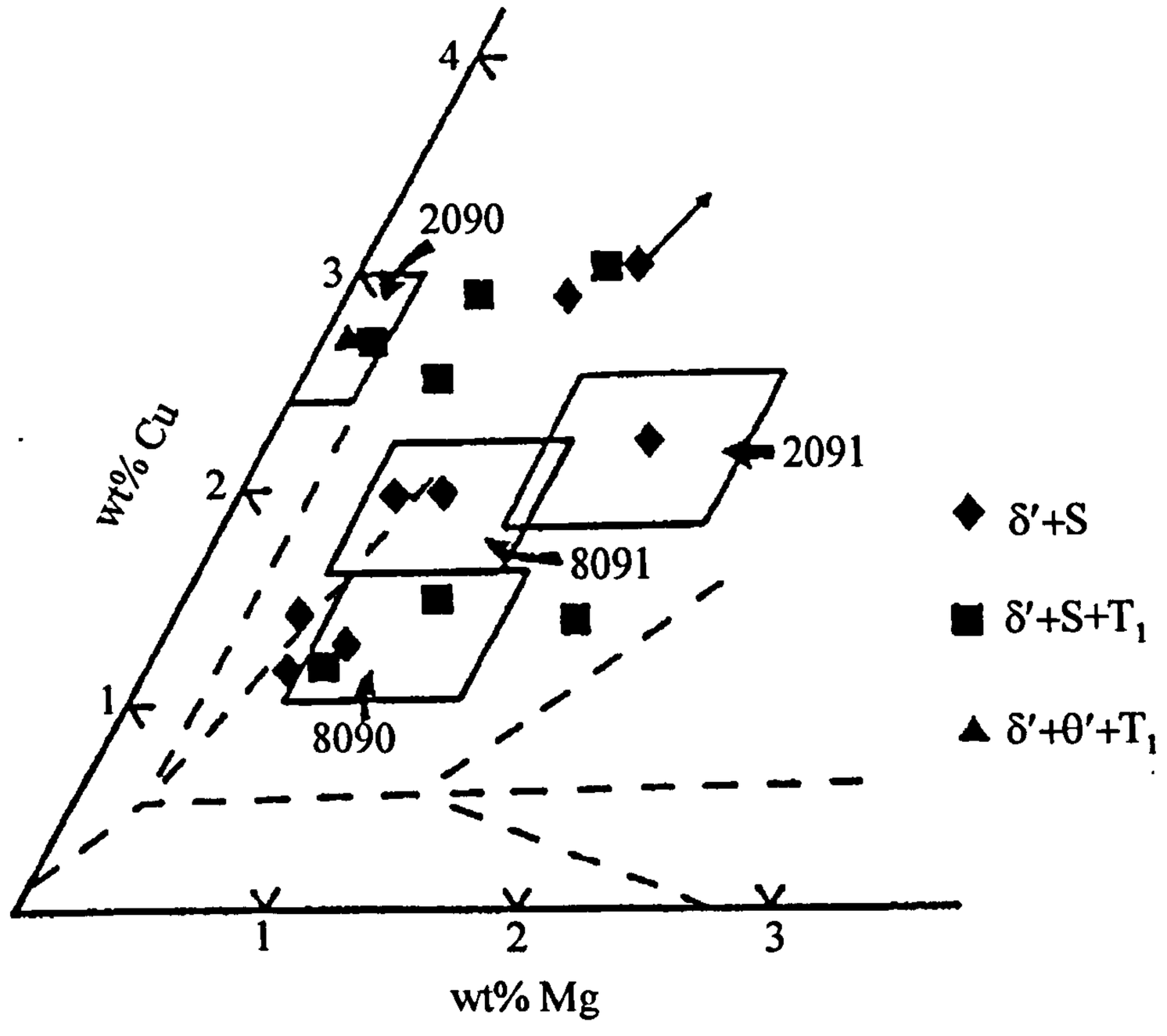

Figure 6.1: Isothermal section at 190°C of the quaternary Al-Cu-Mg alloys containing 2-3wt%Li [23].

CHAPTER 7

Experimental

The alloys studied in this research work had the composition shown in table 7.1. The actual composition was checked to be very near to nominal by measurement of electrical resistivity in the as-quenched state. All the alloys were melted and cast under argon to produce 35mm diameter ingots. The alloys were then homogenised at 510 °C for 8h to remove any segregation and to dissolve the intermetallic phases. The ingots were then scalped, extruded to bar, followed by hot and cold rolling to 1.6 mm strip. In the next paragraphs are described the experimental techniques and methods used to examine the phase transformations which occurred during ageing of the alloys.

7.1 Differential scanning calorimetry (DSC)

The DSC measurements used a power compensated differential scanning calorimeter. The power compensation DSC uses separate furnaces for the sample under study and for the reference sample. Any heat evolved or absorbed by a phase transformation is compensated by a power input to one of the two furnaces. By measuring this power input, the exothermic and endothermic events can be detected in the sample.

The as-quenched DSC-samples were punched out of the 1.6 mm strips giving 6

mm diameter discs. The samples were then solution treated in a salt bath at 540 °C for 15 min. and quenched into ice-brine at -20°C. The discs were then ground to 0.5 mm thickness taking care to avoid heating of the sample. The grinding is very important for removing the depleted-lithium layers from the surfaces of the sample. The discs were then stored in liquid nitrogen to prevent decomposition of the supersaturated solid solution taking place at room temperature. Before placing into the into the Perkin-Elmer series 7 power compensation DSC, the samples were carefully dried to remove any condensation. The DSC furnace temperature was -20°C, and the temperature range used for each scan was from -10°C to 400°C. When the DSC scan had finished the sample was weighed on a Mettler AE 163 balance with an accuracy of 0.01 mg .

For the aged samples the weight was measured before the DSC run. The test procedure is as described above.

7.2 Electrical resistivity

The resistivity samples were machined to dimensions 80 mm (length)x 2 mm x 1.6 mm and resistance measurements were taken using a Cropico DO5 digital ohmmeter employing a four-potentiometric technique. The resistance range was 2 mΩ and the accuracy was ±0.0001 milliohms.

The resistivity ρ was calculated from the equation :

$$\rho = Rbw/l \qquad 7.1$$

where : **R** is the measured resistance

l the length of gauge

b the thickness of the gauge

w the width of the gauge

The resistance was measured with the current flowing through the sample in two directions to eliminate thermal emf's. The average of the measurements was taken.

Two different resistivity methods were used to determine the precipitation characteristics; isothermal measurements and isochronal measurements.

7.2.1 Isochronal resistivity

Samples were solution treated in a salt bath at 540°C for 15 min. and quenched in ice brine (-20°C). The samples were placed in liquid nitrogen immediately after the quench to enable the as-quenched ρ_o value to be measured.

The resistivity samples were step-aged for a constant time (10 min) at increasing temperatures. The temperature range was from 0°C to 560°C employing 20°C temperature intervals. Directly after each step ageing treatment, the samples were quenched into liquid nitrogen.

The 0°C temperature was produced by ice water. For all the other temperatures an air circulation furnace was used.

The resistance measurements were taken in liquid nitrogen using the four point potentiometric technique. The resistivity was calculated by equation 7.1

7.2.2 Isothermal resistivity

After solutionizing, the samples were quenched in ice brine and then immediately transferred into liquid nitrogen in order to measure the as-quenched ρ_o value. Subsequently the samples were aged for increasing times at a constant temperature. After each ageing time, the resistance was measured in liquid nitrogen applying the four-point potentiometric technique. By using equation 7.1, the resistivity was measured.

7.3 X-Ray Diffraction (XRD)

For XRD analysis, samples with dimensions 10 mm × 20 mm were used. The samples were solution treated and subsequently isothermally aged. The ageing temperatures used were 350°C, 150°C. The first temperature was performed in an air circulation furnace and an oil bath was used for the 150°C age.

After ageing, a thickness of 0.5 mm was ground from each side of the 1.6mm strip in order to remove the lithium-depleted surface layers. The samples were then polished to a 1μm finish using diamond paste.

For the XRD analysis, a Siemens D500 diffractometer with Cu K_α radiation (wavelength 1.5406A) was used. The 2θ angle scanned was in the range 10-100° using a step size of 0.01 deg and a dwell time of 5 sec.

7.4 Mechanical tests

Specific alloys were subjected to tensile and tear tests in order to evaluate the 0.2% proof stress and fracture energy respectively after particular heat treatments. For the tensile tests, a Mayes DM/U10 testing machine was used. An external extensometer was used for recording the corresponding strain.

Tear testing was carried out on a Mayes FSH-250 machine. The fracture energy was measured by integrating the area under the stress-strain curve.

It should be noted that for the study of the as-quenched alloys, the samples were kept in liquid nitrogen up to the time they were tested.

7.5 Electron microscopy

7.5.1 Transmission Electron Microscopy (TEM)

From the 1.6 mm alloy sheet, 2 mm×1 mm rectangular samples were cut and aged. The aged samples were ground down from both sides to 0.5 mm. Then 3 mm diameter discs were punched out which, in turn, were further ground to a final thickness of 70-100 μm. Electropolishing of the thin discs was carried out in a Metalthin MK3 twin jet electropolishing aperture using a 30% HNO_3+methanol solution. The samples were examined as soon as possible in a JEM-2000FXII electron microscope using an acceleration voltage of 120kV.

7.5.2 Scanning Electron Microscopy

The study of the fracture surfaces (fractography) of the samples after tensile

testing was carried out in a JSM-6400 Scanning Electron Microscope. All fracture surfaces were ultrasonically cleaned in methanol before examination.

Table 7.1 : Nominal compositions (wt%) of the alloys studied

Alloy Nr	Li	Cu	Mg	Zr	Al
267	1.7	1.2	0	0.07	bal.
268	1.7	1.2	0.7	0.07	bal.
269	1.7	1.2	1.0	0.07	bal.
270	1.7	1.2	1.4	0.07	bal.
271	1.7	1.2	2.0	0.07	bal.
272	1.7	1.2	3.0	0.07	bal.
278	1.7	0	1.2	0.07	bal.
279	1.7	0.6	1.2	0.07	bal.
280	1.7	1.2	1.2	0.07	bal.
281	1.7	2.0	1.2	0.07	bal.
282	1.7	3.0	1.2	0.07	bal.
283	1.7	0	3.0	0.07	bal.
284	1.7	3.0	0	0.07	bal.
381	0	1.2	1.2	0.07	bal.
382	0	1.2	2.0	0.07	bal.
383	1.3	1.2	1.2	0.07	bal.
384	1.3	1.2	2.0	0.07	bal.
385	0	2.0	1.2	0.07	bal.
386	1.3	2.0	1.2	0.07	bal.
380	0	3.0	0	0.07	bal.
319	0	3.0	1.0	0.07	bal.

CHAPTER 8

Precipitation in Al-Li-Mg Alloys

For the interpretation of the effect of magnesium concentration on the precipitation characteristics in the quaternary Al-Li-Cu-Mg system, it is of great importance to first understand the effect of separate additions of magnesium and copper on the binary Al-Li system. In this chapter, the addition of 0.7%, 1.2% and 3% Mg to the binary Al-Li system is considered. The chapter is divided into two main parts:

- Isochronal precipitation characteristics
- Isothermal precipitation characteristics

8.1 Isochronal precipitation characteristics

8.1.1: DSC (as-quenched plots)

DSC thermograms of the as-quenched alloys are shown in **figure 8.1**. In the binary Al-Li alloy with no addition of magnesium, no thermal events were detected. The addition of 1.2% Mg results in the appearance of a small exothermic event (A) due to δ′ precipitation followed by an endothermic event (B) as the δ′ dissolves. As the composition of magnesium increases to 3% the areas under the exothermic and endothermic peaks increase showing that magnesium stimulates the precipitation of δ′.

The δ′ metastable solvus temperature can be equated to the temperature where the δ′ endotherm returns to the baseline (T^{DSC}_{end}). The end temperatures of the endotherms are equal to 205 and 220 °C for alloys 1.7Li1.2Mg and 1.7Li3.0Mg respectively.

For the binary 1.7Li alloy the thermodynamic δ′ metastable solvus is calculated to be 200°C **[16]**. The addition of magnesium has therefore increased the T^{DSC}_{end} temperature by approximately 7°C/wt%Mg. This shift of T^{DSC}_{end} to a higher temperature can be attributed either to an increase of the δ′ metastable solvus, or to an increase of the δ′ particle size. It will be shown later in this chapter that the shift in the end temperature of the endotherm is due to a change in the metastable δ′ solvus.

8.1.2 Isochronal resistivity

Figure 8.2 shows isochronal plots for Al-1.7Li alloys with 0,1.2 and 3.0% Mg. The binary 1.7Li alloy shows a gradual increase in resistivity from 0°C to 40°C which is associated with the formation of δ′ particles that are smaller than the critical size for electron scattering. The following decrease after 40°C can be attributed to the growth of δ′ particles, which are now larger than the critical size. The resistivity decrease extends below the as-quenched value (baseline) and then slowly returns to the baseline at 200°C. This temperature ($T^{Res.}_{end}$) can be equated to the δ′ solvus temperature for the binary 1.7Li alloy.

The addition of magnesium to the alloy does not prevent the formation of the initial resistivity peak but it is delayed to a higher temperature and the height of the peak increases with magnesium concentration (**figure 8.3**).

After δ′ growth, the resistivity returns to baseline at approximately 200°C for the 1.7Li1.2Mg alloy and 220°C for the 1.7Li3.0Mg alloy. These values represent the δ′ solvus temperature for these alloys and they are in excellent agreement with the DSC data (**Table 8.1**).

Note that 1.7Li3.0Mg alloy does not quite reach the as-quenched value because of the onset of precipitation of the equilibrium phases. The $T^{Res.}_{end}$ for this alloy was obtained from the extrapolation of the resistivity plot to the baseline. The equilibrium phases that cause the strong decrease in resistivity in the 1.7Li3.0Mg alloy at 325°C was shown by XRD to be AlLi (δ) and Al_2LiMg (T_M) (**figure 8.4**).

Table 8.1: δ′ solvus temperatures estimated by DSC thermograms and resistivity changes.

Alloy	$T^{Res.}_{end}$	T^{DSC}_{end}
1.7Li	200	200*
1.7Li1.2Mg	200	205
1.7Li3.0Mg	220	225

*Calculated from Noble & Bray [**16**]

8.2 Isothermal precipitation characteristics

The isothermal precipitation characteristics of the Al-Li-Mg system are

considered in this section. Five different heat treatments have been used:

- Ageing at 70,100 and 150°C for 1000h.
- Ageing at 150°C for 24h. This simulates the damage tolerant heat treatment commonly given to alloys based on the Al-Li system.
- Prior ageing at 150°C for 24h following by exposure at 70°C for 1000h. This simulates the conditions that a commercial Al-Li aerospace alloy would be expected to encounter whilst in service.

8.2.1 Ageing at 70°C

Figure 8.5 shows comparative plots of the DSC thermograms after ageing at 70°C for 1000h. As can be seen the addition of magnesium has stimulated the formation of δ′. The temperature at which the dissolution of δ′ is completed (T^{DSC}_{end}) increases by 5°C with the addition of 1.2%Mg to the binary 1.7Li alloy. Raising the magnesium concentration to 3% increases the T^{DSC}_{end} by a further 10°C.

Isothermal resistivity measurements allow the precipitation characteristics of the Al-Li-Mg alloys to be examined during ageing at 70°C, (**figure 8.6**). The resistivity of the binary 1.7Li alloy shows a continuous increase up to 1000h. The isothermal resistivity behaviour of binary Al-Li alloys containing 1.4-2.0 %Li has been investigated by Noble and Bray [**41**]. According to their results a 1.8Li alloy aged at 70°C shows an initial increase followed by a plateau and then a second increase. The binary 1.7Li alloy studied in the present work exhibits a similar trend suggesting that the mechanism of precipitation is similar. Noble and

Bray showed that for alloys containing around 1.8% Li, when aged at 70°C, the δ′ precipitation mechanism is not classical nucleation and growth of δ′. There is a transition stage that involves the nucleation of ordered regions with no change of composition. The initial resistivity increase was attributed to the formation of a high density of fine ordered regions (or domains) which scatter the conduction electrons. The second increase of the resistivity was attributed to the spinodal decomposition of the ordered domains to δ′ which then become more effective scattering centres for the conduction electrons. The continuous increase of resistivity observed in the present work for a 1.7Li alloy implies that spinodal decomposition carries on for a long time and at a slow rate since the δ′ particles do not reach the critical size of electron scattering. The slow kinetics can be attributed to quenched-in vacancies becoming trapped by the nucleation ordered regions and consequently there is a reduced concentration of vacancies to assist the diffusion of lithium to the spinodally decomposing regions.

The addition of 0.7% Mg results in similar resistivity behaviour to the binary 1.7Li alloy up to 50h. Beyond 50h the resistivity increase is more rapid indicating that spinodal decomposition is faster. A resistivity peak is reached after 400h which is followed by a decrease showing that the δ′ has now attained the critical size for electron scattering. The accelerated kinetics of the 1.7Li0.7Mg alloy can be explained by the small increase in the δ′ solvus temperature which will result in a higher driving force for δ′ precipitation.

Increasing the concentration of magnesium to 1.2% produces a resistivity plot that peaks at an earlier time, which again will be due to the increased driving force for δ′ precipitation.

Higher levels of magnesium (3.0%) produce a further increase in the rate of δ′ precipitation. The resistivity peak is reached after 4h ageing which means that spinodal decomposition is very rapid. The following decrease in resistivity is dramatic.

From the above discussion it can be concluded that the addition of magnesium to a binary Al-Li alloy increases the driving force for δ′ precipitation. This causes more rapid spinodal decomposition to take place resulting in a higher volume fraction of δ′ in the alloy.

8.2.2 Ageing at 100°C

DSC thermograms are shown in **figure 8.7** after ageing 1000h at 100°C. Comparison of the peaks shows that there is a small increase of the δ′ dissolution enthalpy as the magnesium concentration is increased. The T^{DSC}_{end} of the 1.7Li3.0Mg alloy is shifted by about 10°C, to a higher temperature compared with the dissolution end of the 1.7Li1.2Mg alloy.

The isothermal resistivity plots for ageing at 100°C are given in **figure 8.8**. All the alloys show an initial increase in resistivity which is followed by a marked

decrease to well below the as-quenched value suggesting nucleation ordering followed by spinodal decomposition to δ′. As the magnesium concentration increases the peak occurs sooner indicating, as for 70°C ageing, that the magnesium promotes enhanced kinetics of δ′ precipitation.

8.2.3 Ageing at 150°C

DSC dissolution plots after ageing at 150°C for 24h and 1000h are presented in **figures 8.9** and **8.10** respectively. **Figure 8.9** shows that once magnesium is added to the binary alloy the δ′ dissolution enthalpy exhibits a marked increase, i.e. there is a significant increase of δ′ volume fraction. This suggests that at short times of ageing at 150°C the addition of magnesium significantly enhances the nucleation of δ′.

Isothermal resistivity plots of these alloys are given in **figure 8.11**. Alloys containing 0-1.2% Mg show a well defined incubation period which is followed by a large decrease of resistivity. This indicates that the mechanism of δ′ formation is following a nucleation and growth process. Because there is no increase in resistivity we can conclude that the critical size for nucleation is greater than the critical size for electron scattering. The 1.7Li3.0Mg alloy does not show a measurable incubation period. This is because the driving force for δ′ precipitation is very large in this alloy, hence the kinetics are very fast and the incubation period has been exceeded by the time the first resistivity measurement

is made.

8.2.4 Effect of magnesium on the α/δ′ solvus

The isothermal resistivity plots in **figure 8.11** show that ageing at 150°C for times >100h will produce the equilibrium volume fraction of δ′. This observation means that **figure 8.10** can be used to calculate the effect of magnesium on the α/δ′ solvus using the following procedure:

- At 150°C, the volume fraction (V_f) of δ′ can be written as

$$V_f = \frac{0.063 - \omega}{0.25 - \omega} \qquad \textbf{(8.1)}$$

where ω is the composition of lithium (atom fraction) at the α/δ′ solvus at 150°C, 0.063 is the analysed lithium composition (atom fraction) of the alloys, and 0.25 is the atom fraction of lithium in δ′. Equation (8.1) follows from the lever rule applied to the Al-Li phase diagram and using the fact that the specific volumes of δ′ and the α solid solution are very nearly equal.

- The equilibrium volume of fraction of δ′ can be calculated from **figure 8.10** using a relation obtained by Noble [**42**]:

$$V_f = \Delta H\ (J/g) / 140 \qquad \textbf{(8.2)}$$

The values are given in table 8.2.

- Hence ω, the atom fraction of lithium at the α/δ′ solvus at 150°C can be calculated by equation (8.1). The resulting values are given in table 8.2.

Table 8.2: Parameters used to calculate the position of the α/δ′ solvus at 150°C.

ALLOY CODE	ΔH (J/g)	V_f	ω (at%)
1.7Li	9.50	0.0679	4.93
1.7Li0.7Mg	10.20	0.0729	4.83
1.7Li1.2Mg	11.67	0.0834	4.60
1.7Li3.0Mg	13.32	0.0952	4.33

- It can be seen from table 2 that increasing the magnesium from zero to 3.0% causes a reduction in ω of 0.6at%.
- Noble and Bray **[16]** have shown that the α/δ′ solvus in binary Al-Li alloys is given by the relation:

$$\ln C_e(at\%) = 4.176 - \frac{9180}{RT} \qquad \textbf{(8.3)}$$

The differentiated form of this equation is:

$$\frac{dT}{dC_e} = 1104 \bullet (4.176 - \ln C_e)^{-2} \bullet C_e^{-1} \qquad \textbf{(8.4)}$$

In the vicinity of 150°C (ω= 4.78at%) the derivative dT/dC_e equals 33.72 °C/at%.

Thus, a reduction in atomic fraction of lithium of 0.6at% corresponds to an increase in the α/δ′ solvus temperature of 20.2°C. This increase in α/δ′ solvus temperature is in excellent agreement with the directly measured value (T^{DSC}_{end}) from **figure 8.1,** which was ~20°C.

- It can be concluded that the addition of magnesium to an 1.7Li alloy increases the α/δ' solvus temperature by 6.7°C /wt%Mg. This value is in good agreement with the value of 5°C/wt%Mg measured by Valentine and Sanders [29]. It also suggests that the value of 20°C/wt%Mg measured by Baumann and Williams [28] is far too high.

8.2.5 Effect of ageing temperature

This section brings together the effect of the ageing temperature on the precipitation characteristics of Al-Li-Mg alloys.

DSC thermograms of the binary alloy (**figure 8.12**) shows that increasing the ageing conditions from 1000 h at 70°C to 1000 h at 150°C does not change the final δ' volume fraction significantly. The isothermal resistivity plots (**figure 8.13**) show that an increase of temperature from 70°C to 150°C not only causes a dramatic decrease of the resistivity but also changes the δ' formation mechanism from nucleation ordering to classical nucleation and growth. From the observation that the final δ' volume fraction is the same after 1000h at 70°C and 1000h at 150°C we can conclude that the 70°C ageing causes a high volume fraction of very fine spinodally decomposed regions with a size smaller than the critical size for electron scattering.

The effect of temperature is similar for the 1.7Li0.7Mg alloy (**figure 8.14**).

For the 1.7Li1.2Mg alloy, the fraction of δ' that precipitates at 70°C and 150°C is again similar, but **figure 8.15** clearly shows that the maximum amount of δ' is

produced at 100°C. Thermodynamically, it would be expected that the volume fraction should increase as the ageing temperature goes from 150 to 100 to 70°C. However, the diffusion coefficient decreases as the temperature is reduced, so that at 70°C the amount of δ′ that forms is limited by kinetic considerations. **Figure 8.16** shows the isothermal resistivity curves for the 1.7Li1.2Mg alloy which, when taken in conjunction with **figure 8.15**, show that the magnitude of the total resistivity decrease at low ageing temperatures cannot be equated to the volume fraction of δ′ that has formed. The small decrease of resistivity to just below the baseline at 70°C indicates that the growth rate of the spinodally decomposed regions is very small and therefore we can conclude that 70°C ageing causes a high volume fraction of fine δ′ particles.

Finally, **figures 8.17** and **8.18** show the DSC and resistivity plots for the 1.7Li3.0Mg alloy. The trends are the same as those for the 1.7Li1.2Mg alloy, but the kinetics are faster and the growth of δ′ particles much larger at all ageing temperatures. It should also be noted that at 150°C the precipitation of δ′ is largely complete by 24h at 150°C (**figure 8.17**). Thus the period 24h to 1000h at 150°C is concerned mainly with δ′ coarsening.

Figure 8.19 summarizes the combined effects of magnesium concentration and ageing temperature on the volume fraction of δ′. The volume fraction was calculated by measuring the dissolution enthalpy and using relation **8.2** given in

the previous section. It can be clearly seen that at all ageing temperatures increasing the magnesium concentration stimulates the formation of δ′. The effect of the ageing temperature for the binary 1.7Li and 1.7Li1.2Mg alloys can be explained by the competition between the thermodynamic driving force and the kinetics of precipitation. The large driving force but slow kinetics for δ′ precipitation at 70°C produces a volume fraction almost equal to that at 150°C where the driving force is lower but the kinetics are faster. The largest volume fraction is produced at 100°C where there is an optimum combination of driving force and diffusivity.

The 1.7Li3.0Mg alloy exhibits a different trend in that the volume fraction of δ′ at 150°C is lower than expected. XRD analysis showed this was due to precipitation of significant amounts of T_M phase (**figure 8.20**). The formation of such a phase requires lithium; therefore a significant fraction of δ′ will dissolve after long term ageing at 150°C.

8.2.6 Size of the δ′ precipitates at 150°C

Increasing the ageing temperature in a given alloy was observed to cause a marked shift of T^{DSC}_{end} to higher temperatures (**figure 8.21**). Because the magnesium concentration remains constant it is likely that the above shift is caused by an increase in the δ′ particle size. In this section evidence will be given that confirms this hypothesis.

Figures 8.22-8.25 show TEM micrographs of 1.7Li1.2-3.0Mg alloys after ageing at 150°C for 24h and 1000h. On these micrographs a large number of particles was measured in order to obtain the normal (Gaussian) particle size distribution of δ′. **Figures 8.26(a,b)** and **8.27(a,b)** show these normal distributions. According to these results, increasing the time of ageing at 150°C from 24h to 1000h caused the mean particle radius to increase from 6 nm to 14 nm for both alloys. Noble and Bray **[43]** have shown that an increase of δ′ radius from 6 nm to 14 nm in a binary 1.7Li alloy will produce a shift of T^{DSC}_{end} of about 20°C. Applying this result to the present work predicts that increasing the ageing time from 24 h to 1000 h at 150°C should produce a shift in the end temperature of the δ′ endotherm of 20°C; **figures 8.15** and **8.17** show this to be the case.

From the above discussion two important things can be noted for **figure 8.21**:

(a) Increasing the ageing temperature for a given alloy produces an increasing shift of T^{DSC}_{end}. This is due to the increasing size of the δ′ precipitates.

(b) The magnitude of the shift increases with increasing magnesium concentration. It is known from TEM that the size of δ′ is independent of magnesium concentration, and therefore the additional shift in high magnesium alloys is due to displacement of the α/δ′ solvus (by approximately 7°C/wt%Mg).

8.2.7 Reversion of the δ′ precipitates

Isochronal reversion resistivity plots after ageing for 1000h at 70°C are given in **figure 8.28**. The binary 1.7Li alloy exhibits a small initial decrease in resistivity (0.4 nΩm) which is attributed to the dissolution of small δ′ precipitates. After 100°C the larger δ′ precipitates grow during the isochronal heating. Because their size is still smaller than the critical size for electron scattering a resistivity increase is observed followed by a decrease to below the baseline when the δ′ precipitates exceed the critical size. At 175°C the resistivity starts increasing again due to the dissolution of δ′ which is completed at 200°C (δ′ solvus temperature). The reversion resistivity plots of the 1.7Li1.2Mg and 1.7Li3.0Mg alloys are similar. Dissolution of the small δ′ particles takes place up to 150°C. Growth of the larger δ′ precipitates occurs up to approximately 180°C. Higher temperatures cause an increase in resistivity due to dissolution of the large δ′ particles and this is complete at 210 and 220°C respectively. The 1.7Li3.0Mg alloy exhibits a marked decrease in resistivity beyond 245°C which can be attributed to the precipitation of large amounts of T_M.

Figure 8.29 presents the comparative reversion plots after isothermal ageing at 150°C. The increase in resistivity observed for all the alloys corresponds to the dissolution of the δ′ that has formed at 150°C. The 1.7Li3.0Mg alloy exhibits a decrease in resistivity beyond 240°C due to precipitation of the equilibrium T_M phase.

As with the DSC dissolution thermograms, the temperature where the reversion

resistivity returns to the baseline ($T^{Rev.}_{end}$) can be equated to the δ′ metastable solvus. Because of the very low equivalent heating rate during reversion (1°C/min) compared with the DSC heating rate (20°C/min) the $T^{Rev.}_{end}$ is observed to be lower than the T^{DSC}_{end}. **Table 8.3** presents the $T^{Rev.}_{end}$ of the alloys after different heat treatments. The effect of ageing temperature on the δ′ solvus temperature as measured by $T^{Rev.}_{end}$ is shown in **figure 8.30**. It can be clearly seen that increasing the magnesium concentration from 0 to 3% produces a 20°C-shift of the δ′ solvus temperature which is very close with the results obtained from the DSC dissolution thermograms (**figure 8.21**) and verifies the conclusion that the addition of magnesium to a 1.7Li binary alloy increases the δ′ metastable solvus temperature by about 7°C/wt%Mg. Increasing the ageing temperature for a given alloy from 70 to 150°C produces a 30°C-shift of $T^{Rev.}_{end}$ to a higher temperature due to increasing size of δ′ precipitates.

Table 8.3: δ′ solvus temperatures estimated by reversion resistivity changes.

	$T^{Rev.}_{end}$ (°C)	
Alloy	**70°C direct age**	**150°C direct age**
1.7Li binary alloy	200	230
1.7Li1.2Mg	210	240
1.7Li3.0Mg	220	250

8.2.8 Exposure at 70°C after prior ageing at 150°C for 24h

This work has been carried out to simulate the service conditions that an Al-Li aerospace alloy may experience. It is known that binary Al-Li alloys undergo a

small amount of embrittlement when alloys are aged 24h at 150°C and then exposed 1000h at 70°C. At the present time no information is available on how the presence of magnesium in the alloy affects the degree of embrittlement. This section is an initial contribution to this lack of knowledge.

All alloys have first been given a standard age of 24h at 150°C. This produces a dispersion of δ′ particles of radius 6 nm (**figures 8.26a, 8.27a**). The alloys have then been exposed for up to 1000 h at 70°C. **Figure 8.31** shows the change in resistivity that occurs during exposure at 70°C. In the 1.7Li binary alloy and the 1.7Li0.7Mg alloy the resistivity increases during exposure, indicating that during exposure very fine δ′ precipitates are forming of a radius <2 nm. In the 1.7Li1.2Mg and 1.7Li3.0Mg alloys the resistivity decreases which either indicates δ′ of a larger size is being nucleated or, in these higher magnesium-containing alloys some of the lithium is adding onto the pre-existing δ′ particles from the 150°C age.

After exposure the alloys were subjected to DSC analysis. **Figures 8.32, 8.33, 8.34** and **8.35** show that the exposure has resulted in an increase in the size of the δ′ endotherm. The increase is very small in the 1.7Li binary alloy and the 1.7Li0.7Mg alloys, but is significant in the higher 1.2% and 3% magnesium alloys. The increase in enthalpy can be converted to an increase in volume fraction of δ′ using the relationship obtained by Noble [**42**] which was referred to in the previous section. The values obtained are plotted in **figure 8.36** and they

show that as the magnesium concentration increases the amount of δ′ produced during exposure increases.

It is interesting to compare these increases in volume fraction with those calculated from the change in the position of the α/δ′ solvus caused by the presence of magnesium. In section 8.2.4 it was shown that at 150°C the solubility of lithium was decreased from 4.93 to 4.33at% by the addition of 3.0%Mg. Using equations 8.3 and 8.4 this corresponds to a decrease from 2.6at% to 2.1at% at 70°C. Use of equation 8.1 shows the volume fraction of δ′ should increase from 0.161 to 0.183, ie by a fraction of 0.022. **Figure 8.36** shows the measured increase in δ′ volume fraction for the 1.7Li3.0Mg alloy to be 0.029. It can be concluded that the increased amounts of δ′ observed during exposure in high magnesium-containing alloys can be largely accounted for by the change in position of the α/δ′ solvus boundary caused by the magnesium addition.

8.2.9 Reversion after exposure

Exposure of the binary 1.7Li alloy after prior ageing 24 h at 150°C results [3] in a bimodal distribution of δ′ particles, ie a distribution with r=6 nm (from the 150°C age) and a distribution with r=2nm (from the exposure). The resistivity results from **figure 8.31** suggest a similar result for the 1.7Li0.7Mg alloy, but the situation is much less clear for the 1.7Li1.2Mg and 1.7Li3.0Mg alloys. In these alloys some growth of the pre-existing δ′ precipitates may occur, or the exposure δ′ is much coarser than in the binary 1.7Li alloy (see **figure 8.31**). It proved

extremely difficult to observe the smaller sized distribution in these alloys with TEM and therefore the relative importance of amount and size of the two distributions are unknown in the high magnesium alloys.

An attempt was made to overcome this problem by dissolving the δ′ in the alloys after exposure, by isochronal reversion. It was hoped that a two step curve would be produced, the first step corresponding to the dissolution of the exposure δ′ and the second step corresponding to dissolution of the δ′ from the 150°C prior age. **Figures 8.37-8.39** give the reversion resistivity plots of the alloys and these are compared with the equivalent plots after a direct age for 1000h at 70°C and a direct age of 24h at 150°C. The isochronal heating of the 1.7Li binary alloy produces a rather complex curve (**figure 8.37**). Taking into consideration the isothermal resistivity change after exposure (**figure 8.31**) the initial decrease of resistivity during reversion can be attributed to the dissolution of very small δ′ precipitates with a size smaller than that for critical electron scattering. The dissolution is completed at 145°C. The coarse 150°C pre-age δ′ particles start dissolving at 150°C and the resistivity returns to the baseline at 200°C where complete dissolution of δ′ has taken place. The reversion curves for the 1.7Li1.2Mg and 1.7Li3.0Mg alloys are shown in **figures 8.38** and **8.39**. In the 1.7Li1.2Mg alloy the reversion of the exposure δ′ is complete at 160°C. This temperature is 15°C higher than the equivalent temperature in the binary alloy (145°C) and this can be explained in three ways:

- the exposure δ′ is larger in the 1.7Li1.2Mg alloy

- the exposure δ′ may grow during reversion in the temperature range 140-160°C
- the δ′ precipitates from the 150°C pre-age may coarsen slightly during exposure in the 1.7Li1.2Mg alloy and hence will dissolve more slowly.

The magnitude of the reversion change due to dissolution of the exposure δ′ is 2 nΩm which is the same as the resistivity decrease during exposure (**figure 8.31**). This suggests that the higher dissolution temperature is probably due to an increase in size of the exposure δ′ (relative to the binary alloy).

In the 1.7Li3.0Mg alloy the reversion of the exposure δ′ is again complete at 160°C. In addition, the magnitude of the reversion change due to dissolution of the exposure δ′ is 5.0 nΩm, which is approximately the same as the resistivity decrease observed during exposure (4.5nΩm, **figure 8.31**).

In both 1.7Li1.2Mg and 1.7Li3.0Mg alloys direct aged at 70°C a decrease in reversion resistivity was observed in the temperature range 150-175°C. This drop in resistivity can be attributed to the growth of large δ′ during isochronal heating. It can be clearly seen from **figures 8.38** and **8.39** that no analogous decrease is observed for the exposed alloys and this can be explained by the lower supersaturation after the 150°C prior age.

The effect of the magnesium concentration on the reversion resistivity curves after exposure at 70°C are given in **figure 8.40**. The increased magnesium

concentration results in a shift of the $T^{Rev.}_{end}$. **Figures 8.40** and **8.41** show that the additions of 1.2 and 3% magnesium cause a displacement of T^{Rev}_{end} of 15°C and 25°C respectively. As shown in section 8.2.4 and was verified in **figure 8.30** the magnesium causes a shift of the δ′ solvus by 6.7°C/wt%Mg which is translated into a displacement of about 10 and 20°C for 1.7Li1.2Mg and 1.7Li3.0Mg alloys respectively. Thus, after exposure the δ′ solvus has been shifted an extra 5°C and this can be attributed to the presence of large δ′ particles caused by the prior age 24h at 150°C.

The exposure curve of the 1.7Li3.0Mg alloy (**figure 8.39**) shows that the as-quenched value is not quite reached after reversion. This is attributed to the formation at 150°C of very small amounts of equilibrium T_M which is, according to the isochronal resistivity changes given in **figure 8.2**, stable up to about 320°C. Reversion temperatures >230°C produce further precipitation of T_M.

For the 1.7Li binary and 1.7Li1.2Mg alloys the baseline is reached after reversion indicating that all the lithium has returned to the matrix and therefore the only phase precipitated during the 150°C pre-age and subsequent exposure is δ′ in these low magnesium alloys.

8.3 Effect of exposure on the mechanical properties of Al-Li-Mg alloys

The changes in proof stress and fracture energy after exposure of the 1.7Li binary, 1.7Li1.2Mg and 1.7Li3.0Mg alloys are shown in **figure 8.42**. The

addition of 1.2%Mg to the binary alloy causes a very small increase in the proof stress (~0.5MPa) whereas the fracture energy exhibits a significant decrement (~16kJ/m^2). Higher levels of magnesium (3%Mg) cause a relatively high increment in the proof stress (4.5MPa) and a marked decrease in fracture energy (48 kJ/m^2). As shown in **figure 8.36,** increasing the magnesium concentration from 1.2 to 3%, the volume fraction of δ′ precipitated during exposure increases approximately two fold. Noble et.al [**3**] studied the effects of exposure on the mechanical properties of binary Al-Li alloys with different lithium contents. According to their results the change in mechanical properties as a result of exposure is the consequence of either the formation of an additional δ′ dispersion, or to the growth of pre-existing δ′ particles from the pre-age, or a combination of the two effects. It has already been shown in a previous section that magnesium additions to the 1.7Li binary alloy do not cause any change in the size of the δ′ precipitates at a given heat treatment. In addition, the reversion resistivity measurements (**figures 8.38, 8.39**) indicate that the exposure does not cause any significant change in the size of pre-age δ′ precipitates (no changes in the $T^{Rev.}_{end}$ are observed). Therefore, it can be concluded that the increase in the proof stress as the magnesium increases from 1.2 to 3% is the result of the formation of larger amounts of fine δ′ precipitates in the matrix between the coarse δ′ particles from the pre-age.

The SEM fractographs taken from the 1.7Li3.0Mg alloy aged 24 h at 150°C and after subsequent exposure at 70°C are shown in **figure 8.43.** It can be seen that

the exposure at 70°C has not caused a significant increase in the amount of grain boundary failure. However, there are less fracture dimples on the fracture surface of the exposed sample indicating increased brittleness. This could be the direct result of the increase in proof stress caused by exposure.

Summary

From the above discussion, the following can be summarised:

- At all ageing temperatures increasing the magnesium concentration stimulates the formation of δ′ due to an increase of the α/δ′ solvus temperature, which in turn results in a higher driving force for δ′ precipitation. It was shown that the α/δ′ solvus temperature increases by 6.7°C/wt%Mg.
- During isothermal ageing at 70 and 100°C the process of δ′ precipitation is nucleation ordering followed by spinodal decomposition. Increasing magnesium concentration from 0 to 3.0% results in more rapid spinodal decomposition and in turn a higher volume fraction of δ′. As the ageing temperature increases from 100 to 150°C the mechanism of δ′ precipitation follows the classical nucleation and growth process.
- For a given alloy, increasing the ageing temperature causes an increase in the mean size of δ′ particles.
- During exposure a fine distribution of very small δ′ precipitates forms. As the magnesium concentration increases from 0 to 3.0% the volume

fraction of exposure δ′ increases as a result of the increase of the α/δ′ solvus temperature. This additional δ′ that is precipitated causes enhanced embrittlement.

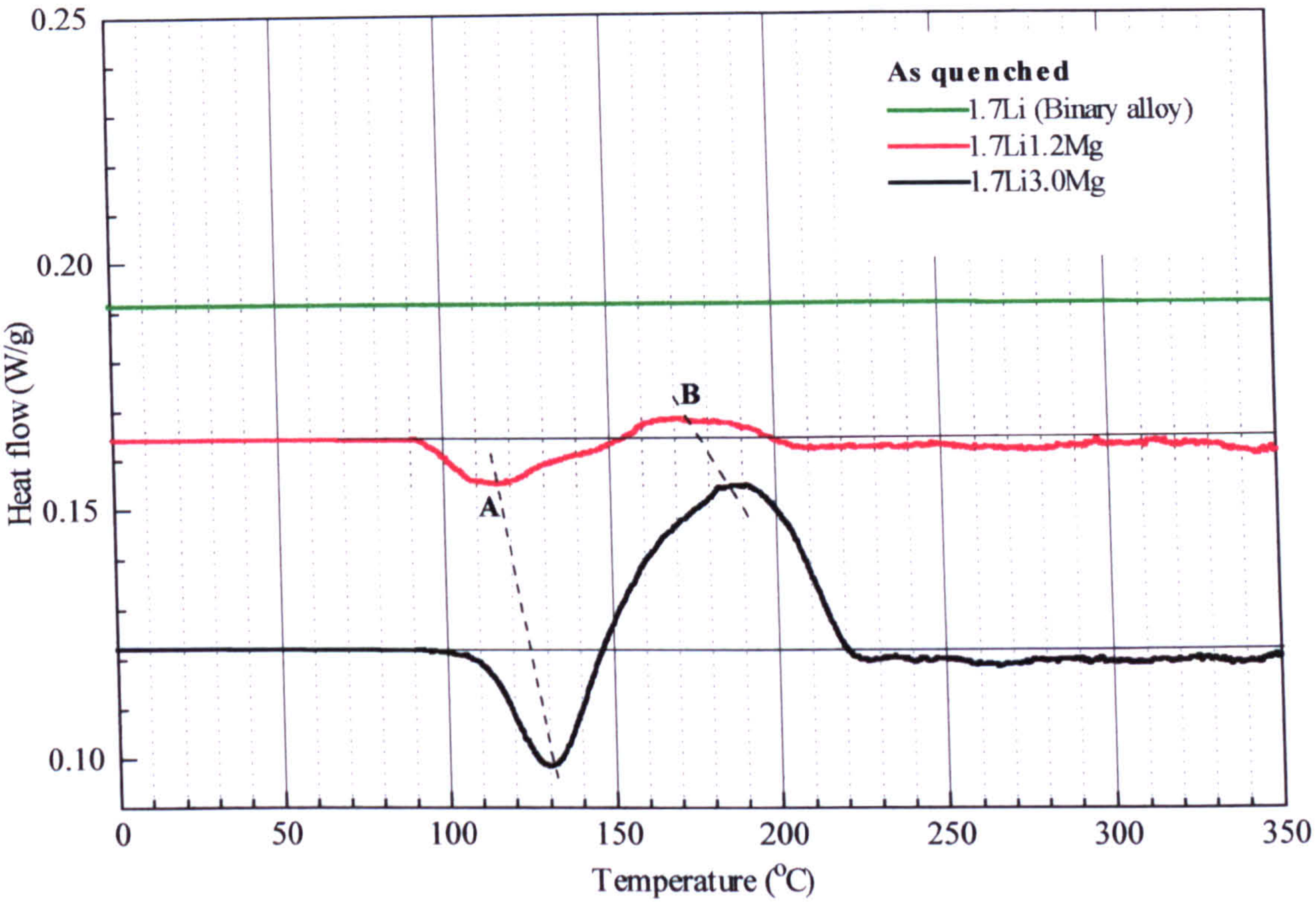

Figure 8.1: Comparative DSC plots of the as-quenched alloys.

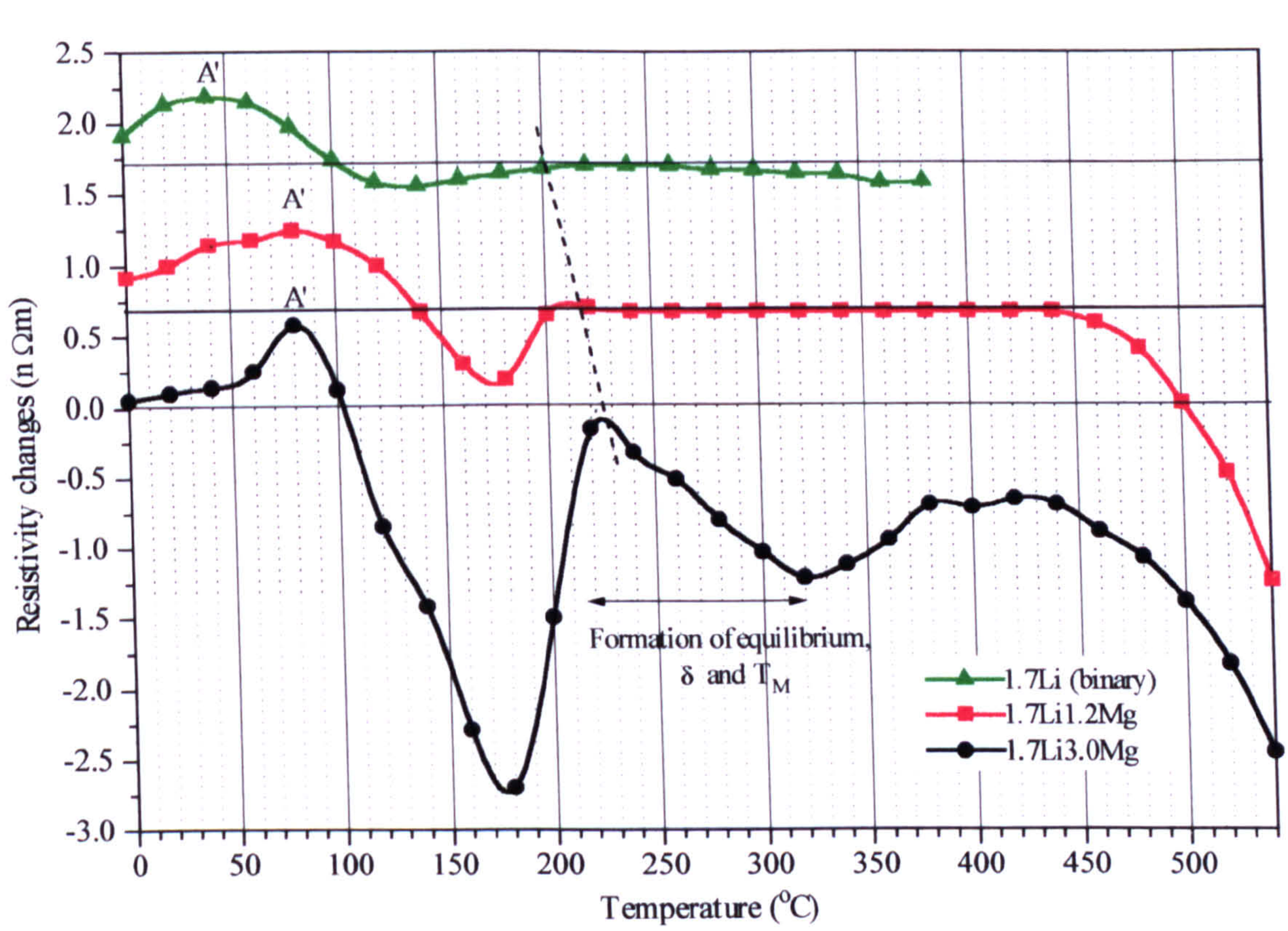

Figure 8.2: Comparison of the isochronal resistivity changes.

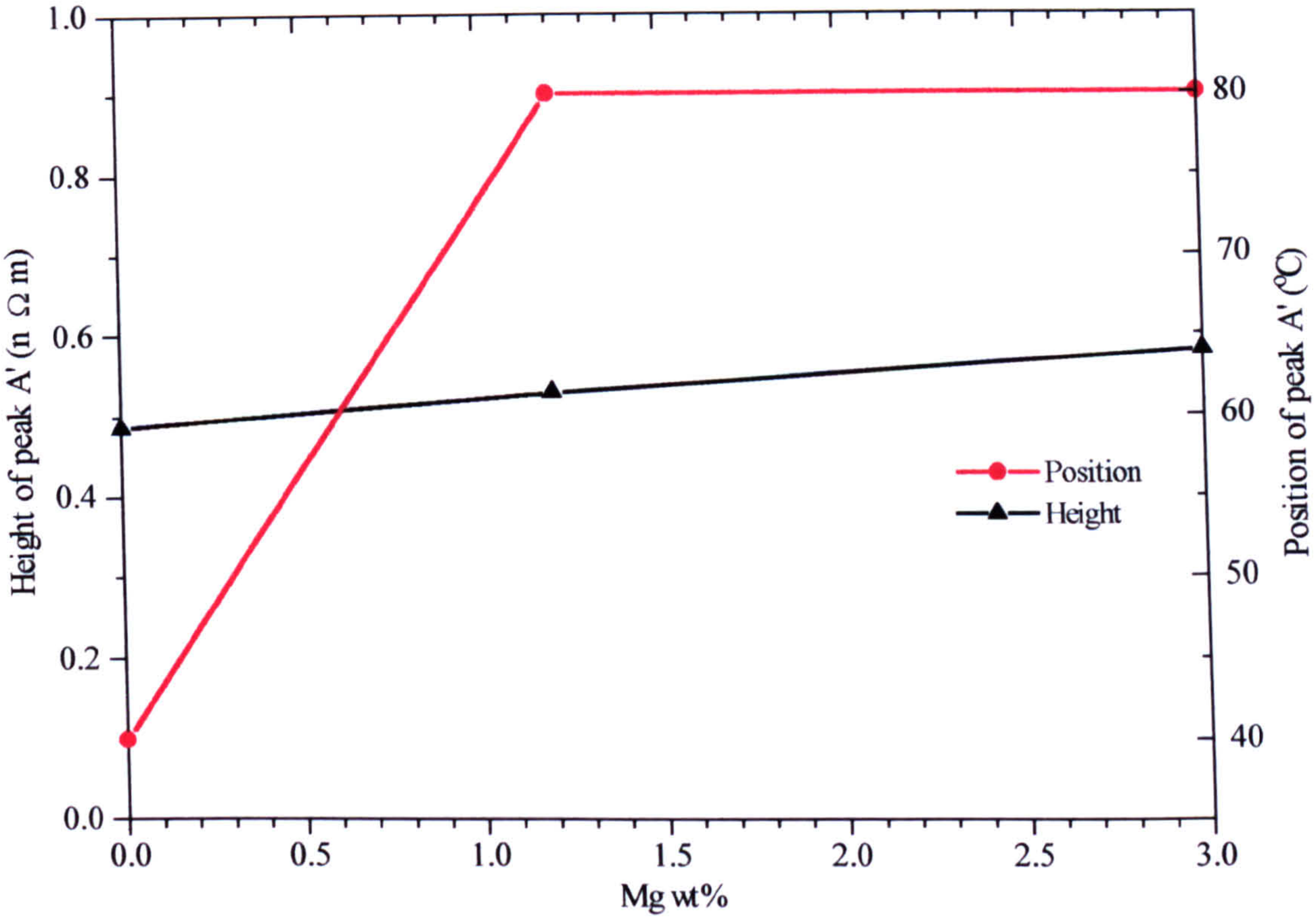

Figure 8.3: Position and height of peak A′.

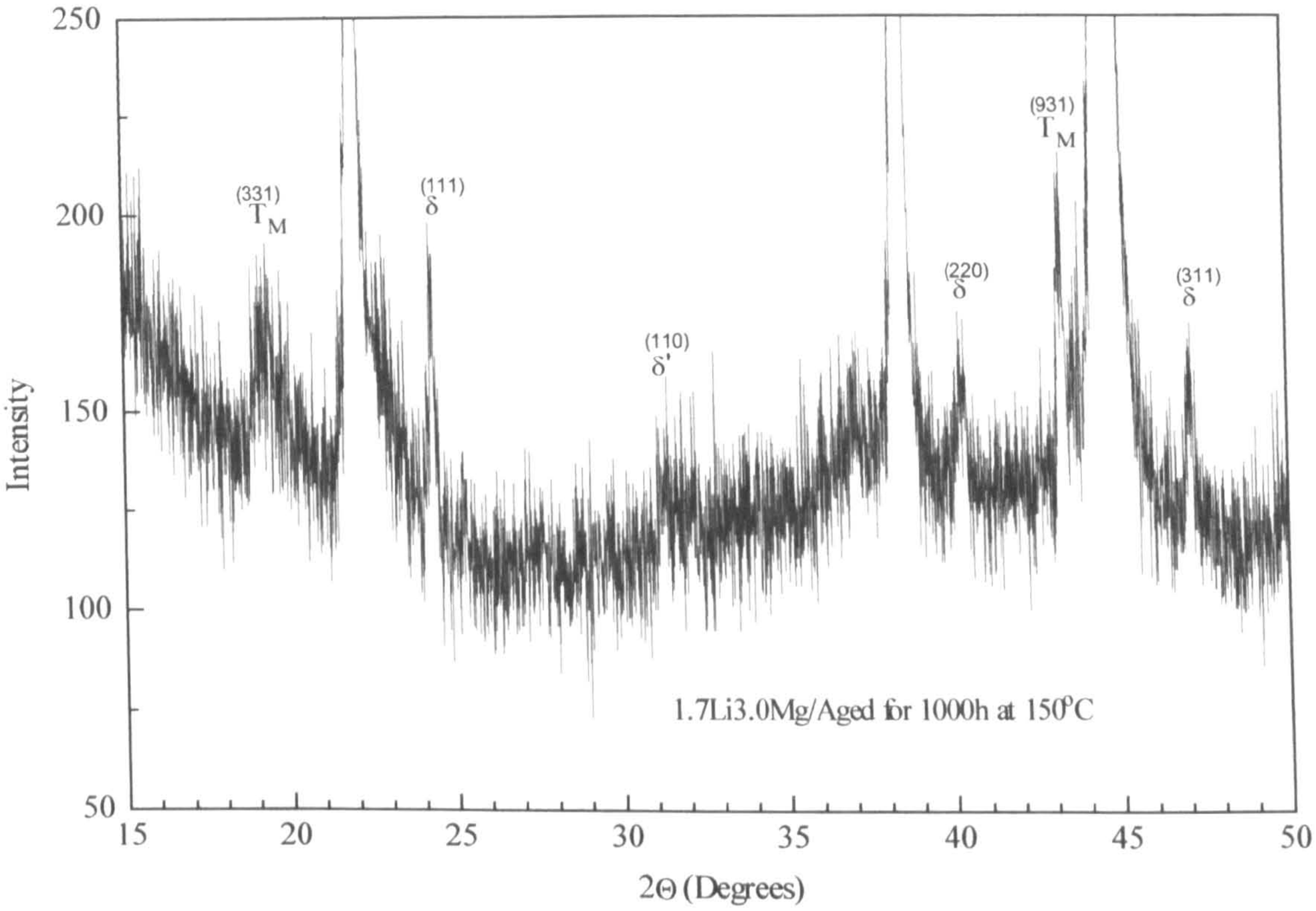

Figure 8.4: XRD-analysis of the 1.7Li3.0Mg alloy after isothermal ageing for 24h 350°C.

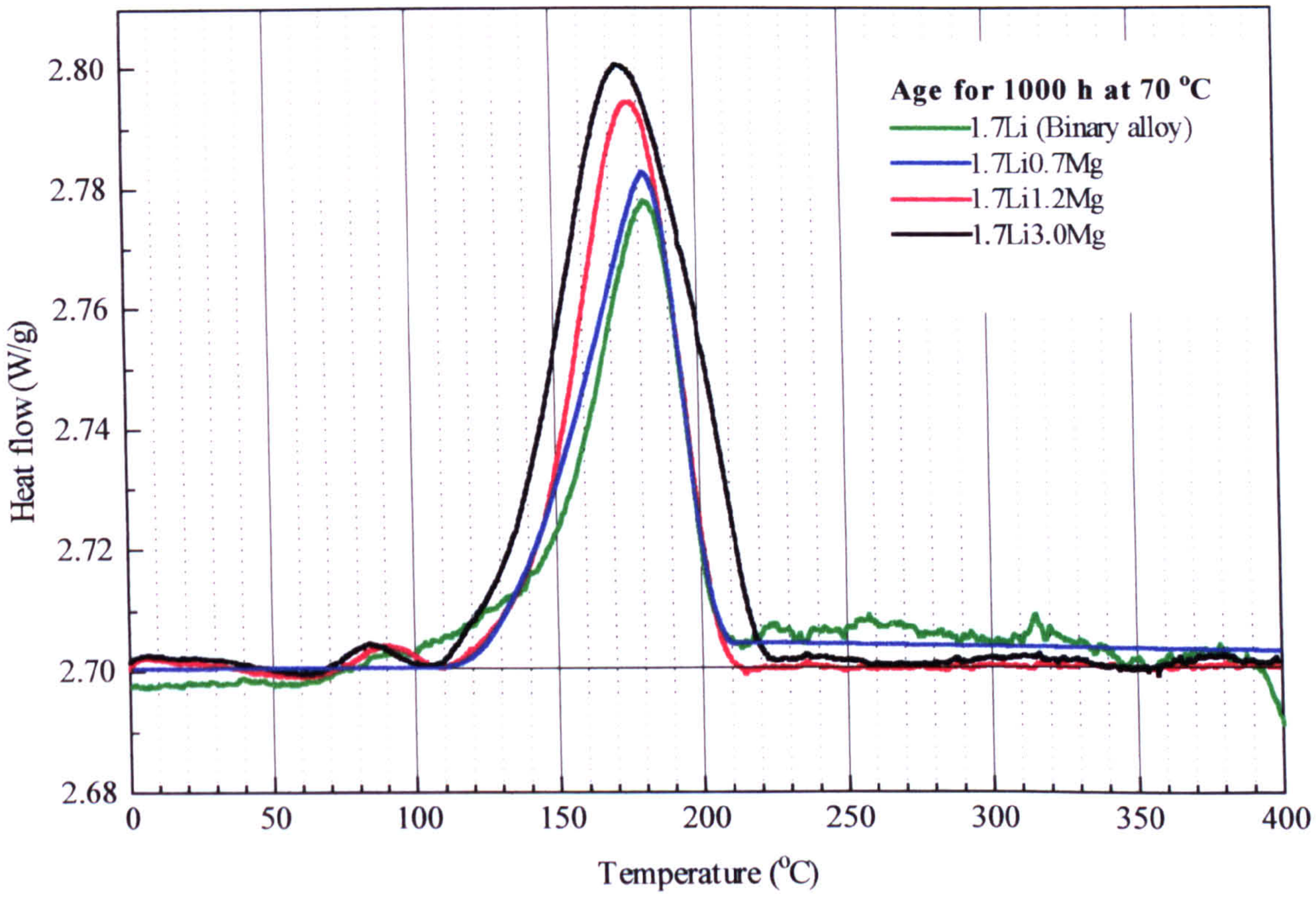

Figure 8.5: Comparative DSC plots of the alloys aged at 70°C for 1000h.

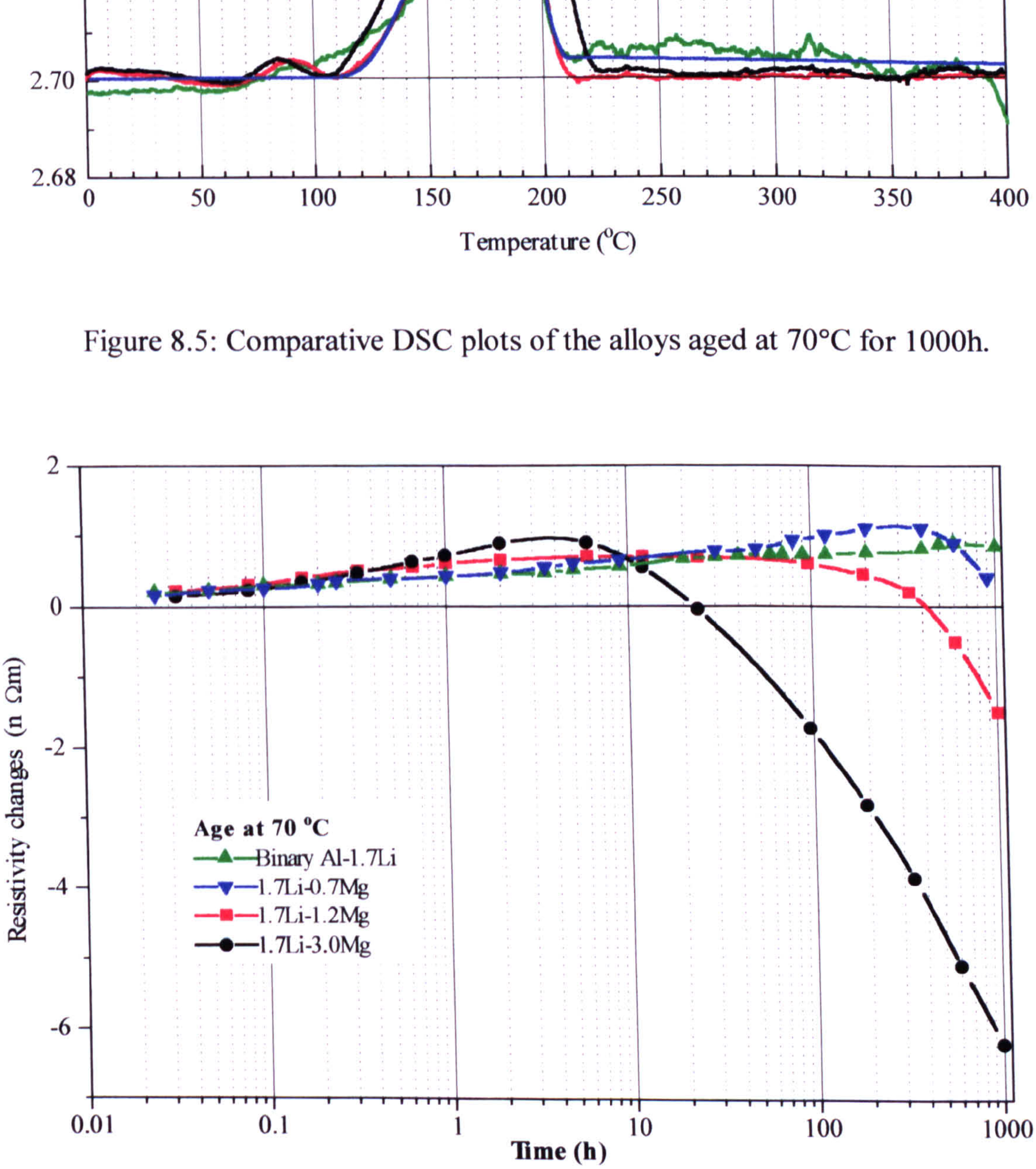

Figure 8.6: Isothermal resistivity changes during ageing at 70°C.

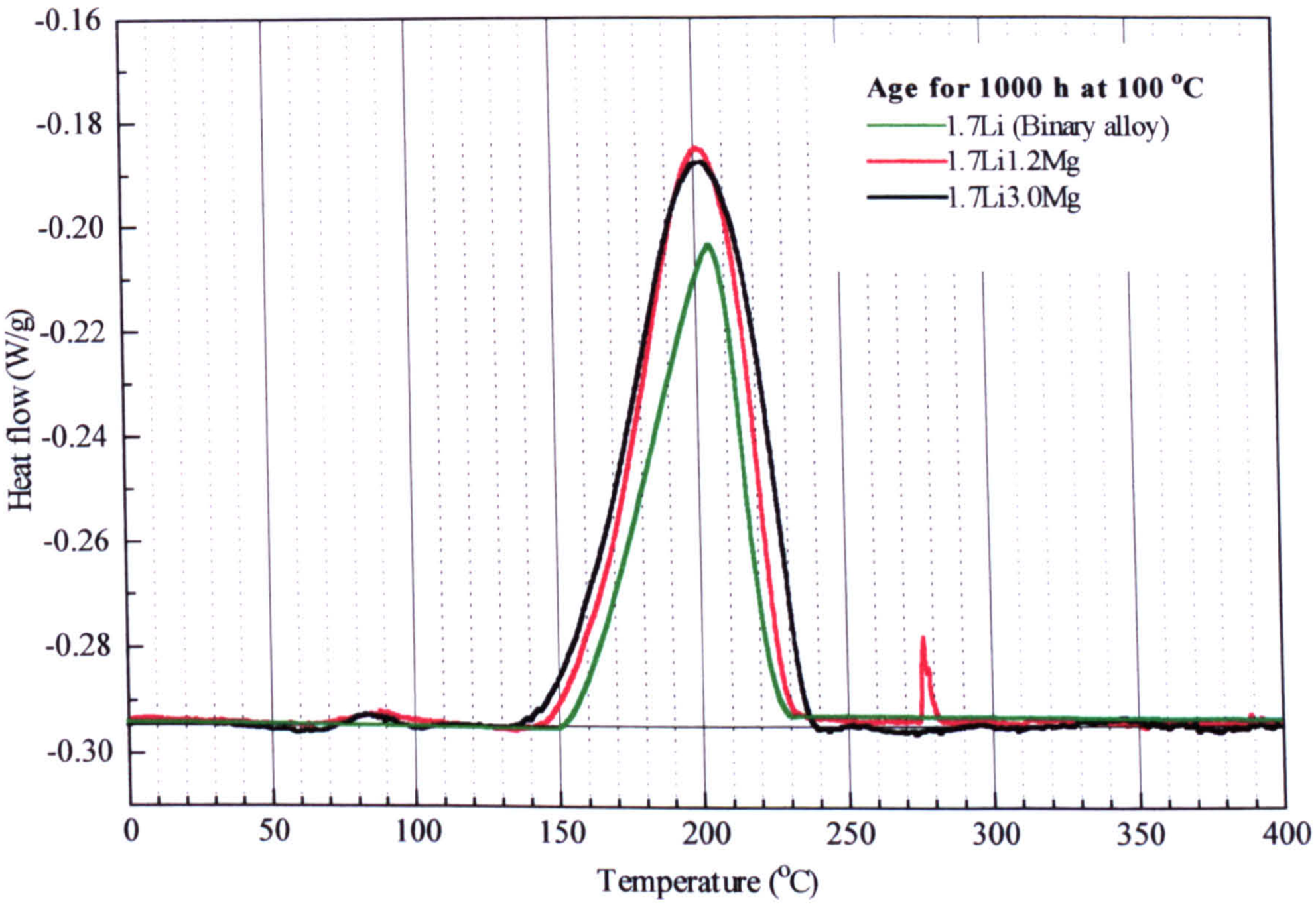

Figure 8.7: Comparative DSC plots of the alloys aged at 100°C for 1000h.

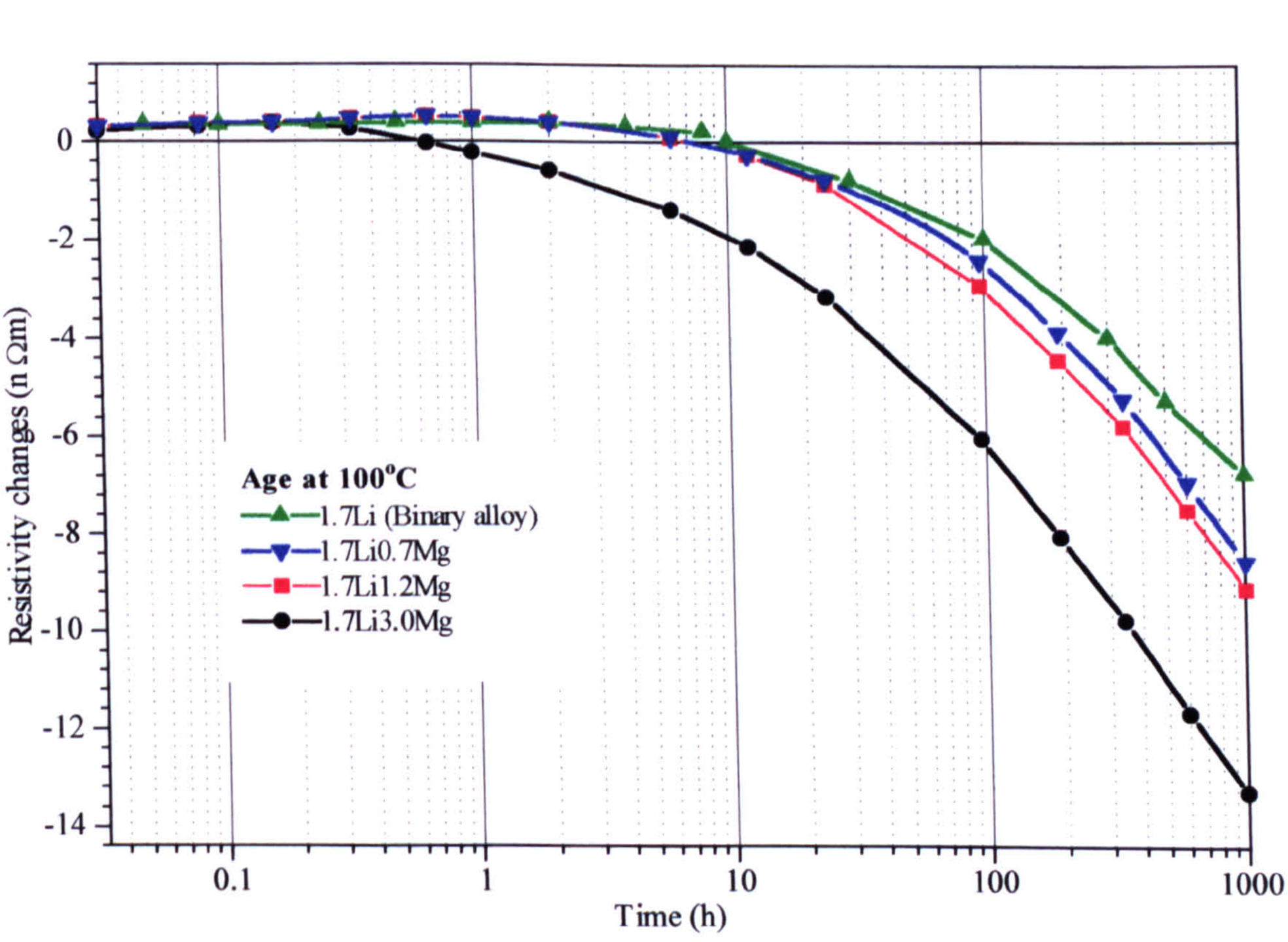

Figure 8.8: Isothermal resistivity changes during ageing at 100°C.

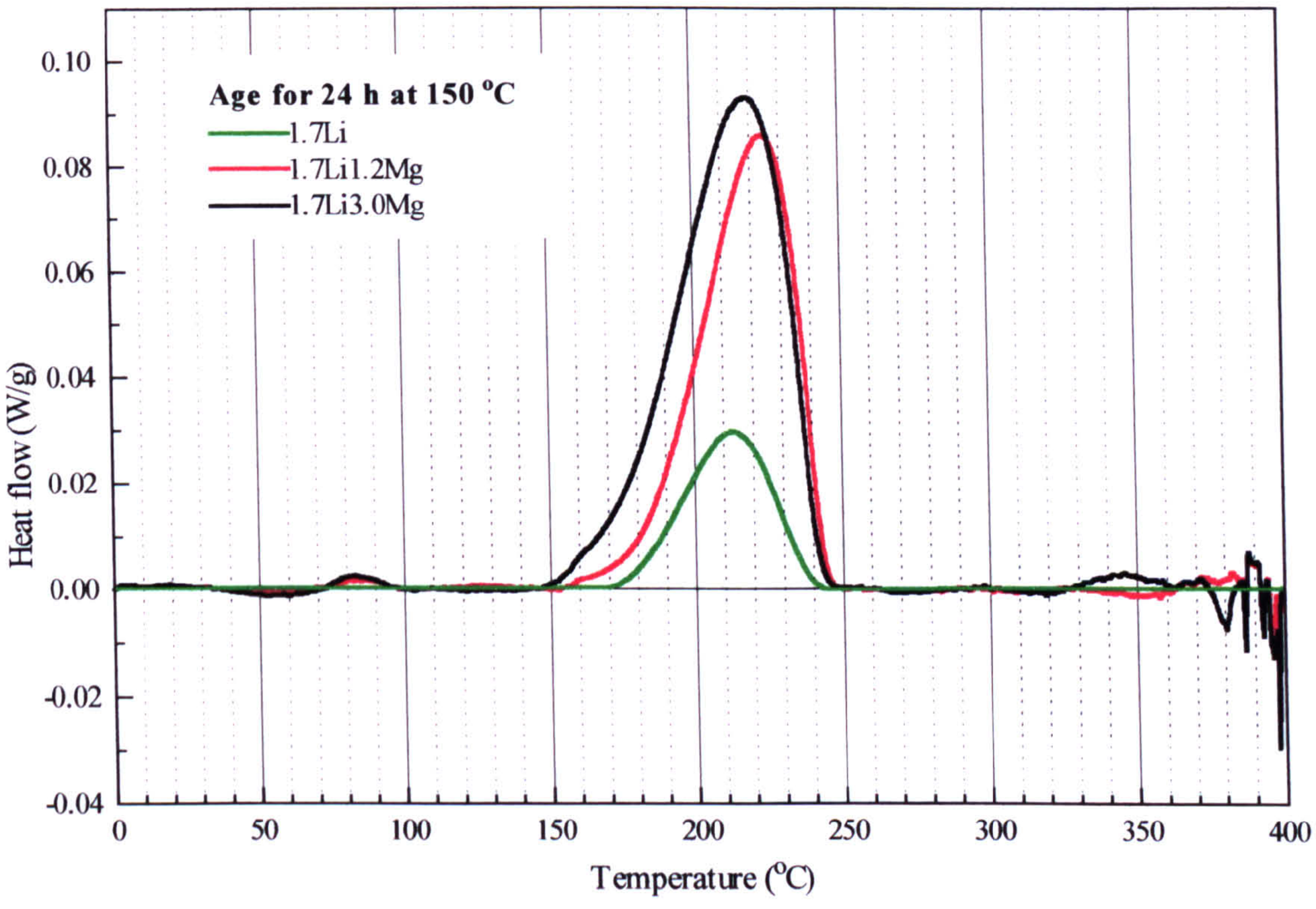

Figure 8.9: Comparative plots of the alloys aged at 150°C for 24h.

Figure 8.10: Comparative DSC plots of the alloys aged at 150°C for 1000h.

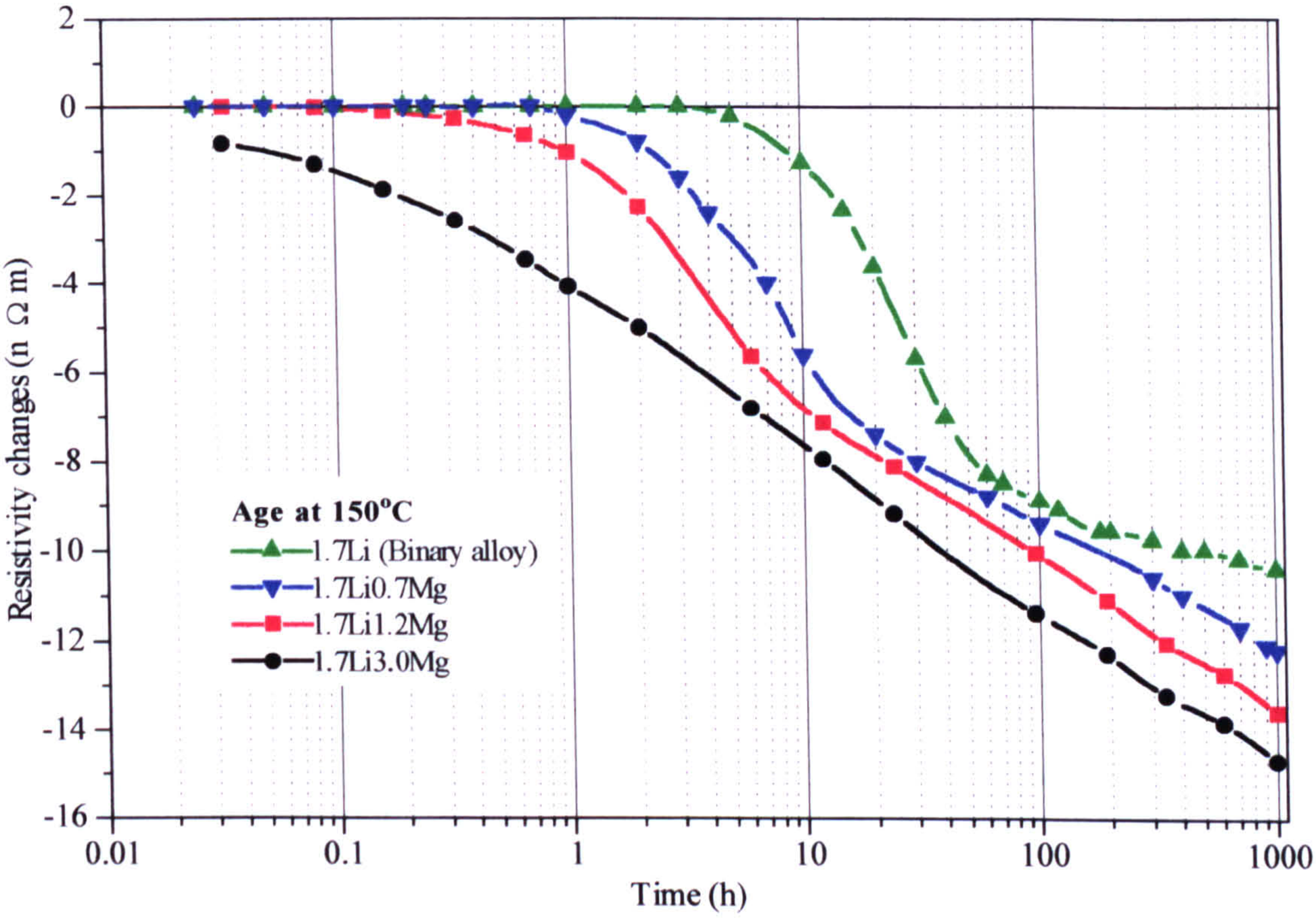

Figure 8.11: Isothermal resistivity changes during ageing at 150°C .

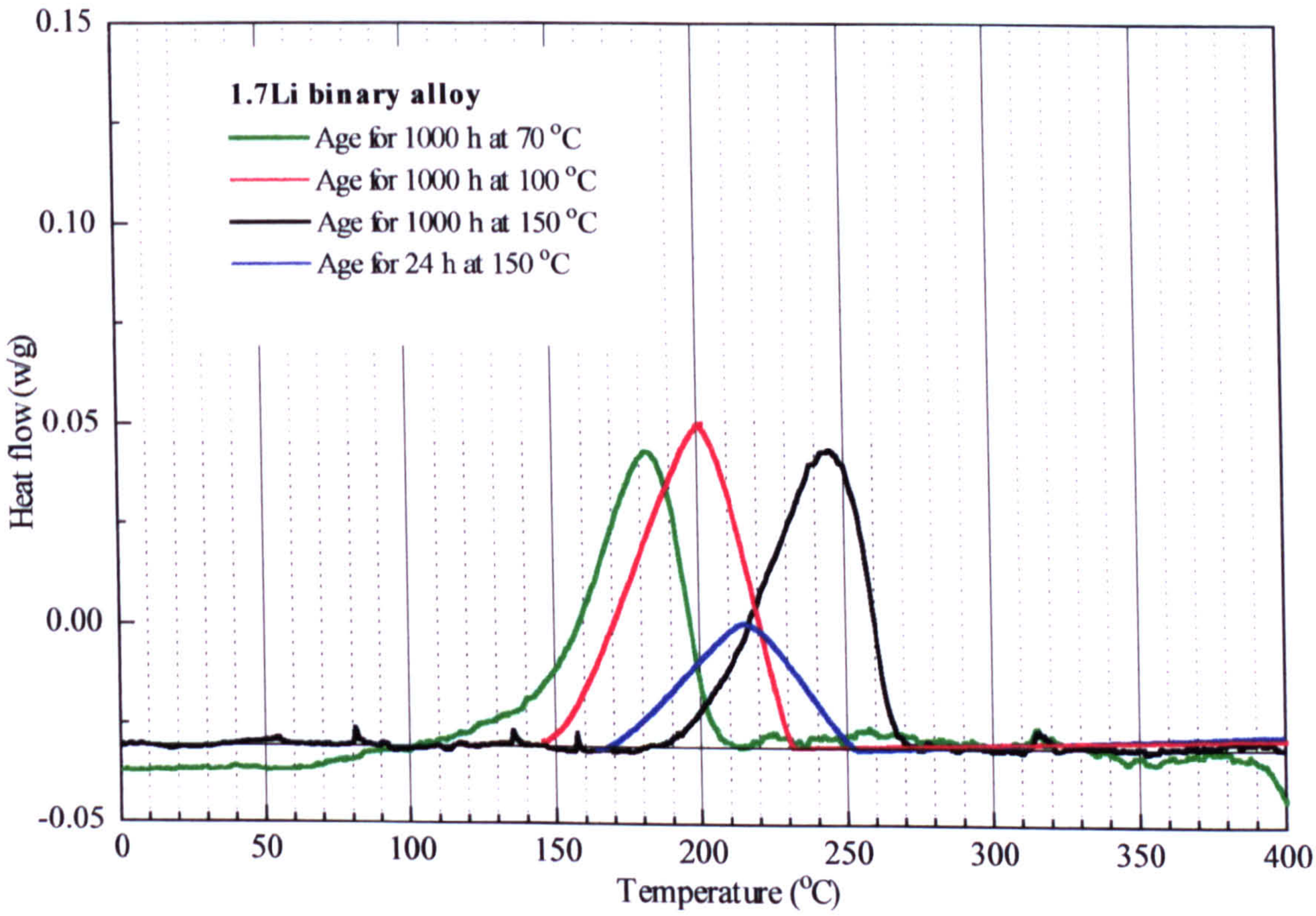

Figure 8.12: Effect of the ageing temperature on the DSC thermogram of the 1.7Li binary alloy.

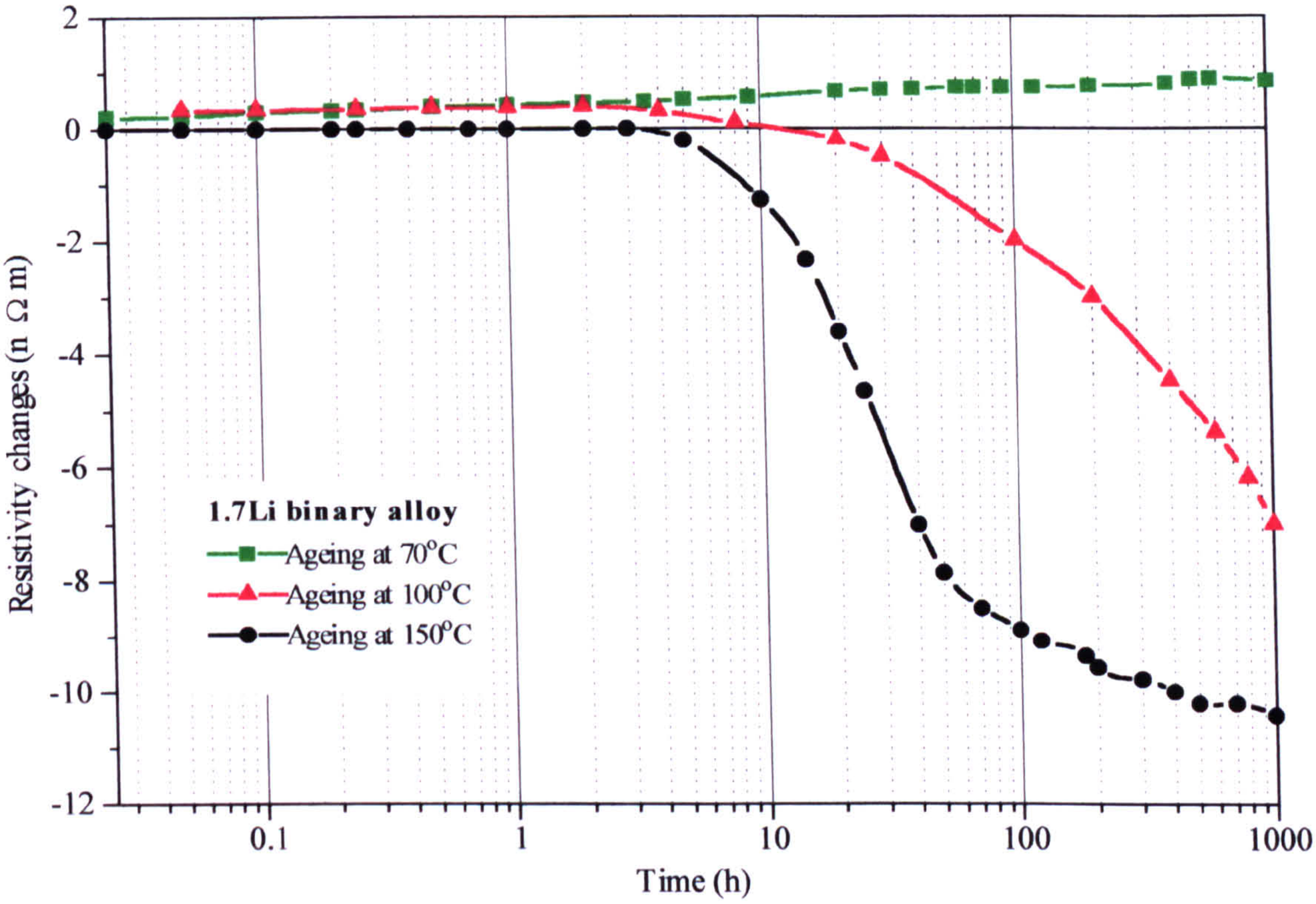

Figure 8.13: Effect of the ageing temperature on the isothermal resistivity of the binary 1.7Li alloy.

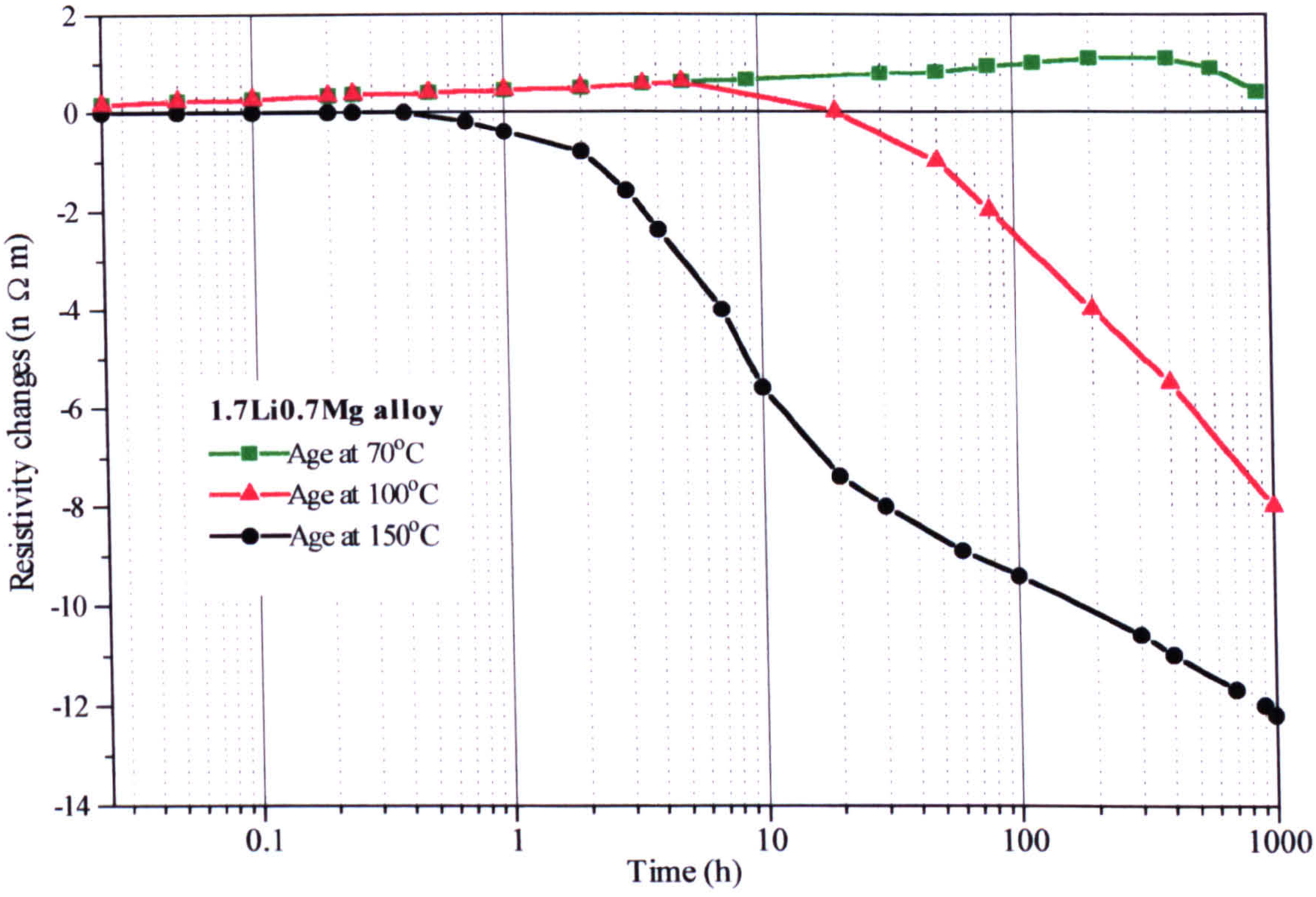

Figure 8.14: Effect of the ageing temperature on the resistivity of the 1.7Li0.7Mg alloy.

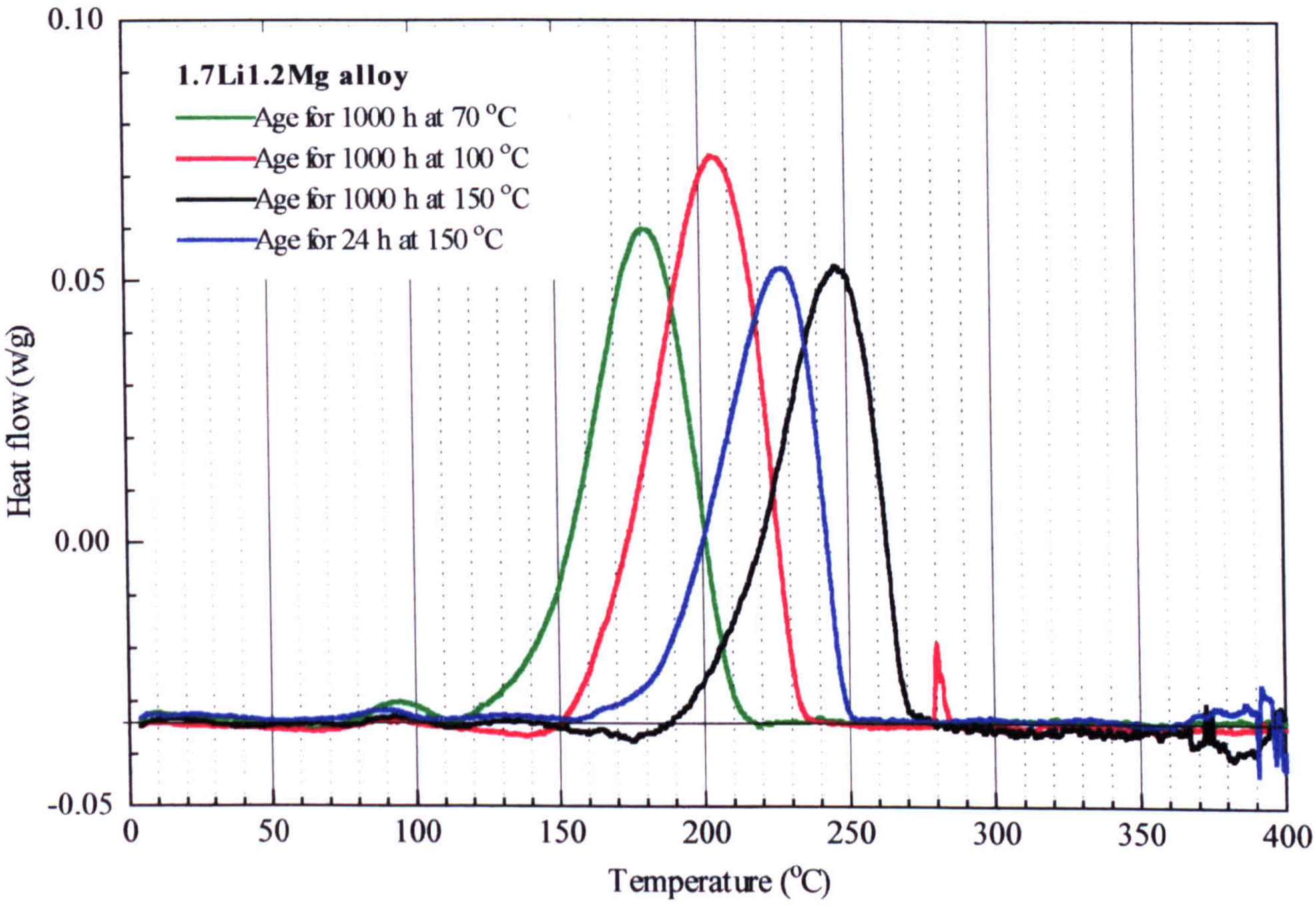

Figure 8.15: Effect of the ageing temperature on the DSC thermogram of the 1.7Li1.2Mg alloy.

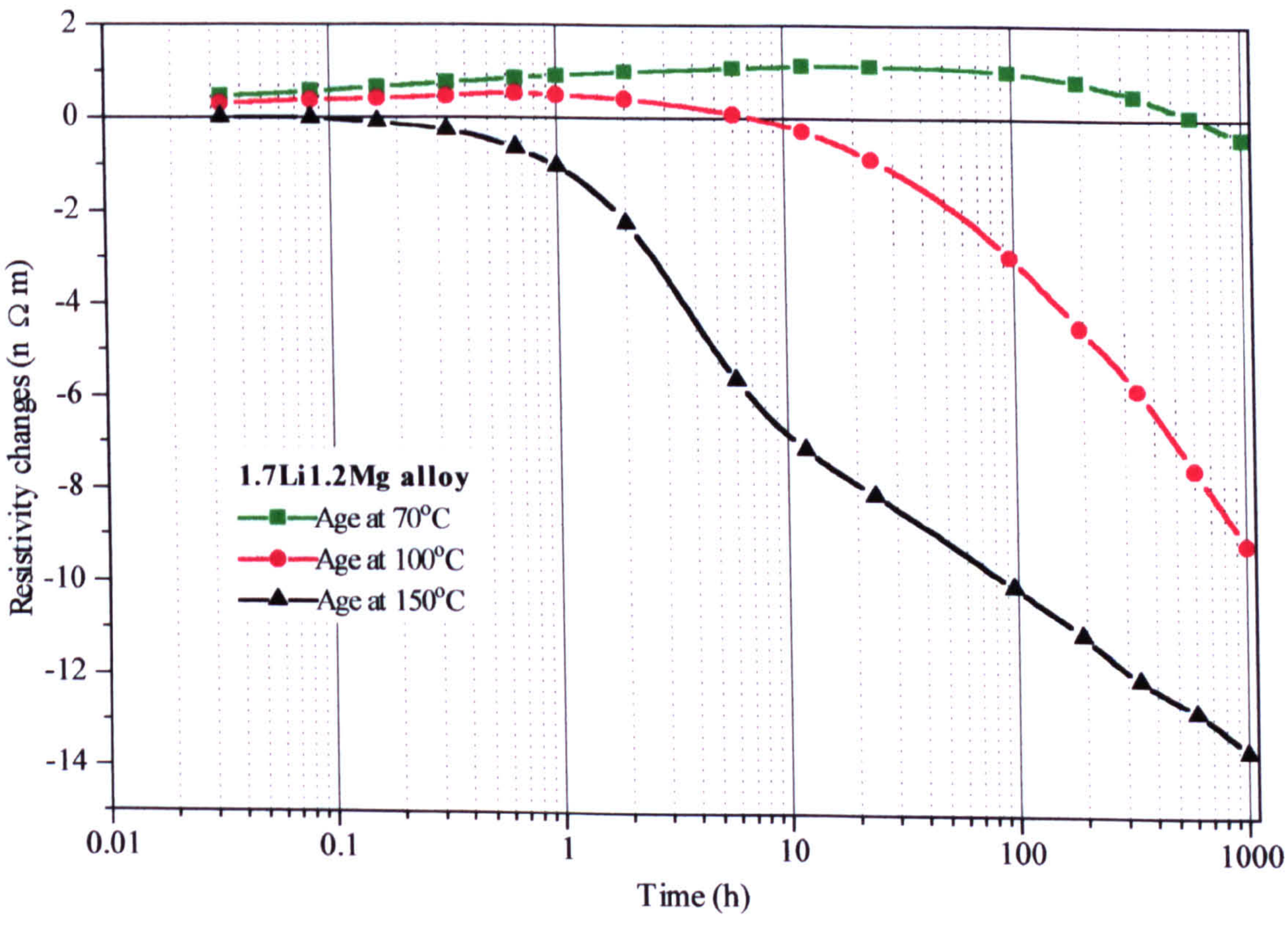

Figure 8.16: Effect of ageing temperature on the resistivity of the 1.7Li1.2Mg alloy.

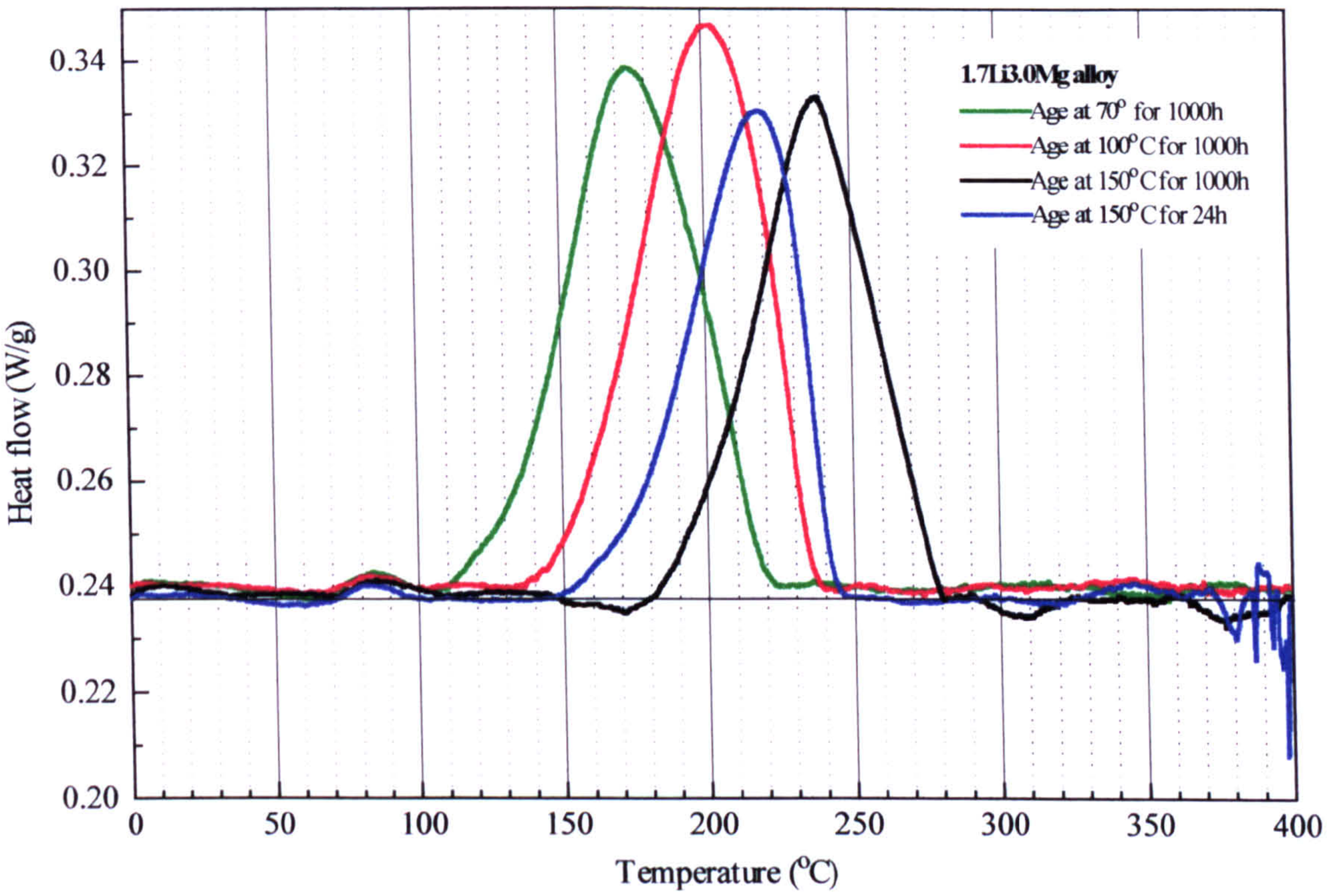

Figure 8.17: Effect of ageing temperature on the DSC thermogram of the 1.7Li3.0Mg alloy.

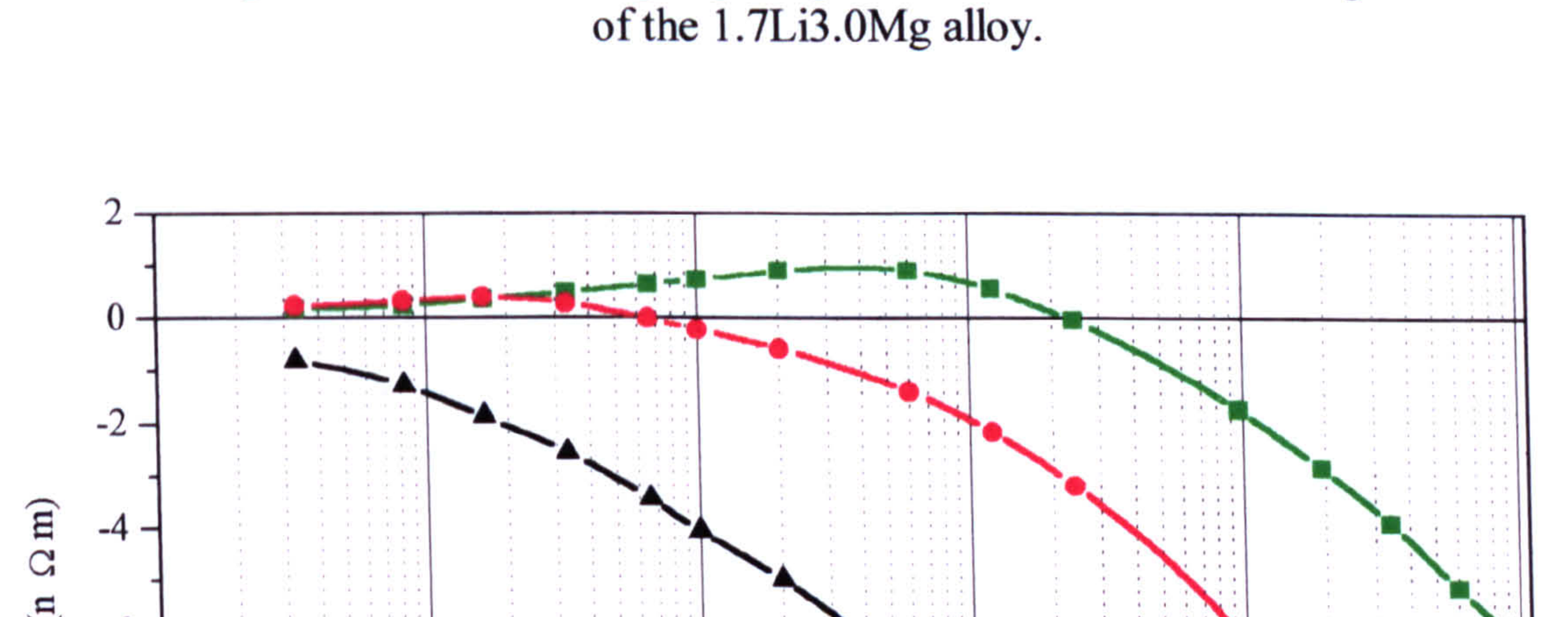

Figure 8.18: Effect of ageing temperature on the resistivity of the 1.7Li3.0Mg alloy.

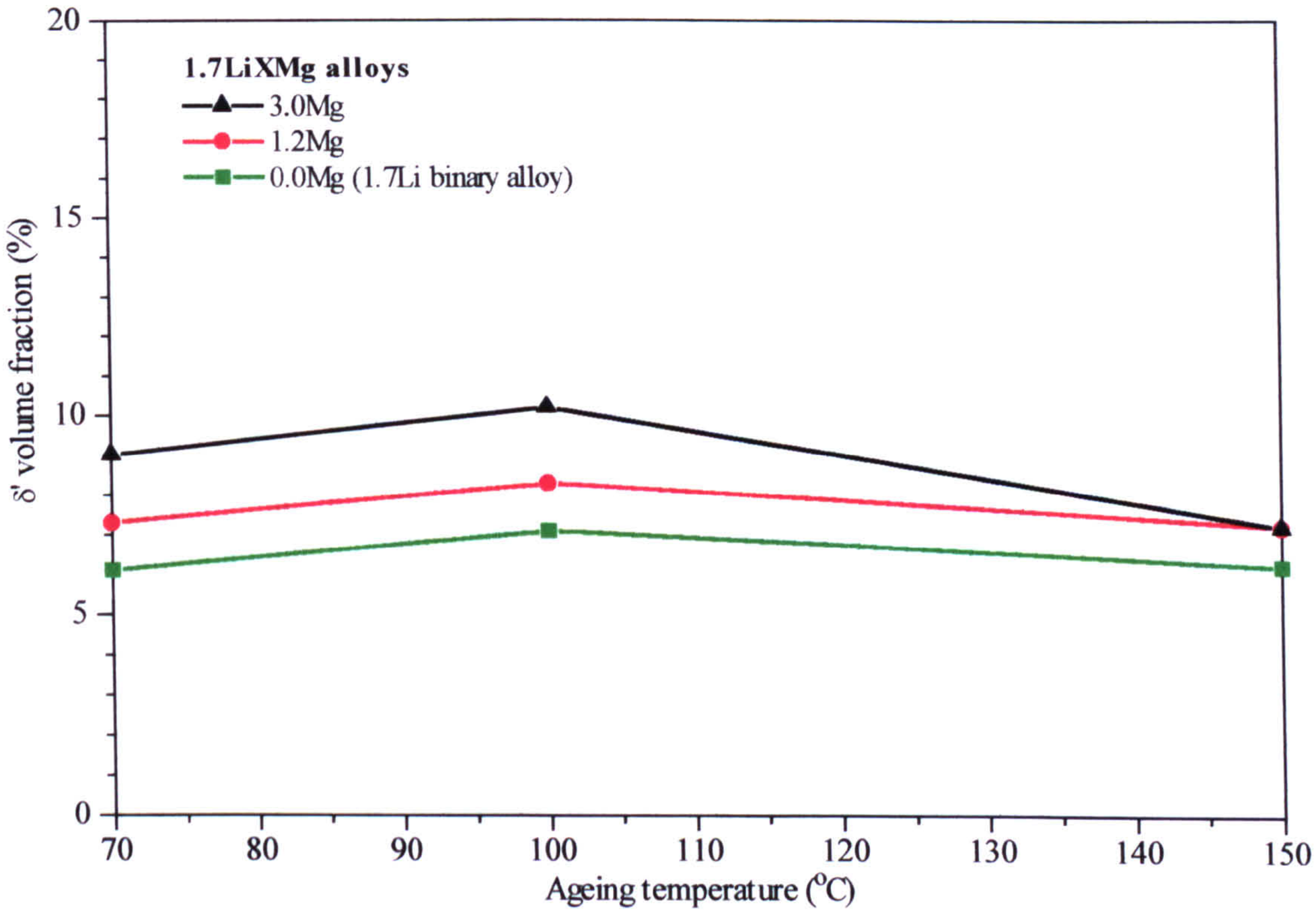

Figure 8.19: Effect of magnesium concentration and ageing temperature on the δ′ volume fraction.

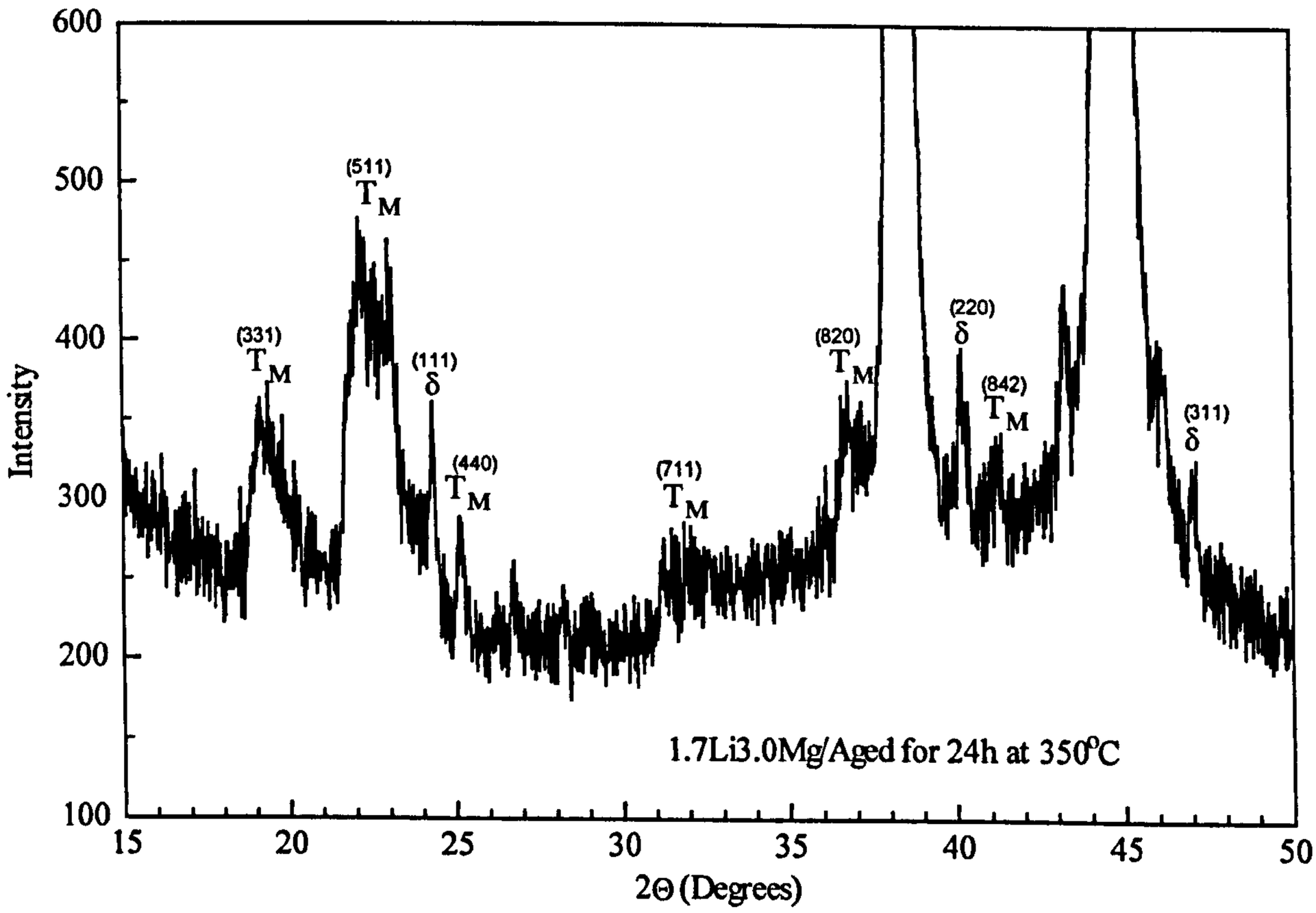

Figure 8.20: XRD-analysis of the 1.7Li3.0Mg alloy after isothermal ageing for 1000h at 150°C.

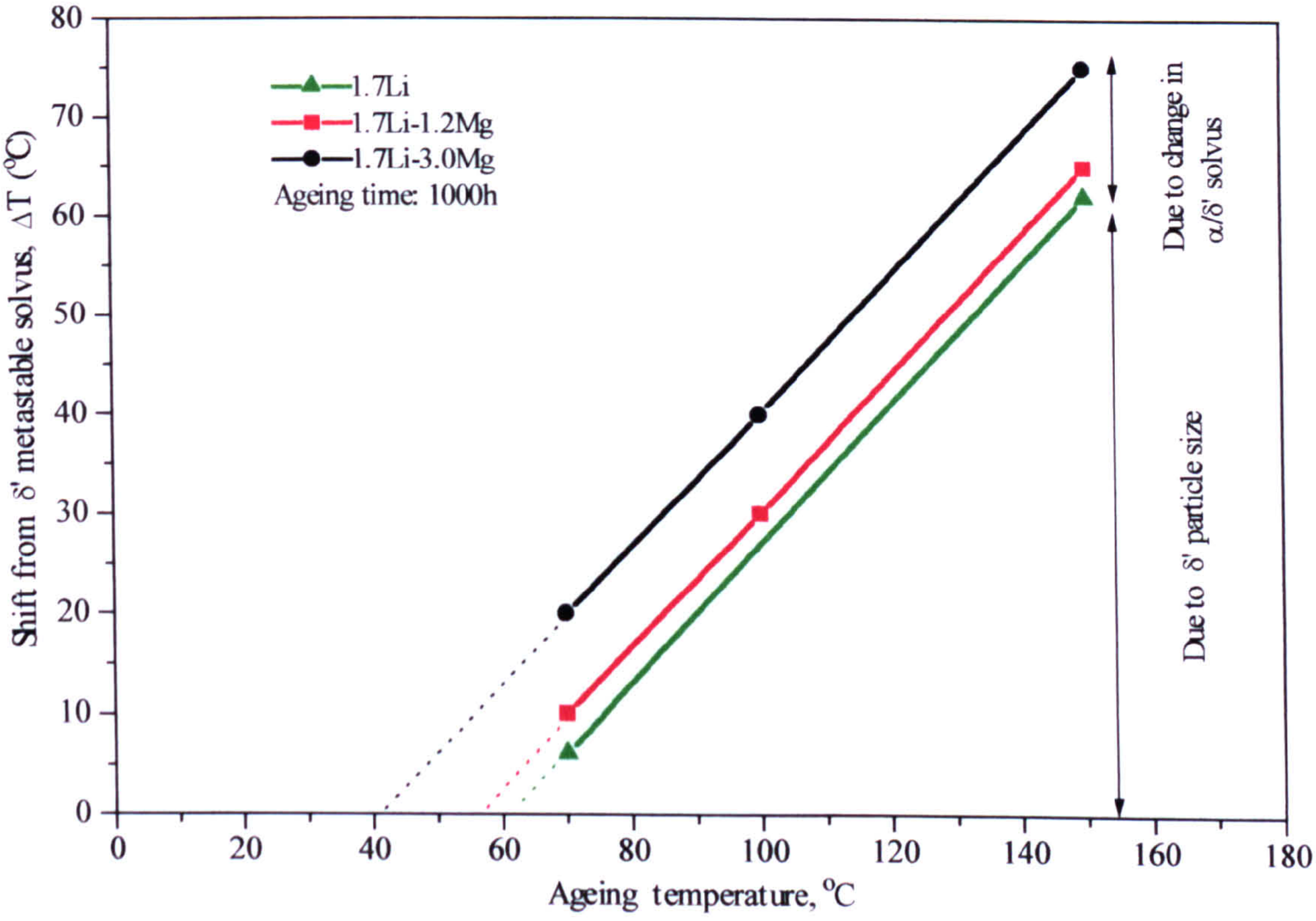

Figure 8.21: Effect of the ageing temperature on T^{DSC}_{end} .

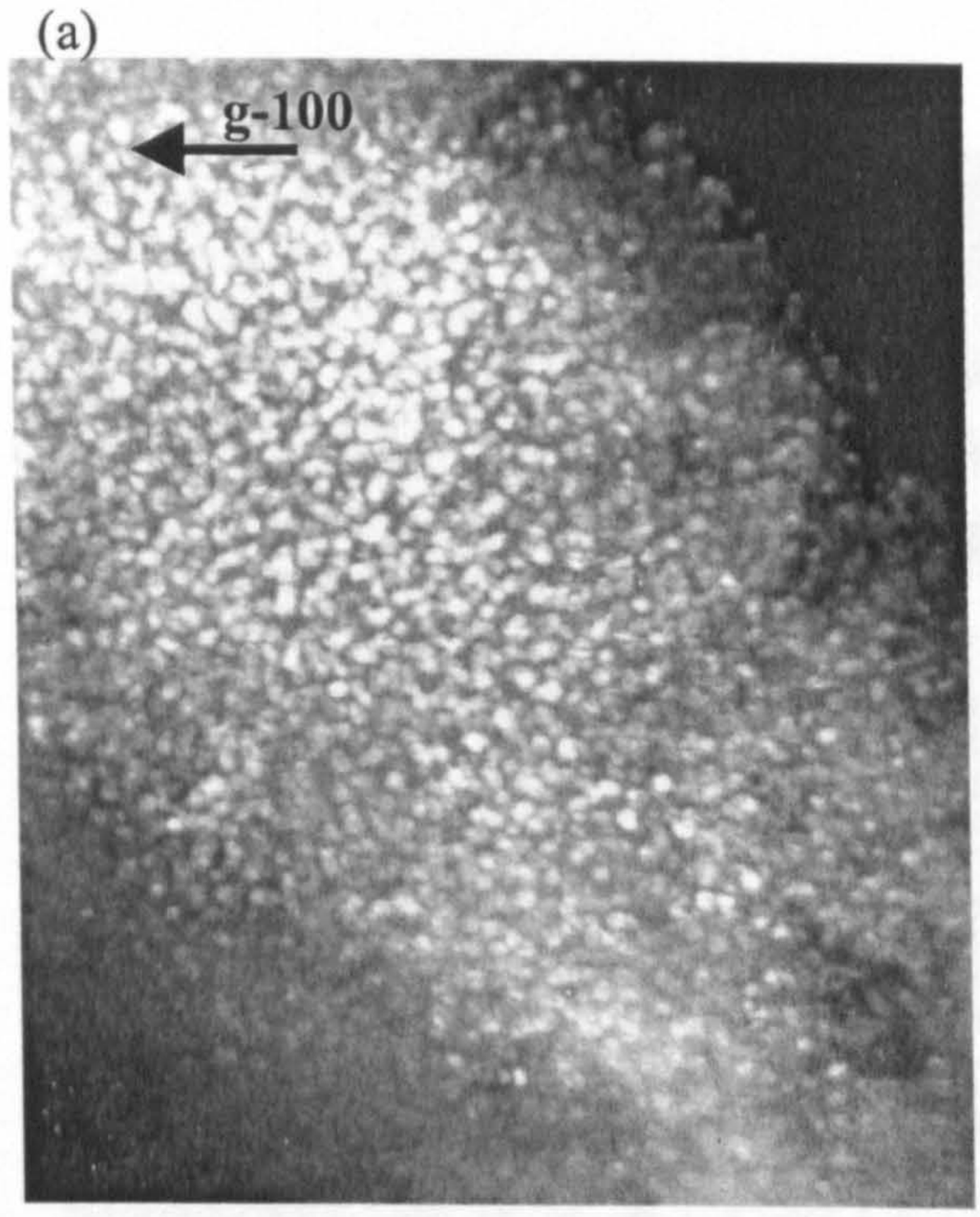

Figure 8.22(a) : TEM image of 1.7Li-1.2Mg alloy aged at 150°C for 24h, ×80K.
<110> zone axis.

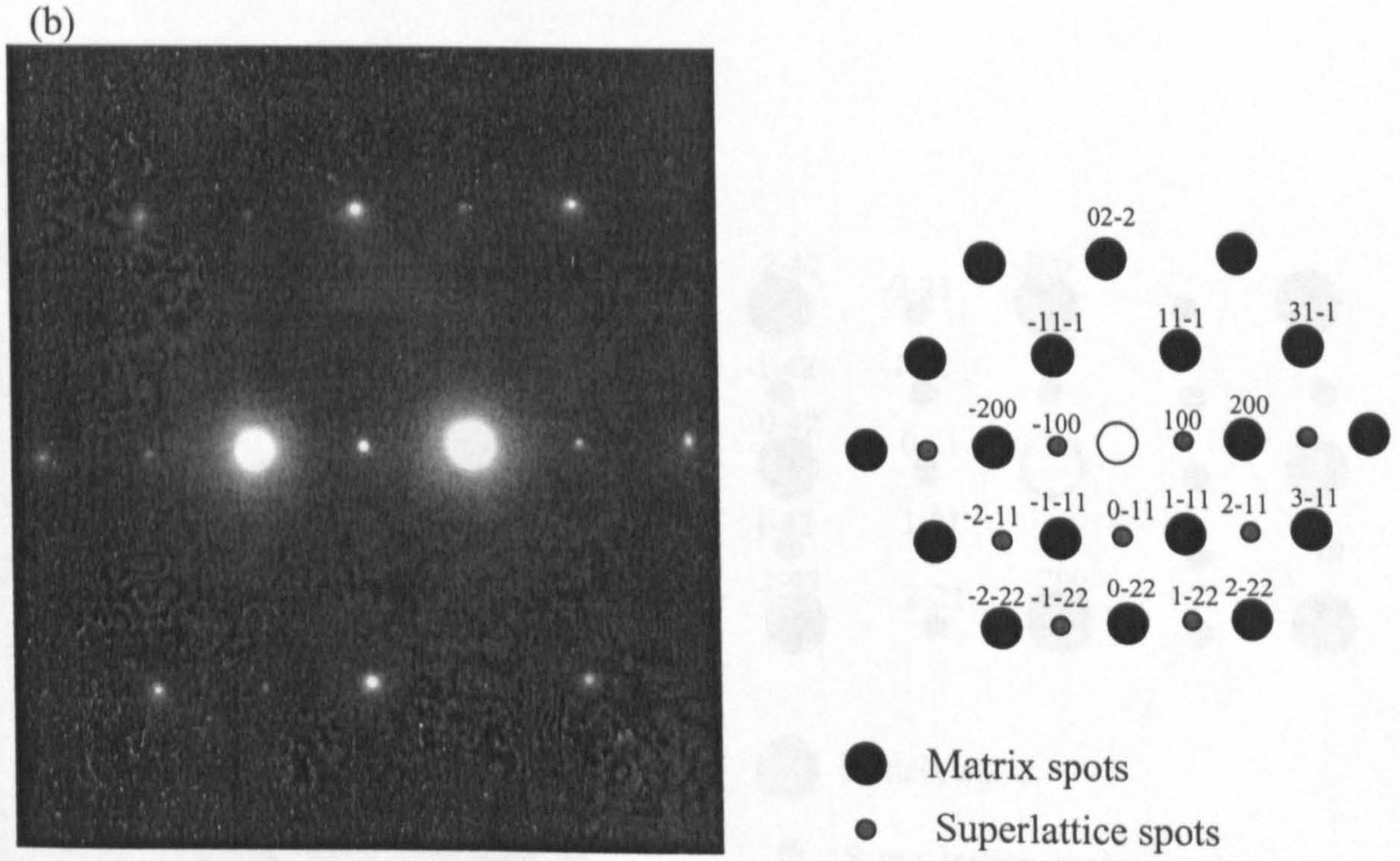

Figure 8.22(b) : SAD pattern of 1.7Li-1.2Mg alloy aged at 150°C for 24h.
<110> zone axis.

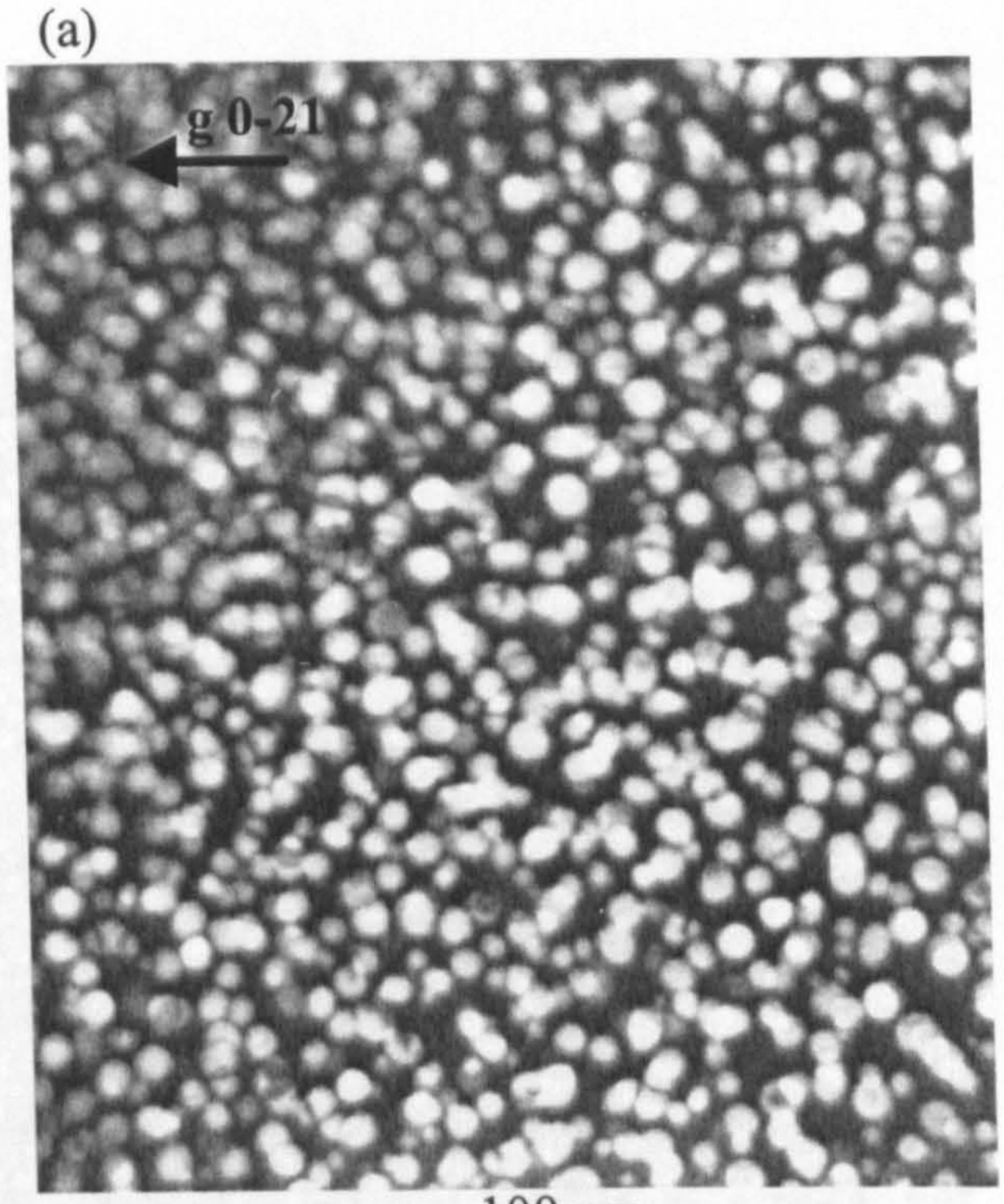

Figure 8.23(a): TEM image of 1.7Li-1.2Mg alloy aged at 150°C for 1000h, ×80K.
<210> zone axis.

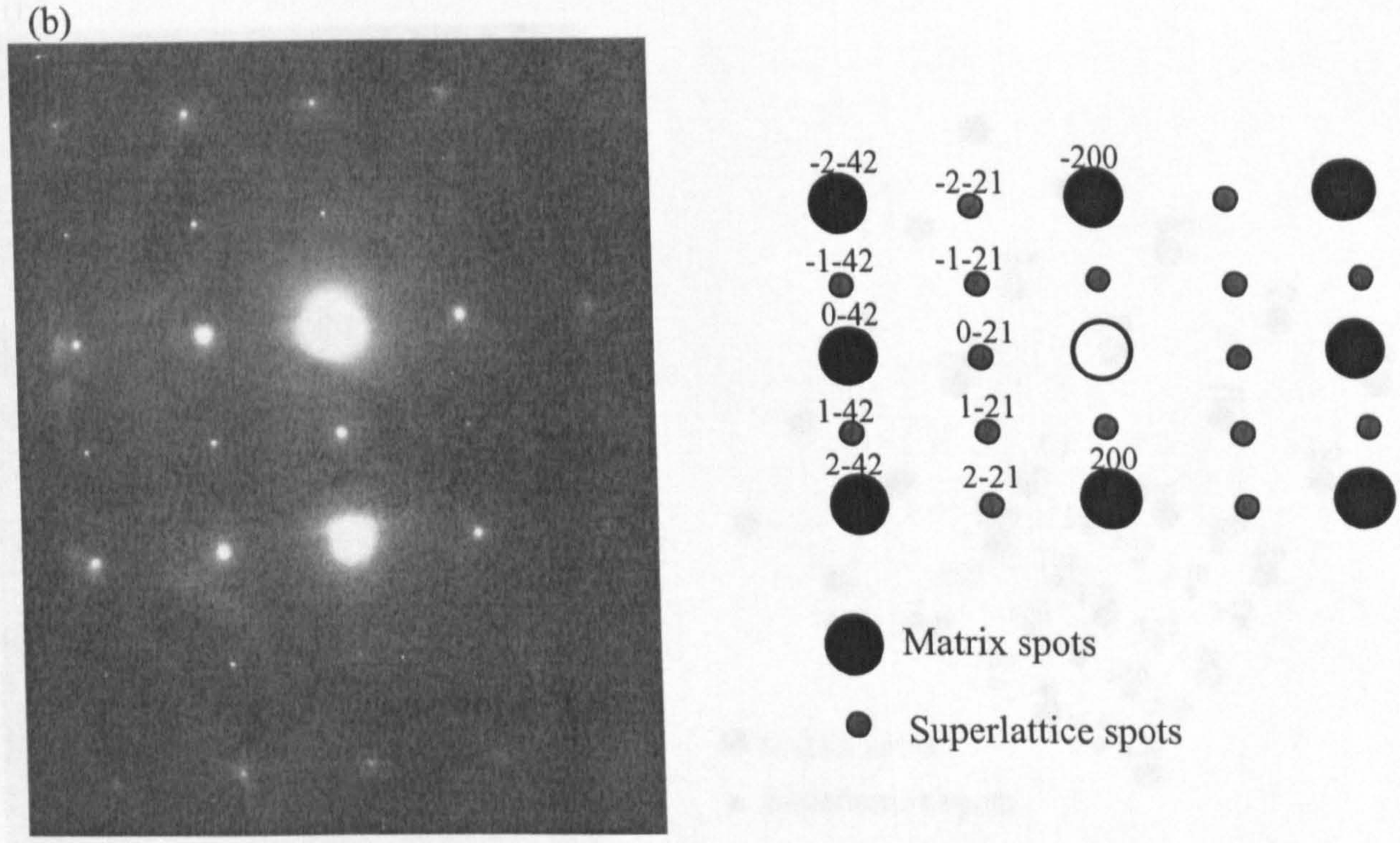

Figure 8.23(b): SAD pattern of 1.7Li-1.2Mg alloy aged at 150°C for 1000h.
<210> zone axis.

Figure 8.24(a): TEM image of 1.7Li-3.0Mg alloy aged at 150°C for 24h, ×80K
<100> zone axis.

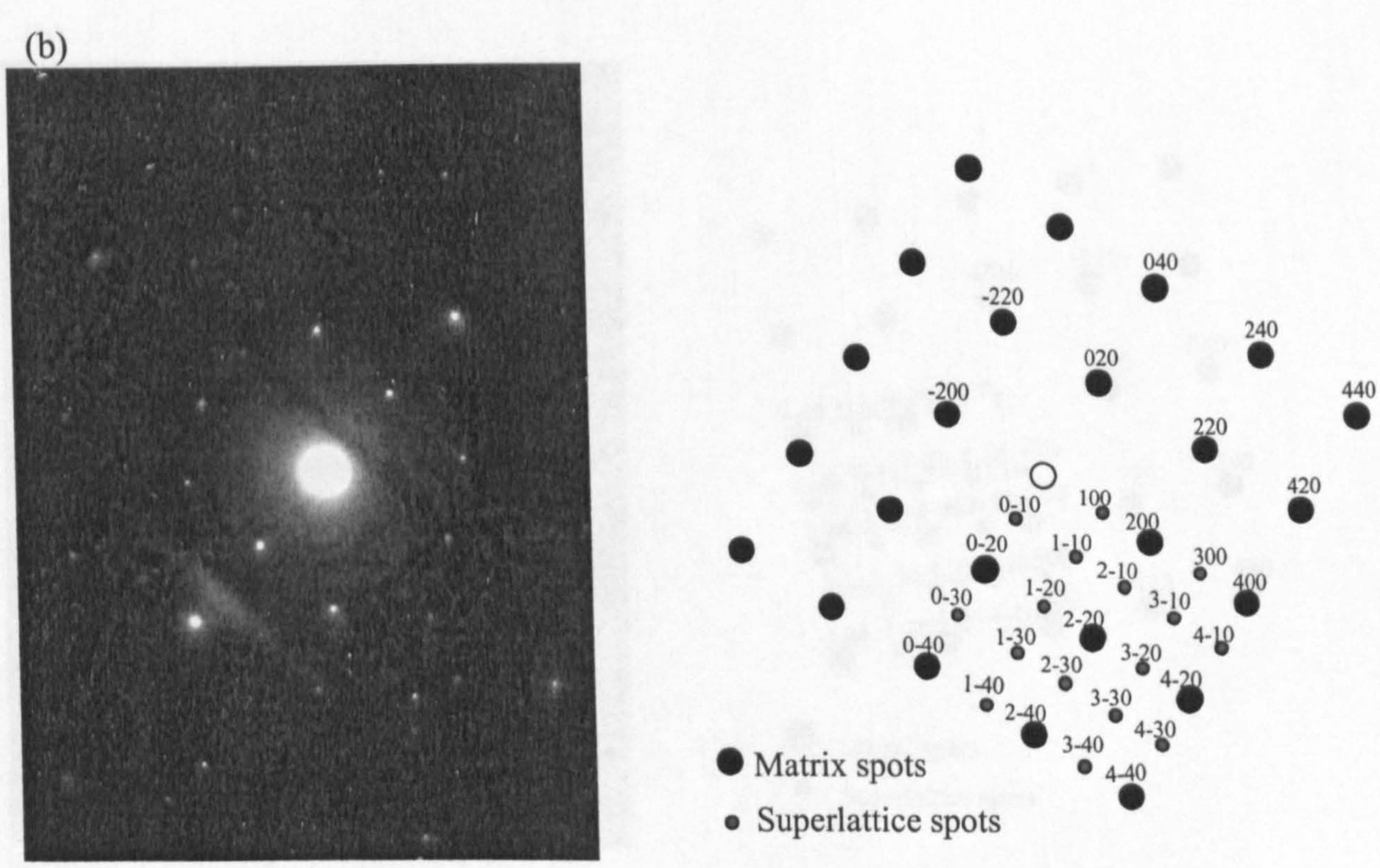

Figure 8.24(b): SAD pattern of 1.7Li-3.0Mg alloy aged at 150°C for 24h.
<100> zone axis.

(a)

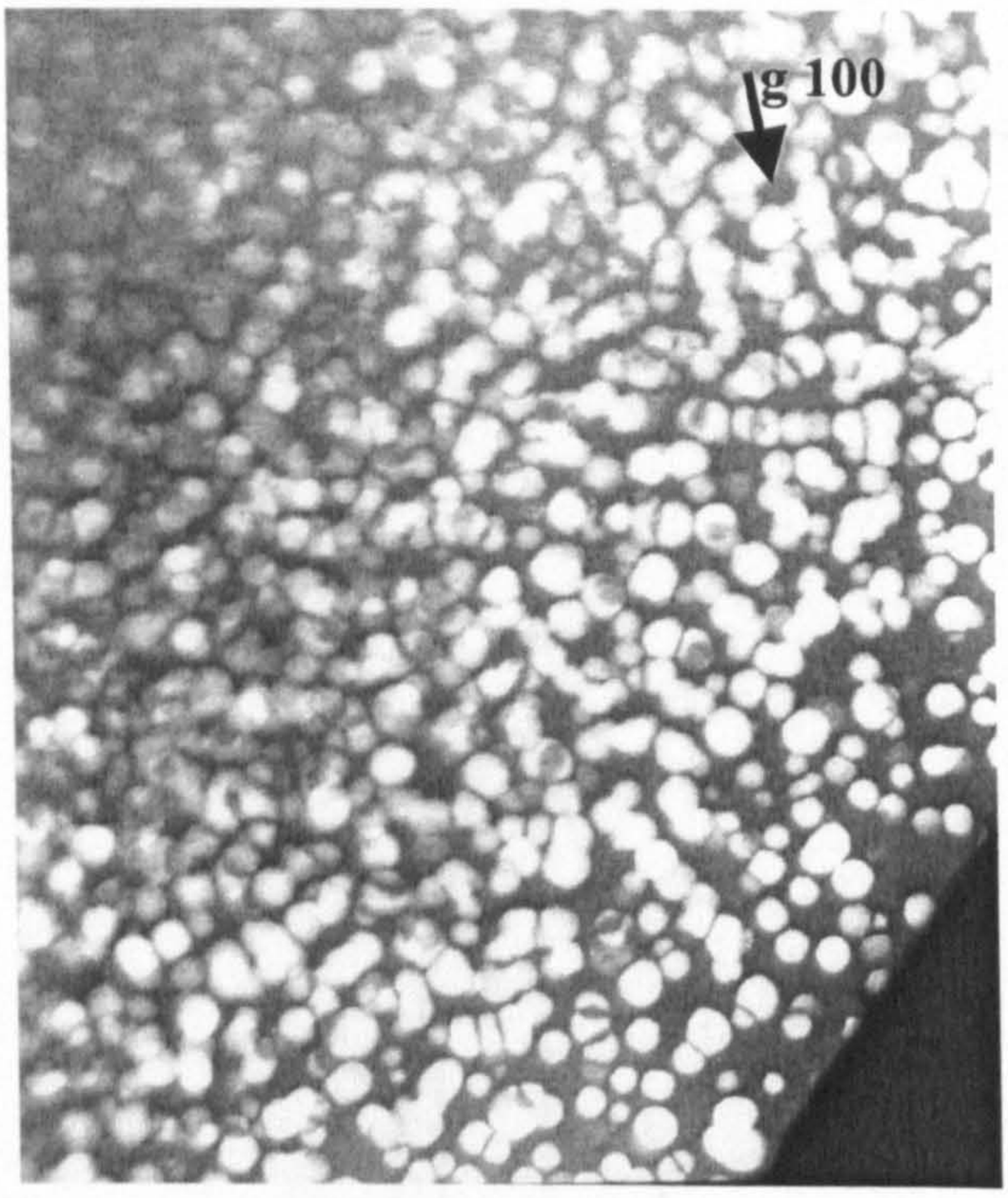

Figure 8.25(a): TEM image of 1.7Li-3.0Mg alloy aged at 150°C for 1000h, ×80K
<100> zone axis.

(b)

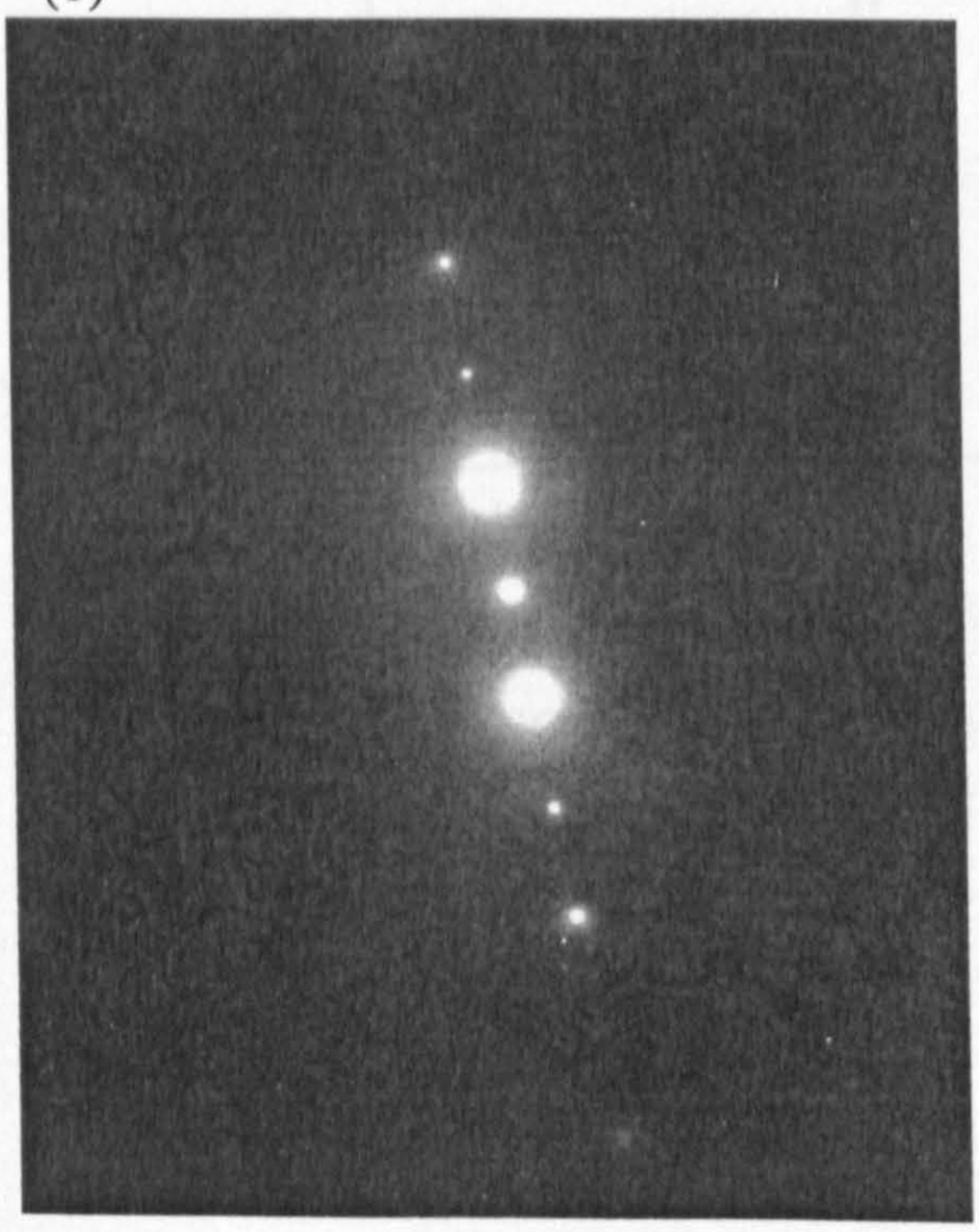

Figure 8.25(b): SAD pattern of 1.7Li-3.0Mg alloy aged at 150°C for 1000h.
<100> zone axis.

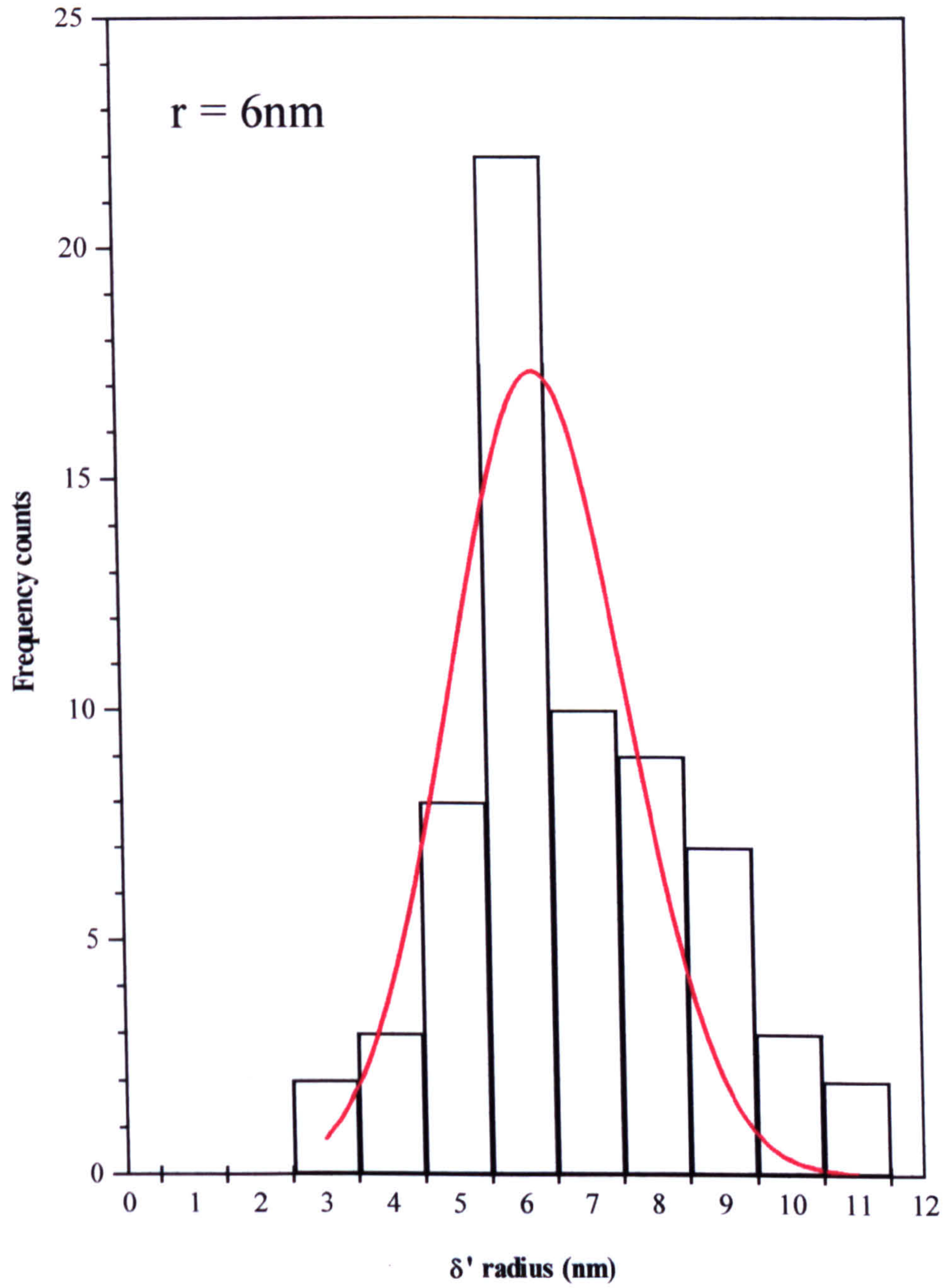

Figure 8.26(a): δ′ particle size distribution for 1.7Li-1.2Mg alloy aged at 150°C for 24h.

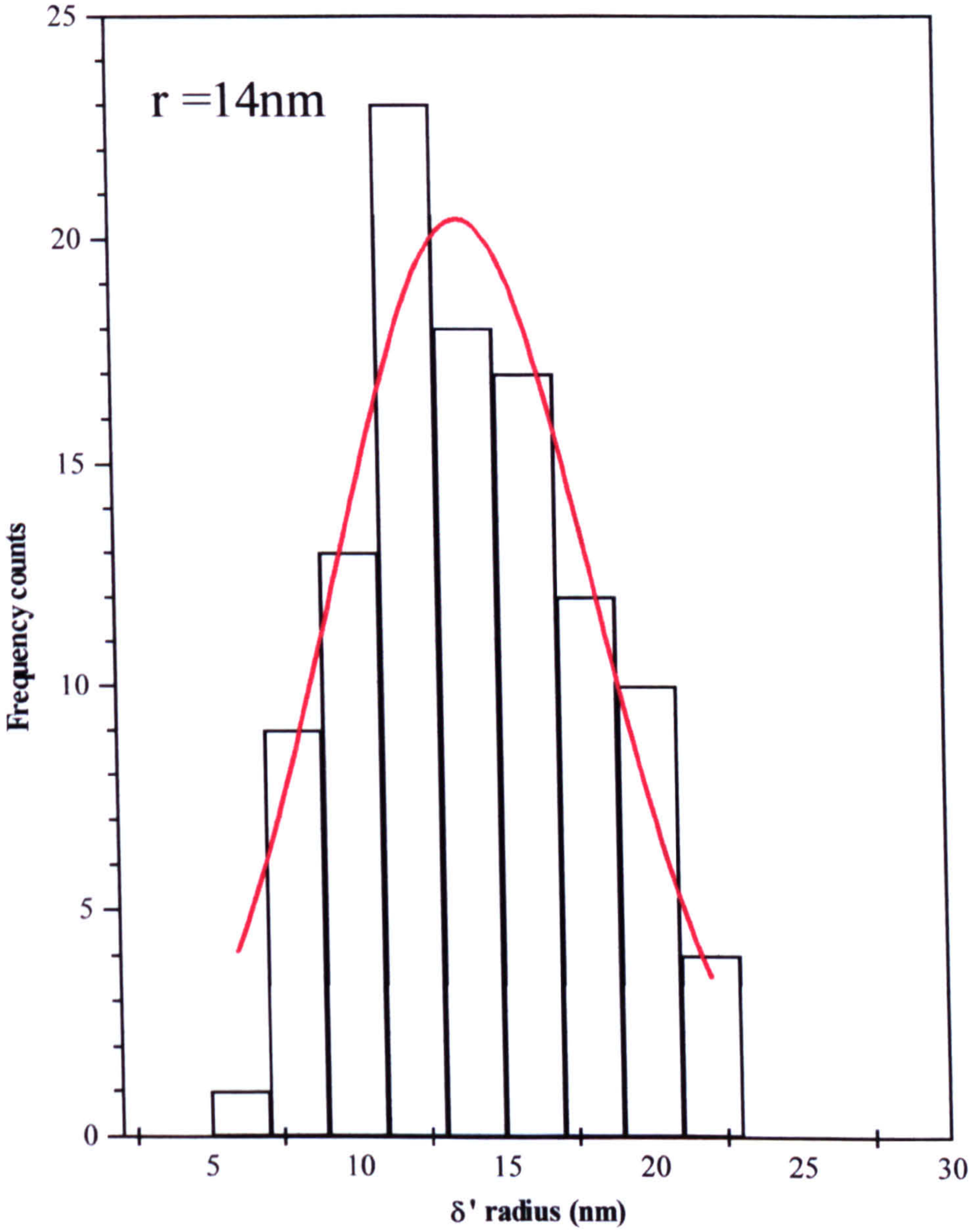

Figure 8.26(b): δ′ particle size distribution for 1.7Li-1.2Mg alloy aged at 150°C for 1000h.

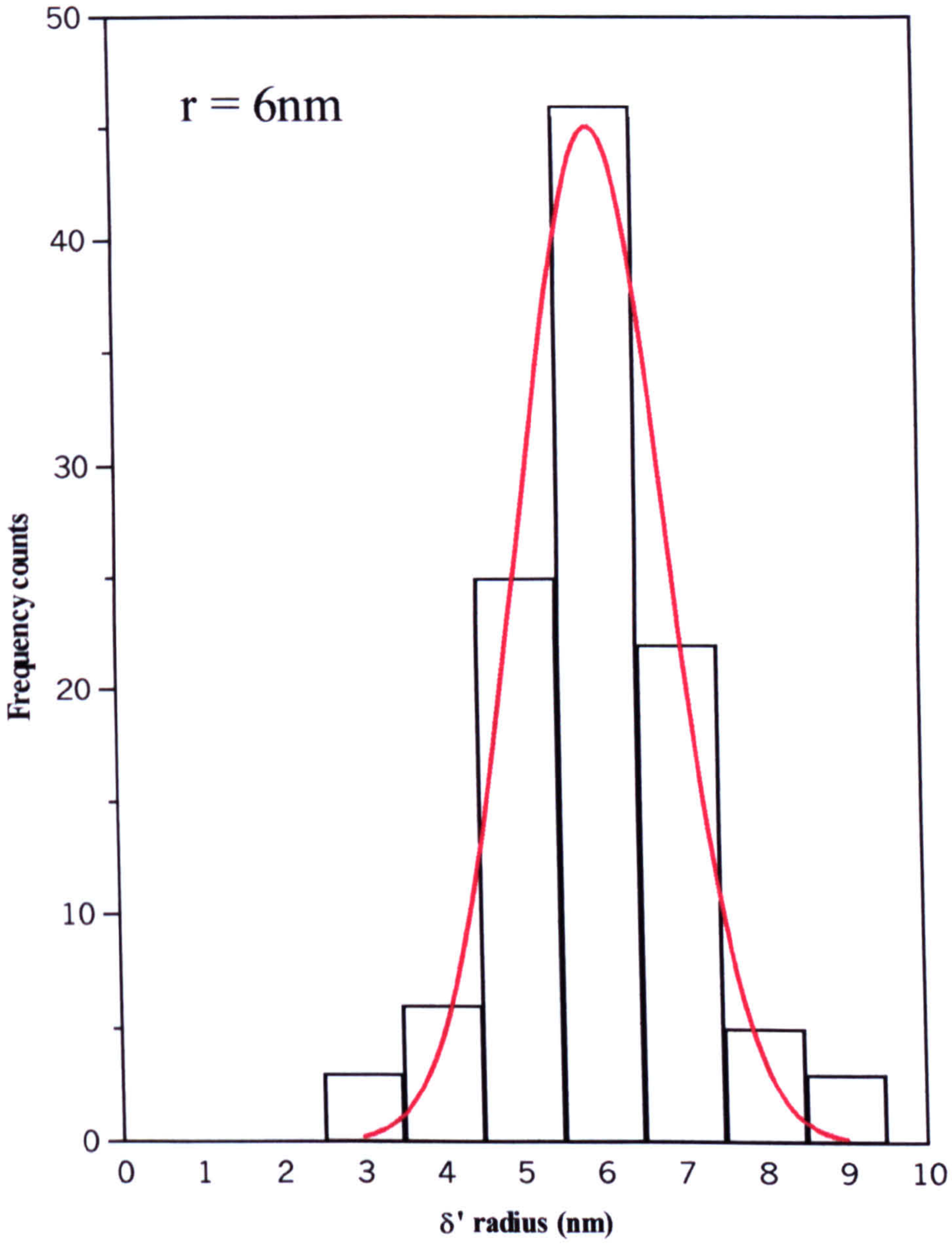

Figure 8.27(a): δ′ particle size distribution for 1.7Li-3.0Mg alloy aged at 150°C for 24h.

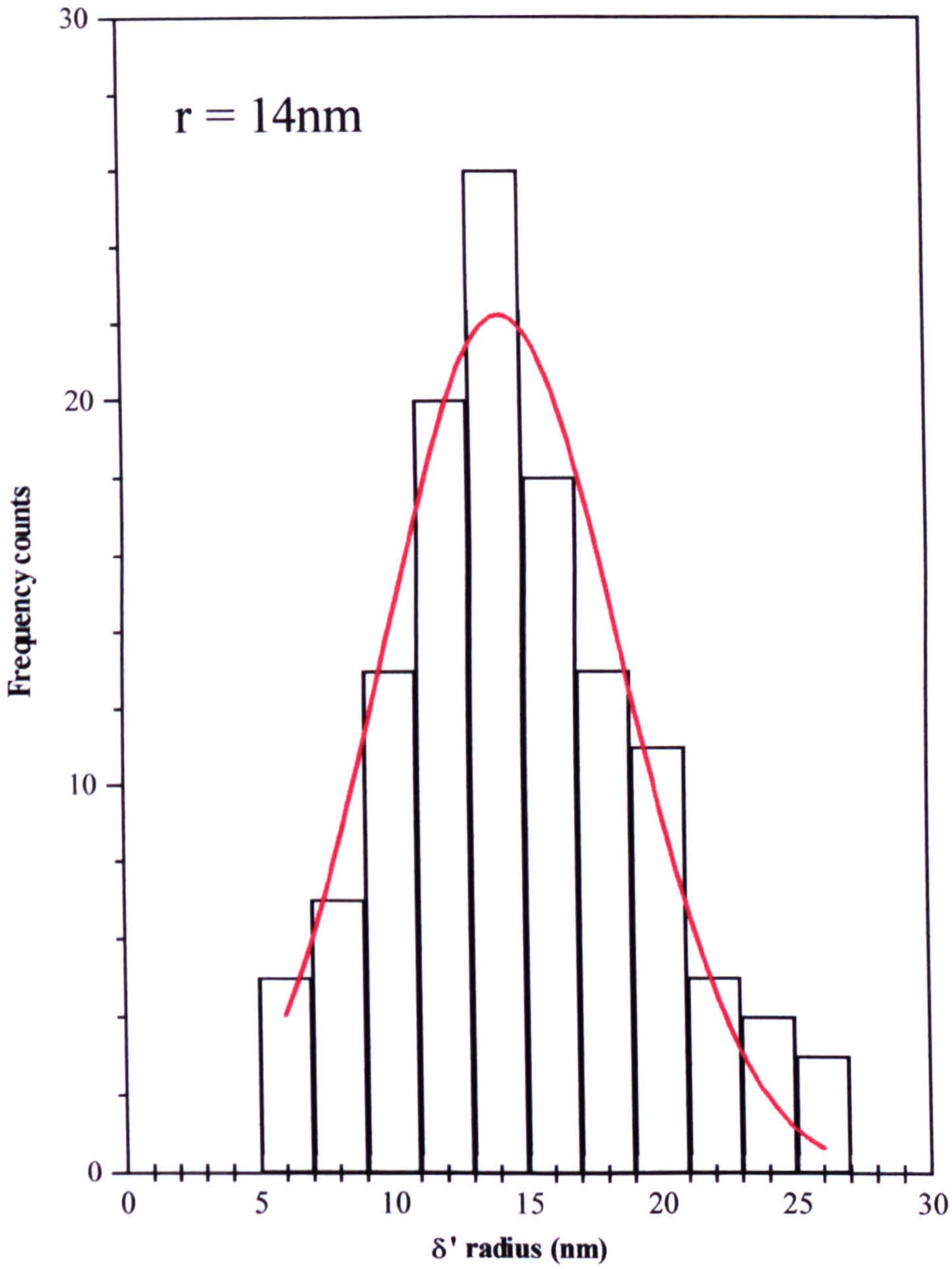

Figure 8.27(b): δ′ particle size distribution for 1.7Li-3.0Mg alloy aged at 150°C for 1000h.

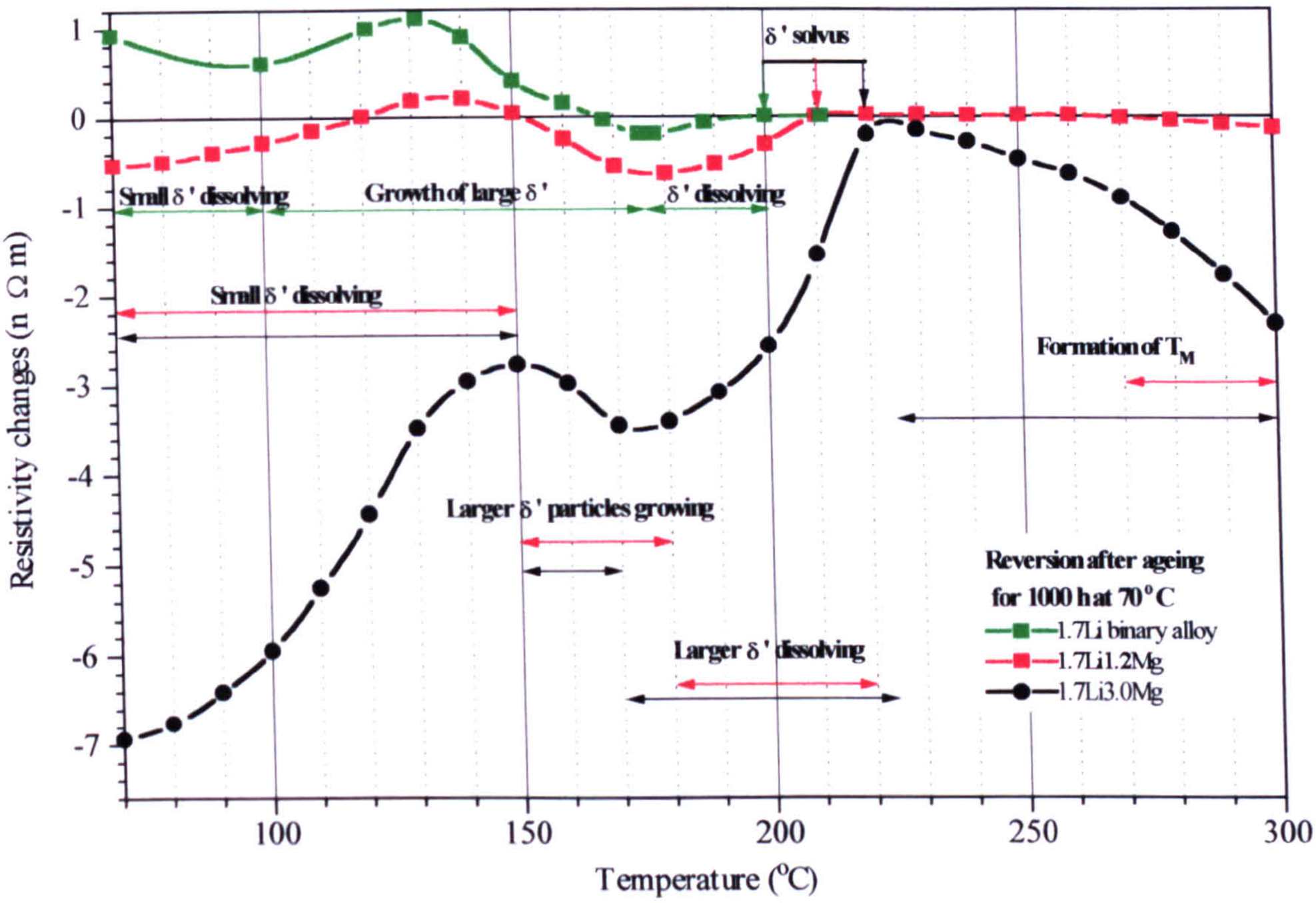

Figure 8.28: Isochronal resistivity reversion after ageing for 1000h at 70°C.

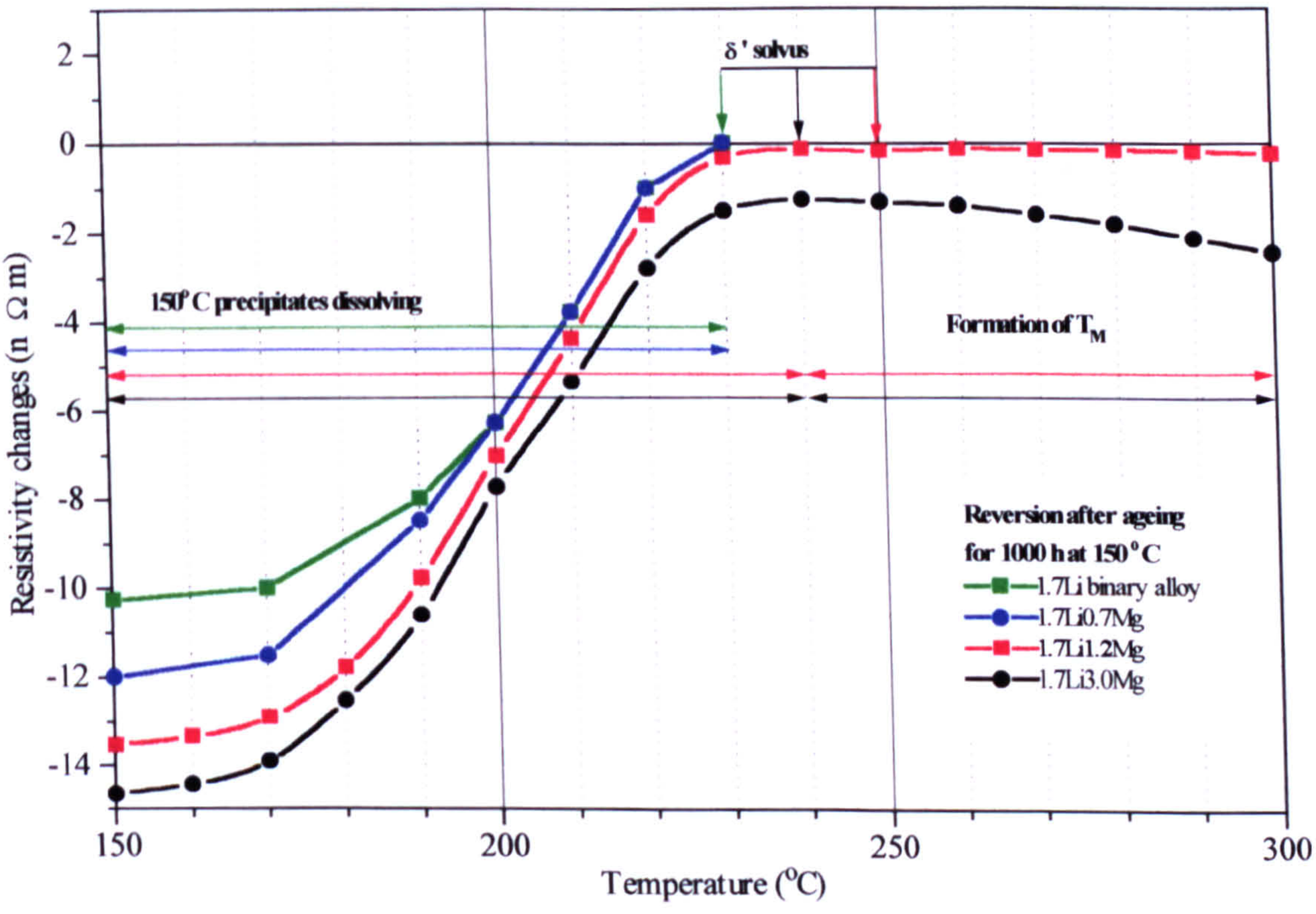

Figure 8.29: Isochronal reversion resistivity after ageing for 1000h at 150°C.

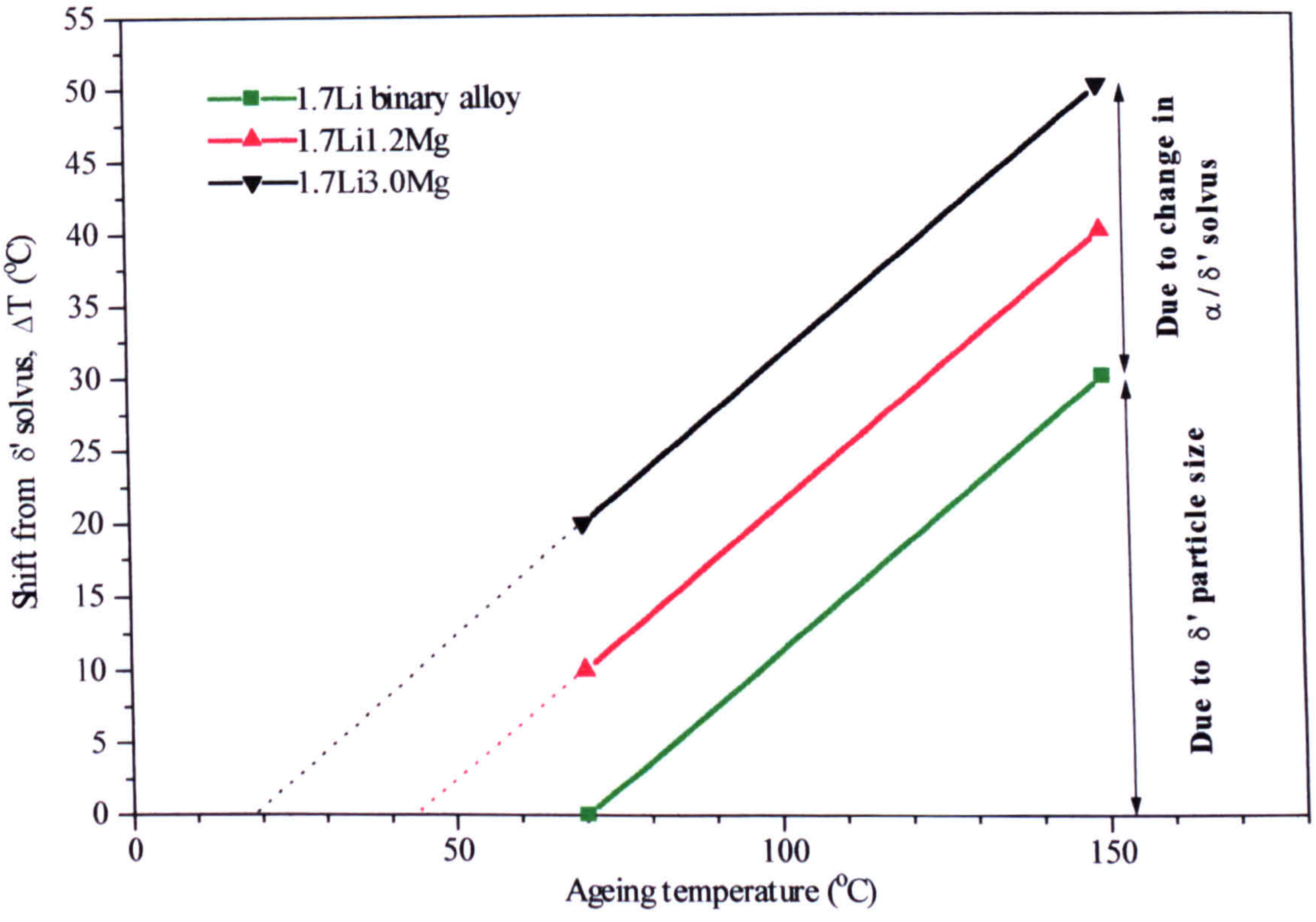

Figure 8.30: Effect of the ageing temperature on the $T^{Rev.}_{end}$.

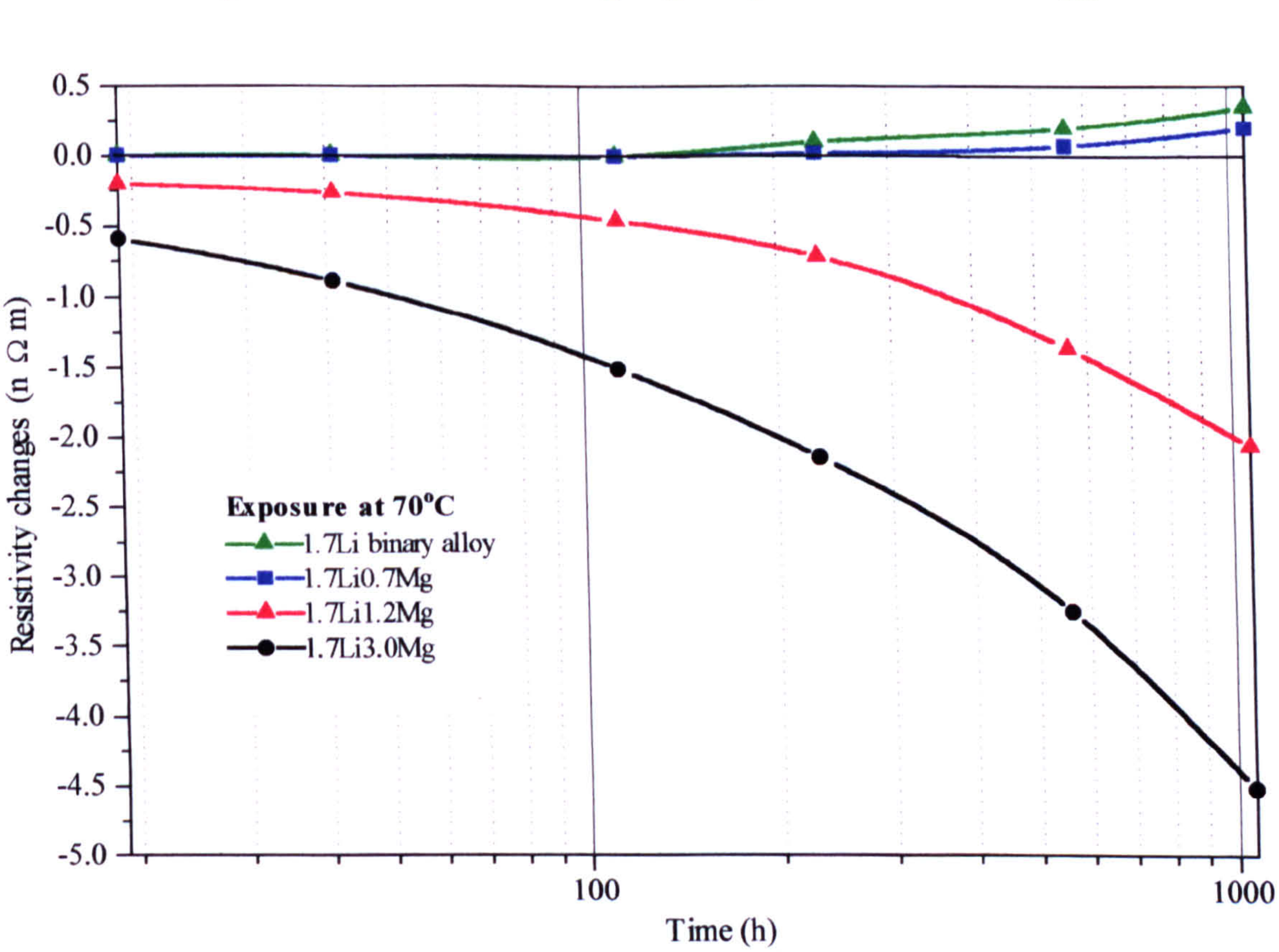

Figure 8.31: Isothermal resistivity changes during exposure at 70°C after prior age at 150°C for 24h.

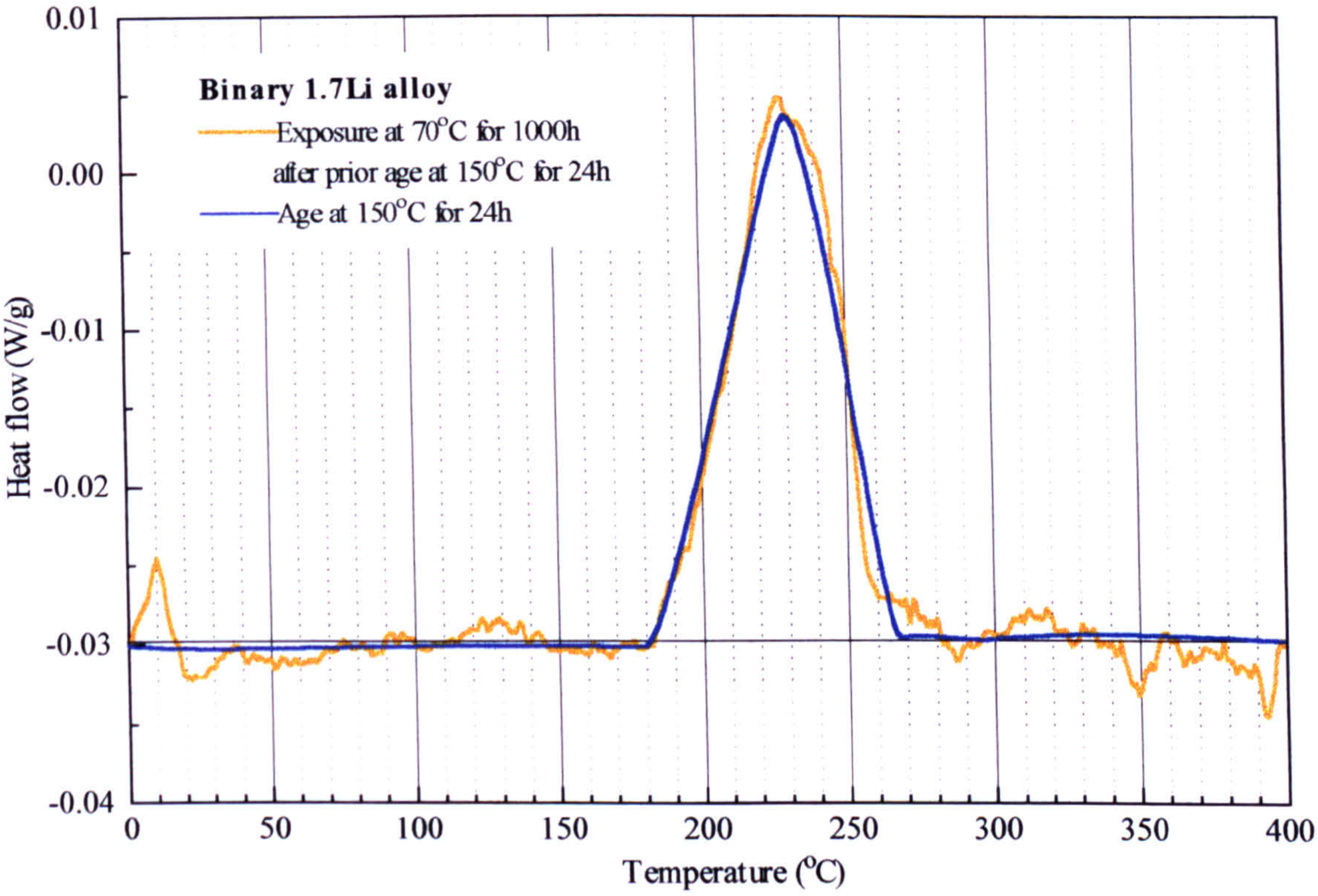

Figure 8.32: Effect of exposure at 70°C on the DSC characteristics of the 1.7Li binary alloy.

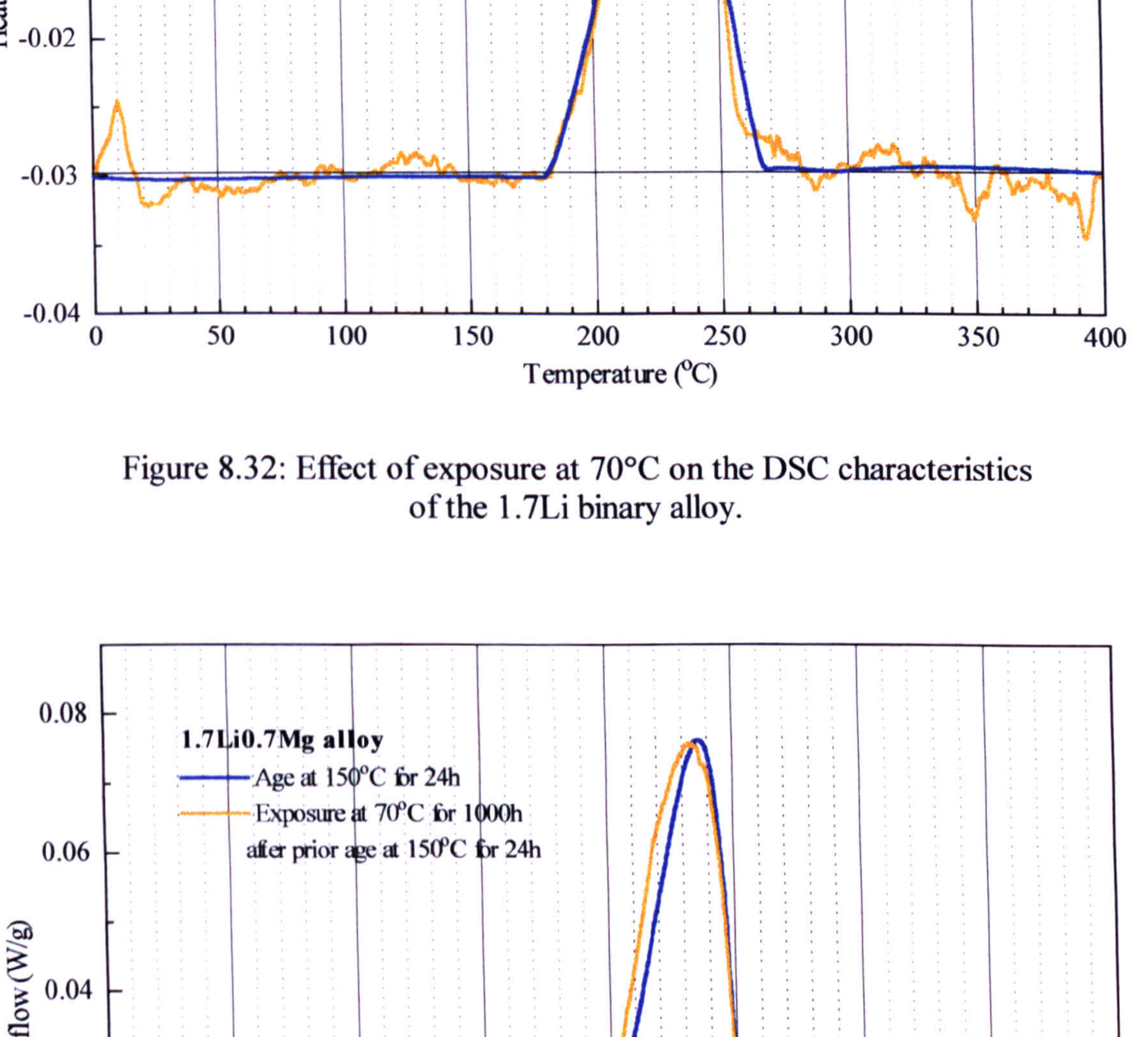

Figure 8.33: Effect of exposure at 70°C on the DSC characteristics of the 1.7Li0.7Mg alloy.

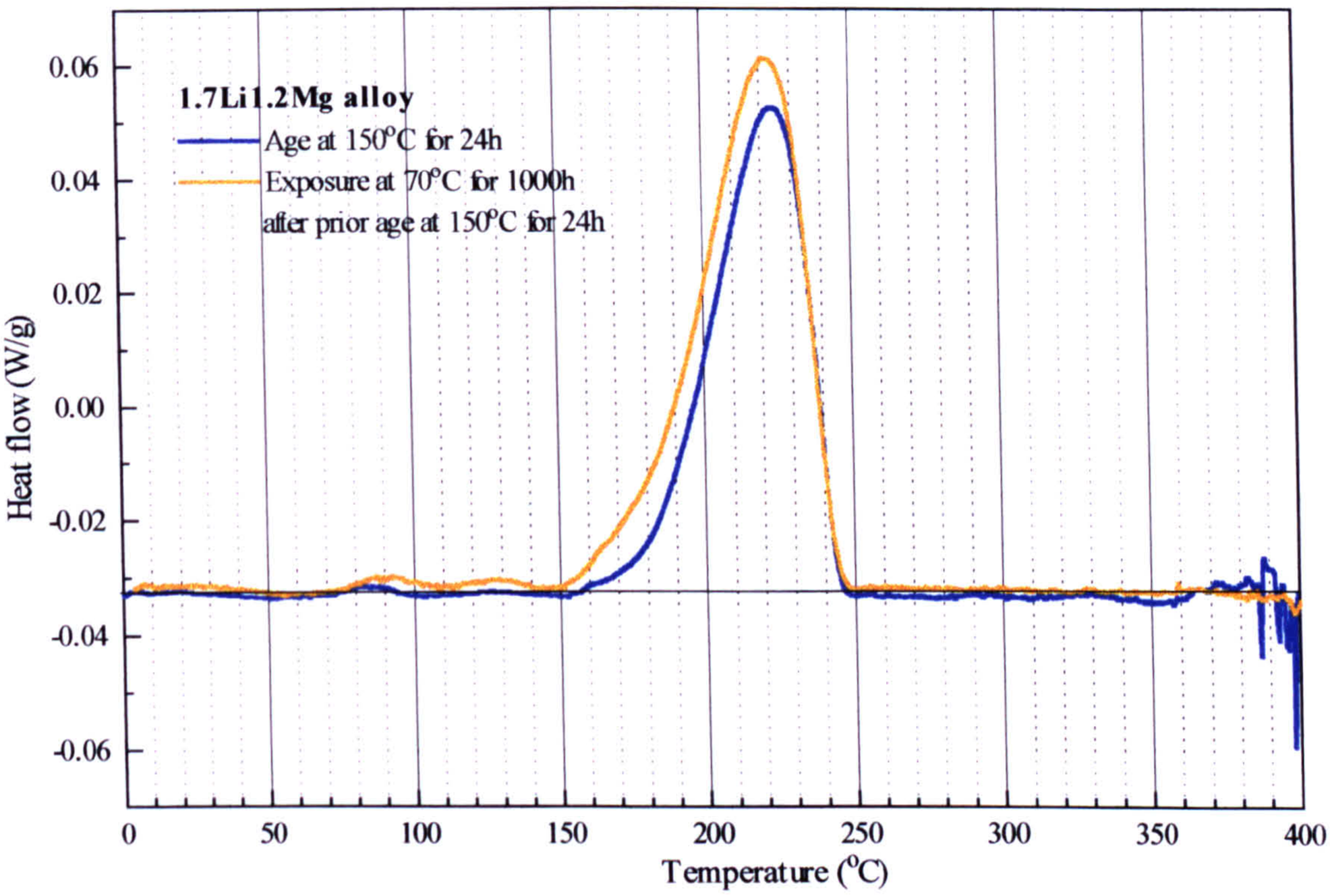

Figure 8.34: Effect of exposure at 70°C on the DSC characteristics of the 1.7Li1.2Mg alloy.

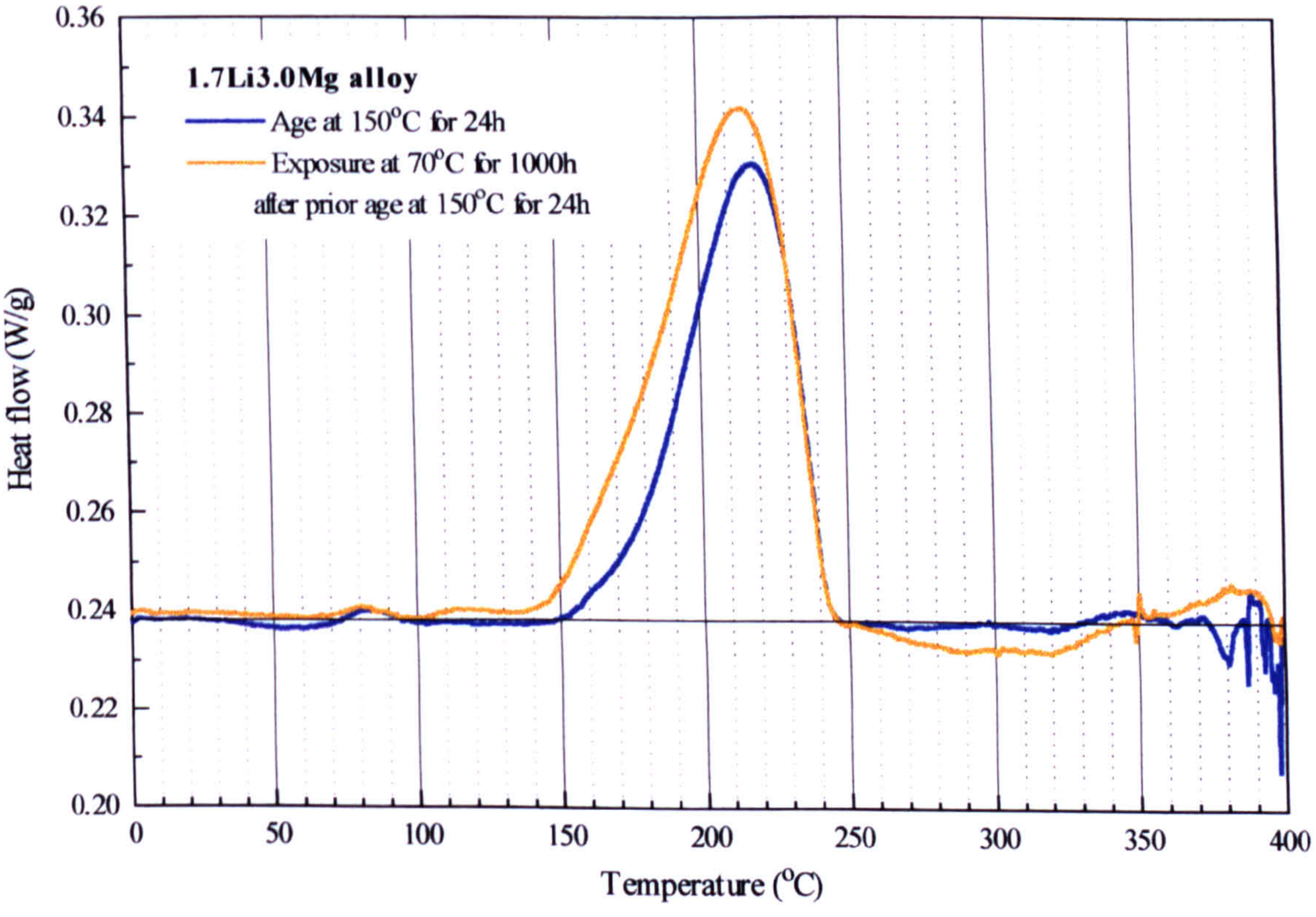

Figure 8.35: Effect of exposure on the DSC characteristics of the 1.7Li3.0Mg alloy.

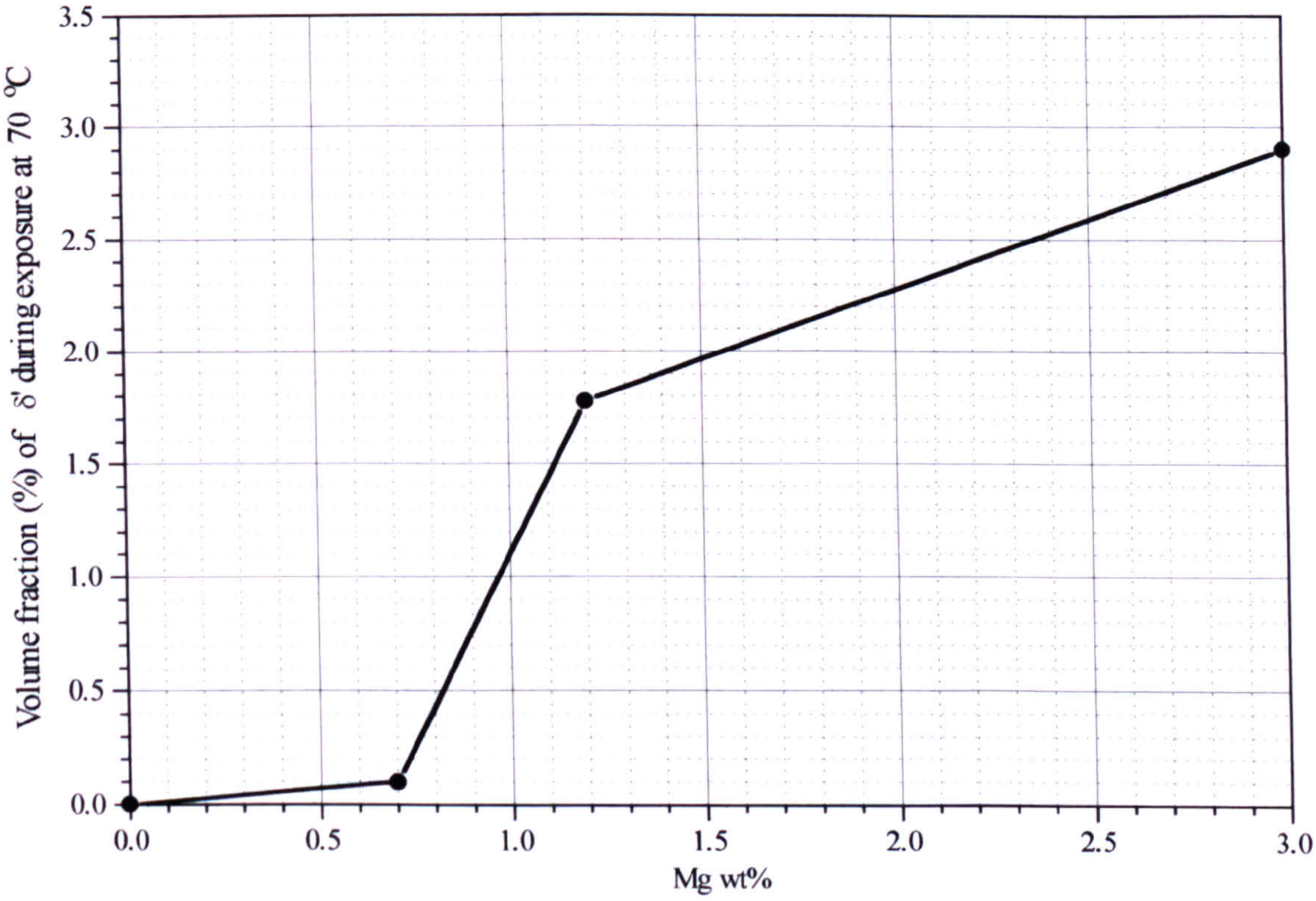

Figure 8.36: Volume fraction of δ′ precipitated during exposure at 70°C in alloys with different magnesium contents.

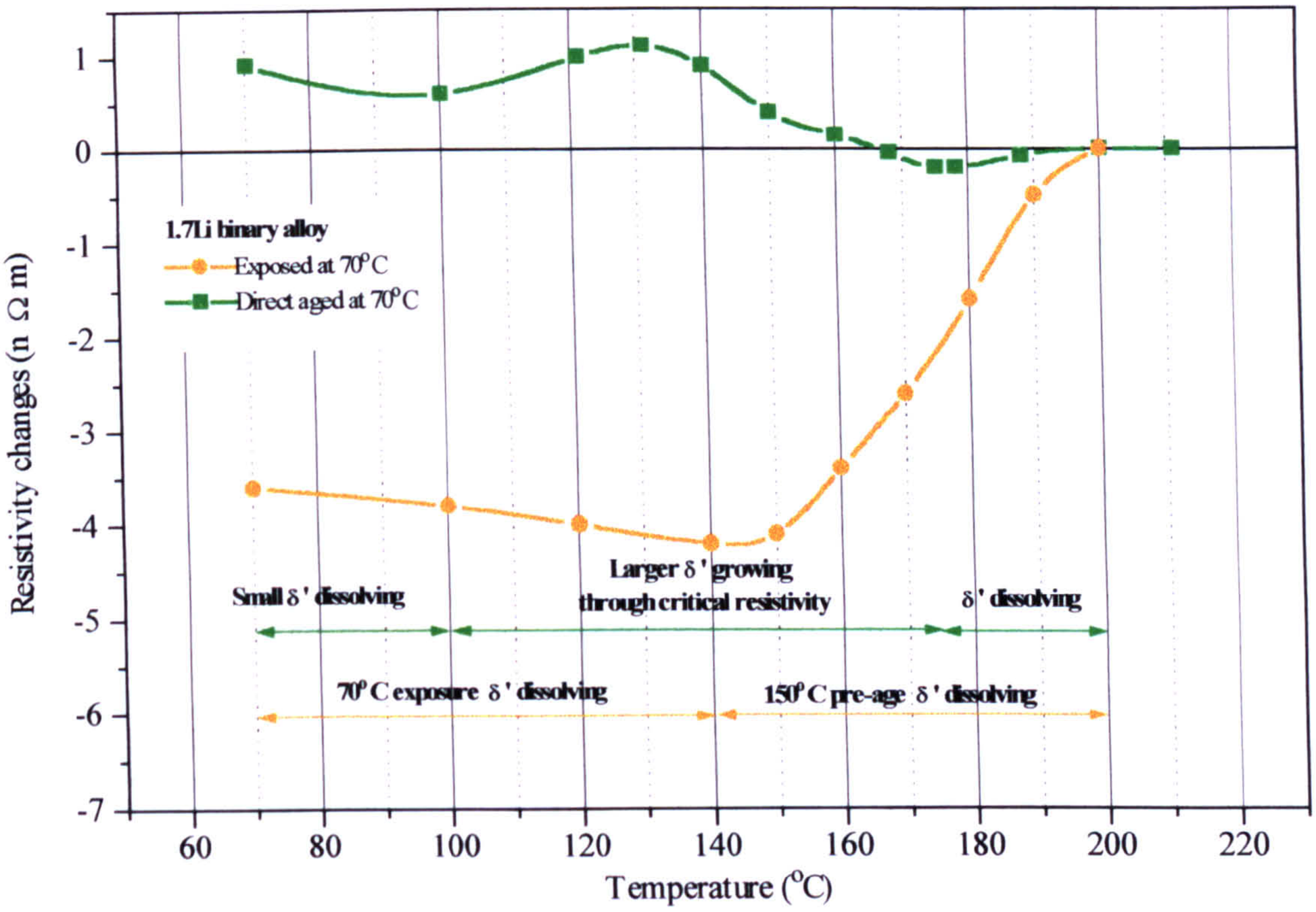

Figure 8.37: Isochronal reversion resistivity of the 1.7Li binary alloy after exposure for 1000h at 70°C with the equivalent plot after direct age at 70°C.

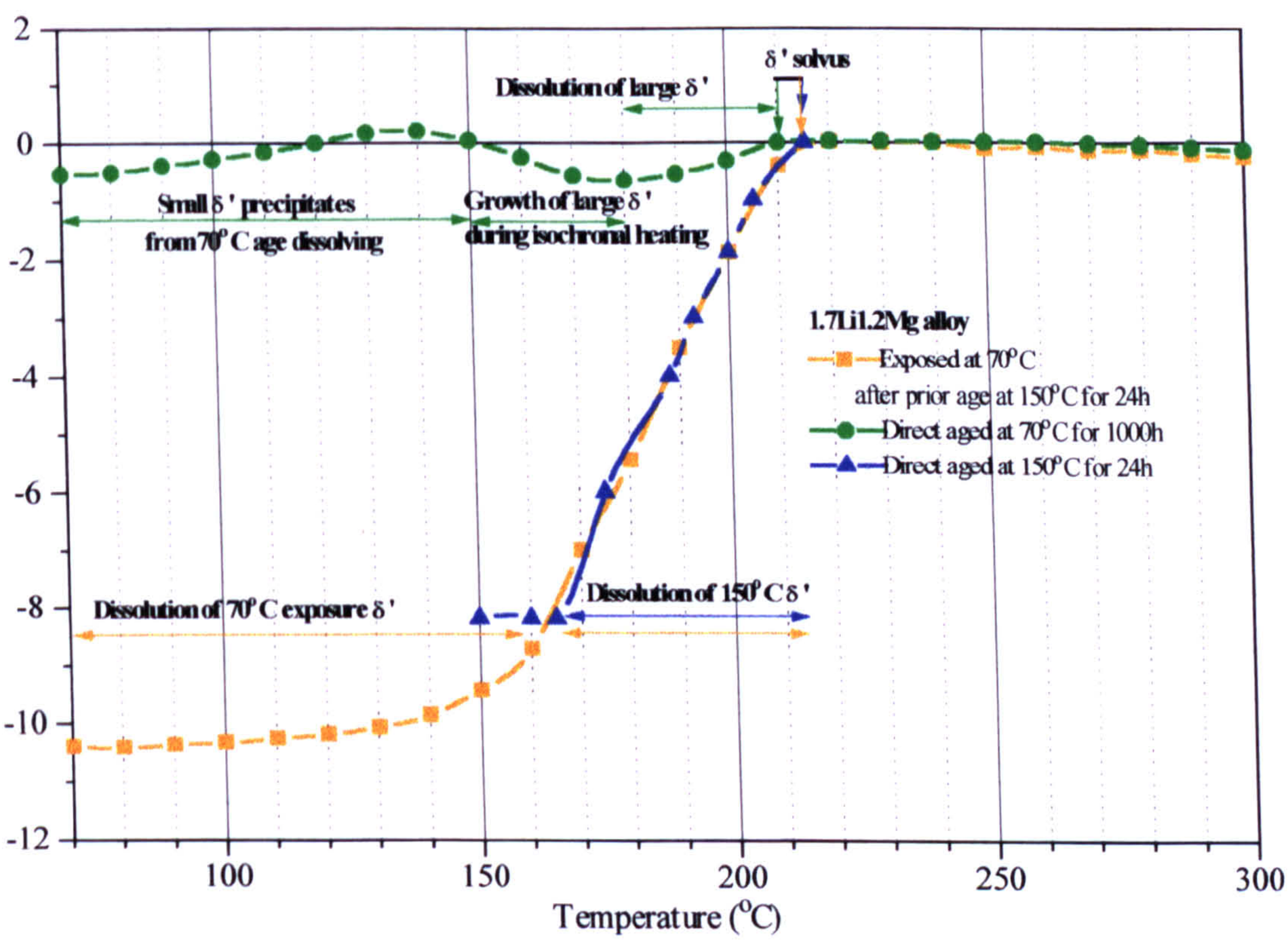

Figure 8.38: Isochronal reversion resistivity of the 1.7Li1.2Mg alloy after exposure for 1000h at 70°C with the corresponding plots after ageing for 1000h at 70°C and 24h at 150°C.

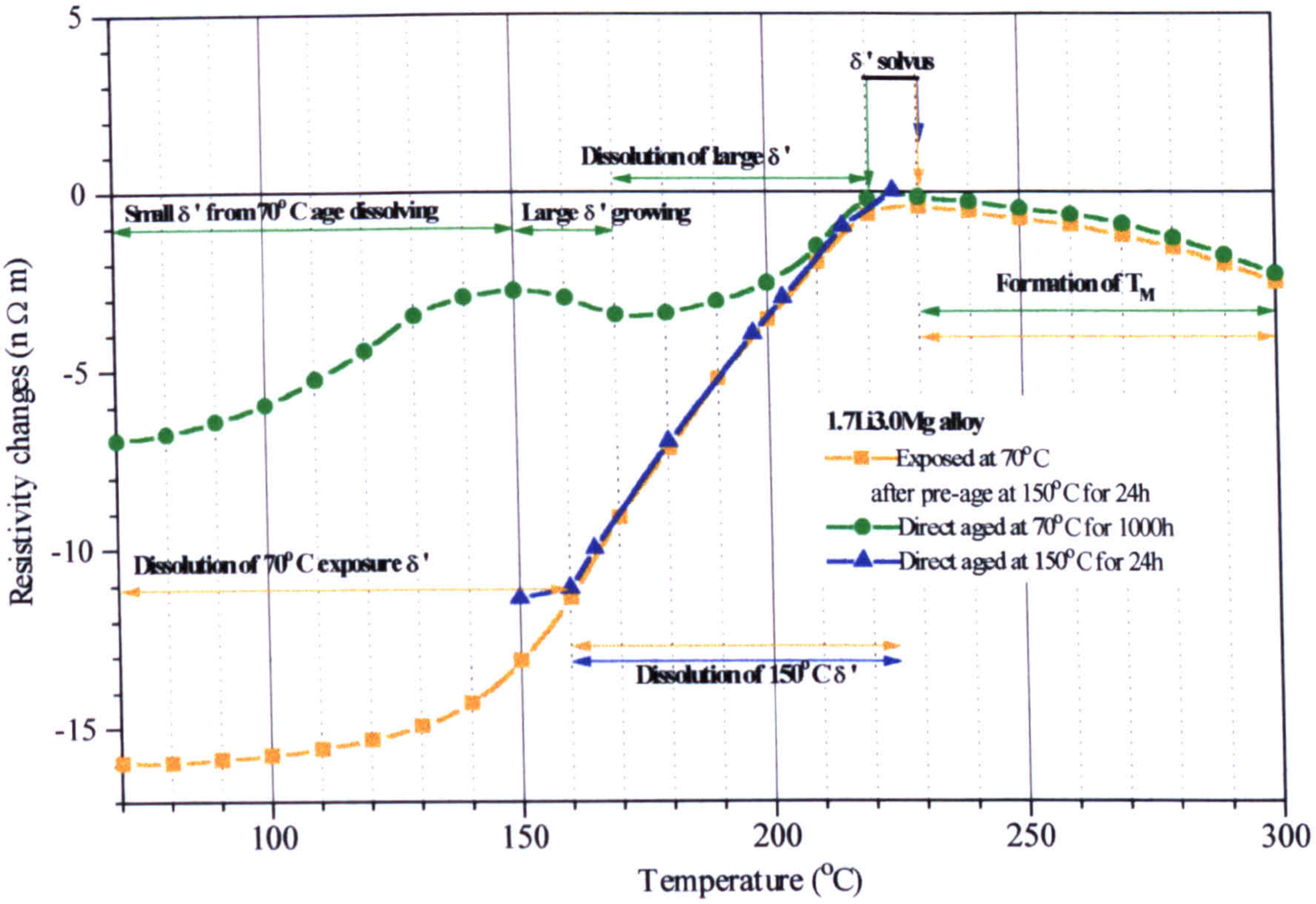

Figure 8.39: Isochronal reversion resistivity plot of the 1.7Li3.0Mg alloy after exposure for 1000h at 70°C with equivalent plots after ageing for 1000h at 70°C and 24h at 150°C.

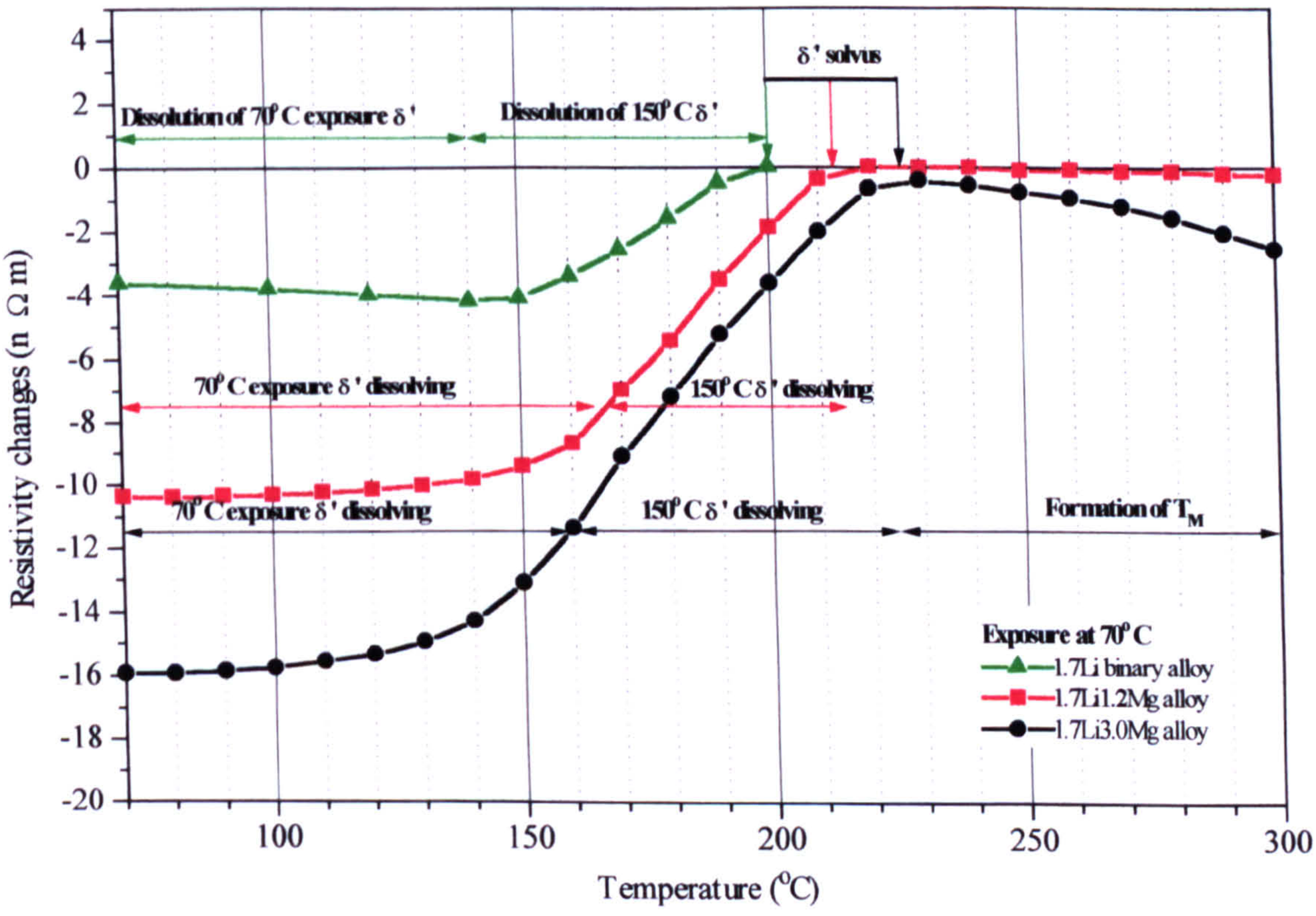

Figure 8.40: Comparative isochronal reversion resistivity plots after exposure for 1000h at 70°C.

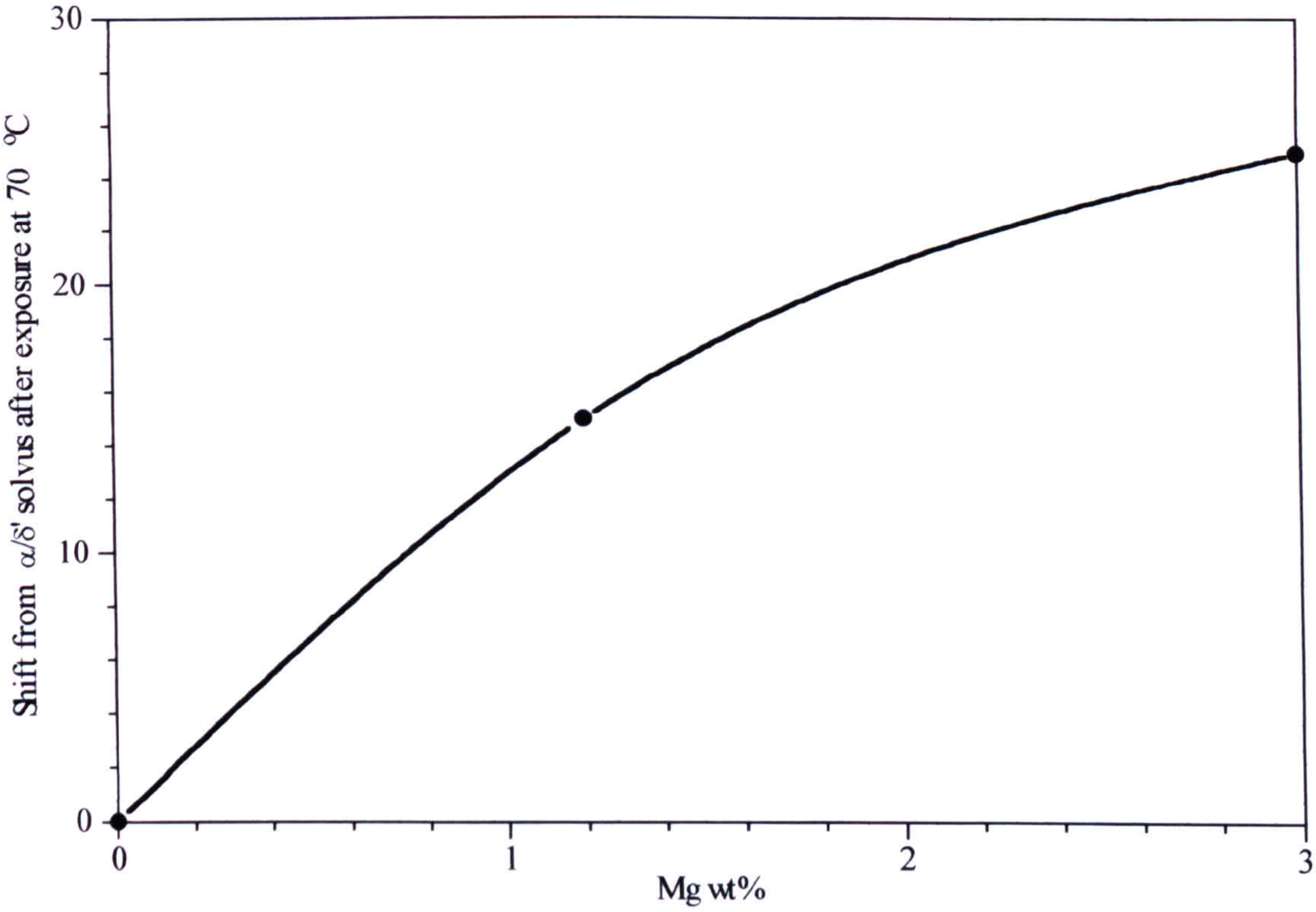

Figure 8.41: Effect of Mg on the $T^{Rev.}_{end}$ after exposure at 70°C.

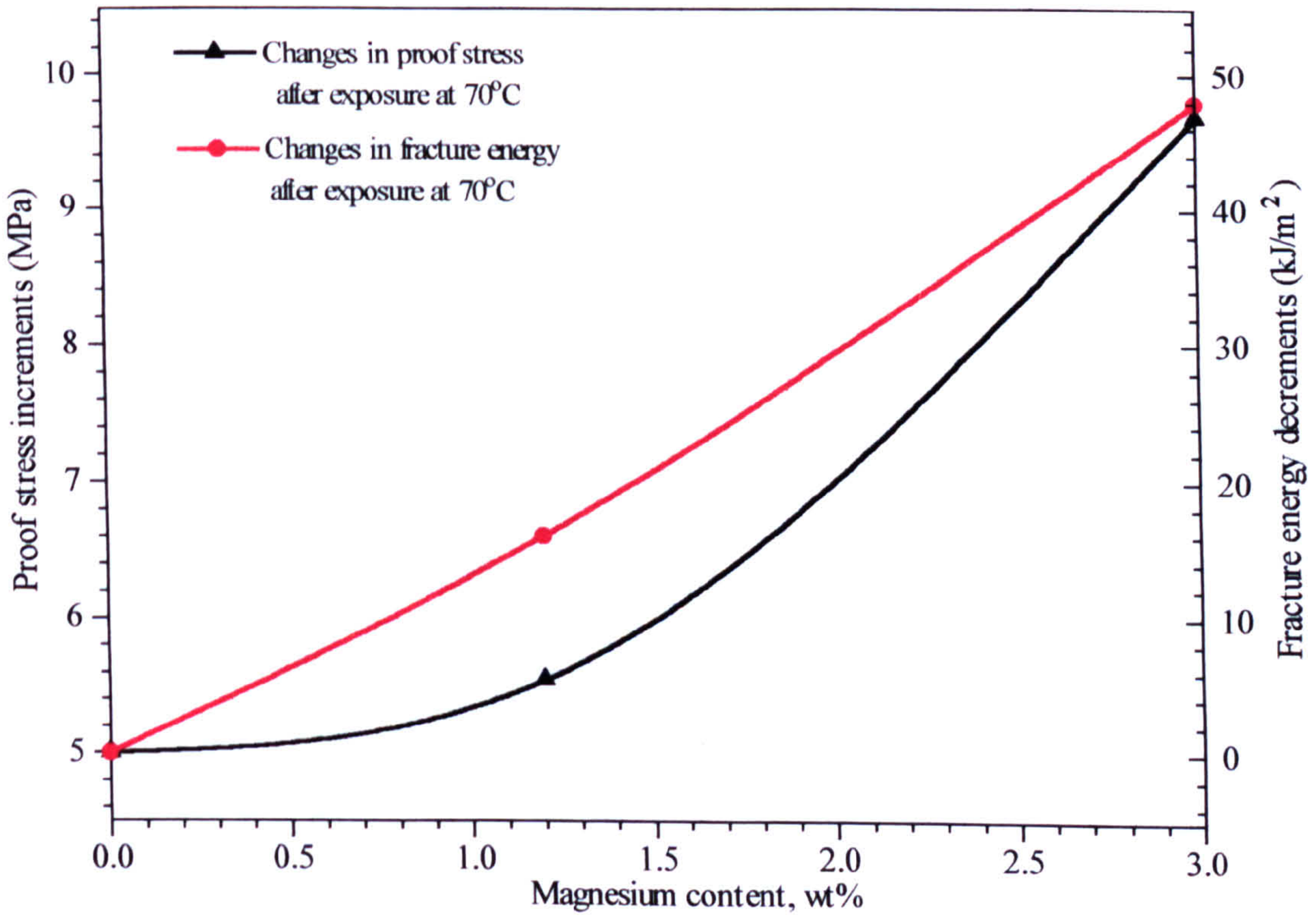

Figure 8.42: Effect of exposure on the mechanical properties of the 1.7Li alloys with different additions of magnesium.

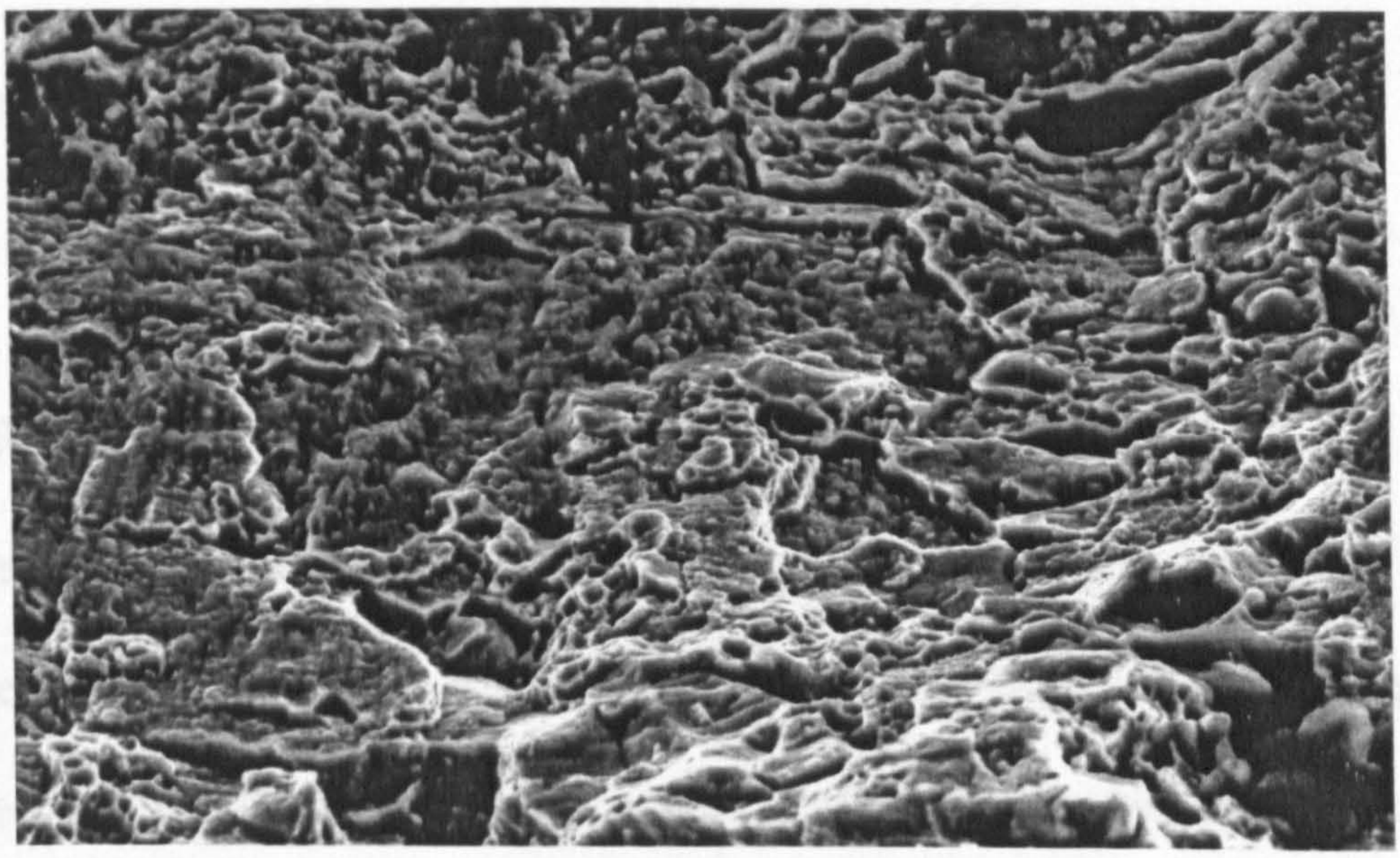

Figure 8.43(a): SEM fractograph of 1.7Li3.0Mg alloy after ageing for 24 h at 150 °C

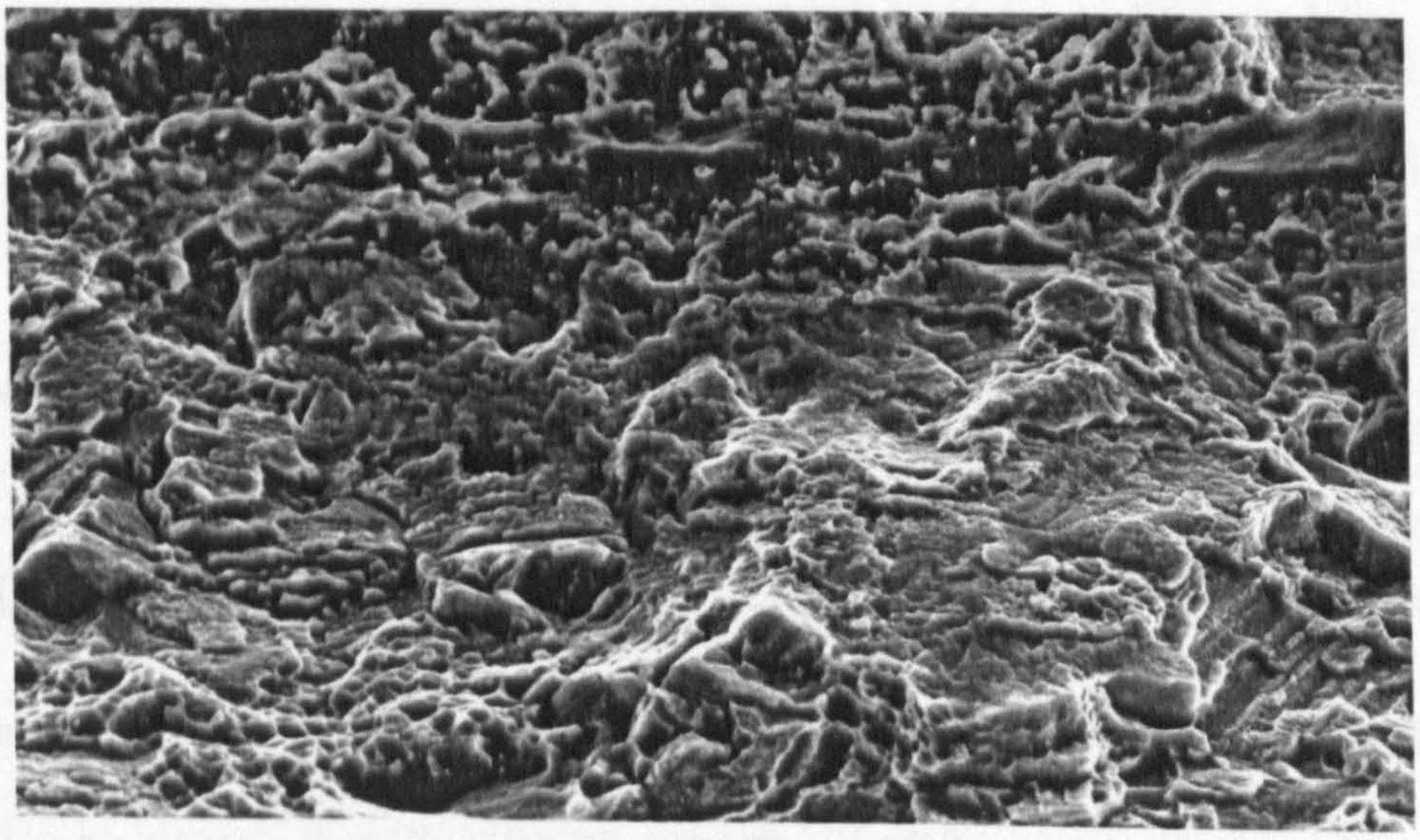

Figure 8.43(b): SEM fractograph of 1.7Li3.0Mg alloy after exposure for 1000 h at 70 °C

CHAPTER 9

Precipitation in Al-Li-Cu alloys

In the previous chapter, the effects of the addition of magnesium on the ageing characteristics of the binary Al-Li system were examined. In the present chapter the effects of the addition of copper on the ageing characteristics of the same system are studied. The addition of 1.2% and 3% Cu is considered.

The chapter is divided into two main parts:

- Isochronal precipitation characteristics
- Isothermal precipitation characteristics

9.1 Isochronal precipitation characteristics

9.1.1: DSC (as-quenched plots)

Figure 9.1 are gives DSC thermograms of the as-quenched alloys. In the binary 1.7Li alloy no thermal events were detected. The addition of 1.2% copper results in the appearance of an exothermic peak (C) at 350°C which, according to XRD **(figure 9.2)**, is due to precipitation of the equilibrium T_1 and T_2 phases. Increasing the addition of copper from 1.2% to 3.0% results in the appearance of an additional exothermic peak (A) at 80°C which is followed by an endothermic

event (B) at 165°C. To assist in the interpretation of the DSC plots a binary Al-3.0%Cu alloy was prepared and subjected to DSC analysis. The DSC plot of this binary 3.0Cu alloy exhibits the presence of an exothermic peak (A′) at 80°C which according to the Al-Cu metastable phase diagram corresponds to the heat evolved during the formation of GP_{Cu} zones. Dissolution of the GP_{Cu} zones results in the development of an endothermic event (B′) at 160°C. Comparing the areas under peaks A and A′ and the temperature range where these peaks take place it is readily evident that they are coincident. Peak A is slightly larger and therefore it is likely to be a mixture of GP_{Cu} and δ′ precipitation.

The area under the exothermic peak (C) increases significantly with copper concentration, showing that the high copper addition stimulates the formation of the equilibrium T_1 and T_2 phases. XRD verifies extensive precipitation of T_1 and T_2 **(figure 9.3).**

9.1.2 Isochronal resistivity

The isochronal plots for 1.7Li alloys with 0, 1.2 and 3.0% Cu and the binary 3.0% Cu alloy are shown in **figure 9.4.** The isochronal plot of the binary 1.7Li alloy has already been discussed in the previous chapter. The initial gradual increase in resistivity up to 40°C observed in the binary alloy is associated with the formation of δ′ particles that are smaller than the critical size for electron scattering. The decrease after 40°C is attributed to the formation or growth of δ′

particles which are larger than the critical size. The resistivity decrease extends below the baseline and then slowly returns to the baseline at 200°C (T^{Res}_{end}) which is equated to the δ′ solvus temperature for the binary 1.7Li alloy.

The addition of 1.2% Cu results in a small reduction of the height of the initial resistivity peak (**figure 9.5**). The as-quenched resistivity value is attained at 200°C (**figure 9.4**), showing that the addition of 1.2%Cu does not shift the δ′ metastable solvus boundary. The fact that the resistivity of the 1.7Li1.2Cu alloy does not decrease below the baseline suggests a slower rate of growth of δ′ compared to the binary alloy. This is also supported by the position of peak A″ which is reached at a temperature 20°C higher in the 1.7Li1.2Cu alloy (**figure 9.5**). As the temperature increases from 200°C to 370°C a decrease in resistivity is observed which consists of two stages, 200-300°C (stage I) and 300-370°C (stage II). Stage I corresponds to a slow decrease in resistivity which may be the result of the precipitation and growth of T_1 plates. In stage II, precipitation of T_1 continues but this is accompanied by the formation and growth of T_2. This latter phase (Al_6CuLi_3) requires 3 times the amount of lithium for each molecule of precipitate compared to the T_1 phase (Al_2CuLi) and this results in a large decrease of resistivity. X-Ray diffraction analysis of the 1.7Li1.2Cu alloy confirmed the presence of the equilibrium T_1 and T_2 phases after ageing for 24h at 350°C (**figure 9.2**). Higher temperatures result in the dissolution of T_1 and T_2.

Increasing the copper concentration to 3% increases the size of the initial

resistivity peak significantly without changing its position (**figure 9.5**). The resistivity plot of the binary Al-3.0Cu alloy indicates that a small fraction of the resistivity increase in the 1.7Li3.0Cu alloy is due to the formation of GP_{Cu} zones. Calculation from the relative heights of peak A'' (**figure 9.5**) shows that 25% of the height is due to GP_{Cu} zones, 37% to δ′, leaving a remainder of 38% that has to be attributed to the stimulation of either δ′ or GP_{Cu}. It will be shown later in the chapter that it is due to stimulation of δ′.

In the previous section it was shown by means of DSC that very little stimulation of δ′ took place. This discrepancy can be explained by the significantly higher heating rate during the DSC run (20°C/min) compared to the mean heating rate of the isochronal resistivity experiment (2.0°C/min) and the higher sensitivity of the latter.

The resistivity drop after peak A'' extends below the baseline as growth of δ′ and GP_{Cu} takes place, but does not return to the baseline due to the commencement of precipitation of another phase.

As the temperature increases beyond 200°C up to 260°C a resistivity increase is observed in the 1.7Li3.0Cu alloy. Temperatures >260°C result in a dramatic decrease in resistivity which ends at 360°C. Noble and Thompson [**31**] have investigated the precipitation characteristics of the Al-Li-Cu system. According to their results, ageing of a 1.5Li3.5Cu alloy at 190°C caused precipitation of T_1 from very early times. The temperature stability of this phase was estimated to be

180-350°C. Thus the increase in resistivity at 200-260°C observed in the present 1.7Li3.0Cu alloy can be attributed to the formation of small T_1 plates. Further evidence is provided by TEM analysis of the 1.7Li3.0Cu alloy after ageing for 0.5h at 260°C. The bright field images **(figure 9.6)** show very clearly the precipitation of T_1 plates. The fringes observed in micrograph **9.6 (b)** correspond to T_1 precipitates with an inclined habit plane relative to the foil surface. The marked decrease of resistivity over the range 260-350°C is caused by co-precipitation of T_1 and T_2 phases. X-Ray diffraction analysis of the 1.7Li3.0Cu alloy verified the presence of T_1 and T_2 phases after ageing for 24h at 350°C **(figure 9.3)**. Temperatures higher than 350°C cause dissolution of T_1 and T_2.

9.2 Isothermal precipitation characteristics

In this section the isothermal precipitation characteristics of the Al-Li-Cu system are considered. Five different heat treatments have been used:

- Ageing at 70, 100 and 150°C for 1000 h
- Ageing at 150°C for 24 h. This is the damage tolerant heat treatment commonly given to alloys based on the Al-Li system.
- Prior ageing at 150°C for 24 h following by exposure at 70°C for 1000 h. This is intended to simulate the condition that a commercial Al-Li aerospace alloy would be expected to encounter whilst in service.

9.2.1 Ageing at 70°C

Figure 9.7 shows comparative DSC thermograms after ageing at 70°C for 1000 h. In the binary 1.7Li alloy the large endotherm at 190°C represents the dissolution of the δ′ phase. The addition of 1.2% Cu to the binary 1.7 Li alloy produces a small increase in the area of the dissolution peak. However, the addition of 3% copper results in a dramatic increase in the size of the endotherm. This increase in the size of the endotherm could be due to three effects:

- A significant contribution to the endotherm from the dissolution of GP_{Cu} zones.
- Dissolution of an enhanced volume fraction of δ′ that has resulted from the copper addition.
- A combination of the above two effects.

TEM of the 1.7Li3.0Cu alloy after ageing 1000 h at 70°C showed the presence of δ′ (**figure 9.8 a**) and electron diffraction analysis showed continuous streaking through {001} diffraction spots, thus confirming the presence of GP_{Cu} zones (**figure 9.8 b**).

To determine the size of the contribution of GP_{Cu} zones to the dissolution endotherm in **figure 9.7**, a binary Al-3.0Cu alloy was aged for 1000h at 70°C and DSC analysis carried out. The plot is shown on **figure 9.7** from which it can be calculated that the increase in the size of the endotherm in the 1.7Li3.0Cu alloy relative to the 1.7Li alloy is the combined result of

- precipitation of GP_{Cu} zones (45%)

- copper stimulating δ′ precipitation (55%)

Isothermal resistivity plots for ageing at 70°C are given in **figure 9.9**.

The resistivity plot of the binary 1.7Li alloy consists of an initial increase followed by a plateau and then a second increase. The initial resistivity increase can be attributed to the formation of a high density of fine ordered regions (or domains) which scatter the conduction electrons. The second increase can be attributed to the spinodal decomposition of the ordered domains which produce more effective scattering centres for the conduction electrons. The continuous increase of resistivity implies that the spinodal decomposition carries on for a long time and at a slow rate since the δ′ particles do not reach the critical size for electron scattering even after ageing for 1000h. The slow kinetics can be attributed to quenched-in vacancies becoming trapped by the ordered regions and therefore there is a reduced concentration of vacancies to assist the diffusion of lithium to the spinodally decomposing regions.

The resistivity behaviour changes slightly with the addition of 1.2% Cu. After 1000 h a large resistivity increase is observed but the resistivity peak is still not reached. This implies a slightly increased number-density of small-sized δ′ particles compared to the binary Al-1.7Li alloy.

The addition of 3% Cu to the binary alloy results in a large two-step increase of resistivity.

Based on the DSC results of the previous section, this enhanced resistivity change is due to a combination of enhanced δ′ precipitation and GP_{Cu} zone

formation. Resistivity measurements of the binary Al-3.0Cu alloy aged at 70°C show little change in resistivity and therefore it can be surmised that the majority of the enhanced resistivity change is due to stimulation of δ′ precipitation.

The question now arises as to why δ′ precipitation should be stimulated by the presence of copper in the alloy. It has already been shown (**figure 9.8**) that GP_{Cu} zones are present in the 1.7Li3.0Cu alloy aged at 70°C and that copper does not move the α/δ′ boundary (**figure 9.4**). Furthermore, TEM observation (**figure 9.10**) showed that no such zones are present in the 1.7Li1.2Cu alloy (as evidenced by the absence of <001> streaking in **figure 9.10b**). This suggests that it is the presence of GP_{Cu} zones and not simply the presence of copper, that is stimulating δ′ formation. A careful examination of the dark field image of **figure 9.8a** shows that the δ′ precipitates are elongated in the <001> directions. This suggests that δ′ may be forming (heterogeneously) on GP_{Cu} zones in the 1.7Li3.0Cu alloy. At this stage, it is difficult to be certain of this interpretation since the δ′ and GP_{Cu} zones that form at 70°C are extremely small (~ 4nm diameter). In the following sections ageing at a higher temperature is considered and this casts more light on the precipitation mechanism.

9.2.2 Ageing at 100°C

DSC thermograms are presented in **figure 9.11** after ageing for 1000h at 100°C. Comparison of the peaks from the different alloys shows that, as at 70°C, there is a small increase in the δ′ dissolution enthalpy with the addition of 1.2%Cu. Further addition of copper (3%) results in a large increase of the peak area. DSC

analysis of a binary Al-3.0Cu alloy aged for 1000 h at 100°C shows that all the increase in the size of the endotherm in the 1.7Li3.0Cu alloy relative to the 1.7Li alloy can be accounted for by the dissolution of GP_{Cu} zones. The resistivity plots in **figure 9.14** show that after 1000 h almost the same amount of δ′ has been precipitated in 1.7Li and 1.7Li3.0Cu alloys which again indicates that there has been no stimulation of δ′ in the 1.7Li3.0Cu alloy after ageing for 1000h at 100°C.

The question now arises as to why the volume fraction of δ′ is increased by the addition of copper when the alloy is aged 1000 h at 70°C but not when the alloy is aged 1000 h at 100°C. This can be explained by the following observations:

- The *equilibrium* fraction of δ′ precipitated at a given temperature is the same in 1.7Li, 1.7Li1.2Cu and 1.7Li3.0Cu alloys since copper does not affect the position of the α/δ′ boundary.
- The kinetics of δ′ precipitation are speeded-up by the addition of copper since this produces GP_{Cu} zones which act as heterogeneous nucleation centres.
- With ageing at 70°C, the equilibrium volume fraction of δ′ is not attained, hence, after 1000h ageing, the volume fraction of δ′ in the 1.7Li3.0Cu alloy is considerably higher than that in the 1.7Li alloy.
- With ageing at 100°C, the equilibrium volume fraction of δ′ is reached (or closely approached) after 1000h, hence, the volume fractions of δ′ in the 1.7Li3.0Cu and 1.7Li alloys are identical.

TEM analysis showed the presence of δ′ in the 1.7Li1.2Cu and 1.7Li3.0Cu alloys, (**figure 9.12, 9.13**). The size of the δ′ in the 1.7Li1.2Cu and 1.7Li3.0Cu alloys is approximately the same (~10nm diameter). In the 1.7Li3.0Cu alloy, in addition to δ′, streaking in <001> directions on the diffraction pattern indicated the presence of GP_{Cu} zones. Evidence for GP_{Cu} zones in the 1.7Li1.2Cu alloy was much less strong. As at 70°C, the δ′ in the 1.7Li3.0Cu alloy was elongated in the <001> directions, again indicating the possibility of heterogeneous nucleation of δ′ on GP_{Cu} zones.

Figure 9.14 shows the isothermal resistivity plots for ageing at 100°C. All the alloys exhibit an initial increase of resistivity which is followed by a marked decrease to well below the as-quenched value. According to the sub-phase regions of the Al-Li phase diagram determined by Noble and Bray **[44]**, the 1.7Li binary alloy lies in the nucleation-ordered region of the phase diagram when the alloy is aged at 100°C. The initial increase in resistivity of the binary alloy can therefore be attributed to the electron scattering from ordered regions developing in the matrix. Addition of 1.2%Cu to the alloy produces a small increase in the magnitude of the resistivity and the resistivity remains positive for a longer period. This may be the result of a finer dispersion of δ′ particles being produced by nucleation on Cu clusters or GP_{Cu} zones.

For the period 300-1000 h ageing, the resistivity curves for the 1.7Li and 1.7Li1.2Cu alloys are identical which, as mentioned earlier, indicates that after

long ageing times (>300h) the amount of δ′ produced in the two alloys is the same.

Addition of 3%Cu to the alloy results in a significant change to the isothermal resistivity characteristics (**figure 9.14**). A well defined peak in resistivity occurs after ageing 1h at 100°C and the magnitude of the peak is significantly higher than the resistivity increase observed in the 1.7Li and 1.7Li1.2Cu alloys. It is proposed that δ′ nucleates heterogeneously on GP_{Cu} zones similar to that described for the 1.7Li1.2Cu alloy but with increased number density; this then explains the larger resistivity increase. After long ageing times, >300h, the resistivity decrease falls to that observed in the 1.7Li and 1.7Li1.2Cu alloys.

9.2.3 TEM analysis of the effect of GP_{Cu} zones on the precipitation of δ′ during ageing at moderate temperatures.

In the previous sections it was shown that the addition of 3% copper (and possibly 1.2%Cu) results in the formation of GP_{Cu} zones during ageing at 70 and 100°C which, in turn, affect the kinetics of δ′ precipitation. In this section the role of the GP_{Cu} zones on the enhanced precipitation of δ′ in a 1.7Li3.0Cu alloy is considered in more detail after ageing at the above temperatures. It has already been shown that ageing at 70 and 100°C results in continuous streaking in the <001> directions of electron diffraction patterns (**figures 9.8b, 9.13b**) confirming the presence of GP_{Cu} zones. These zones cannot be seen in the dark field image

but it is noted that not all δ′ particles are spherical in shape. It can be observed that some of the larger δ′ particles are elongated in <001> directions, suggesting that δ′ may have nucleated on the GP_{Cu} zones producing composite precipitates consisting of an inner plate of GP_{Cu} and an outer shell of δ′. Further TEM analysis was carried out in an attempt to investigate this further. It was hoped that a second ageing treatment at a temperature higher than 100°C would result in an increase of the size of δ′ and enable the elongated particles to be seen more easily. Therefore, TEM thin foils were prepared after treating the 100°C sample for 48h (2days) and 192h (8 days) at 130°C. This temperature was selected in order to avoid possible co-precipitation of T_1 which is known to occur at 150°C. The micrographs are presented in **figures 9.15** and **9.16**. At the longer ageing time, the GP_{Cu} zones can be clearly seen in the bright field image (**figure 9.16b**) together with their <001> streaking in **figure 9.16c**. In dark field imaging (**figure 9.16a**) using a δ′ superlattice spot, composite particles consisting of plates of GP_{Cu} zones surrounded by a sheath of δ′ can be clearly seen. Between these composite particles are spherical δ′ particles that have either nucleated in the matrix without the aid of GP_{Cu} zones, or nucleated on small GP_{Cu} zones and subsequently coarsened into a spherical shape.

A similar effect can be seen at the shorter age time of 48h at 130°C but, due to the smaller size of particle, the effect is less obvious (**figure 9.15**).

It can therefore be concluded that δ′ nucleates on GP_{Cu} zones after secondary

ageing at 130°C. It is therefore likely that similar heterogeneous nucleation takes place at the lower ageing temperatures, i.e. 70 and 100°C, thus explaining the enhanced kinetics of δ′ formation that is observed in copper-containing Al-Li alloys when aged at low temperatures.

9.2.4 Ageing at 150°C

DSC plots after ageing at 150°C for 24h and 1000h are given in **figures 9.17** and **9.18** respectively. **Figure 9.17** shows that with increase of the copper concentration from 0 to 3%, the δ′ dissolution peak exhibits a marked increase in area. TEM micrographs of 1.7Li1.2Cu and 1.7Li3.0Cu alloys after ageing for 24h at 150°C (**figures 9.19 and 9.20** respectively) showed the presence of δ′. In addition the 1.7Li3.0Cu alloy showed the formation of a small number of coarse GP_{Cu} zones (**figure 9.20**). The low density of the GP_{Cu} zones is consistent with the Al-Cu phase diagram which predicts a very small driving force for GP_{Cu} formation at 150°C.

The XRD spectra of 1.7Li1.2Cu and 1.7Li3.0Cu alloys are shown in **figures 9.21** and **9.22.** The intensity of the T_1 peaks suggest that as copper increases from 1.2% to 3.0% the precipitation of T_1 is stimulated. TEM analysis confirmed the precipitation of T_1 plates with habit plane {111} **(figures 9.20a, b).**

The precipitation characteristics change dramatically after ageing at 150°C for 1000h. An addition of 1.2%Cu to the binary alloy produces a small decrease in the dissolution peak (**figure 9.18**). According to the X-Ray diffraction data of **figure 9.23** this small decrease is due to the formation of T_1, the precipitation of which causes dissolution of some δ′ during the age at 150°C. Increasing the copper addition to 3% produces a large decrease in the area of the δ′ endotherm peak, i.e. there is now a significant decrease of δ′ volume fraction (**figure 9.18**). X-Ray diffraction analysis of the 1.7Li3.0Cu alloy showed that after ageing for 1000h at 150°C formation of a significant fraction of equilibrium T_1 and T_2 has taken place (**figure 9.24**) and therefore the large decrease in δ′ volume fraction can be attributed to δ′ dissolution during the age at 150°C. The exothermic event in the DSC plot of **figure 9.18** at about 310°C is caused by further precipitation of T_1 and T_2 phases as evidence by the X-ray data of **figure 9.3**.

Isothermal resistivity plots for ageing at 150°C are presented in **figure 9.25**. All the alloys exhibit an incubation period which is followed by a decrease of resistivity. This suggests that the mechanism of δ′ formation is occurring by a nucleation and growth process. The incubation period becomes shorter as the copper concentration increases from 0 to 3%, indicating that the copper promotes enhanced δ′ precipitation kinetics. No increase in resistivity is observed during the early stages of precipitation and therefore it can be concluded that the critical size for nucleation is larger than the critical size for electron scattering. In the

binary 1.7Li alloy the δ′ precipitation reaction is complete by ~100h ageing at 150°C. Similarly, in the 1.7Li1.2Cu alloy the δ′ precipitation reaction is complete after 100h ageing but this is followed by a small increase in resistivity due to precipitation of T_1 phase which is known to cause appreciable electron scattering **[30]**.

In the 1.7Li3.0Cu alloy, before the δ′ reaction is complete, significant T_1 precipitation occurs so that the total resistivity drop is reduced and this is followed by a large increase in resistivity from precipitation of a large volume fraction of T_1.

9.2.5 Effect of ageing temperature

This section discusses the effect of ageing temperature on the precipitation characteristics of Al-Li-Cu alloys.

The effect of the ageing temperature on the 1.7Li binary alloy has already been considered in section **8.2.5.** This can be summarised as follows:

- An increase of ageing temperature from 70°C to 150°C changes the δ′ formation mechanism from nucleation-ordering to classical nucleation and growth.
- 70°C ageing causes a high volume fraction of very fine spinodally decomposed regions with a size smaller than the critical size for electron scattering.

- Changing the ageing conditions from 1000h at 70°C to 1000h at 150°C does not change significantly the final volume fraction of δ′ that is precipitated.

Figure 9.26 presents the DSC thermograms of the 1.7Li1.2Cu alloy after ageing at different temperatures. It can be clearly seen that the maximum amount of δ′ is precipitated at 100°C. Thermodynamically, it would be expected that the volume fraction would increase as the ageing temperature decreases from 150 to 100 to 70°C. However, the diffusivity decreases as the temperature drops, so that at 70°C the amount of δ′ that forms is limited by kinetic considerations.

The isothermal resistivity curves for the 1.7Li1.2Cu alloy are shown in **figure 9.27**. These resistivity plots show:

- Very small δ′ particles are produced at 70°C of a size <2 nm, ie a resistivity peak is not reached.
- Small δ′ particles are also produced at 100°C but, in this case, a size of 2 nm is exceeded after ageing for approximately 30h.
- At 150°C a long incubation period indicates that classical nucleation and growth of δ′ is the dominant process.

These results suggest that at 70°C and 100°C, δ′ is forming on fine GP_{Cu} zones but, at 150°C, the dispersion of GP_{Cu} zones is so coarse that their influence on δ′ precipitation is minimal.

When the isothermal resistivity curves in **figure 9.27** are considered along with

the DSC plot of **figure 9.26,** it can be seen that the magnitude of the total resistivity decreases at 100°C and 150°C cannot be equated to the volume fraction of δ′ that has formed at 100°C and 150°C. The highest volume fraction of δ′ is produced at 100°C but this does not correspond to the largest decrease of resistivity, which is observed to occur for ageing at 150°C. By means of TEM the diameter of δ′ particles was measured after ageing for 1000 h at 100°C (**figure 9.12**) and for 24h at 150°C (**figure 9.19**) and were found to be ~10 nm and ~40 nm respectively. Therefore, the reason for the smaller decrease in resistivity during ageing at 100°C is due to the considerably smaller δ′ particle size which will make a positive contribution to the electrical resistivity; the resistivity at 100°C will therefore fall more slowly than that at 150°C.

DSC thermograms and resistivity curves for the 1.7Li3.0Cu alloy are presented in **figures 9.28** and **9.29,** respectively. It can be seen from **figure 9.28** that ageing 1000h at 70 and 100°C produces almost the same amount of δ′. After ageing 1000h at 150°C the amount of δ′ that forms is reduced dramatically due to precipitation of T_1 during the age. The resistivity plots at 150°C in **figure 9.29** indicate that at 70°C and 100°C very fine δ′ is formed during the early stages of ageing probably nucleated on GP_{Cu} zones. At 150°C classical nucleation and growth of δ′ appears to be taking place.

Figure 9.30 summarises the combined effects of copper concentration and

ageing temperature on the δ′ volume fraction that is developed after ageing 1000h. The volume fraction was calculated by measuring the dissolution enthalpy, correcting for the presence of GP_{Cu} zones, and using relation **8.2** given in **chapter 8**. The trend in **figure 9.30** is that the volume fraction of δ′ increases with copper concentration when alloys are aged at 70°C and 100°C, and there is a decrease in δ′ volume fraction when ageing is at 150°C. The trends at 70°C and 100°C are the result of copper additions affecting the kinetics of δ′ precipitation (as described earlier). The trend at 150°C is the result of progressively higher rates of T_1 precipitation with increasing copper concentration.

9.3 Exposure at 70°C after prior ageing at 150°C for 24h

This part of the work simulates the service conditions that an Al-Li aerospace alloy may experience i.e. prolonged exposure to 70°C during flight or whilst standing on a runway in the hot sun. It is known that binary Al-Li alloys undergo a small amount of embrittlement when alloys are aged 24h at 150°C and then exposed 1000h at 70°C [**3**]. In this section the effects of copper additions on exposure embrittlement are studied.

The DSC thermograms of 1.7Li, 1.7Li1.2Cu and 1.7Li3.0Cu alloys after ageing 24h at 150°C and exposing 1000h at 70°C are presented in **figures 9.31, 9.32** and **9.33**. Exposure has not caused an increase in the dissolution endotherm of the 1.7Li binary alloy (**figure 9.31**) but there are clear increases in area of the

endotherm in the 1.7Li1.2Cu and 1.7Li3.0Cu alloys (**figures 9.32, 9.33**). It should be noted that the DSC thermogram of the 1.7Li3.0Cu alloy displays a clear double peak (A and B) after exposure (**figure 9.33**). Peak (A) represents dissolution of the fine distribution of precipitates produced during exposure, and peak B represents dissolution of a coarse fraction of δ′ particles resulting from the 24h ageing at 150°C. The earlier work described in this chapter has shown that a considerable amount of GP_{Cu} zones can be produced in the 1.7Li3.0Cu alloy during ageing at 70°C. Therefore, the endothermic peak A will represent dissolution of both fine δ′ and GP_{Cu} zones. To determine the enthalpy due to dissolution of δ′ only, the area of the dissolution peak of an Al-3.0Cu alloy aged 24h at 150°C followed by 1000h at 70°C has been subtracted from the area of the peak caused by the 'exposure precipitates'. The area under the dissolution peak of the Al-3.0Cu alloy was found to be 4.0 J/g. This amount of energy represents 1/3 of the heat absorbed by dissolution of the exposure precipitates and therefore the other 2/3 of the energy can be attributed to δ′ dissolution. This δ′ enthalpy can be converted to an increase in volume fraction of δ′ produced by exposure at 70°C by using relation 8.2 referred to in the previous chapter. The volume fractions obtained are displayed in **figure 9.34** and they show that as the copper concentration increases from 1.2 to 3% the amount of δ′ precipitated during exposure increases significantly.

TEM on samples of 1.7Li3.0Cu alloy aged 24h at 150°C and samples exposed at 70°C showed the presence of coarse δ′ (~15nm diameter), coarse GP_{Cu} zones (~65nm diameter) and T_1 phase (**figure 9.35**). Also, in the matrix of the exposed alloy, very fine precipitation of δ′ and GP_{Cu} zones can just be resolved. In order to study this exposure precipitation, and in particular to see if exposure δ′ had been formed by nucleation on GP_{Cu} zones, the exposed 1.7Li3.0Cu alloy was aged for a week at 100°C in order to coarsen the exposure precipitates. **Figure 9.36** shows the result of this additional ageing. The exposure precipitation can now be clearly seen and it appears to be δ′ precipitated on fine GP_{Cu} zones of 13nm diameter (see section 9.2.3).

Isothermal resistivity curves for alloys during exposure at 70°C are shown in **figure 9.37.** The resistivity increase in the 1.7Li binary alloy indicates that very small δ′ precipitates are forming during exposure, of a diameter <2nm (critical size for electron scattering). No increase is observed for the 1.7Li1.2Cu alloy; the resistivity decreases smoothly as exposure progresses. Assuming that δ′ is forming on GP_{Cu} zones, then this resistivity behaviour suggests that at the 1.2%Cu level, the size of the GP_{Cu} zones on which the δ′ nucleates is larger than the critical size for electron scattering.

The 1.7Li3.0Cu alloy exhibits a different resistivity behaviour. Here the exposure causes an initial increase in resistivity followed by a relatively large decrease. The DSC and TEM results described earlier showed that in this alloy a

large number-density of GP_{Cu} zones are produced, on which the δ′ phase is nucleated. The resistivity behaviour suggests that at the 3.0%Cu level the size of the GP_{Cu} zones on which the δ′ nucleates is now less than the critical size for electron scattering.

9.4 Mechanical properties after long term service exposure

The effects of exposure for 1000h at 70°C on the mechanical properties of the 1.7Li, 1.7Li1.2Cu and 1.7Li3.0Cu alloys are shown in **figure 9.38**. It can be clearly seen that exposure causes only a very small change in the proof stress of the binary 1.7Li alloy whereas no change is observed for the fracture energy. Increasing the copper addition from 0 to 3% results in a marked increment of proof stress and a corresponding decrement in the fracture energy. This exposure embrittlement must be caused by either δ′ forming during exposure, GP_{Cu} zones forming during exposure, or a combination of the two effects. It is known from the literature that GP_{Cu} zones cause little or no embrittlement in Al-Cu alloys; this leaves δ′ to consider. **Figure 9.34** shows that as the copper addition increases from 0 to 3.0% the volume fraction of δ′ formed during exposure increases significantly. In addition, from the DSC thermograms in **figures 9.32** and **9.33** it is clear that exposure does not produce a shift of T^{DSC}_{end} of the dissolution endotherm indicating that little or no growth of the pre-age δ′ particles has taken place during exposure. This was also confirmed by TEM (**figures 9.20, 9.35**). Thus we can conclude that the changes in proof stress and fracture energy are due only to the formation of large amounts of fine δ′ between the coarse δ′

precipitates produced by the prior age at 150°C for 24h. The high volume fraction of δ′ produced by exposure results an increase in proof stress and a corresponding decrease in fracture energy. It may also cause an intensification of planar slip in the copper-containing alloys causing stress concentrations at grain boundaries and an increasing tendency for grain boundary failure. SEM has therefore been carried out to see if the degree of grain boundary fracture increases in the exposed alloy. **Figure 9.39** compares SEM fractographs taken from the 1.7Li3.0Cu alloy aged 24h at 150°C and after subsequent exposure at 70°C. These do not show a marked increase in the amount of grain boundary failure, but they do indicate an increased brittleness in that there are less ductile fracture dimples on the fracture surface of the exposed sample. This is probably the direct result of the increase in proof stress caused by exposure.

9.5 Summary and comparison of copper additions with those of magnesium

In the previous chapter it was shown that at all ageing temperatures, increasing the magnesium concentration stimulated the formation of δ′ due to an increase of the α/δ′ solvus temperature which in turn results in a higher driving force for δ′ precipitation. It was found that the α/δ′ solvus temperature increased by 6.7°C/wt%Mg.

Copper additions to an 1.7Li alloy have a different effect. It has been shown in the present chapter that copper has no effect on the α/δ′ solvus temperature.

However, the addition of copper results in the formation of GP_{Cu} zones which can act as very effective nucleation centres for δ′ phase. This has the effect of increasing the rate of δ′ precipitation. The increased rate of δ′ precipitation is clearly apparent even after ageing times of 1000h at 70°C. At 100°C the increased rate of δ′ precipitation is observed only during the early stages of ageing.

In both the Al-Li-Cu and Al-Li-Mg alloys the increased rate of δ′ precipitation resulting from copper and magnesium additions, causes an increased volume fraction of fine δ′ to form during exposure at 70°C. This means that the higher the copper concentration or magnesium concentration in the alloy, the greater the degree of embrittlement during exposure.

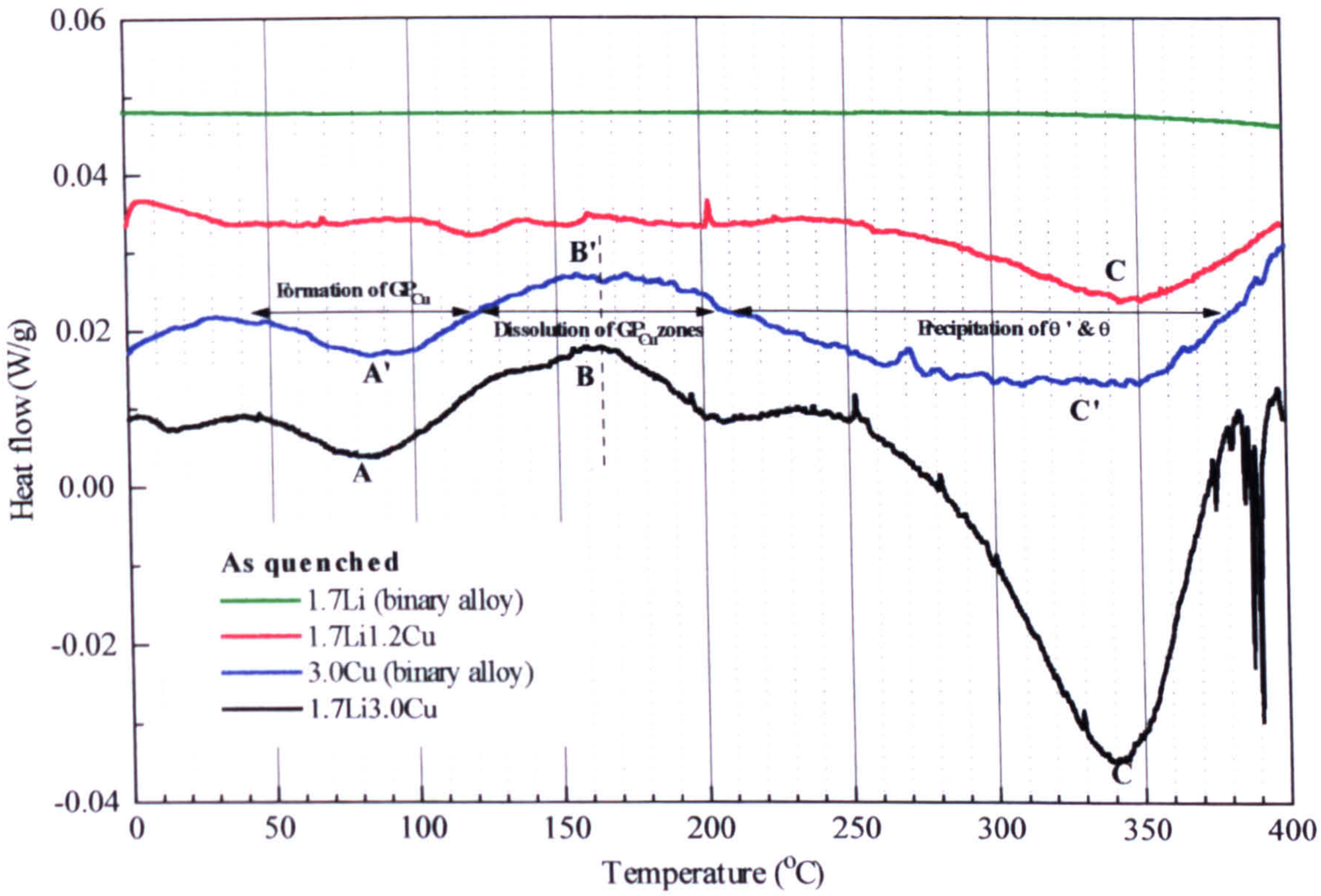

Figure 9.1: Comparative DSC plots of the as-quenched alloys.

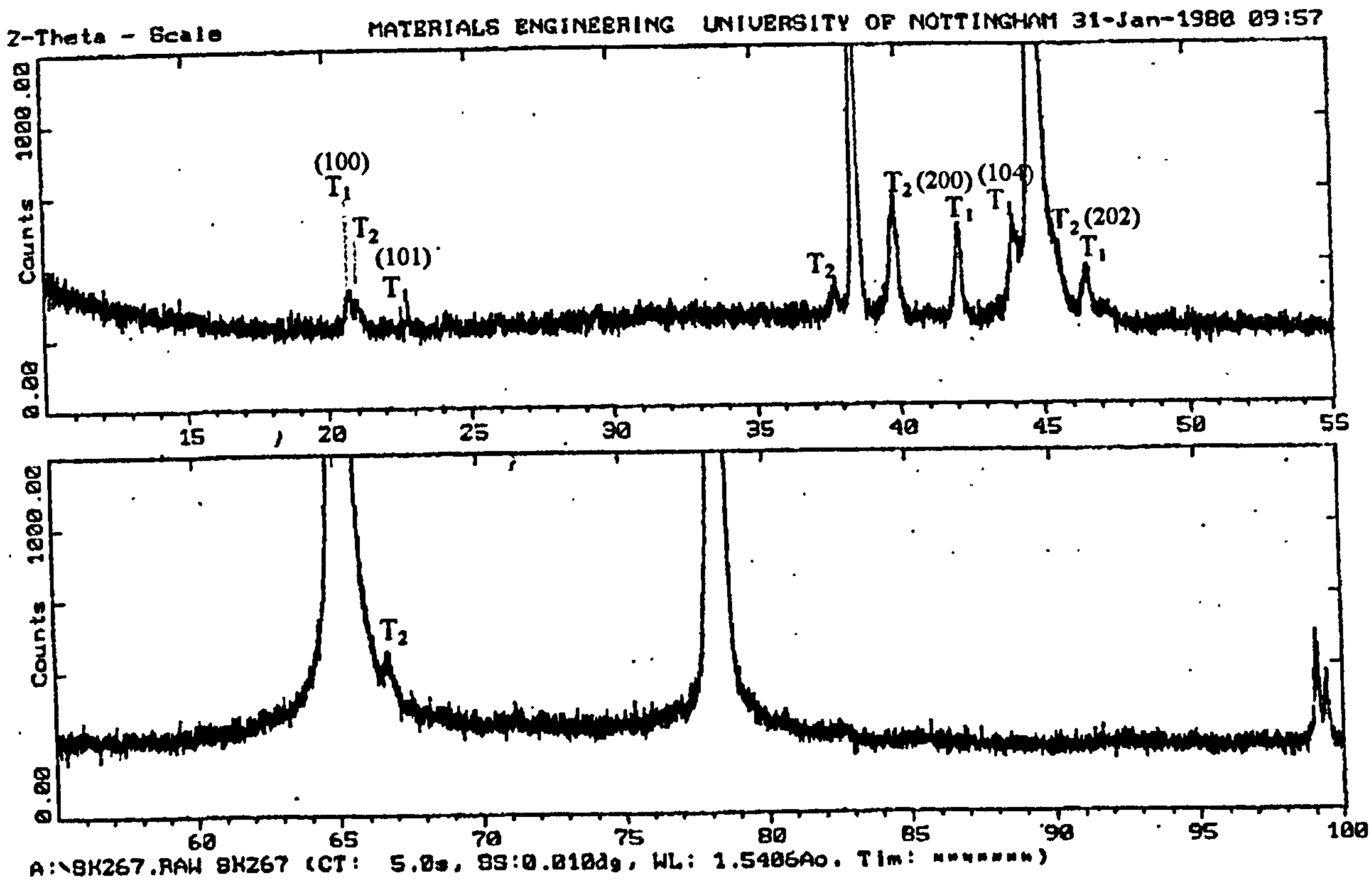

Figure 9.2: XRD spectrum of 1.7Li1.2Cu alloy after ageing for 24h at 350°C.

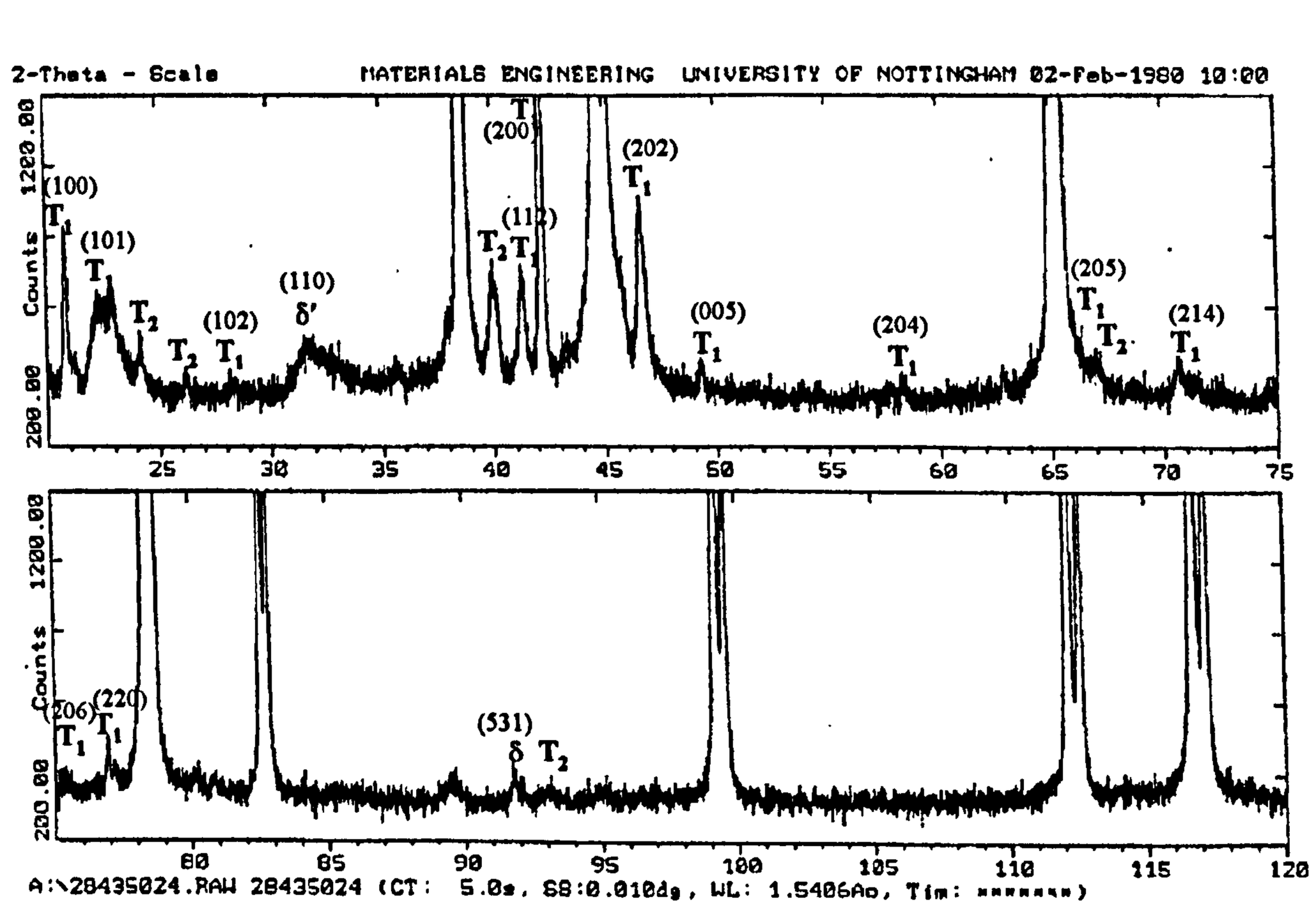

Figure 9.3: XRD spectrum of 1.7Li3.0Cu alloy after ageing for 24h at 350°C.

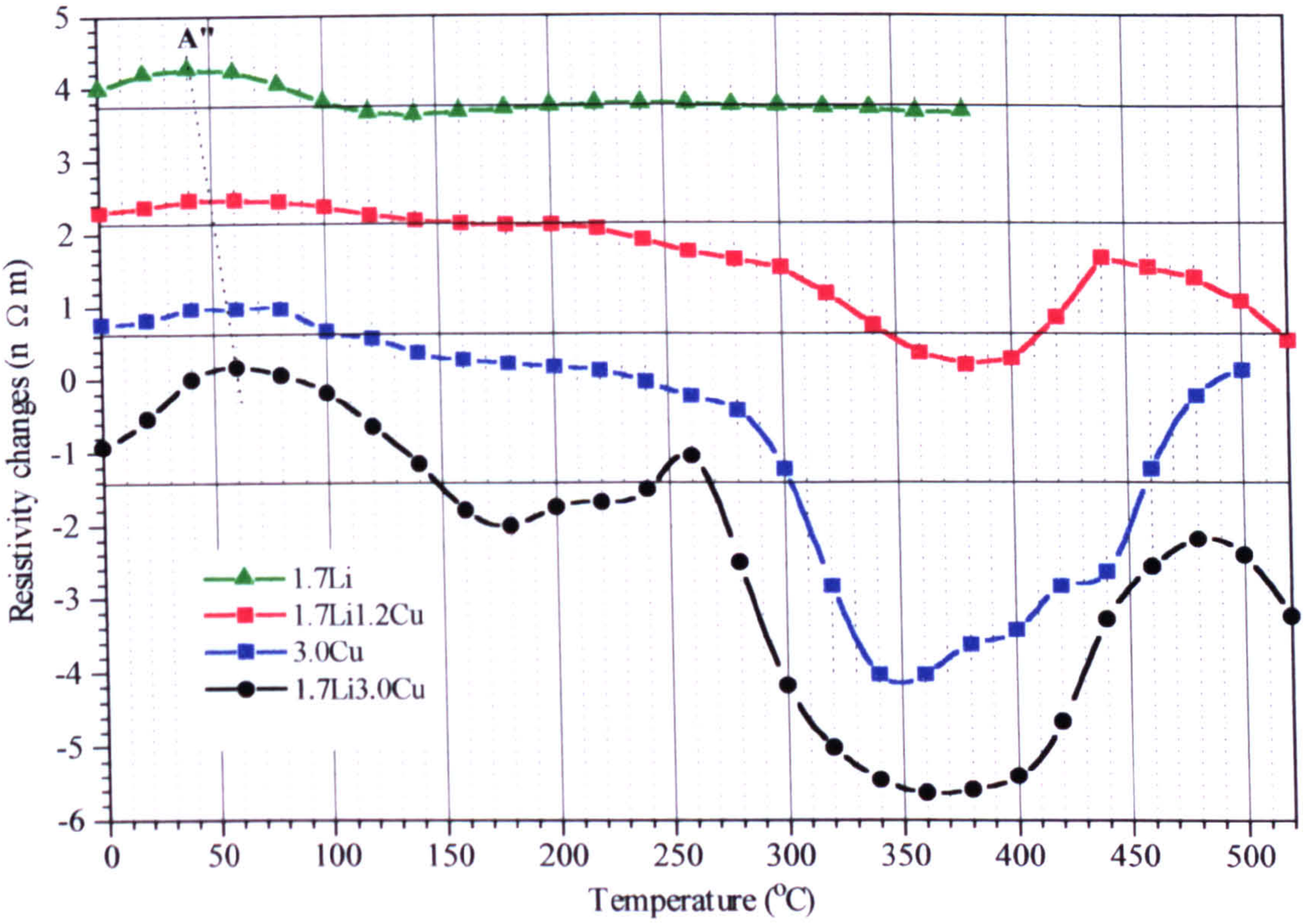

Figure 9.4: Comparison of the isochronal resistivity changes.

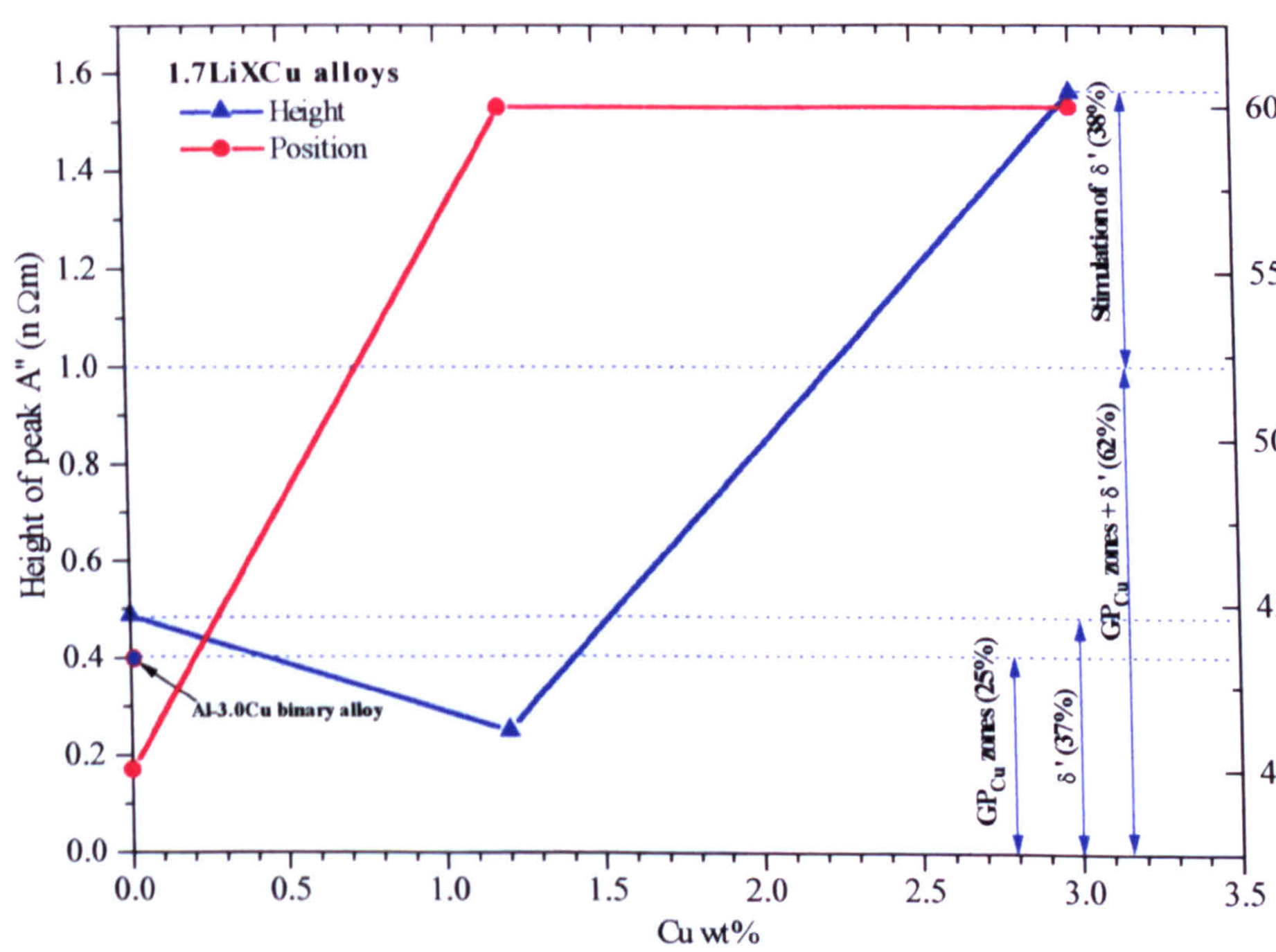

Figure 9.5: Height and position of peak A''.

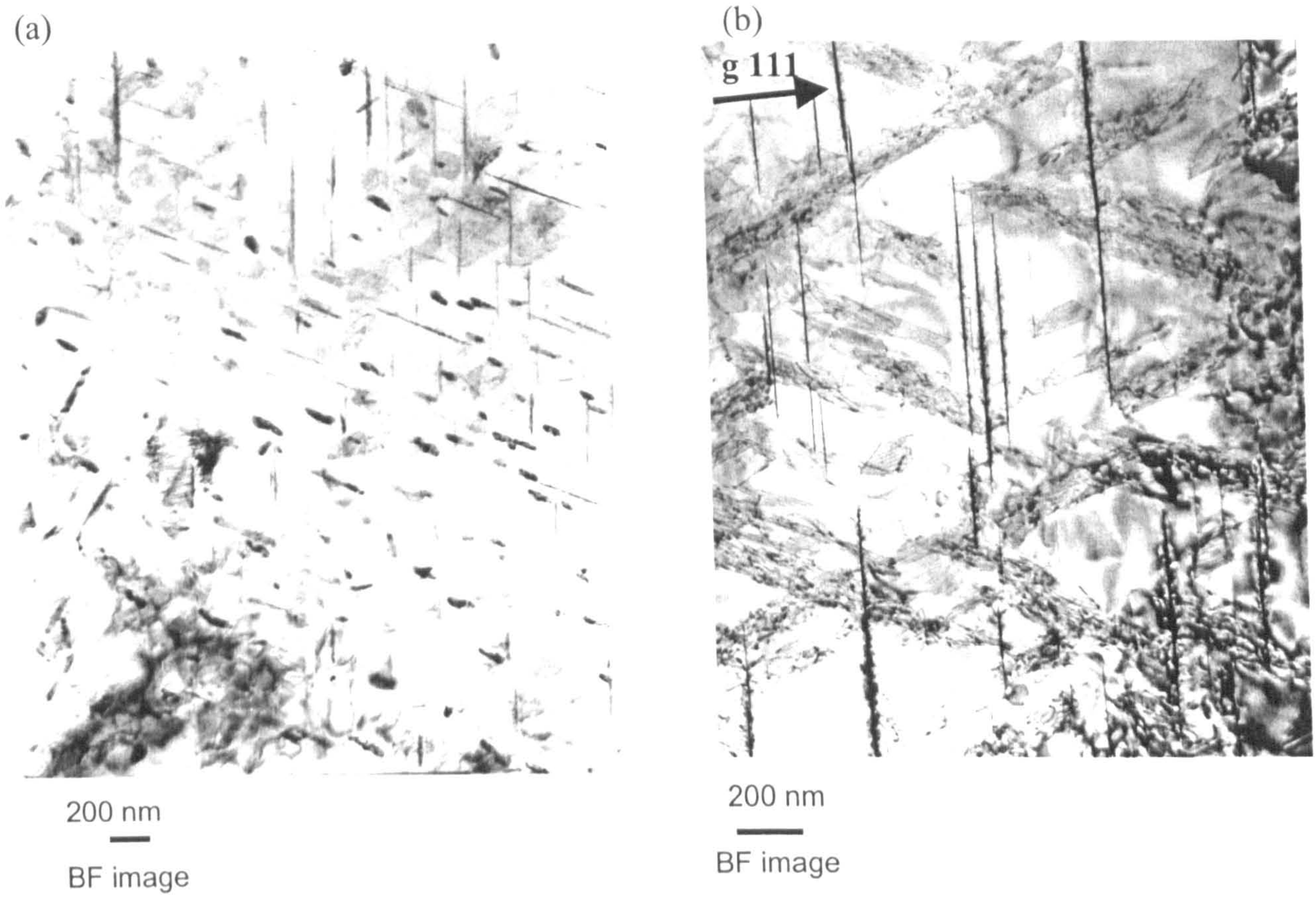

Figure 9.6 (a, b): TEM image of 1.7Li3.0Cu alloy after ageing for 0.5h at 260°C. Zone axis <$\bar{1}\bar{1}2$ >.

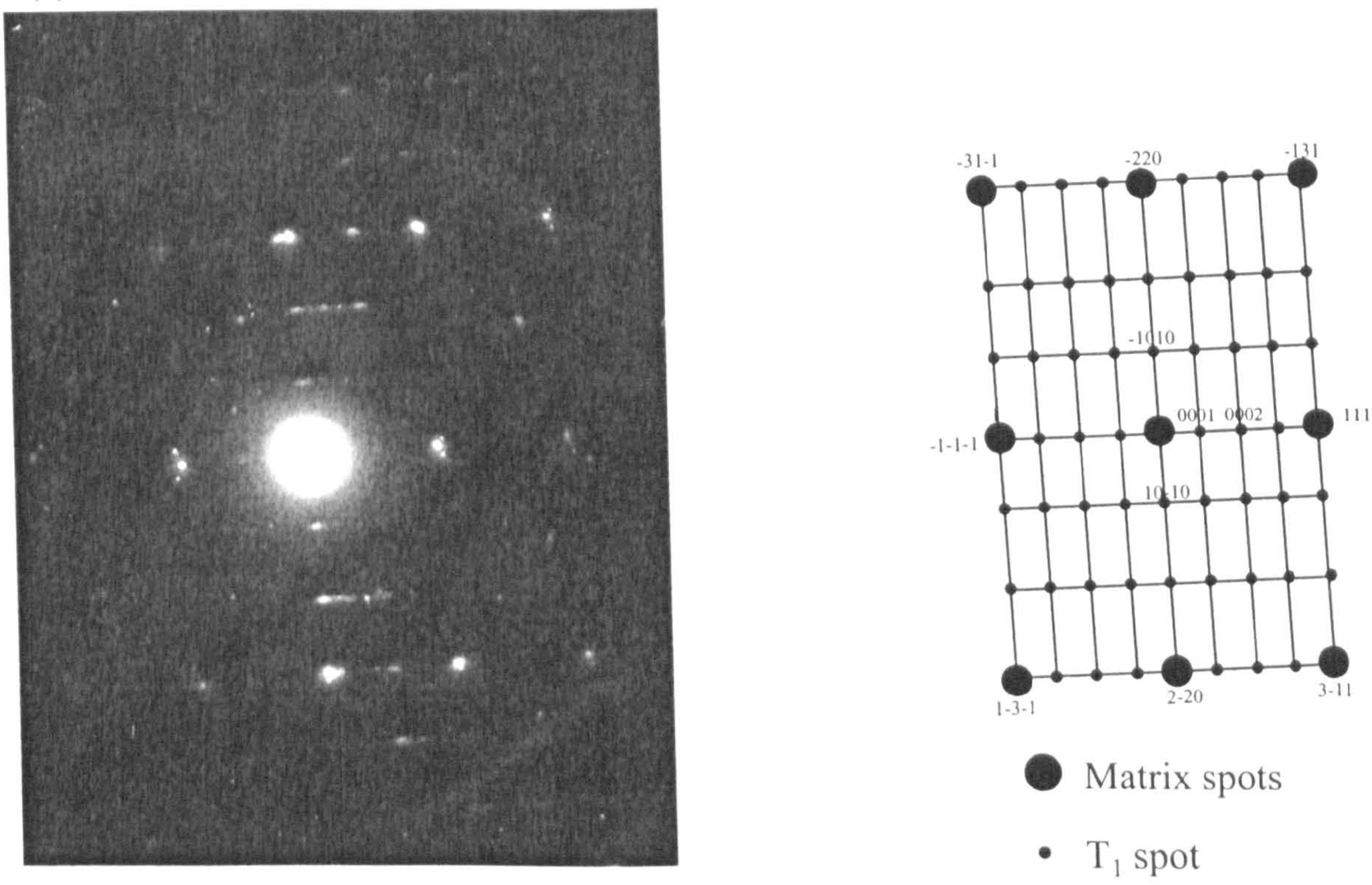

Figure 9.6 (c): SAD pattern of 1.7Li3.0Cu alloy after ageing for 0.5h at 260°C. Zone axis <$\bar{1}\bar{1}2$>.

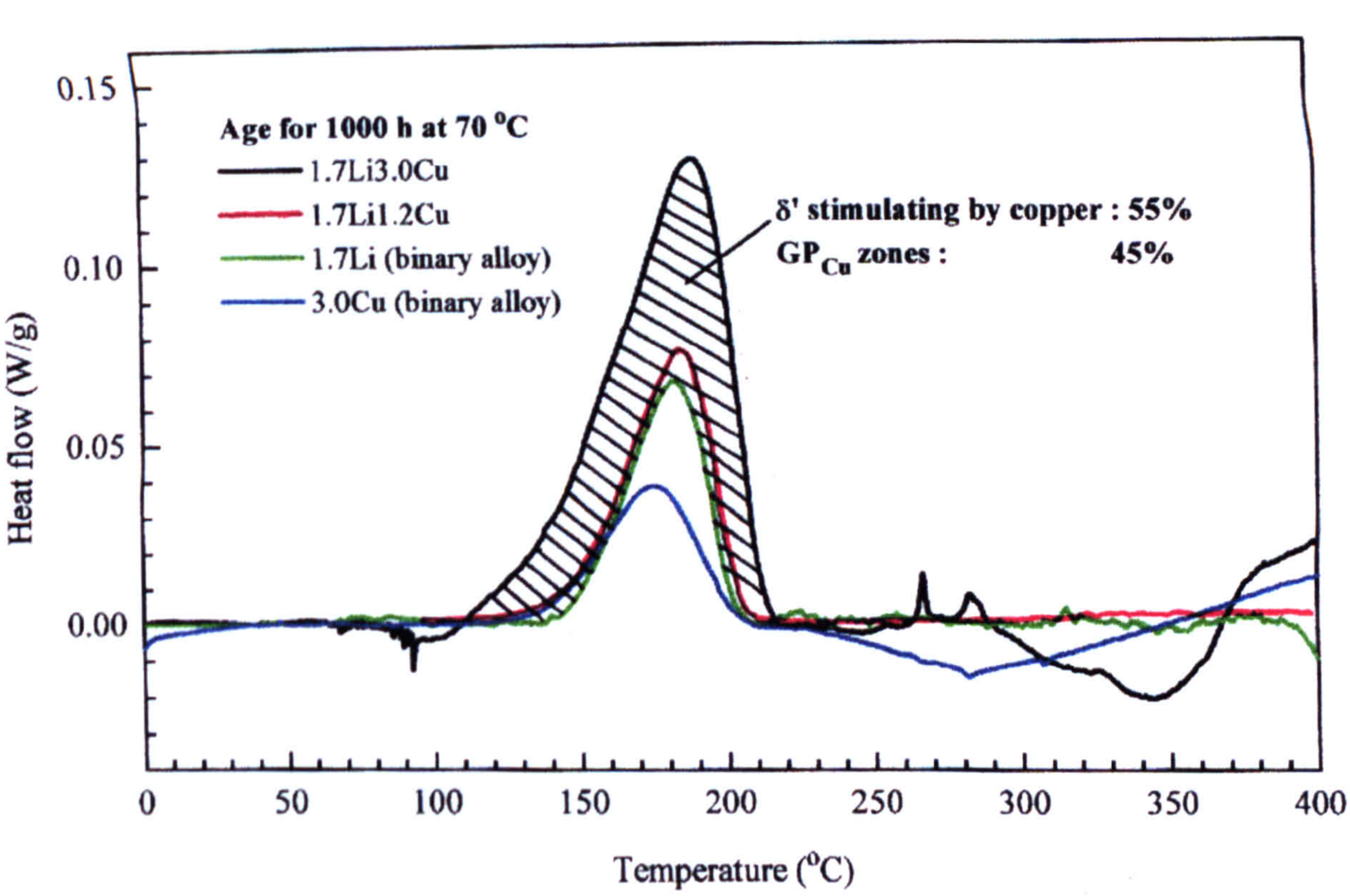

Figure 9.7: DSC comparative plots of the alloys aged at 70°C for 1000h.

(a)

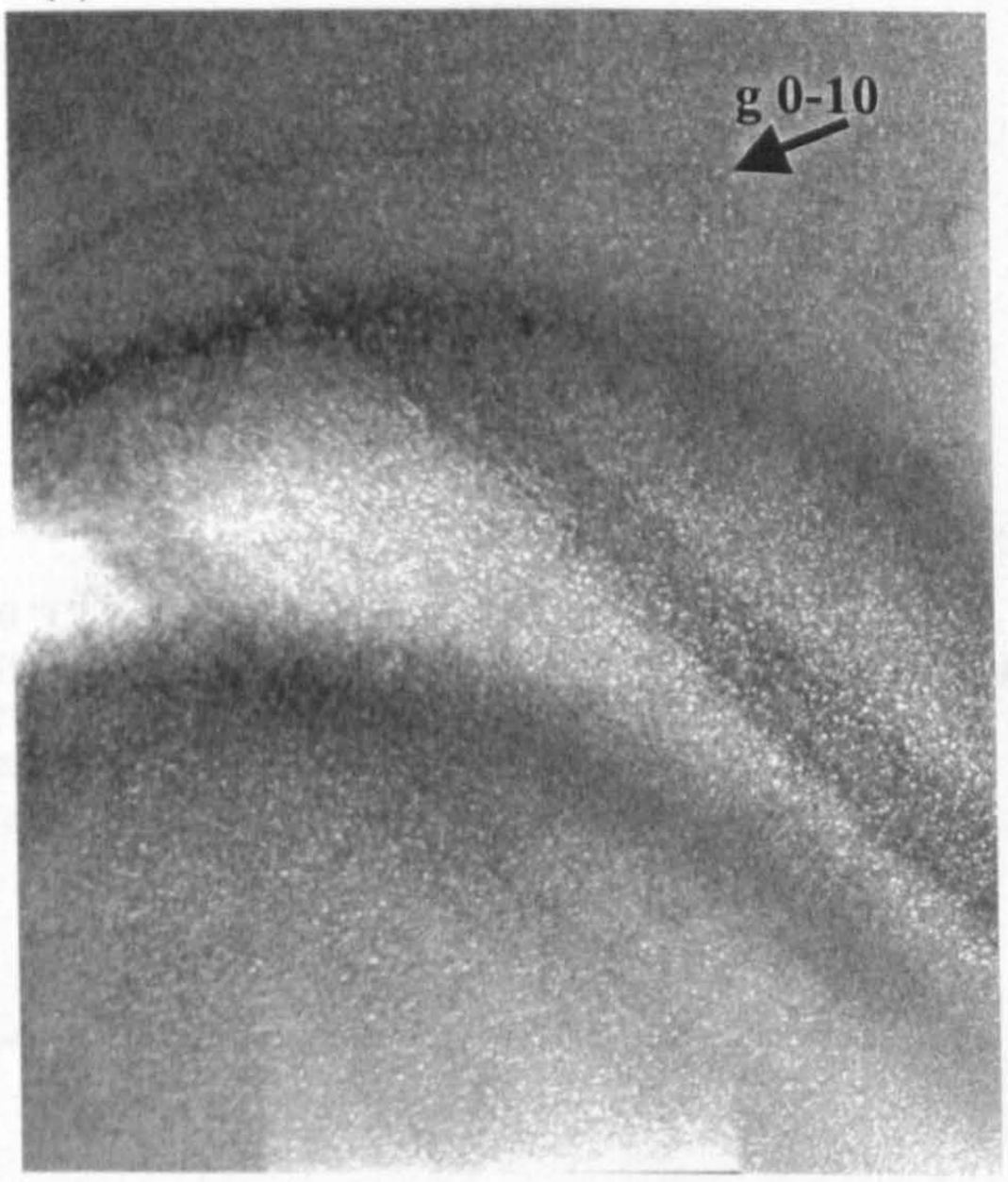

Figure 9.8 (a): TEM image of 1.7Li3.0Cu alloy after ageing for 1000h at 70°C.
Zone axis <001>.

(b)

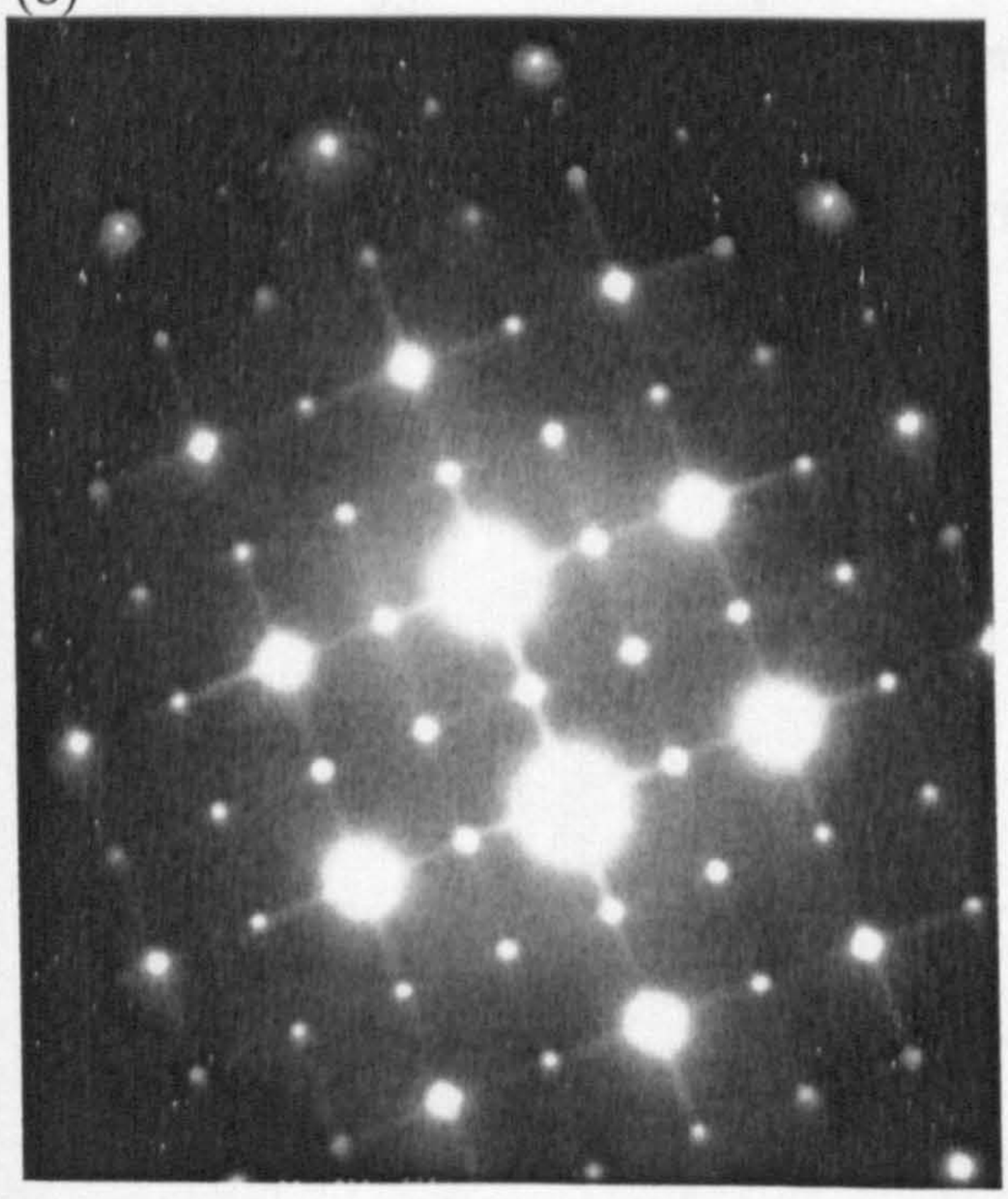

Figure 9.8 (b):SAD pattern of 1.7Li3.0Cu alloy after ageing for 1000h at 70°C.
Zone axis <001>.

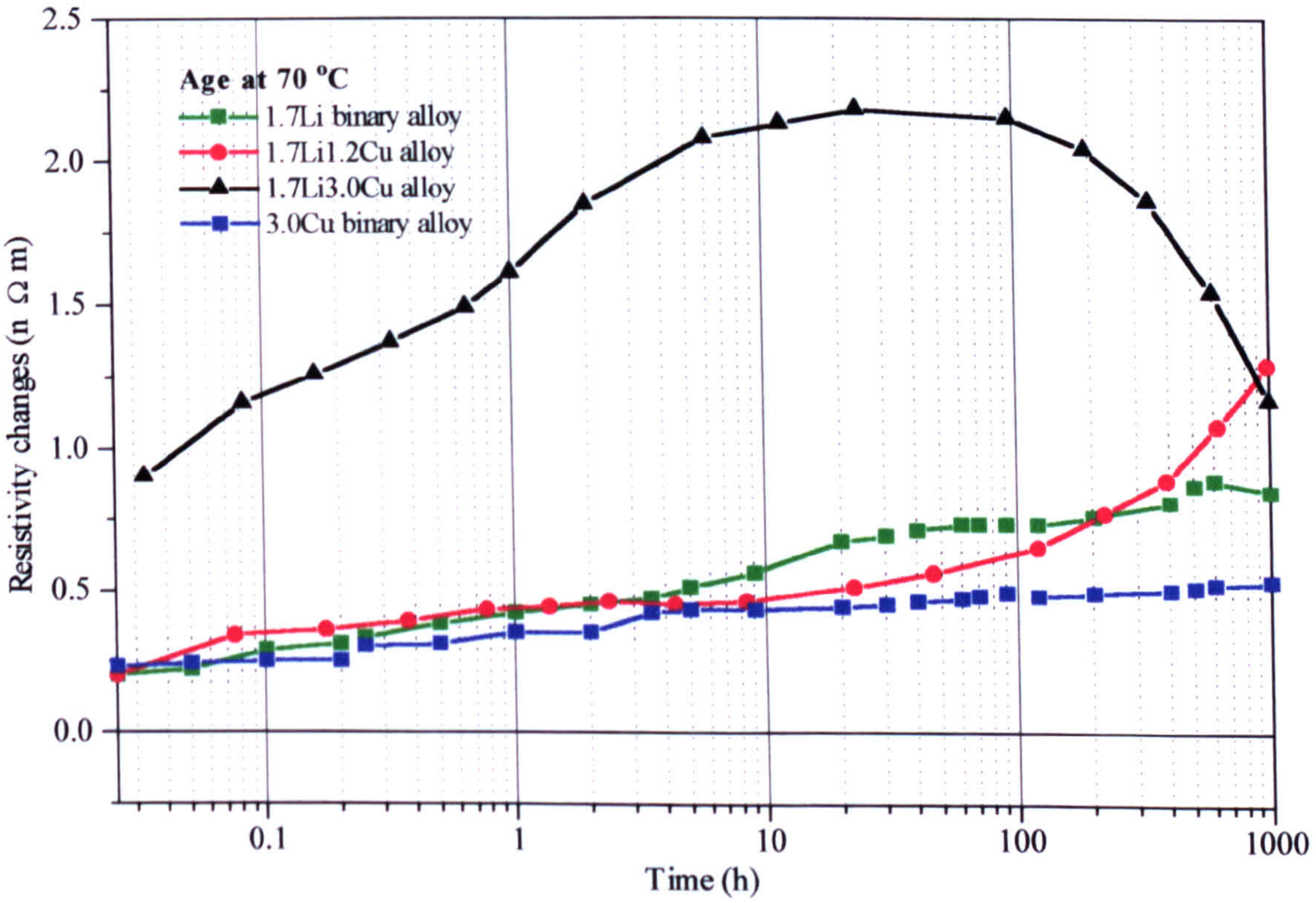

Figure 9.9 : Isothermal resistivity changes during ageing at 70°C.

(a)

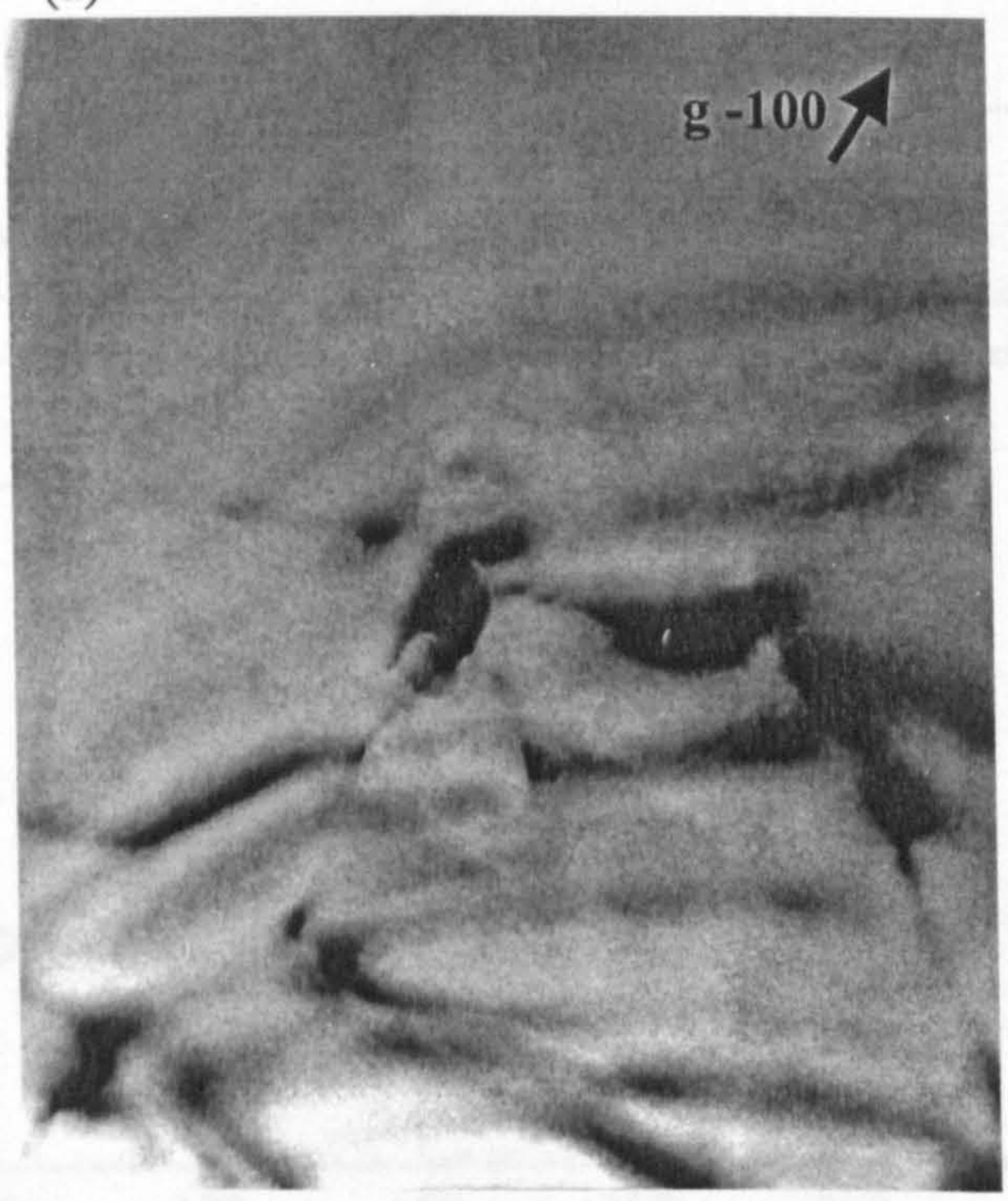

Figure 9.10 (a): TEM image of 1.7Li1.2Cu alloy after ageing for 1000h at 70°C. Zone axis <011>.

(b)

Figure 9.10 (b): SAD pattern of 1.7Li1.2Cu alloy after ageing for 1000h at 70°C. Zone axis <011>.

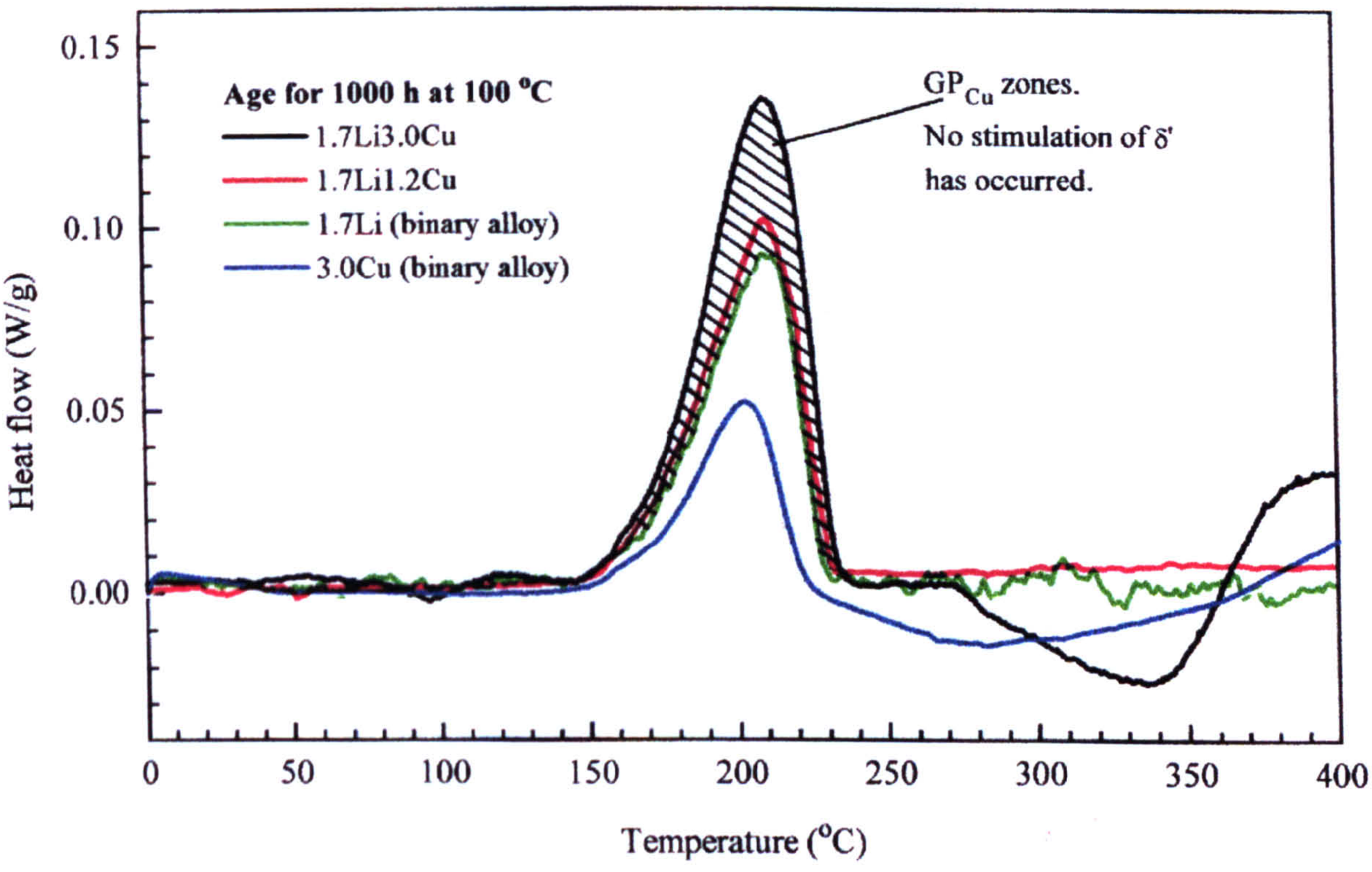

Figure 9.11: DSC comparative plots of the alloys aged at 100°C for 1000h.

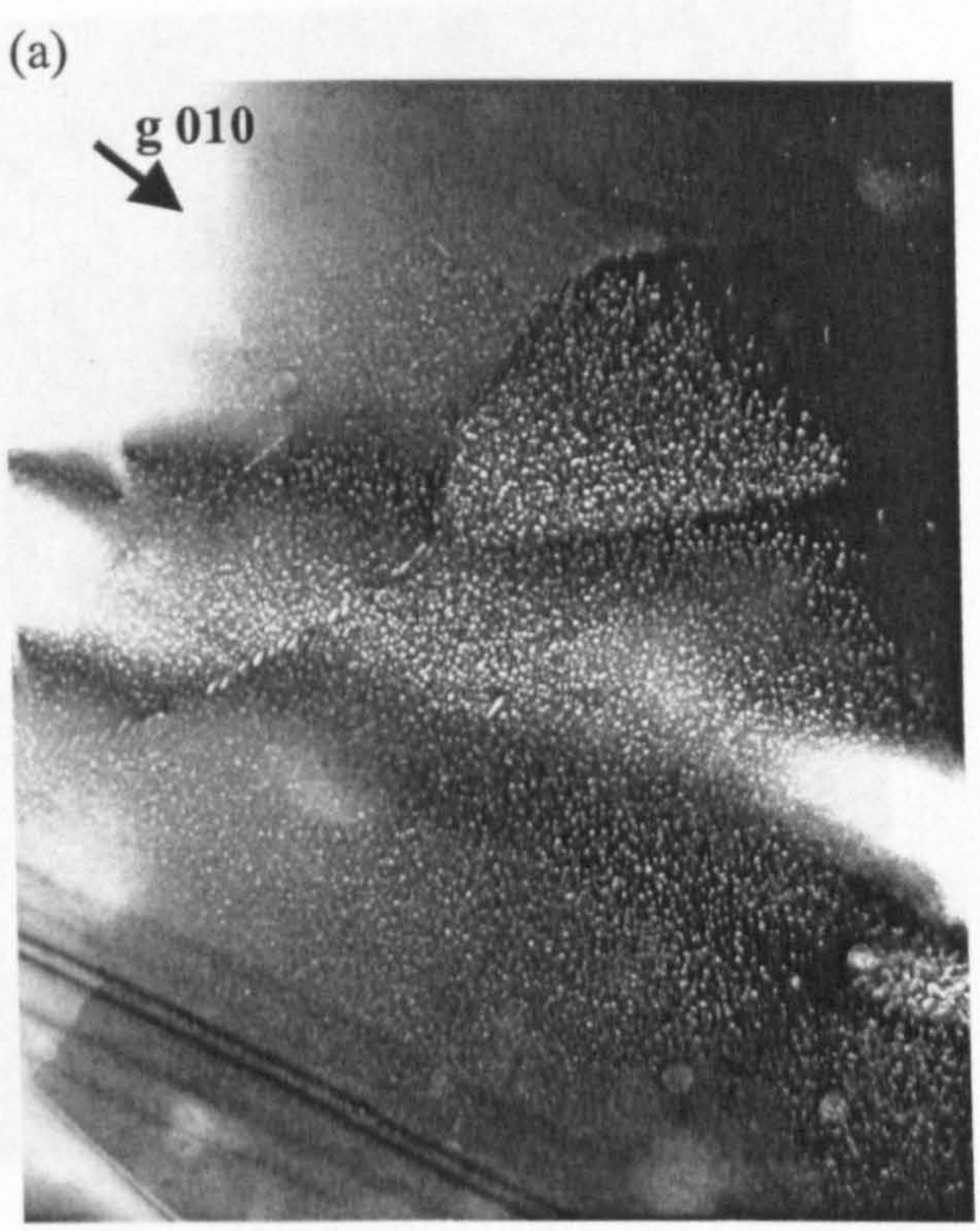

Figure 9.12 (a): TEM image of 1.7Li1.2Cu alloy after ageing for 1000h at 100°C.
Zone axis <001>.

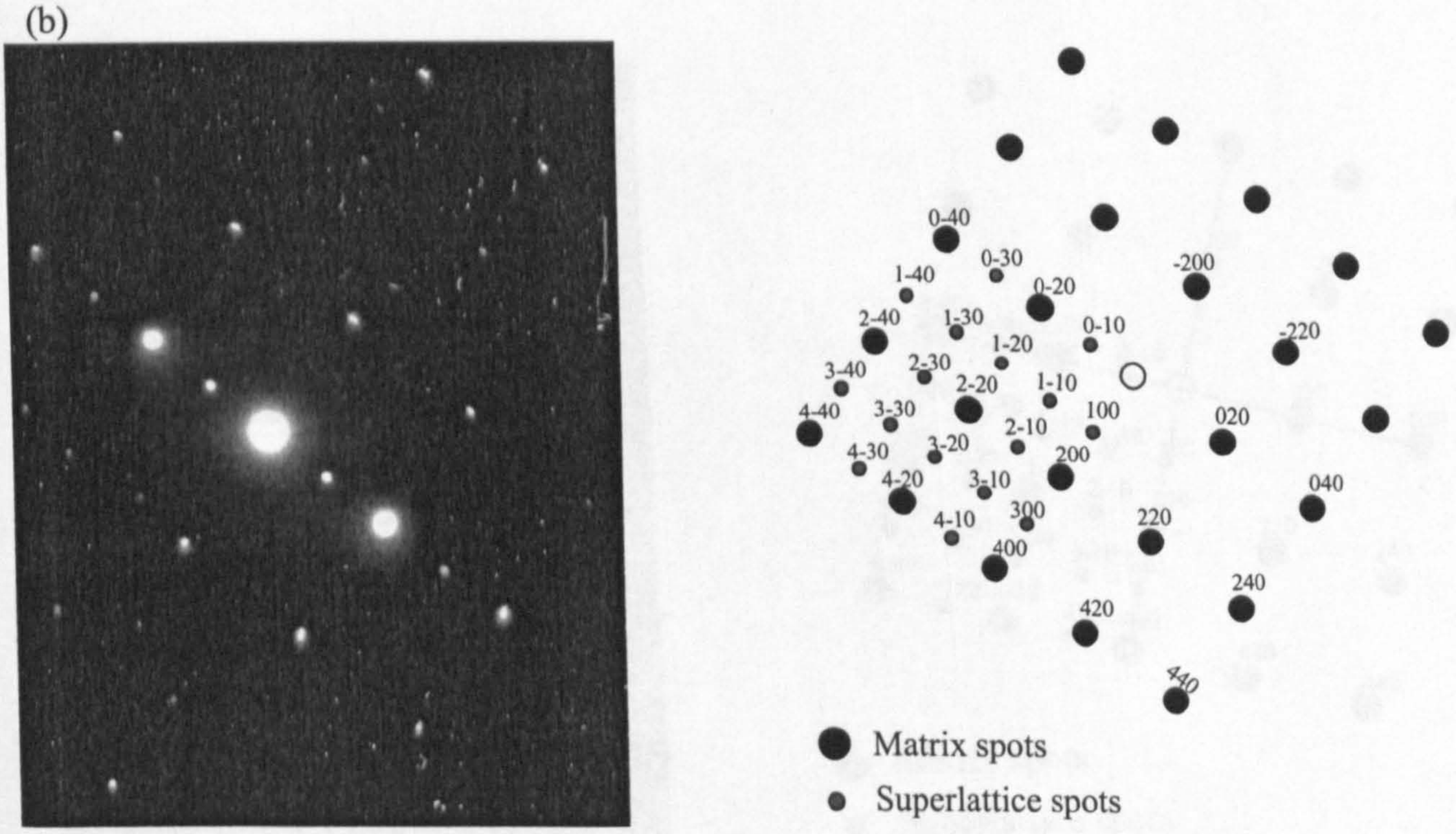

Figure 9.12 (b): SAD pattern of 1.7Li1.2Cu alloy after ageing for 1000h at 100°C.
Zone axis <001 >.

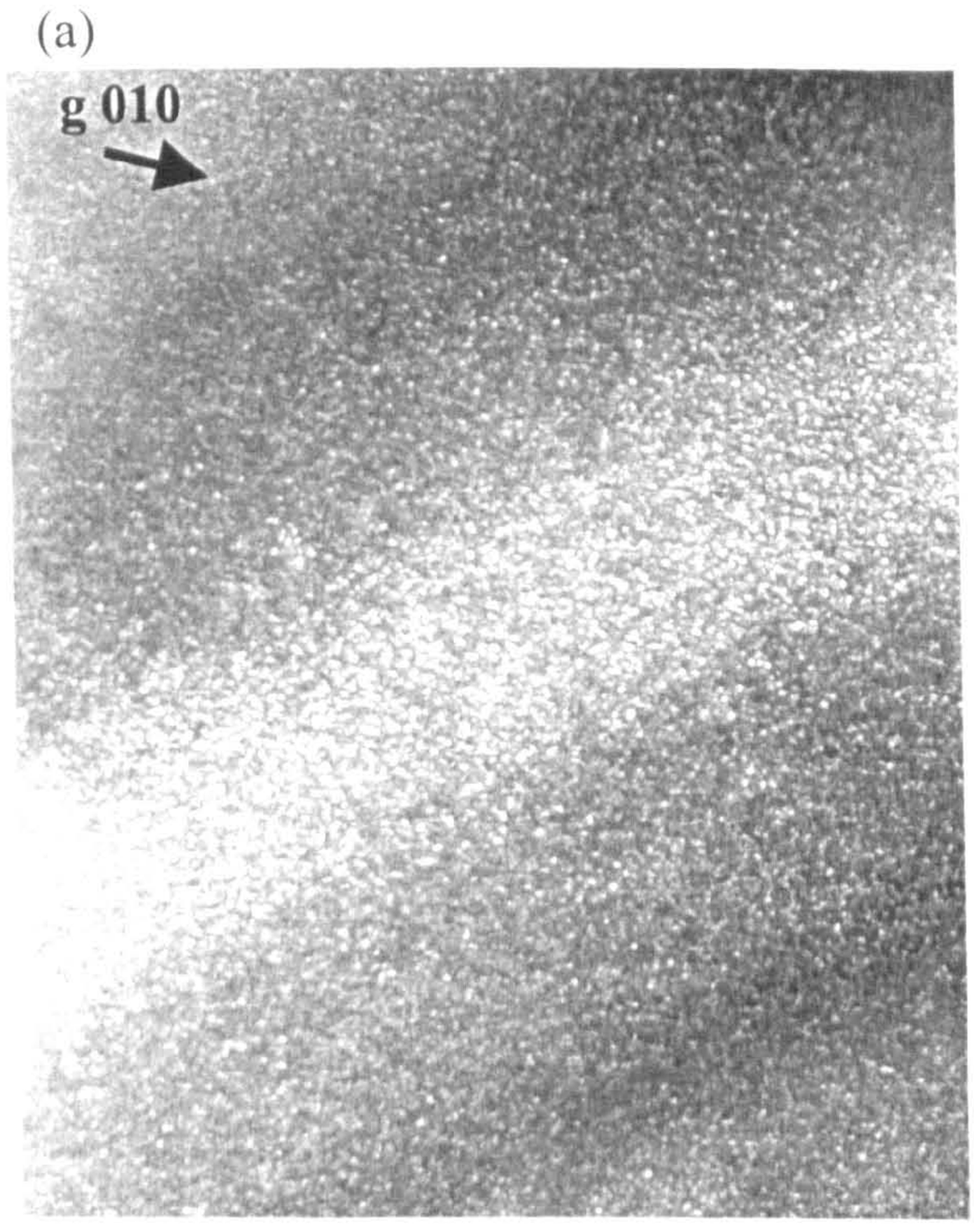

Figure 9.13 (a): TEM image of 1.7Li3.0Cu alloy after ageing for 1000h at 100°C. Zone axis <001>.

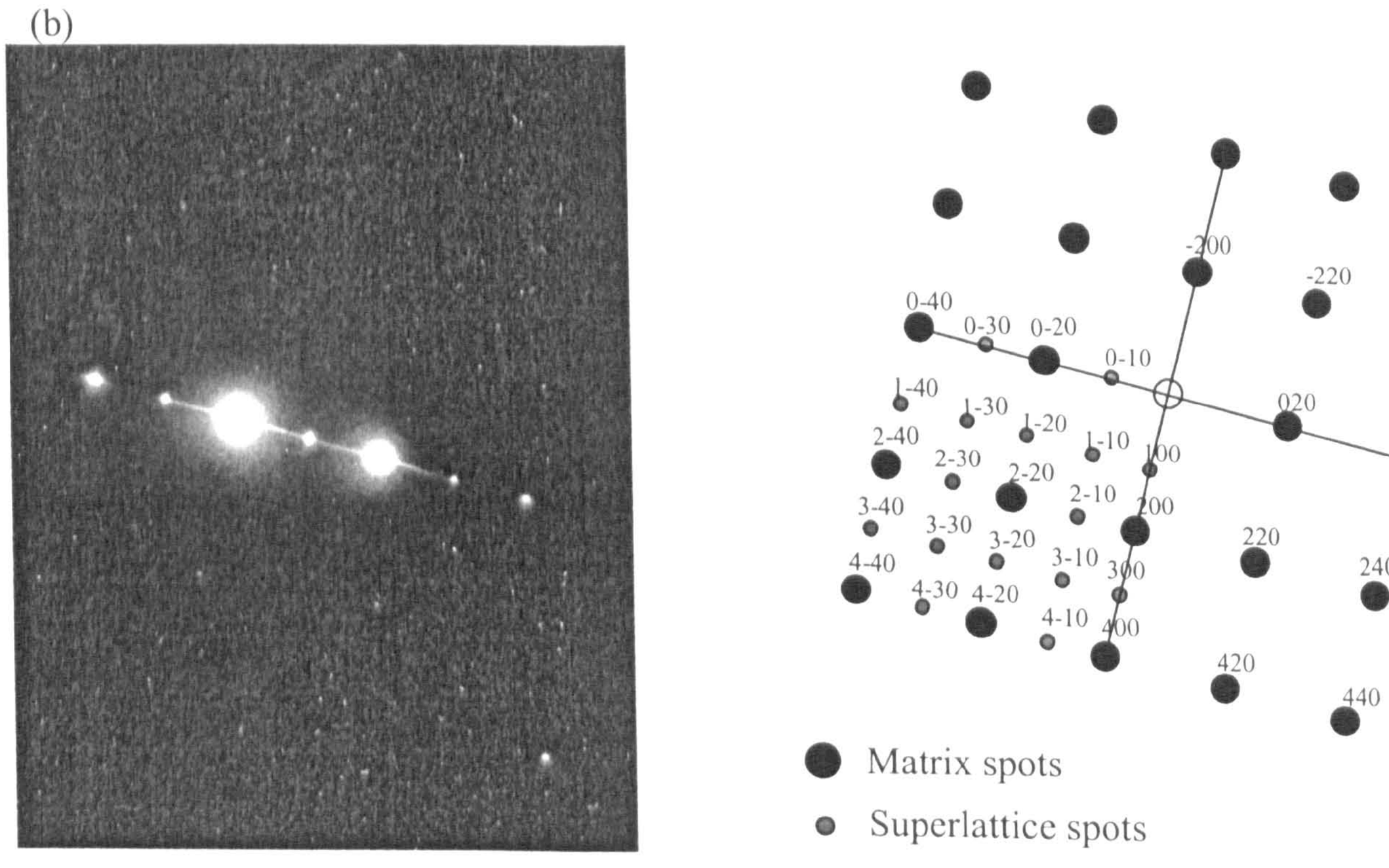

Figure 9.13 (b): SAD pattern of 1.7Li3.0Cu alloy after ageing for 1000h at 100°C. Zone axis <001>.

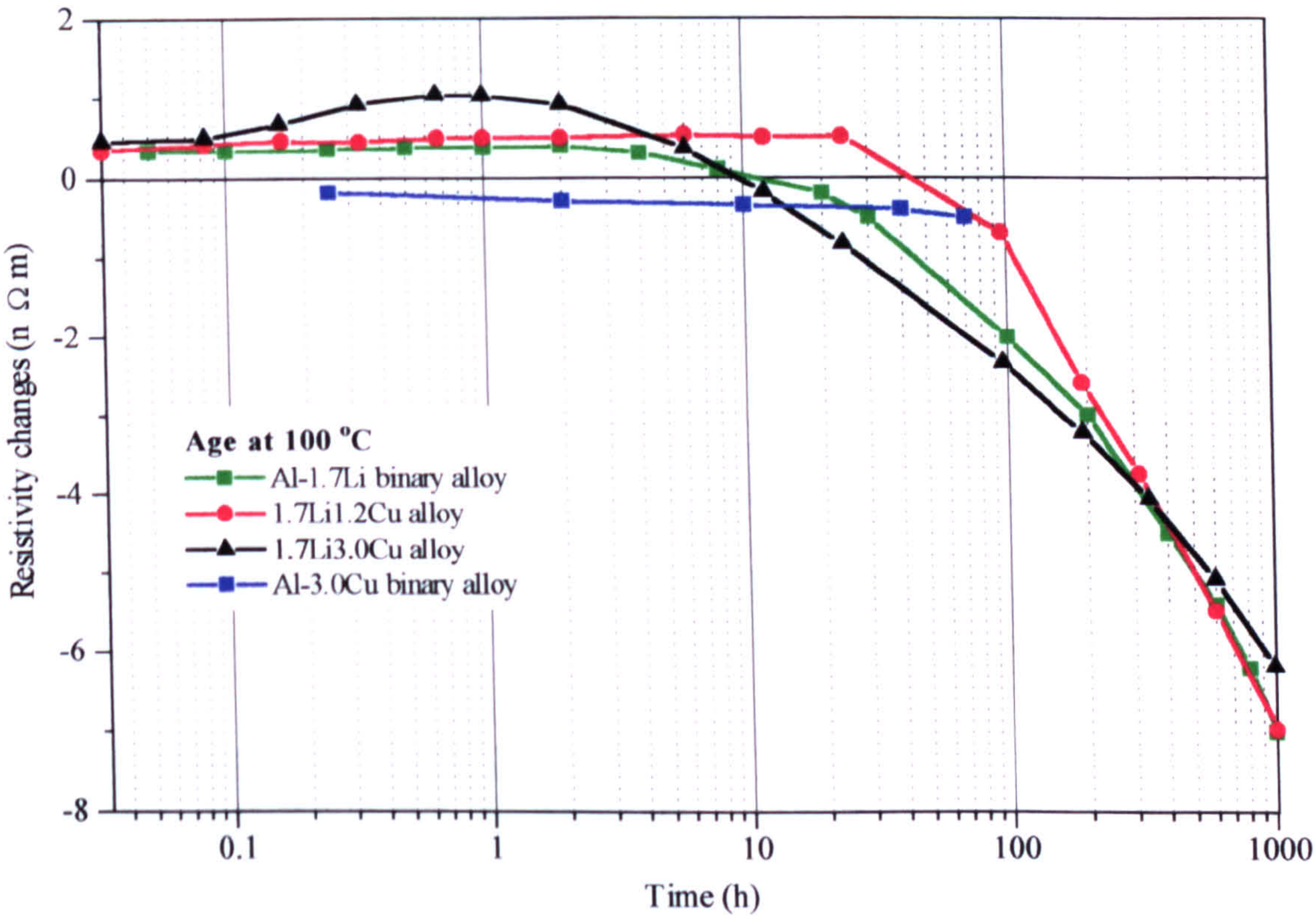

Figure 9.14: Isothermal resistivity changes during ageing at 100°C.

(a)

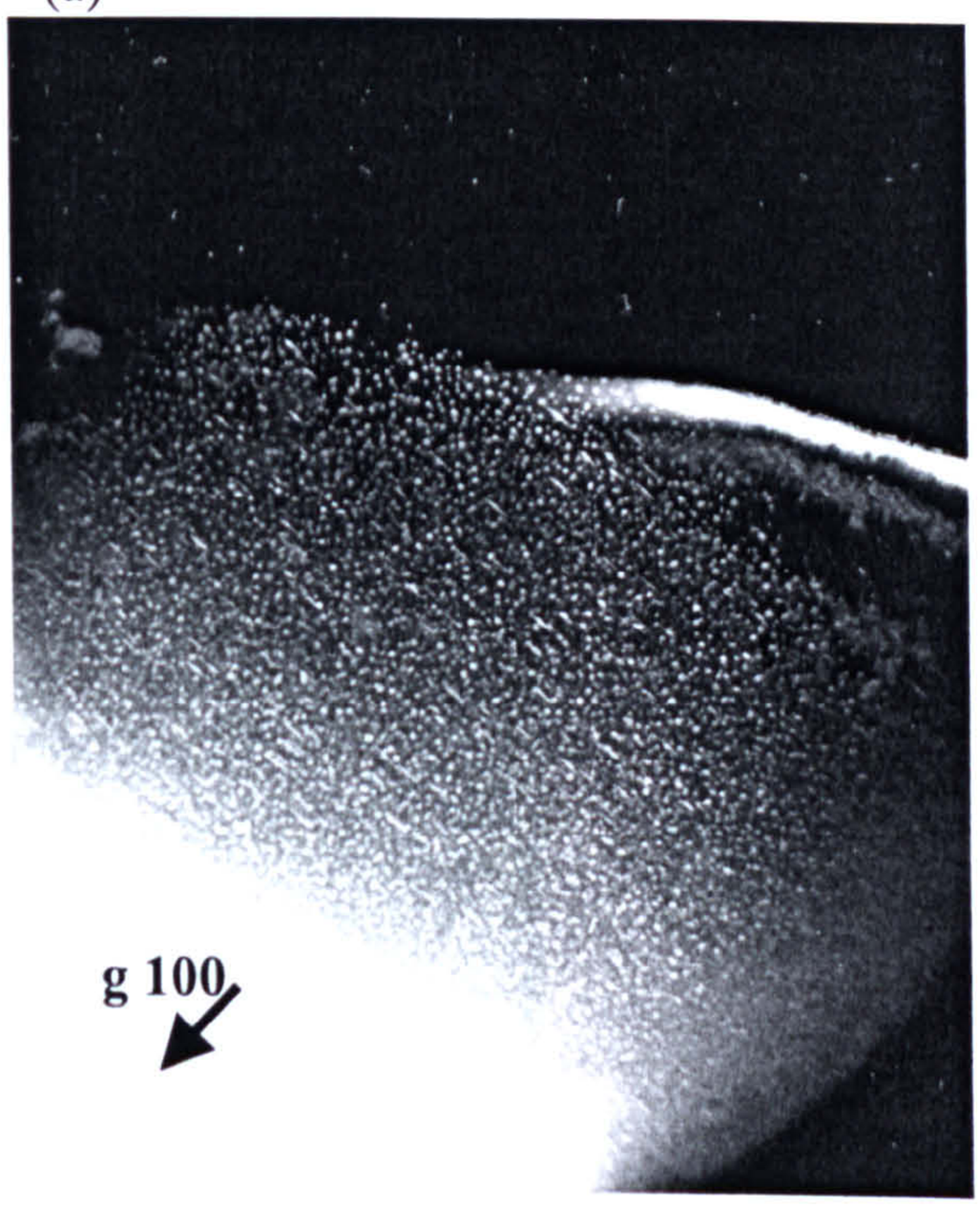

Figure 9.15 (a): TEM image of 1.7Li3.0Cu alloy after ageing for 48h at 130°C. Zone axis <011>.

(b)

Figure 9.15 (b): SAD pattern of 1.7Li3.0Cu alloy after ageing for 48h at 130°C. Zone axis <011>.

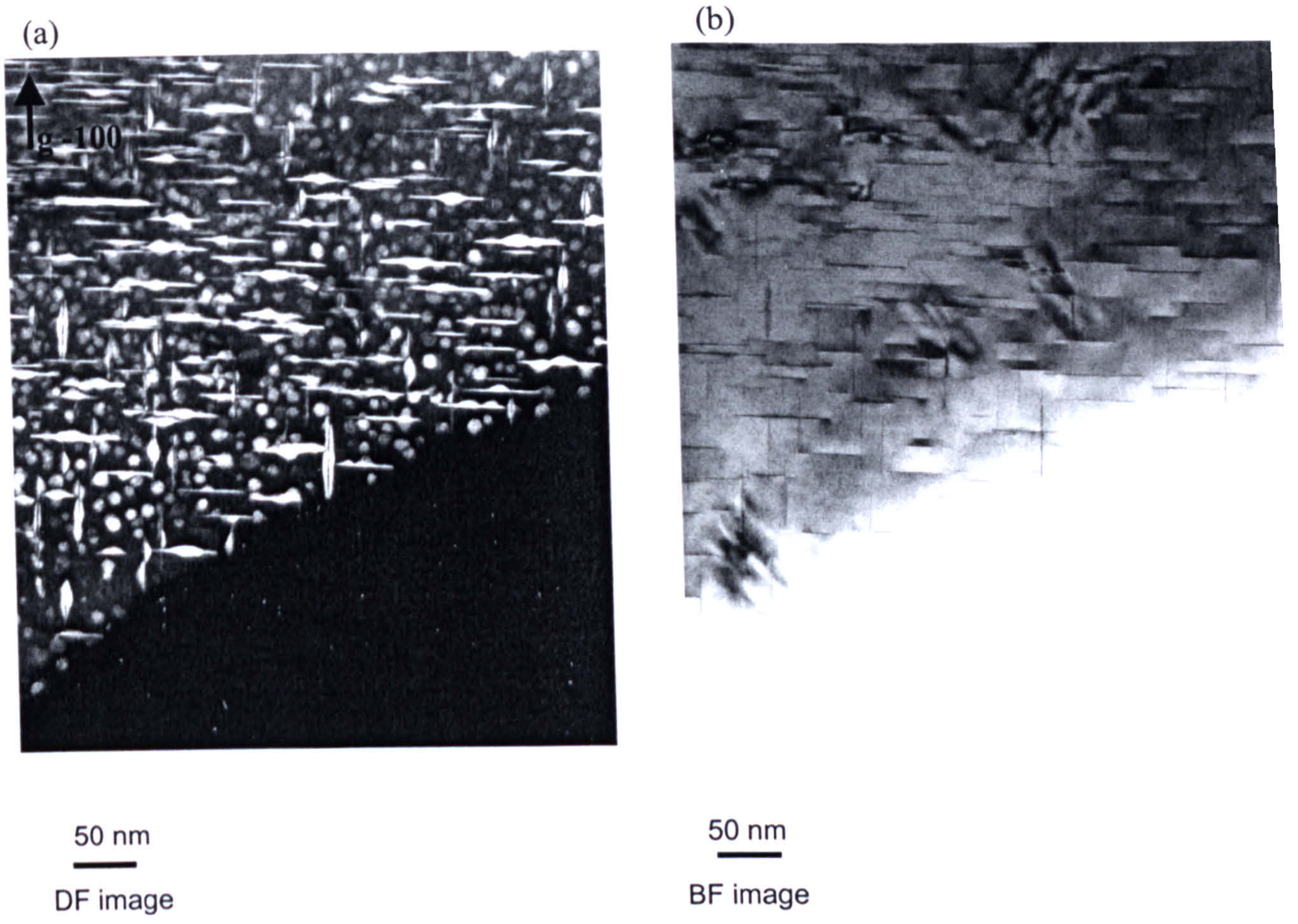

Figure 9.16 (a), (b): TEM image of 1.7Li3.0Cu alloy after ageing for 192h at 130°C. Zone axis <001>.

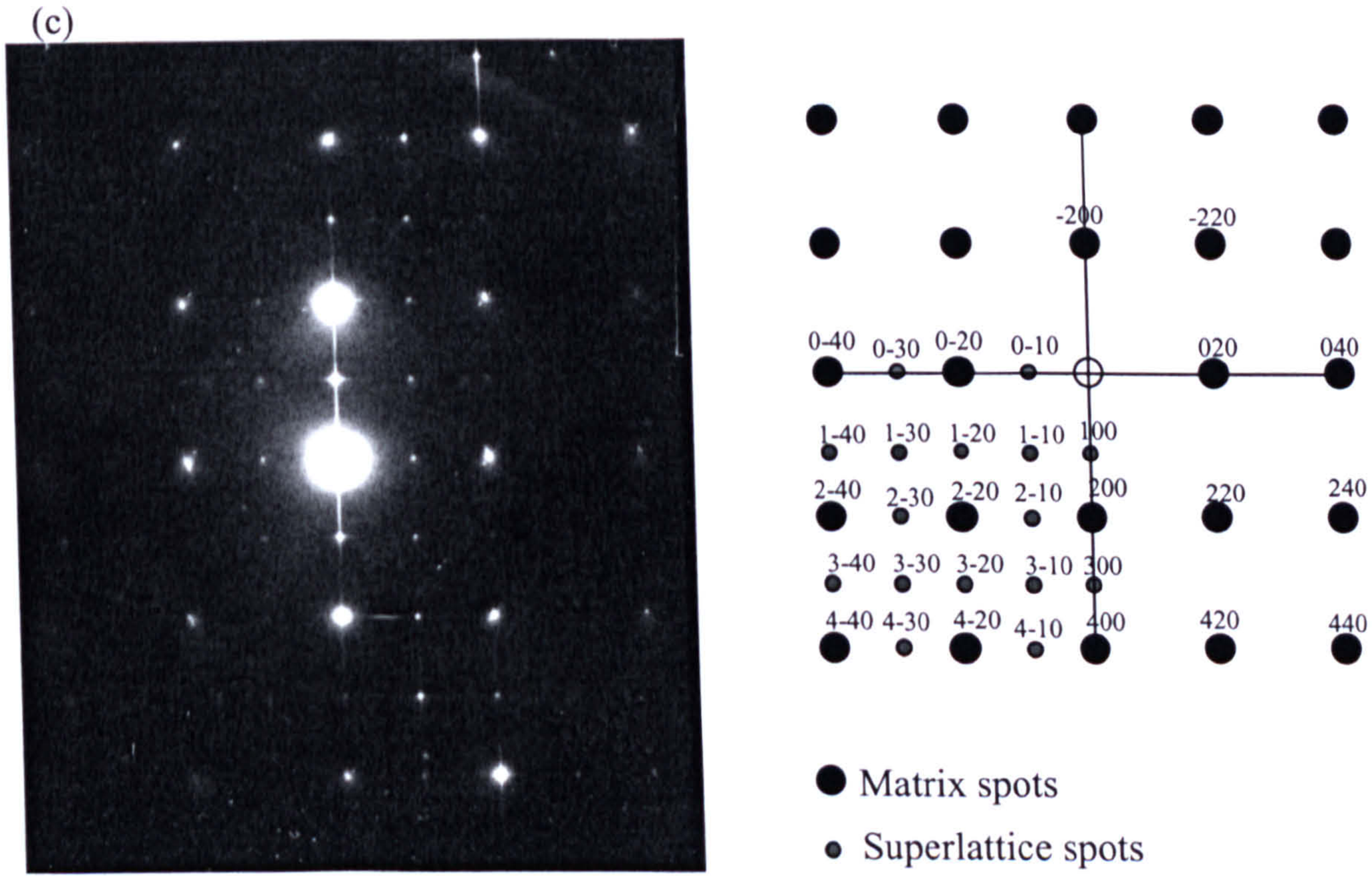

Figure 9.16 (c): SAD pattern of 1.7Li3.0Cu alloy after ageing for 192h at 130°C. Zone axis <001>.

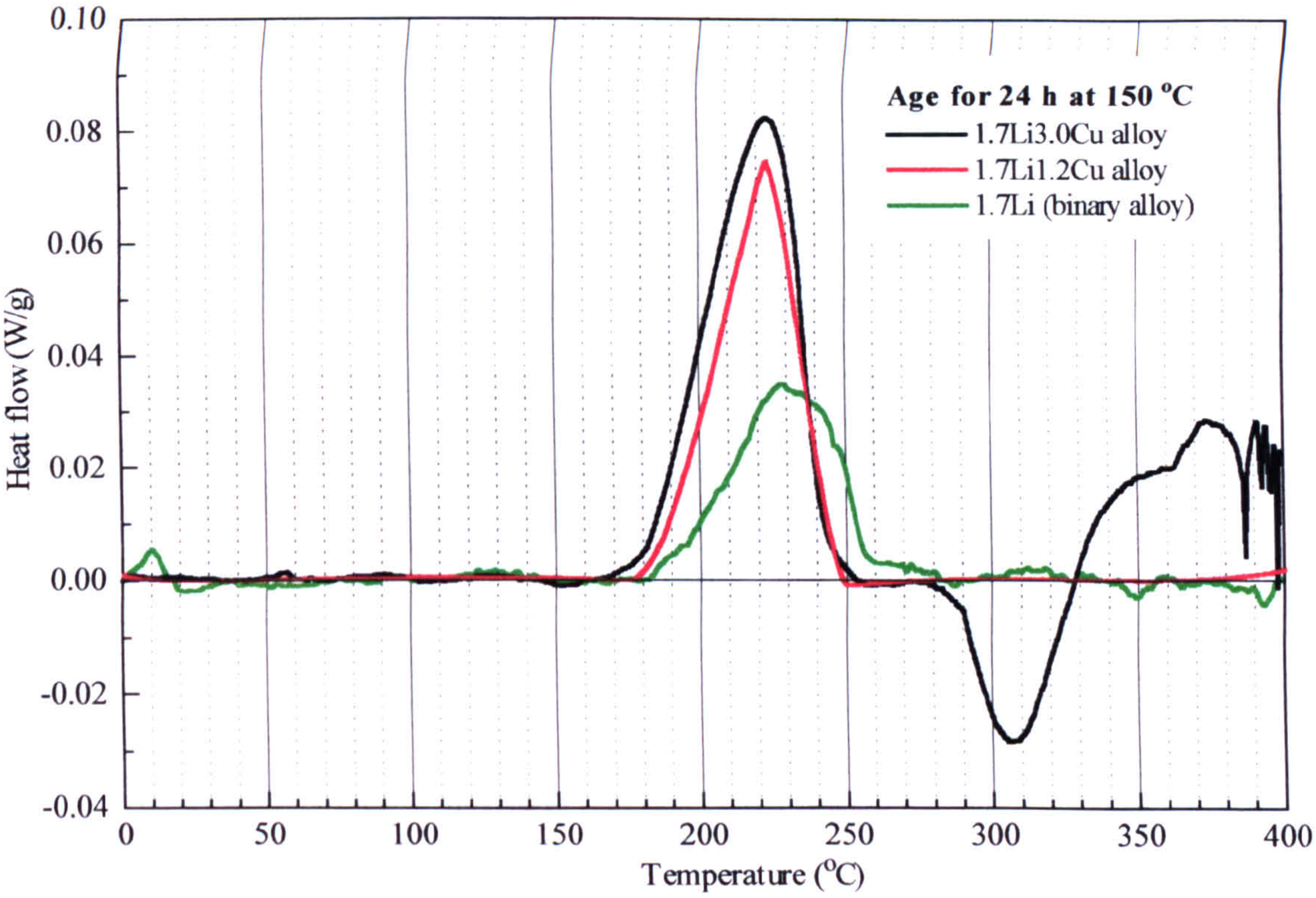

Figure 9.17: DSC comparative plots of alloys aged at 150°C for 24h.

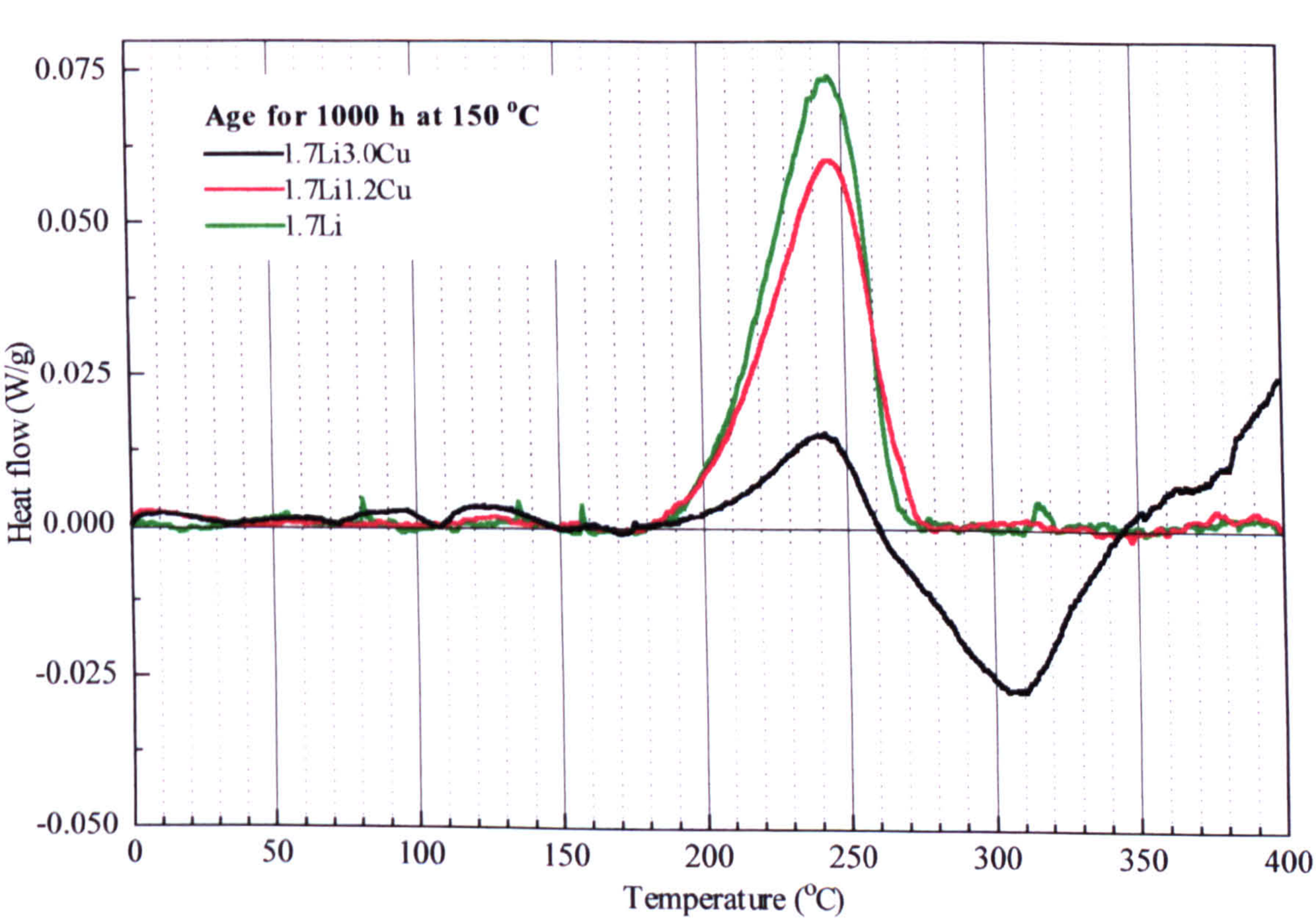

Figure 9.18:DSC comparative plots of alloys aged at150°C for 1000h.

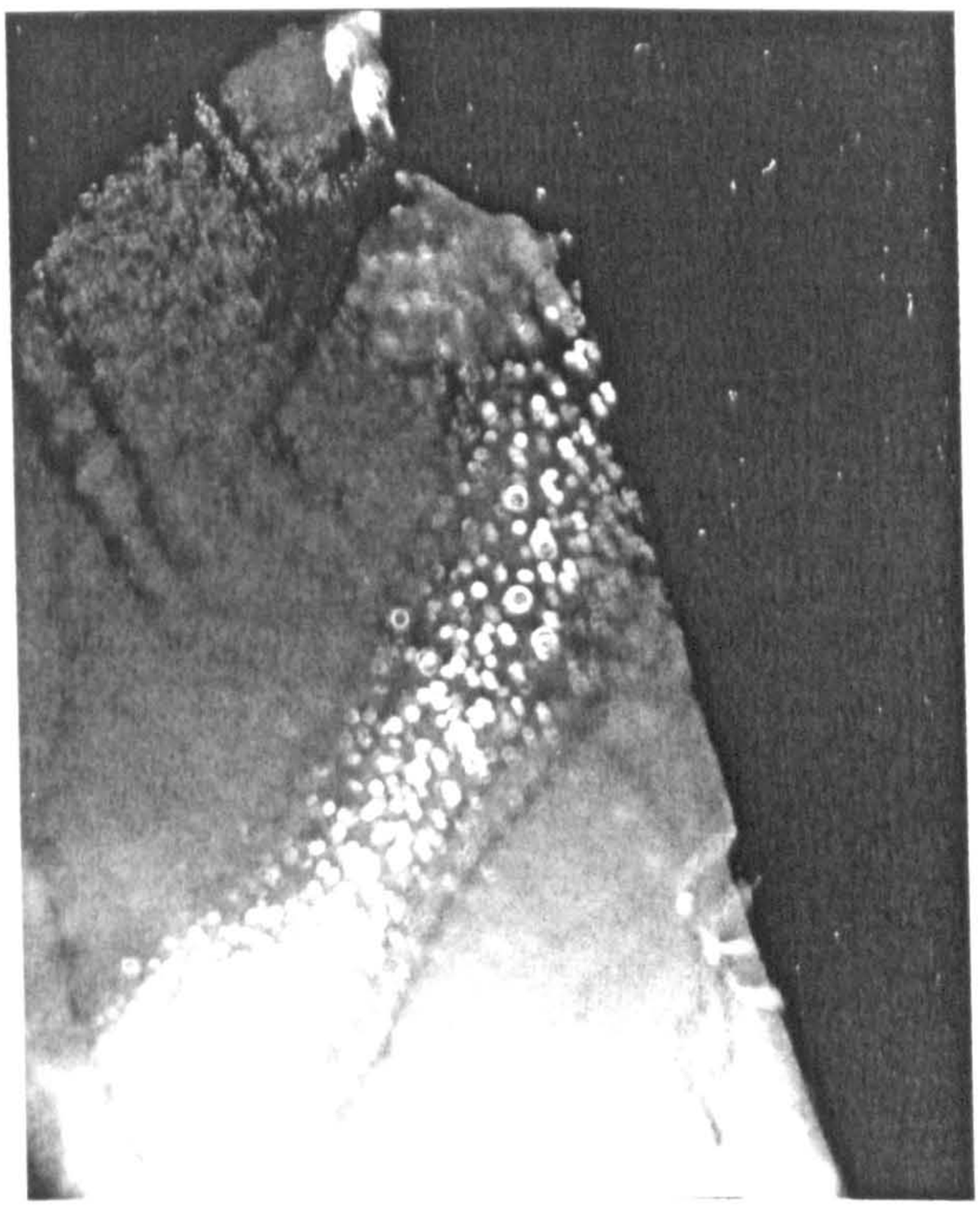

Figure 9.19: TEM image of 1.7Li1.2Cu alloy after ageing for 24h at 150°C. Zone axis <011>.

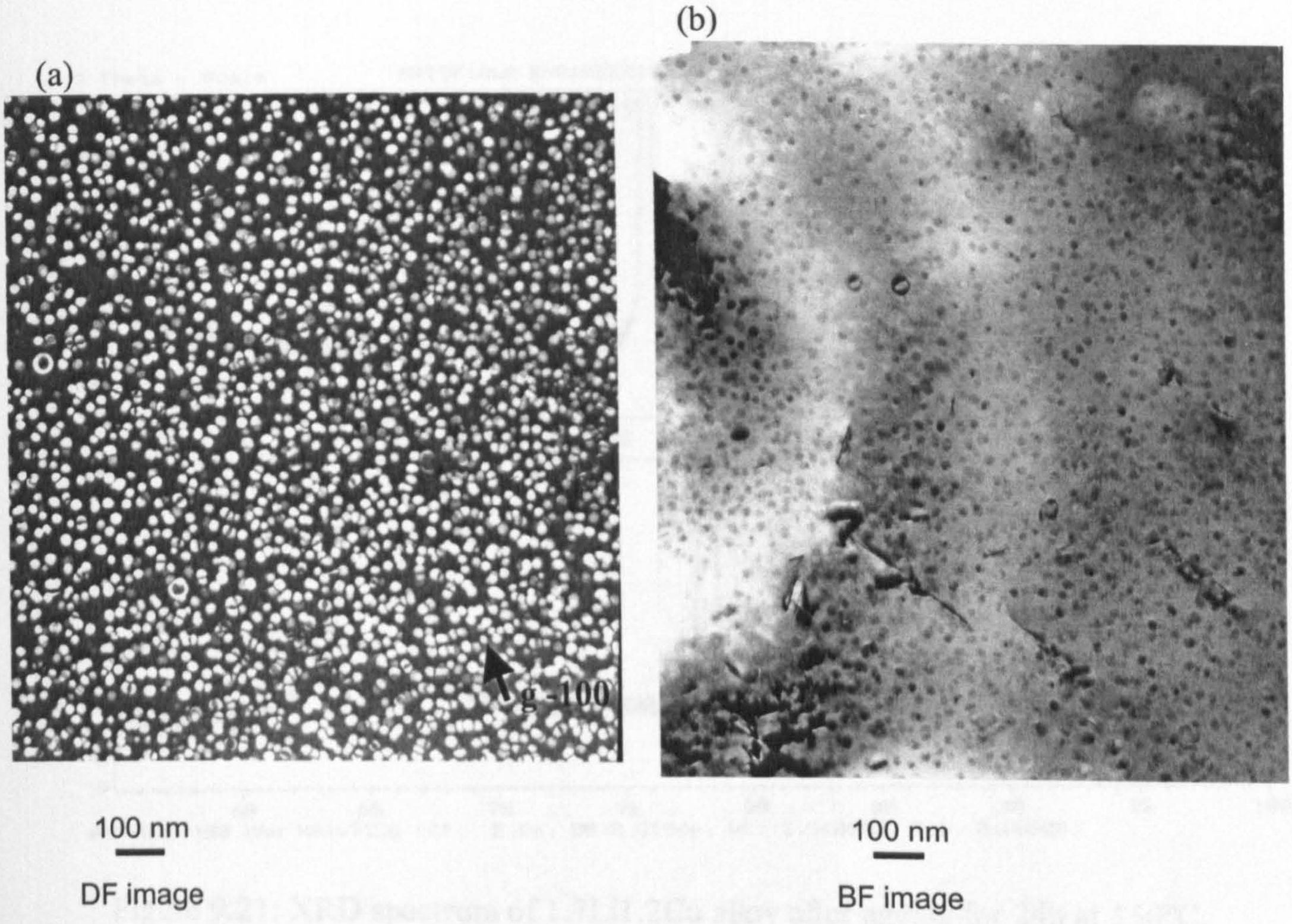

Figure 9.20 (a, b): TEM image of 1.7Li3.0Cu alloy after ageing for 24h at 150°C. Zone axis <011>.

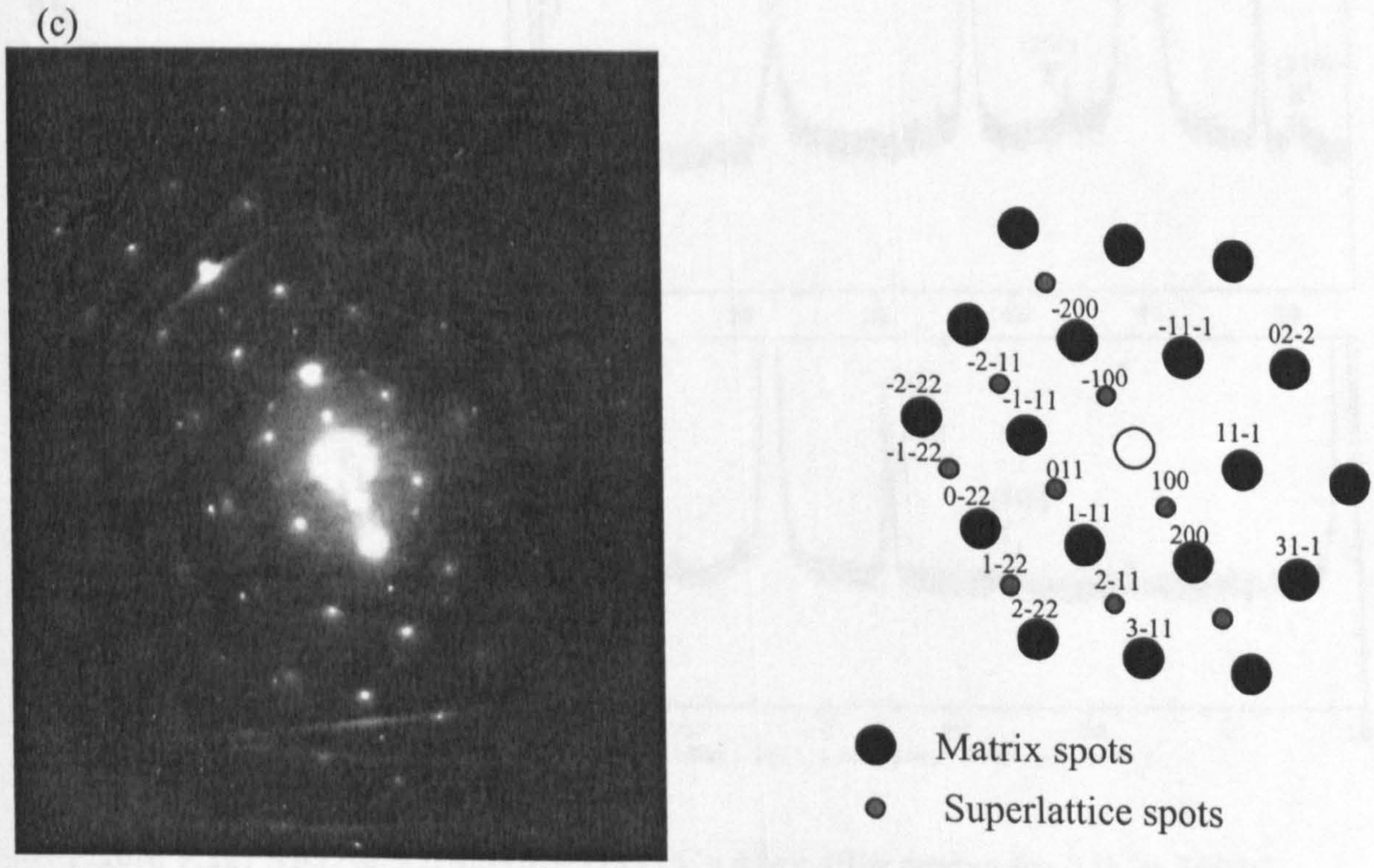

Figure 9.20 (c): SAD pattern of 1.7Li3.0Cu alloy after ageing for 24h at 150°C. Zone axis <011>.

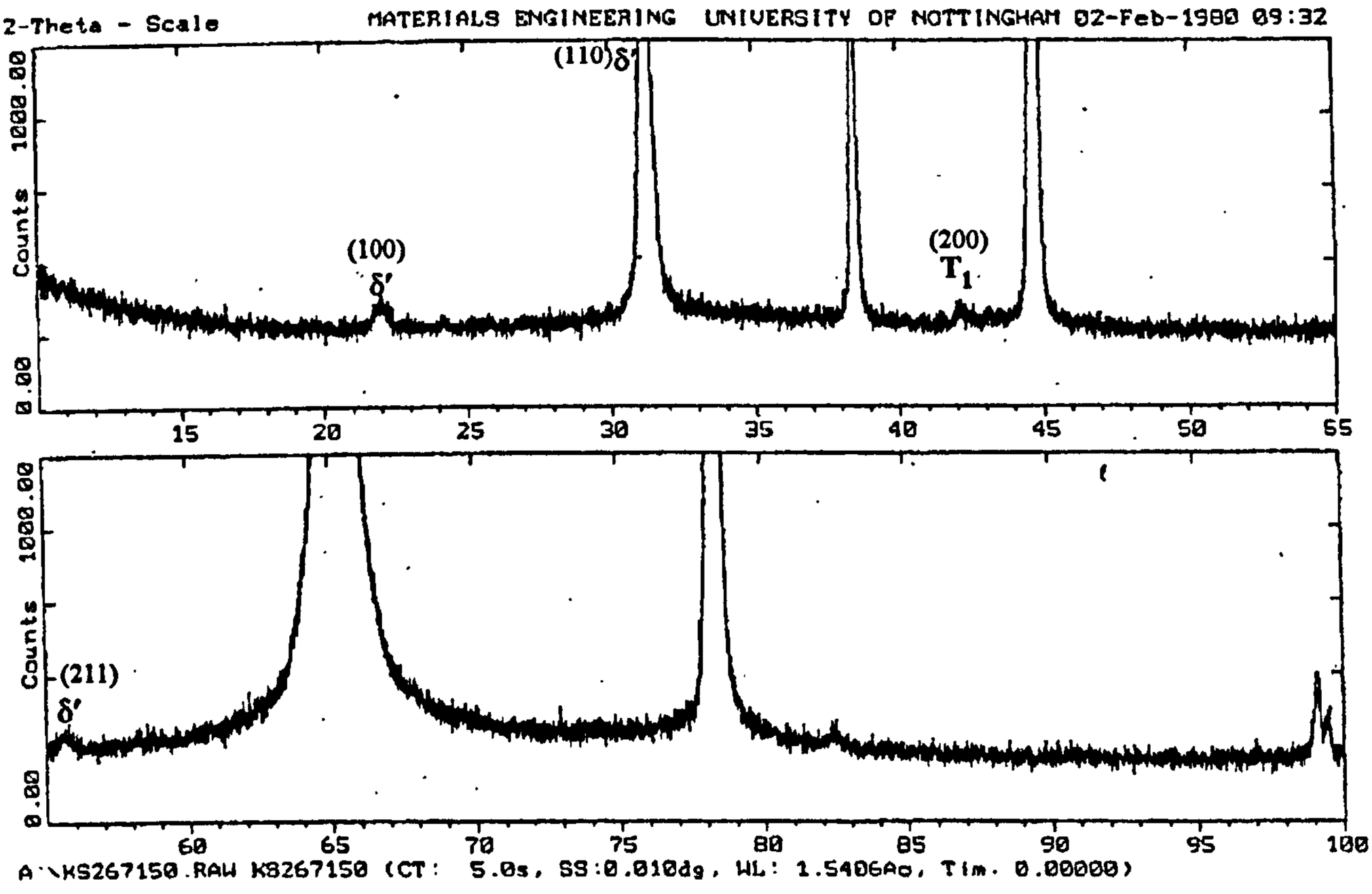

Figure 9.21: XRD spectrum of 1.7Li1.2Cu alloy after ageing for 24h at 150°C.

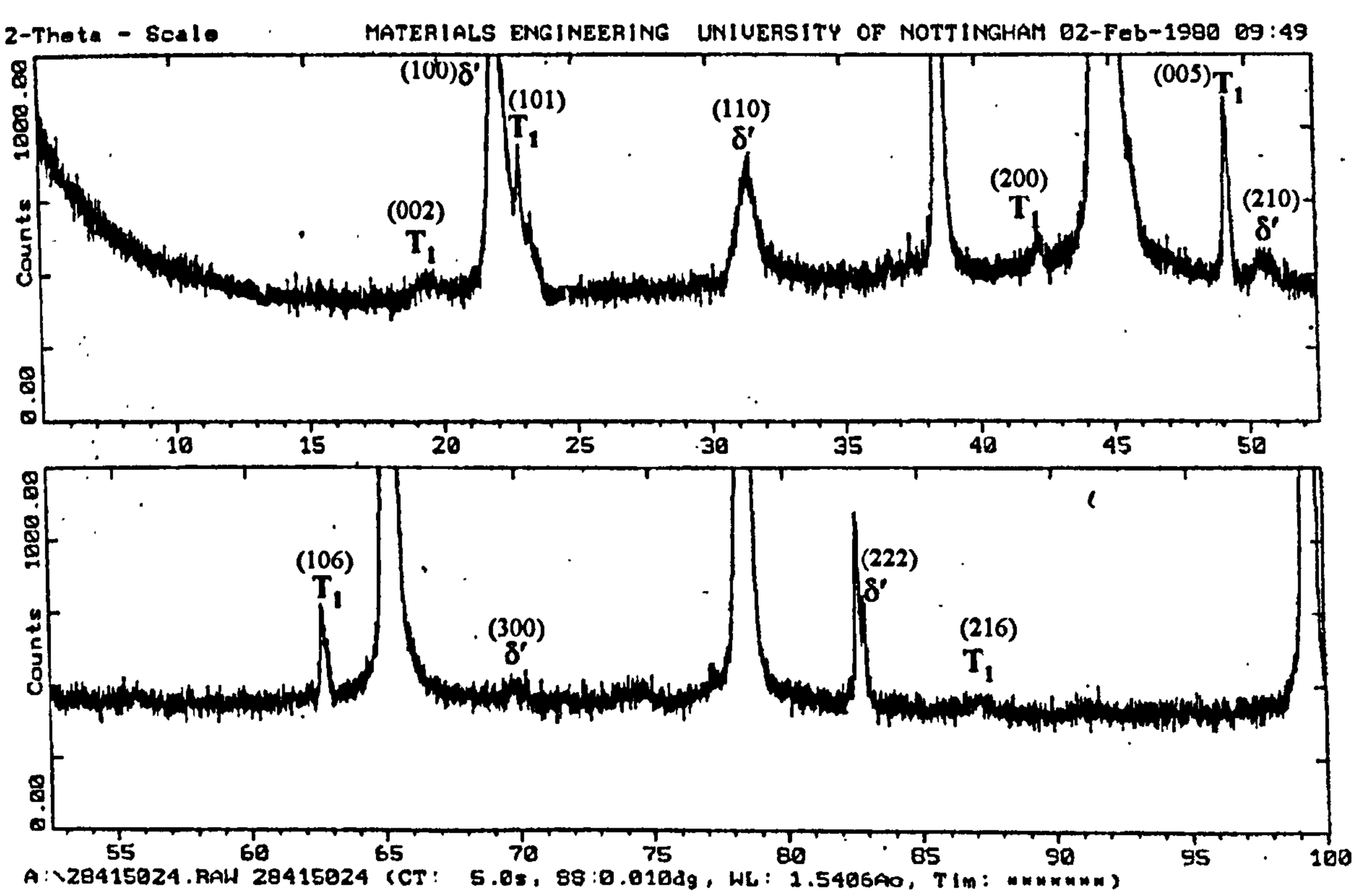

Figure 9.22: XRD spectrum of 1.7Li3.0Cu alloy after ageing for 24h at 150°C.

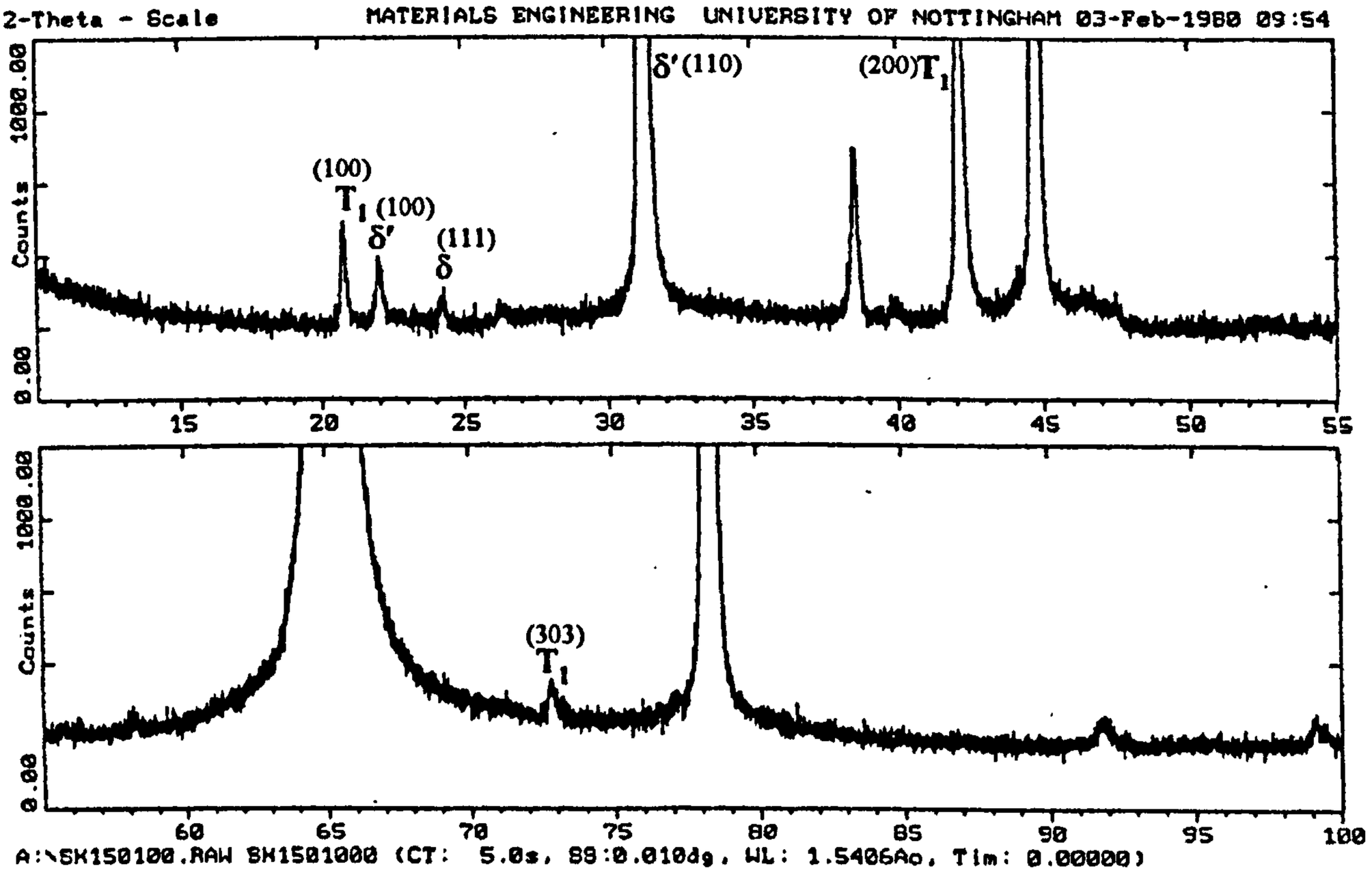

Figure 9.23: XRD spectrum of 1.7Li1.2Cu alloy after ageing for 1000h at 150°C.

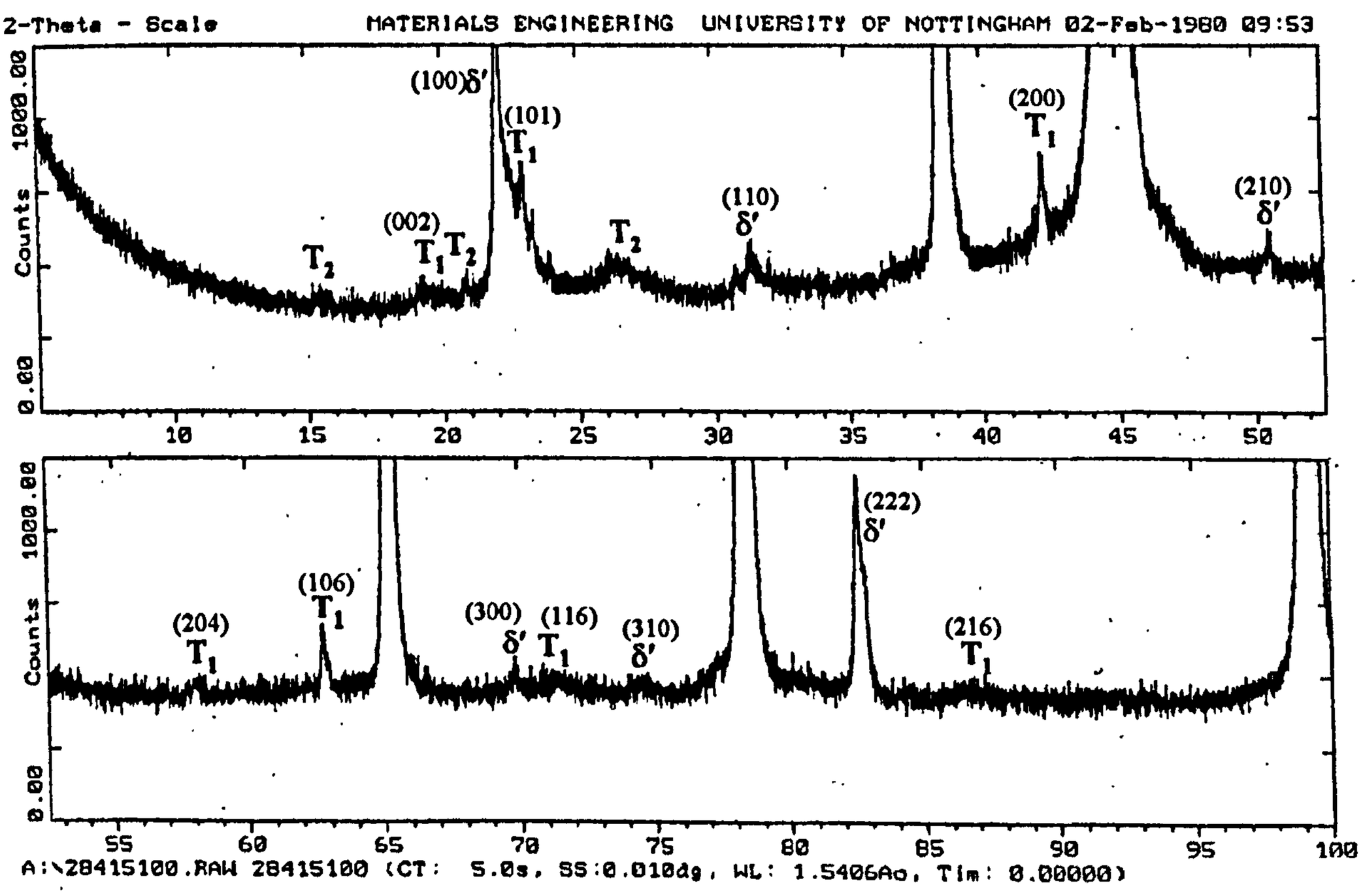

Figure 9.24: XRD spectrum of 1.7Li3.0Cu alloy after ageing for 1000h at 150°C.

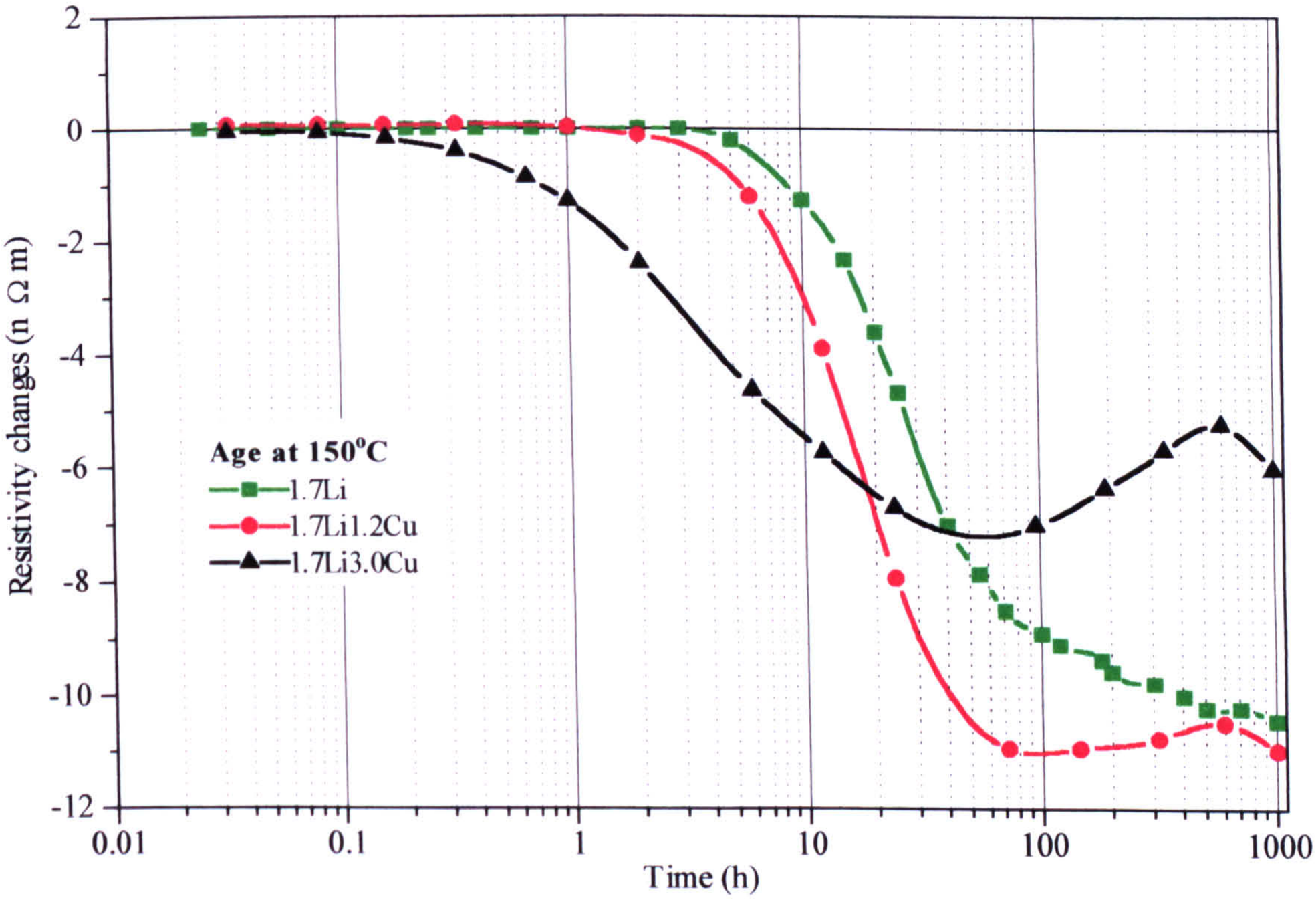

Figure.9.25: Isothermal resistivity changes during ageing at 150°C

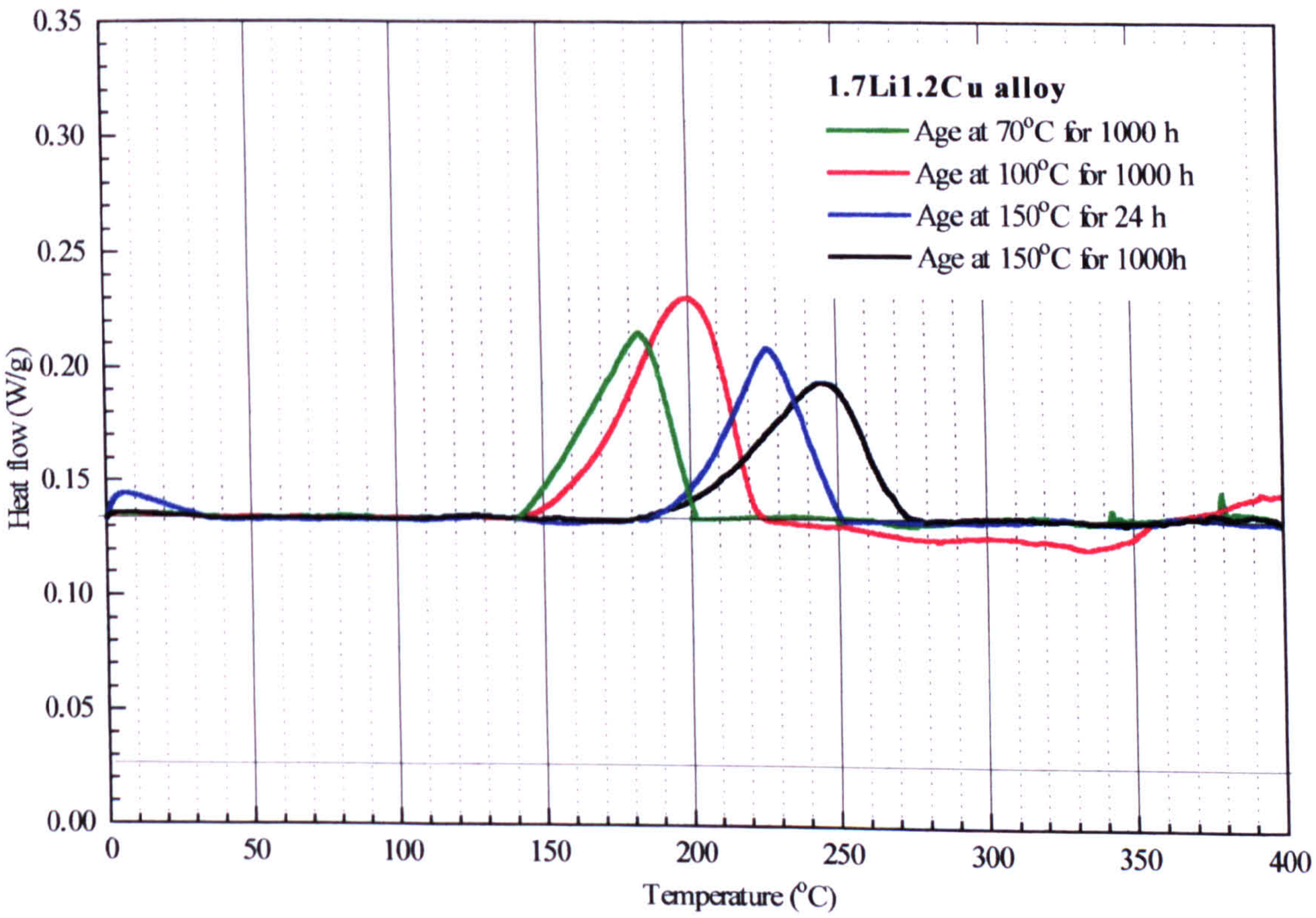

.Figure.9.26: Effect of the ageing temperature on the DSC thermogram. of an 1.7Li1.2Cu alloy.

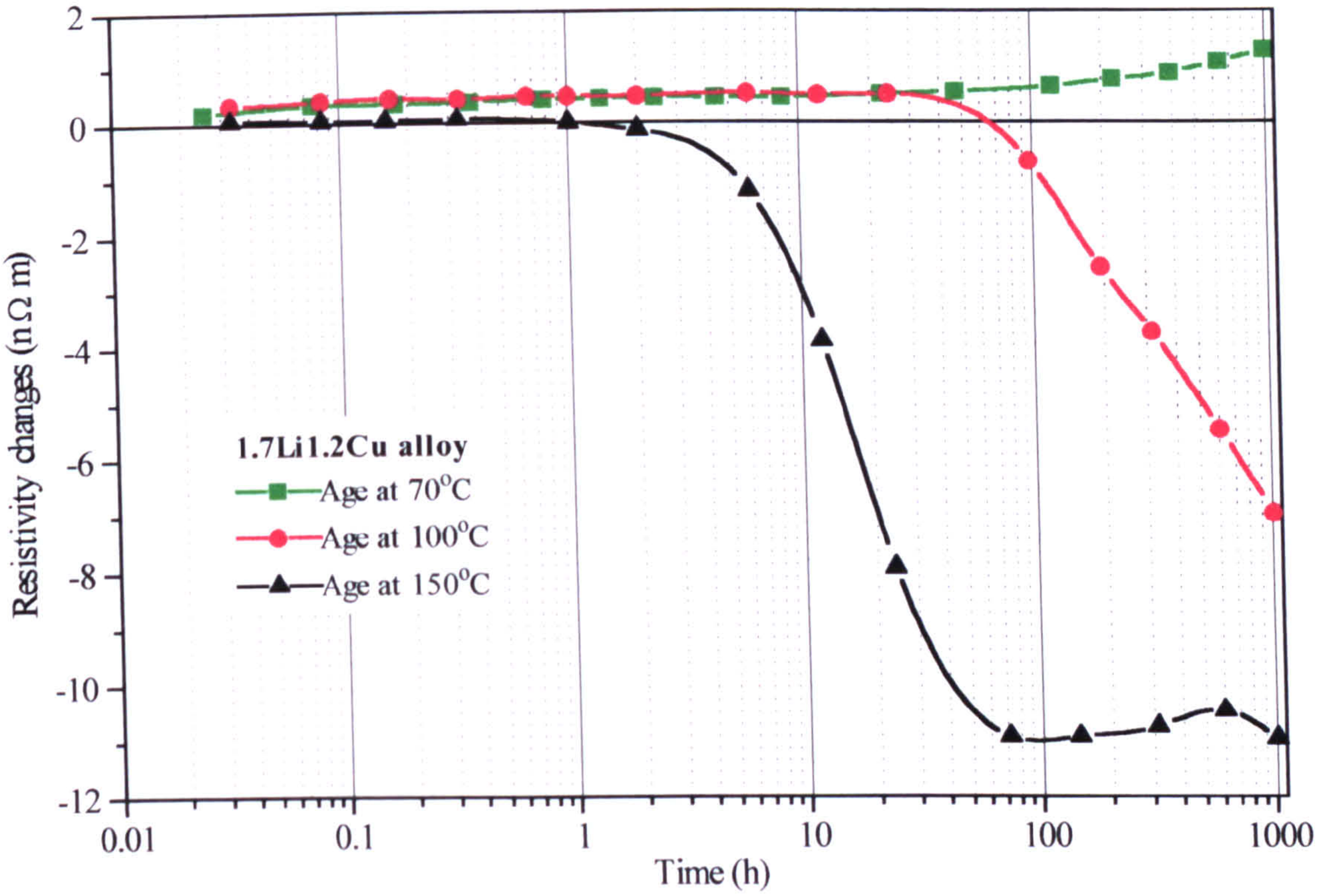

Figure.9.27: Effect of the ageing temperature on the resistivity of an 1.7Li1.2Cu alloy.

Figure.9.28: Effect of the ageing temperature on the DSC thermogram of an1.7Li3.0Cu alloy.

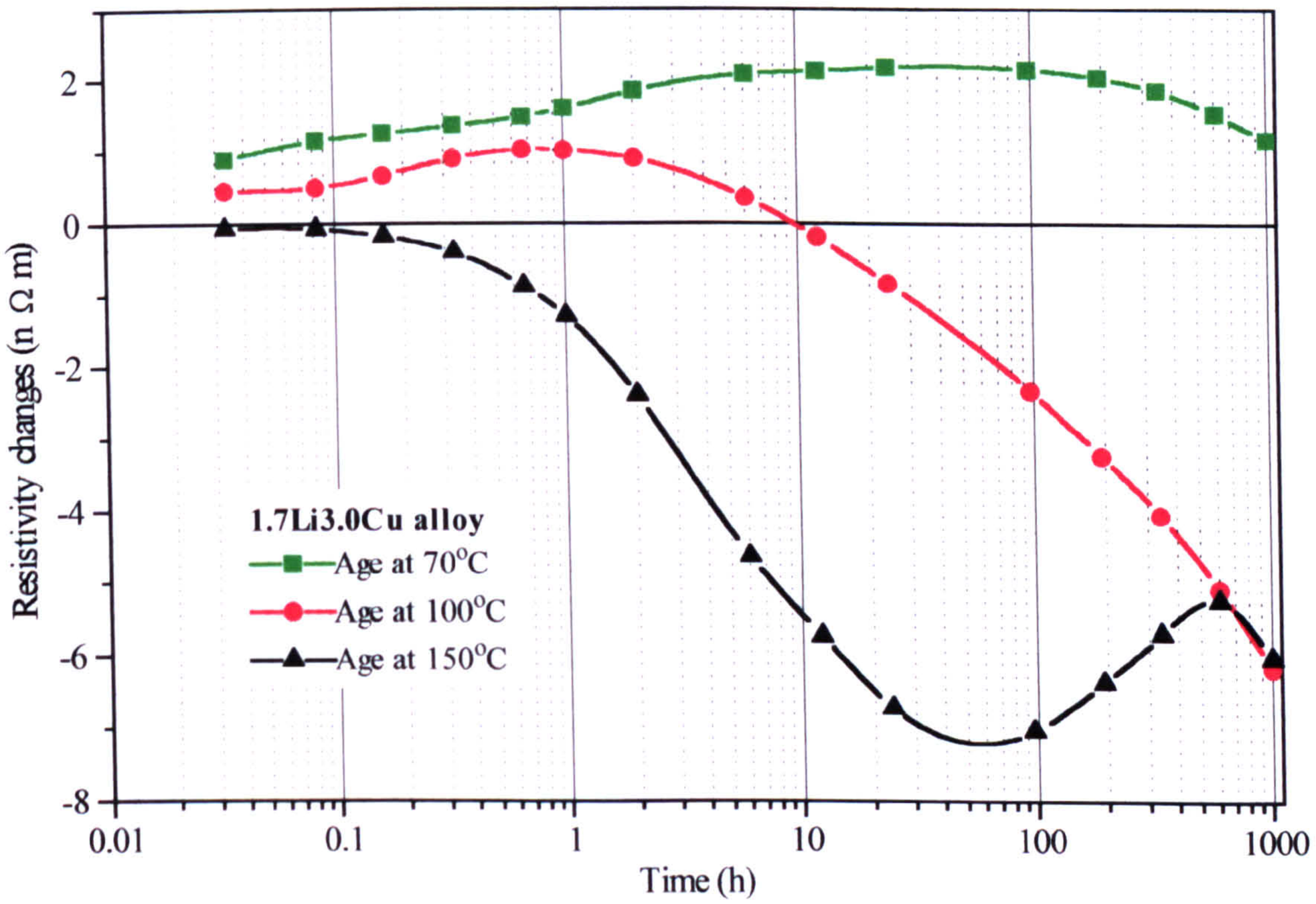

Figure.9.29: Effect of ageing temperature on the resistivity of an 1.7Li3.0Cu

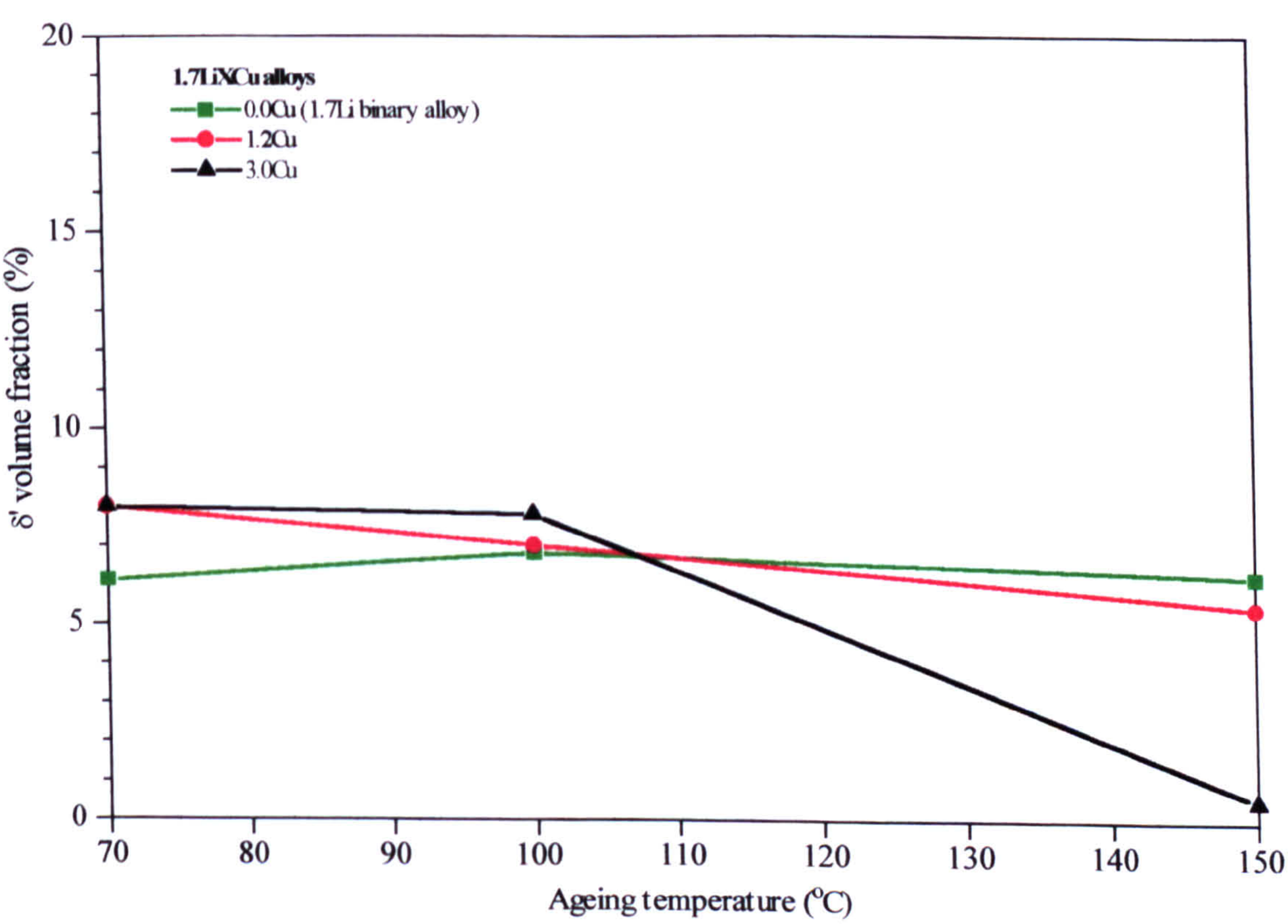

Figure 9.30: Effect of copper concentration and ageing temperature on the δ′ volume fraction.

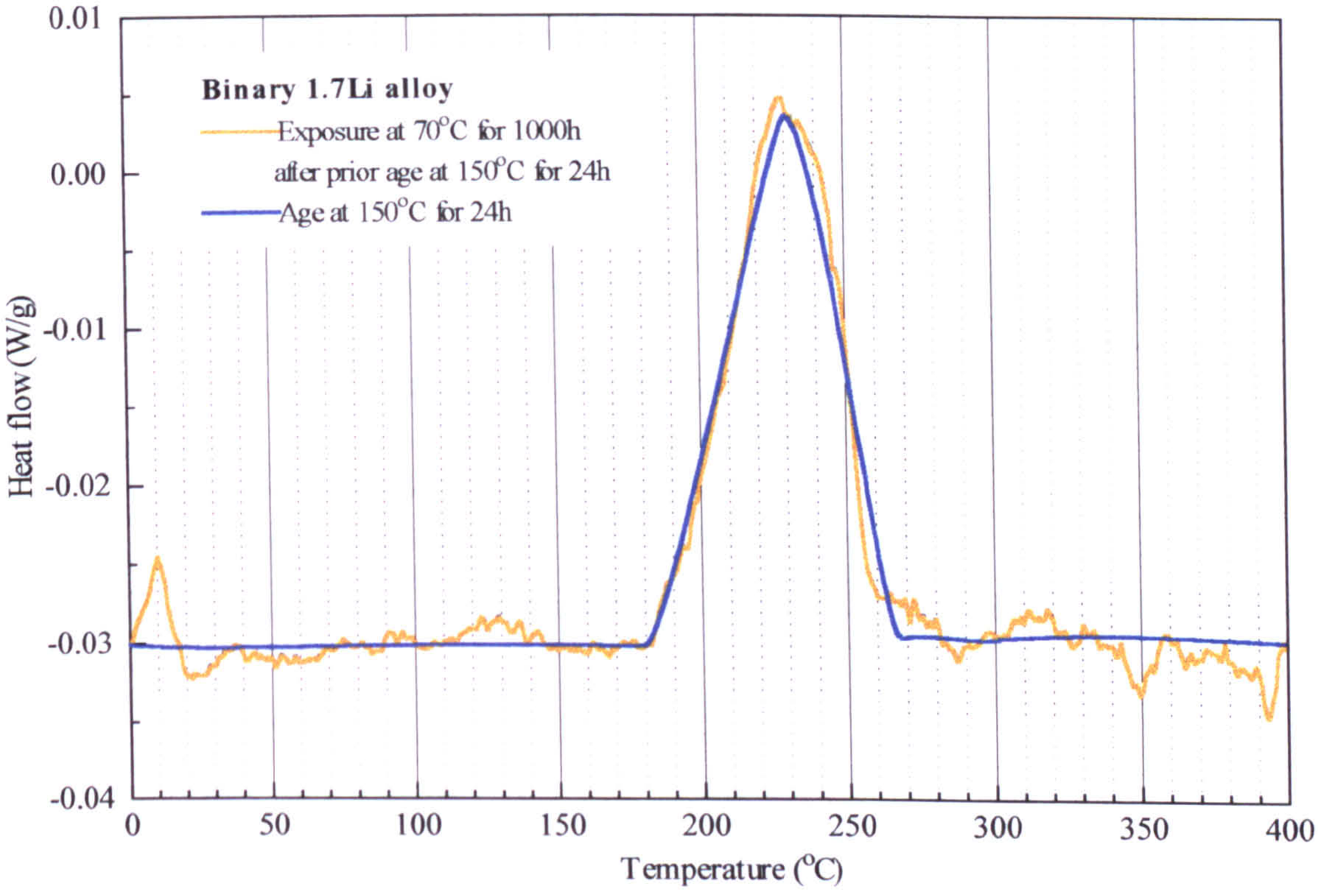

Figure 9.31: Effect of exposure on the 1.7Li binary alloy.

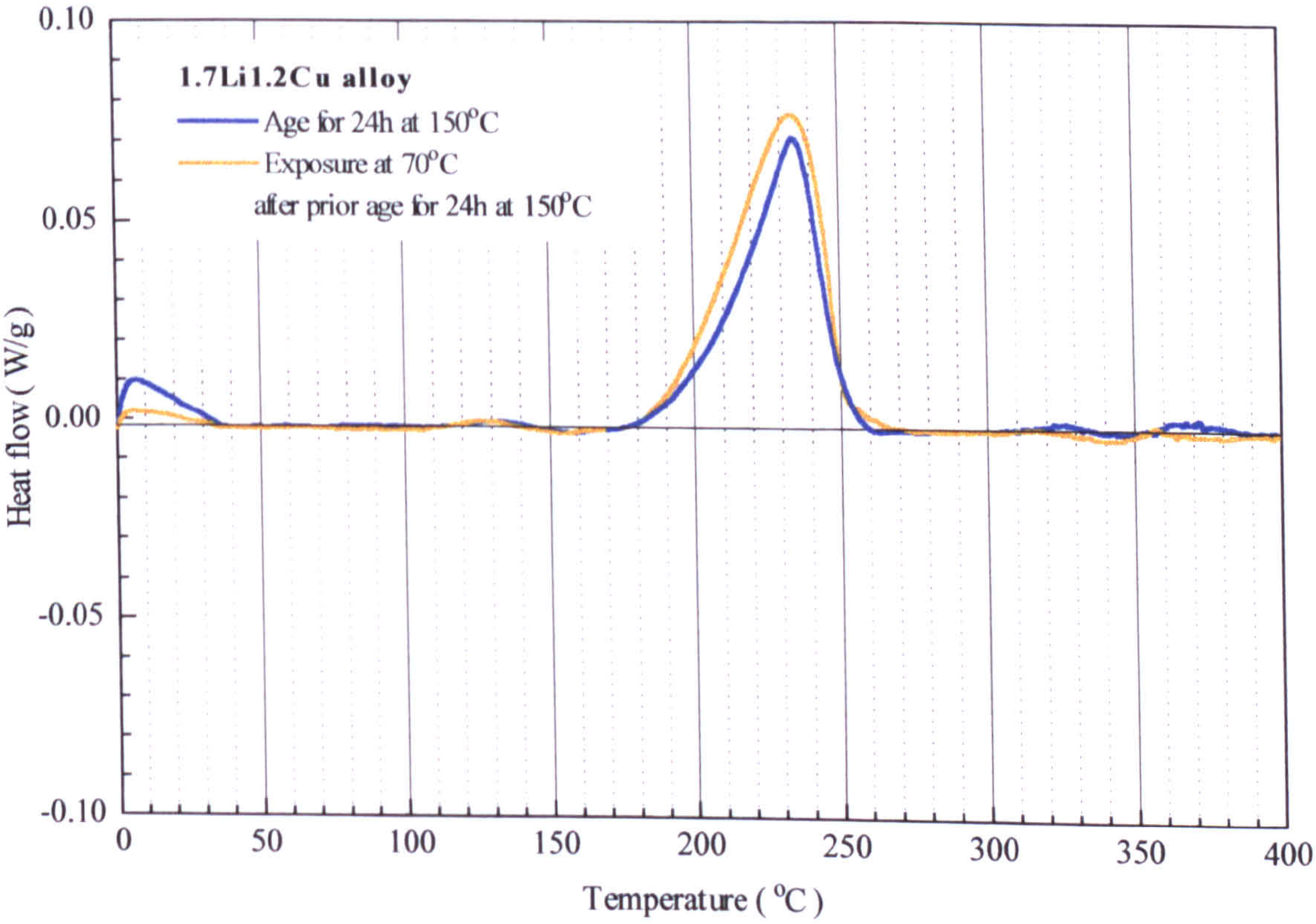

Figure.9.32: Effect of exposure on the 1.7Li1.2Cu alloy.

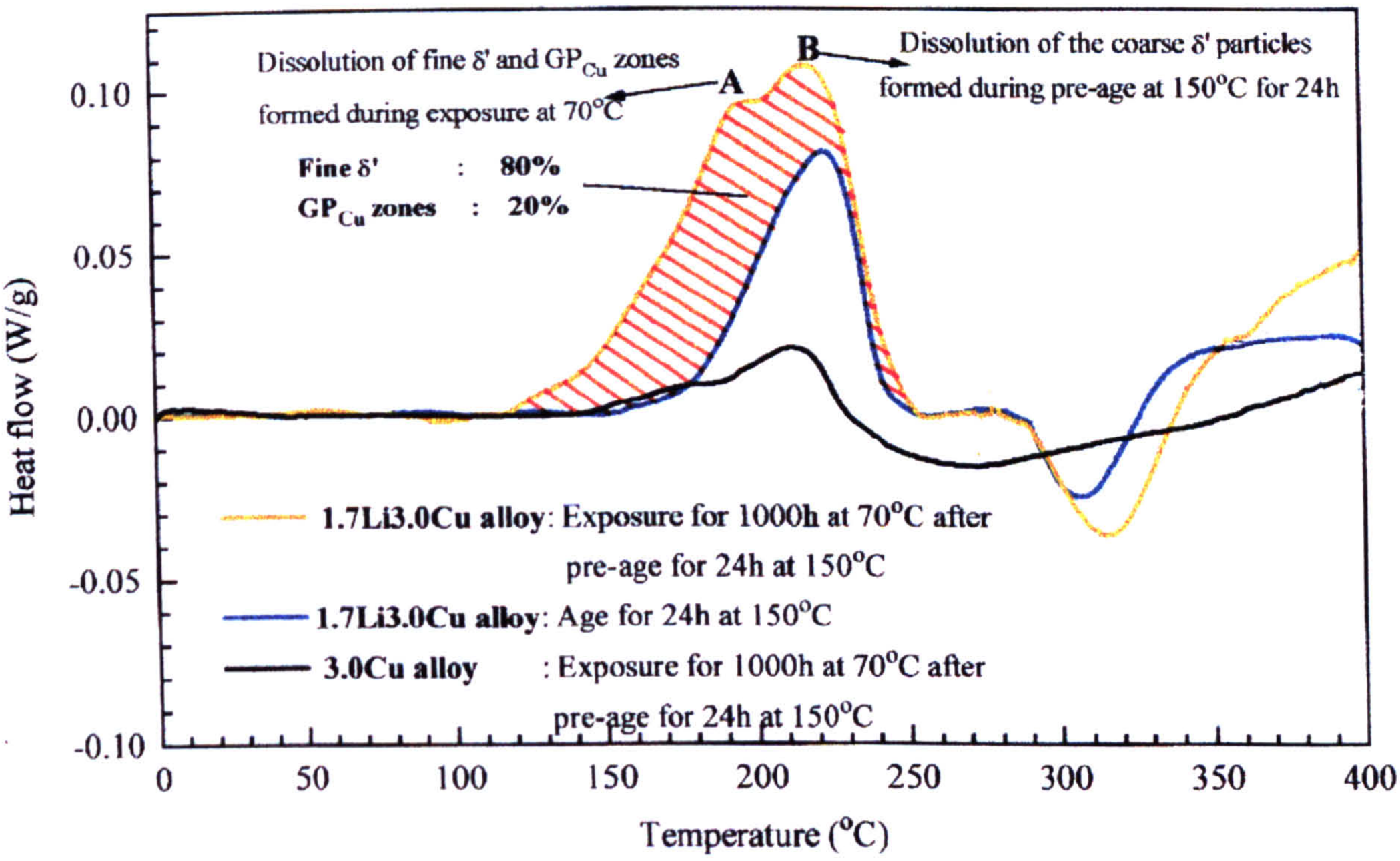

Figure.9.33: Effect of exposure on the 1.7Li3.0Cu alloy.

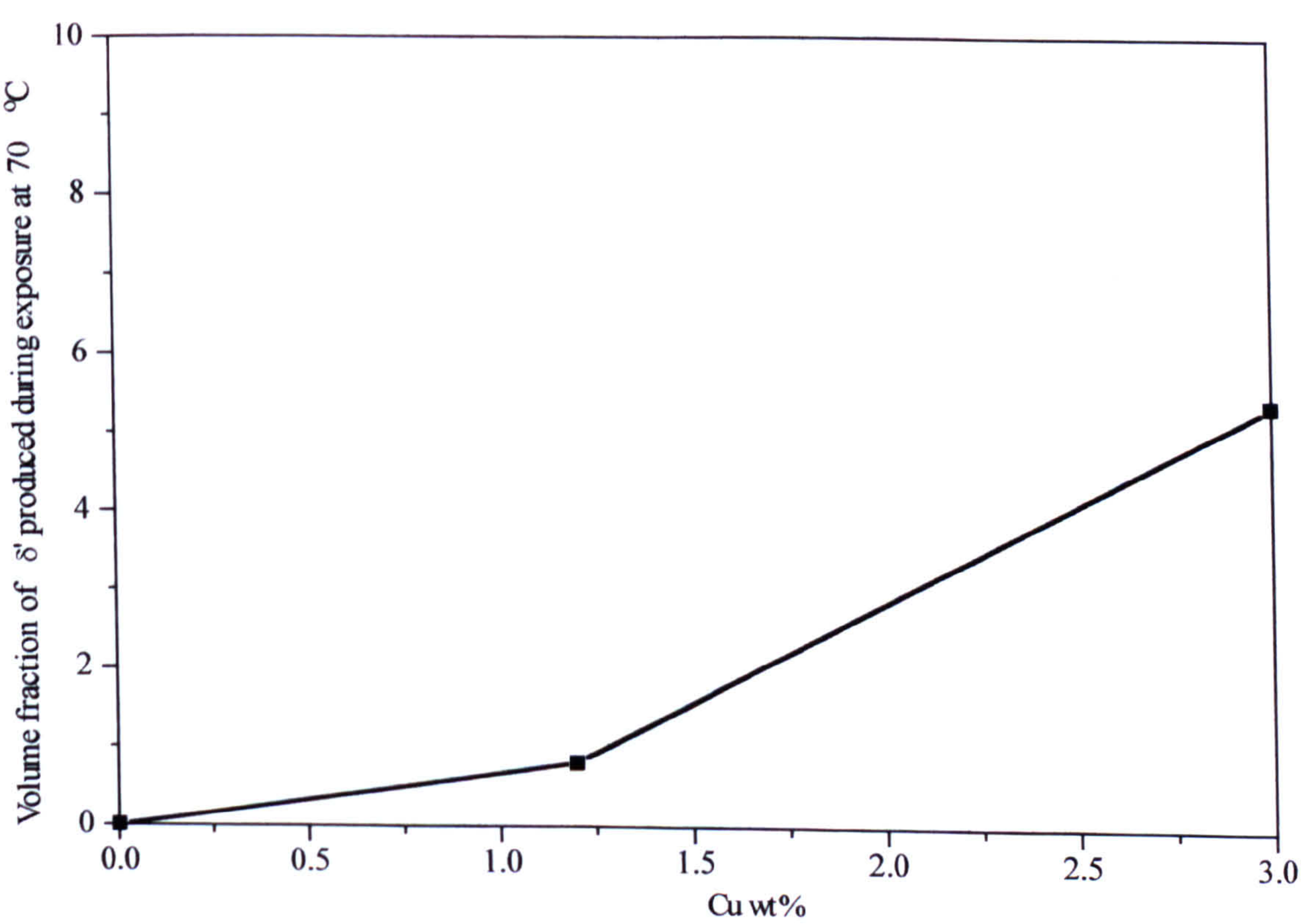

Figure 9.34: Volume fraction of δ′ produced by exposure at 70°C in alloys with different copper contents.

(a)

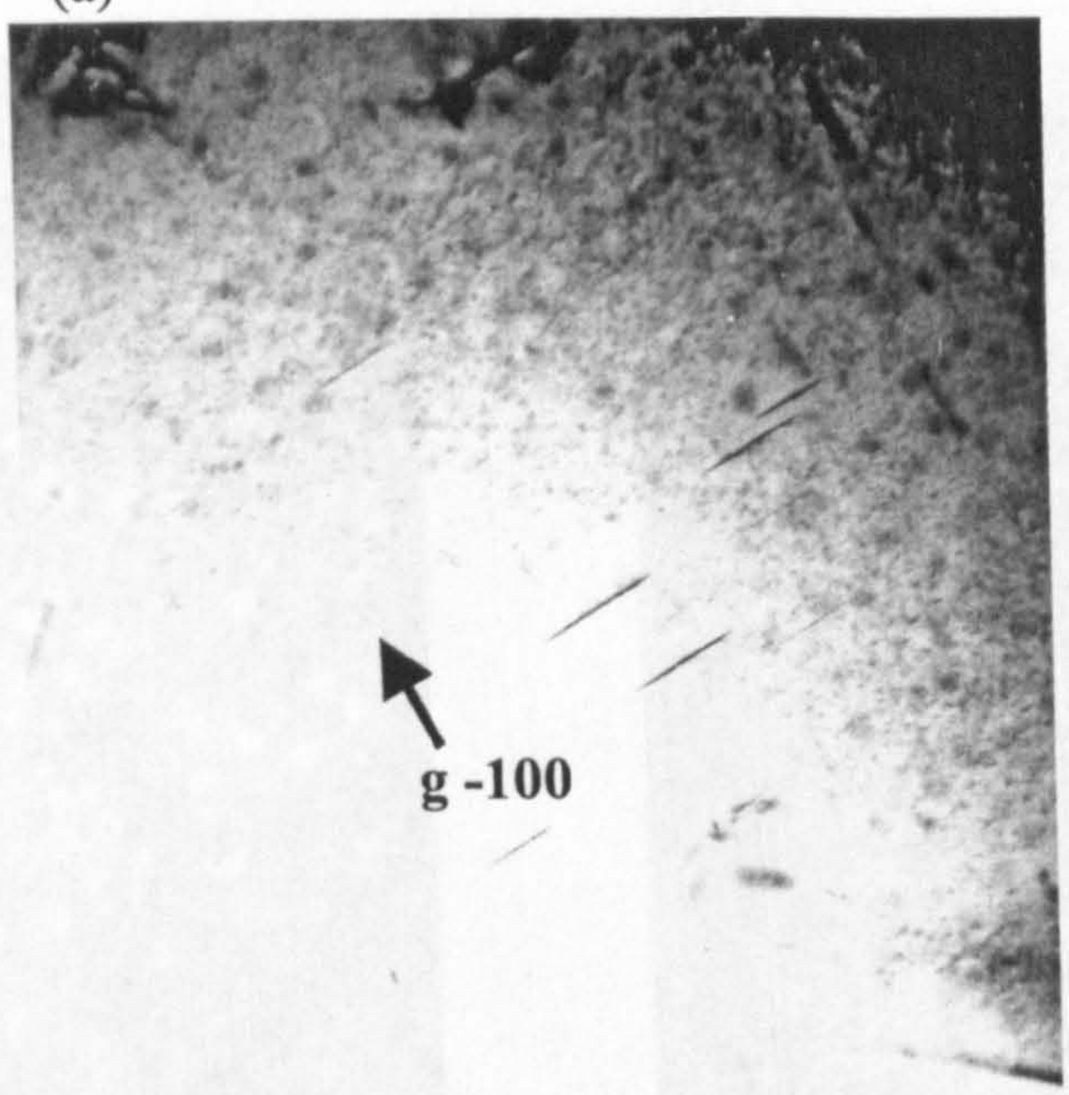

Figure 9.35 (a): TEM images of 1.7Li3.0Cu alloy after exposure for 1000h at 70°C . Zone axis <013>.

(b)

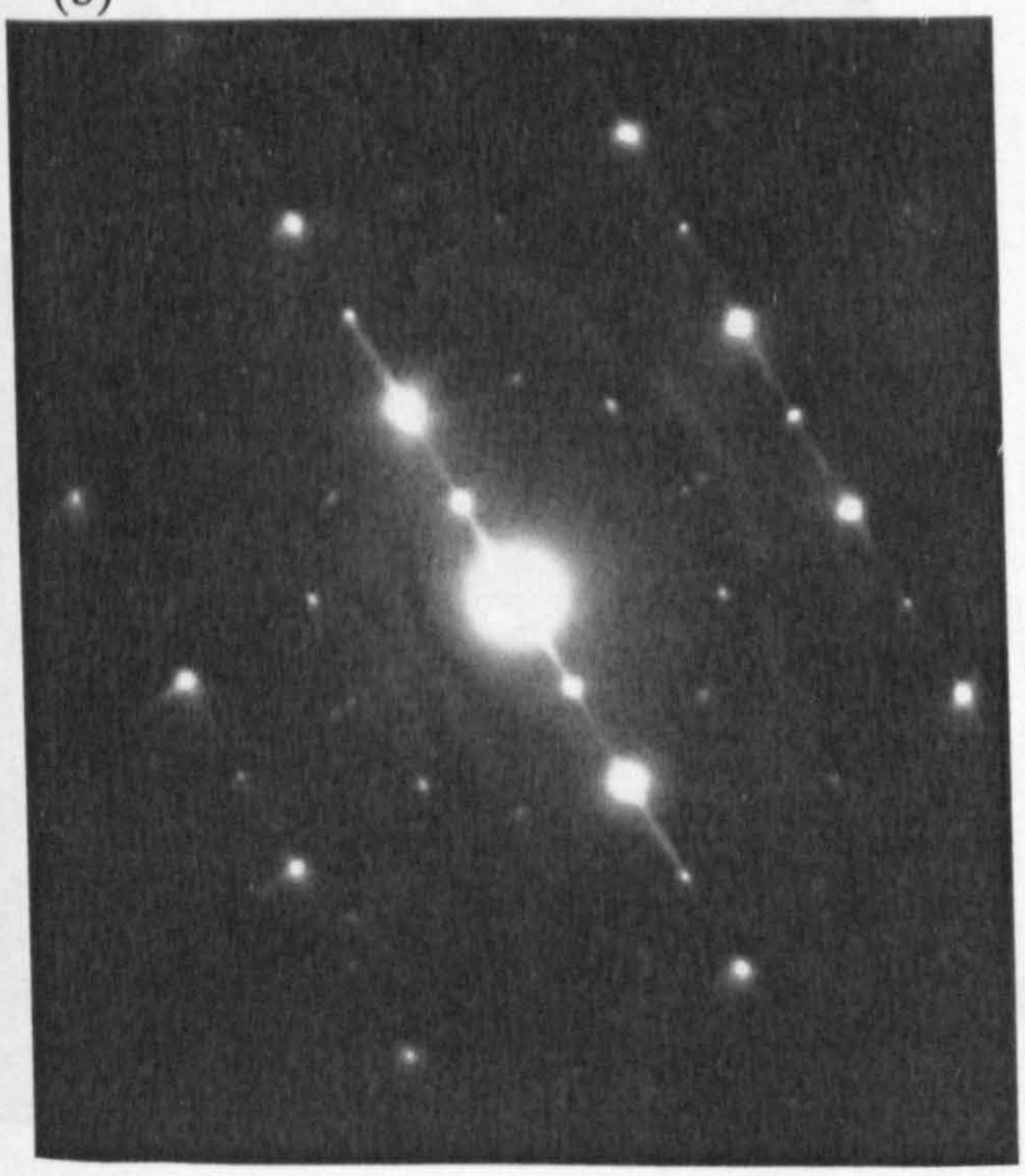

Figure 9.35 (b): SAD pattern of 1.7Li3.0Cu alloy after exposure for 1000h at 70°C . Zone axis <013>.

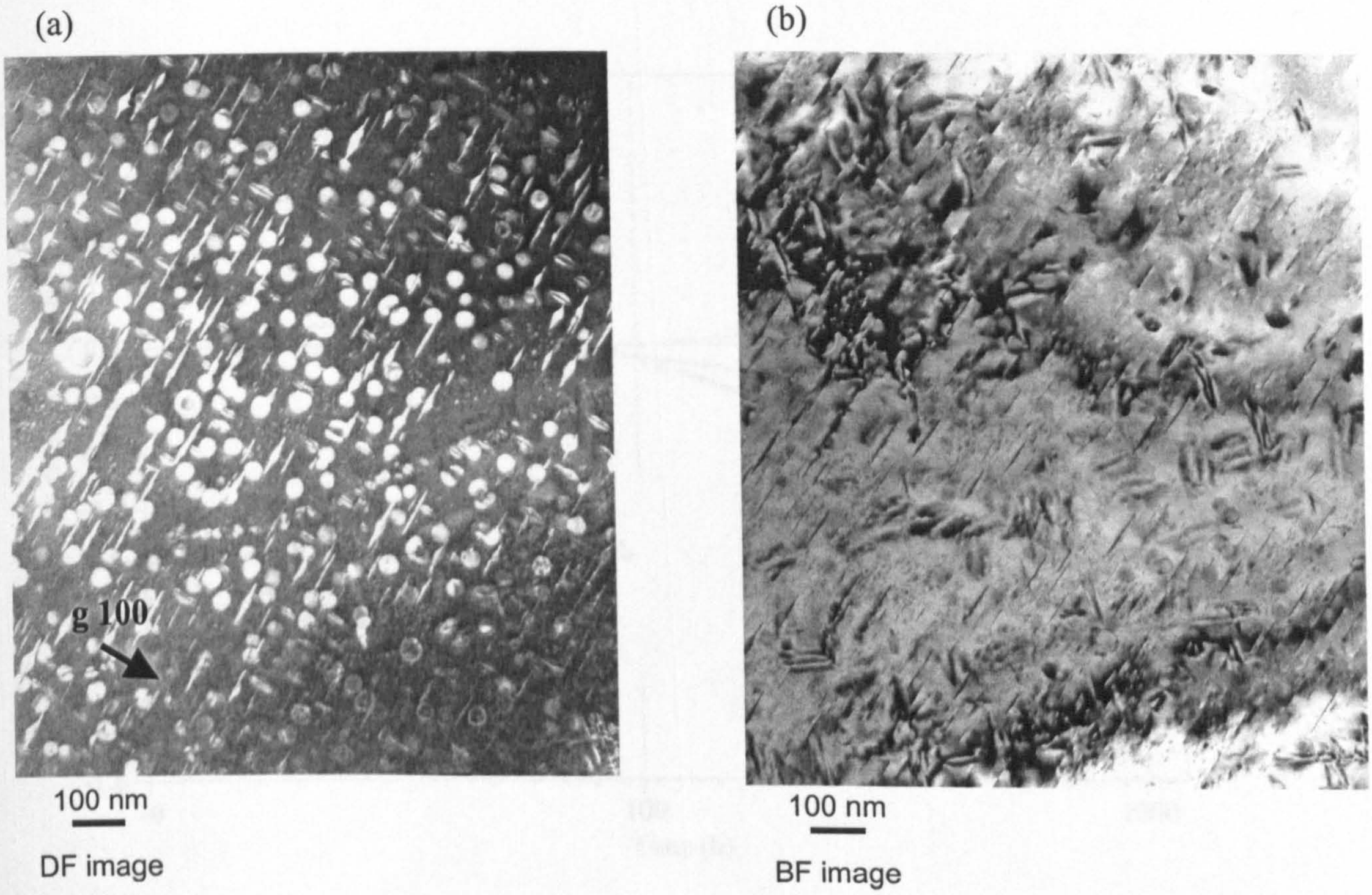

Figure 9.36 (a, b): TEM images of 1.7Li3.0Cu alloy aged for 7 days at 100°C after exposure for 1000h at 70°C .
Zone axis <001>.

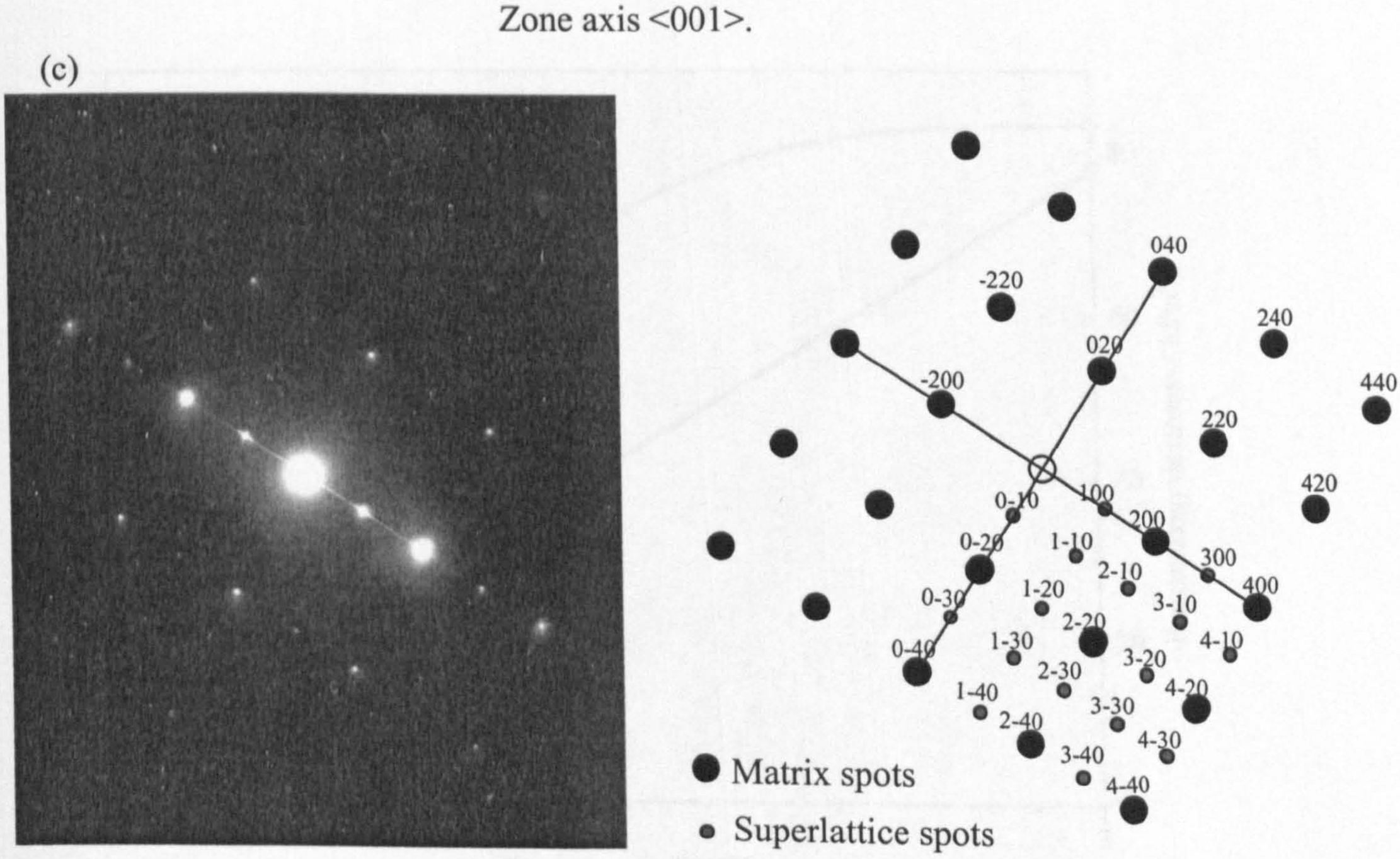

Figure 9.36 (c): SAD pattern of 1.7Li3.0Cu alloy aged for 7 days at 100°C after exposure for 1000h at 70°C .
Zone axis <001>.

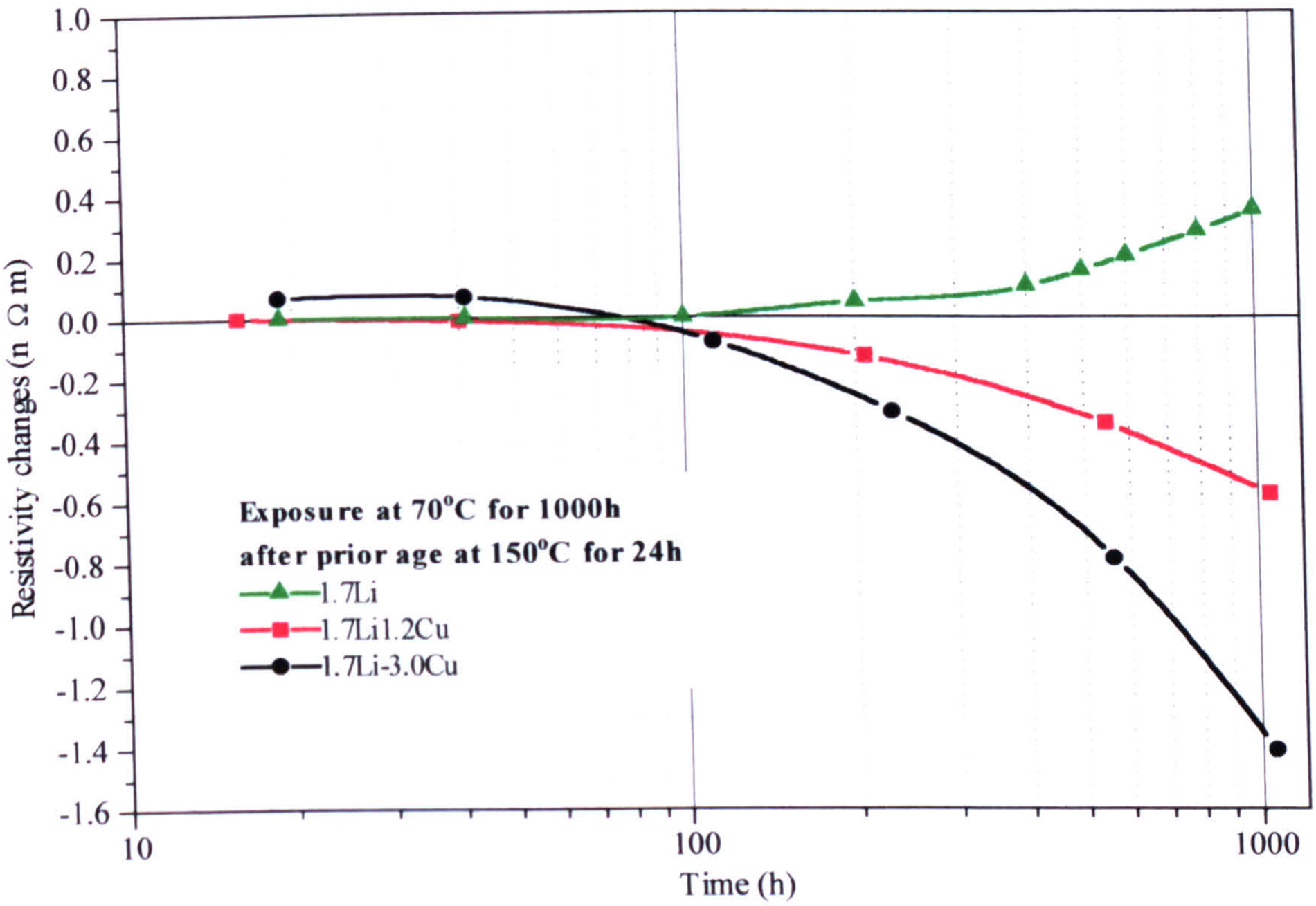

Figure.9.37: Isothermal resistivity changes during exposure at 70°C after prior ageing at 150°C 24h.

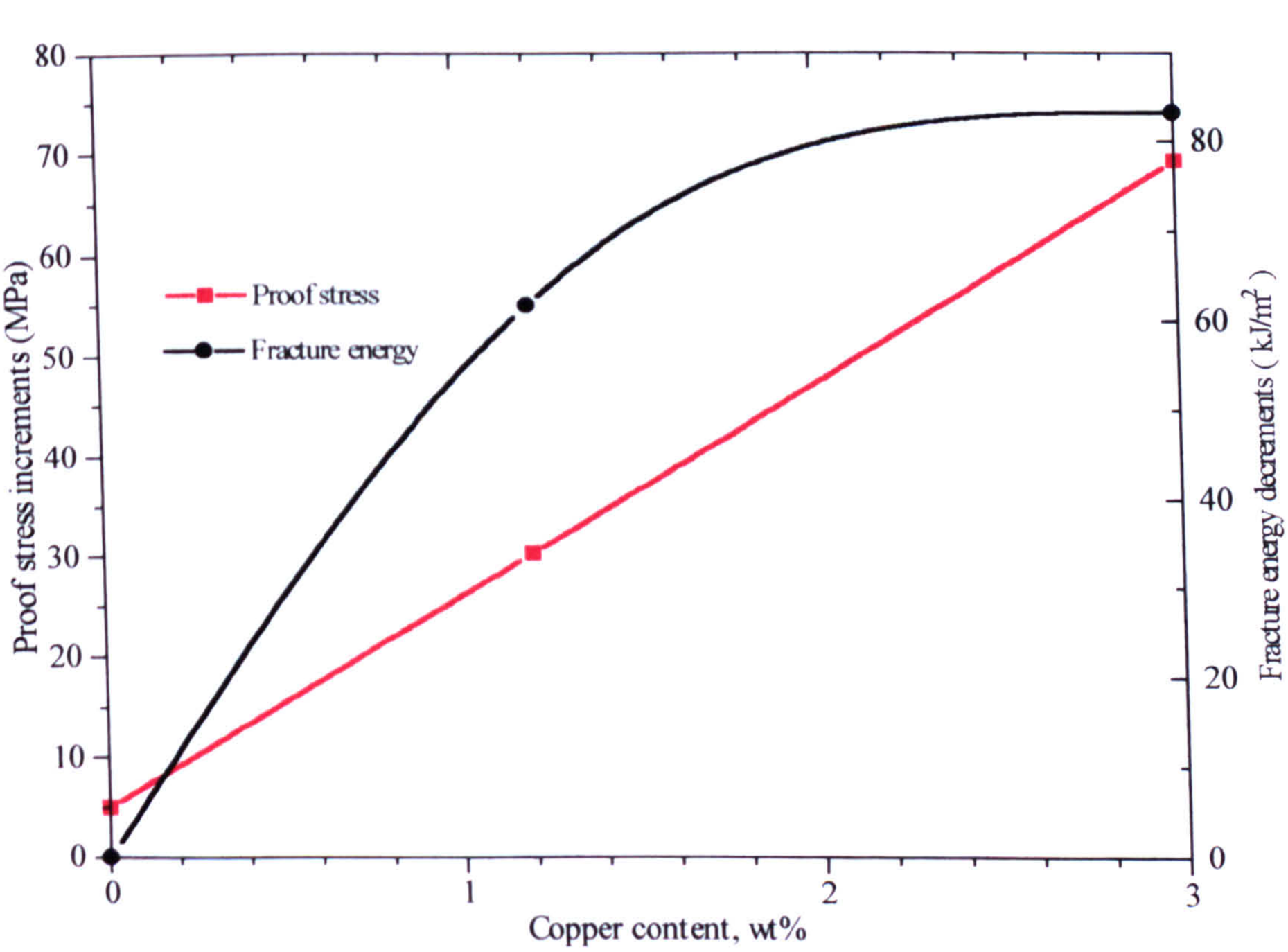

Figure 9.38: Effect of exposure at 70°C on the mechanical properties of the Al-Li-Cu alloys.

(a)

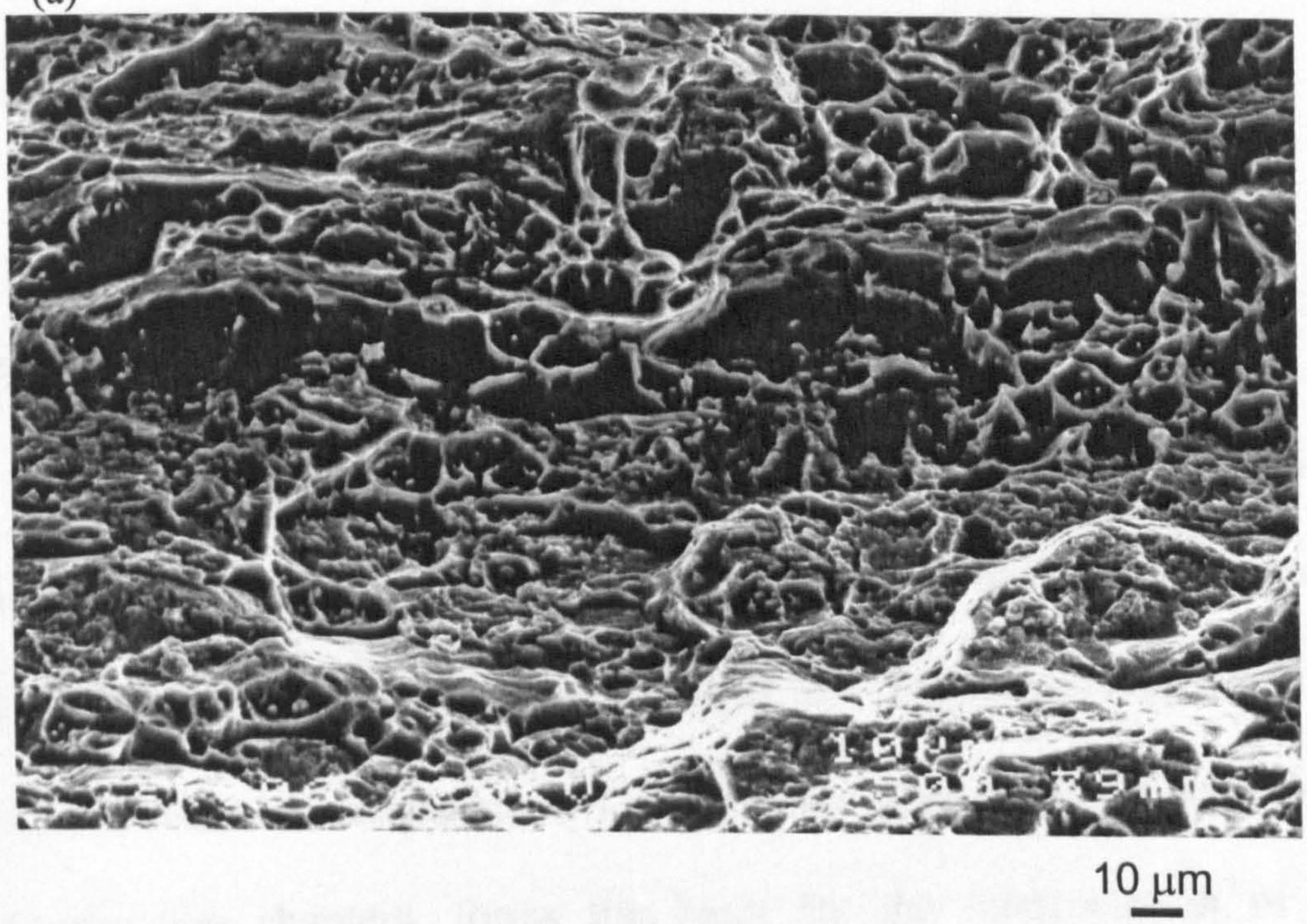

Figure 9.39 (a): SEM fractograph of 1.7Li3.0Cu alloy for 24h at 150°C.

(b)

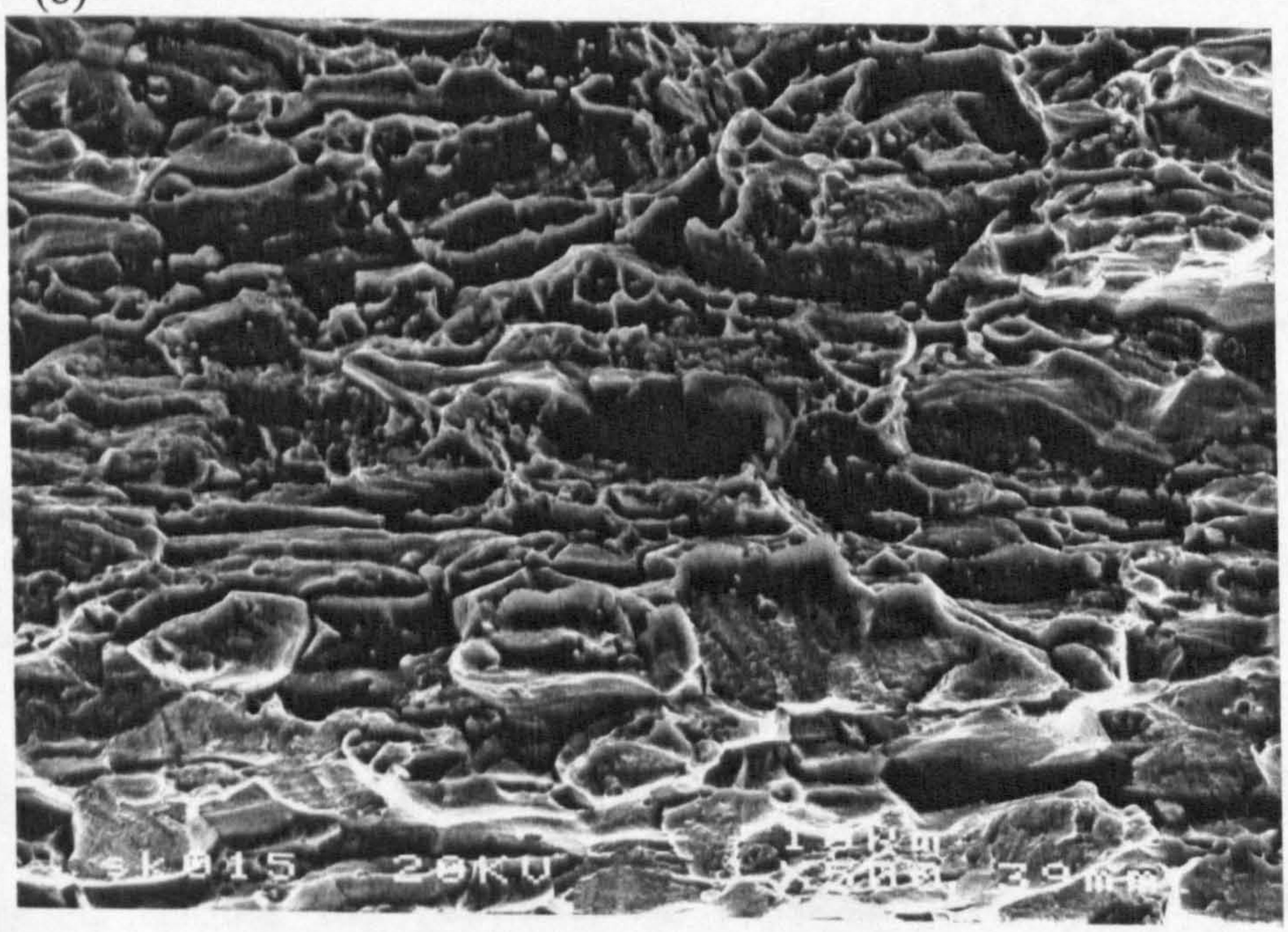

Figure 9.39(b): SEM fractograph of 1.7Li3.0Cu alloy after exposure for 1000h at 70°C.

CHAPTER 10

Precipitation characteristics in Al-Cu-Mg alloys

In the previous chapters the effects of copper and magnesium on the precipitation characteristics of the ternary Al-Li-Cu and Al-Li-Mg systems were examined. The present chapter considers the effects of copper and magnesium on the ageing characteristics of the Al-Cu-Mg system. This analysis, in combination with those of the previous two chapters, forms the basis for the interpretation of the complicated phase transformations that take place in quaternary Al-Li-Cu-Mg alloys.

The chapter is divided into two main sections:

- Isochronal precipitation characteristics
- Isothermal precipitation characteristics

10.1 Brief review on the latest studies of phase transformations in Al-Cu-Mg alloys

Before the interpretation of the results exhibited in the following paragraphs, it is important to outline the positions of different researchers on the phase transformations taking place in dilute Al-Cu-Mg alloys.

Ringer et al **[45, 46, 47, 48]** have proposed that the initial very rapid increase in

hardness in a 2.8Cu2.26Mg alloy at 150°C is due to the clustering of solute atoms that precedes GPB zone formation, and that further ageing up to 100 h causes the formation of rod-like GPB zones and heterogeneously precipitated S. Their HREM and CTEM results showed that GPB zones are present only after ageing for greater than 50 h at 150°C, i.e. clustering dominates the first 50 h of ageing.

Zahra et al **[49, 49(4, 5, 6)]** using DSC, HREM, and EDS experiments on a similar alloy to that used by Ringer et al showed that GPB zones can form at very short ageing times at all temperatures below 200°C. They accepted that an early clustering reaction took place, but this lasted only for the first few seconds of ageing. They also confirmed the presence of the metastable S″ phase.

Although Ringer et al continued to argue against the early formation of GPB zones and the existence of S″ **[50]**, the latest, most complete work carried out by Charai et al **[51]** gives strong evidence for the early appearance of GPB zones and the existence of S″. It also suggests that the early clusters that form during the first few seconds of ageing are rich in magnesium. The results and conclusions of this latest study will be used as a basis for the interpretation of the results presented in the remainder of the chapter.

10.2 Isochronal characteristics

10.2.1 The effect of different copper additions

To study the effect of copper concentration, the magnesium content has been kept constant at approximately 1.2% and the copper varied from 1.2 to 3.0%.

10.2.1.1 DSC (as-quenched plots)

Figure 10.1 gives comparative DSC plots of the as-quenched alloys. The 1.2Cu1.2Mg DSC plot exhibits a very early exothermic peak (A) of which only the end-part is detected. This exothermic peak is attributed to the formation of magnesium rich Mg-Cu clusters **[51]**. Further heating results in the development of an exothermal effect at about 110°C (peak E) that is due to the formation of copper-rich clusters, i.e. GPB zones. As the temperature increases a series of endothermic and exothermic effects arise in the temperature range 170-260°C. The endothermic effect B, at approximately 180°C is attributed to the dissolution of Mg-Cu clusters. At about 220°C the dissolution of fine GPB zones takes place (peak G) but the coarser fraction of these grows during DSC heating into S″ (exotherm O). Dissolution of this S″ phase occurs at 250 °C (peak H). Exothermic peak U is attributed to the precipitation of the semicoherent phase S′ (~285°C) and the equilibrium phase S (~320°C).

As the copper concentration increases from 1.2 to 2.0% (2.0Cu1.2Mg alloy) changes in the size and position of all thermal events are observed. The degree of

each change is given in **table 10.1**. For peak A, no firm conclusions can be extracted because only part of the peak is visible. However, the corresponding cluster dissolution peak B suggests an increase in the volume fraction of these clusters. These clusters are considered rich in magnesium **[51]** but the present results suggest the copper content of the clusters also has an important role to play in their development. Exothermic peak E exhibits a displacement to a lower temperature by 10°C indicating that acceleration of the GPB zone kinetics has taken place. This can be explained by **figure 10.2** which shows the section of the ternary Al-Cu-Mg phase diagram at 190°C. It can be easily seen that the increase in copper concentration from 1.2 to 2.0% results in a larger supersaturation relative to the S phase which, in turn, suggests a higher driving force for the rate of nucleation of GPB zones. The GPB zone dissolution endotherm and the S″ dissolution endotherm are both increased in size as the copper increases from 1.2% to 2.0%, thus indicating an increase in volume fraction of GPB zones and the S″ which forms from these zones during DSC heating. There is little or no change in the positions of these peaks. Finally, the small enlargement of exothermic peak U indicates that the larger supersaturation has caused a higher volume fraction stimulation of S′ and S precipitation.

A copper increase beyond 2.0% (3.0Cu1.2Mg alloy) caused a marked increase in heat effect E and its position exhibits a 10°C shift to a lower temperature. This behaviour can be attributed to the further increase of supersaturation (**figure 10.2**) which results in a higher driving force for GPB zone formation. The cluster dissolution peak B suggests that further stimulation of the Mg-Cu clustering

process has been caused by the increase of copper. The endothermic event which accompanies the dissolution of GPB zones (peak G) exhibits a significant increase as would be expected. This increased volume fraction of GPB zones has caused an increase in the amount of S″ (peak H). In this high copper-containing alloy the exothermic events corresponding to S′ precipitation and S precipitation (peak U) have increased in size, again consistent with increased supersaturation.

10.2.1.2 Isochronal resistivity

The resistivity plots of 1.2Cu1.2Mg, 2.0Cu1.2Mg and 3.0Cu1.0Mg alloys are presented in **figure 10.3**. The 1.2Cu1.2Mg alloy exhibits a resistivity peak (A′) at 140°C which, following the DSC results, can be attributed to the formation of GPB zones that are smaller than the critical size for electron scattering (2 nm). Higher temperatures than 140 °C cause a decrease in resistivity as growth of the zones takes place. The decrease of resistivity continues up to 340°C due to precipitation of S″, S′and S. Further heating causes dissolution of these phases which is accompanied by an increase of resistivity towards the baseline. By increasing the copper concentration to 2.0% (2.0Cu1.2Mg alloy), the height of peak A′ rises significantly without any change in its position (**figure 10.4**). This suggests that a higher number density of GPB zones form. This result is in good agreement with the DSC results presented in the last section. Surprisingly, the resistivity measurements do not appear to detect formation of the Mg-Cu clusters which are suspected to form at temperatures lower than 0 °C.

As the copper addition increases beyond 2 % (3.0Cu1.2Mg alloy), a further increase in the height of peak A′ is observed and there appears to be an additional earlier peak at 80°C, peak A′′, which could be the result of GP_{Cu} zones since the alloy is in (or very near) the α+S+θ phase field (**figure 10.2**). The decrease in resistivity in the temperature range 140-230°C is again attributed to the growth of GPB zones. In this high copper alloy precipitation of S′′, S′ and S phases cause a dramatic drop of resistivity in the temperature range 230-290 °C followed by an increase in resistivity at temperatures higher than 290°C as dissolution of these phases takes place.

It will be noted that no reference has been made during the discussion of the isochronal resistivity results about the phase transformations that correspond to heat effects B, G, O, and H observed in the DSC traces. The form of the isochronal resistivity plots in **figure 10.3** makes it very difficult to draw any conclusions about these phase transformations. In order to overcome this difficulty the resistivity plots have been differentiated to enable a direct comparison to be made with the DSC thermograms. Any minimum or maximum on a differentiated plot corresponds to the highest rates of resistivity increase or decrease, whereas each baseline point corresponds to a maximum or minimum in the conventional resistivity plot. **Figures 10.5, 10.6,** and **10.7** give the comparative DSC/differentiated resistivity plots of 1.2Cu1.2Mg, 2.0Cu1.2Mg, and 3.0Cu1.0Mg alloys. The differentiated plot of the 1.2Cu1.2Mg alloy exhibits two maxima at 80 and 390°C (peaks E′ and Y′) and a minimum at approximately

280°C (peak U′). Peaks E′ and U′ correspond to the DSC peaks E and U which were attributed to the formation of GPB zones and precipitation of S′ and S respectively. Peak Y′ is the result of the dissolution of the latter phases. It can be readily seen that the resistivity peaks described above are shifted to lower temperatures compared with the corresponding DSC peaks. This can be explained by the lower mean heating rate of the isochronal resistivity experiment (2 °C/min) compared with that of the DSC run (20°C/min). The small resistivity inflection that is observed at a temperature of 220°C could be the result of the formation of S″ from GPB zones. The increase of copper concentration from 1.2% to 3% (2.0Cu1.2Mg and 3.0Cu1.0Mg alloys) produced stronger inflections on the differentiated plots. In the 3.0Cu1.0Mg alloy these resistivity inflections can be related to the DSC peaks B, G, O and H (**figure 10.7**). **Figure 10.8** compares the differentiated resistivity plots for the various alloys. It can be easily seen that the increase of copper has caused an increase in the area of peak E′ and its position has shifted to lower temperature. This mirrors the DSC results and indicates that the increase in copper supersaturation has resulted in an increase in the driving force for GPB zone formation which in turn has accelerated its formation kinetics. The changes in the area and position of peak U′ exhibit a similar trend, confirming that increasing copper concentration has increased the volume fraction and rate of formation of S′ and S. Finally, as the copper concentration increases, the reactions relating to cluster dissolution, GPB dissolution, GPB→S″ transformation and S″ dissolution, are all shifted to a

lower temperature.

10.2.2 The effect of magnesium concentration

To study the effect of magnesium concentration on precipitation in Al-Cu-Mg alloys, the concentration of copper was fixed at 1.2% and the magnesium varied from 1.2 to 2.0%.

10.2.2.1 DSC (as-quenched plots)

The as-quenched plots of 1.2Cu1.2Mg and 1.2Cu2.0Mg alloys are given in **figure 10.9**.

Exotherm A is significantly increased in size suggesting that the increased magnesium concentration has stimulated the formation of Mg-Cu clusters. No changes were detected for exothermal peak E in respect to its size and position. This is expected as GPB zones are rich in copper and therefore an increase in magnesium concentration should not have a significant effect on their formation. Endothermic peak B is increased in size which is in keeping with the higher volume fraction of Mg-Cu clusters formed at lower temperatures. Although the overlapping effects of peaks G, O, and H make difficult the determination of the size of peak G it is believed that there is little change in its size, ie consistent with no change in exothermic peak E. The apparent increased height of this peak is attributed to overlapping effects. The case appears to be the same for endothermal effect H. The characteristics of this peak (height and position) remain the same with the increase of magnesium and this is in agreement with

previous experimental results **[51]**. GPB zone formation is a necessary step before the zones transform to S″ during DSC heating. Thus if there is little change in GPB zone formation there should be little change in S″ formation.

10.2.2.2 Isochronal resistivity

Figure 10.10 shows the isochronal resistivity plots of 1.2Cu1.2Mg and 1.2Cu2.0Mg alloys. As discussed in the previous sections the initial increase in resistivity is attributed to the formation of GPB zones with size smaller than the critical size for electron scattering (2 nm). The resistivity reaches a peak at 140°C (peak A′). The plots show that the increase in magnesium addition to 2.0% results in a small increase of peak A′ without any changes in its position. This suggests that a slightly larger volume fraction of GPB zones has formed in the 1.2Cu2.0Mg alloy. This result is not consistent with the DSC results where no change in the size of the GPB exothermic peak E was detected (**figure 10.9**). However this can be explained by the higher sensitivity of the resistivity technique. The marked drop of resistivity beyond 240°C is attributed to the precipitation of S″, S′ and S. It can be seen that the high magnesium alloy exhibits a larger decrease of resistivity suggesting a larger volume fraction of S″, S′ and S precipitates. Higher temperatures cause dissolution of these phases which increases the resistivity towards the baseline.

Differentiation of the resistivity plots produced clear peaks corresponding to the precipitation of GPB zones, S′ and S but inflections corresponding to cluster dissolution, GPB dissolution, GPB→S″ transformation and S″ dissolution were

not detected in the 1.2Cu2.0Mg alloys (**figure 10.11**). **Figure 10.12** compares the differentiated resistivity plot of 1.2Cu1.2Mg and 1.2Cu2.0Mg alloys where it can be seen that the increase in magnesium concentration results in a small increase in the area of peak E′ suggesting a larger volume fraction of GPB zones due to the larger driving force. The area of peak U′ is also enlarged with increasing magnesium concentration indicating that stimulation of S′ and S has occurred.

From the above results the following can be outlined for the effect of copper and magnesium on the isochronal precipitation characteristics of Al-Cu-Mg alloys:

Effect of copper concentration

- Increase of copper additions results in significant stimulation of GPB-zones, S′ and S formation, resulting from an increase in supersaturation.
- The DSC results indicate that as copper increases from 1.2 to 3.0% the temperature of GPB zone formation decreases by approximately 10°C/wt%Cu.
- The resistivity results indicate that increase of copper from 1.2 to 3.0% produces a higher number density of GPB zones and faster precipitation kinetics.

Effect of magnesium concentration

- Increase of magnesium additions stimulates the Mg-Cu clustering process.
- The effect on GPB-zone formation is smaller than that observed with increasing copper concentration.

10.3 Ageing at 70°C

10.3.1 Varying copper concentration

Figure 10.13 gives the comparative DSC plots of 1.2Cu1.2Mg, 2.0Cu1.2Mg and 3.0Cu1.0Mg alloys after ageing 1000 h at 70 °C.

The DSC thermogram of 1.2Cu1.2Mg alloy exhibits a broad endotherm in the temperature range 150-270°C. Careful observation leads to the conclusion that the endotherm consists of three endothermic events, peaks B, G, H at 175, 210, and 250°C respectively and an exothermic peak O at approximately 240 °C. Endothermic peaks B, G are attributed to the dissolution of Mg-Cu clusters and GPB zones that have formed during the age at 70°C. Exothermic peak O is due to the transformation of large GPB zones into S″ during DSC heating, and the endotherm H is caused by dissolution of this S″. The high-temperature exothermal effect U (290 °C) is attributed to the precipitation of S′ and S phases followed by their dissolution at temperatures >350°C.

An increase of copper from 1.2 to 2.0 % results in an enlargement of exothermal effect G together with a 10°C shift to a lower temperature. The increase in the area under peak G suggests that stimulation of GPB zones has taken place as a result of the higher driving force caused by the larger supersaturation of copper **(figure 10.2)**. The 10°C shift to a lower temperature indicates a smaller size of the zones. Endothermal effect H also exhibits an increase in its size which is expected to occur as a result of the stimulation of GPB zones.

The high temperature exothermic peak U exhibits an increase in its size suggesting an increase in the volume fraction of S′ and S phases.

Higher copper concentrations (3.0Cu1.0Mg alloy) resulted in a further increase in the size of exothermal effect G. Also, there is a further shift of 20°C to a lower temperature. The above behaviour indicates that the increase in copper concentration to 3% caused the precipitation of a higher volume fraction of smaller-sized GPB zones. A corresponding increase in the size of endotherm H (S″ dissolution) was also noted. Exothermal effect U exhibits a large increase in its size indicating a further increase in the volume fraction of S′ and S phases occurred with increasing copper concentration.

Figure 10.14 presents comparative resistivity plots of 1.2Cu1.2Mg, 2.0Cu1.2Mg and 3.0Cu1.0Mg alloys. Alloy 1.2Cu1.2Mg exhibits an initial increase in resistivity up to 2 h of ageing that is attributed to the nucleation and growth of GPB zones with size smaller than the critical size for electron scattering. According to the DSC results a small amount of Mg-Cu clusters may have formed during ageing at 70°C. Therefore, it is believed that in the first minutes of ageing the resistivity increase is due to a combination of Mg-Cu clusters and GPB zones.

After 2 h, the rate of increase becomes very low and, after 6 h, a plateau is reached. No further changes are observed even after 1000 h of ageing at 70°C. This resistivity behaviour suggests that after 6 h the rate of growth of GPB zones is very small.

As the copper addition increases from 1.2 to 2% the increase in resistivity is enhanced, indicating faster GPB zone kinetics, supporting the DSC results (**figure 10.13**). The resistivity attains a plateau after 10 h and thereafter there is little or no further growth of GPB zones. The resistivity difference between the two plateaus after 1000 h of ageing is the result of an increase in the volume fraction of GPB zones, which is consistent with the DSC results (**figure 10.13**).

An increase of copper concentration beyond 2% (3.0Cu1.0Mg alloy) results in a further increase of resistivity, suggesting that the rates of nucleation and growth of GPB zones are again accelerated. Similar to the other two alloys the resistivity reaches a plateau, this time after 1 h of ageing which is much faster than that observed in the 2.0Cu1.2Mg alloy where the plateau was attained after 10 h. This suggests that the GPB zone reaction was completed much earlier. There is again a resistivity difference after 1000h of ageing between 2.0Cu1.2Mg and 3.0Cu1.0Mg alloys indicating that a higher volume fraction of GPB zones has been formed; this is in agreement with the DSC results presented in **figure 10.13**.

10.3.2 Varying magnesium concentration

The comparative DSC plots of 1.2Cu1.2Mg and 1.2Cu2.0Mg alloys after ageing 1000 h at 70°C are given in **figure 10.15.**

The DSC thermogram of 1.2Cu1.2Mg alloy has already been discussed in the previous section. It was shown that the thermal event appearing in the temperature range 150-270°C consists of three endothermic peaks (B, G, H) and

an exothermic peak (O). Peaks B, G correspond to the dissolution of Mg-Cu clusters and GPB zones that have formed during the 70°C age. Peak O is caused by the transformation of GPB zones to S″during DSC heating and peak H is the dissolution of this S″. The high-temperature exothermic peak U at 290°C was attributed to the precipitation of S′ and S.

Increase in magnesium concentration from 1.2 to 2.0% causes a very small enlargement of peak B. This behaviour would be expected as these clusters are rich in magnesium and therefore an increase in magnesium supersaturation will cause further clusters to develop during the 70°C age. The remainder of the peaks appeared to be little affected by magnesium concentration.

The comparative resistivity plots of 1.2Cu1.2Mg and 1.2Cu2.0Mg alloys during ageing at 70 °C alloys are given in **figure 10.16.** The resistivity plot of 1.2Cu1.2Mg alloy has already been discussed in the previous section. The increase in resistivity up to 2 h of ageing was attributed principally to the formation of GPB zones with size smaller than the critical size for electron scattering. However it is believed that the increase in resistivity in the very early stages of ageing may be due to a combination of Mg-Cu clusters and GPB zones. After 6 h of ageing, the resistivity reaches a plateau and there are no further significant changes observed even after 1000 h of ageing. As the magnesium concentration increases from 1.2 to 2.0% a small decrease in the rate of resistivity increase is observed up to 10 min of ageing indicating that the

nucleation and growth of GPB zones is slower. It is well known that the binding energy between magnesium atoms and vacancies is higher than that between copper atoms and vacancies. Therefore the slower kinetics for GPB zone formation in the 1.2Cu2.0Mg alloy during the first 10 min of ageing can be attributed to the reduced number of mobile vacancies available for copper diffusion. After 10 min, the resistivity continues to increase for the 1.2Cu2.0Mg alloy whereas it slows down for the 1.2Cu1.2Mg alloy. After 6 h of ageing both alloys reach a plateau and a resistivity difference of ~0.5 nΩm is developed. The higher resistivity in the 1.2Cu2.0Mg alloy may be the result of a larger number of Mg-Cu clusters co-existing with GPB zones in the higher magnesium alloy.

10.4 Ageing at 100°C

10.4.1 Varying copper concentration

The DSC plots of 1.2Cu1.2Mg, 2.0Cu1.2Mg, and 3.0Cu1.0Mg alloys are shown in **figure 10.17** after ageing 1000 h at 100°C.

The DSC thermogram of 1.2Cu1.2Mg alloy exhibits a broad endotherm in the temperature range 190-270°C that consists of two endothermic peaks, peaks G and H, at 220 and 255 °C respectively and an exothermic peak, peak O, at approximately 240 °C. The endotherm B present after ageing at 70°C is now absent.

Increasing the copper concentration to 2% results in a significant increase in the size of peak G indicating that a larger volume fraction of GPB zones is being produced during ageing. This stimulation can be explained by the increase in copper supersaturation that results in a larger driving force for GPB zone formation. The position of this peak is shifted by ~5°C to a lower temperature suggesting a decrease in the size of the zones. Endothermal effect H exhibits an enlargement of its size suggesting an increase in S″ volume fraction; this is to be expected since a larger volume fraction of GPB zones have been produced in the alloy. The significant increase of the size of peak U indicates that the larger copper concentration has resulted in a larger volume fraction of S′ and S. No changes in the position of this peak were detected.

Higher additions of copper (3.0Cu1.0Mg alloy) results in a very small increase of the area under peak G. The size of peak H was essentially unchanged. This follows from the effect of 3.0% copper on the size of the GPB zone peak which showed only a very small increase relative to the 2.0% copper alloy.

The comparative resistivity plots of 1.2Cu1.2Mg, 2.0Cu1.2Mg, and 3.0Cu1.0Mg alloys aged at 100°C are presented in **figure 10.18**. The 1.2Cu1.2Mg alloy exhibits an increase in resistivity in the first hour of ageing that is attributed to the formation of GPB zones of size smaller than the critical size for electron scattering. After 1 h of ageing the rate of resistivity increase is very low suggesting that growth of GPB zones at 100°C is very sluggish. As the copper

addition increases from 1.2 to 2.0 and 3.0 % (2.0Cu1.2Mg and 3.0Cu1.0Mg alloys) the early resistivity increase accelerates indicating that enhancement of GPB zones kinetics has occurred. Similar to the 1.2Cu1.2Mg alloy the resistivities in the 2.0Cu1.2Mg and 3.0Cu1.0Mg alloys attain a plateau after ageing 1 h suggesting little growth of GPB zones after this ageing period.

10.4.2 Varying magnesium concentration

The DSC thermograms of 1.2Cu1.2Mg and 1.2Cu2.0Mg alloys after ageing 1000 h at 100°C are shown in **figure 10.19.** As already shown in the previous sections the two endothermic peaks G and H appearing in the 1.2Cu1.2Mg alloy correspond to the dissolution of GPB zones and S″ respectively. As the magnesium increases from 1.2 to 2.0% there is minimal change in both peaks.

In **figure 10.20** are given the resistivity plots of 1.2Cu1.2Mg and 1.2Cu2.0Mg alloys aged at 100°C. The resistivity plot of the 1.2Cu1.2Mg alloy has already been discussed in the previous section. As the magnesium concentration increases from 1.2 to 2.0% the general resistivity changes are similar to those observed at 70 °C; extrapolating the curves to very short ageing times shows that the increased magnesium concentration reduces the rate of GPB zone formation in the very early stages of ageing. As with the results at 70°C the height of the resistivity plateau is increased in the 1.2Cu2.0Mg alloy, possibly due to the presence of Mg-Cu clusters co-existing with the GPB zones.

10.5 Ageing at 150 °C

10.5.1 Varying copper concentration

Figure 10.21 shows DSC comparative plots of 1.2Cu1.2Mg, 2.0Cu1.2Mg and 3.0Cu1.0Mg alloys after ageing for 24 h at 150°C. The DSC thermogram of the 1.2Cu1.2Mg alloy exhibits a large endothermic peak, peak G, at approximately 230°C which is attributed to the dissolution of GPB zones formed during ageing. The S″ dissolution peak H is present but is much smaller than that observed in the DSC thermograms of 1.2Cu1.2Mg alloy after ageing for 1000 h at 70 and 100 °C (**figure 10.13** and **10.17**)

Increasing the copper concentration from 1.2 to 2.0% and 2.0% to 3.0% results in an increase in the area under peak G indicating that a larger volume fraction of GPB zones has been produced. The same remarks apply to the exothermal effect U, the marked enlargement of its size suggesting that the volume fraction of S′ and S has also been increased.

The resistivity results in **figure 10.23** show a resistivity difference of about 1 nΩm is developed after 24 h of ageing as the copper concentration increases from 1.2 to 2.0%. This indicates the formation of a higher volume fraction of GPB zones with size smaller than the critical size for electron scattering, which is in agreement with the DSC results.

The DSC comparative plots of the above alloys after ageing for 1000 h at 150°C are presented in **figure 10.22.** The DSC thermogram of the 1.2Cu1.2Mg alloy

illustrates endothermal effects in the temperature range 190-275°C that consists of peaks G and H, at 235 and 260°C respectively. Peak G is again attributed to the dissolution of GPB zones whereas peak H is due to the dissolution of S″ formed during ageing (see next section). The small exothermic peak U at approximately 285°C corresponds to the precipitation of S′ and S. Heating to temperatures higher than 385°C causes dissolution of these precipitates resulting in an endothermal effect. It can be easily seen that the size of this endotherm is larger than the size of exotherm U this being the result of precipitation of S′ and S taking place during ageing.

Increasing the copper concentration from 1.2 to 2.0% did not cause an increase in the size of the GPB dissolution peak or the S″ dissolution peak. A further increase in the copper addition from 2.0 to 3.0% results in a decrease in the size of the GPB dissolution peak which will be the result of enhanced S′ precipitation in the 3.0Cu1.0Mg alloy during ageing at 150°C. This is further confirmed by the reduced size of the exotherm U in the 3.0Cu1.0Mg alloy.

10.5.2 Varying magnesium concentration

The comparative DSC plots of 1.2Cu1.2Mg and 1.2Cu2.0Mg alloys after ageing for 24 h at 150°C are presented in **figure 10.24.** Increasing magnesium concentration from 1.2 to 2.0% results in only a very small increase in the GPB dissolution peak showing that the increase in magnesium supersaturation does

not have any significant effect on the formation of GPB zones. This is to be expected since GPB zones are rich in copper atoms. The apparent increase in the size of peak H is due to the displacement of peak G to higher temperatures (as result of larger GPB zones) thus causing an overlap with peak H. The resistivity plots shown in **figure 10.26** show that after ageing 24 h at 150°C the resistivity increase is higher in the 1.2Cu2.0Mg alloy suggesting a larger population of GPB zones (less than the critical scattering size) exists in the higher magnesium alloy. This may be the result of the lower mobile vacancy concentration in the 1.2Cu2.0Mg alloy.

Figure 10.25 presents the comparative DSC plots of 1.2Cu1.2Mg and 1.2Cu2.0Mg alloys after ageing for 1000 h at 150°C. As the magnesium concentration increases from 1.2 to 2.0% (1.2Cu2.0Mg alloy) the endothermic peak G and endothermic peak H merge into an "apparent" single peak. The increase in magnesium results in an increase in the area of the combined G and H peaks. Finally, the enlarged peak U suggests that a larger amount of S′ and S forms during DSC heating.

10.6 Effect of ageing temperature

DSC thermograms of 1.2Cu1.2Mg alloy (**figure 10.27**) show that the largest volume fraction of GPB zones is produced at 100°C where there is an optimum combination of driving force and diffusivity. As the ageing temperature goes

from 70 to 100 to 150°C the position of the GPB dissolution peak G shifts to higher temperatures indicating that the size of GPB zones increases with ageing temperature. Increase of ageing temperature from 70 to 100°C does not produce any significant change in the size of the S″ dissolution peak H, although it would be expected to increase following the increase in GPB zone volume fraction. This can be explained by the larger-sized GPB zones requiring a higher temperature to dissolve and therefore giving less opportunity for the zones to transform to S″. As the ageing conditions increase to 24h/150°C the transformation into S″ is dramatically suppressed by the even larger size of GPB zones which therefore now transform to S′. Based on this interpretation, after 1000 h at 150°C endothermic peak H would be expected to be absent. However **figure 10.27** shows the presence of a significant sized S″ peak. This suggests that S″ is now forming during the prior ageing at 150°C. The isothermal resistivity plots (**figure 10.28**) show that after 1000h of ageing at 70 and 100°C the resistivity increase is approximately the same. However, from the DSC results it is known that at 100°C a significantly larger volume fraction of GPB zones has formed (ΔH=4.1 J/g compared with 3.6 J/g at 70°C). A possible reason for this difference is that resistivity measurements are measuring the number of sub-critical precipitates for electron scattering (≤ 2 nm) and not their total volume fraction. Increasing the ageing temperature to 150°C results in a drop of resistivity below the baseline after 90 h of ageing due to the formation of S″, S′, and S phases.

The 2.0Cu1.2Mg, and 3.0Cu1.0Mg and 1.2Cu2.0Mg alloys exhibit similar trends to the 1.2Cu1.2Mg alloy (**figures 10.29-10.34**). The largest volume fraction of GPB zones is formed during ageing at 100°C. As in the 1.2Cu1.2Mg alloy, the effect of ageing temperature on S″ appears to be more complicated. **Figure 10.35** presents the combined effects of ageing temperature on the enthalpy absorbed (ΔH) during the dissolution of S″ (peak H). Although exact values of ΔH cannot be extracted because peak H is an overlapping peak, the general trends can be easily seen. For all the alloys, changing the ageing conditions from 70°C/1000h to 150°C/24h reduces the S″ enthalpy, implying that a smaller amount of S″ forms. As shown earlier in this paragraph this can be explained by the larger-sized GPB zones that require higher temperatures for their dissolution thus decreasing the temperature range where transformation into S″ can take place, and therefore GPB zones transform to S′ instead of S″. The plots also show that ageing the 2.0Cu1.2Mg and 3.0Cu1.0Mg alloys for a 1000 h at 150°C causes a reduction in the S″ enthalpy. This could be the result of either less S″ forming during DSC heating (due to the larger size of GPB zones) or to S′ forming during the age at 150°C. However, with the 1.2Cu1.2Mg alloy, ageing for a 1000 h at 150°C causes an increase in the S″ enthalpy and this can only be explained by S″ forming during the age (along with S′). It is therefore likely that some S″ forms at 150°C in the 2.0Cu1.2Mg and 3.0Cu1.0Mg alloys, but the optimum alloy composition for forming S″ at 150°C (after 1000 h age) appears to be the dilute 1.2Cu1.2Mg alloy.

Increase of ageing time at 150°C from 24 to 1000 h causes a dramatic decrease of peak U (**figures 10.27, 10.29, 10.31, 10.33**) indicating that S′ and S has been precipitated during ageing. Further confirmation comes from the results of Charai et al **[51]** where after 96 h (4 days) at 150°C considerable amounts of S′ had precipitated in a 2.0Cu1.2Mg alloy. It is believed that either clusters or regions rich in magnesium and copper remain after GPB zone and S″ reversion and these regions act as nucleation sites for S′ [51].

From the above results the following can be concluded:

- The largest volume fraction of GPB zones is formed during ageing at 100°C where there is an optimum combination of thermodynamic driving force and diffusivity.
- Increasing the ageing conditions from 70°C/1000h to 150°C/24h causes a retardation of S″ formed during the DSC run. This is attributed to larger-sized GPB zones that form during ageing which require higher temperatures for their dissolution thus decreasing the temperature range where their transformation into S″ can take place. As the ageing temperature increases there is therefore an increasing tendency for less S″ and more S′ to form during the DSC run.
- As the ageing time at 150°C increases there is an increasing tendency for S″ and S′ formation to take place during ageing.

10.7 Effect of exposure at 70°C

In this section the effect of exposure at 70°C after prior ageing 24 h at 150°C has been studied. The conclusions reached for these simple Al-Cu-Mg alloys will help for the better understanding of the role of GPB zones in the embrittlement that occurs in commercial Al-Li-Cu-Mg alloys after exposure at low temperatures [**40**].

10.7.1 Varying copper concentrations

Figures 10.36-10.38 display the DSC thermograms of 1.2Cu1.2Mg, 2.0Cu1.2Mg and 3.0Cu1.0Mg alloys exposed for 1000 h at 70°C after pre-ageing for 24 h at 150°C.

None of the alloys exhibit a significant increase in the size of endothermal effect G indicating that any GPB zone formation that may be taking place during exposure is not being detected by the DSC technique. However, a very small increase in resistivity in 1.2Cu1.2Mg and 2.0Cu1.2Mg alloys (**figure 10.39**) suggests that GPB zones with size smaller than 2 nm (critical size for electron scattering) is forming during exposure, but the volume fraction is very small.

An interesting observation can be made if the DSC plots of the exposed 1.2Cu1.2Mg and 2.0Cu1.2Mg alloys are compared with those after a straight age of 1000 h at 70°C (**figures 10.36, 10.37**, and **10.13**). In both cases the GPB dissolution peak occurs at 10-20°C higher in the exposed case. This is because the GPB zones in the exposed alloy have been nucleated at 150°C and therefore

have a larger size. The area of the GPB peak in the straight aged (70°C) alloy and in the exposed alloy are approximately the same. However, the area of the S″ peak is much smaller in the exposed alloy compared to the straight aged alloy. This is consistent with results described earlier in this chapter, i.e. the larger the GPB zone diameter the less chance there is for it to transform to S″ during DSC heating.

10.7.2 Varying magnesium concentration

Increasing magnesium concentration from 1.2% (1.2Cu1.2Mg alloy) to 2.0% (1.2Cu2.0Mg alloy) does not cause any changes in the effect of exposure on the formation of GPB zones i.e. only a very small amount of GPB zones precipitate during exposure (**figures 10.40, 10.41**).

It should be noted by comparing the DSC plots for the 1.2Cu2.0Mg alloy in the straight aged and exposed conditions, the same effects appear as in the 1.2Cu1.2Mg and 2.0Cu1.2Mg alloys. That is, the exposed alloy exhibits a larger diameter of GPB zone and reduced S″ peak size.

Summary

From the above analysis the following is proposed:

Effect of copper

- The as-quenched DSC and isochronal resistivity results suggest that increasing copper addition from 1.2% to 3.0% causes significant stimulation of GPB zone formation and enhanced kinetics. The increase of copper also leads to a higher number-density of GPB zones.
- Ageing for 1000 h at 70 and 100°C and 24 h at 150°C causes stimulation of GPB zones as copper concentration increases from 1.2 to 3.0%. However increasing the ageing conditions to 1000 h at 150°C results in retardation of GPB zones with increasing copper concentration from 1.2 to 3.0% due to enhanced precipitation of S′.
- Copper concentration in the range 1.2-3.0% appears to have no effect on the amount of GPB zones formed during exposure at 70°C.

Effect of magnesium

- The as-quenched DSC and isochronal resistivity plots indicated that increasing magnesium concentration stimulates the Mg-Cu clustering process. The effect of magnesium on GPB-zone formation is smaller than that observed with increasing copper concentration.
- At all ageing temperatures (70,100,150°C) magnesium appears to have

little effect on the formation of GPB zones.

- The concentration of magnesium in the range 1.2-2.0% has no effect on the amount of GPB zones formed during exposure.

Effect of ageing temperature (for all the alloys)

- The largest volume fraction of GPB zones is formed during ageing at 100°C.
- Changing the ageing conditions from 70°C/1000h to 150°C/24h results in retardation of S″ formed during ageing due to the formation of larger-sized GPB zones that require higher temperatures for their dissolution, thus decreasing the temperature range where transformation into S″ can occur. Increasing the ageing time at 150°C from 24 h to 1000 h results in an increasing tendency for S″ and S′ formation during ageing. The dilute 1.2Cu1.2Mg alloy appears to have the optimum composition for forming S″ during ageing at 150°C/1000 h.

Table 10.1: Changes in the size and position of the thermal effects during heating of the as-quenched Al-Cu-Mg alloys

		PEAKS						
Copper increase		**A**	**E**	**B**	**G**	**O**	**H**	**U**
1.2→2.0%	**Size changes**	—	SI	SI	SI		SI	SI
	Shift(°C)	—	-10	-10	-10		No shift	-20
2.0→3.0%	**Size changes**	—	LI	LI	LI		LI	SI
	Shift(°C)	—	-10	-10	-10		No shift	-10

SI : Small Increase
LI : Large Increase

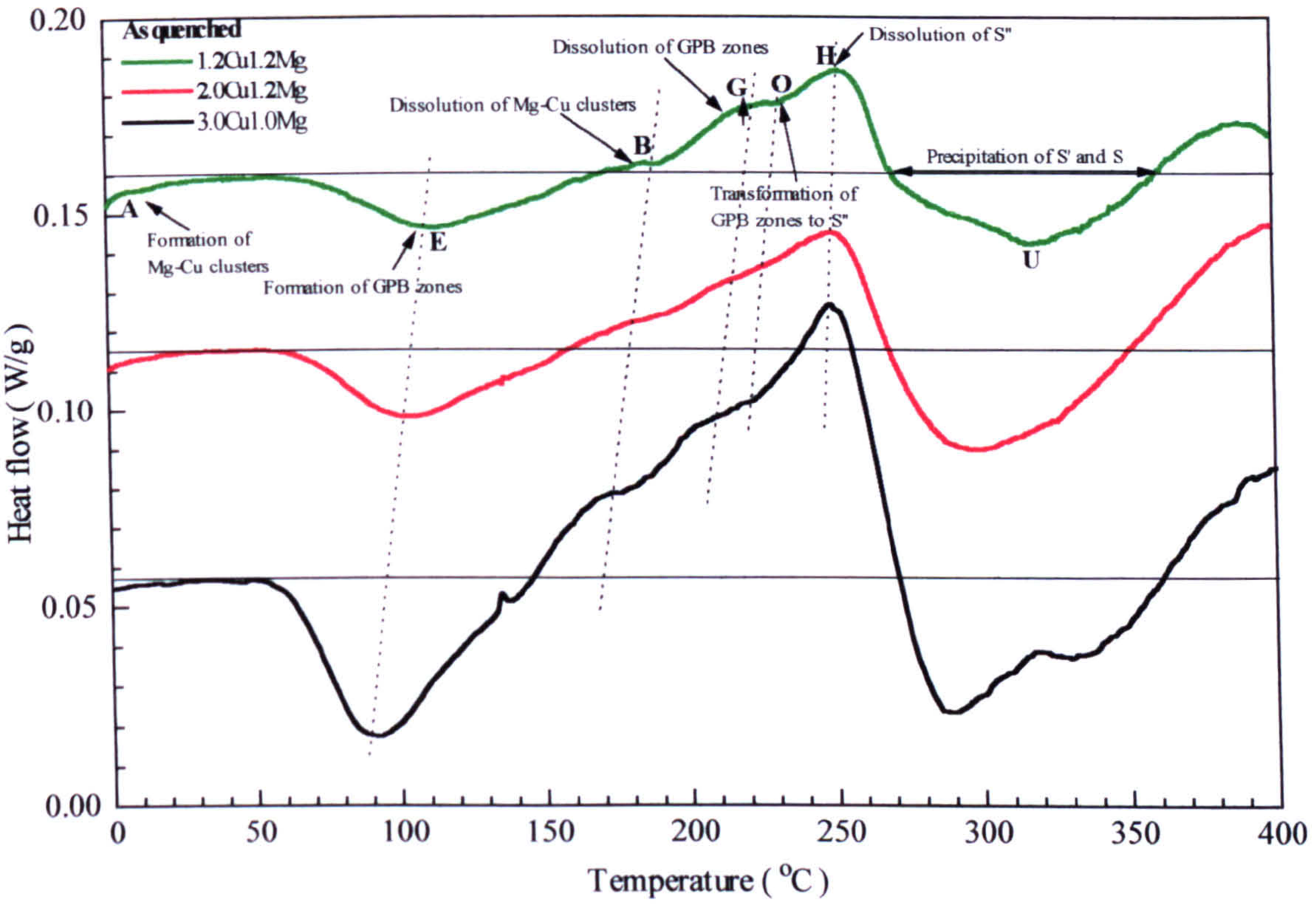

Figure 10.1: DSC comparative plots of the as-quenched alloys with varying copper addition.

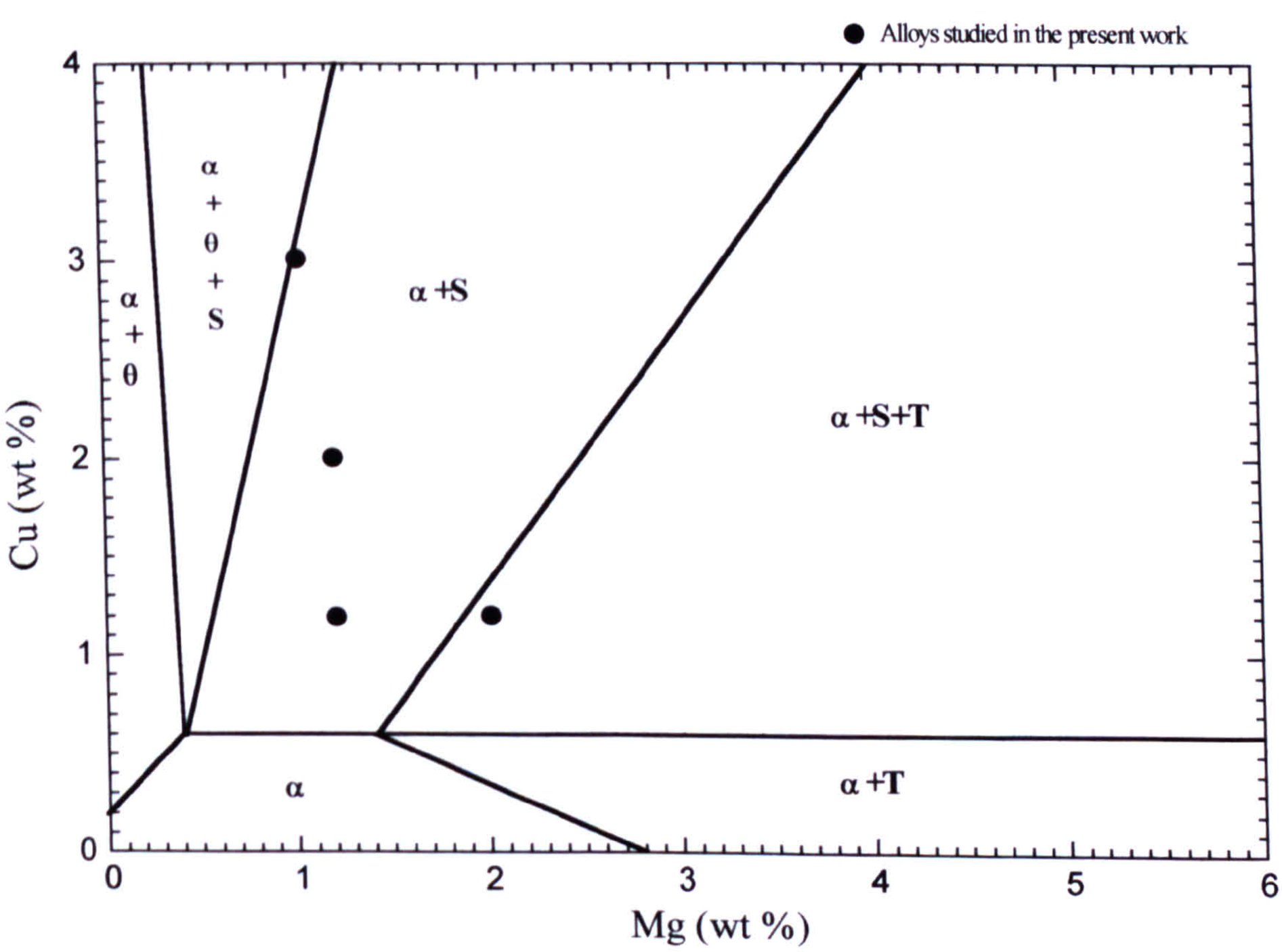

Figure 10.2: Isothermal section of the ternary Al-Cu-Mg phase diagram at 190°C

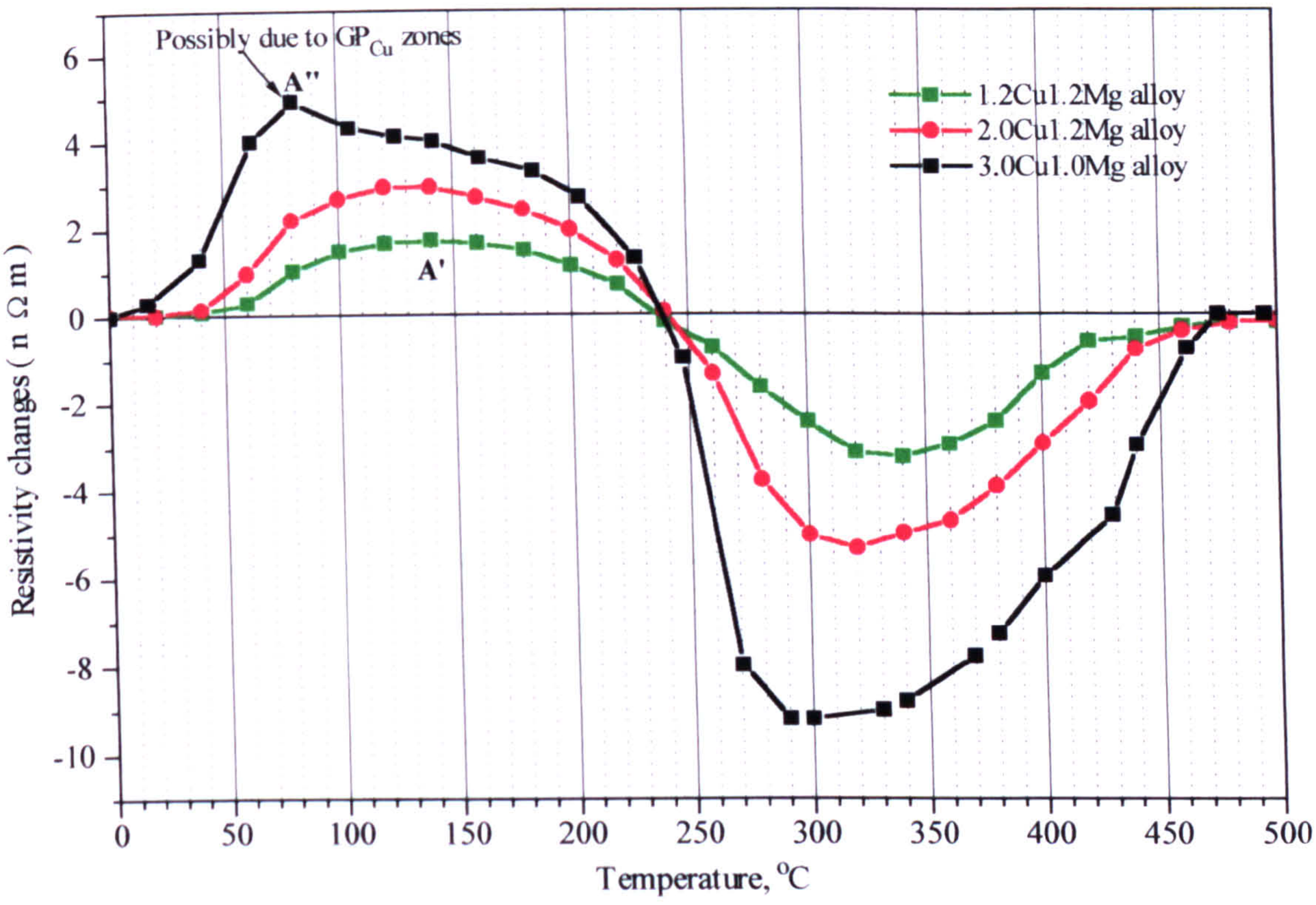

Figure 10.3: Comparison of the isochronal resistivity changes of the alloys with varying copper addition.

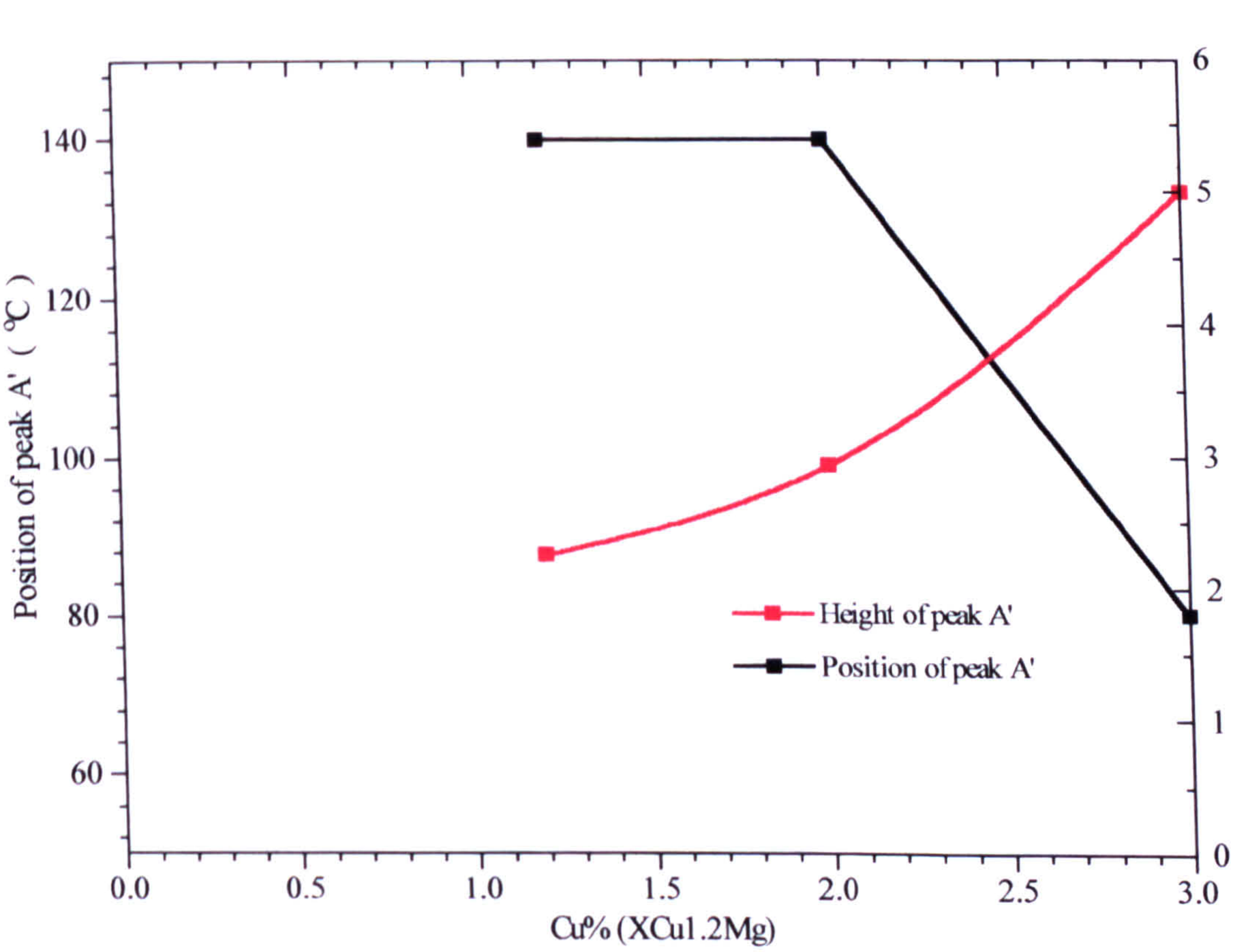

Figure 10.4: Height and position of peak A′.

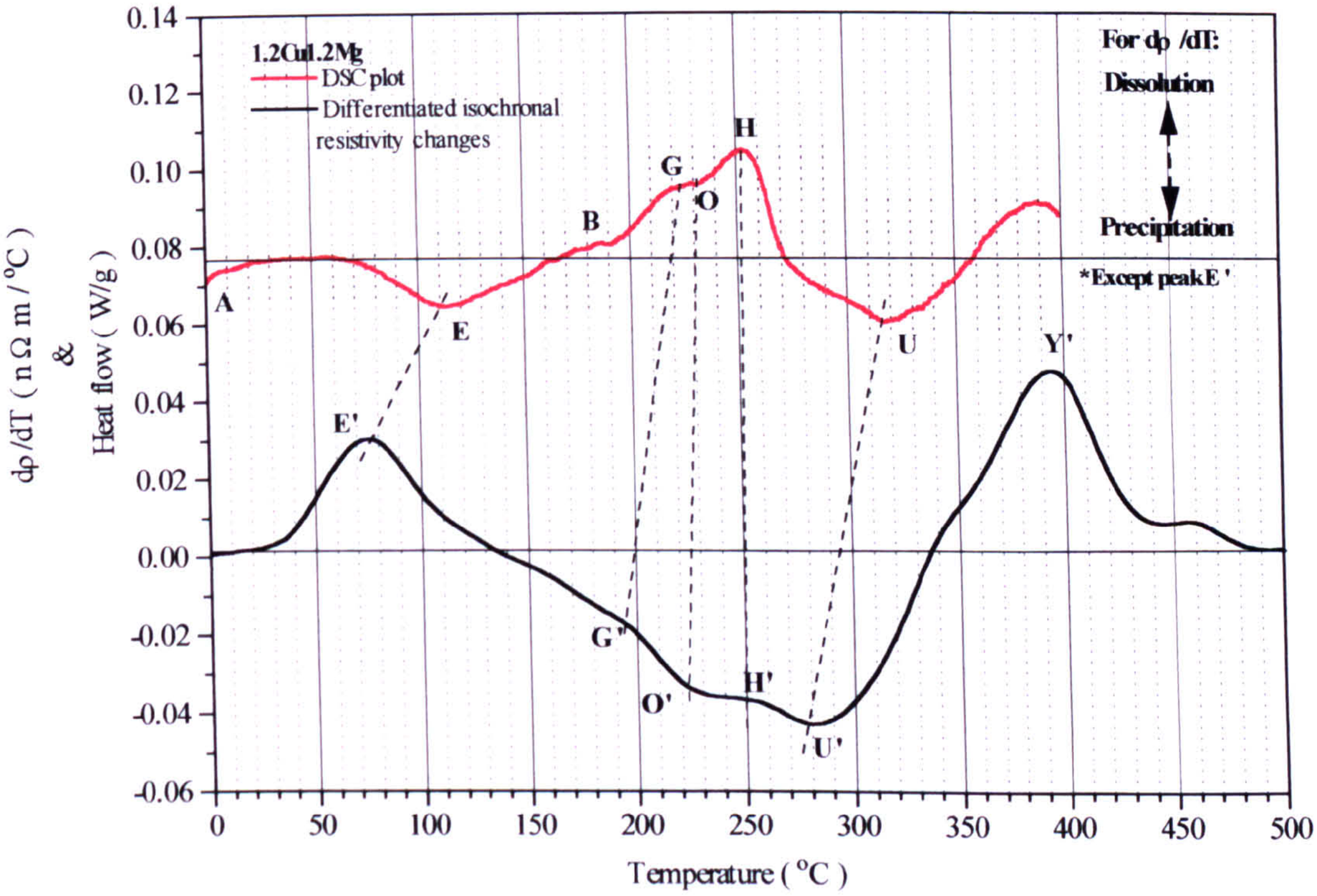

Figure 10.5: Comparative DSC/Differentiated resistivity plots of 1.2Cu1.2Mg alloy.

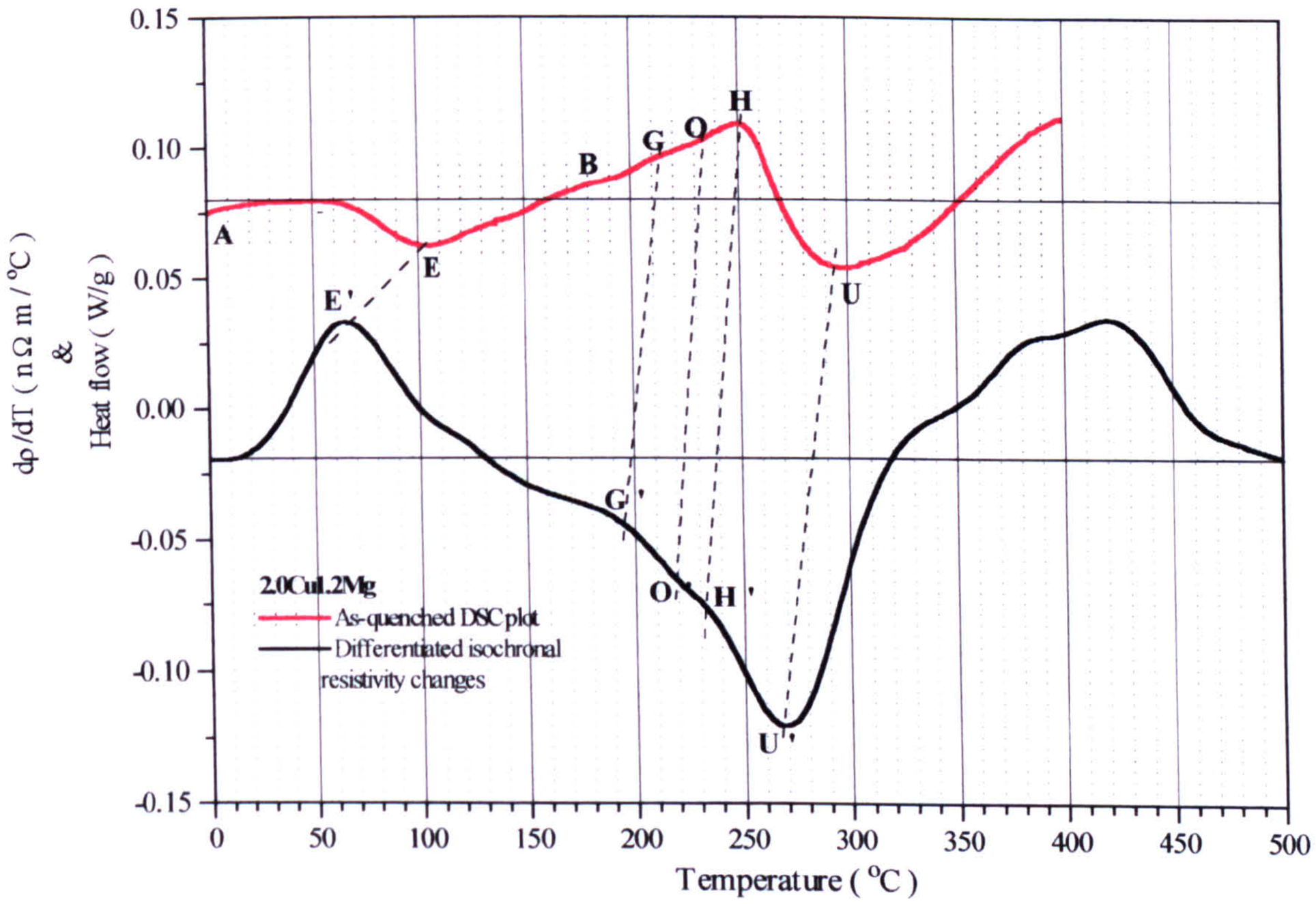

Figure 10.6: Comparative DSC/Differentiated resistivity plots of 2.0Cu1.2Mg alloy.

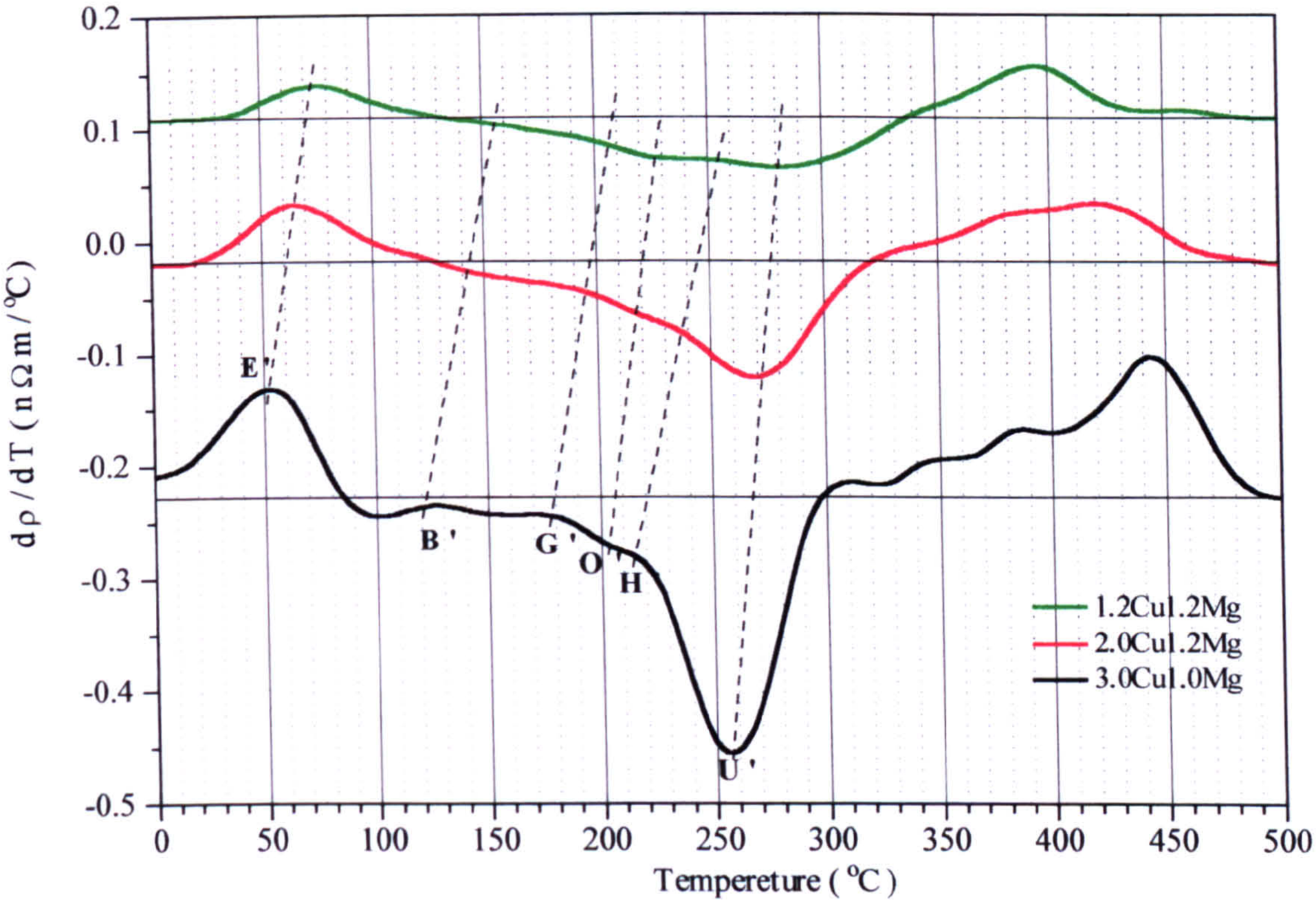

Figure 10.8: Comparative differentiated resistivity plots of the alloys with varying copper addition.

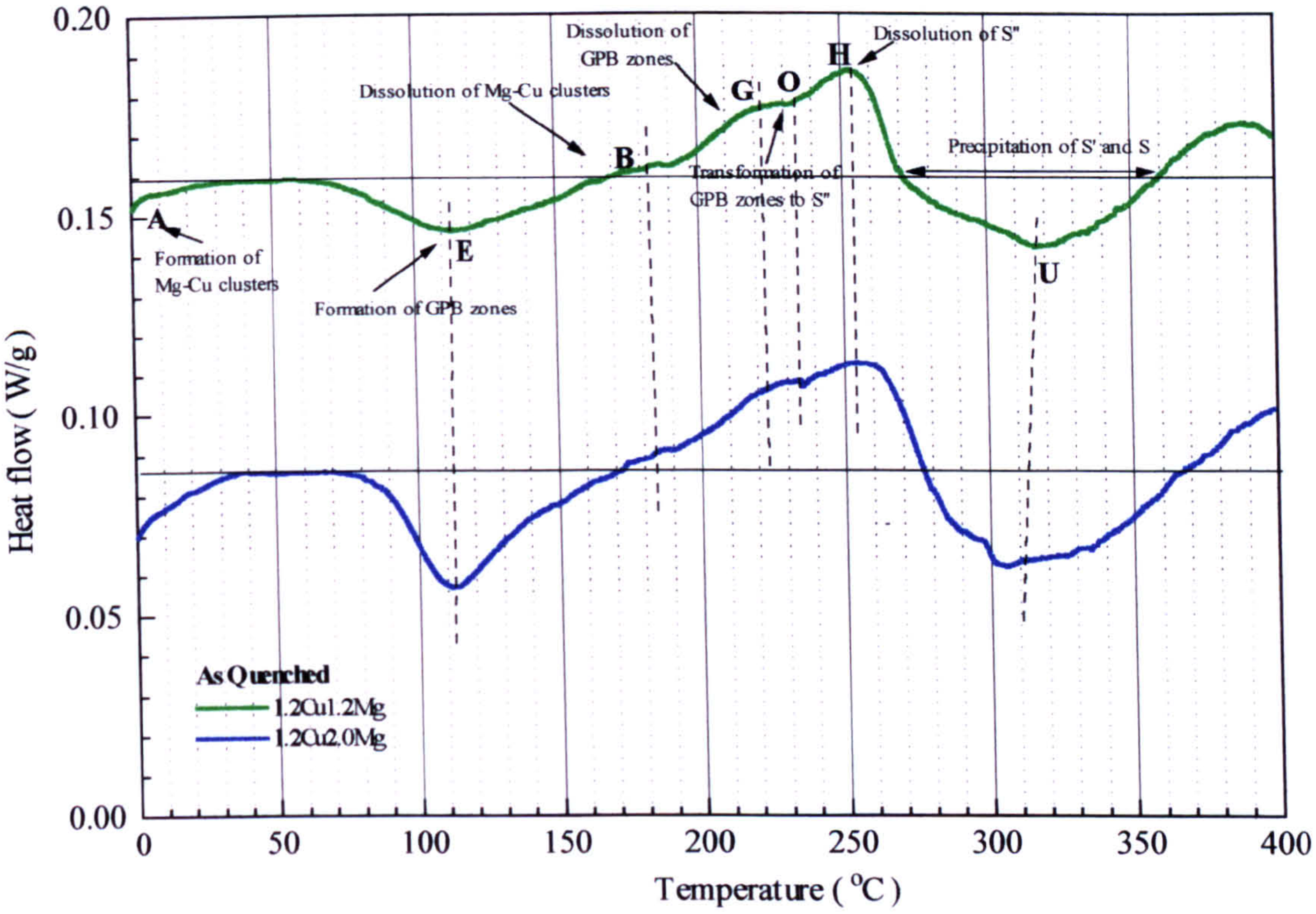

Figure 10.9: DSC comparative plots of the as-quenched alloys with varying magnesium addition.

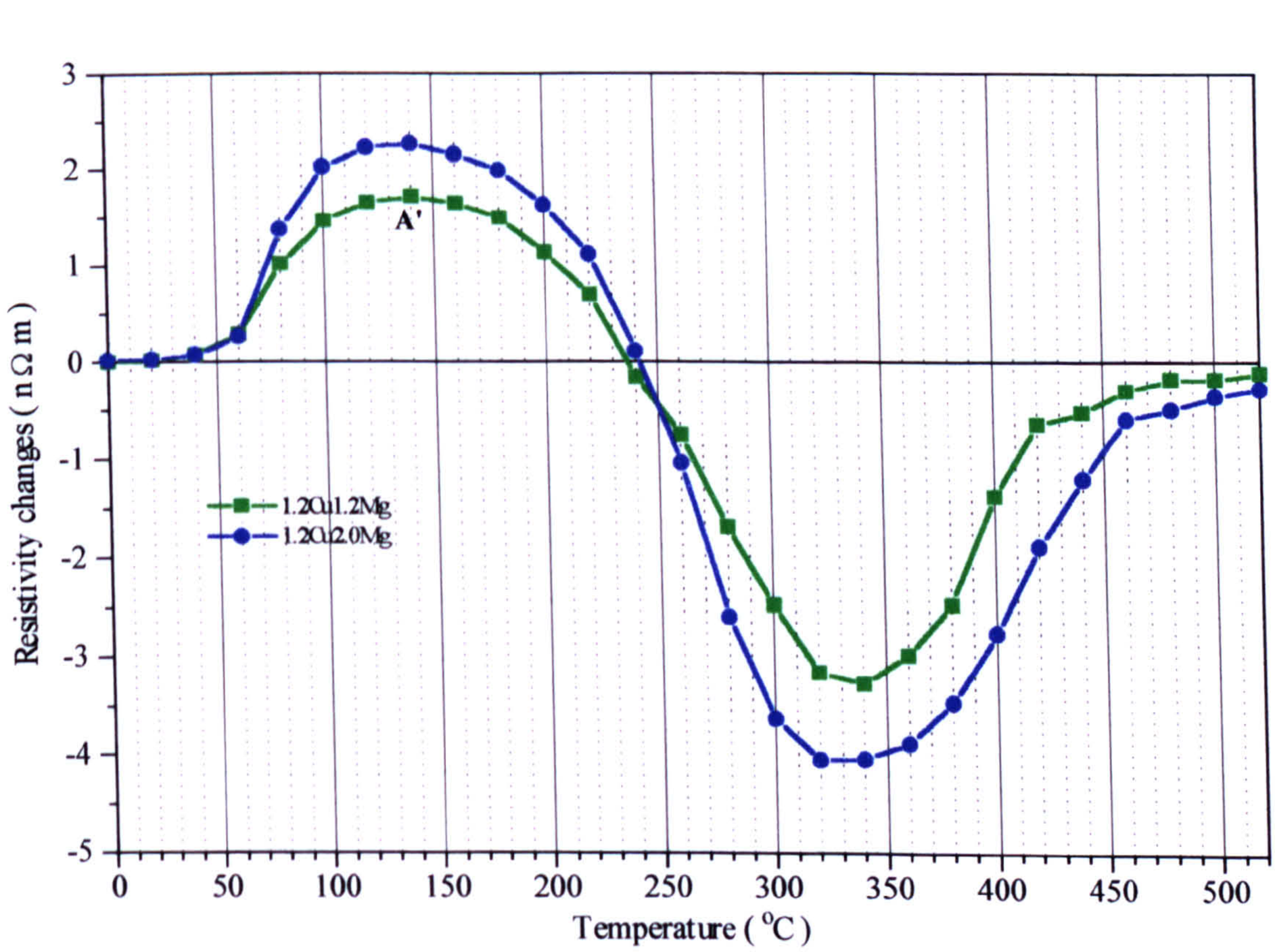

Figure 10.10: Comparison of the isochronal resistivity changes of the alloys with varying magnesium addition.

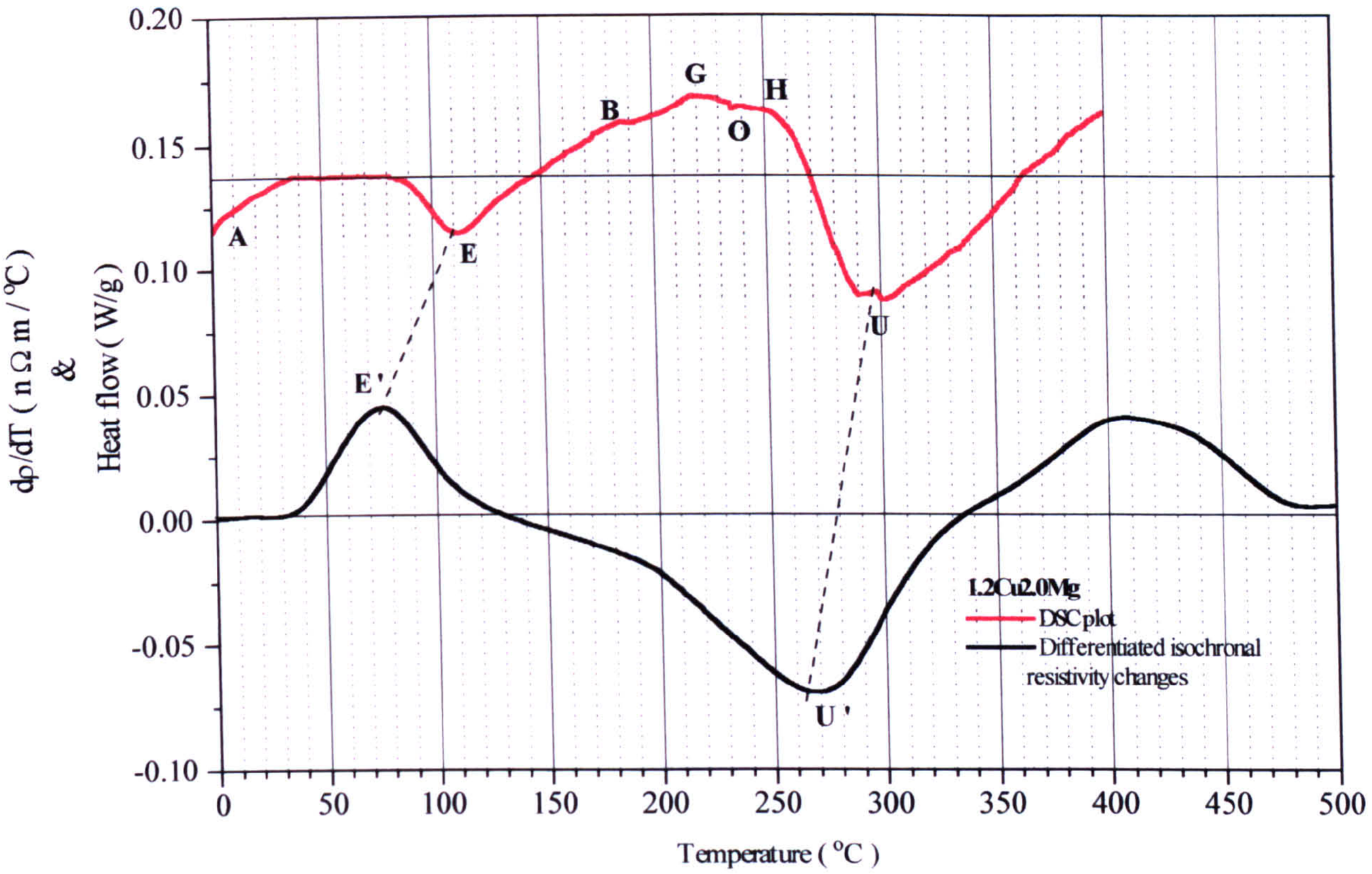

Figure 10.11: Comparative DSC/Differentiated resistivity plots of 1.2Cu2.0Mg alloy.

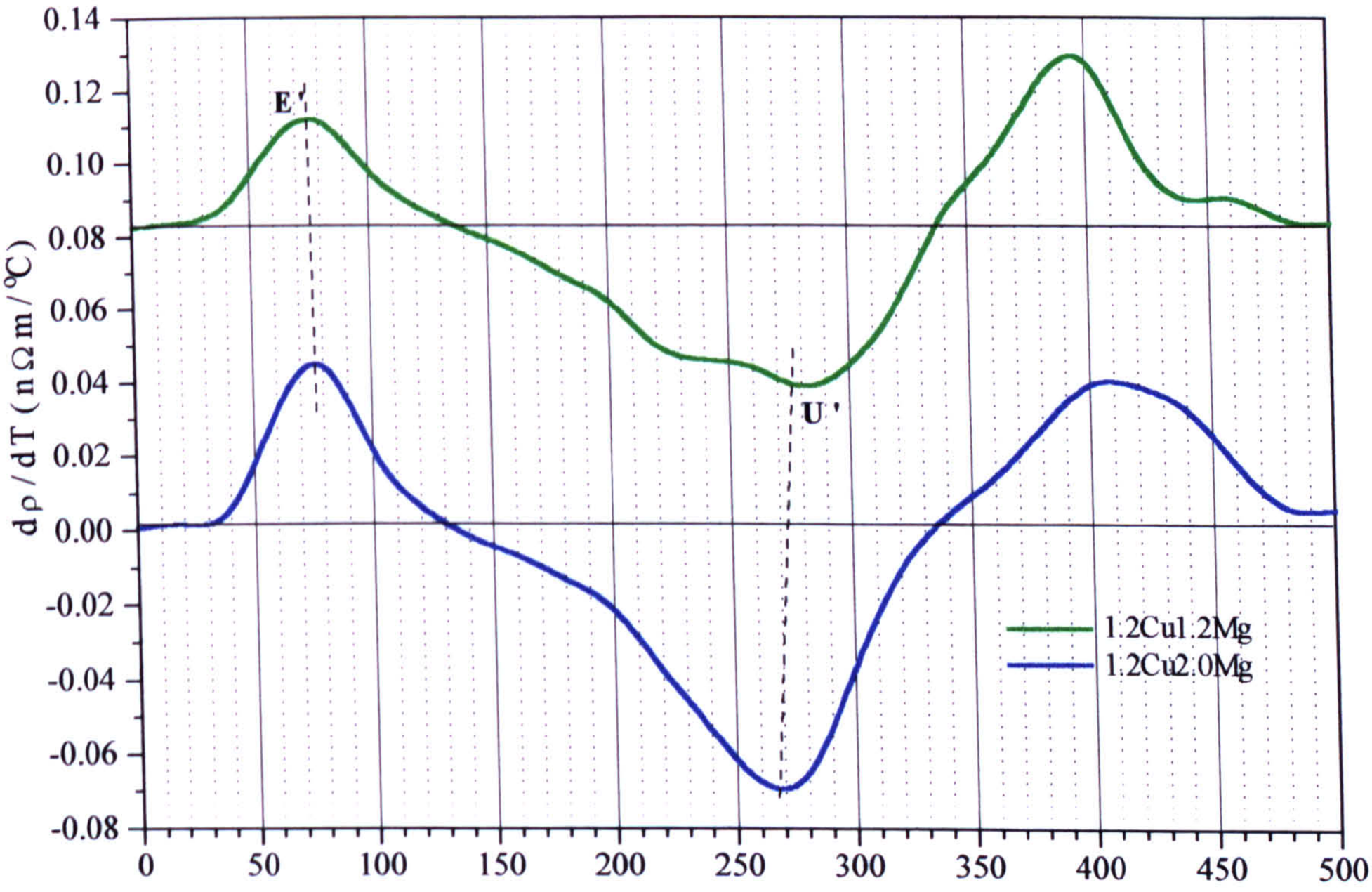

Figure 10.12: Comparative differentiated resistivity plots of the alloys with varying magnesium addition.

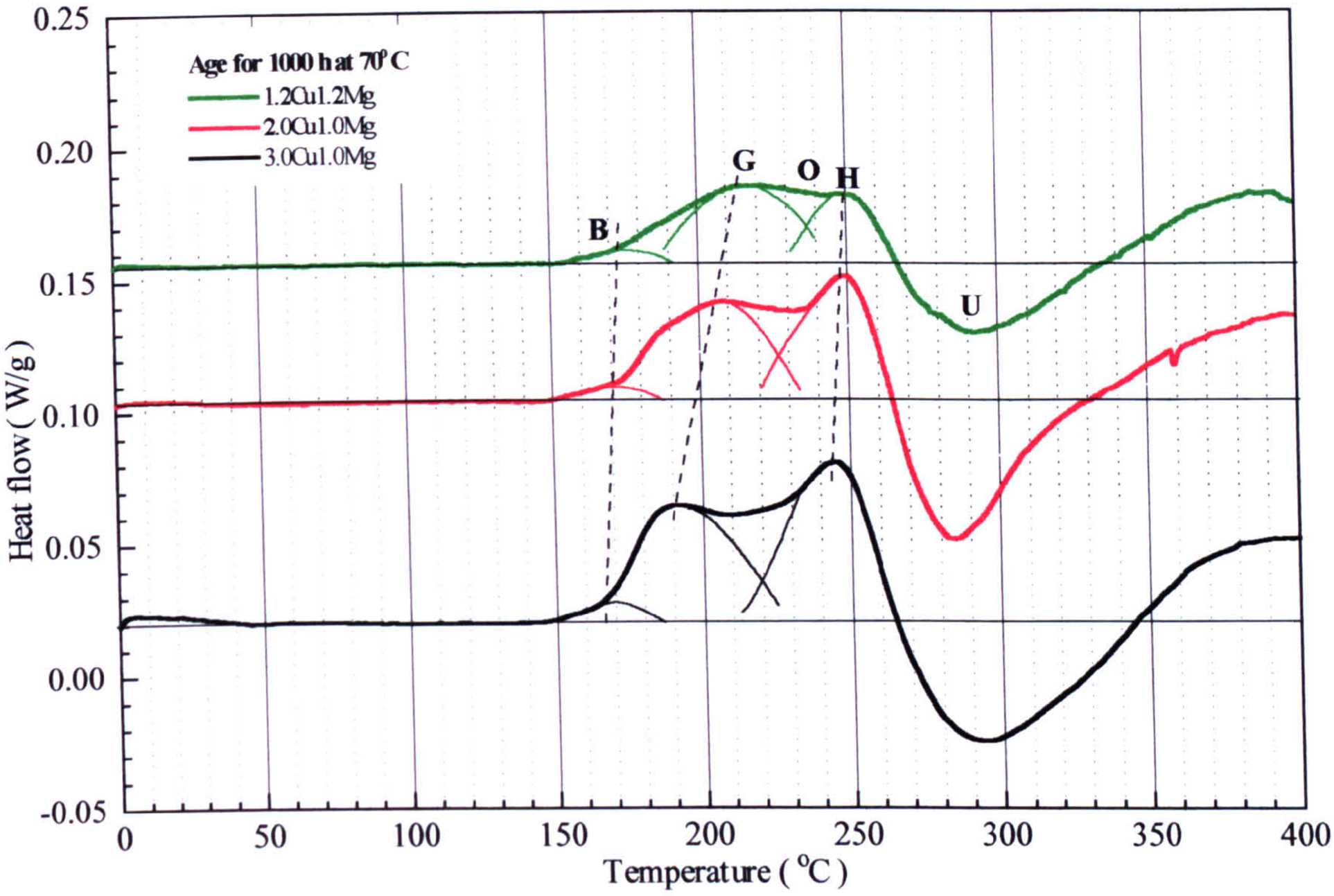

Figure 10.13: DSC comparative plots of the alloys with varying copper concentration after ageing for 1000 h at 70°C.

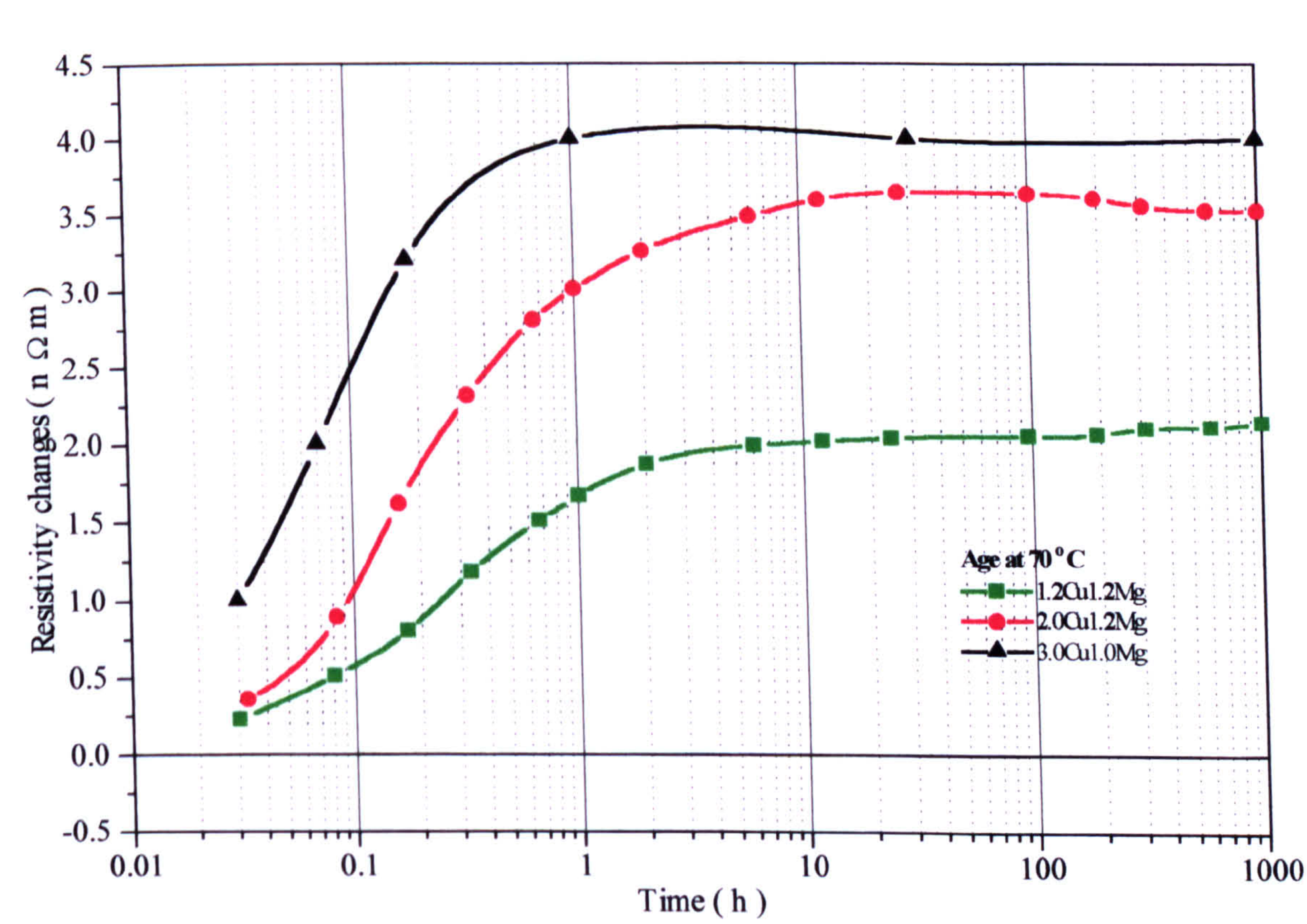

Figure 10.14: Isothermal resistivity changes of the alloys with varying copper concentration during ageing at 70°C.

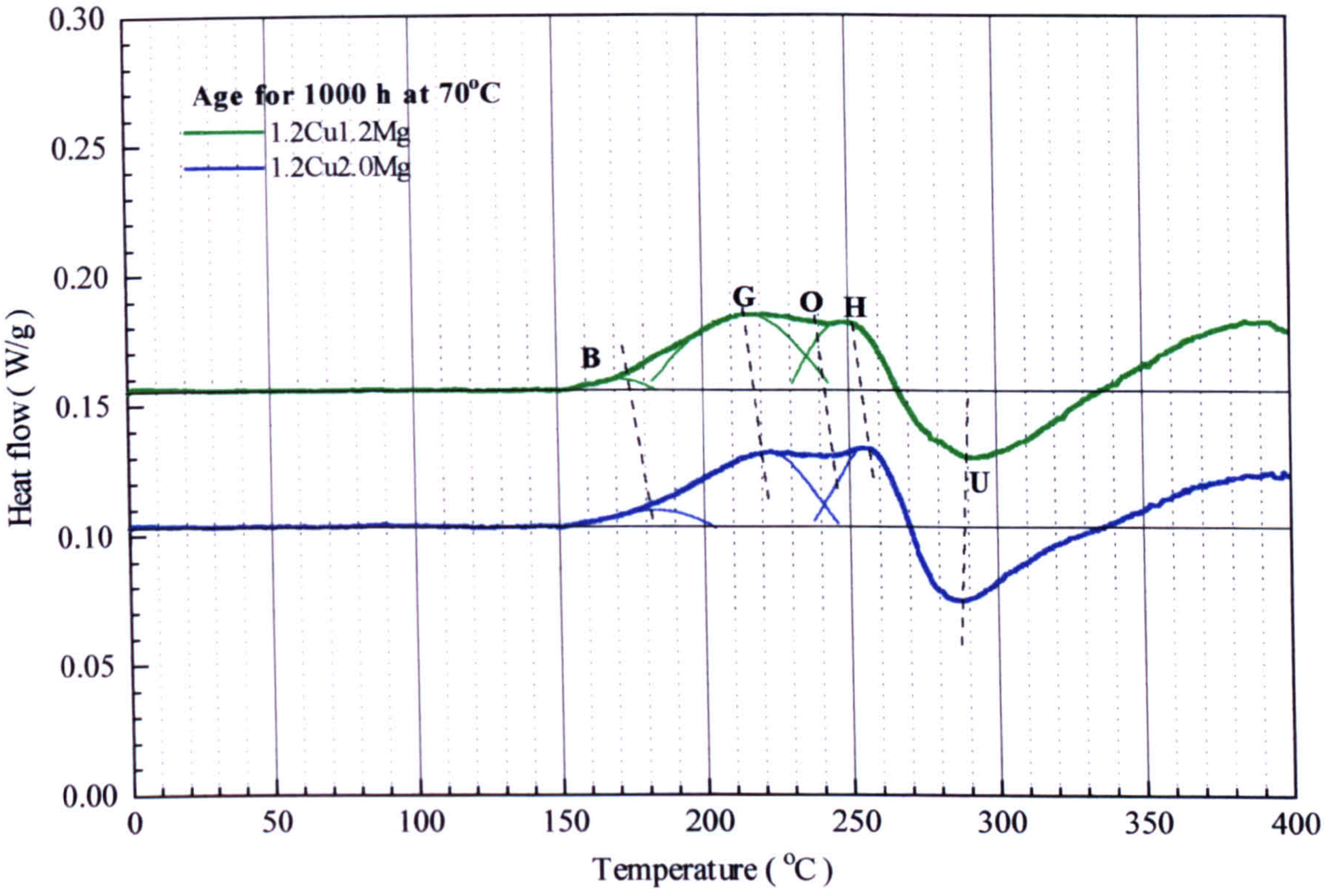

Figure 10.15: DSC comparative plots of the alloys with varying magnesium concentration after ageing for 1000 h at 70°C.

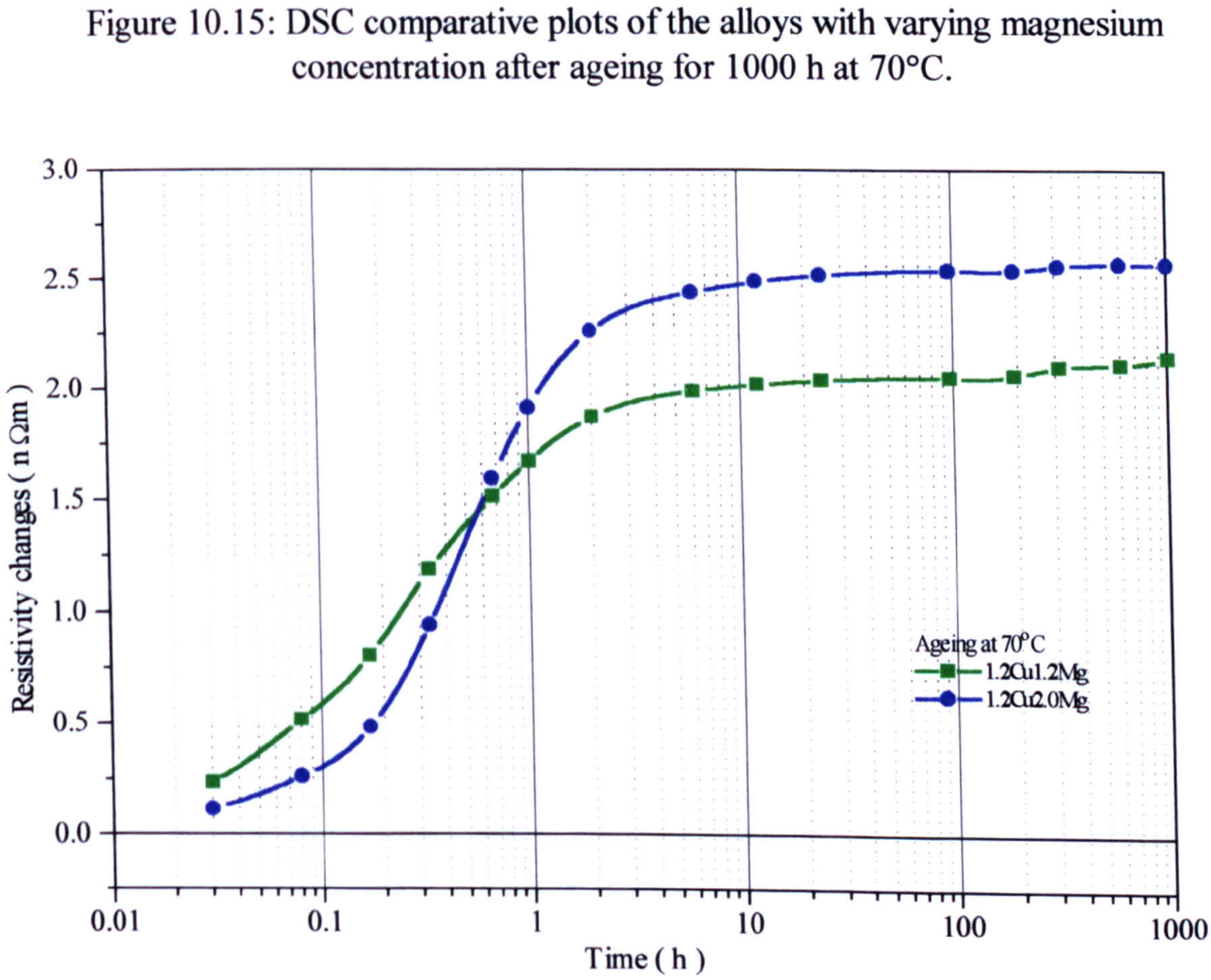

Figure 10.16: Isothermal resistivity changes of the alloys with varying magnesium concentration during ageing at 70°C.

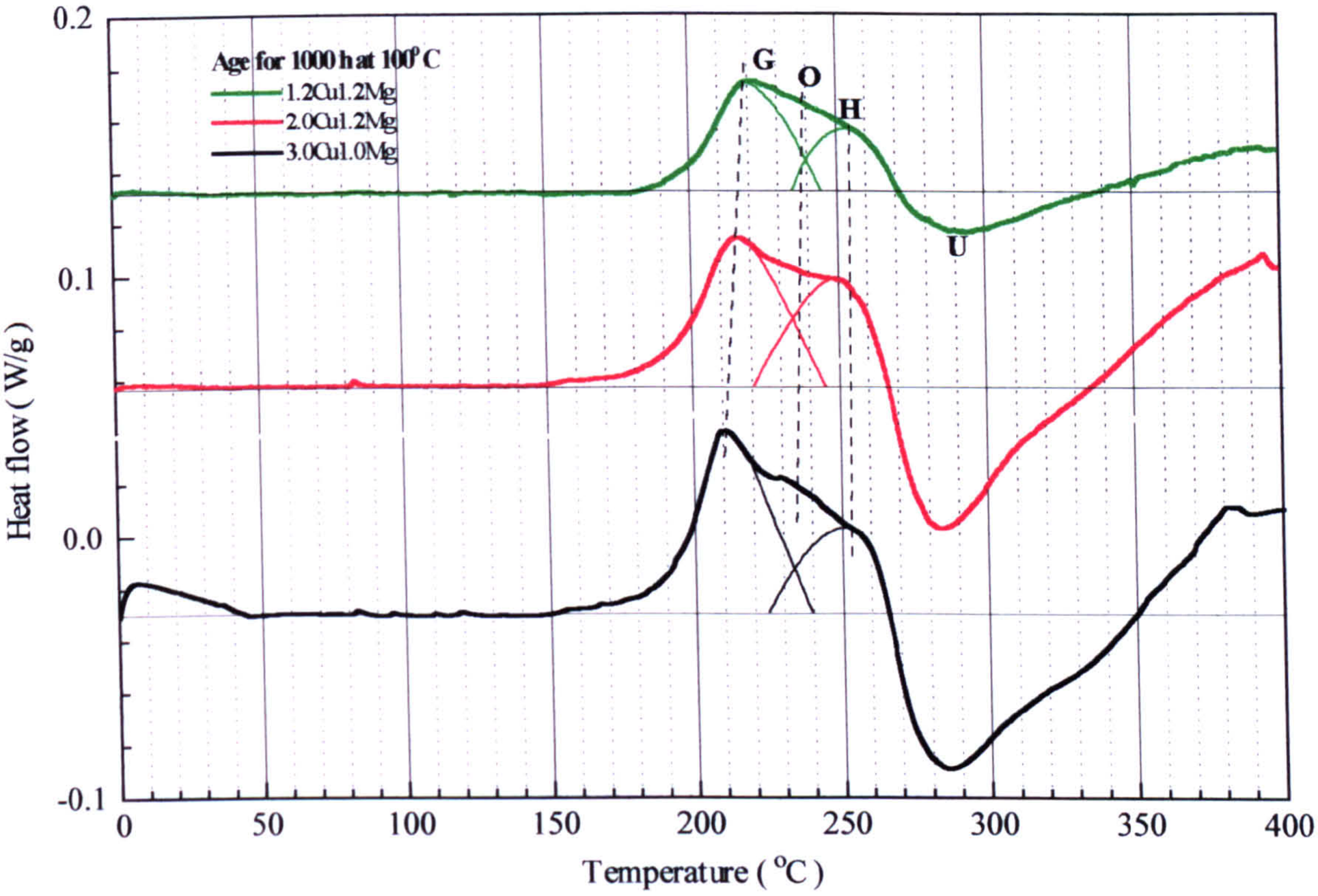

Figure 10.17: DSC comparative plots of the alloys with varying copper concentration after ageing for 1000 h at 100°C.

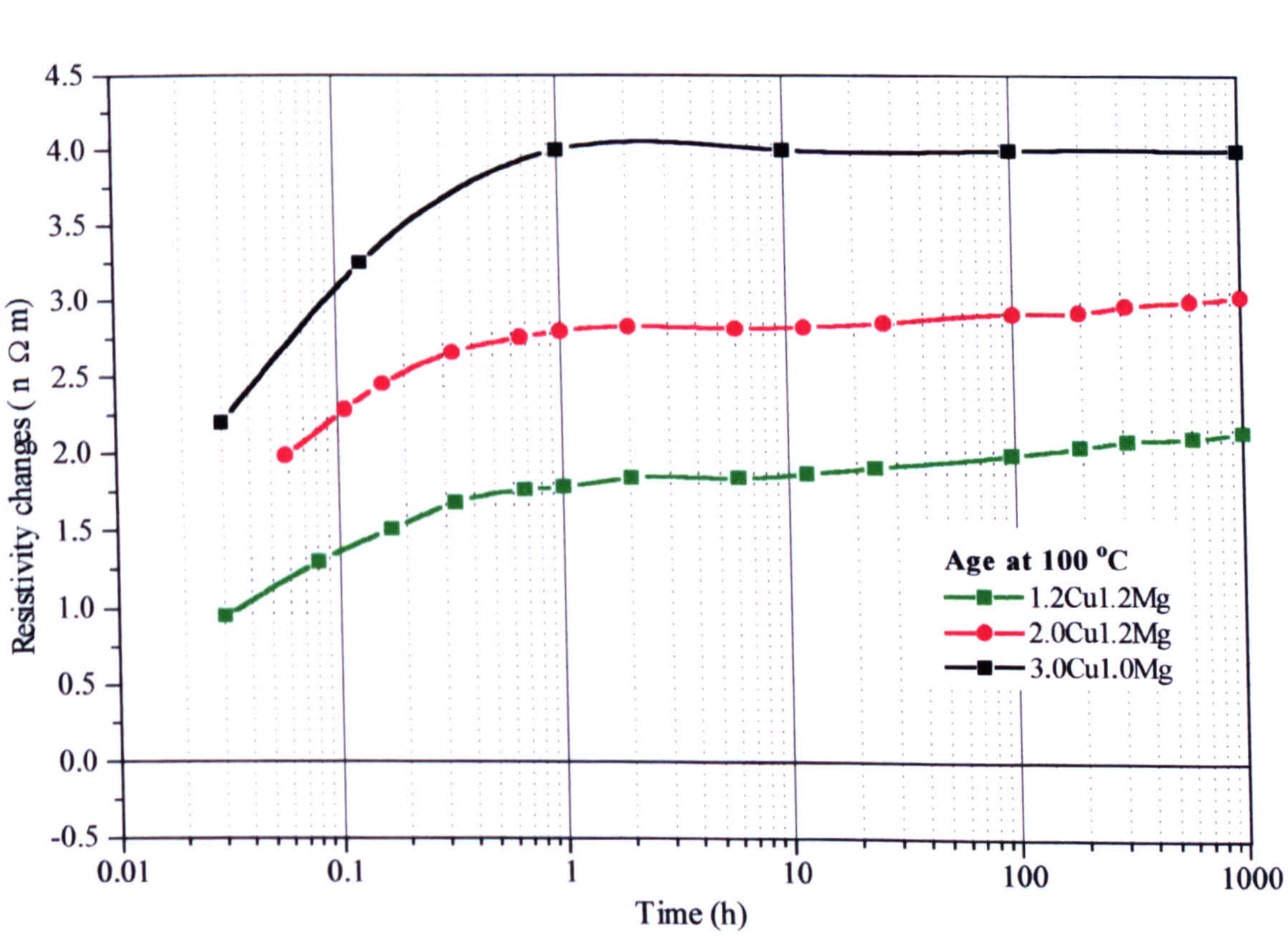

Figure 10.18: Isothermal resistivity changes of the alloys with varying copper concentration during ageing at 100°C.

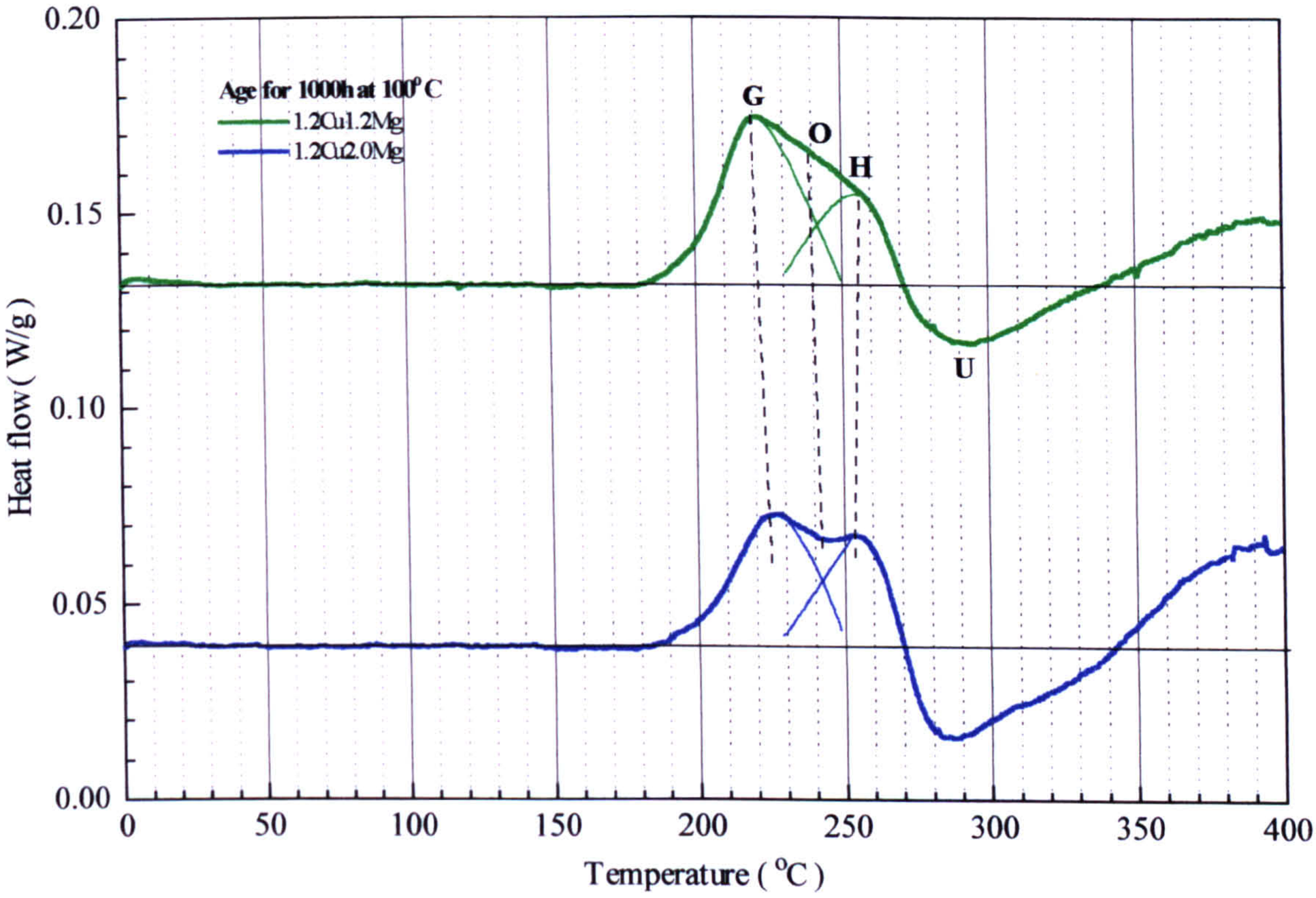

Figure 10.19: DSC comparative plots of the alloys with varying magnesium concentration after ageing for 1000 h at 100°C.

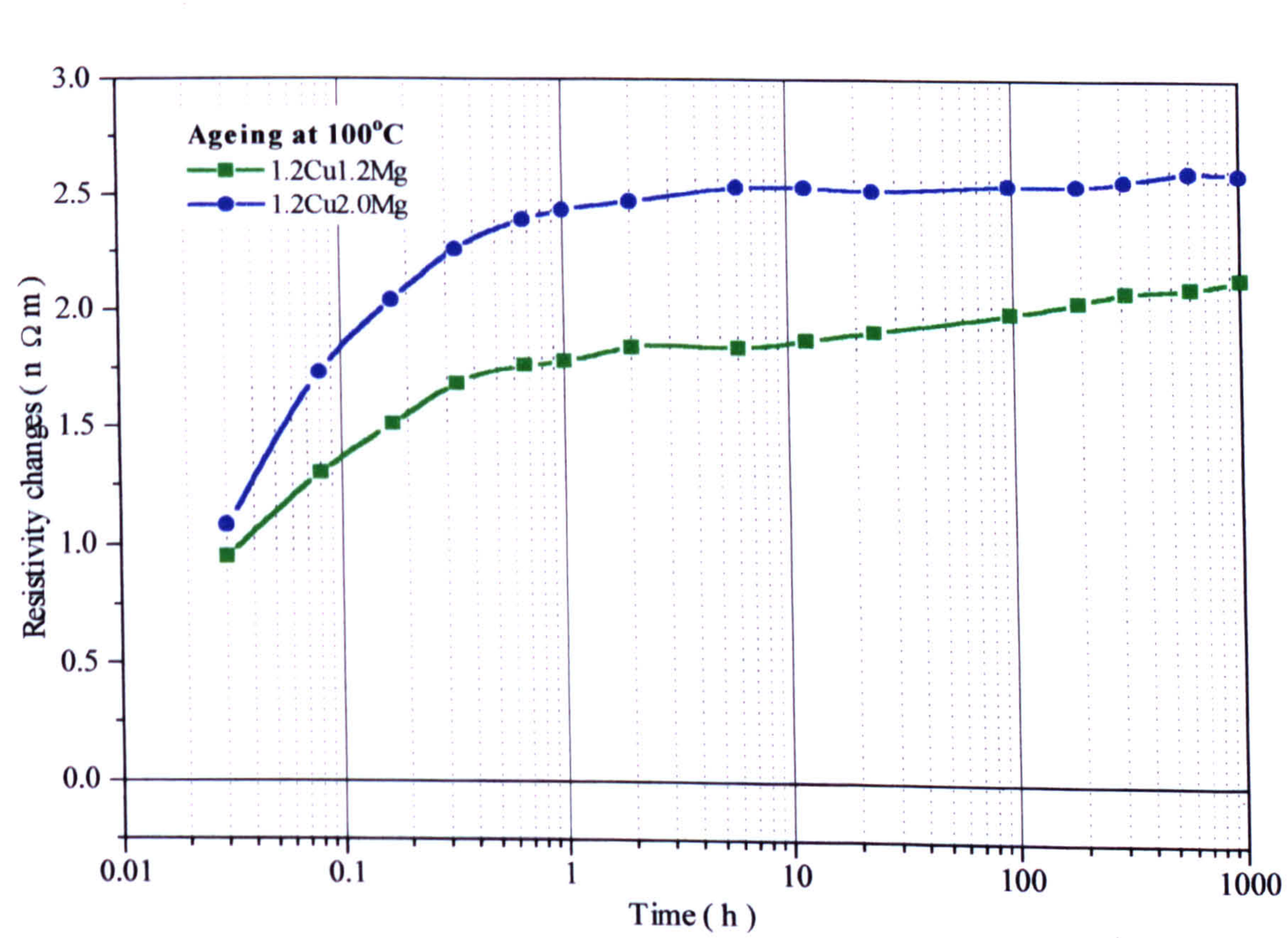

Figure 10.20: Isothermal resistivity changes of the alloys with varying magnesium concentration during ageing at 100°C.

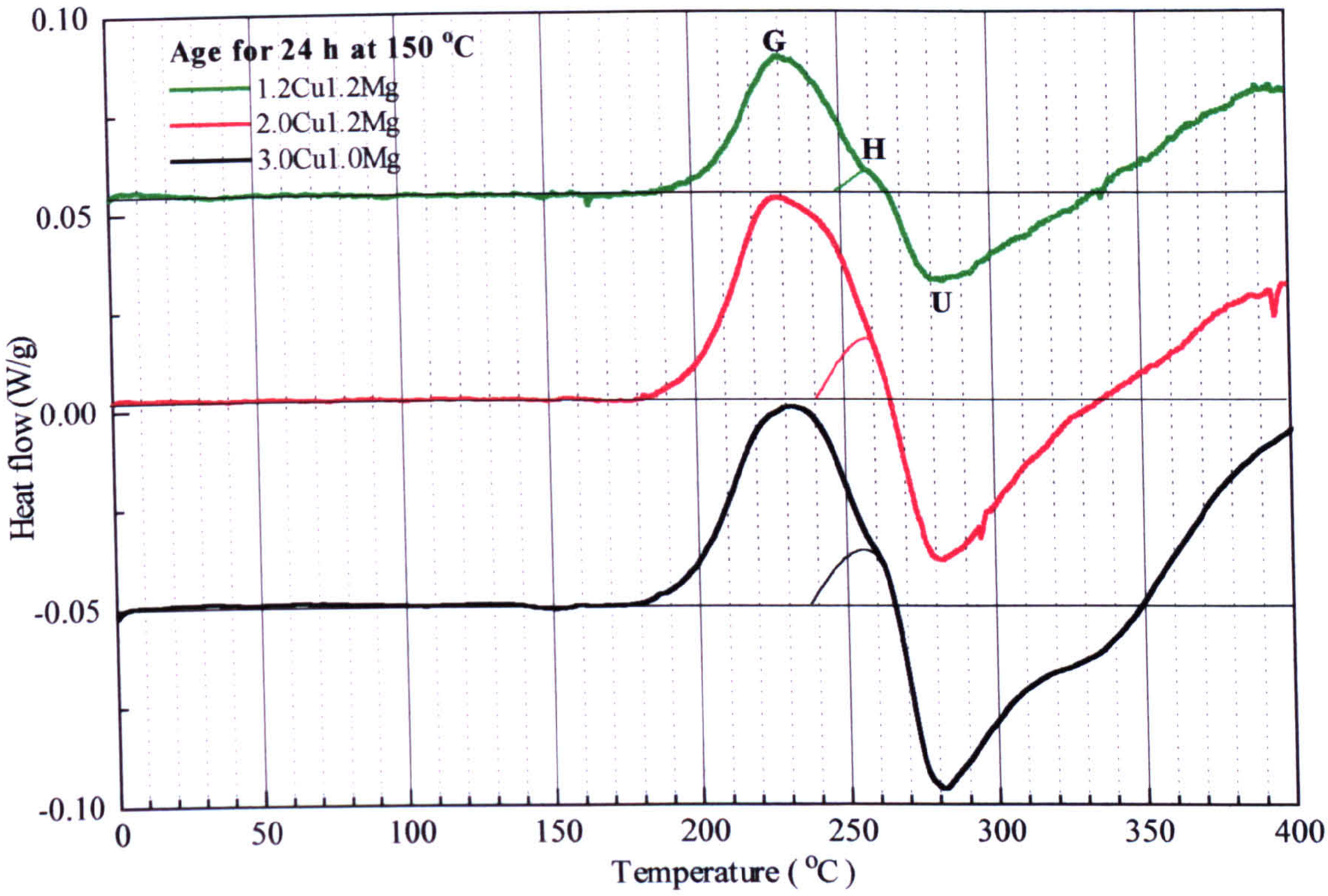

Figure 10.21: DSC comparative plots of the alloys with varying copper concentration after ageing for 24 h at 150°C.

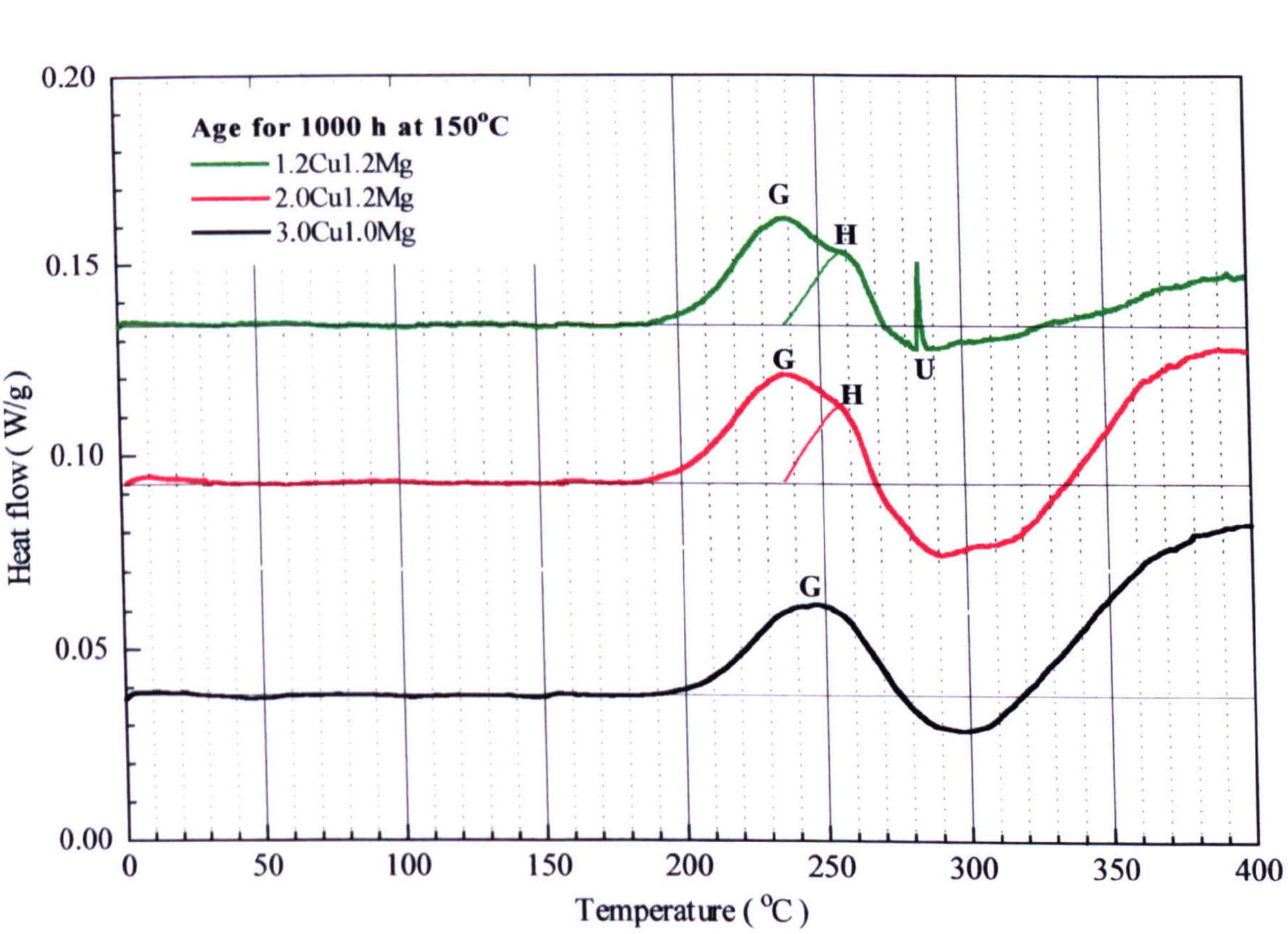

Figure 10.22: DSC comparative plots of the alloys with varying copper concentration after ageing for 1000 h at 150°C.

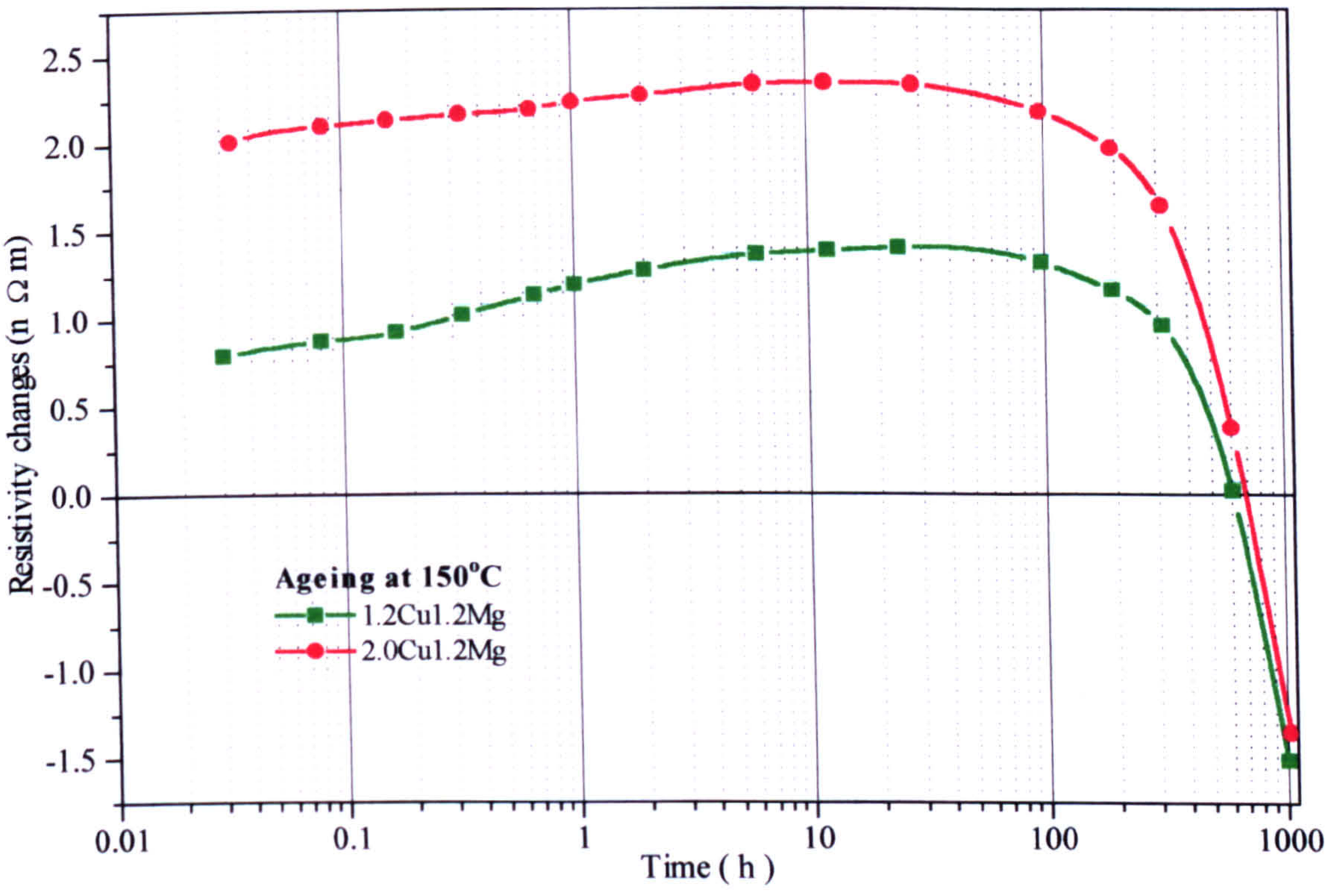

Figure 10.23: Isothermal resistivity changes of the alloys with varying copper concentration during ageing at 150°C.

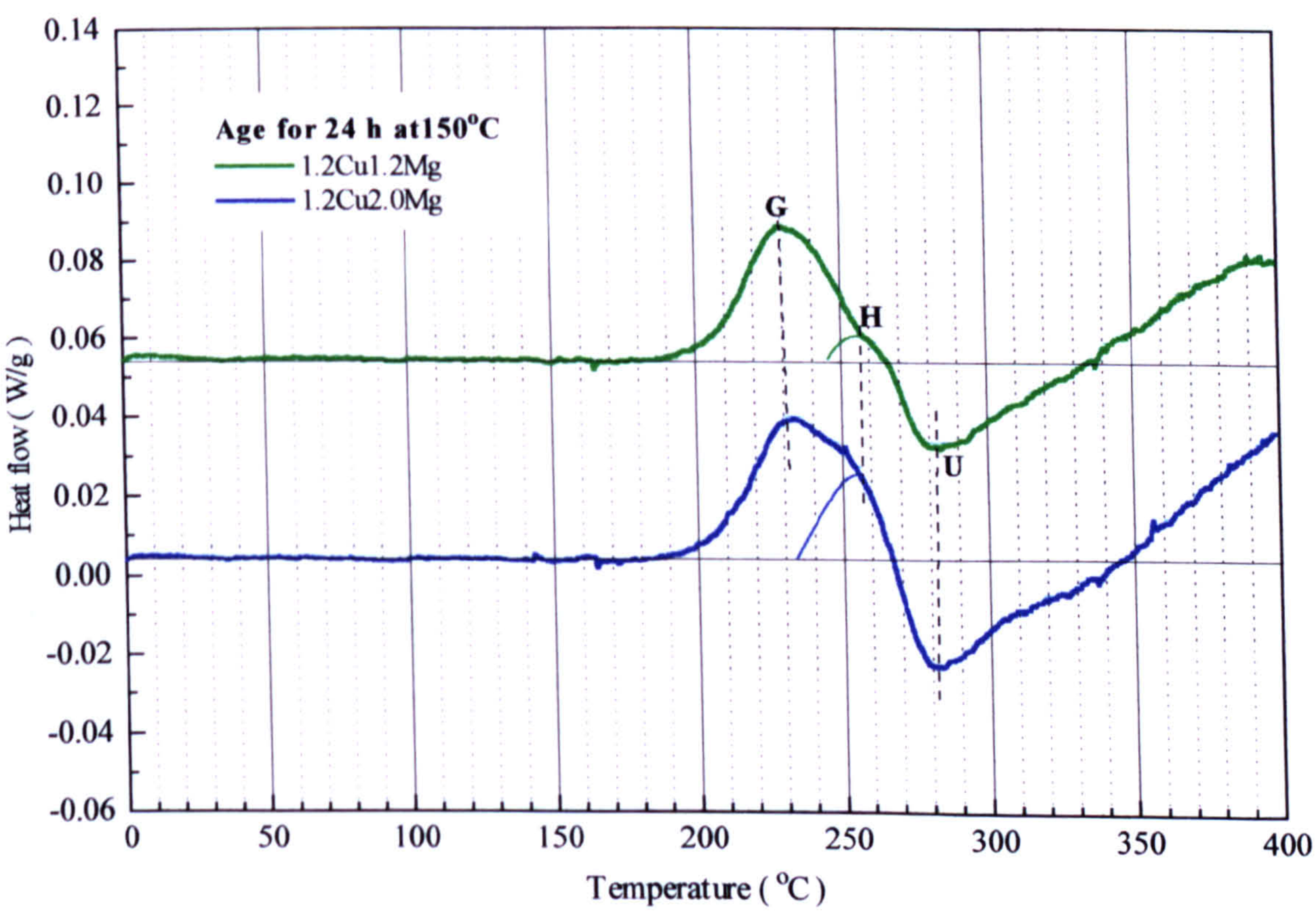

Figure 10.24: DSC comparative plots of the alloys with varying magnesium concentration after ageing for 24 h at 150°C.

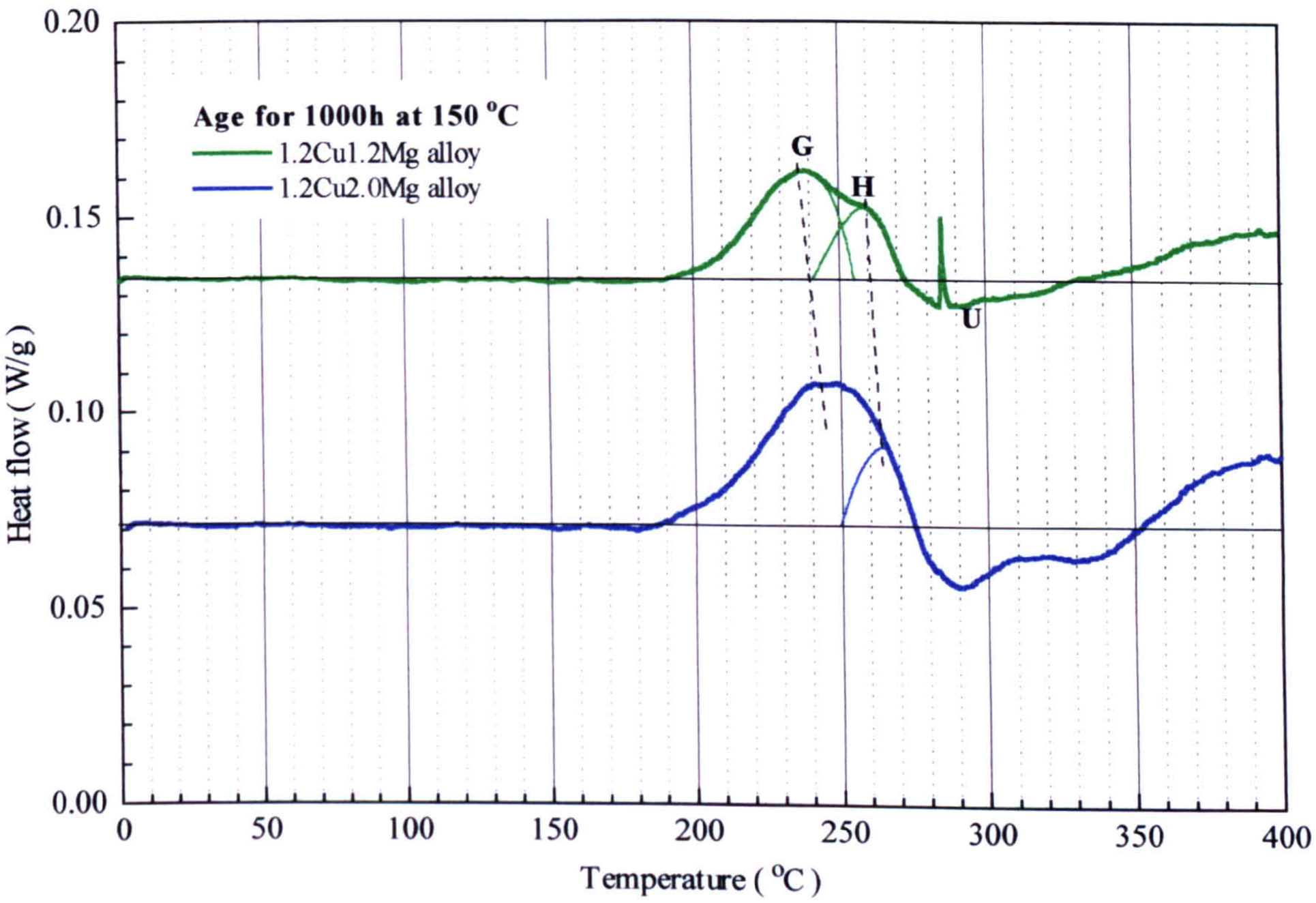

Figure 10.25: DSC comparative plots of the alloys with varying magnesium concentration after ageing for 1000 h at 150°C.

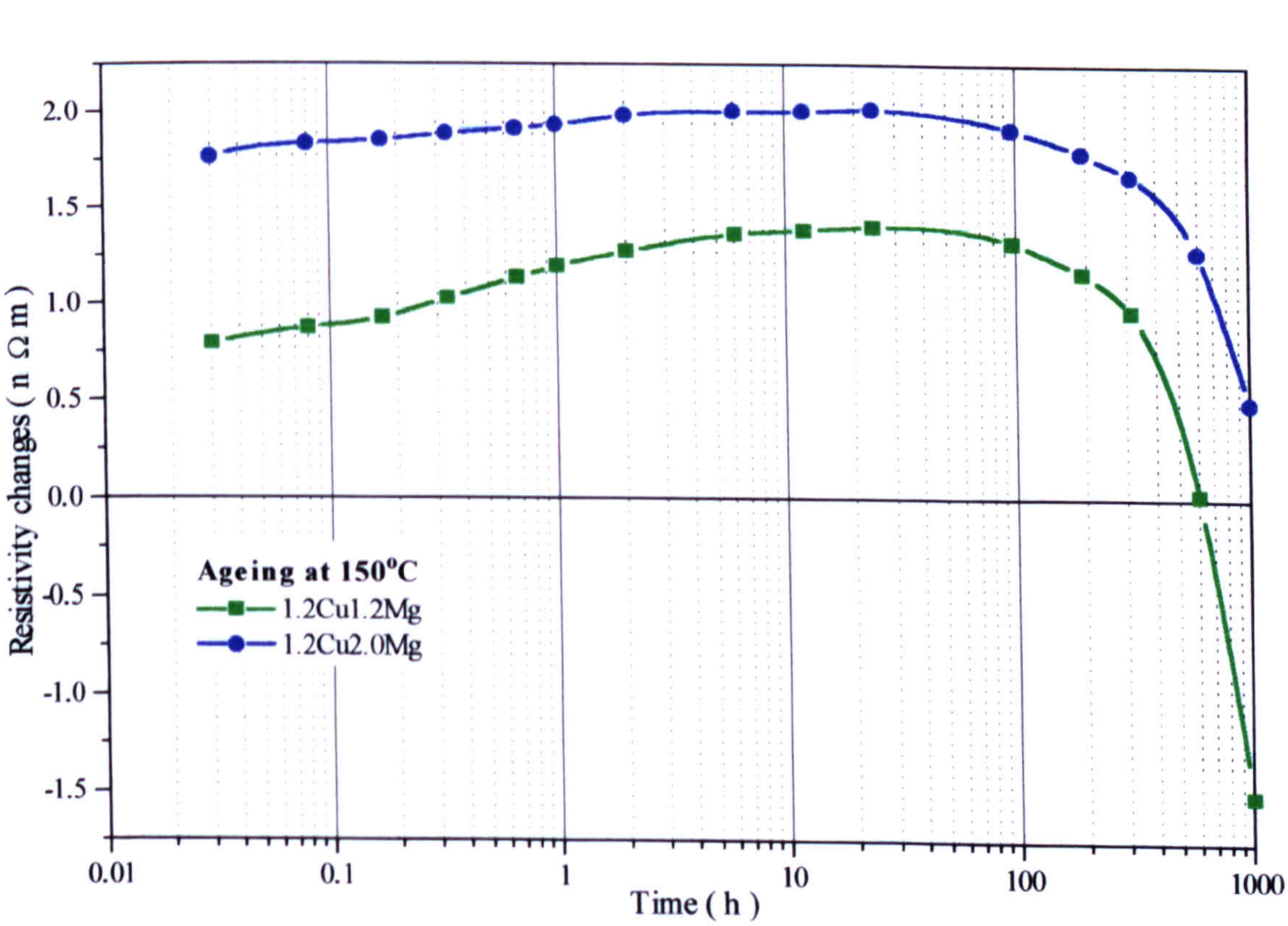

Figure 10.26: Isothermal resistivity changes of the alloys with varying magnesium concentration during ageing at 150°C.

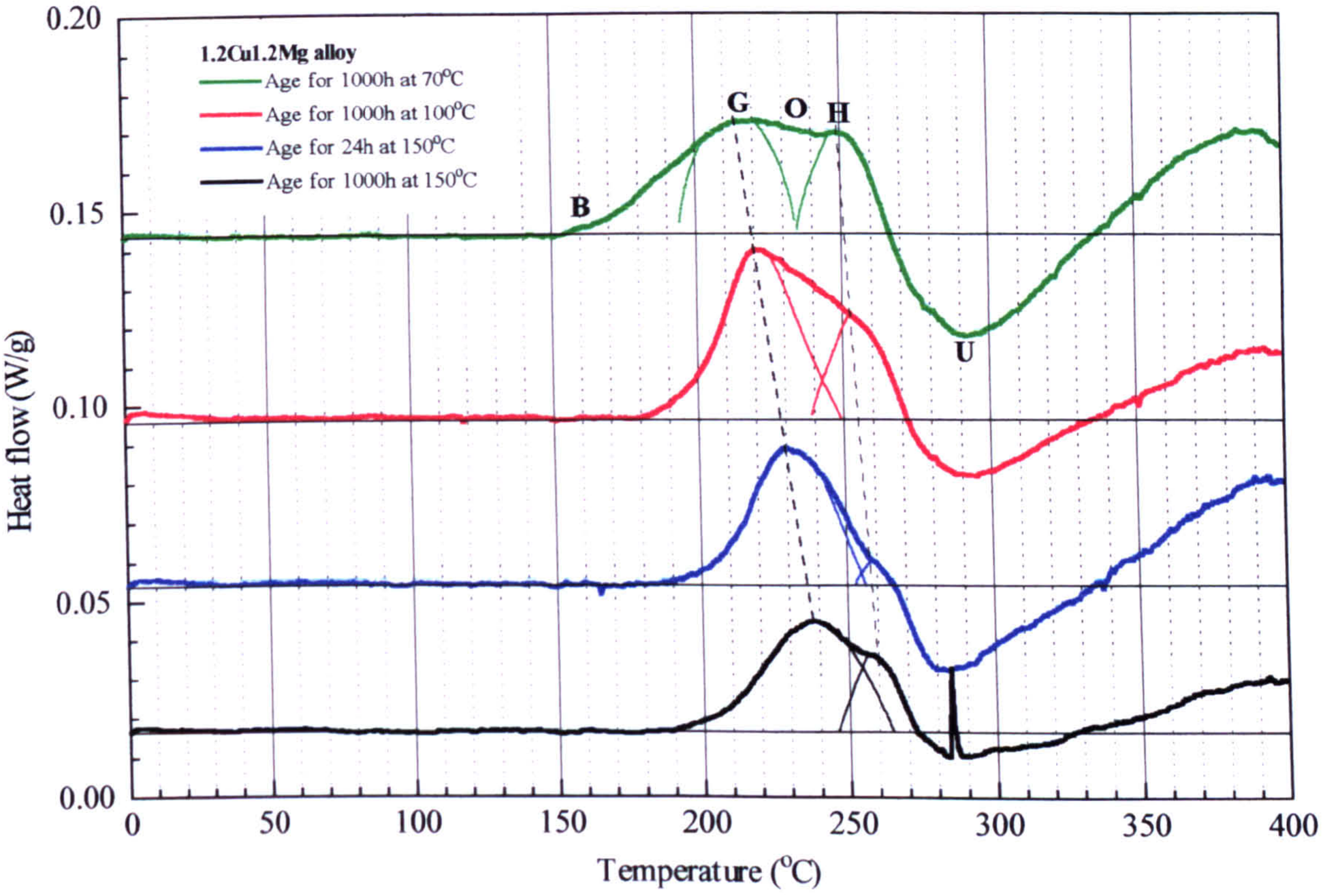

Figure 10.27: Effect of the ageing temperature on the DSC thermogram of an 1.2Cu1.2Mg alloy.

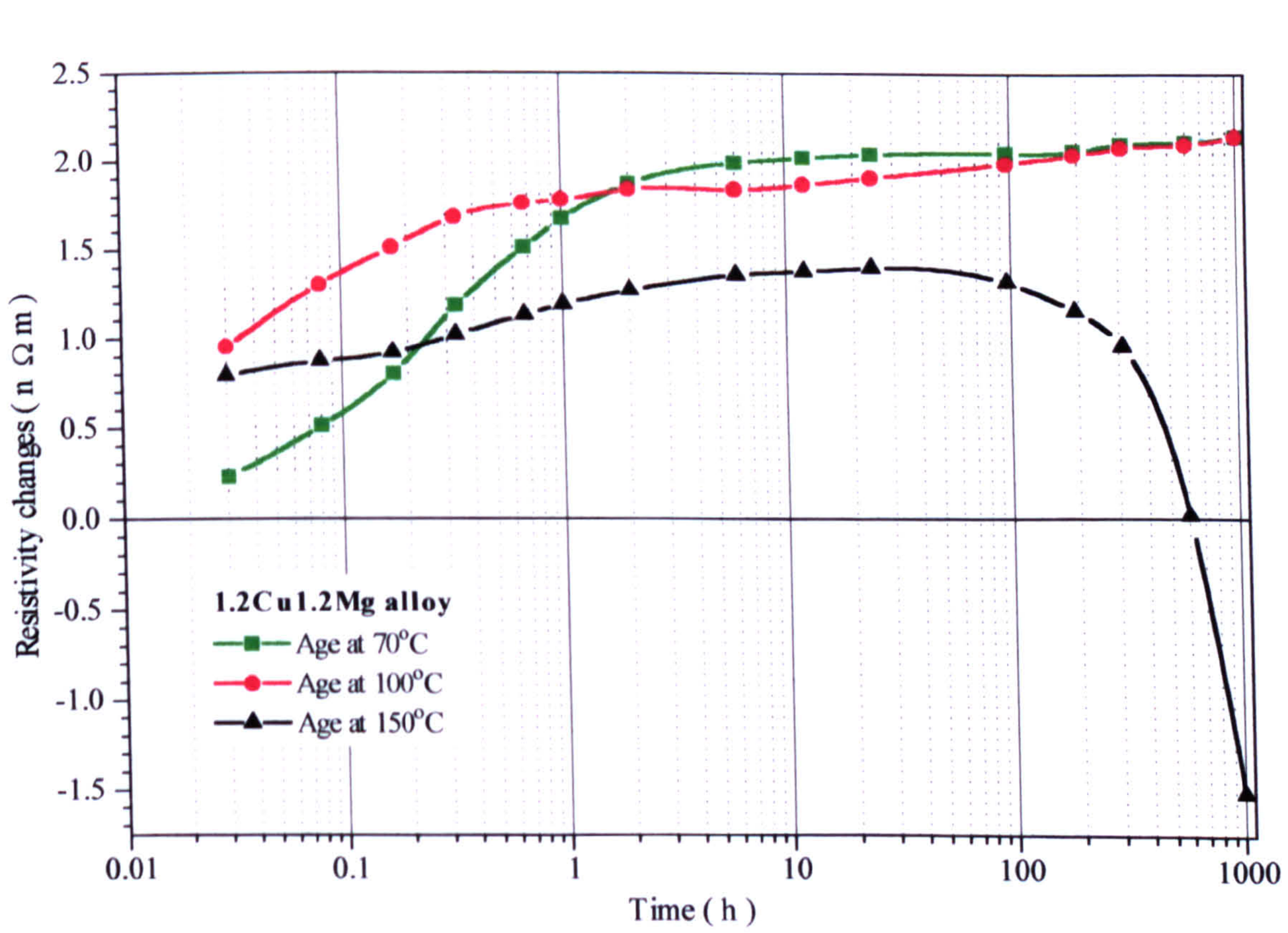

Figure 10.28: Effect of the ageing temperature on the resistivity of an 1.2Cu1.2Mg alloy.

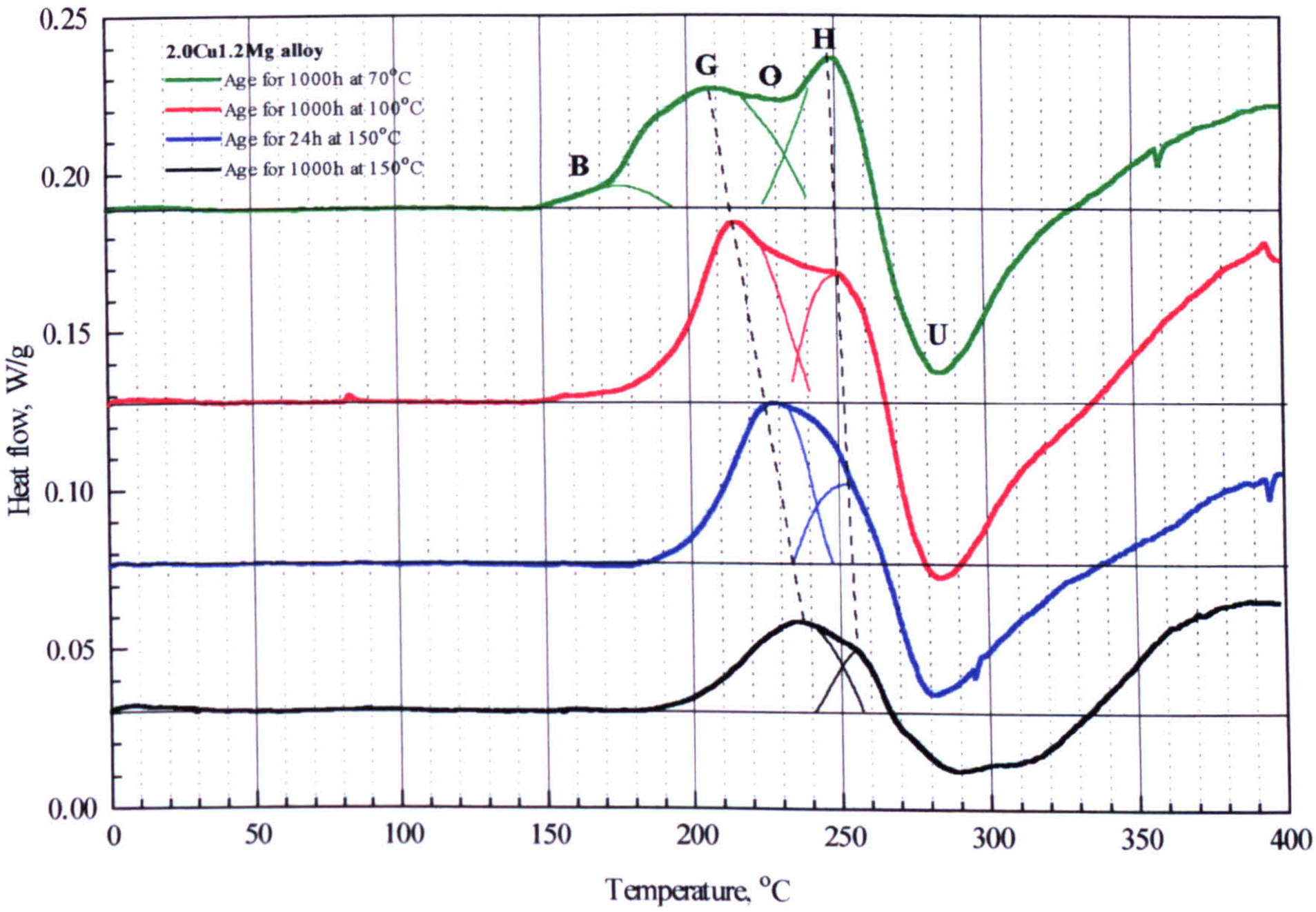

Figure 10.29: Effect of the ageing temperature on the DSC thermogram of an 2.0Cu1.2Mg alloy.

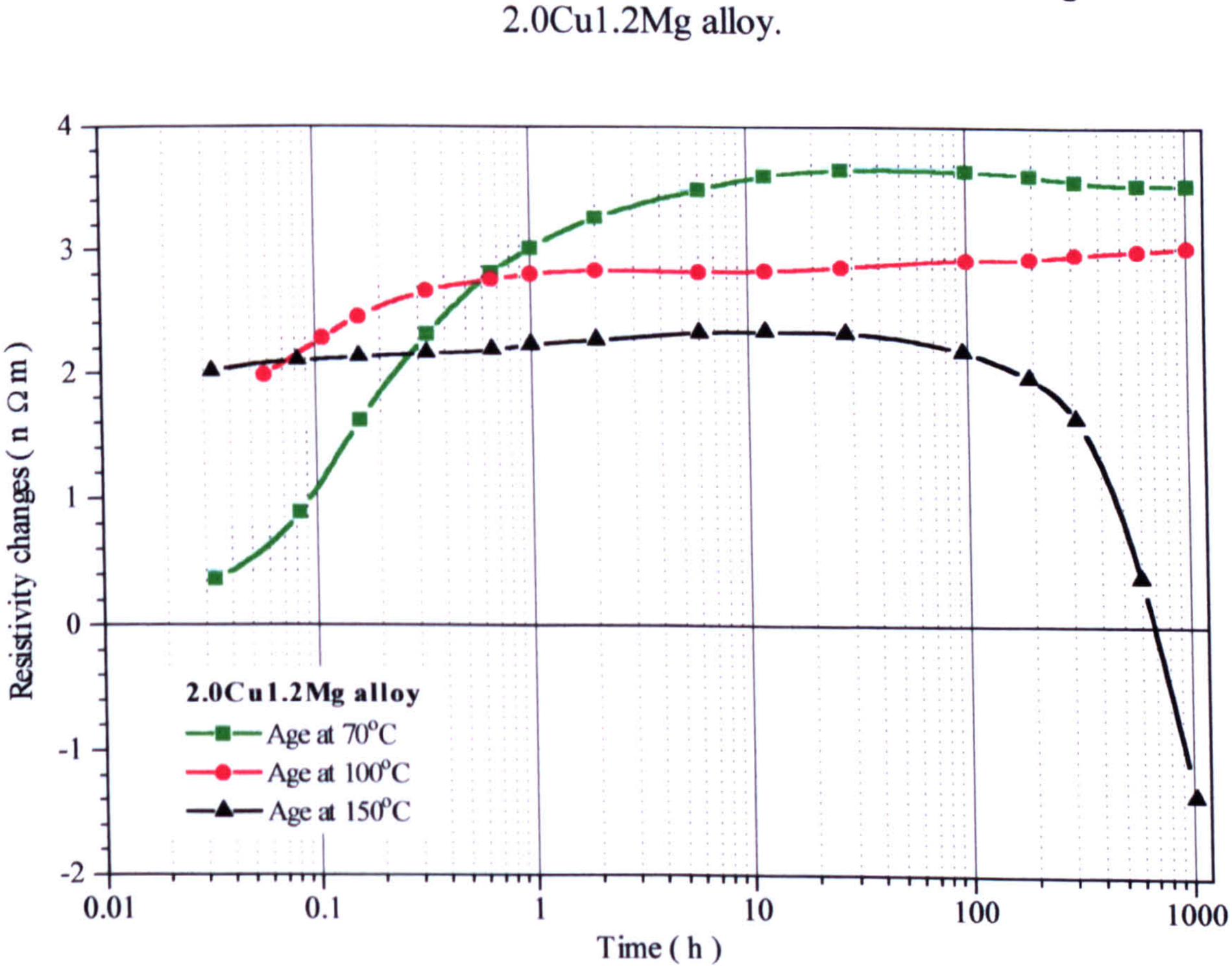

Figure 10.30: Effect of the ageing temperature on the resistivity of an 2.0Cu1.2Mg alloy.

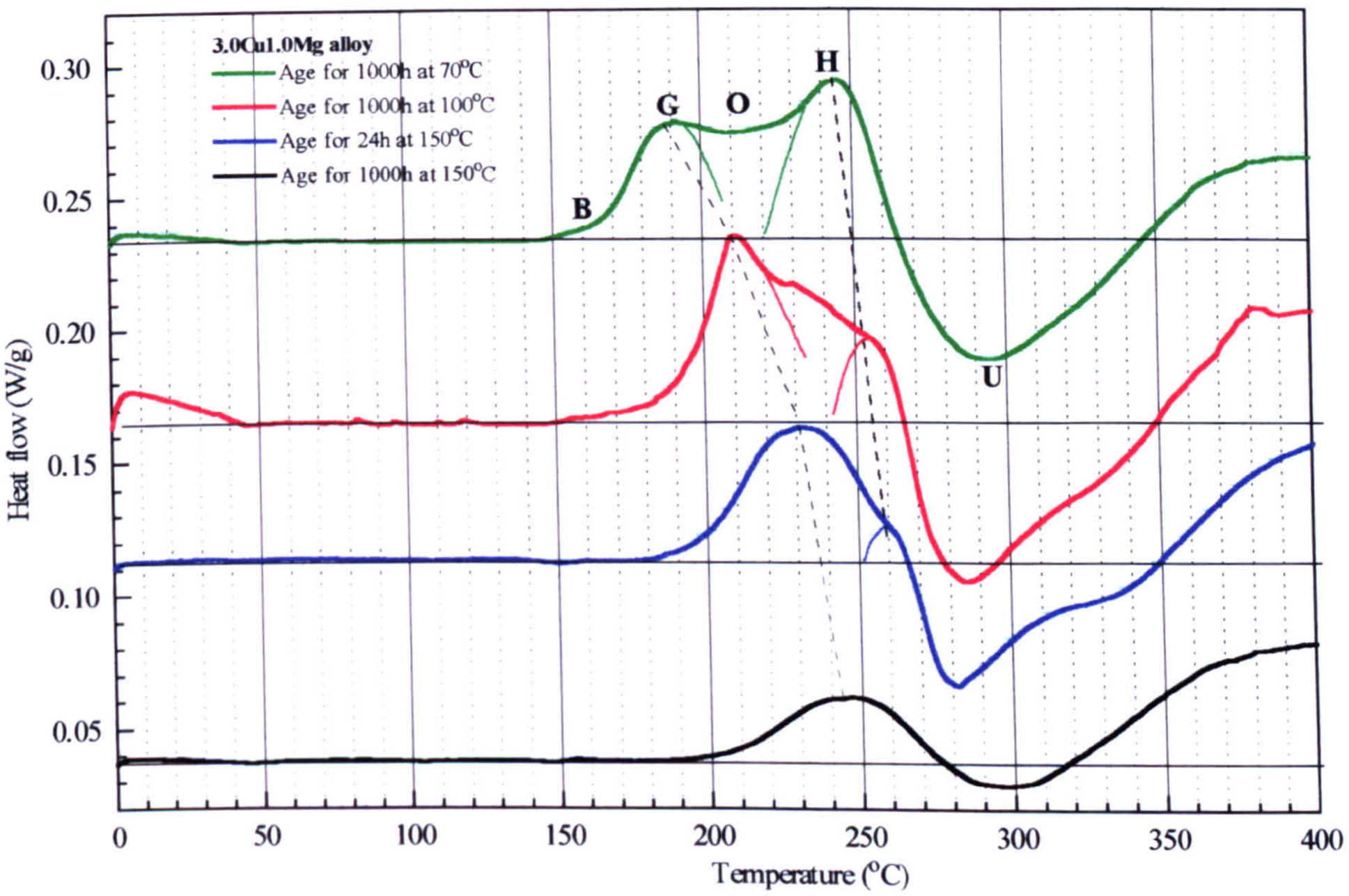

Figure 10.31: Effect of the ageing temperature on the DSC thermogram of an 3.0Cu1.0Mg alloy.

Figure 10.32: Effect of the ageing temperature on the resistivity of an 3.0Cu1.0Mg alloy.

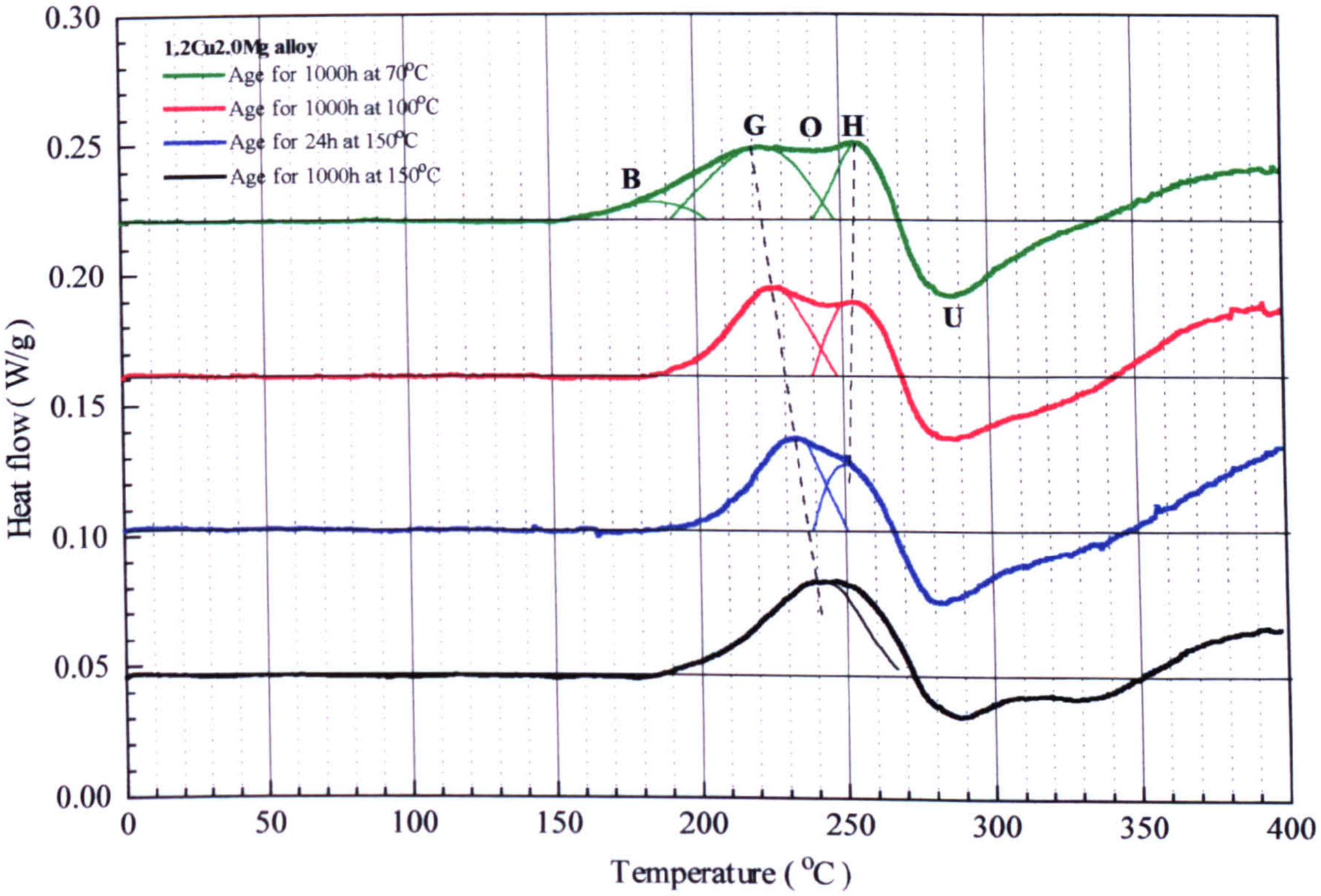

Figure 10.33: Effect of the ageing temperature on the DSC thermogram of an 1.2Cu2.0Mg alloy.

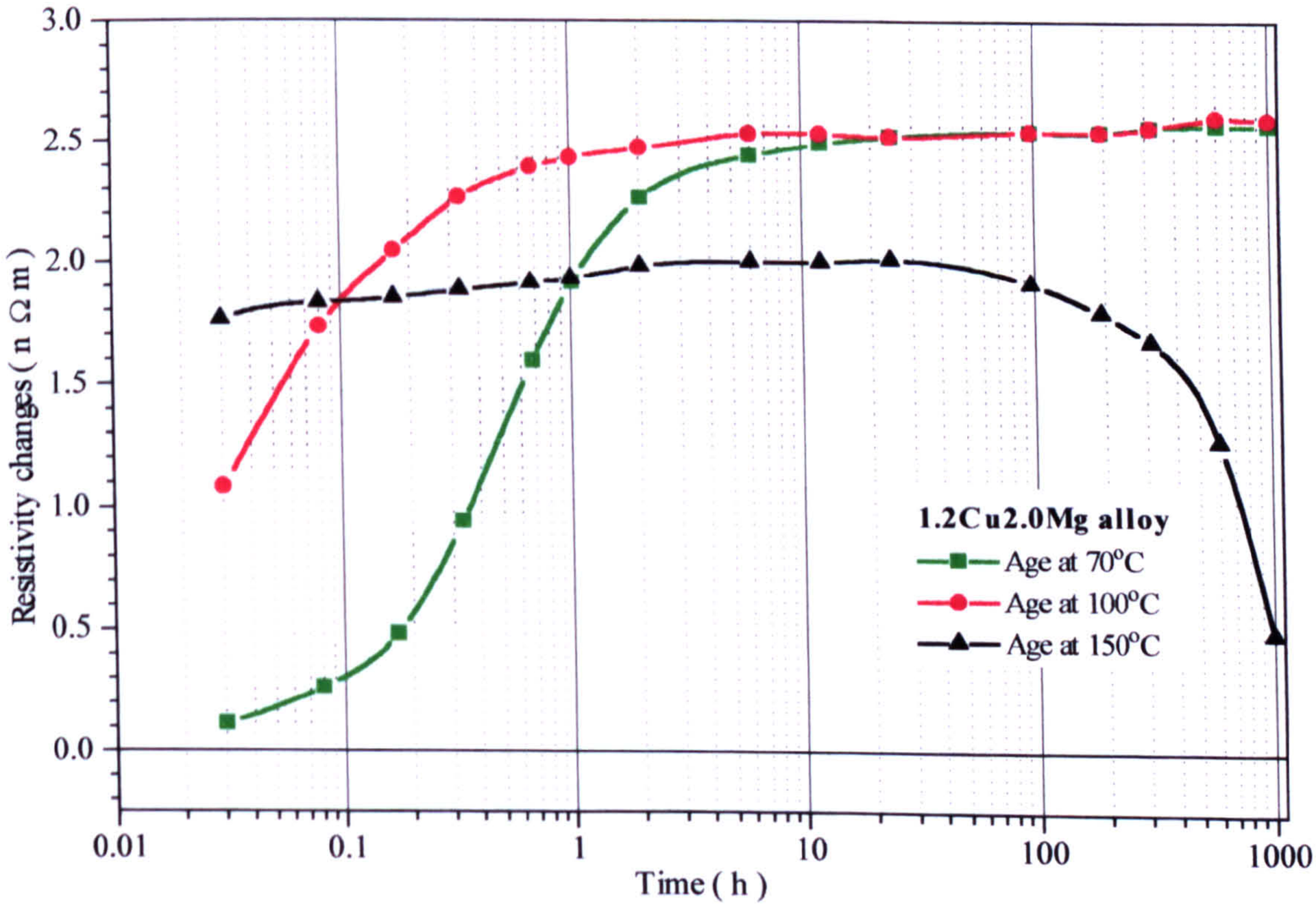

Figure 10.34: Effect of the ageing temperature on the resistivity of an 1.2Cu2.0Mg alloy.

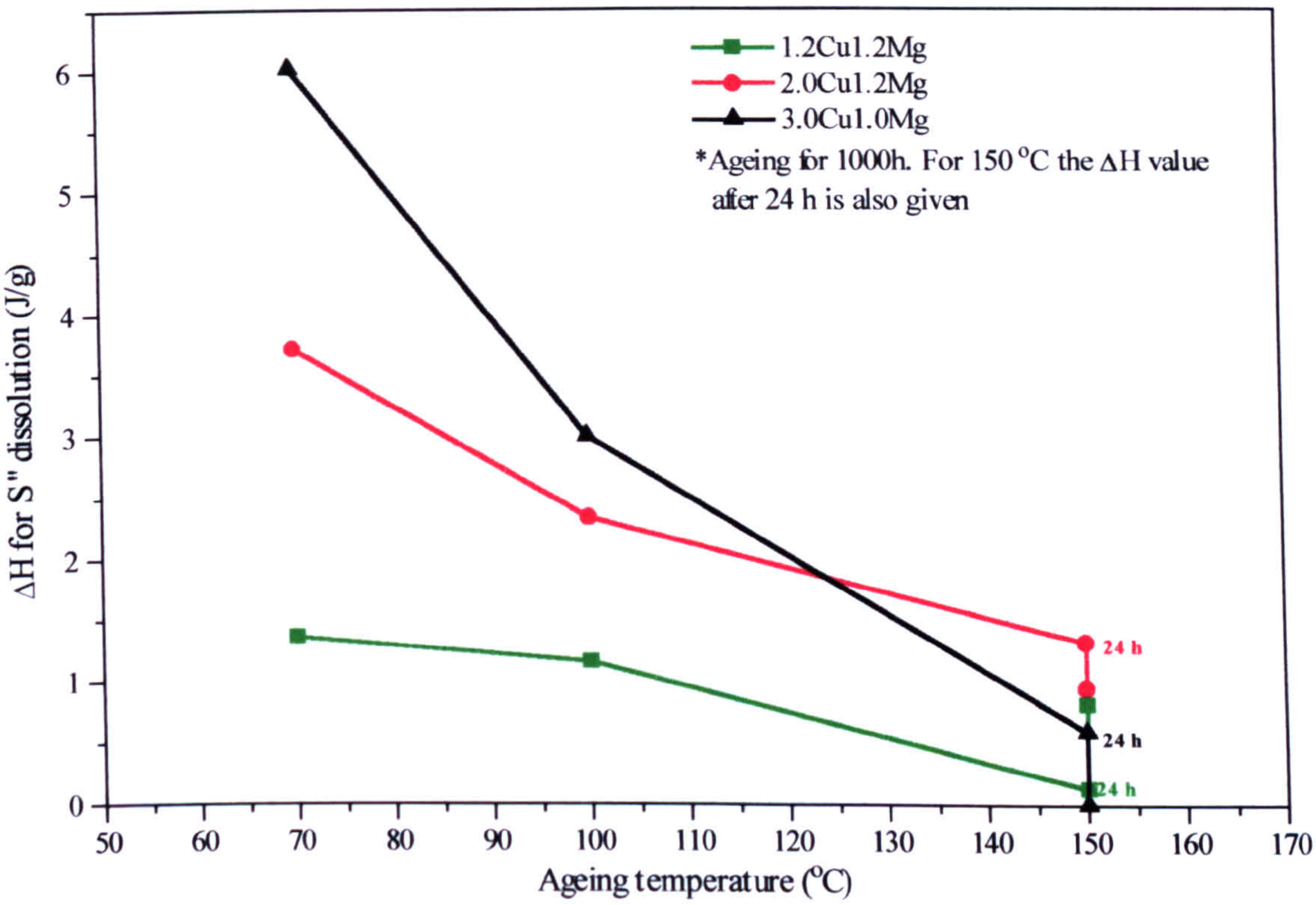

Figure 10.35: Effect of copper concentration and ageing temperature on the S″ dissolution enthalpy.

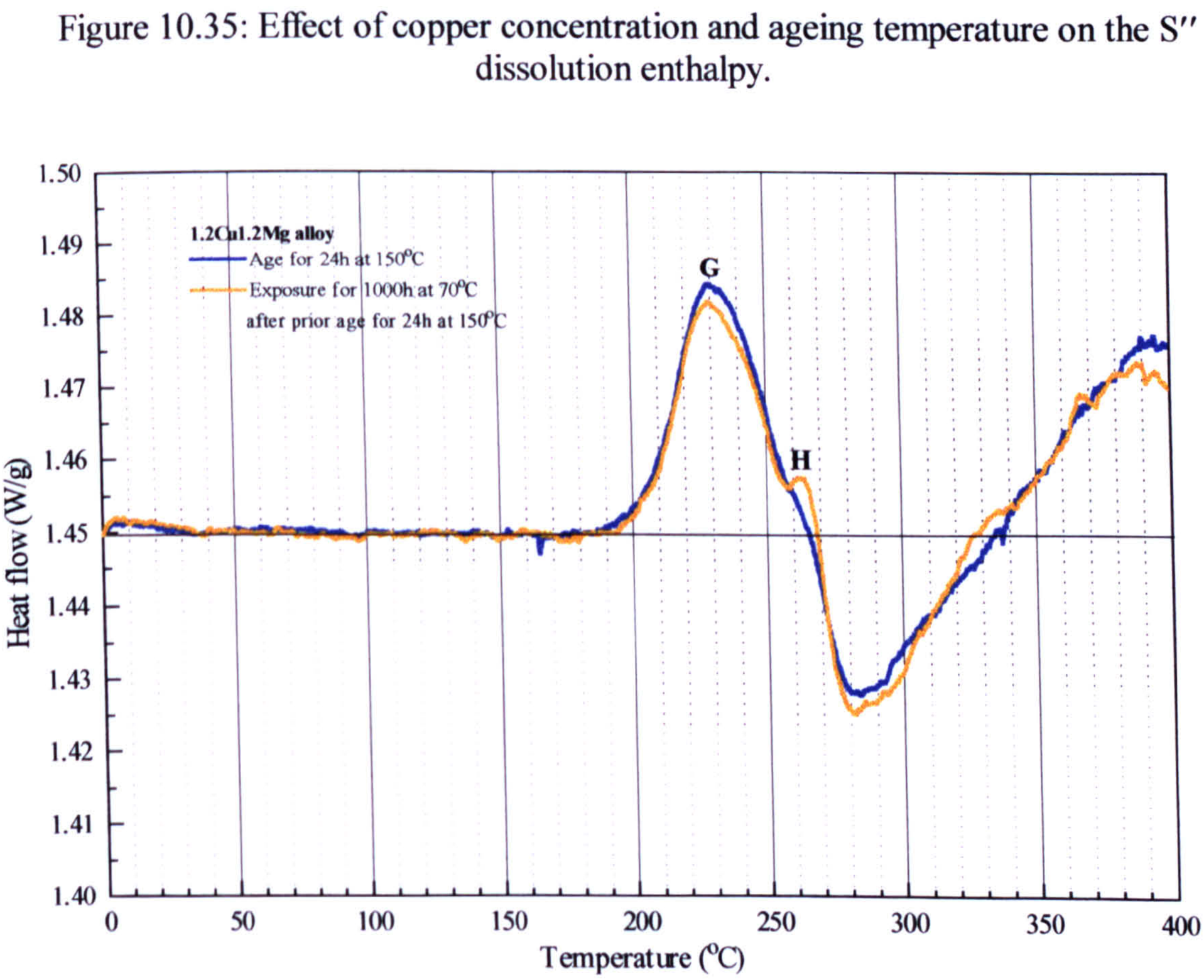

Figure 10.36: Effect of exposure at 70°C on the 1.2Cu1.2Mg alloy.

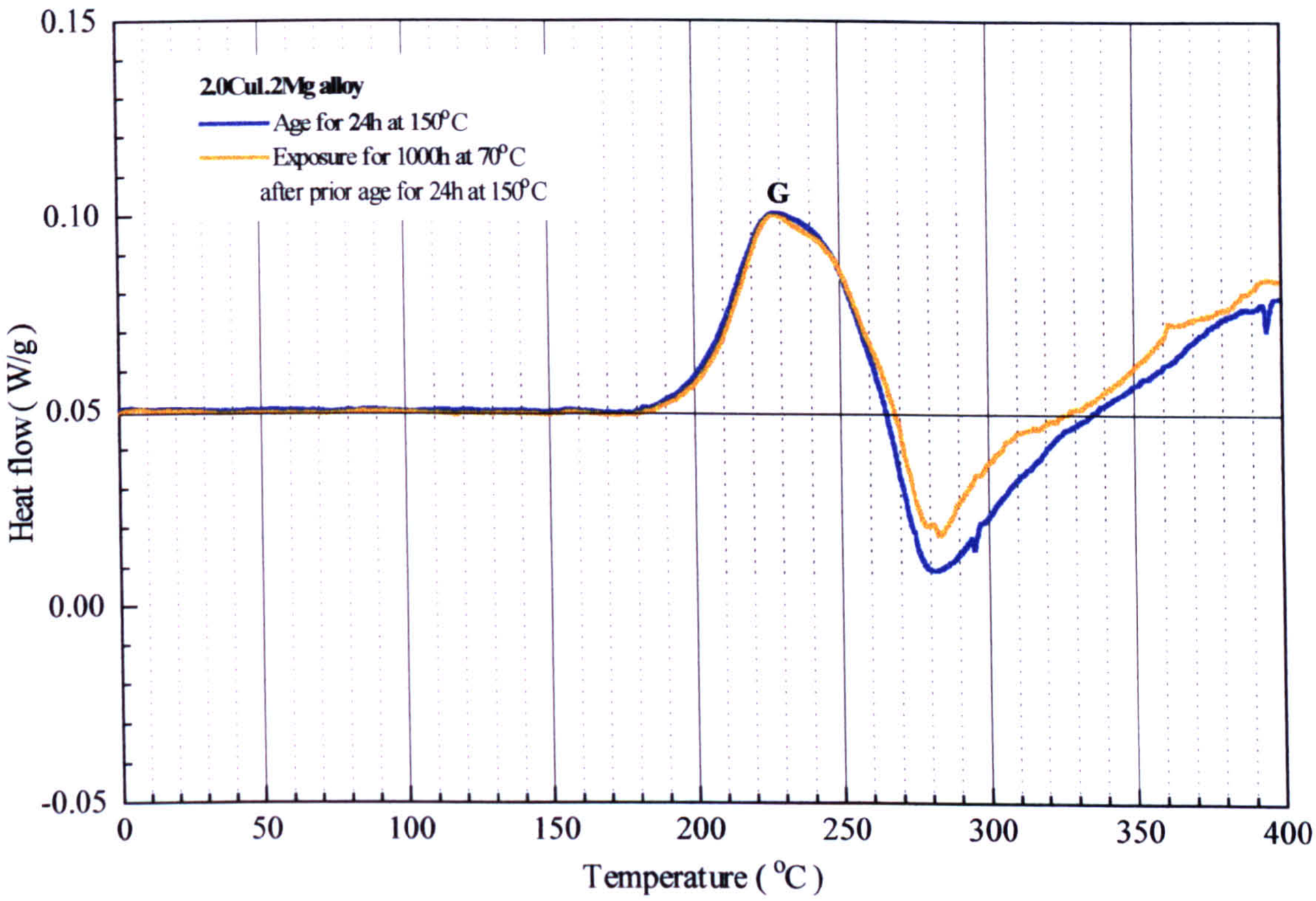

Figure 10.37: Effect of exposure at 70°C on the 2.0Cu1.2Mg alloy.

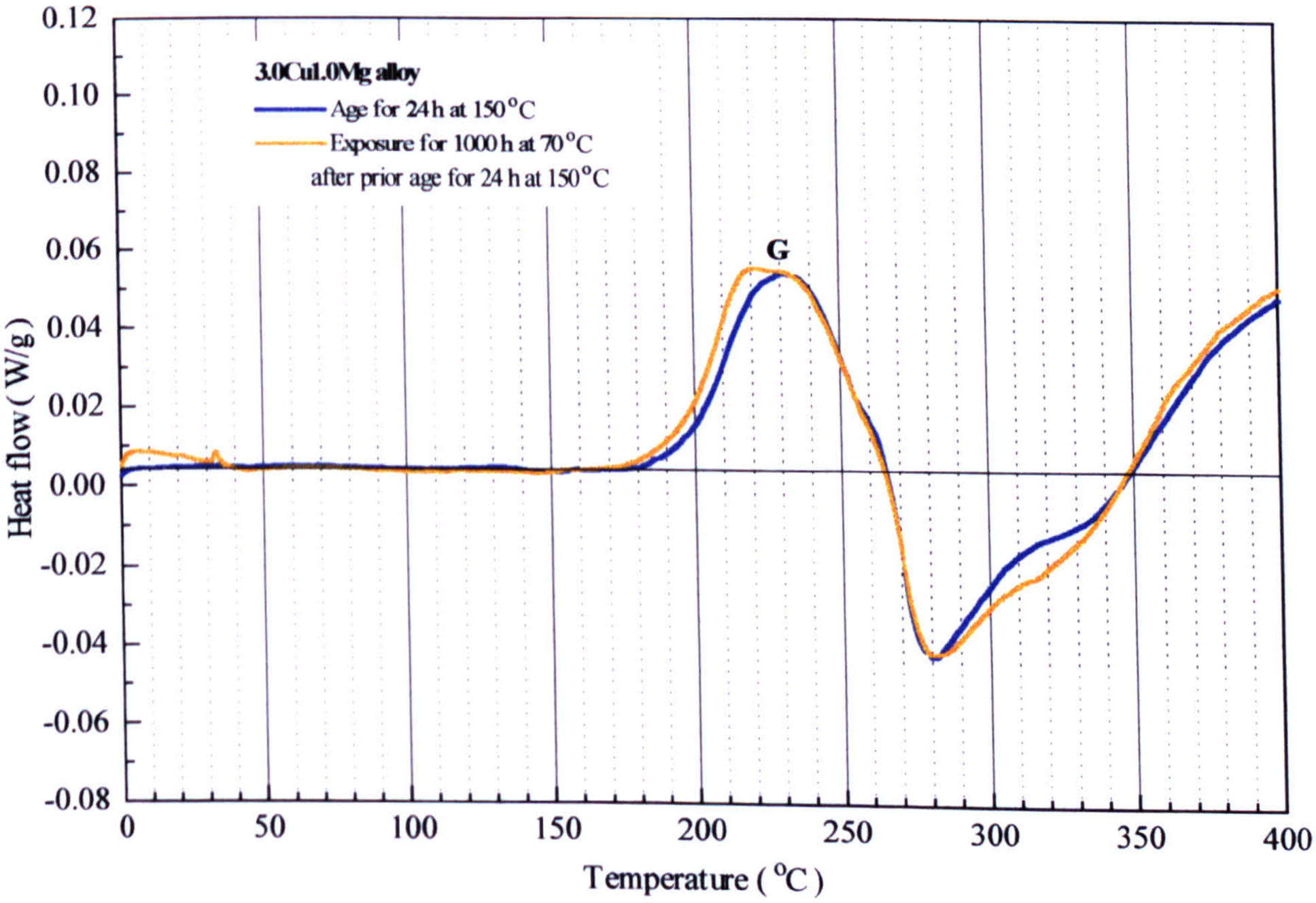

Figure 10.38: Effect of exposure at 70°C on the 3.0Cu1.0Mg alloy.

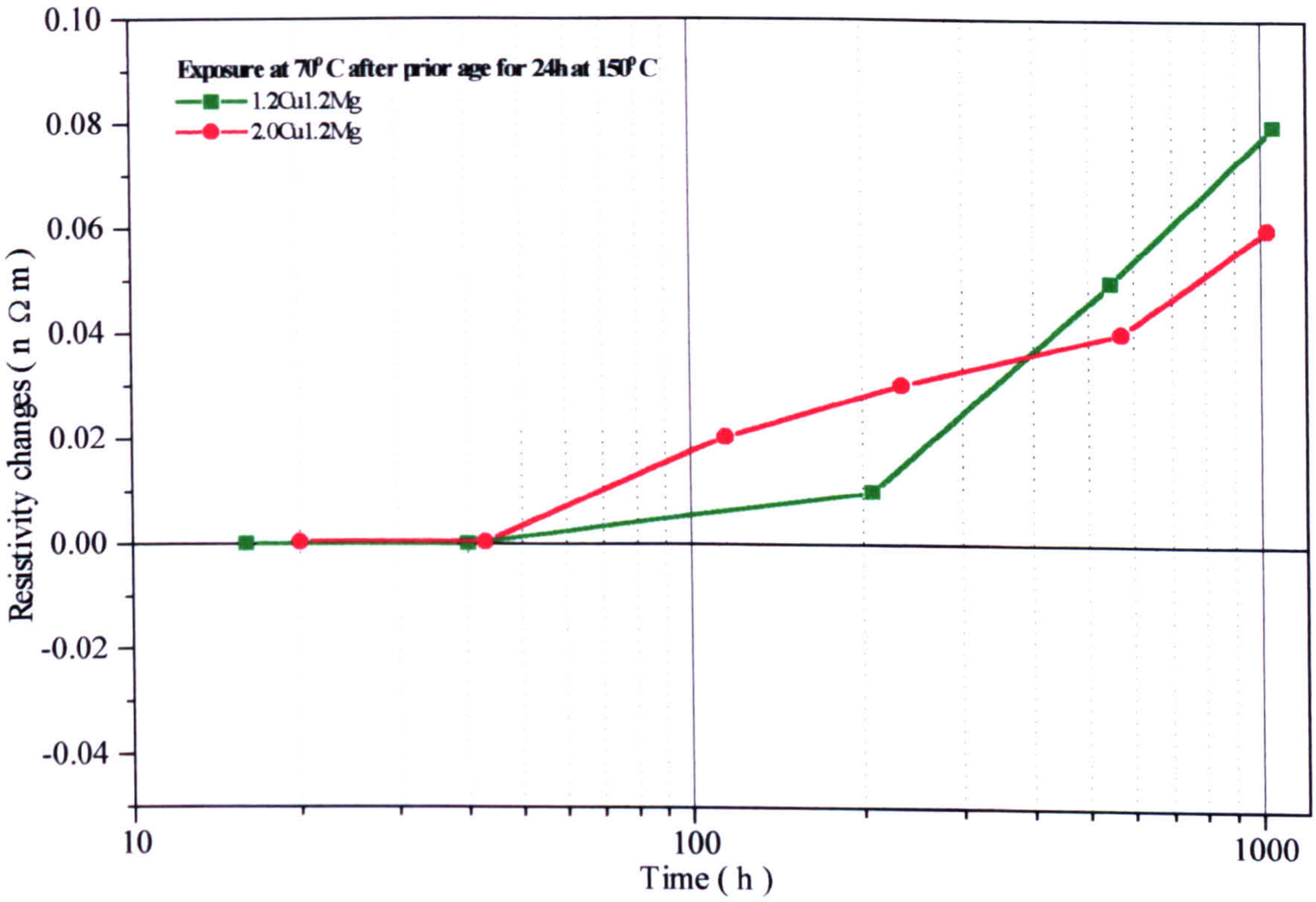

Figure 10.39: Isothermal resistivity changes of the alloys with varying copper concentration during exposure at 70°C.

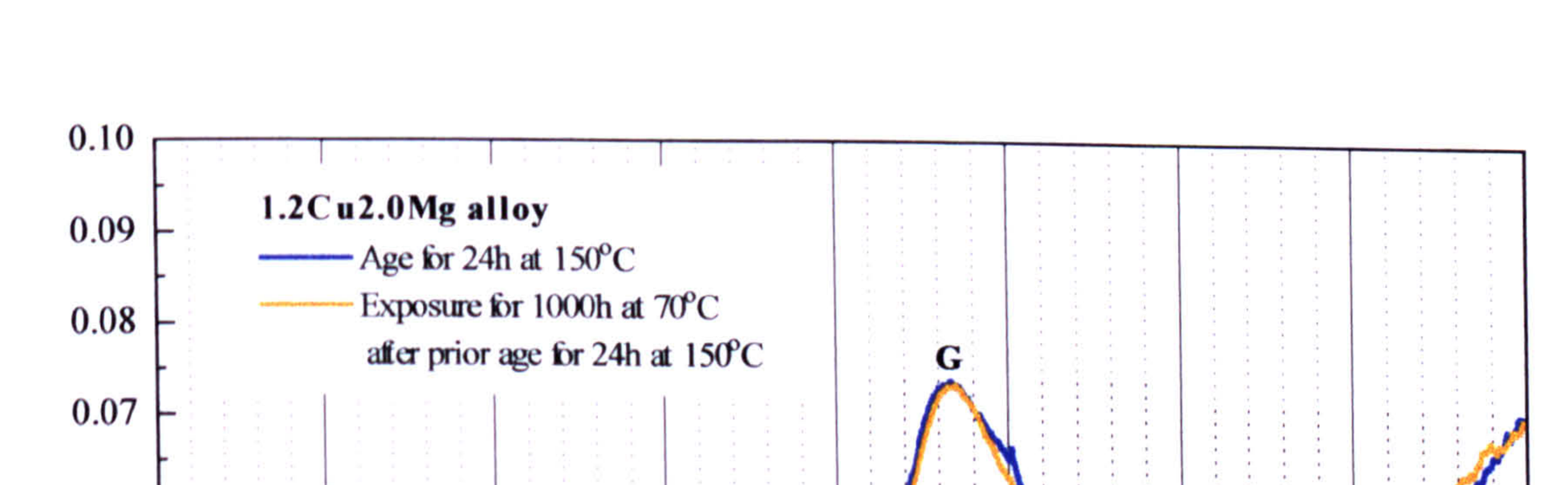

Figure 10.40: Effect of exposure at 70°C on the 1.2Cu2.0Mg alloy.

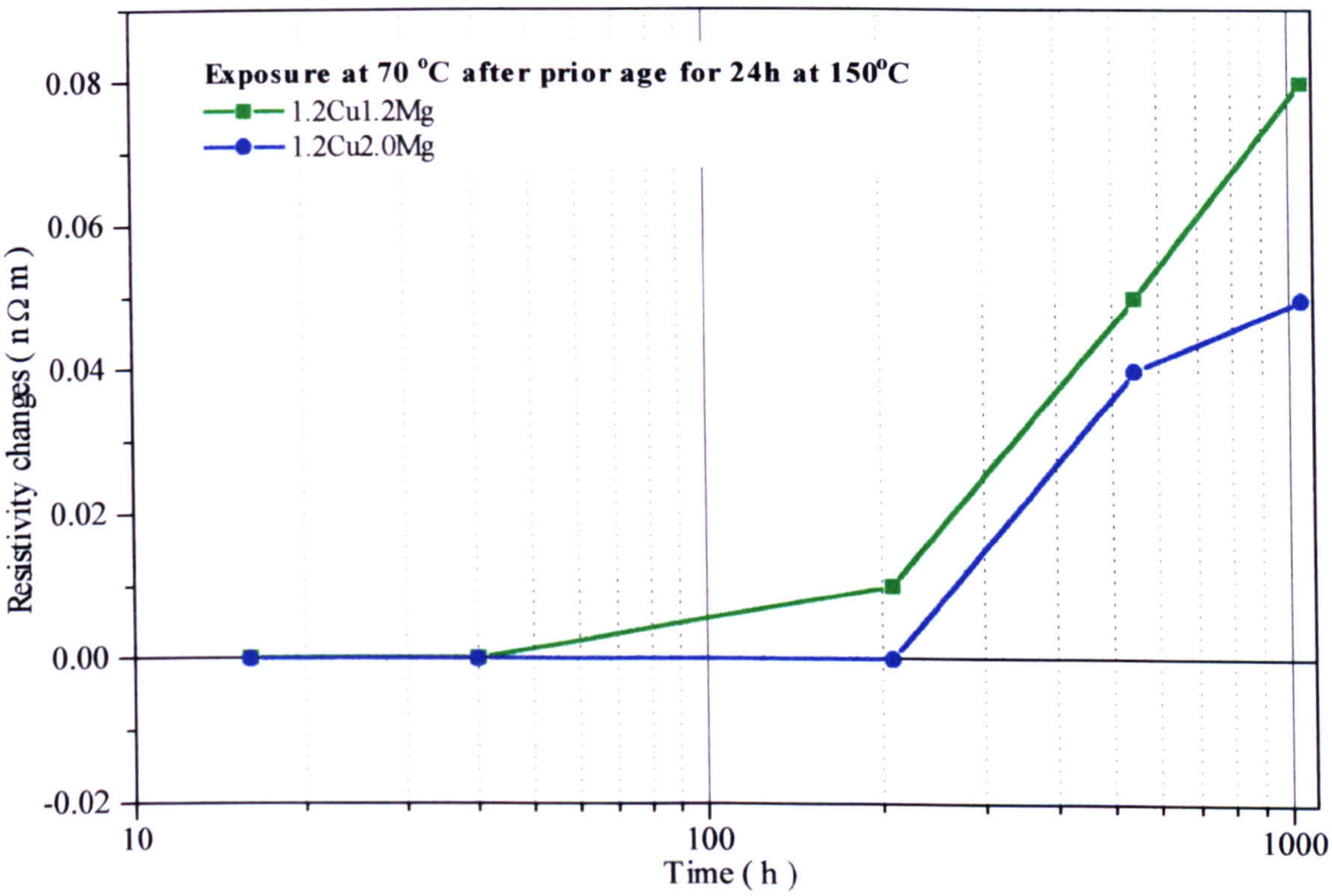

Figure 10.41: Isothermal resistivity changes of the alloys with varying magnesium concentration during exposure at 70°C.

CHAPTER 11

Effect of magnesium concentration on the ageing characteristics of Al-Li-Cu-Mg alloys

Chapters 8, 9 and 10 have examined the effects of copper and magnesium in the ternary Al-Li-Mg, Al-Li-Cu, and Al-Cu-Mg systems. The conclusions extracted from these chapters will be the basis for the interpretation of the precipitation characteristics that take place in the more complicated quaternary Al-Li-Cu-Mg system. The following sections analyse the role of magnesium on the precipitation reactions occurring in 1.7Li1.2CuXMg alloys. For this, six different alloys with increasing magnesium additions from 0 to 3% were used. The chapter is divided into three main parts:

- State of the as-quenched solid solutions.
- Isochronal precipitation characteristics.
- Isothermal precipitation characteristics.

11.1 General survey of the as-quenched solid solutions

The Al-1.7Li-1.2Cu-XMg-0.07Zr alloys have first been examined in the as-quenched state. XRD traces showed only the aluminium peaks indicating that the solution treatment and quenching procedure had dissolved and kept in solution all the majority of the solute.

The next step was to determine whether any association of magnesium atoms with other solute atoms was taking place in the as-quenched solid solution, e.g. Mg-Li, Mg-Cu, or Mg-Li-Cu associations. This was done by measuring the as-quenched resistivity, ρ_o, and applying Matthiessen's rule to the ρ_o values.

11.1.1 Resistivity of as-quenched alloys

The electrical resistivities of pure metals and dilute alloys can be described in terms of Matthiessen's rule. Matthiessen's rule states that the total resistivity is the sum of two independent contributions; the residual resistivity ρ_o caused by scattering of electrons from alloying elements/impurities and structural imperfections, and the thermal resistivity ρ_i produced by scattering from phonons. The electrical resistivity arising from structural imperfections, e.g. dislocations and grain boundaries, is much smaller than that produced by a concentration, C, of solute atoms. Hence, we can express Matthiessen's rule by the relation:

$$\rho(T,C) = \rho_i(T) + \rho_o(C) \qquad 11.1$$

For the as-quenched measurement, the alloy is in the solid solution state and because the samples are kept in liquid nitrogen the alloy remains in the solid solution state. All measurements are taken in liquid nitrogen so the thermal resistivity is very low.

Matthiessen's rule can therefore be written:

$$\rho(T,C) = \rho_o(C) \qquad 11.2$$

For i different solute atoms equation 11.2 has the form:

$$\rho(T,C) = \Sigma\rho_o(Ci) \qquad \textbf{11.3}$$

For the Al-Li-Cu -Mg-Zr system, equation 11.3 has the analytical form :

$$\rho(T,C) = \Sigma\rho_o(Ci) = \rho_o(C_{Al}) + \rho_o(C_{Li}) + \rho_o(C_{Cu}) + \rho_o(C_{Mg}) + \rho_o(C_{Zr}) \qquad \textbf{11.4}$$

Equation 11.4 will now be used to calculate the theoretical resistivity of the various Al-Li-Cu-Mg-Zr alloys, and this value will then be compared with the experimentally measured values.

The change in the resistivities of binary alloys of Al-Li, Al-Cu, Al-Mg and Al-Zr as a function of solute addition are available in the literature **[53]**. The values are:

Al-Li: 8.73 nΩm/at%Li

Al-Cu: 8.19 nΩm/at%Cu

Al-Mg: 4.86 nΩm/at%Mg

Al-Zr: 58.6 nΩm/at%Zr

In order to use these values the compositions of the Al-Li-Cu-Mg-Zr alloys have to be converted from wt% to at%. This has been done using the relation:

$$at\%i = \frac{2637916656w_i}{(977730.4137w_{Al} + 1085115.86w_{Mg} + 6981119.563)A_i} \qquad \textbf{11.5}$$

where i : Al, Li, Cu, Li, Mg, Zr

A_i : atomic mass of i

w_i : weight percent of i

Equation 11.4 can take the form:

$$\rho(T,C) = \Sigma\rho_o(Ci) = \rho_o(C_{Al}) + \rho^*_{Li} \times at\%_{Li} + \rho^*_{Cu} \times at\%_{Cu} + \rho^*_{Mg} \times at\%_{Mg} + \rho^*_{Zr} \times at\%_{Zr} \quad \textbf{11.6}$$

where:

ρ^* is the contribution each single element (nΩm/at%) makes to the resistivity.

$\rho_o(C_{Al})$ is the resistivity value for pure aluminium in liquid nitrogen and is equal to 2.30 nΩm.

The resistivity calculations of atomic percent and the resistivity contribution from each element are given in **table 11.1**. By adding all the individual contributions the theoretical resistivities of the alloys are obtained and these are shown in **table 11.2**.

The experimental and theoretical resistivity data of the Al-Li-Cu-Mg-Zr alloys are plotted as a function of magnesium concentration in **figure 11.1**.

It can be seen that the experimental plot is in good agreement with the theoretical data. This means that in the quenched solid solution the magnesium atoms are behaving as though they were in a simple Al-Mg solid solution, i.e. immediately after the quench the magnesium atoms do not appear be associating with other solute atoms, i.e Li, Cu, Zr.

11.2 Isochronal precipitation characteristics

The isochronal results presented in this section show that increasing concentrations of magnesium in the Al-Li-Cu-Mg alloys produce increasing amounts of δ′ phase. The mechanism by which this comes about could be one of the following:

- Increasing magnesium concentration shifts the δ′ metastable solvus line to higher temperatures by ~7.0°C/wt%Mg (see chapter 8).
- In magnesium-containing alloys, GPB zones will be produced (see chapter 10). If δ′ were to be forming on the GPB zones in a manner similar to that described for δ′ growing on GP_{Cu} zones (chapter 9), then this could also cause an increase in the volume fraction of δ′ observed during a DSC run.
- In magnesium-containing alloys, ageing may cause the formation of Li-Cu-Mg clusters capable of nucleating δ′. Increasing the concentration of magnesium would increase the number of such clusters and therefore increase the amount of δ′ produced during ageing.

At this stage of the thesis it is impossible to say which is the correct mechanism. However, as the results are presented in the chapter, each mechanism will be considered and it is hoped that by the end of this chapter there will be a body of evidence that indicates which is the correct mechanism.

11.2.1 DSC (as-quenched plots)

Figure 11.2 presents DSC comparative plots of the as-quenched alloys.

The 1.7Li1.2Cu alloy exhibits only a small high temperature exothermic peak at approximately 340°C (peak O) that is attributed on the basis of XRD results to the precipitation of T_1 (Al_2LiCu) and T_2 (Al_6Li_3Cu) phases (**figure 11.12**). Although this alloy will precipitate δ′ phase during isothermal ageing, the fast heating rate used for the DSC run does not allow sufficient time for the precipitation of detectable amounts of δ′. Increasing the magnesium addition from 0 to 3% results in the appearance of exothermic peaks in the temperature range 120-130°C and 330-370°C with endothermic peaks at intermediate temperatures. The initial exothermic peak I according to TEM and XRD results is due to the precipitation of δ′ (**figures 11.7-11.11**). It will be shown later that a significant amount of the heat evolved during peak I is also due to the formation of GPB zones; these zones are not detected by TEM or XRD analysis. The high temperature exotherm O is attributed to the precipitation of phase T_2 on the basis of XRD analysis (**figures 11.13-11.16**).

Careful observation of the intermediate endothermal effect leads to the conclusion that it consists of three overlapping endothermic peaks, designated K, G, and H. The size and position of these endotherms varies with increasing magnesium concentration. To assist in the identification of these overlapping peaks, DSC and resistivity measurements have been made on two low lithium alloys (1.3Li1.2Cu1.2Mg and 1.3Li1.2Cu2.0Mg) in the as-quenched condition. The low lithium concentration reduces the amount of δ′ that forms and therefore there is less masking of the peaks from this phase. These results are now considered.

11.2.2 Investigation of low lithium alloys

Figure 11.18 presents as-quenched DSC plots of 1.2Cu1.2Mg, 1.3Li1.2Cu1.2Mg and 1.7Li1.2Cu1.2Mg alloys. The DSC plot of 1.2Cu1.2Mg alloy has already been discussed in the last chapter. The initial exothermic peak E is attributed to the formation of Mg-Cu clusters and GPB zones whereas the overlapping endothermal effects B, G, and H correspond to the dissolution of Mg-Cu clusters, GPB zones, and S″ (the latter forming during the DSC heating). The addition of 1.3Li to the 1.2Cu1.2Mg alloy (1.3Li1.2Cu1.2Mg alloy) results in a larger initial exothermic event, peak I and the appearance of a larger overlapping endothermal effect, peak K, that has substituted for peak B. These changes in the 1.3Li1.2Cu1.2Mg alloy are likely to be caused by the precipitation of a small amount of δ′ (since this is the temperature range where δ′ precipitation is expected). Such δ′ precipitation would have to have been stimulated in some way since DSC analysis does not detect any δ′ precipitation in as-quenched binary Al-1.3Li alloys. This δ′ stimulation could be the result of any of the three mechanisms outlined in the previous section, i.e. shift of the δ′ solvus due to the presence of magnesium, precipitation of δ′ on GPB zones, and precipitation of δ′ from Li-Cu-Mg clusters.

As the addition of lithium increases from 1.3 to 1.7% (1.7Li1.2Cu1.2Mg alloy) significant stimulation of peaks I and K has taken place. This behaviour can be explained by the increased supersaturation of lithium that results in a higher driving force for δ′ precipitation. It should be noted that the size of the GPB

dissolution peak G has decreased in the 1.7Li1.2Cu1.2Mg alloy. This could be explained if δ′ is nucleating from Li-Cu-Mg clusters since in this case less copper and magnesium atoms would be available for GPB zone formation.

The isochronal resistivity plots of the low lithium alloys are shown in **figure 11.19.** Also included is the isochronal resistivity plot of a 1.7Li binary alloy. The resistivity peak A′ at about 140°C observed in the 1.2Cu1.2Mg alloy is due to the formation of Mg-Cu clusters and GPB zones that are smaller than the critical size for electron scattering (see previous chapter). Taking into consideration the DSC results (**figure 11.18**) the significant increase in the height of peak A′ caused by adding 1.3%Li to the 1.2Cu1.2Mg alloy (1.3Li1.2Cu1.2Mg alloy) can be attributed to the formation of fine δ′ that co-exists with the GPB zones. The fine δ′ and GPB zones then make approximately the same contributions to the resistivity (**figure 11.20**). Increasing the temperature beyond 140°C causes the resistivity to start decreasing due to growth of the fine δ′ and GPB zones. As the δ′ solvus temperature (~200°C) is approached the fine δ′ starts dissolving and GPB zones continue to grow. At about 250 °C, dissolution of the small GPB zones occurs whereas the larger ones transform into S″ as described in the previous chapter for 1.2Cu1.2Mg alloys.

Increasing the lithium addition to 1.7% (1.7Li1.2Cu1.2Mg alloy) results in the formation of a double resistivity peak at 70 and 200°C, peaks B′ and C′ respectively. The early peak B′ corresponds to the formation of fine δ′ that grows through the critical electron scattering size very fast due to the large driving force

for δ′ precipitation (large supersaturation of lithium). However, the positive contribution to resistivity from the presence of GPB zones prevents the resistivity from dropping below the baseline. As the temperature increases beyond 100°C the GPB zones grow and become more effective scattering centres for electrons resulting in a second increase of resistivity. As the temperature approaches the δ′ metastable solvus temperature (~200°C) dissolution of δ′ commences, until at 200°C only GPB zones remain. Temperatures higher than 200°C result in dissolution of GPB zones and formation of S″.

Finally, comparison of the 1.7Li1.2Cu1.2Mg alloy with the 1.7Li binary alloy shows that the increase of resistivity observed in the binary alloy at 0°C, which can be attributed to the formation of ordered domains, is absent (**figure 11.19**). It can be concluded that in Al-Li-Cu-Mg alloys the nucleation ordering is likely to have been suppressed and δ′ formation now takes place either from Li-Cu-Mg clusters or is nucleated on GPB zones.

The effect of lithium on the precipitation characteristics of the higher magnesium alloy (1.2Cu2.0Mg alloy) appears to be very similar to that described above i.e. the increase in lithium concentration from 0 to 1.7% causes stimulation of fine δ′ precipitation with enhanced kinetics (**figures 11.21** and **11.22**). The only change is on the isochronal resistivity plot of 1.3Li1.2Cu2.0Mg. This alloy exhibits a double resistivity peak at 110 and 180°C, peaks B′ and C′ respectively, which was not observed for the lower magnesium alloy (1.3Li1.2Cu1.2Mg alloy) (**figure 11.23**). This could be explained by assuming a slightly higher lithium

concentration in the 1.3Li1.2Cu2.0Mg alloy.

The results from the low lithium Al-Li-Cu-Mg alloys have shown:

- The presence of copper and magnesium in these alloys enhances the kinetics of δ′ formation. The mechanism by which the kinetics are enhanced is not clear at this stage of investigation.
- Increasing the lithium concentration from 1.3 to 1.7% results in a further increase of fine δ′ precipitation with enhanced reaction kinetics.

11.2.3 Investigation of 1.7Li1.2CuXMg alloys

Referring back to **figure 11.2,** it can be seen that increasing magnesium concentration from 0.7 to 2.0% results in a significant increase in the size of peak K indicating that stimulation of δ′ has taken place. The GPB zone dissolution peak G also appears to increase in size and this will be discussed later since it is an unexpected result (it was found in the last chapter that in lithium-free alloys magnesium did not effect GPB zones). By subtracting the enthalpy for GPB zone formation in an as-quenched 1.2Cu1.2Mg alloy (peak E, **figure 11.18**) from the enthalpy of exothermal effect I and using **equation 8.2** it is possible to estimate the volume fraction of δ′ precipitated in 1.7Li1.2Cu0.7-3.0Mg alloys (**figure 11.4**). It should be noted that the 1.2Cu1.2Mg alloy was chosen because, as shown in the last chapter, the amount of Mg-Cu clusters formed in this alloy is very small and therefore the results of the subtraction are more accurate. The calculations were based on the exothermal effect I because there are less overlapping effects to influence the calculation of δ′ volume fraction. According

to **figure 11.4** the δ′ volume fraction exhibits only a small increase with increasing magnesium concentration from 0 to 1.2%. As the magnesium concentration increases further from 1.2 to 1.4% to 2.0% the δ′ volume fraction increases sharply. Further increase of magnesium beyond 2.0% causes a drop in the volume fraction of δ′. From **figure 11.4** it can be seen that the volume fraction of δ′ precipitated in 1.7Li1.2CuXMg alloys is slightly larger compared with 1.7LiXMg alloys for concentrations up to 1.2%. The difference increases dramatically with a further increase in magnesium concentration from 1.2 to 1.4 and 2.0%.

These results enable the following comments to be made on the mechanism by which magnesium stimulates δ′ precipitation in 1.7Li1.2CuXMg alloys.

- Shift of the δ′ solvus boundary to a higher temperature is not the primary cause of δ′ stimulation (compare the plots of Al1.7LiXMg with Al-1.7Li1.2CuXMg).
- The small amount of δ′ enhancement over the range 0-1.2%Mg in the 1.7Li1.2CuXMg alloys could be caused by precipitation on GPB zones since it is known that the number of GPB zones will be increasing over this composition range.
- The very large stimulation of δ′ that occurs over the range 1.4-3.0% in the 1.7Li1.2CuXMg alloys cannot be the result of precipitation on GPB zones since it is known from the previous chapter that the number of GPB zones is not increasing over this composition range. This means that the

stimulation of δ′ in Al-Li-Cu-Mg alloys containing ≥1.4Mg is probably the result of the formation of Li-Cu-Mg clusters which are capable of rapidly developing into δ′ precipitates (hereafter referred to as CLδ′). It is interesting to note that this cluster development occurs only after >1.2%Mg has been added. It may be that up to 1.2%Mg most of the magnesium is used in producing GPB zones; beyond 1.2%Mg "free" magnesium is available in the matrix to gather both copper and lithium thus forming Li-Cu-Mg clusters. This implies that Mg is the dominating species that controls Li-Cu-Mg cluster formation.

- Although the primary cause of the increased volume fraction of δ′ in Al-Li-Cu-Mg alloys is not due to shift of the δ′ solvus boundary, the shift of the boundary may have a contributory effect on δ′ precipitation. A shift in the boundary will cause an increase in the driving force for δ′ precipitation, i.e. an increased driving force for the Li-Cu-Mg clusters to transform to CLδ′.

The precipitation characteristics change as the level of magnesium reaches 3.0% (1.7Li1.2Cu3.0Mg alloy). From **figure 11.2** it can be clearly seen that the decrease in the size of peak I is accompanied by a 20°C-shift to a higher temperature. Endothermic peak G exhibits also a decrease in its size, suggesting that retardation of both δ′ and GPB zones has occurred. At about 270°C a new endothermic peak (peak J) has been developed. The double peak at 310°C and

340°C is attributed on the basis of XRD results to T_M (Al_2LiMg) and T_2 phases (**figure 11.17**). From the above the following changes can be summarised with increasing magnesium concentration from 2.0 to 3.0%:

- Retardation of δ′ and GPB zones.
- Development of a new endothermic peak at approximately 270°C, peak J.
- Precipitation of the equilibrium phase Al_2LiMg (T_M) at about 310°C.

It is believed that all these changes relate to each other. **Figure 11.3** gives the isothermal section of the Al-Li-Mg system at 200°C. It can be seen that the 3.0Mg alloy lies well within the $\alpha+T_M$ area suggesting that the thermodynamic state is different from that in lower magnesium alloys. The high driving force for T_M precipitation is confirmed by the XRD results. It is postulated that a precursor of the equilibrium T_M phase (T'_M) may co-precipitate with δ′ and GPB zones during the early stages of the isochronal heating (peak I) that consumes lithium and magnesium atoms at the expense of δ′ and GPB zones. This can also explain the 20°C-displacement of peak I to a higher temperature as now the activation energy for the formation of both δ′ and GPB zones is larger.

11.2.4 Determination of the activation energy for δ′ formation

In order to cast more light on the process of CLδ′ nucleation, it is useful to determine the activation for δ′ formation in these alloys. This has been done using DSC analysis and assuming that the majority of the initial exotherm is the result of δ′ precipitation.

Kissinger [**52**] has shown that the activation energy of a reaction occurring during heating at a constant rate can be measured. For DSC experiments (non-isothermal heating) it can be shown, that the relation between the temperature for a fixed stage of transformation, T_f, and the heating rate, Φ, is given by the following equation:

$$\ln(T_f^2/\Phi) = (E_A/k_B T_f) + \ln\beta_f \qquad \textbf{11.1}$$

where : β_f is the state variable fully determining that fixed state of transformation

E_A is the activation energy of the process

k_B is Boltzmann's constant

Thus, the activation energy for δ′ formation can be obtained from the slope of the plot:

$$\ln(T_f^2/\Phi) \text{ vs } 1/T_f \qquad \textbf{11.2}$$

where T_f is the temperature of the exothermic peak in K and Φ the heating rate of the DSC run in deg/sec.

Table 11.3 records the T_f data for each Φ and the $\ln(T_f^2/\Phi)$, $1/T_f$ values for the 1.7Li1.2Cu2.0Mg alloy.

From linear regression of the data in **table 11.3** it was found that the activation energy of δ′ formation is equal to 62 kJ/mol (**figure 11.5**). This value is much lower than that associated with diffusion of lithium in aluminium (130 kJ/mol) but is in the range of activation energies measured for the movement of vacancies in aluminium alloys, that is 45-65 kJ/mol. Therefore, it can be concluded that δ′ precipitation in Al-Li-Cu-XMg alloys is controlled by the presence of excess

vacancies quenched-in from solution heat treatment. It is postulated that these vacancies bind with "free" magnesium in solid solution; these Mg-vacancy pairs then diffuse and gather copper and lithium atoms thus producing Li-Cu-Mg clusters which are capable of nucleating δ′.

11.2.5 Isochronal resistivity

Comparative resistivity plots of all the alloys are presented in **figure 11.24**. The 1.7Li1.2Cu alloy exhibits a small resistivity peak at 40°C that is attributed to the formation of a small volume fraction of δ′ with size smaller than the critical size for electron scattering. Higher temperatures result in growth of δ′ and the resistivity drops towards the baseline (~120°C). In the temperature range 120-200°C the resistivity traces the baseline as δ′ dissolution occurs. As the temperature increases from 200°C to 370°C the resistivity decreases below the baseline due to the precipitation of T_1 and T_2 phases.

The addition of magnesium to the alloy results in the appearance of two well developed peaks at approximately 80 and 200°C, peaks B′ and C′. As already shown in the section on low lithium alloys, peak B′ is due to the formation of fine δ′, probably CLδ′, that occurs rapidly at low temperatures and peak C′ is due to GPB formation. There must be a contribution to peak B′ from GPB but **figures 11.19** and **11.22** suggest that their contribution at low temperatures is small. As the temperature increases beyond 80°C CLδ′ grows causing a resistivity drop. At these higher temperatures the contribution from GPB zones becomes dominant

and the resistivity starts increasing again. As the temperature approaches the metastable solvus temperature of δ′ (~200°C) dissolution of CLδ′ occurs. More copper and magnesium atoms therefore become available to grow the GPB zones. GPB zones attain the critical size for electron scattering at 200°C (peak C′). This suggests that GPB zones follow a low rate of growth due to the fact that the majority of copper and magnesium atoms are captured by the initial development of Li-Cu-Mg clusters.

As the magnesium concentration increases from 0.7 to 2.0% the height of peak B′ increases (**figure 11.25**) suggesting that stimulation of CLδ′ has occurred, this being in agreement with the DSC results. The position of this peak remains unchanged indicating that no changes in the reaction kinetics have taken place.

As the magnesium increases to 3.0%, peak B′ exhibits a marked decrease in its size and a 20°C-shift to a higher temperature. This behaviour indicates that significant retardation of δ′ has occurred and that the kinetics for CLδ′ precipitation are slowed down which is in perfect agreement with the DSC results. As discussed earlier this is probably due to movement from a δ–containing phase field into the $\alpha+T_M$ phase field thereby resulting in the formation of pre-cursor T'_M phases. Further work is required to confirm these ideas.

Peak C′ is attributed to the formation of GPB zones with size smaller than the critical size for electron scattering, and surprisingly this exhibits an increase in its

height with increasing magnesium, suggesting that stimulation of GPB zones has occurred (**figure 11.26**). In lithium-free alloys, such stimulation of GPB zones by magnesium was not observed. It may be that in lithium-containing alloys, Mg-Cu clusters do not form (they are replaced by Li-Cu-Mg clusters which evolve into δ′). The absence of Mg-Cu clusters may have the effect of increasing the driving force for GPB zones, with their volume fraction therefore increased. Additionally, as the CLδ′ dissolves, the copper and magnesium atoms that are released are available for the formation of further GPB zones.

11.3 Isothermal precipitation characteristics

This section examines the effect of magnesium on the isothermal precipitation characteristics of Al-Li-Cu-Mg alloys. In order to overcome the problem of overlapping DSC effects that makes difficult the identification of the phases that precipitate during isothermal ageing, low lithium alloys (1.3Li1.2CuXMg) were also examined.

Five different heat treatments have been used:

- Ageing for 1000 h at 70, 100 and 150 °C.
- Ageing for 24 h at 150 °C. This simulates the damage tolerant heat treatment applied to alloys based on the Al-Li system.
- Prior ageing for 24 h at 150 °C following by exposure for 1000 h at 70 °C. This double heat treatment simulates the conditions that a commercial aerospace alloy encounters under service conditions.

11.3.1 Age at 70°C

11.3.1.1 Investigation of low lithium alloys

Figure 11.27 presents the DSC comparative plots of 1.2Cu1.2Mg and 1.2Cu2.0Mg alloys with lithium concentrations of 1.3 & 1.7%. The addition of 1.3% Li to the 1.2Cu1.2Mg alloy results in the appearance of a well developed endotherm (peak K) at approximately 190°C that is the result of the formation of δ′ during the age at 70°C. The addition of lithium has also caused a shift of endothermic peak G to a higher temperature by 15°C indicating that larger-sized GPB zones have formed. This can be explained by the high binding energy between lithium atoms and vacancies that results in a decrease in the concentration of excess free vacancies and in turn to a lower nucleation rate of GPB zones in the early stages of ageing. As the concentration of lithium increases from 1.3% to 1.7% additional δ′ precipitation takes place (enlargement of peak K) as a result of the higher supersaturation of lithium. In addition, peak K exhibits a 10°C-shift to a lower temperature which will be the result of a finer dispersion of δ′ due to the larger driving force for δ′ precipitation.

The resistivity measurements on 1.2Cu1.2Mg alloys with additions of 1.3,1.7%Li during ageing at 70°C (**figure 11.28(a)**) show that GPB zones make a significant contribution to the total resistivity changes in the lithium-containing alloys, partly masking the effect of δ′. By subtracting the effect of GPB zones it can be seen (**figure 11.28(b)**) that in the 1.3Li1.2Cu1.2Mg alloy the resistivity attains a peak after 4 h of ageing due to the precipitation of fine δ′ of size ≤2 nm (critical

size for electron scattering). Longer ageing times cause a drop of resistivity below the baseline as growth of δ′ over the critical electron scattering size occurs. As the lithium concentration increases to higher levels (1.7Li1.2Cu1.2Mg alloy) the resistivity reaches the critical size for electron scattering in much shorter ageing times due to the larger supersaturation of lithium that causes significant enhancement of δ′ precipitation reaction kinetics.

The situation is not significantly different for the higher magnesium alloys. The addition of 1.3% Li to 1.2Cu2.0Mg alloy causes an increase in the endothermal effect K at about 180°C due to the dissolution of δ′. Again, the addition of lithium has resulted in a displacement of the endothermic peak G to a higher temperature by 10°C indicating that a coarser distribution of GPB zones has formed. Increasing the lithium addition from 1.3 to 1.7% results in additional δ′ precipitation as a result of the higher driving force for δ′ precipitation.

The resistivity plots (**figure 11.28(b)**) show that the 1.3Li1.2Cu2.0Mg alloy attains a resistivity peak after about 2.5 h of ageing. As the lithium concentration increases from 1.3% to 1.7% (1.7Li1.2Cu2.0Mg alloy) a resistivity peak is attained at much earlier ageing times (~0.4 h) suggesting that considerable acceleration of δ′ precipitation reaction kinetics has occurred.

The isothermal resistivity plots of 1.3Li1.2Cu1.2Mg and 1.3Li1.2Cu2.0Mg

alloys show that during the first hour of ageing at 70°C the reaction kinetics for δ′ precipitation is reduced as the magnesium concentration increases from 1.2% to 2.0% (**figure 11.28(b)**). This suggests that the additional magnesium has not significantly changed the position of the α/δ′ solvus boundary (this would increase the δ′ precipitation rate). A possible explanation is that clusters of Li-Cu-Mg rapidly form during the early stages of ageing resulting in a short delay in the formation of δ′ (which form from the clusters). Once δ′ starts evolving from the clusters a fine dispersion of δ′ results with higher volume fraction than that observed in the 1.3Li1.2Cu1.2Mg alloy, i.e. as evidenced by the DSC results after ageing 1000 h.

From the above the following can be summarised:

- The phases that precipitate during ageing at 70°C in the lithium-containing alloys are δ′ and GPB zones.

- As the lithium concentration increases from 1.3 to 1.7% the driving force for δ′ precipitation becomes larger, producing a higher volume fraction of finer δ′. The precipitation reaction kinetics of δ′ are also significantly enhanced.

- The addition of lithium to 1.2Cu1.2Mg and 1.2Cu2.0Mg alloys produces a coarser distribution of GPB zones. This can be explained by a decrease in the concentration of free vacancies due to the high binding energy with lithium atoms that results in a lower nucleation rate of GPB zones.

- The increase of magnesium concentration from 1.2% to 2.0% in the low lithium alloys slows the reaction kinetics of δ′ precipitation during the early stages of ageing at 70°C. This suggests that magnesium is not significantly increasing the α/δ′ solvus temperature, but is promoting the formation of Li-Cu-Mg clusters. After 1000 h of ageing a larger volume fraction of finer δ′ has formed in the higher magnesium alloy. This may be the result of nucleation of δ′ on Li-Cu-Mg clusters.

11.3.1.2 Investigation of 1.7Li1.2CuXMg alloys

The DSC comparative plots of the 1.7Li1.2CuXMg alloys after ageing for 1000 h at 70°C are given in **figure 11.29**. The 1.7Li1.2Cu alloy exhibits an endothermic peak at 180°C, peak K, due to the dissolution of δ′.

The addition of 0.7%Mg causes a marked increase in the size of endothermal effect K indicating significant stimulation of δ′ precipitation. The overlapping endothermal effects G and H correspond to the dissolution of GPB zones and S″ (the latter having formed during the DSC run). DSC heating to higher temperatures results in the appearance of a broad exotherm (260-380°C) with peaks at 280 and 350°C, that correspond to the precipitation of equilibrium δ and T_2 phases respectively.

Increasing magnesium concentration from 0.7% to 3.0% causes enlargement of the area of peak K, suggesting that further stimulation of δ′ has taken place. By measuring the dissolution enthalpy (area of peak K) and applying **equation 8.2,**

the volume fraction of δ′ was estimated for each alloy. The results obtained are presented in **figure 11.30** where the volume fraction of δ′ is plotted versus the magnesium concentration. Also included is the corresponding plot for 1.7LiXMg alloys (i.e. no copper addition). It can be seen that the addition of 0.7%Mg causes a very small increase in the volume fraction of δ′ suggesting that slight stimulation of δ′ precipitation has occurred. This could be explained by the presence of GPB zones that act as sites for heterogeneous nucleation of δ′ in a manner similar to GP_{Cu} zones in Al-Li-Cu alloys (see chapter 9). As the magnesium concentration increases from 0.7% to 1.2% there is little change in the δ′ volume fraction. On the basis of the DSC results, it is believed that in this concentration range all the magnesium is consumed by GPB zone formation, resulting in a slight increase in their size without having any effect on their number density and therefore on the nucleation rate of δ′.

Increasing magnesium concentration from 1.2% to 1.4% results in a sharp rise in the volume fraction of δ′. It is postulated that all the magnesium added beyond 1.2% enters solid solution rather than forming GPB zones and now forms vacancy rich Li-Cu-Mg clusters that are capable of nucleating δ′ much more effectively than GPB zones. Levels of magnesium higher than 1.4% do not produce further increments in δ′ volume fraction indicating that the maximum volume fraction of δ′ (as determined by the α/δ′ solvus boundary) has already been attained for 1.4% Mg additions.

Comparison with the 1.7LiXMg alloys plot leads to the conclusion that up to

1.2% magnesium the volume fraction of δ′ precipitated in the 1.7Li1.2CuXMg alloys is very close to that formed in the 1.7LiXMg alloys, suggesting that the shift of the α/δ′ solvus line to higher temperatures results in almost the same stimulation of δ′ precipitation as that from GPB zones. However, the presence of copper in the 1.7Li1.2CuXMg alloys for magnesium concentrations higher than 1.2% appears to cause a dramatic stimulation of δ′ precipitation, via the formation of Li-Cu-Mg clusters, that cannot be achieved in the non-copper 1.7LiXMg alloys by a shift of the δ′ metastable solvus line to higher temperatures.

The resistivity plots of the 1.7Li1.2CuXMg alloys during ageing at 70°C and the same plots after subtraction of the effect of GPB zones are presented in **figures 11.31(a) and 11.31(b)** respectively. The resistivity plot of 1.7Li1.2Cu alloy has already been discussed in chapter 9. The initial increase of resistivity in this alloy can be attributed to ordered domains which scatter the conduction electrons. Spinodal decomposition of the ordered domains produces more effective scattering centres for the conduction electrons causing a second increase of resistivity. A resistivity peak is not reached even after 1000 h of ageing as the spinodal decomposition occurs at a slow rate. It is believed that quenched-in vacancies becoming trapped by ordered domains and therefore the diffusion of lithium atoms to the spinodally decomposing regions is difficult.

Increasing the magnesium concentration from 0 to 0.7% results in a resistivity peak (peak A′) after 0.4 h of ageing suggesting that the reaction kinetics of δ′

precipitation are significantly enhanced. As the magnesium concentration increases from 0.7% to 1.0% to 1.2% no further changes are observed with respect to the position and magnitude of peak A′; this is in agreement with the DSC results (**figure 11.29**). As the magnesium concentration increases from 1.2% to 1.4% the height (but not position) of peak A′ exhibits a dramatic increase. This suggests that significant stimulation of δ′ has taken place producing a large volume fraction of fine δ′ (higher number density) that can scatter the conduction electrons much more effectively. This stimulation of δ′ is attributed to the formation of Li-Cu-Mg clusters that result in an increase in the nucleation rate of δ′. The fact that the position of peak A′ does not change suggests that Li-Cu-Mg clusters do not affect the growth rate of δ′ precipitation and consequently the critical size for electron scattering is reached after the same ageing time. A further increase in magnesium concentration from 1.4% to 2% does not cause any additional change in the magnitude and position of peak A′, indicating that the number of Li-Cu-Mg clusters does not increase further and therefore the same number density of δ′ is produced.

Higher levels of magnesium beyond 2.0% (1.7Li1.2Cu3.0Mg alloy) cause a dramatic change in the resistivity behaviour. The early stages of ageing show a clear double peak (at 1 and 10h ageing) **figure 11.31(a)**. The reasons for this behaviour need further investigation with TEM but it is thought that the cause of this behaviour is connected with a shift from α phase field containing δ into the $\alpha+T_M$ phase field as the level of magnesium reaches 3%.

11.3.2 Age at 100°C

11.3.2.1 Investigation of low lithium alloys

According to **figure 11.32,** the addition of 1.3% Li to 1.2Cu1.2Mg (1.3Li1.2Cu1.2Mg alloy) results in the appearance of an endothermic peak at about 210°C (peak K) that is due to the dissolution of δ′. Increasing the lithium concentration to higher levels (1.7Li1.2Cu1.2Mg alloy) causes enlargement of the size of peak K due to additional δ′ precipitation as the lithium supersaturation becomes larger. No changes are observed for endothermal peak G.

The resistivity plots of the above alloys are presented in **figure 11.33(a)** and in **figure 11.33(b)** after subtracting the effect due to GPB zones. The 1.3Li1.2Cu1.2Mg alloy exhibits an initial increase of resistivity and a peak is reached after 2 h of ageing that is due to the formation of δ′ of size equal to that for the critical size for electron scattering (≤2nm) (**figure 11.33(b)**).

Increasing the lithium concentration to 1.7% (1.7Li1.2Cu1.2Mg alloy) causes a rapid drop of resistivity to below the baseline at very short ageing times (0.1 h) indicating that the reaction kinetics of δ′ precipitation have been dramatically accelerated.

The same trends are observed for the higher magnesium alloys (XLi1.2Cu2.0Mg). As expected, higher levels of lithium (1.7Li1.2Cu2.0Mg alloy) cause a significant increase in the size of endothermic peak K as additional precipitation of δ′ occurs. Comparison of the resistivity plots of

1.3Li1.2Cu1.2Mg and 1.3Li1.2Cu2.0Mg alloys (**figure 11.33(b)**) suggests that δ′ precipitation kinetics are slower in the higher magnesium alloy in the early stages of ageing (up to ~1 h) and this could again, be due to the formation of Li-Cu-Mg clusters in the early stages of ageing. These clusters subsequently develop into δ′ precipitates giving enhanced δ′ precipitation after moderate times of ageing (i.e. CLδ′). However after 1000 h ageing at 100°C the DSC results (**figure 11.32**) show that the δ′ volume fraction is the same in both alloys, showing that magnesium is influencing the kinetics of δ′ precipitation and not the thermodynamics i.e. the position of the α/δ′ solvus boundary.

From the above the following can be summarised:

- The phases that precipitate in Al-Li-1.2Cu-Mg alloys containing 1.3-1.7Li and 1.2-2.0Mg during ageing for 1000 h at 100°C are CLδ′ and GPB zones.
- Independently of the magnesium levels, the increase in lithium concentration results in additional δ′ precipitation and enhanced kinetics due to the larger driving force for δ′ precipitation as the lithium supersaturation increases.
- The addition of lithium to the ternary Al-Cu-Mg alloys causes an increase in the size of the GPB zones that is attributed to a decrease in their nucleation rate.
- Comparison of the low lithium alloys reveals that magnesium causes a

retardation of the δ′ precipitation kinetics in the very early stages of ageing that can be attributed to the prior formation of Li-Cu-Mg clusters.

11.3.2.2 Investigation of 1.7Li1.2CuXMg alloys

The DSC comparative plots of 1.7Li1.2CuXMg alloys are shown in **figure 11.34.** The 1.7Li1.2Cu alloy exhibits an endothermic peak, peak K, at 200°C that is caused by the dissolution of δ′. As the magnesium concentration increases from 0 to 0.7 % the endothermic event K becomes broader due to the additional dissolution of GPB zones and S″ (the latter being formed during the DSC heating). Because the dissolution events overlap it is extremely difficult to determine the positions and the areas of the endothermal effects that correspond to GPB zones and S″. Nevertheless, based on the DSC results of chapter 10 it was feasible, by subtracting the enthalpy of GPB zones and S″ from the whole endotherm K, to estimate the heat absorbed by the dissolution of δ′ only. Then, by using **equation 8.2**, the volume fraction of δ′ was calculated. The data obtained were plotted as a function of magnesium concentration (**figure 11.35**). As can be seen, increasing magnesium concentration from 0 to 1.2% produces only a very small increase in the volume fraction of δ′, probably the result of the shift of the α/δ′ solvus boundary or possibly formation of δ′ on GPB zones. As the magnesium concentration increases from 1.2% to 1.4%, excess magnesium (over that to form GPB zones) becomes available for the formation of Li-Cu-Mg clusters resulting in significant stimulation of δ′ precipitation. A further increase

in magnesium concentration to 2.0% does not result in a further increase in the δ′ volume fraction, suggesting that the equilibrium δ′ volume fraction (as determined by the α/δ′ solvus boundary) has already been reached at the 1.4% Mg level. An increase in magnesium from 2.0 to 3.0% causes a decrease in the volume fraction of δ′ indicating that retardation of δ′ precipitation has happened. This is probably the result of T_M or precursor to T_M forming during the age at 100°C; such phases would consume a significant amount of lithium atoms at the expense of δ′.

Comparing the δ′ volume fraction plots of 1.7Li1.2CuXMg and 1.7LiXMg alloys (**figure 11.35**), it can be seen that, as with ageing at 70°C, as the magnesium concentration increases from 1.2% to 1.4% the presence of copper causes a marked stimulation of δ′ precipitation through the formation of Li-Cu-Mg clusters; such stimulation is considerably greater than that caused by the shift of the α/δ′ solvus to higher temperatures (that takes place in the non-copper alloys).

The resistivity plots of the 1.7Li1.2CuXMg alloys are presented in **figures 11.36 a, b**. The resistivity plot of 1.7Li1.2Cu alloy has already been discussed in chapter 9. The increase of resistivity is attributed to the combined effect of ordered regions and fine δ′ particles being produced on GP_{Cu} zones. After 50 h of ageing the critical electron scattering size is attained and the resistivity drops below the baseline. Once magnesium is added to 1.7Li1.2Cu (1.7Li1.2Cu0.7Mg alloy) a dramatic enhancement of the kinetics of δ′ precipitation takes place and

the critical size for electron scattering is reached at or before the first resistivity measurement taken. The other magnesium containing alloys (1.0-2.0 Mg) exhibit a similar trend. The form of the 1.7Li1.2Cu3.0Mg resistivity plot is different from the lower magnesium alloys in that a pronounced resistivity peak appears after ageing for 0.5 h at 100°C. This could be caused by a precursor to T_M; a TEM investigation is required to research this further.

11.3.3 Age at 150°C

11.3.3.1 Investigation of low lithium alloys

Comparative DSC plots are given in **figure 11.37.** The addition of 1.3% Li to 1.2Cu1.2Mg alloy causes a very small increase in the size of the initial endotherm (200-265°C) due to the dissolution of a small amount of δ′ in addition to GPB zones. This is to be expected because at 150°C a concentration of 1.3% Li lies on or very near to the δ′ metastable solvus line and therefore there is only a very small driving force for δ′ precipitation.

Increasing the lithium addition to beyond 1.3% (1.7Li1.2Cu1.2Mg alloy) results in considerable enlargement of the endotherm due to the dissolution of a significantly larger volume fraction of δ′ (endothermic peak K). No conclusions can be extracted for GPB zone formation because endothermal effect G is totally overlapped by endothermic peak K.

Figure 11.38a presents the resistivity plots of the alloys during ageing at 150°C. After the subtraction of the effect of GPB zones (1.2Cu1.2Mg alloy) (**figure**

11.38b), it can be seen that the 1.3Li1.2Cu1.2Mg alloy exhibits an increase in resistivity that is due to the formation of a small volume fraction of δ′ with size smaller than that for the critical size for electron scattering (≤ 2 nm). A resistivity peak is attained only after 24 h indicating that the kinetics are very slow, as expected by the very small driving force for δ′ precipitation. Higher levels of lithium (1.7Li1.2Cu1.2Mg alloy) causes the resistivity to commence decreasing after ageing approximately 1 h. This behaviour is attributed to the significant acceleration of the kinetics due to the increased driving force for δ′ precipitation; this is in perfect agreement with the DSC results.

The higher magnesium alloys (1.3,1.7Li1.2Cu2.0Mg) exhibit very similar trends as the lithium concentration increases from 0 to 1.3 to 1.7% **(figures 11.38a, b)** i.e. additional δ′ precipitation takes place with enhanced kinetics.

Finally, comparison between the resistivity plots of 1.3Li1.2Cu1.2Mg and 1.3Li1.2Cu2.0Mg alloys suggests that the increase in magnesium concentration from 1.2% to 2.0% has not caused any changes in the reaction kinetics of δ′ precipitation.

It should be noted that the study of the above alloys was limited to ageing at 150 for 24 h because, as shown in the last chapter, longer ageing times at 150°C produce extensive precipitation of equilibrium phases.

From the above results the following can be summarised for ageing for 24h at 150°C:

- The phases that precipitate in 1.3,1.7Li1.2Cu1.2,2.0Mg alloys for ageing up to 24h at 150°C are CLδ′ and GPB zones.
- Increasing the lithium addition from 1.3% to 1.7% results in a large increase in the volume fraction of δ′ that is produced.
- No changes were observed for the reaction kinetics of δ′ precipitation in 1.3Li1.2CuXMg alloys as the magnesium concentration was increased from 1.2 to 2.0%.

11.3.3.2 Investigation of 1.7Li1.2CuXMg alloys

The DSC comparative plots of 1.7Li1.2CuXMg alloys are shown in **figure 11.39.** The 1.7Li1.2Cu alloy exhibits an endothermic peak (peak K) at about 245°C that is due to the dissolution of δ′. Increasing magnesium concentration from 0 to 0.7% results in a wider endothermal effect (170-275°C) due to the additional dissolution of GPB and S″ phase. The amount of energy that corresponds to the dissolution of δ′ was calculated by subtracting the contribution of GPB zones and S″ given by the DSC results of the lithium-free alloys given in the last chapter. By applying **equation 8.2** to the data obtained the volume fraction of δ′ was calculated for each alloy and plotted as a function of the magnesium concentration **(figure 11.40)**. The 1.7Li1.2CuXMg alloys do not exhibit any increase in the volume fraction of δ′ for magnesium concentrations up to 1.2%. As the magnesium concentration increases from 1.2% to 1.4% the δ′ volume fraction increases considerably suggesting that stimulation of δ′ precipitation has

occurred. Again, this is attributed to the formation of Li-Cu-Mg clusters that are capable of nucleating δ′ much more effectively than GPB zones. A further increase of magnesium concentration to 2.0% does not produce any further increase in δ′ volume fraction suggesting that the equilibrium volume fraction of δ′ has already been attained for the 1.4% Mg level. Higher levels of magnesium (1.7Li1.2Cu3.0Mg alloy) result in a significant decrease in δ′ volume fraction. As already referred in the previous section, this decrease is probably related to the precipitation of T_M precursors that consume lithium atoms at the expense of δ′.

The resistivity plots for ageing up to 24 h at 150°C show that in the presence of magnesium the δ′ precipitation kinetics are greatly enhanced (**figure 11.41a, b**). At low magnesium concentrations the enhancement of kinetics is likely to be the result of precipitation of δ′ on GPB zones, but at higher magnesium concentrations it is likely to be the result of CLδ′ formation. A more detailed comparison of the resistivity data is difficult since the magnitude of the resistivity decrease is a function not only of δ′ volume fraction, but also of δ′ precipitate size.

11.4 Effect of ageing temperature

This section considers the effect of ageing temperature on the precipitation characteristics of 1.7Li1.2CuXMg alloys. The effect of ageing temperature on 1.7Li1.2Cu0.0Mg alloy has already been discussed in detail in chapter 9 (section

9.2.5). In this alloy the DSC thermograms showed that the maximum amount of δ′ is precipitated at 100°C (**figure 11.42**). This was attributed to the optimum combination of thermodynamics and kinetics at this ageing temperature. The isothermal resistivity curves (**figure 11.51**) indicated that at 70°C and 100°C, δ′ forms on fine GP_{Cu} zones (resistivity increases) whereas at 150°C the dispersion of GP_{Cu} zones is so coarse that their influence on δ′ precipitation is minimal and the dominant process is classical nucleation and growth (long incubation period). It should also be noted that the highest volume fraction of δ′ is produced at 100°C but this does not correspond to the largest decrease of resistivity (largest decrease is at 150°C). TEM examination showed that this was due to the much finer distribution of δ′ that forms during ageing at 100°C and this makes a positive contribution to the electrical resistivity.

Figures 11.43-11.47 give the DSC plots of 1.7Li1.2Cu0.7-2.0Mg alloys. As can be seen from **figure 11.49** the largest volume fraction of δ′ (peak K) is formed at 100°C. Again, this is the result of the optimum combination of thermodynamics and kinetics. The displacement of peak K to higher temperatures with increasing ageing temperature (**figure 11.50**) is the result of the formation of a coarser dispersion of δ′.

The 1.7Li1.2Cu3.0Mg alloy does not follow the trend of the rest of the alloys i.e. the amount of δ′ decreases as the ageing temperature increases from 70°C to 100°C (**figure 11.48**). Once again, it is believed that the reason for this behaviour

is the precipitation of T_M precursors at temperatures ≥100°C resulting in a reduction of the volume fraction of δ′ precipitation.

The resistivity plots of the 1.7Li1.2Cu0.7-2.0Mg alloys are presented in **figures 11.52-11.56.** All the alloys exhibit during ageing at 70 °C an initial resistivity increase ending after short ageing times (~0.4 h) in a resistivity peak. This is the result of the formation of very fine δ′ of size smaller than the critical size for electron scattering. Longer ageing times cause a drop of resistivity below the baseline as growth of δ′ occurs. As the ageing temperature increases from 70 to 100 to 150°C, due to the enhanced ageing kinetics, the electron scattering critical size is attained before the first measurement can be taken.

The resistivity plots of 1.7Li1.2Cu3.0Mg alloy are shown in **figure 11.57**. As can be seen the resistivity peak B′, that is attained after a small drop of resistivity below the baseline, shifts to earlier ageing times as the ageing temperature increases from 70°C to 100°C. Presumably a similar peak occurs at 150°C after very short ageing times but this has not been detected due to the extremely rapid ageing kinetics at this temperature. A detailed TEM analysis needs to be carried out on this alloy in order to determine the cause of the resistivity peak.

11.5 Exposure at 70°C after prior ageing at 150°C for 24 h

This section examines the effects of varying magnesium concentrations on the embrittlement that an aged (24 h 150°C) Al-Li-Cu-Mg aerospace alloy

undergoes after prolonged exposure at 70°C during service.

The DSC comparative plots, after ageing for 24 h at 150°C and after exposure for 1000 h at 70°C of each 1.7Li1.2CuXMg alloy are shown in **figures 11.58-11.64.** In order to measure the enthalpy that corresponds to the dissolution of δ′ formed during exposure, the area of the dissolution peak after ageing for 24 h at 150°C was subtracted from the area of the peak after exposure for 1000 h at 70°C. By using **equation 8.2,** this enthalpy was converted to volume fraction of δ′. The volume fractions obtained are displayed in **figure 11.65**. It can be seen that as magnesium concentration increases from 0 to 1.2 % the volume fraction of δ′, that is produced during exposure, increases. However, further increase of magnesium from 1.2% to 1.4% results in a reduced volume fraction of δ′ after exposure.

For magnesium concentrations higher than 1.4% (1.7Li1.2Cu2.0Mg alloy) the δ′ volume fraction is actually reduced after subsequent exposure at 70°C. This behaviour could be explained by:

- Dissolution of δ′ caused by the formation of another Li-rich phase during exposure at 70°C.
- Li-Cu-Mg clusters form at 150°C. Due to the high binding energy between Li Cu Mg atoms, these clusters require a high amount of enthalpy for their dissolution. It is postulated that during subsequent exposure at 70°C these clusters transform into δ′ which in turn requires a reduced amount of enthalpy for dissolution.

11.6 Effect of exposure on the mechanical properties of 1.7Li1.2CuXMg alloys

Figure 11.66 shows the changes in proof stress and fracture energy after exposure for 1000 h at 70°C. It can be clearly seen that for magnesium levels up to ~1.0% the proof stress exhibits a significant increase that is accompanied by an analogous decrease in fracture energy. As the magnesium concentration increases beyond 1.0% the proof stress starts decreasing and finally for magnesium levels ≥2% no increase in proof stress is observed. In the same composition range (1.0-2.0%) the fracture energy increases indicating less embrittlement during exposure. This behaviour is in good agreement with the DSC results presented in the last paragraph where the largest volume fraction of exposure δ′ was observed at 1.2%Mg. As the magnesium concentration increases beyond 1.2% the amount of δ′ precipitated during exposure decreases resulting in a softer more ductile material.

Summary

The following is a summary of the results found in the present chapter.

As quenched alloys

- In the as-quenched condition magnesium atoms behave as though they are in a simple binary Al-Mg solid solution, i.e. the magnesium atoms do not

associate with other solute atoms, i.e. Li, Cu, Zr.

- In the low lithium Al-1.3Li-Cu-Mg alloys the presence of copper and magnesium enhances the kinetics of δ′ formation. Increasing the lithium concentration from 1.3% to 1.7% results in an increase of fine δ′ precipitation with enhanced reaction kinetics.
- In the 1.7Li1.2CuXMg alloys the dominant mechanism for δ′ stimulation is not the shift of δ′ solvus boundary to a higher temperature.
- The small stimulation of δ′ in 1.7Li1.2CuXMg alloys over the range 0-1.2%Mg can be attributed to heterogeneous nucleation and growth on GPB zones.
- The marked enhancement of δ′ precipitation in the 1.7Li1.2CuXMg alloys over the composition range 1.4-3.0%Mg is due to the formation of Li-Cu-Mg clusters which are capable of rapidly developing into δ′ precipitates. It is important to be noted that the clustering process starts only after >1.2Mg has been added. It is believed that for magnesium levels up to 1.2% the magnesium is used in producing GPB zones; beyond 1.2%Mg 'free' magnesium is available in the matrix to gather both lithium and copper thus developing into Li-Cu-Mg clusters.
- The activation energy for δ′ formation in 1.7Li1.2Cu2.0Mg alloy was 62kJ/mol, which is in the range of activation energies measured for the movement of vacancies in aluminium. This suggests that δ′ precipitation in Al-Li-Cu-XMg alloys is controlled by the presence of excess vacancies

that have been quenched-in after solutionising.

- It is postulated that the retardation of δ′ and GPB zone formation that occurs in 1.7Li1.2Cu3.0Mg alloy is due to the formation of a precursor of the equilibrium T_M phase (T'_M).

Isothermal ageing

- At all ageing temperatures, increasing the lithium concentration in Al-Li-Cu-Mg alloys from 1.3 to 1.7% results in stimulation of δ′ precipitation due to the increased supersaturation of lithium. During ageing at 70°C and 100°C, an increase in magnesium concentration from 1.2 to 2.0% in the low lithium alloys (1.3Li1.2CuXMg) results in a delay in the precipitation of δ′ due to the rapid formation of Li-Cu-Mg clusters in the early stages of ageing.
- Isothermal ageing at 70, 100, and 150°C causes significant enhancement of δ′ precipitation in 1.7Li1.2CuXMg alloys as the magnesium concentration increases beyond 1.2%.
- At all ageing temperatures (70, 100, 150°C) retardation of δ′ takes place in the 1.7Li1.2Cu3.0Mg alloy.
- The largest volume fraction of δ′ forms at 100°C where there is an optimum combination of thermodynamics and kinetics. Increasing the ageing temperature from 70 to 100 to 150°C results in a coarser dispersion of δ′.

- The volume fraction of δ′ that is produced in the 1.7Li1.2CuXMg alloys during exposure at 70°C increases as the magnesium concentration increases from 0 to 1.2%. A further increase of magnesium results in a reduced volume fraction of δ′ after exposure.
- The maximum embrittlement after exposure at 70°C is observed for the 1.7Li1.2Cu1.2Mg alloy and is attributed to the maximum volume fraction of δ′ that precipitates in this alloy during exposure.

Table 11.1: Compositions of the alloys in at% and the corresponding contribution to resistivity from each element

Alloy Nr	267	268	269	270	271	272
Mg wt%	0	0.7	1	1.4	2	3
at%	0	0.75	1.01	1.50	2.14	3.21
4.86 nΩm/at%						
Li wt%	1.7	1.7	1.7	1.7	1.7	1.7
at%	6.35	6.35	6.35	6.36	6.36	6.37
8.73 nΩm/at%						
Cu wt%	1.2	1.2	1.2	1.2	1.2	1.2
at%	0.49	0.49	0.49	0.49	0.49	0.49
8.19 nΩm/at%						
Zr wt%	0.07	0.07	0.07	0.07	0.07	0.07
at%	0.02	0.02	0.02	0.02	0.02	0.02
58.6 nΩm/at%						

Table 11.2: The experimental resistivity values (ρ_o exper.) and the theoretical values extracted from equation 11.6.

%Mg	ρ_o Theor.	ρ_o exp.
0	60.57	63.59
0.7	64.23	63.3
1	65.82	63.22
1.4	67.93	68.79
2	71.08	72.96
3	76.34	77.13
*ρ_o:n.ohm.m		

Table 11.3: Data used in Kissinger method (see text)

T_f (K)	Φ(K/min)	$\ln(T_f^2/\Phi)$	$1/T_f$
487.013	5.0	10.767	0.00205
494.062	10.0	10.103	0.00202
501.454	20.0	9.439	0.00199
513.222	40.0	8.793	0.00195
520.157	60.0	8.414	0.00192
529.204	80.0	8.161	0.00189

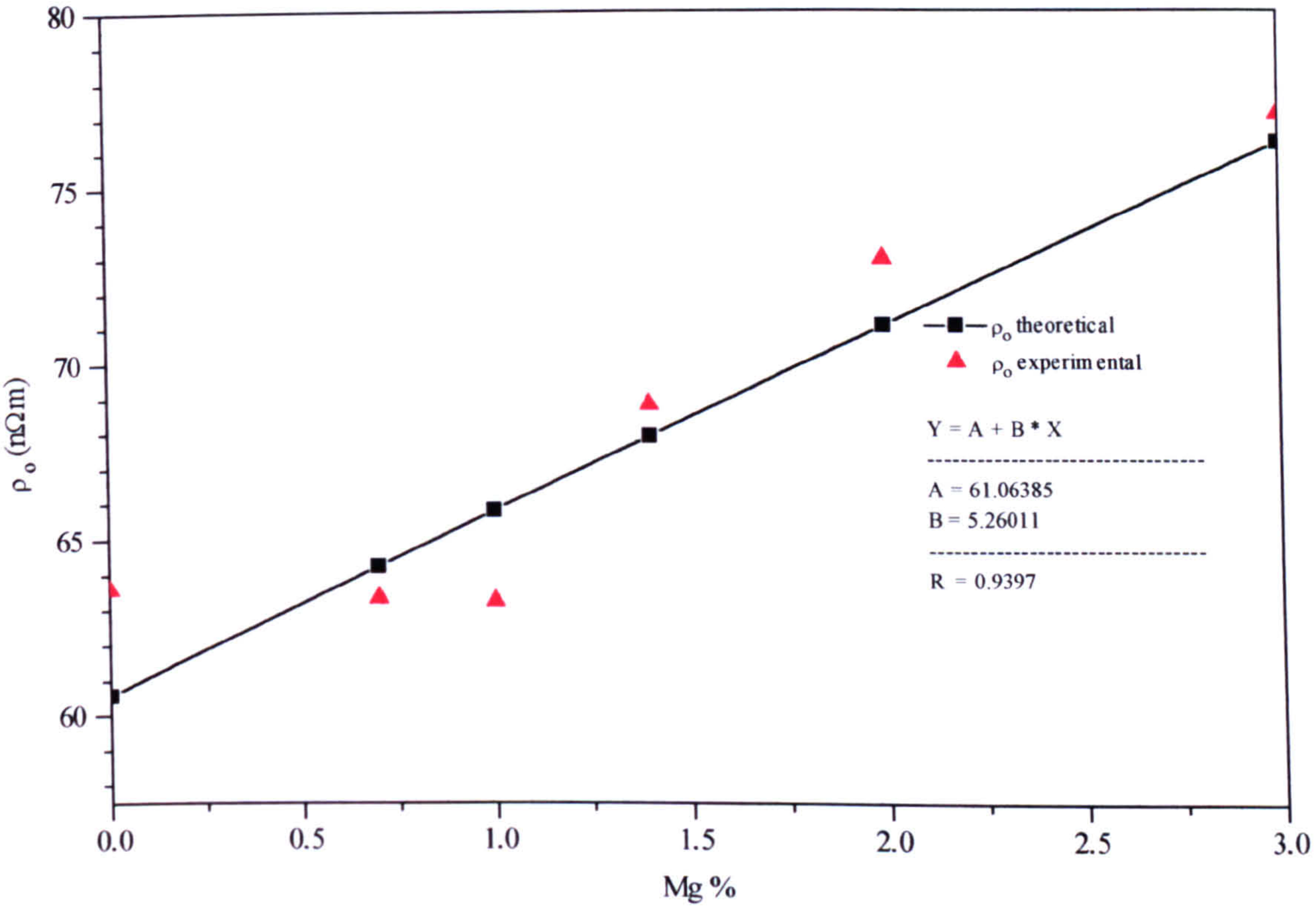

Figure 11.1: Effect of magnesium concentration on the residual resistivity ρ_o.

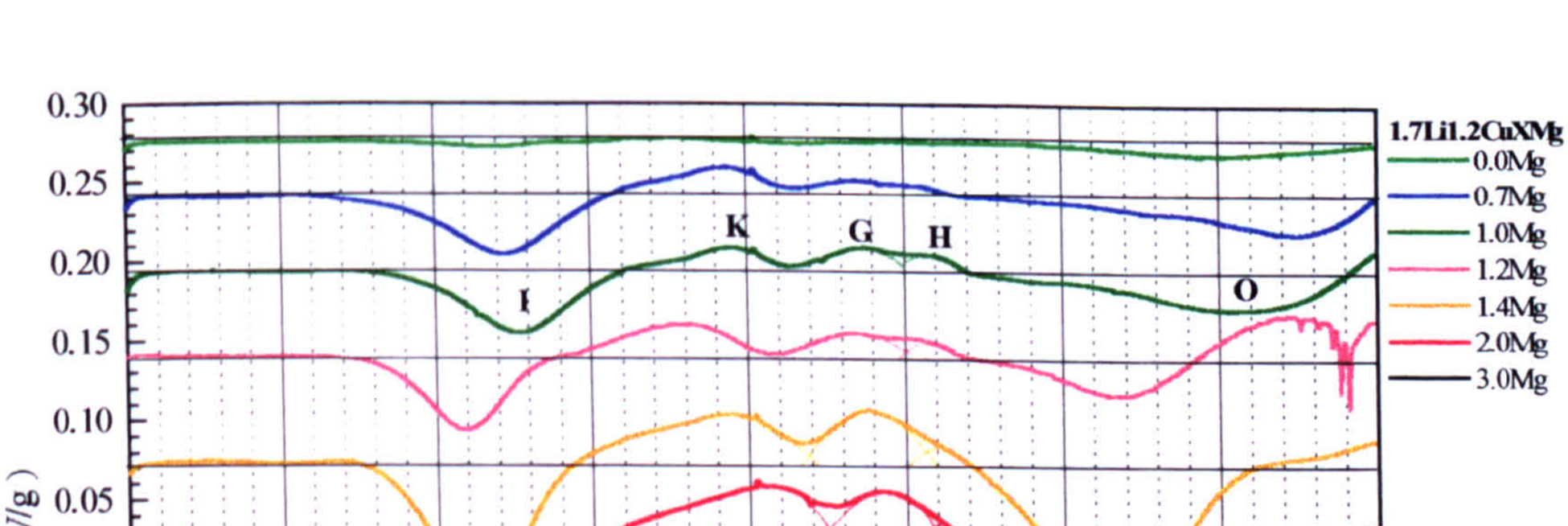

Figure 11.2: Comparative DSC plots of the as-quenched 1.7Li1.2CuXMg alloys.

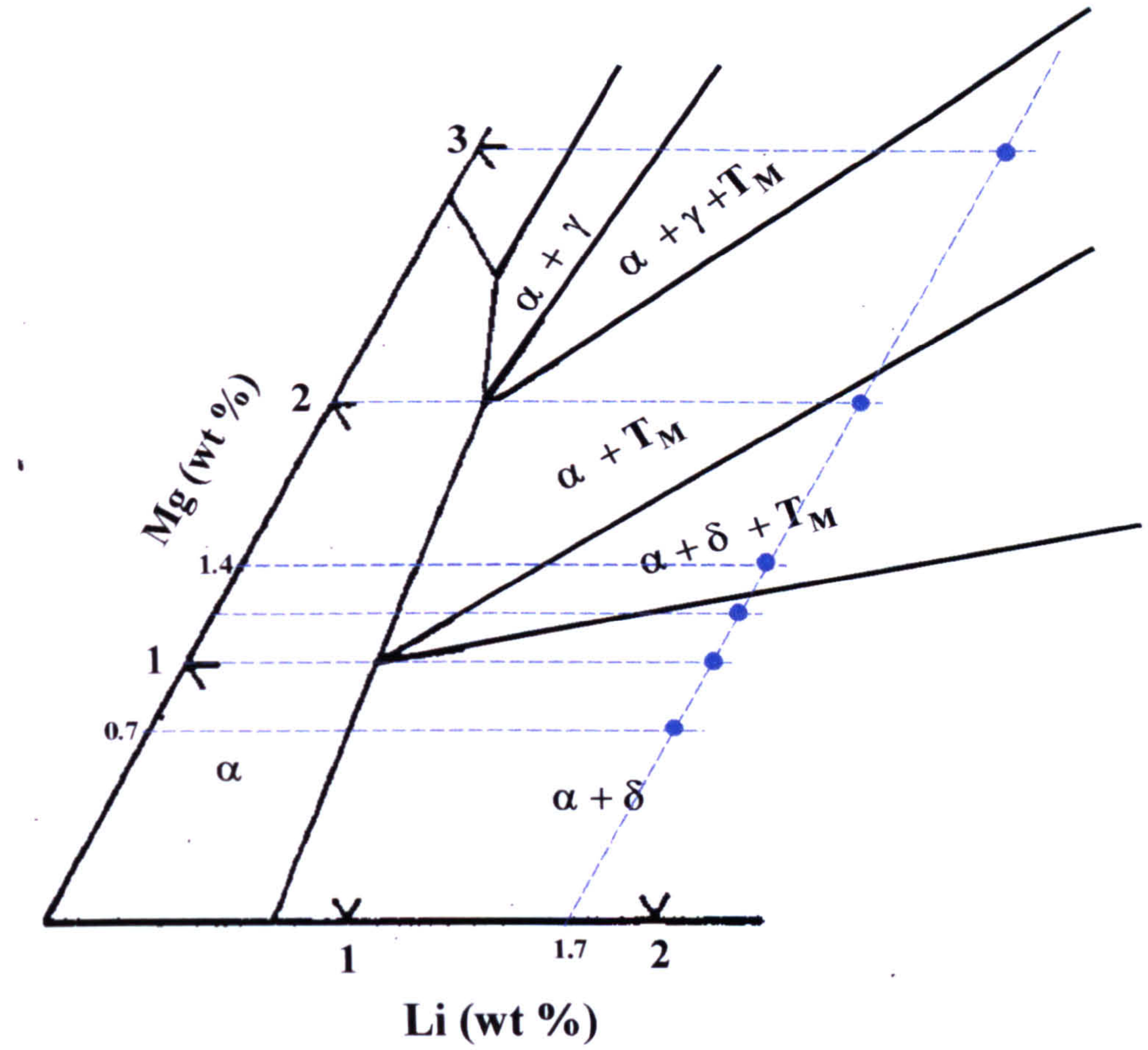

Figure 11.3: Isothermal section of the ternary Al-Li-Mg system at 200°C.

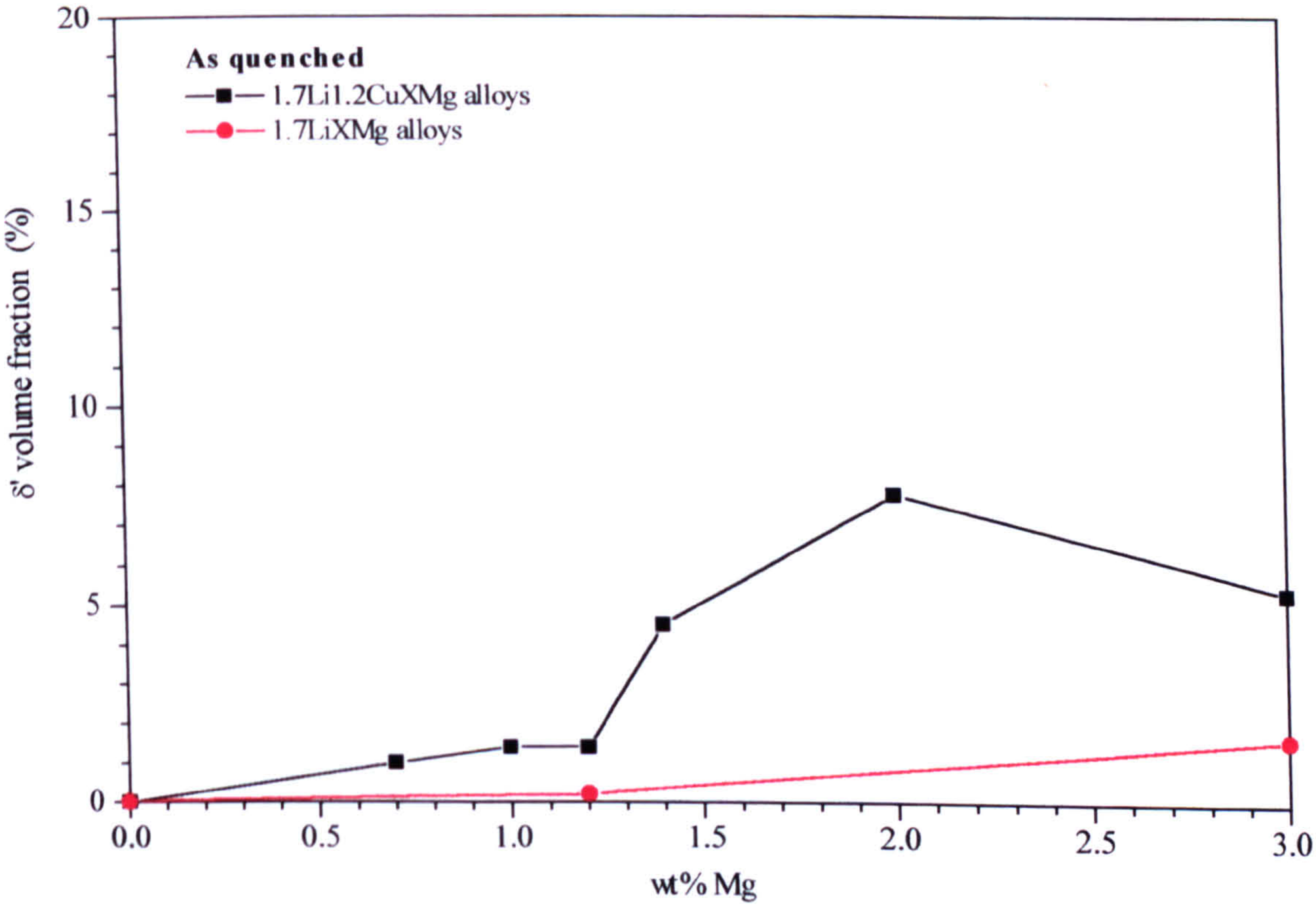

Figure 11.4: Volume fraction of δ′ produced during DSC heating of the as-quenched 1.7Li1.2CuXMg alloys.

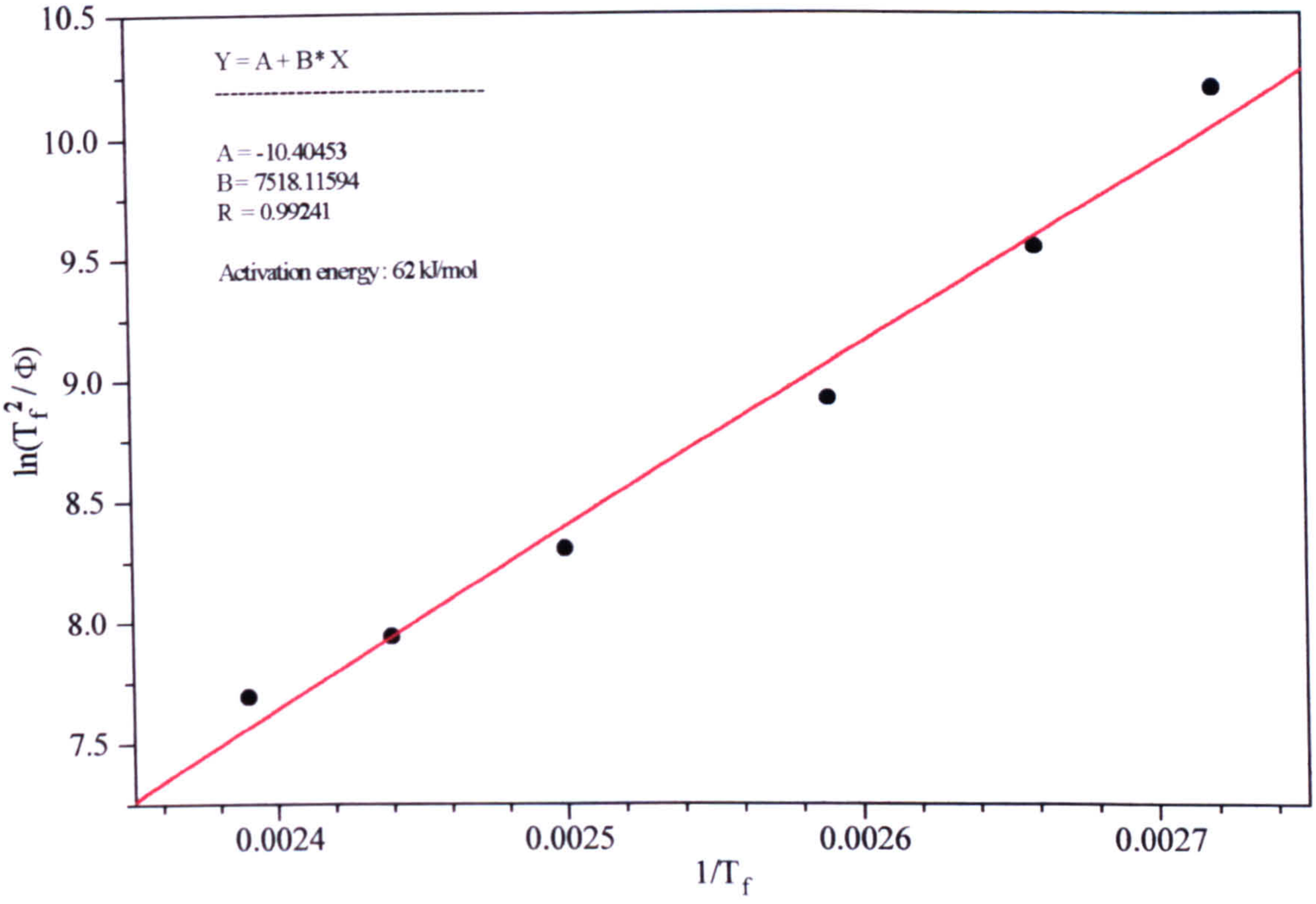

Figure 11.5: Calculation of δ′ activation energy by applying linear regression on the data obtained by using Kissinger analysis [77].

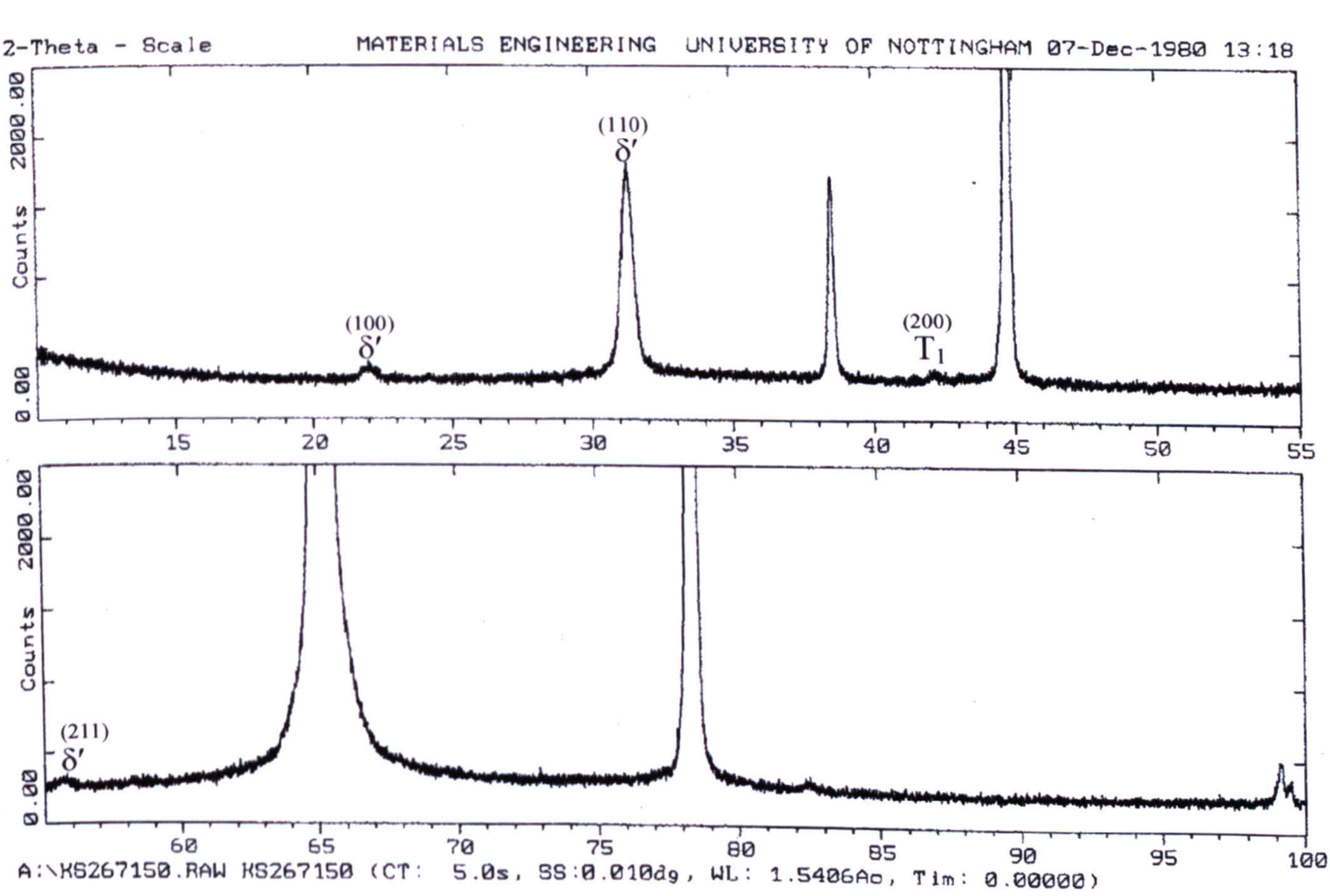

Figure 11.6: XRD spectrum of 1.7Li1.2Cu0.0Mg alloys after ageing for 24 at 150°C.

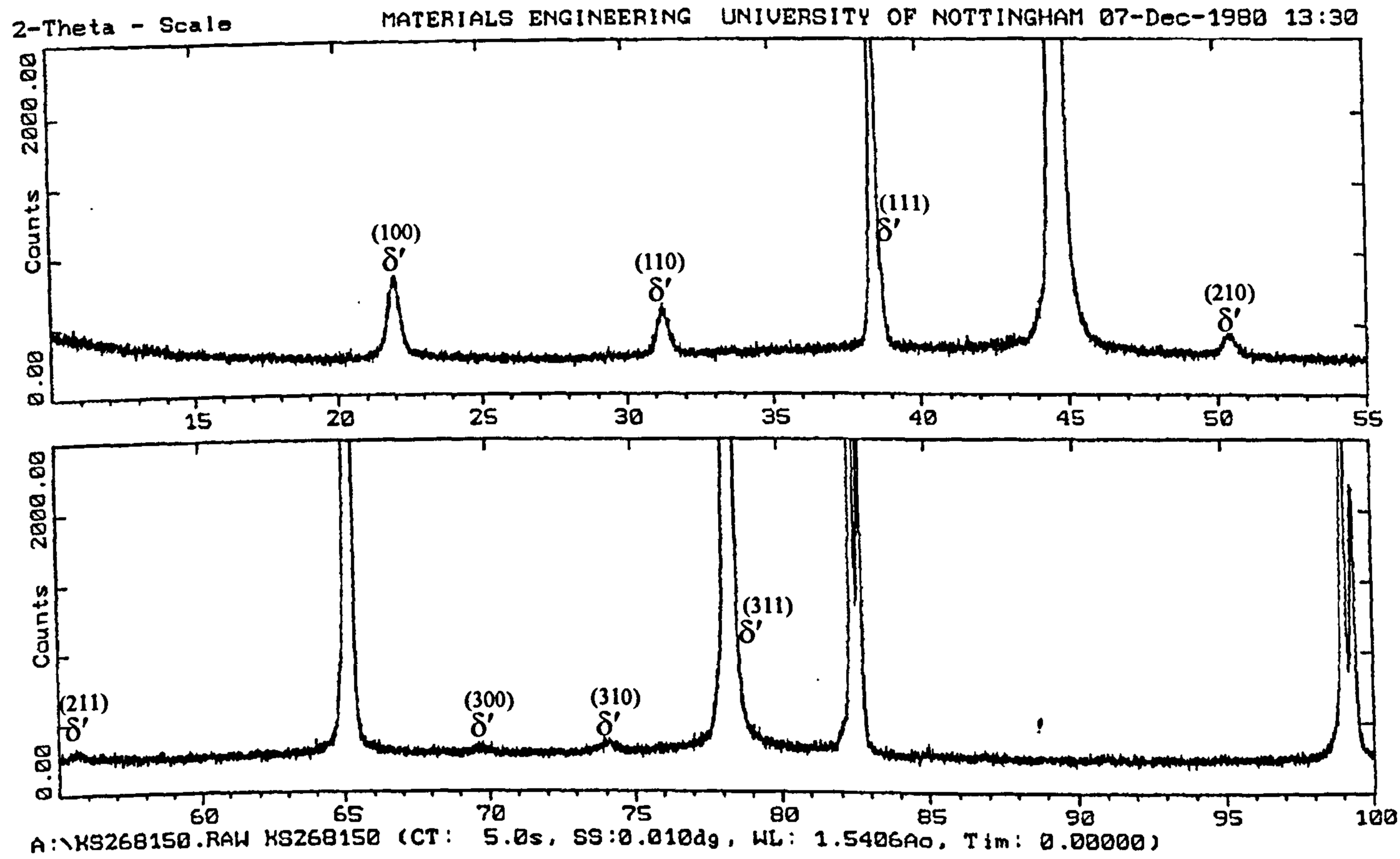

Figure 11.7: XRD spectrum of 1.7Li1.2Cu0.7Mg alloys after ageing for 24 at 150°C.

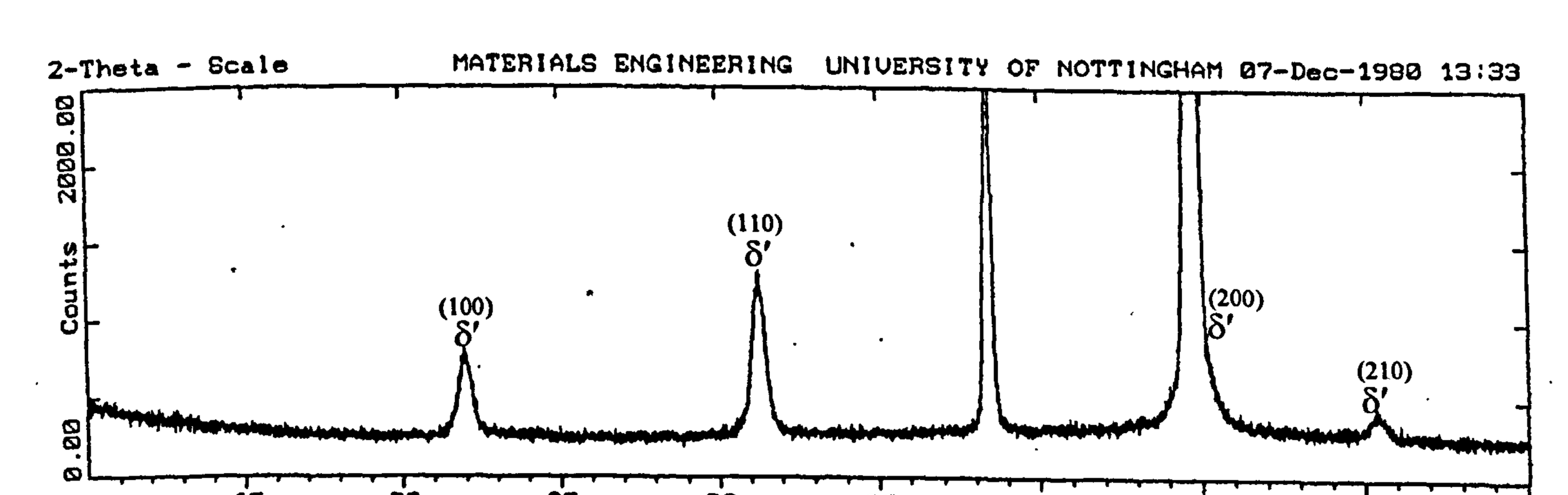

Figure 11.8: XRD spectrum of 1.7Li1.2Cu1.0Mg alloys after ageing for 24 h at 150°C.

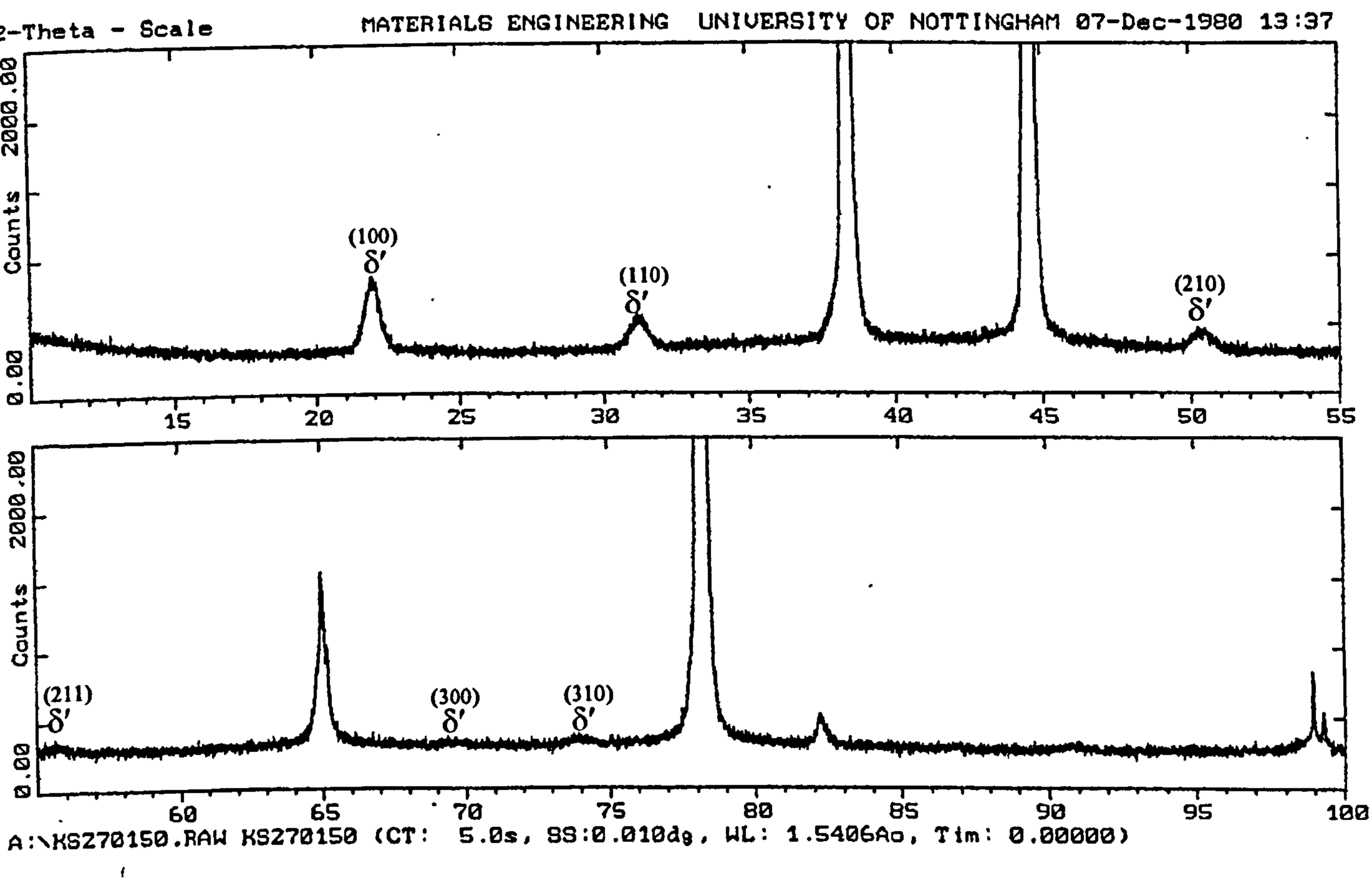

Figure 11.9: XRD spectrum of 1.7Li1.2Cu1.4Mg alloys after ageing for 24 at 150°C.

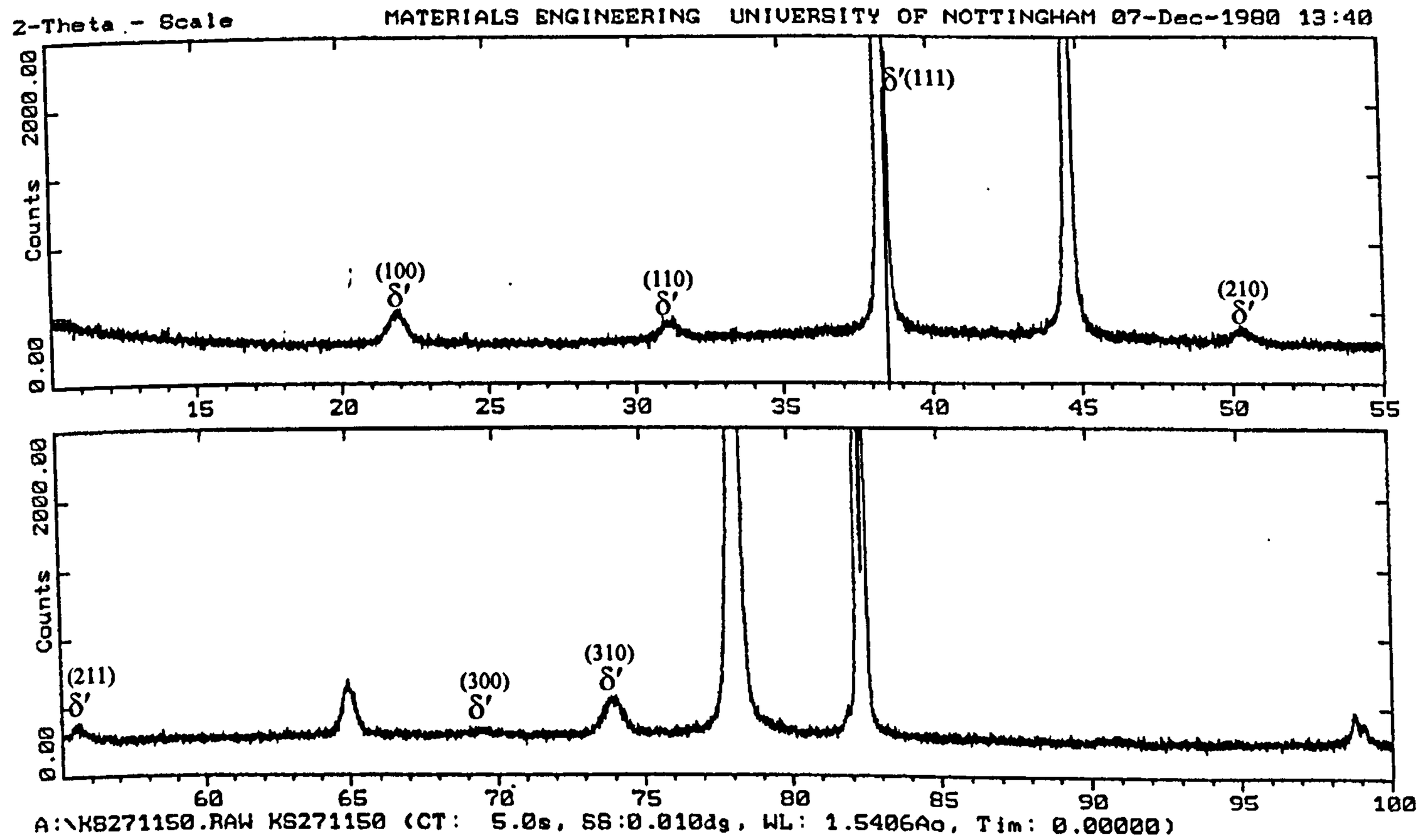

Figure 11.10: XRD spectrum of 1.7Li1.2Cu2.0Mg alloys after ageing for 24 at 150°C.

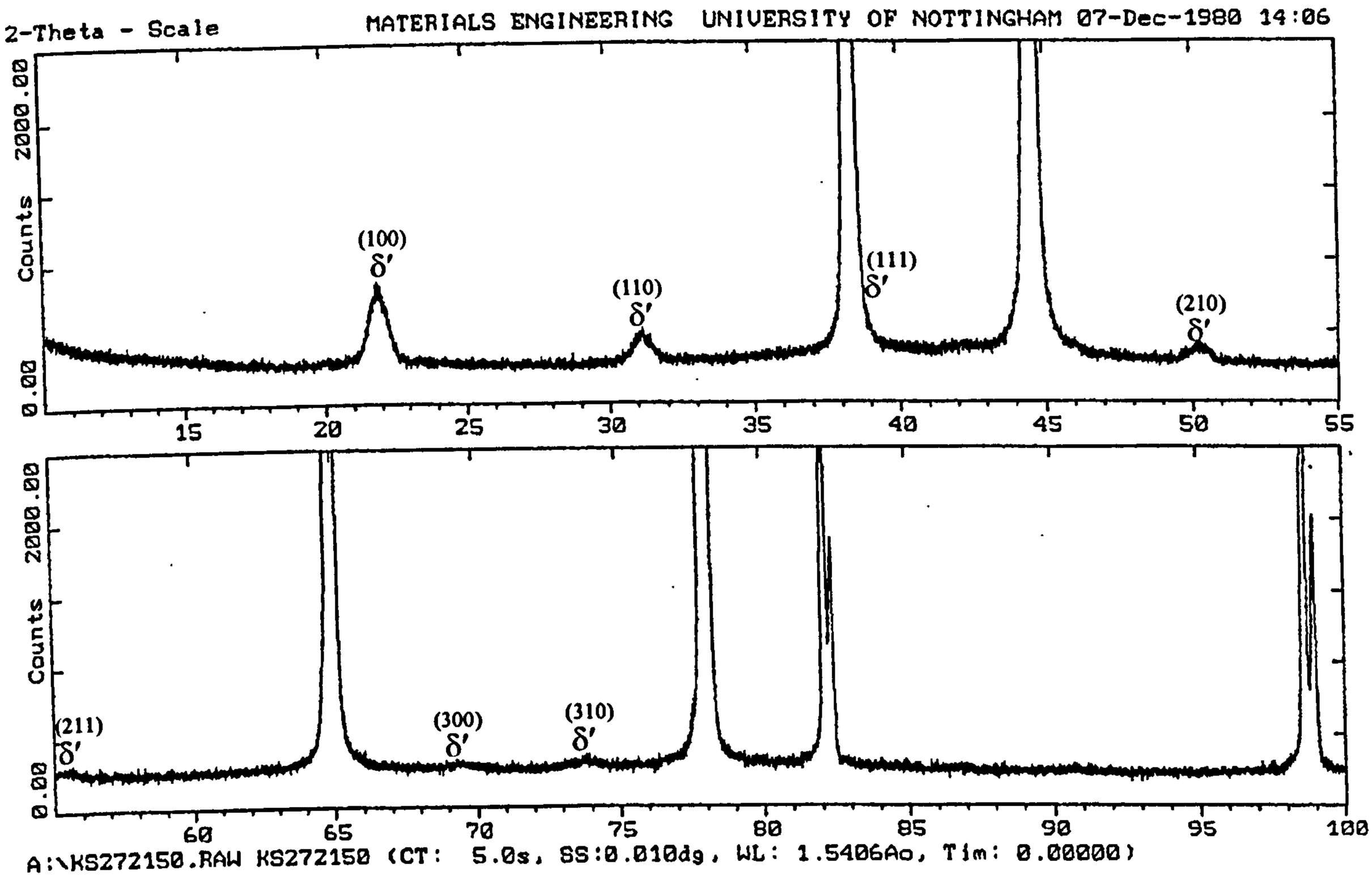

Figure 11.11: XRD spectrum of 1.7Li1.2Cu3.0Mg alloys after ageing for 24 at 150°C.

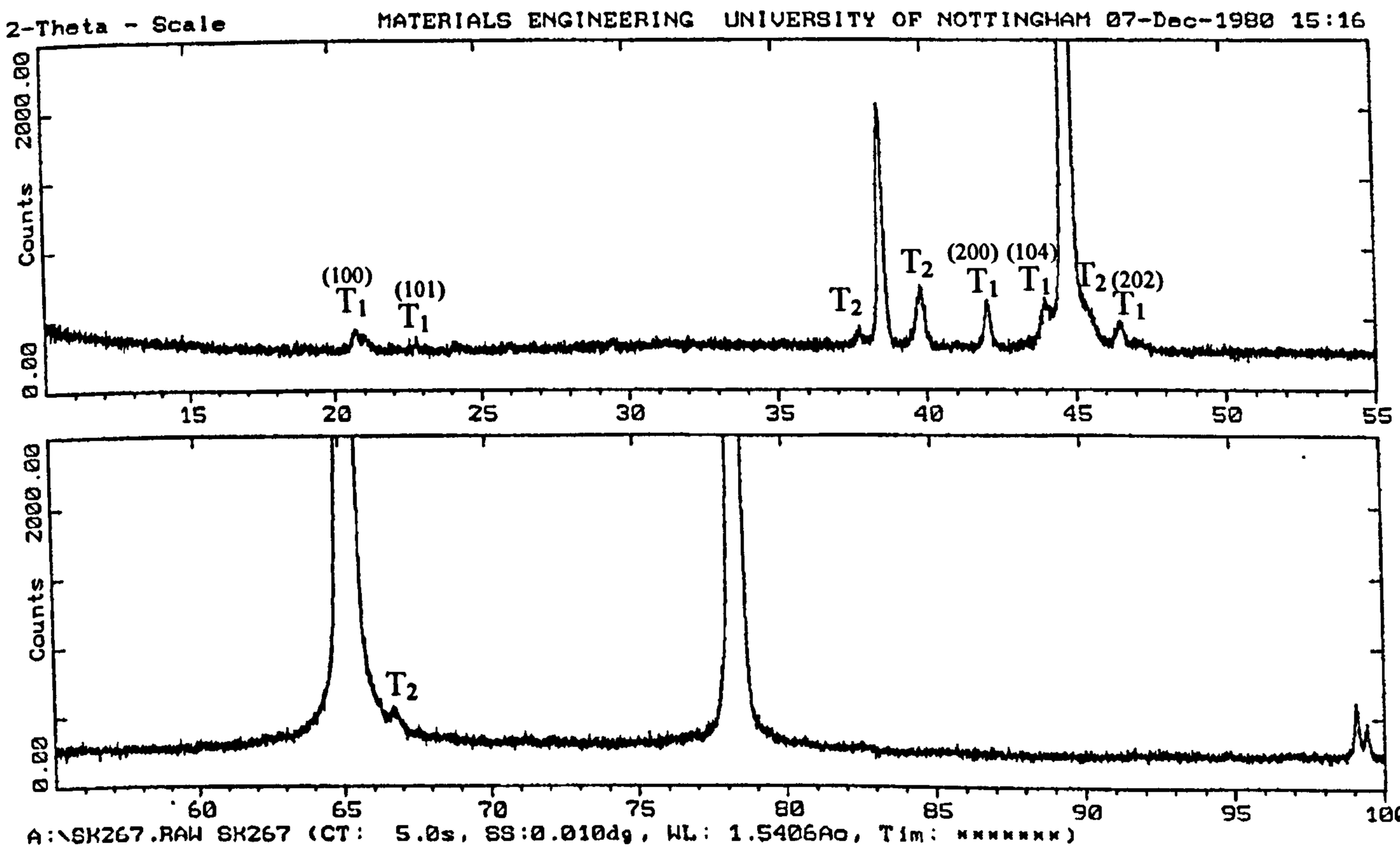

Figure 11.12: XRD spectrum of 1.7Li1.2Cu0.0Mg alloy after ageing for 24 h at 350°C.

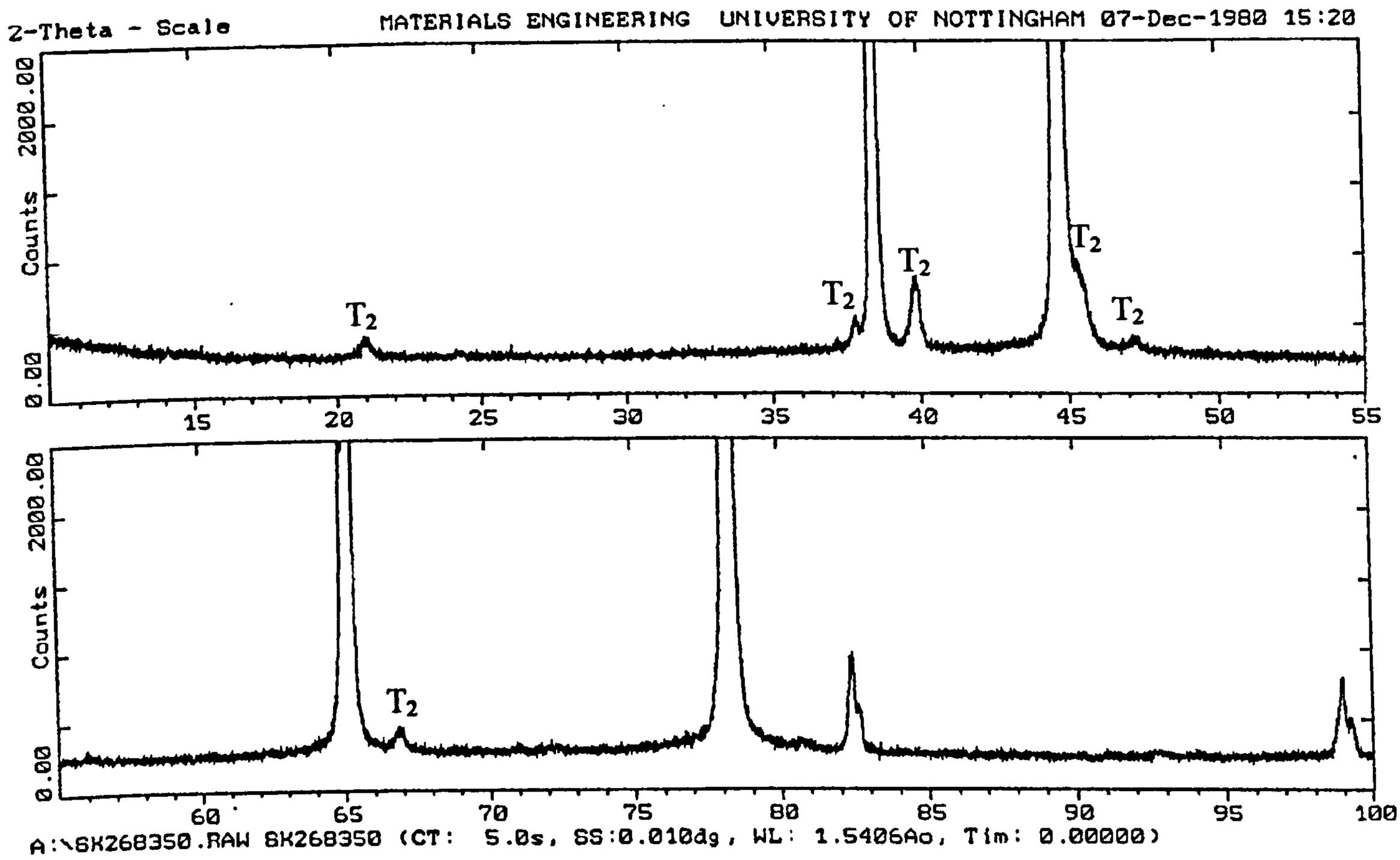

Figure 11.13: XRD spectrum of 1.7Li1.2Cu0.7Mg alloy after ageing for 24 h at 350°C.

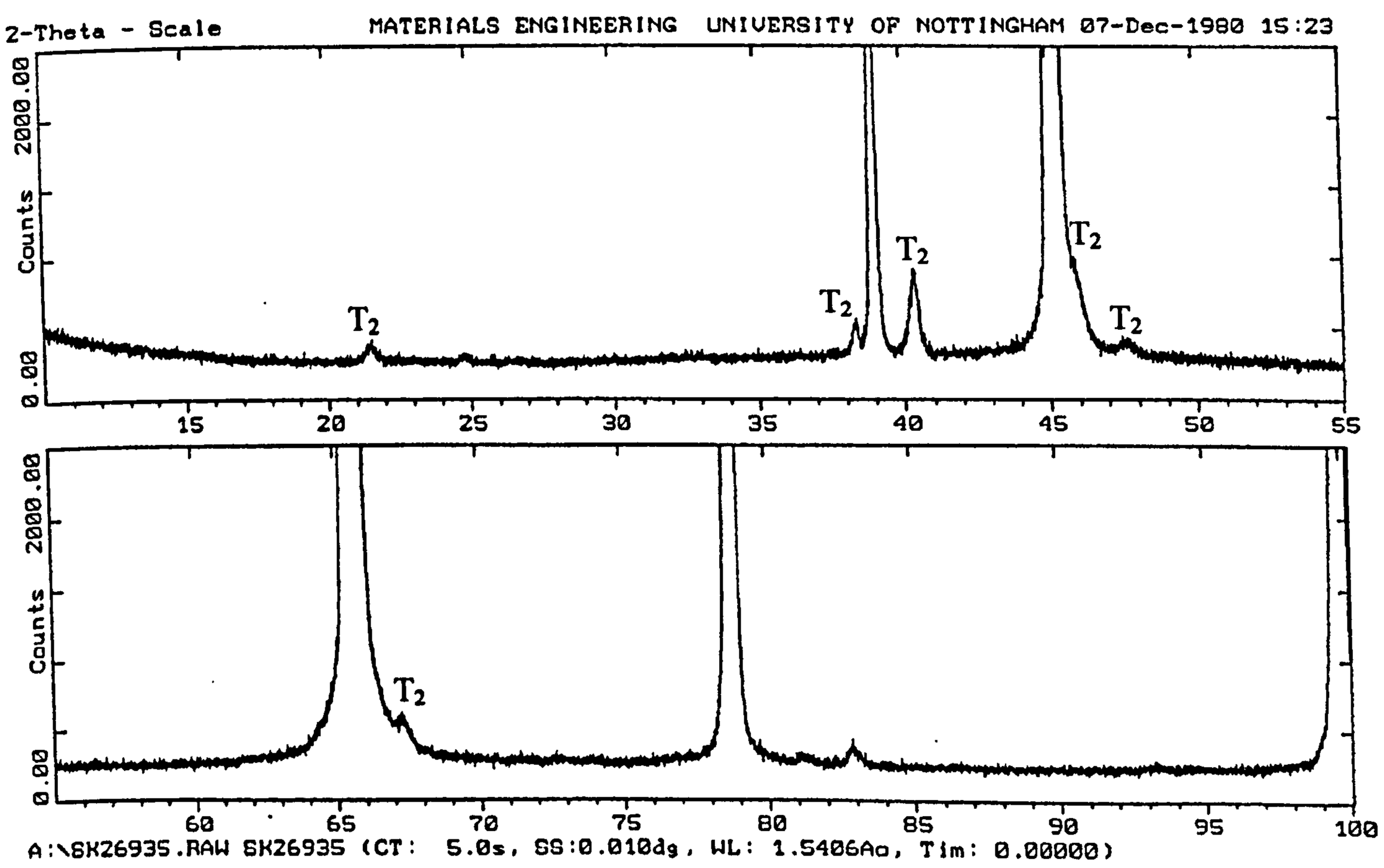

Figure 11.14: XRD spectrum of 1.7Li1.2Cu1.0Mg alloy after ageing for 24 h at 350°C.

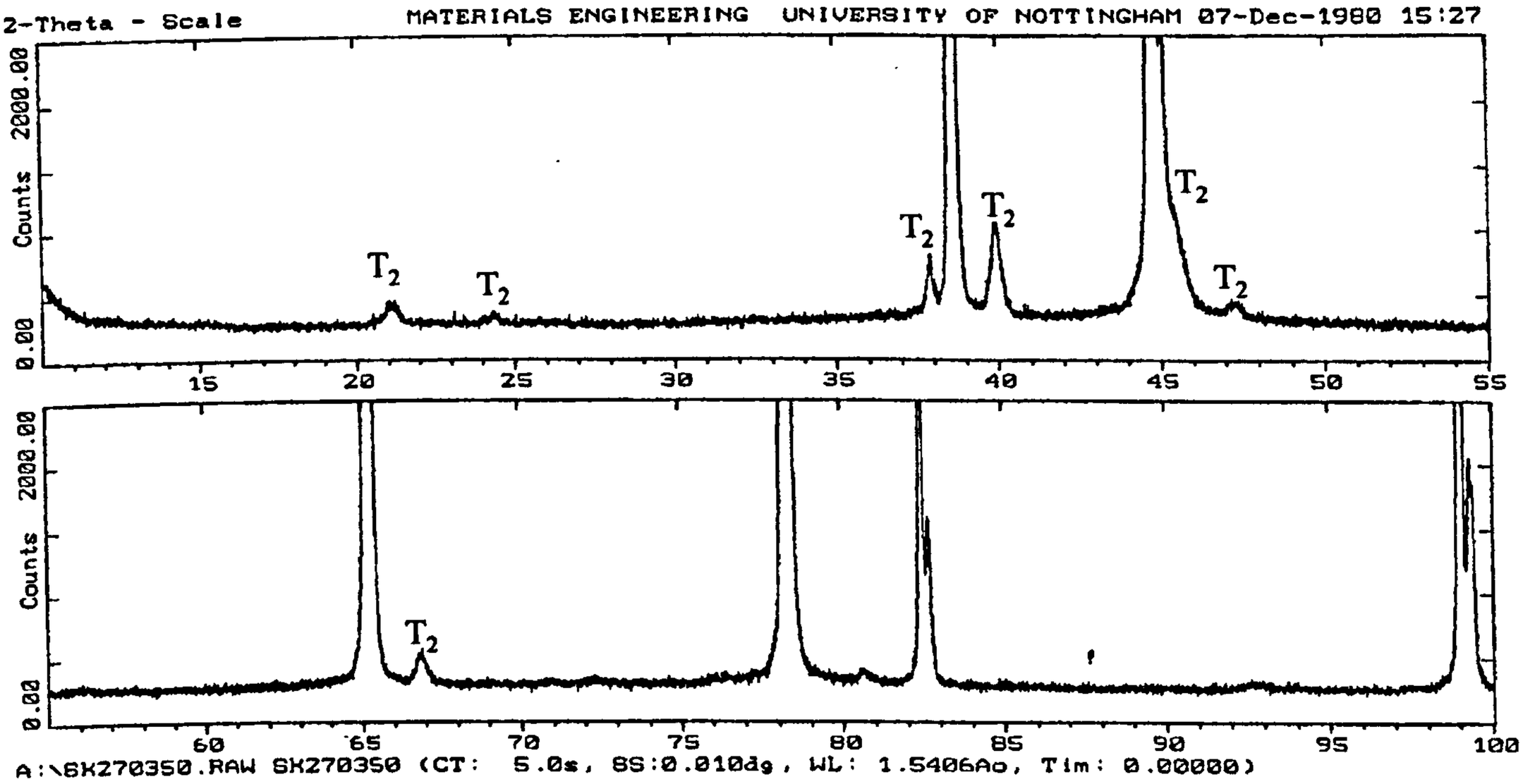

Figure 11.15: XRD spectrum of 1.7Li1.2Cu1.4Mg alloy after ageing for 24 h at 350°C.

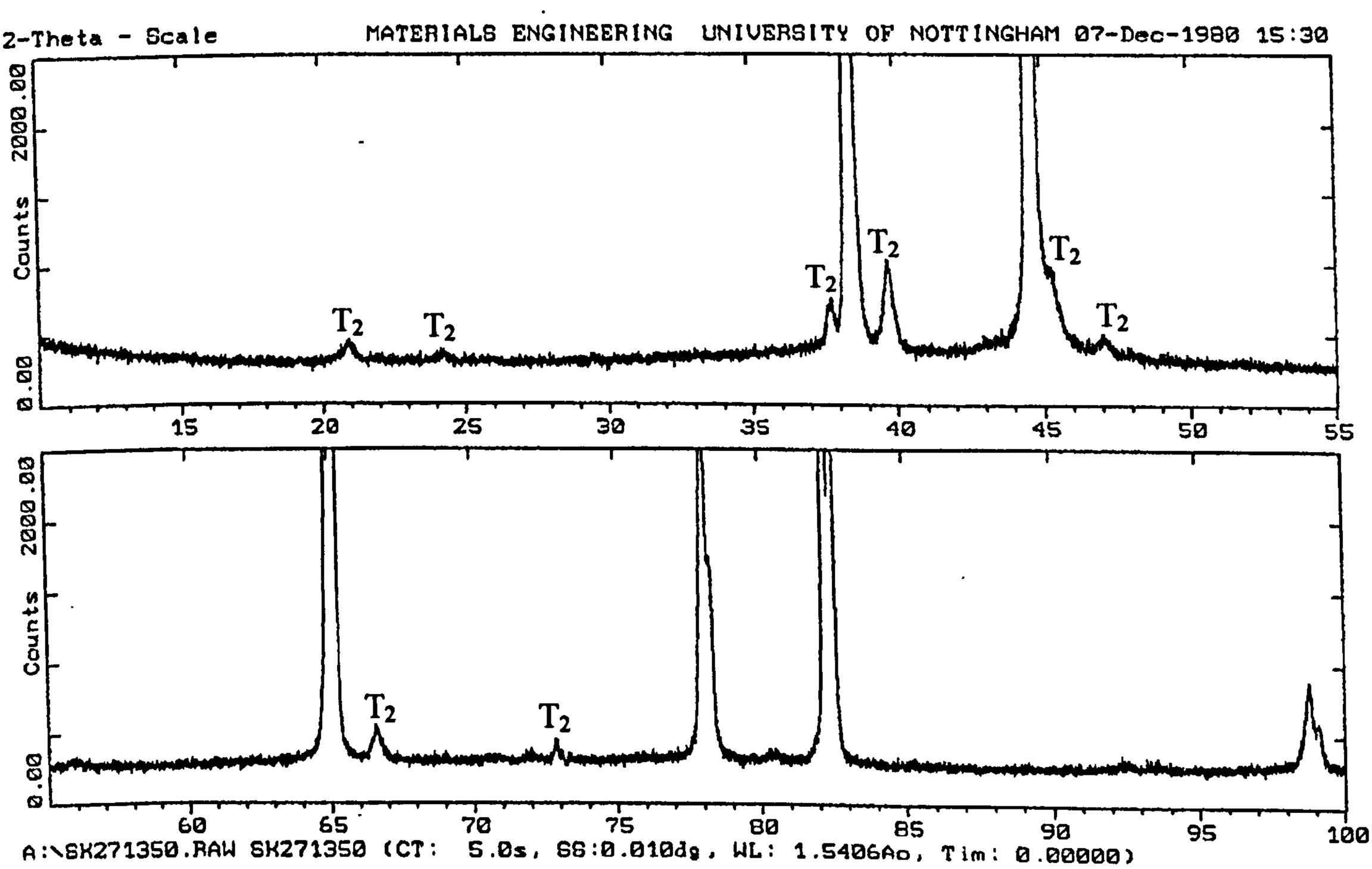

Figure 11.16: XRD spectrum of 1.7Li1.2Cu2.0Mg alloy after ageing for 24 h at 350°C.

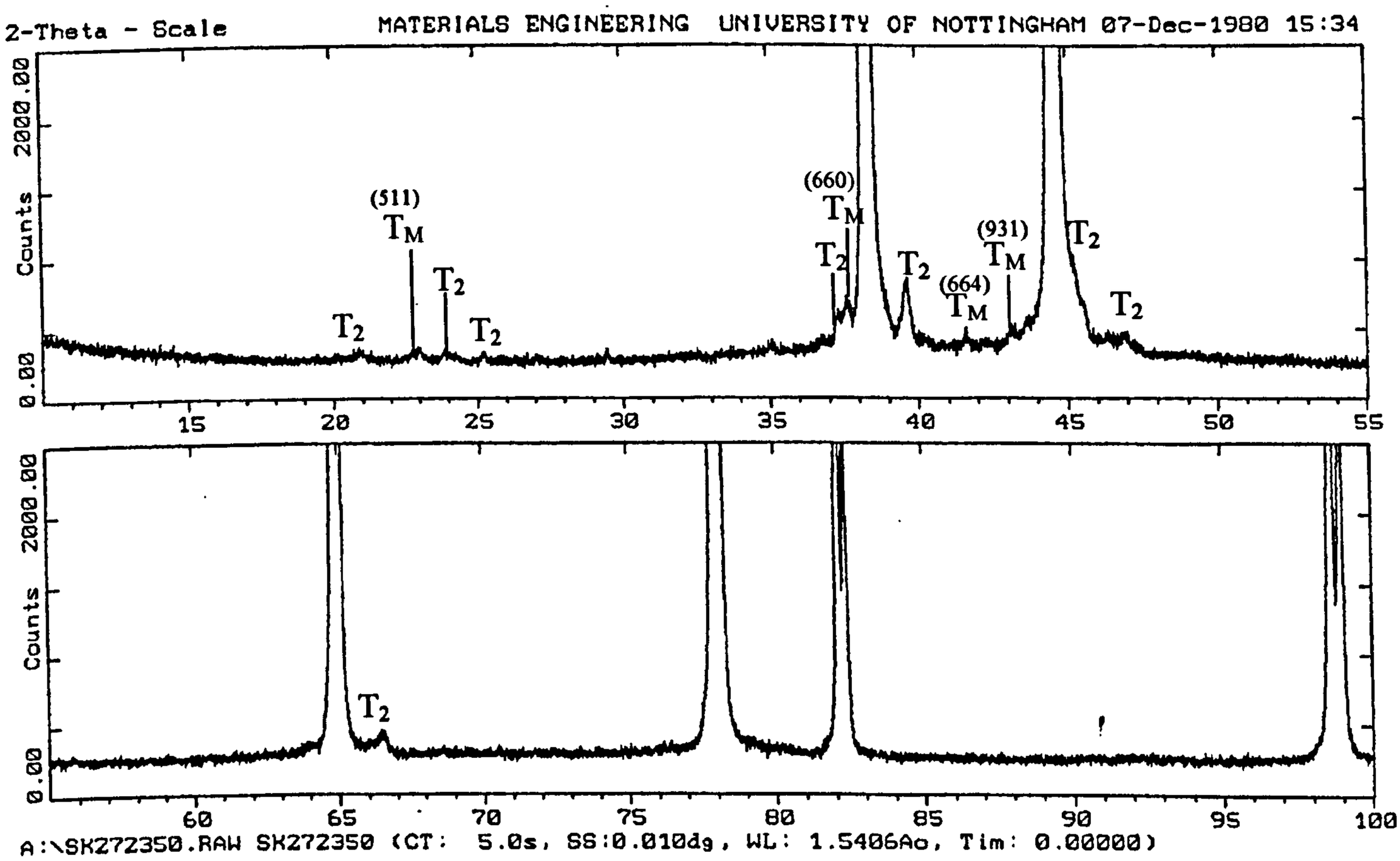

Figure 11.17: XRD spectrum of 1.7Li1.2Cu3.0Mg alloy after ageing for 24 h at 350°C.

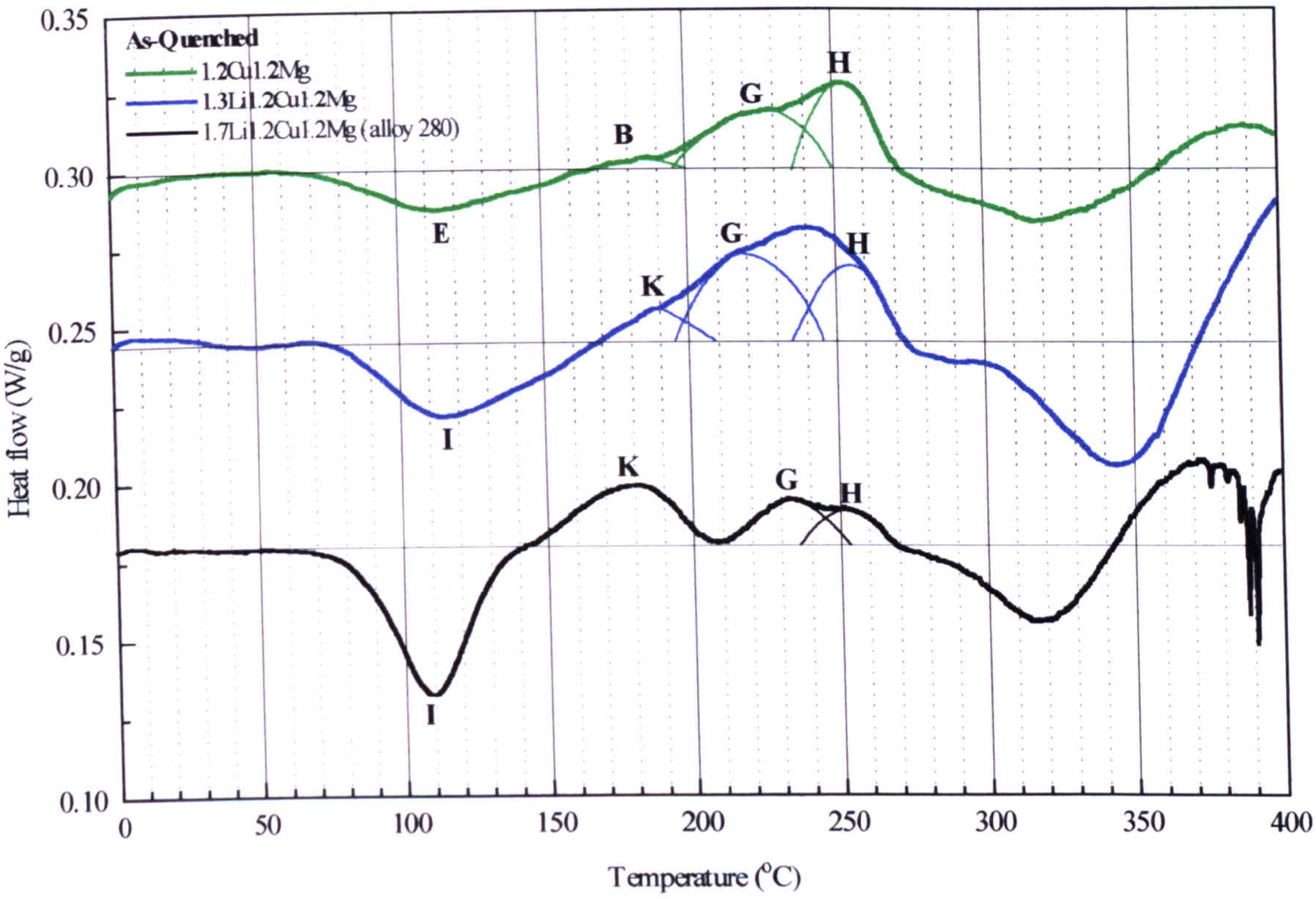

Figure 11.18: Comparative DSC plots of the as-quenched 1.2Cu1.2Mg, 1.3Li1.2Cu1.2Mg, and 1.7Li1.2Cu1.2Mg alloys.

Figure 11.19: Comparative isochronal resistivity plots of 1.7Li binary, 1.2Cu1.2Mg, 1.3Li1.2Cu1.2Mg, and 1.7Li1.2Cu1.2Mg alloys.

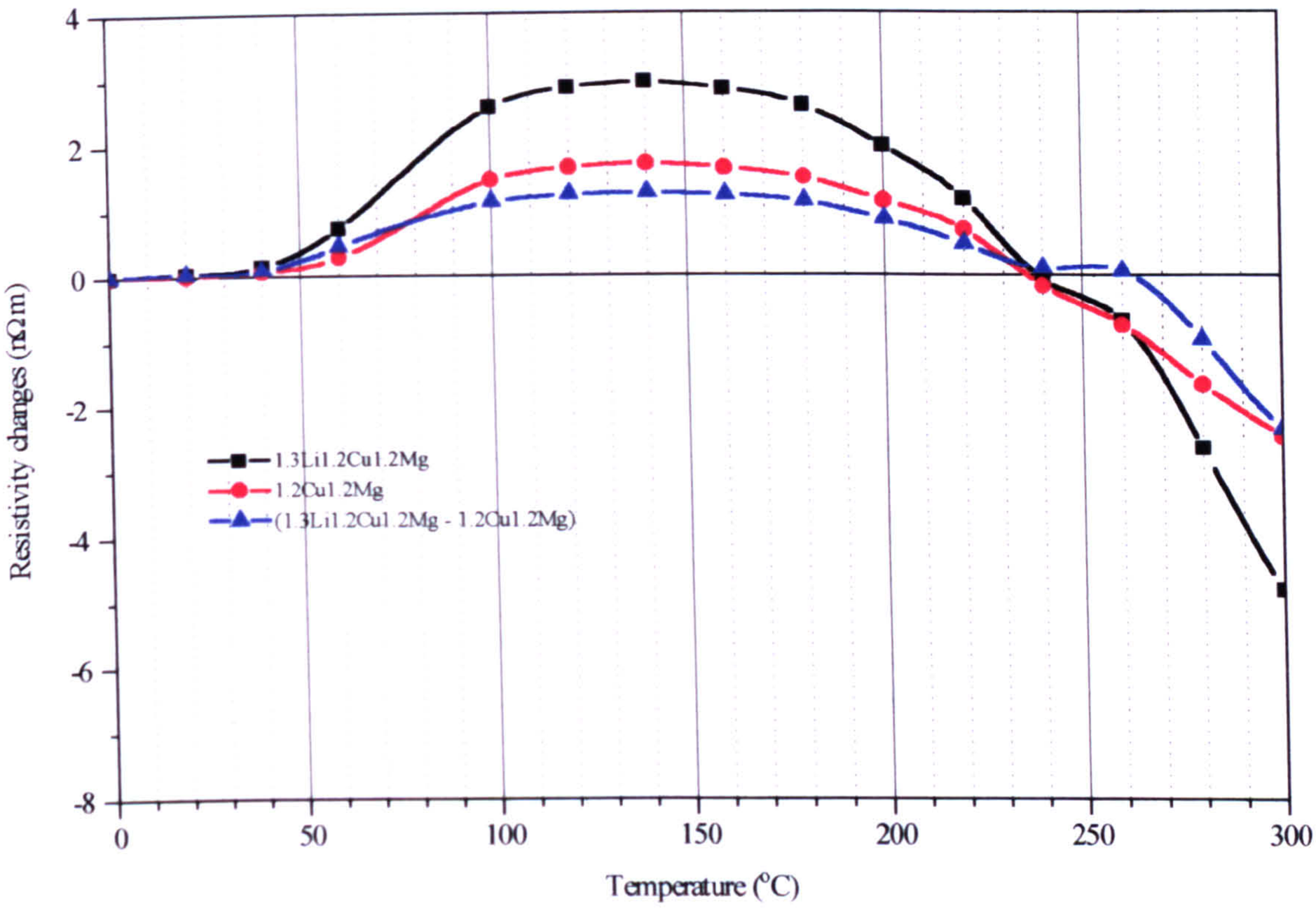

Figure 11.20: Subtraction of the effect of GPB zones from the isochronal resistivity plot of a 1.3Li1.2Cu1.2Mg alloy and comparison with the isochronal resistivity plot of a 1.2Cu1.2Mg alloy. (Data derived from ***figure 11.19)***

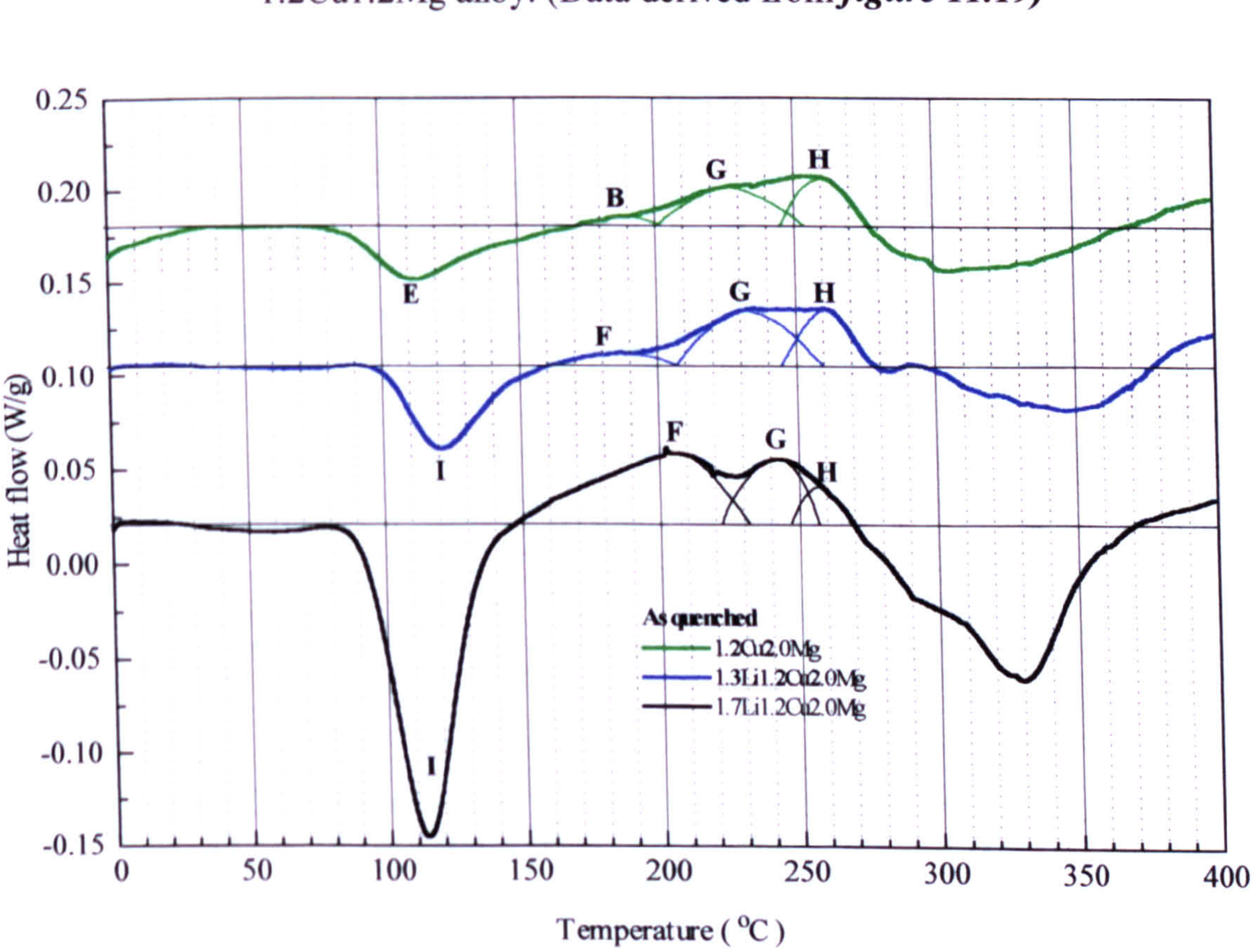

Figure 11.21: Comparative DSC plots of the as-quenched 1.2Cu2.0Mg, 1.3Li1.2Cu1.2Mg and 1.7Li1.2Cu2.0Mg alloys.

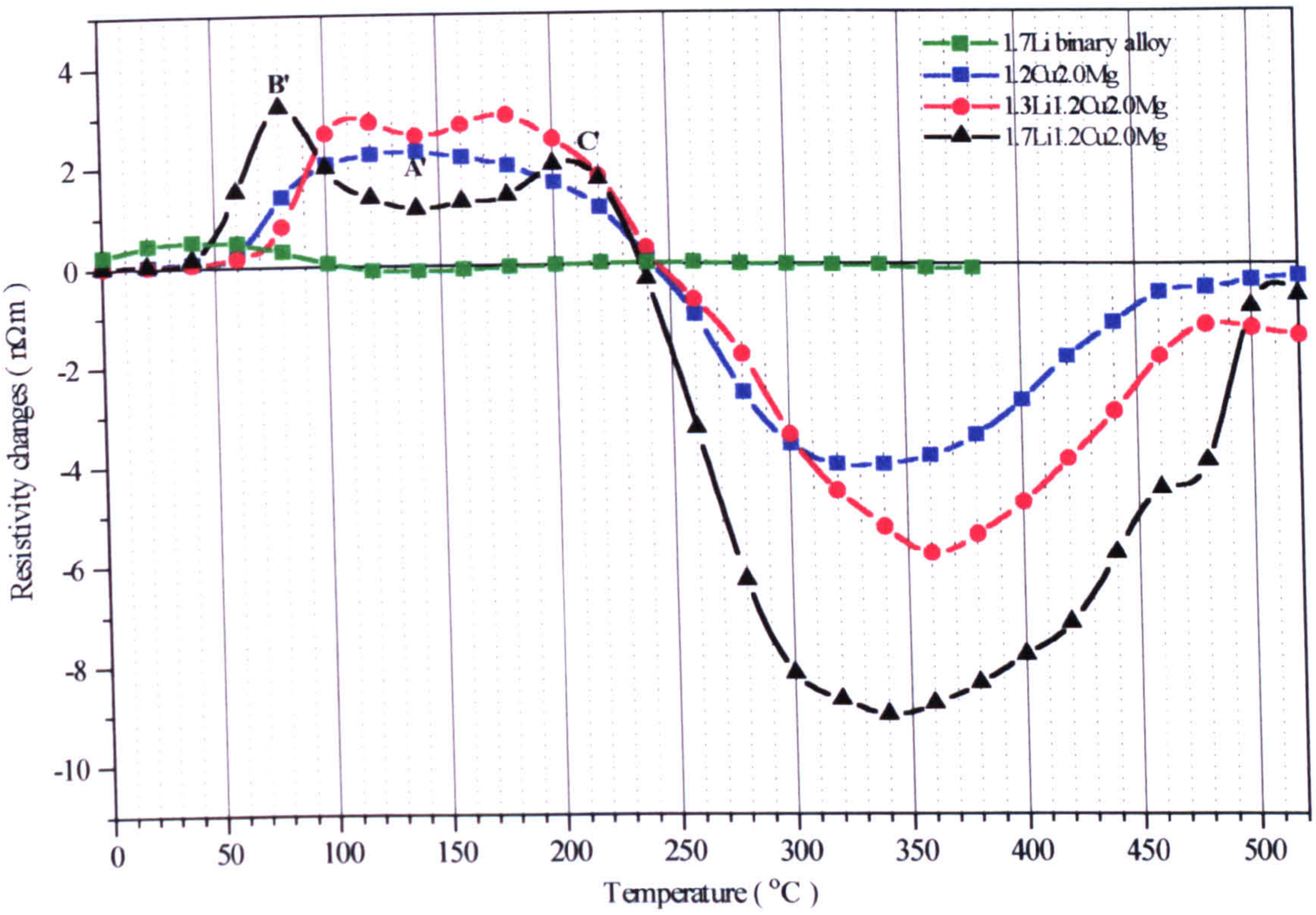

Figure 11.22: Comparative isochronal resistivity plots of 1.2Cu2.0Mg, 1.3Li1.2Cu2.0Mg, and 1.7Li1.2Cu2.0Mg alloys.

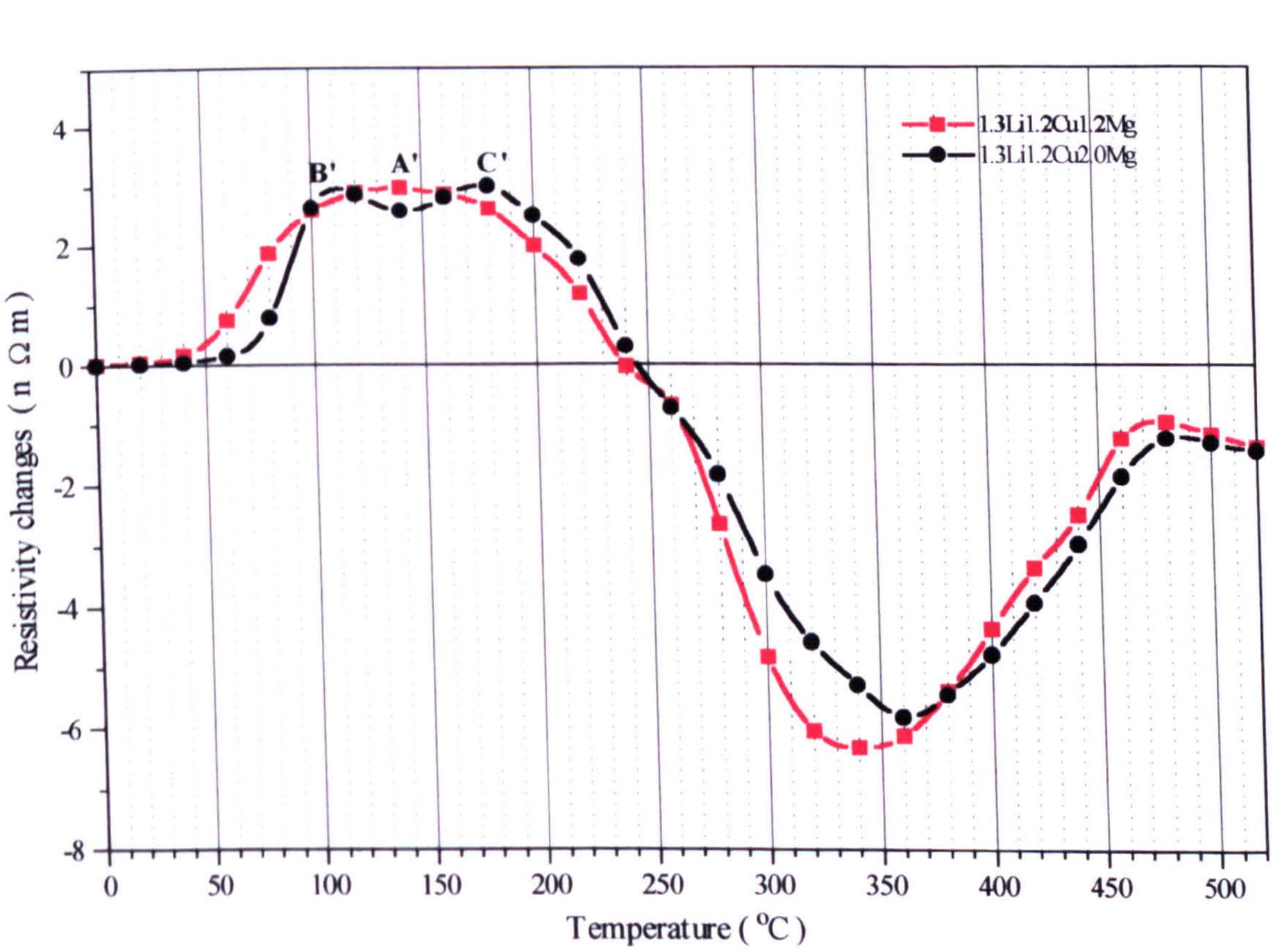

Figure 11.23: Comparative isochronal resistivity plots of 1.3Li1.2Cu1.2Mg and 1.3Li1.2Cu2.0Mg alloys.

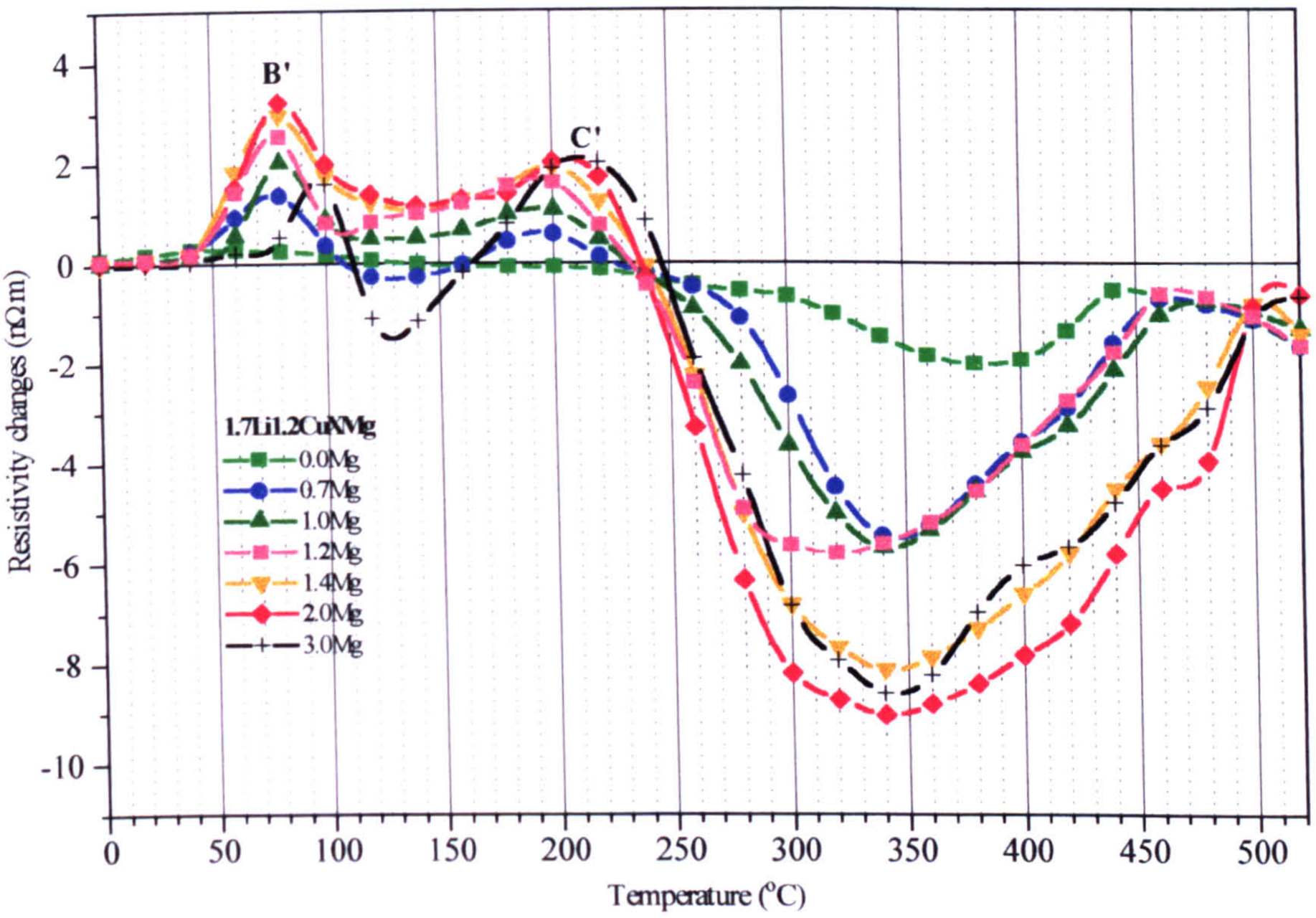

Figure 11.24: Comparative isochronal resistivity plots of 1.7Li1.2CuXMg alloys.

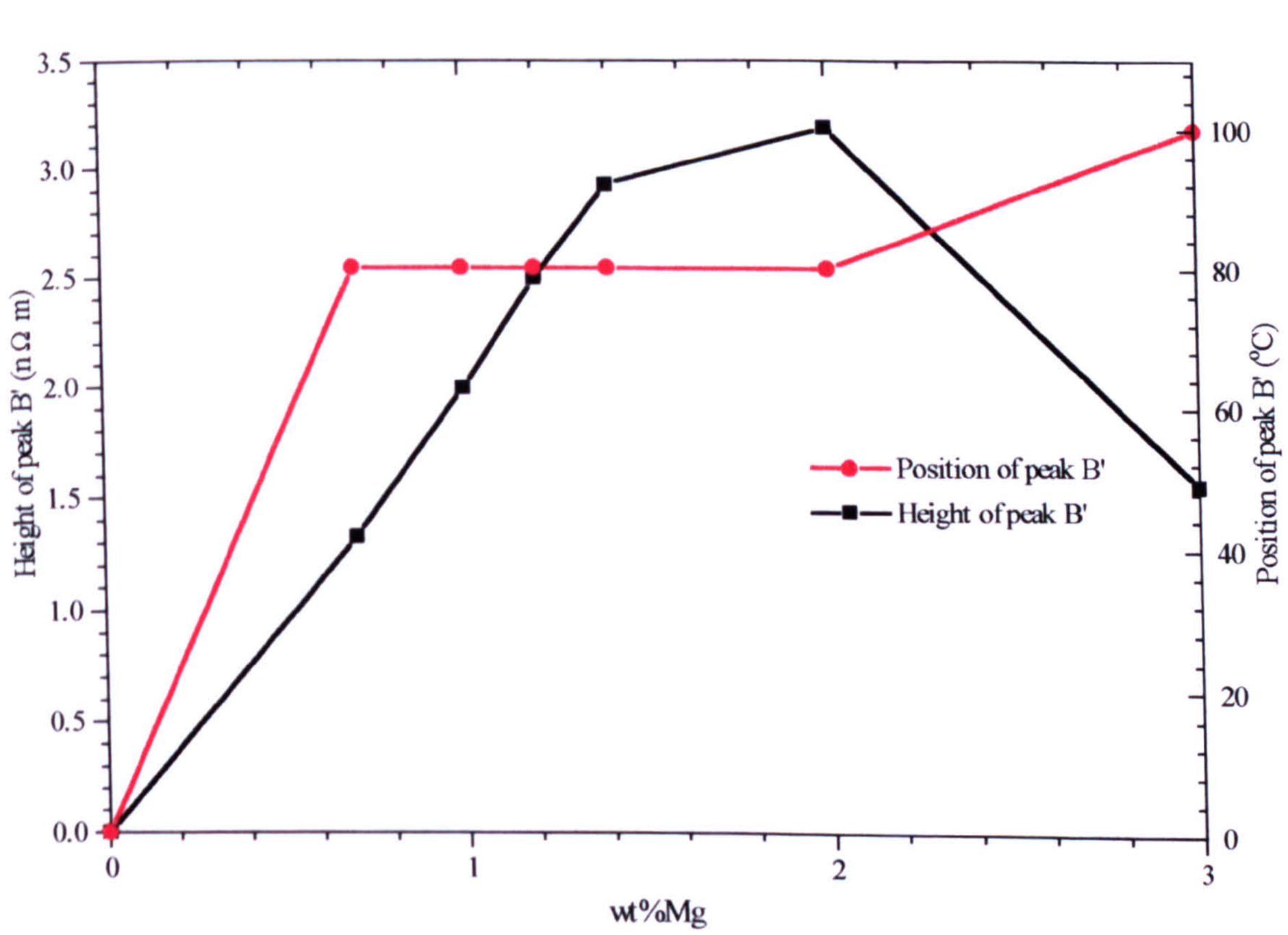

Figure 11.25: Height and position of isochronal resistivity peak B′.

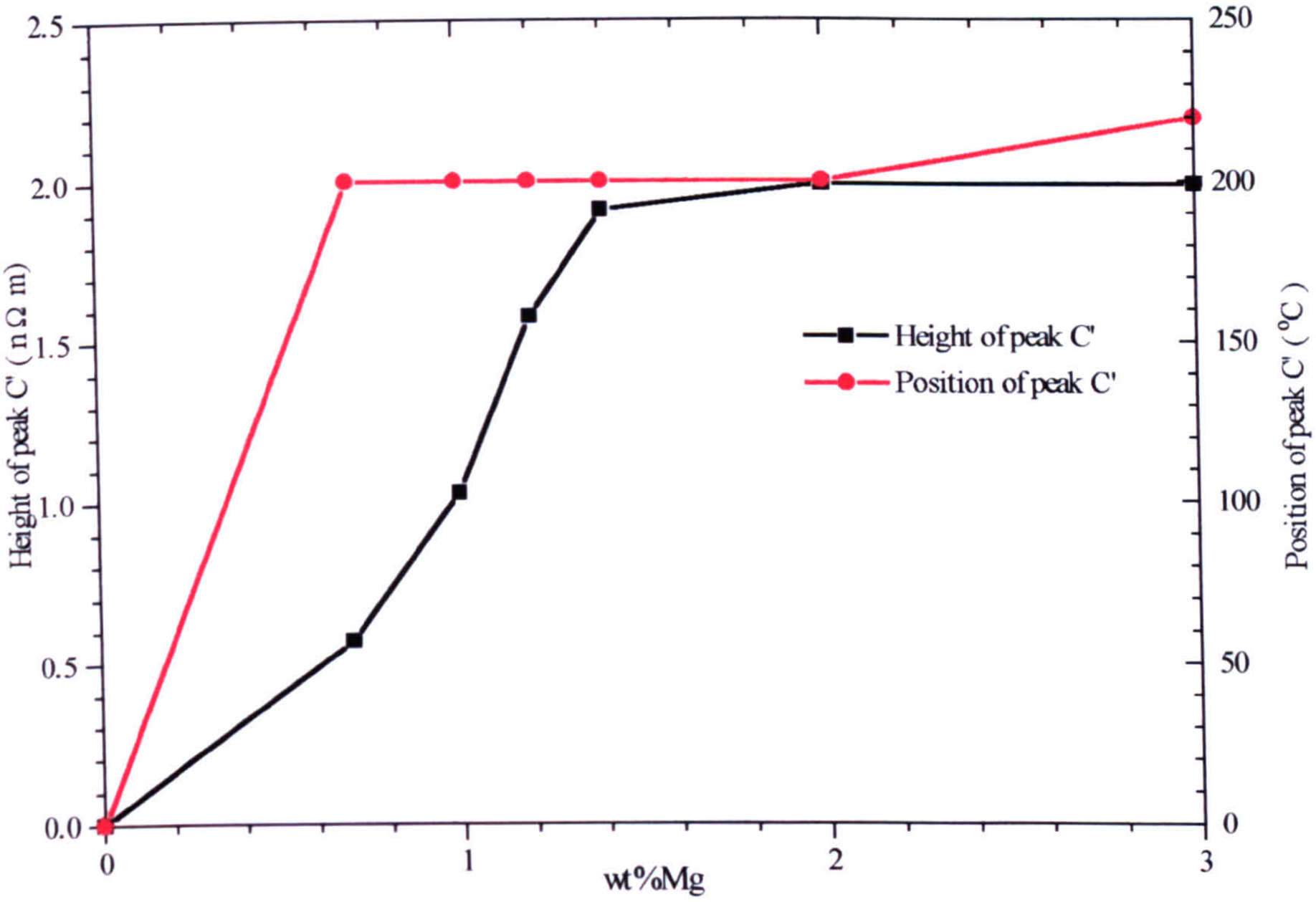

Figure 11.26: Height and position of isochronal resistivity peak C′.

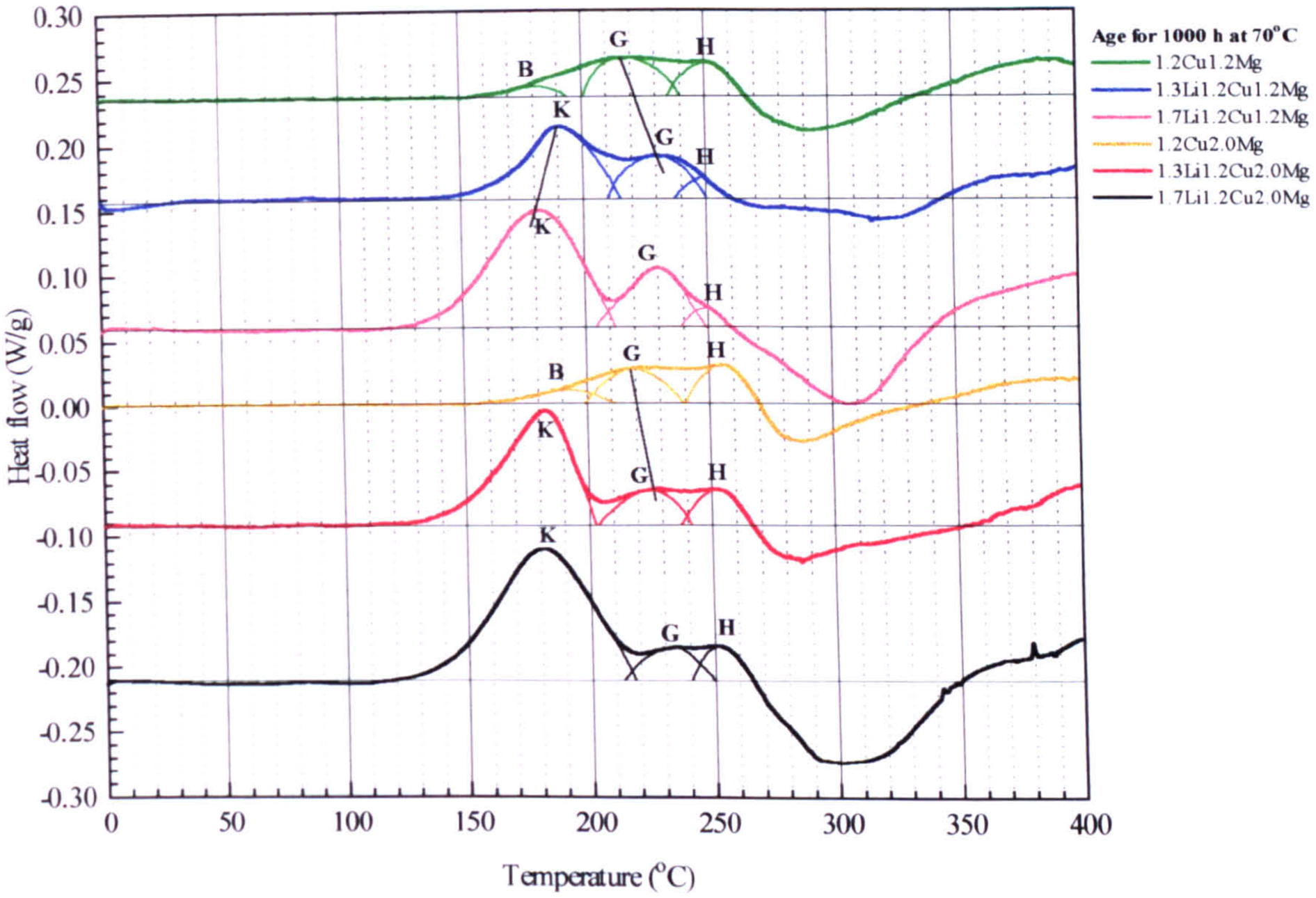

Figure 11.27: Comparative DSC plots of 1.2Cu1.2Mg and 1.2Cu2.0Mg alloys with lithium concentrations of 1.3 and 1.7% after ageing for 1000h at 70°C.

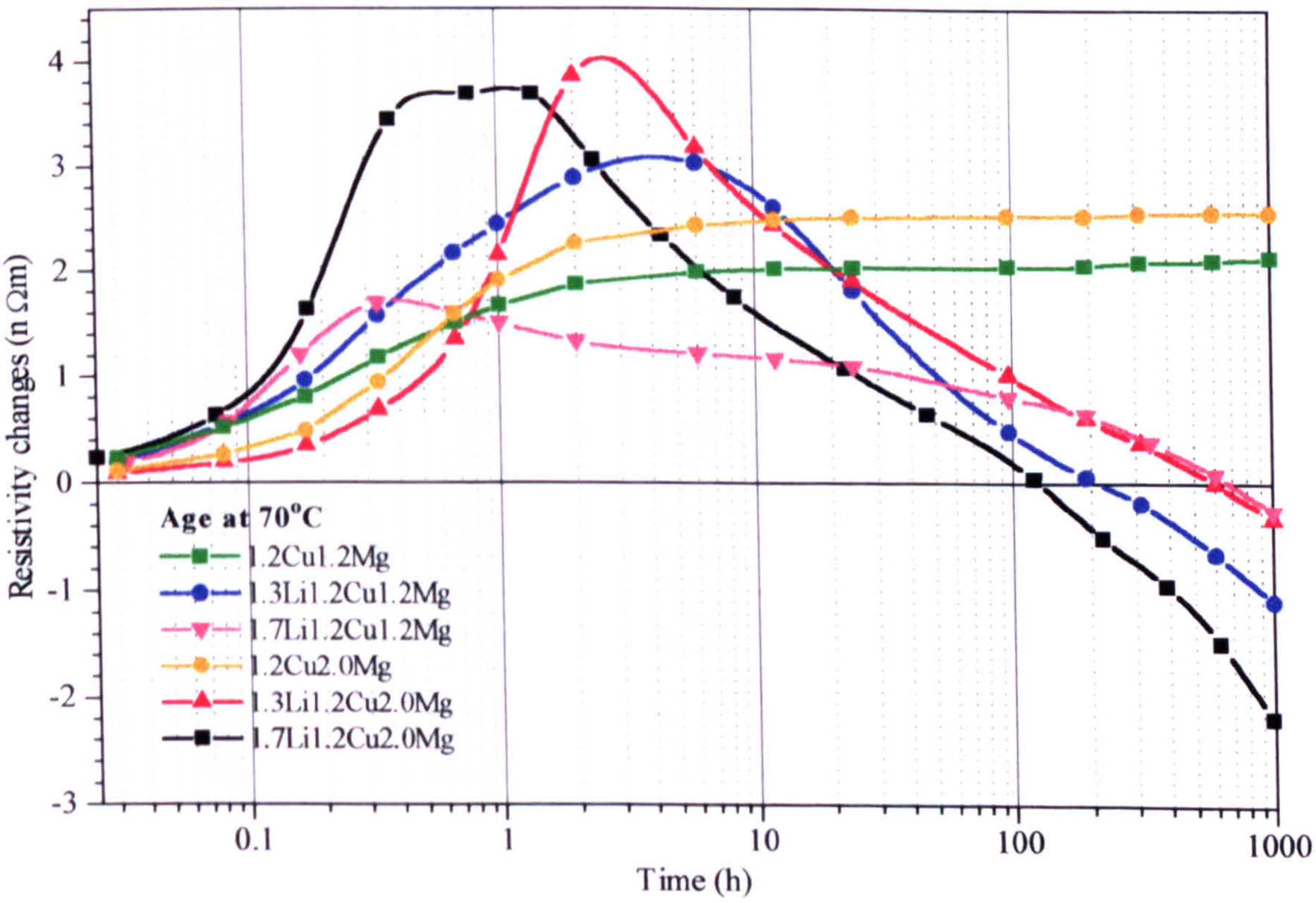

Figure 11.28 (a): Comparative isothermal resistivity plots of 1.2Cu1.2Mg and 1.2Cu2.0Mg alloys with lithium concentrations of 1.3% and 1.7% during ageing at 70°C.

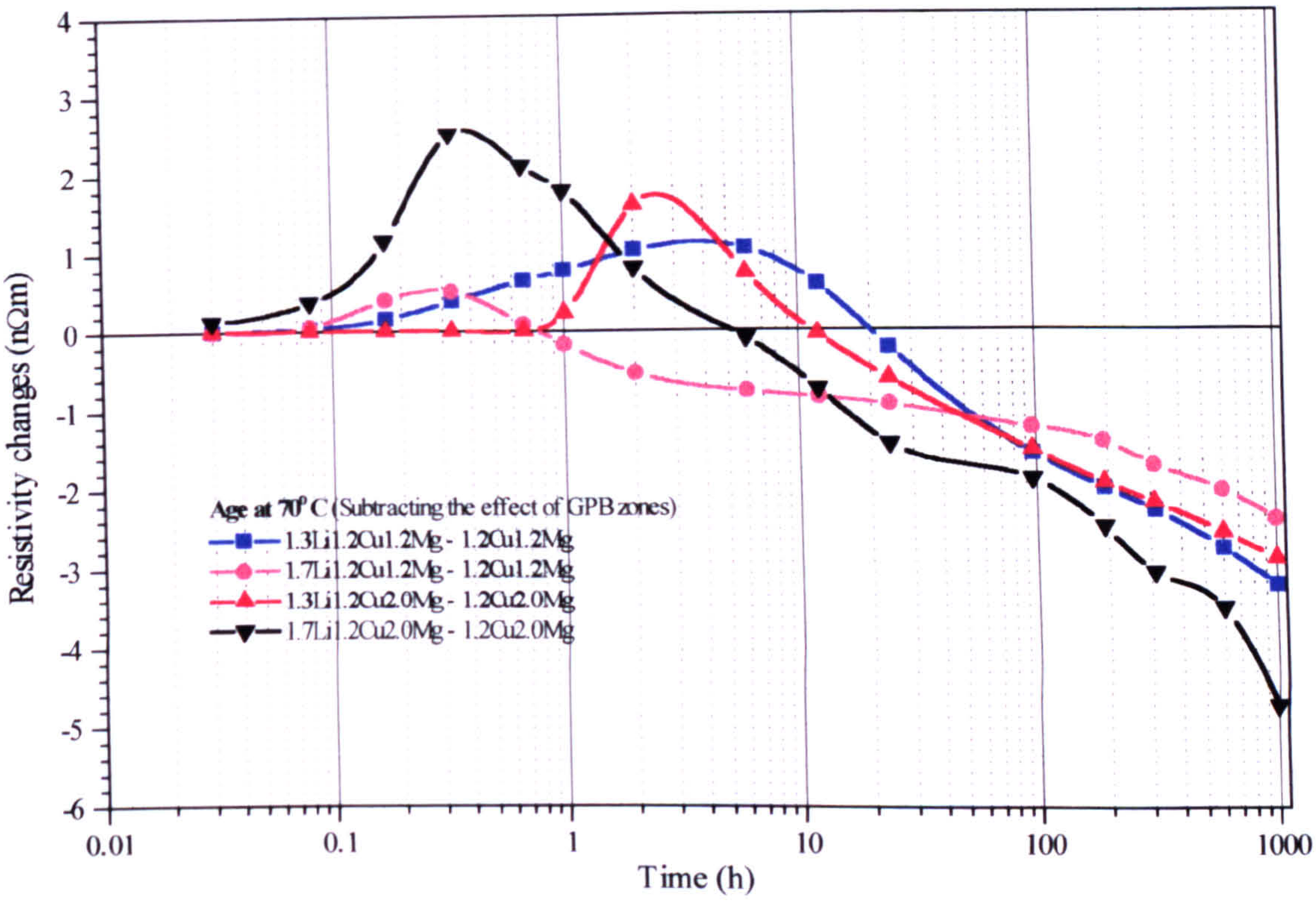

Figure 11.28 (b): Comparative isothermal resistivity plots of 1.2Cu1.2Mg and 1.2Cu2.0Mg alloys with lithium concentrations of 1.3% and 1.7% during ageing at 70°C after the subtraction of the effect of GPB zones.

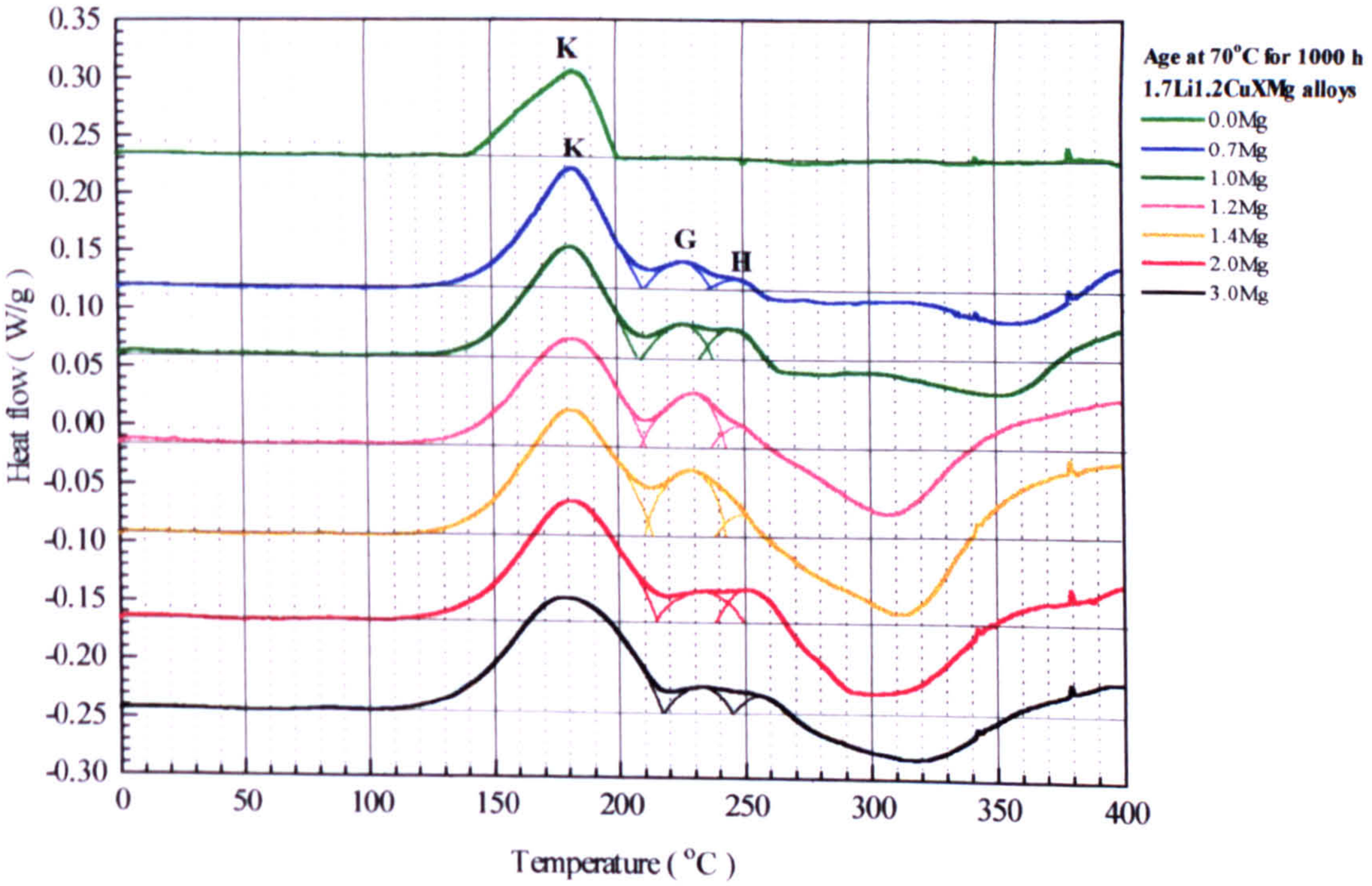

Figure 11.29: Comparative DSC plots of 1.7Li1.2CuXMg alloys after ageing for 1000 h at 70°C.

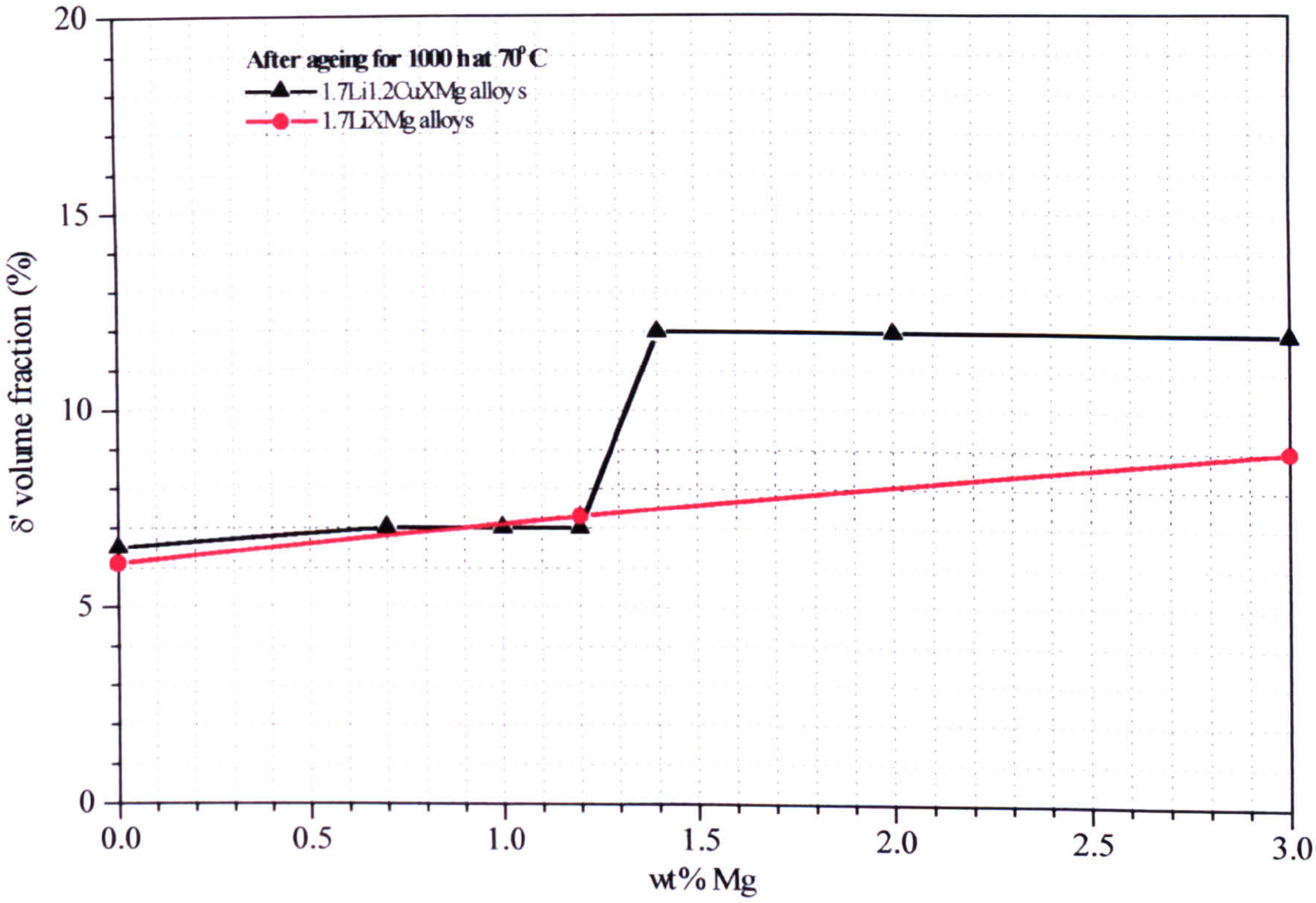

Figure 11.30: δ′ volume fraction produced in 1.7Li1.2CuXMg and 1.7LiXMg alloys after ageing for 1000 h at 70°C.

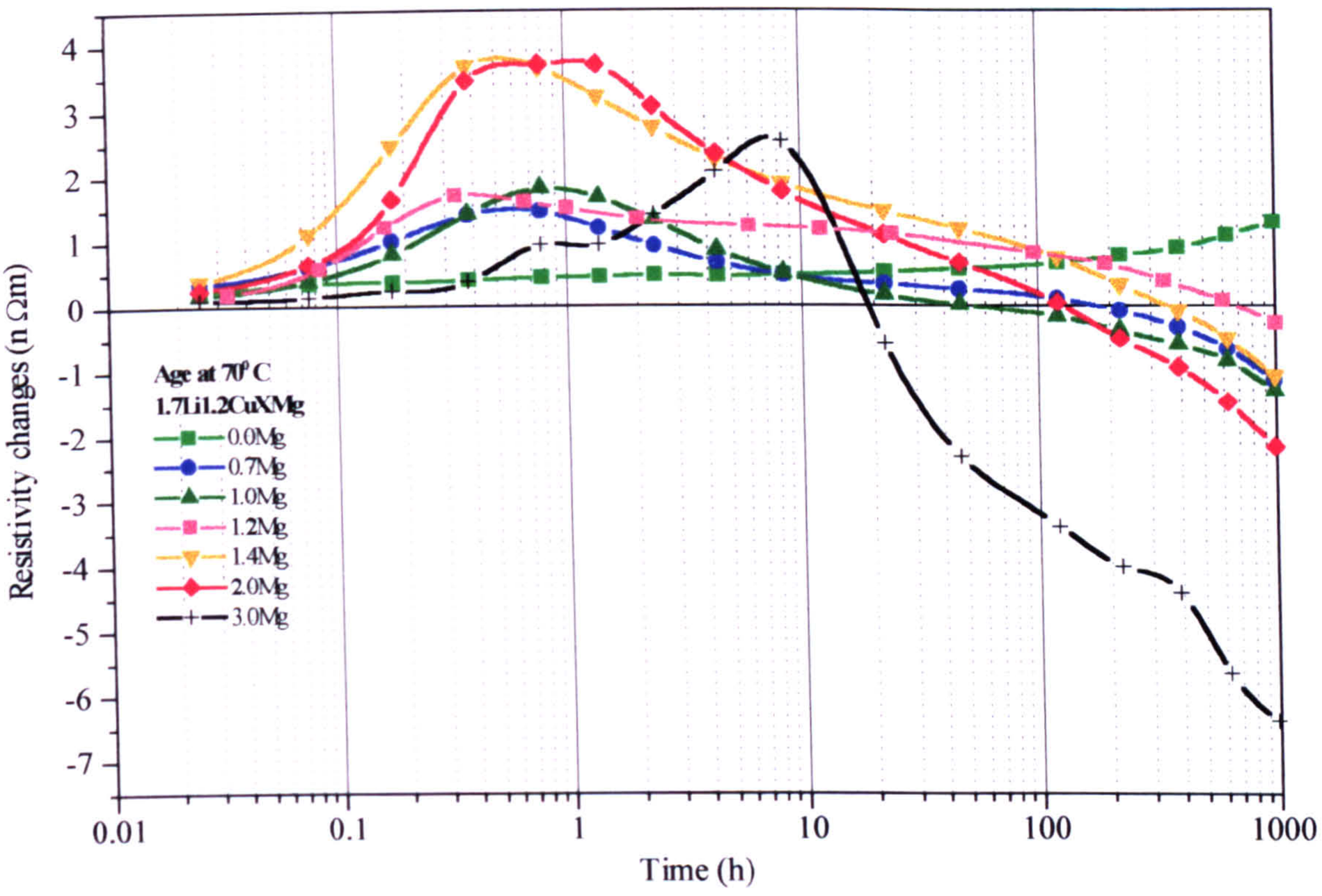

Figure 11.31 (a): Isothermal resistivity changes of 1.7Li1.2CuXMg alloys during ageing at 70°C.

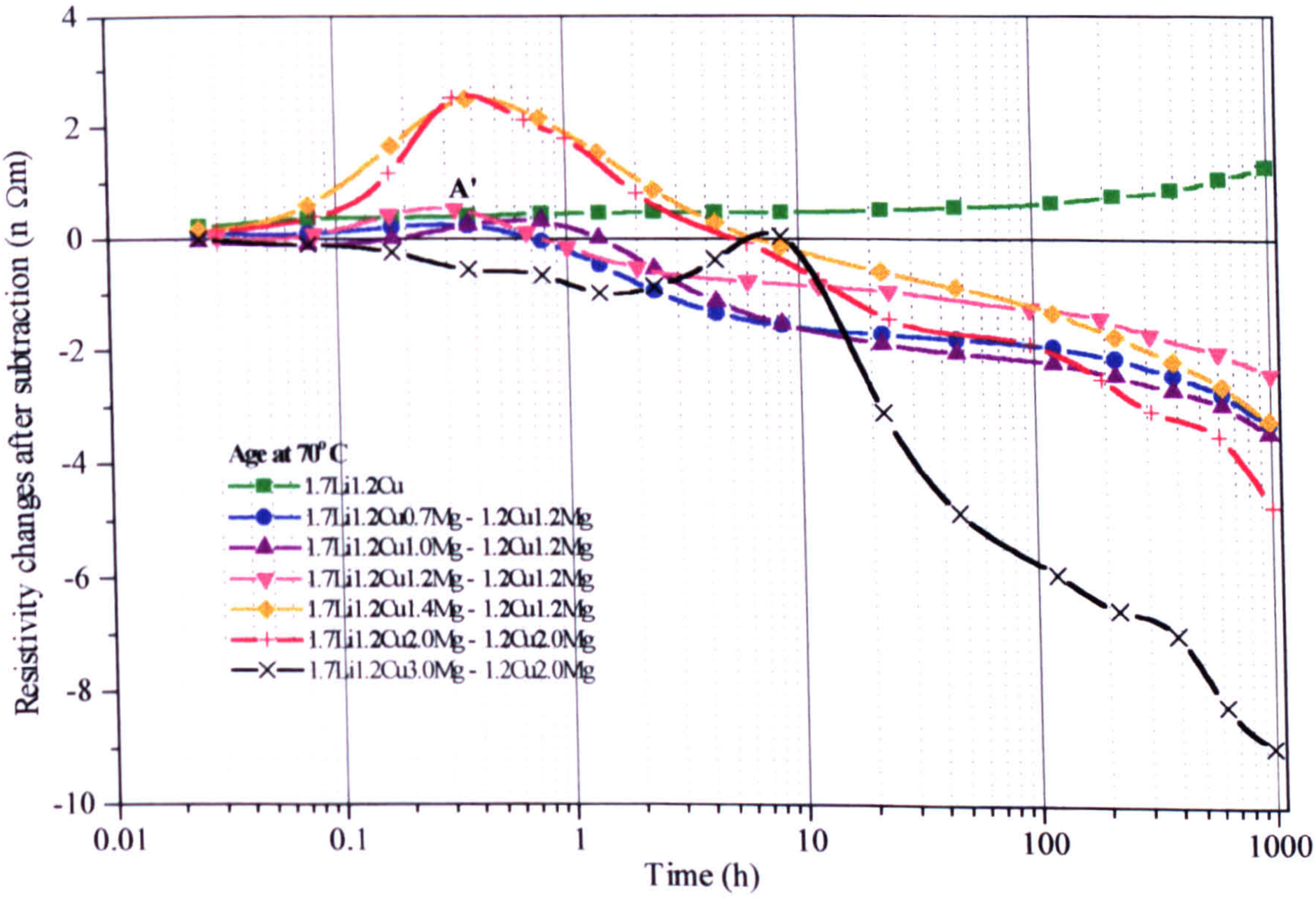

Figure 11.31 (b): Isothermal resistivity changes of 1.7Li1.2CuXMg alloys during ageing at 70 °C after the subtraction of GPB zones.

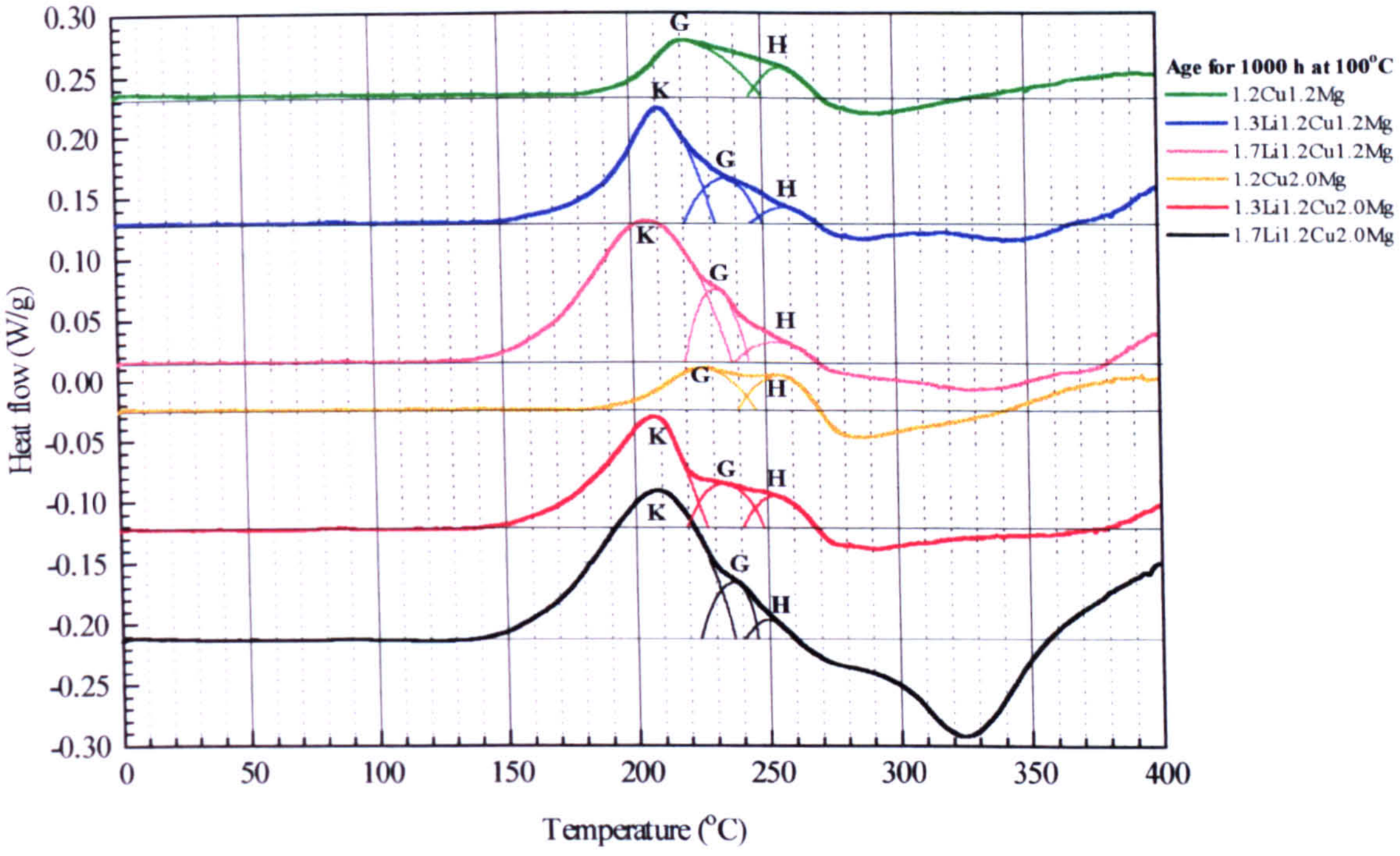

Figure 11.32: Comparative DSC plots of 1.2Cu1.2Mg and 1.2Cu2.0Mg alloys with lithium concentrations of 1.3 and 1.7% after ageing for 1000 h at 100°C.

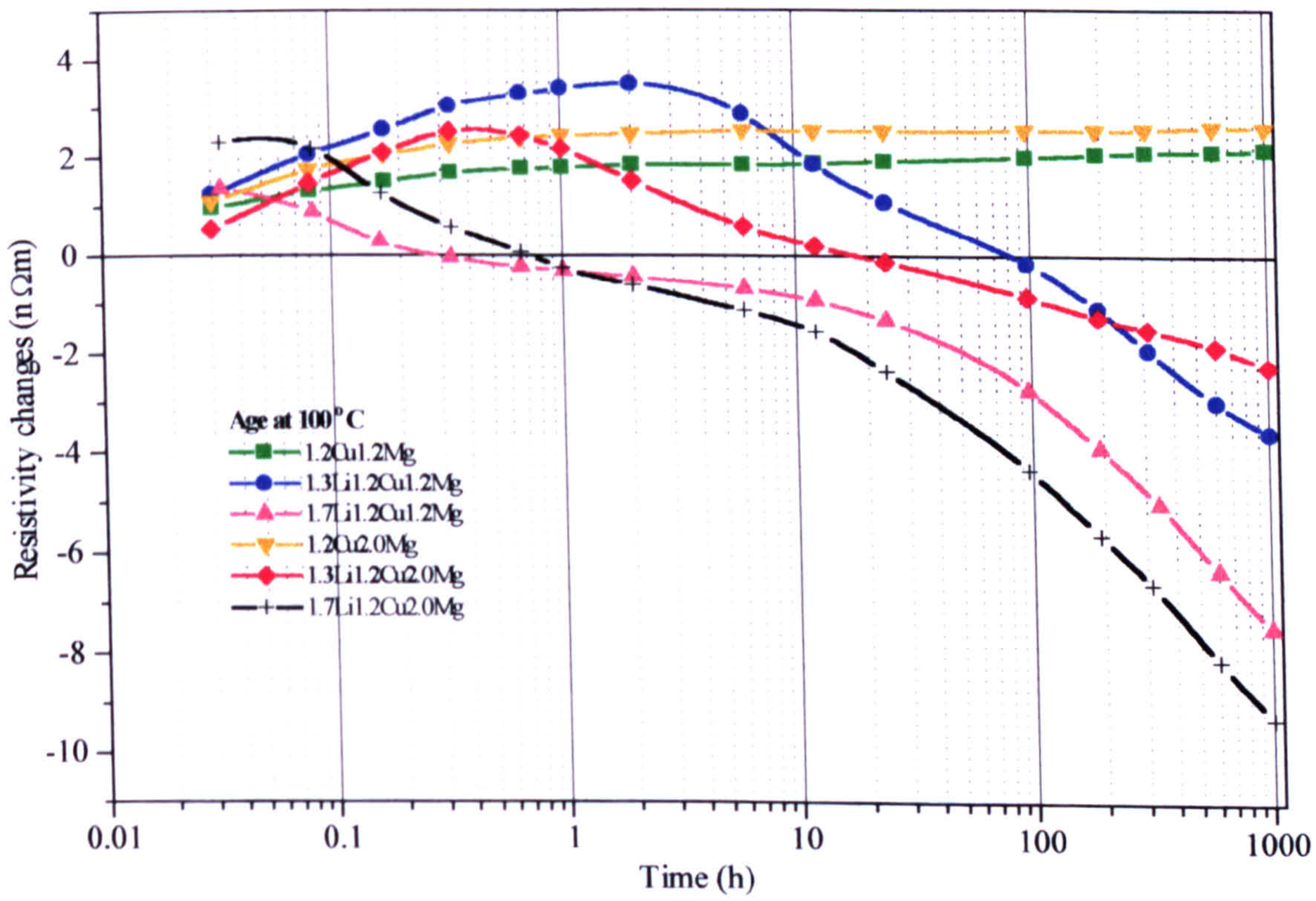

Figure 11.33 (a): Comparative isothermal resistivity plots of 1.2Cu1.2Mg and 1.2Cu2.0Mg alloys with lithium concentrations of 1.3% and 1.7% during ageing at 100°C.

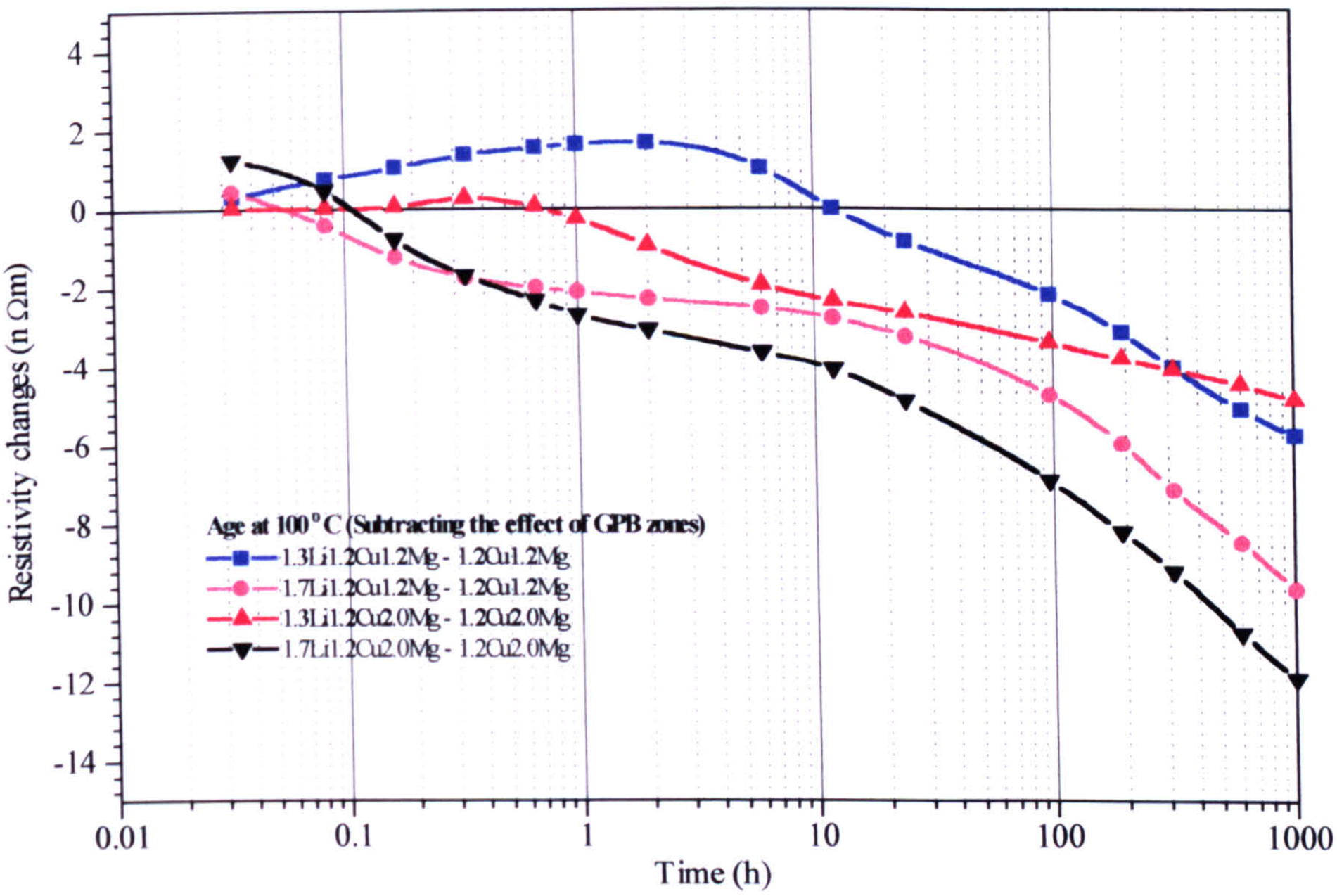

Figure 11.33 (b): Comparative isothermal resistivity plots of 1.2Cu1.2Mg and 1.2Cu2.0Mg alloys with lithium concentrations of 1.3% and 1.7% during ageing at 100°C after the subtraction of the effect of GPB zones.

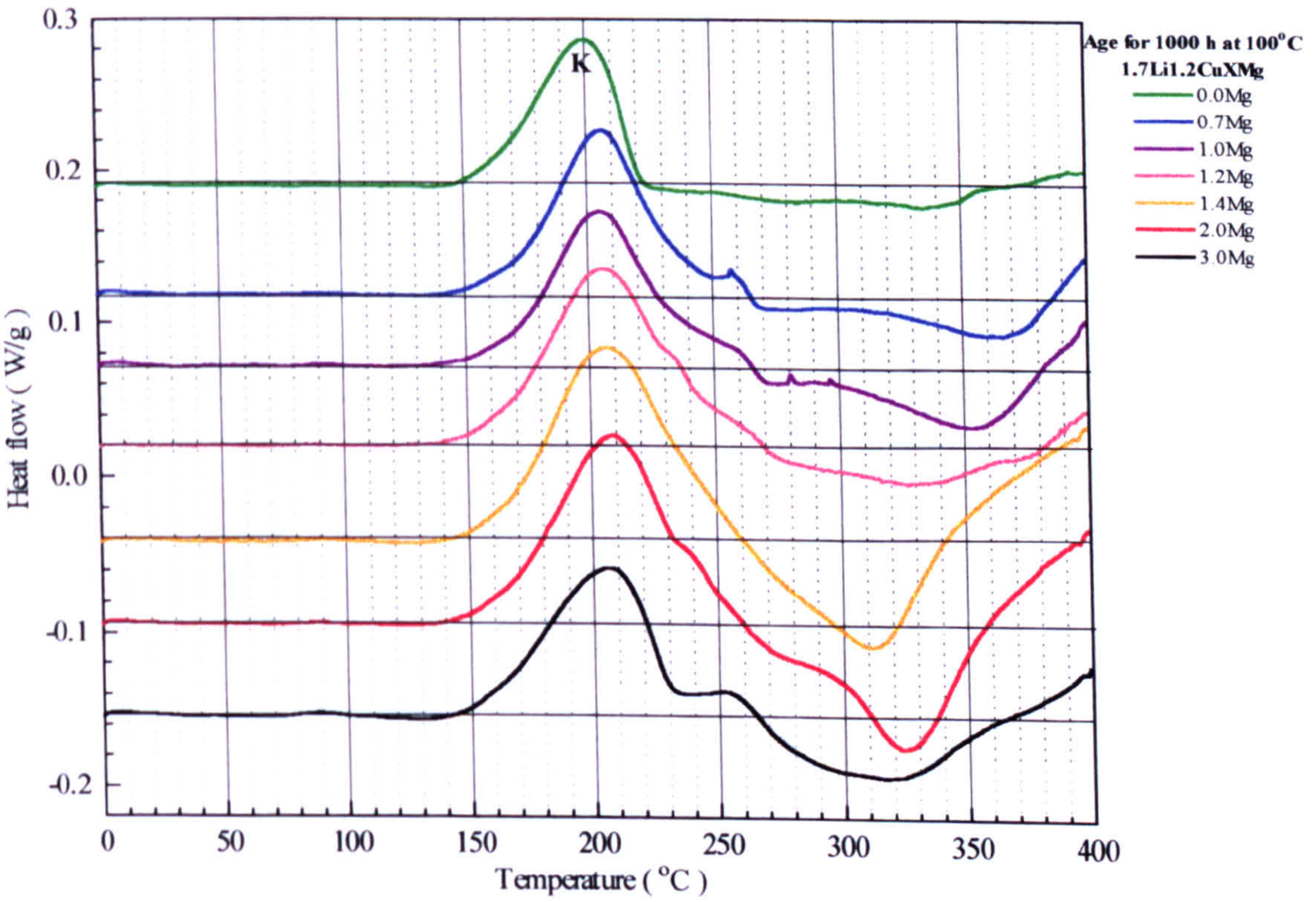

Figure 11.34: Comparative DSC plots of 1.7Li1.2CuXMg alloys after ageing for 1000 h at 100°C.

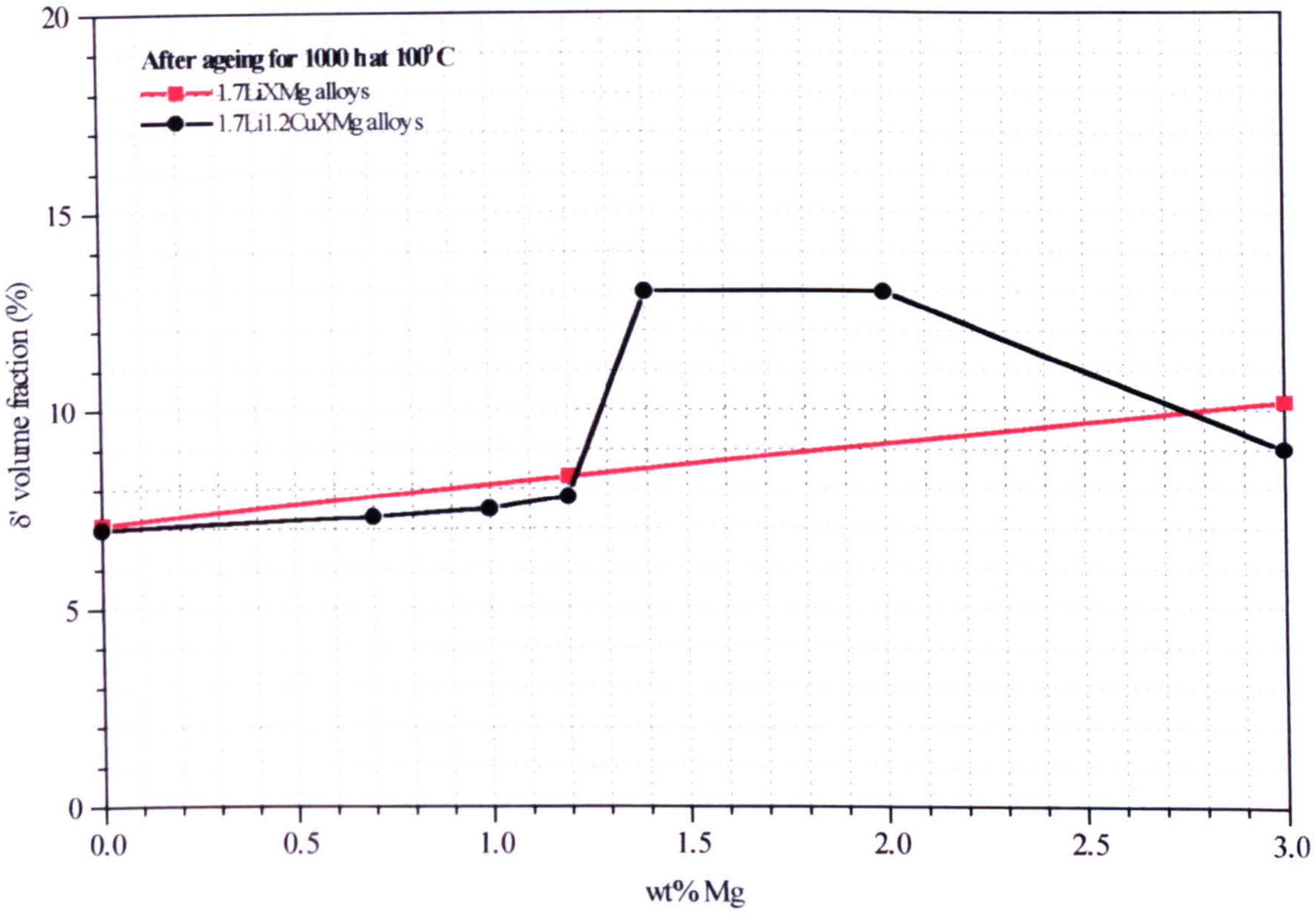

Figure 11.35: δ′ volume fraction produced in 1.7Li1.2CuXMg and 1.7LiXMg alloys after ageing for 1000 h at 100°C.

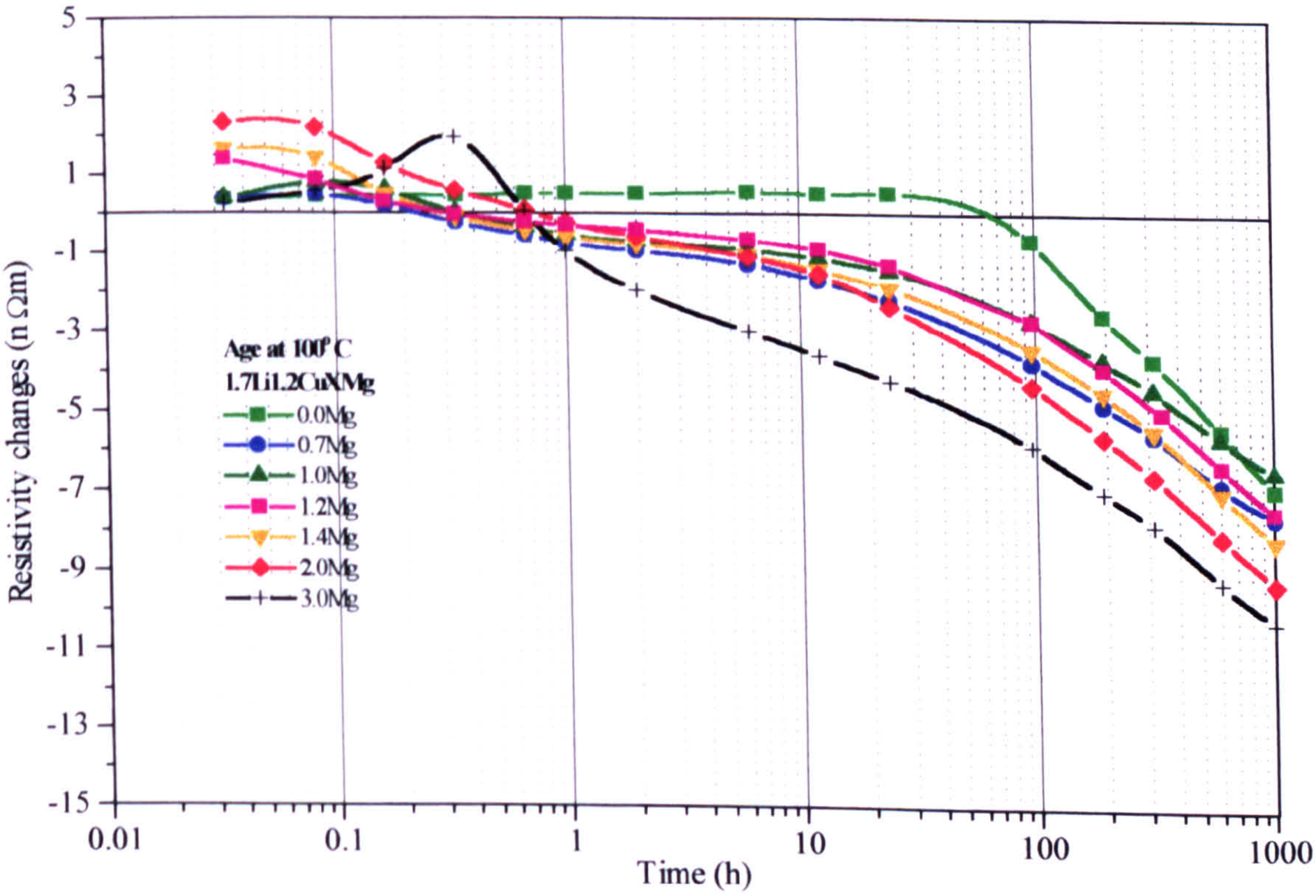

Figure 11.36 (a): Isothermal resistivity changes of 1.7Li1.2CuXMg alloys during ageing at 100°C.

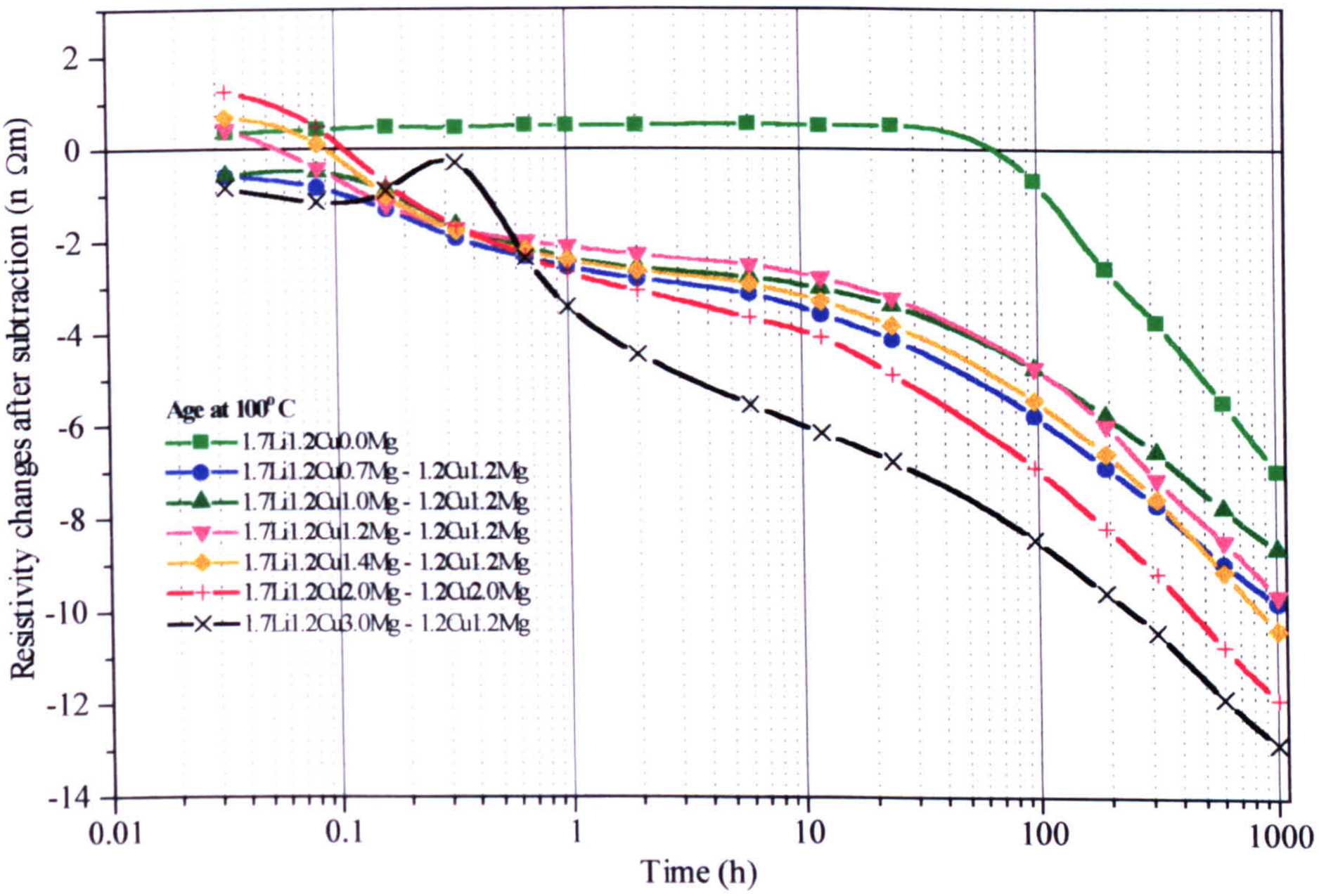

Figure 11.36 (b): Isothermal resistivity changes of 1.7Li1.2CuXMg alloys during ageing at 100 °C after the subtraction of GPB zones.

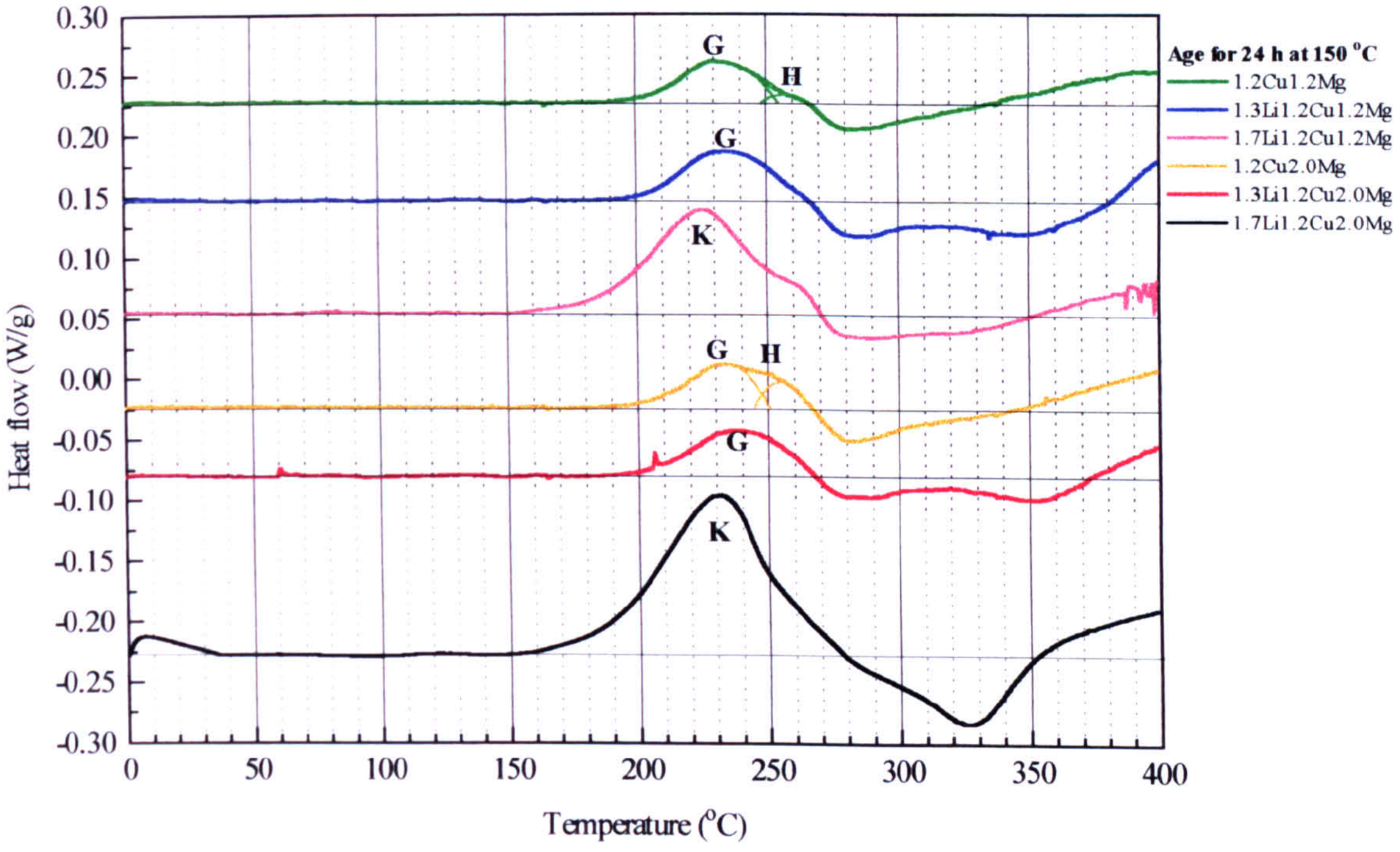

Figure 11.37: Comparative DSC plots of 1.2Cu1.2Mg and 1.2Cu2.0Mg alloys with lithium concentrations of 1.3 and 1.7% after ageing for 24h at 150°C.

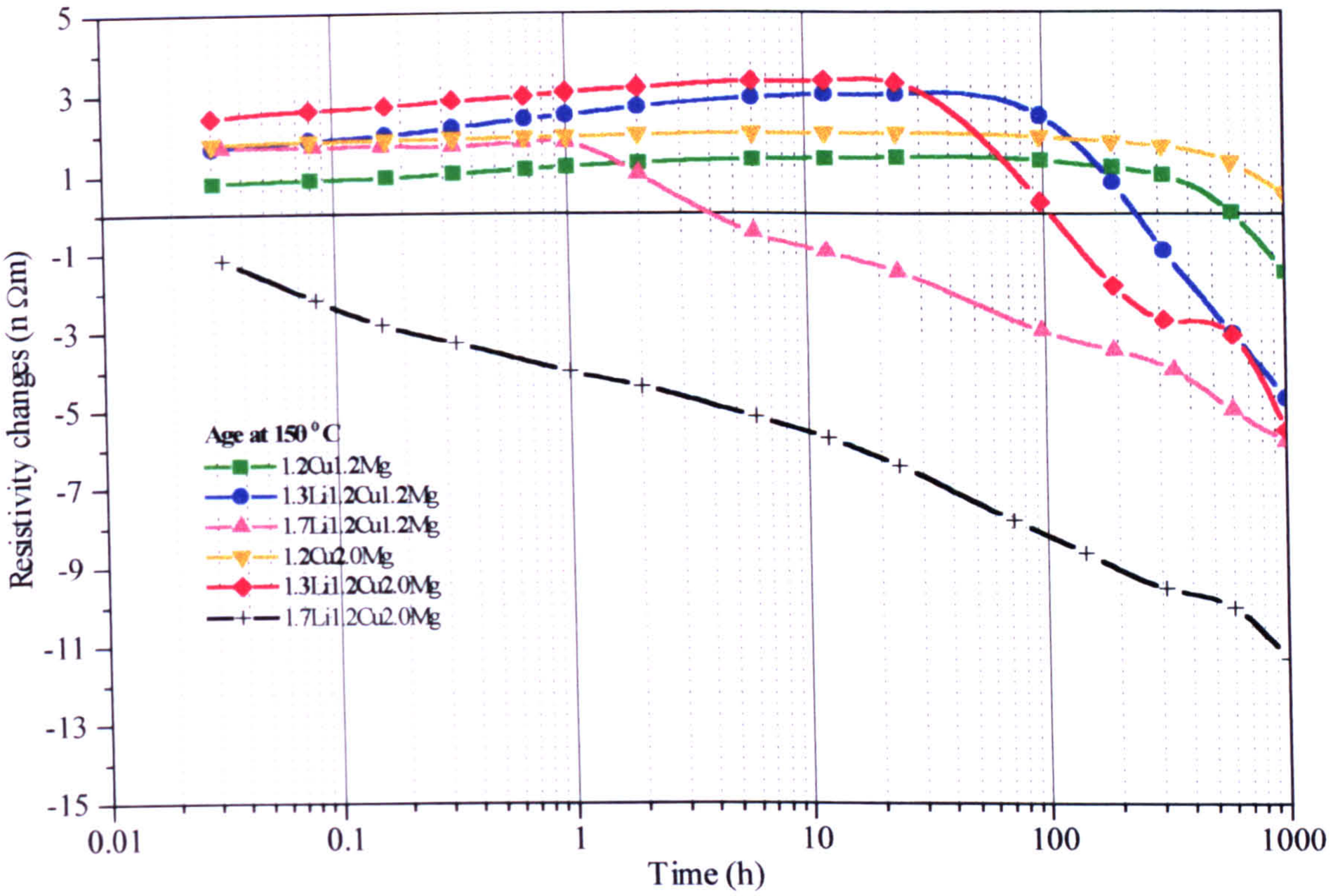

Figure 11.38 (a): Comparative isothermal resistivity plots of 1.2Cu1.2Mg and 1.2Cu2.0Mg alloys with lithium concentrations of 1.3% and 1.7% during ageing at 150°C.

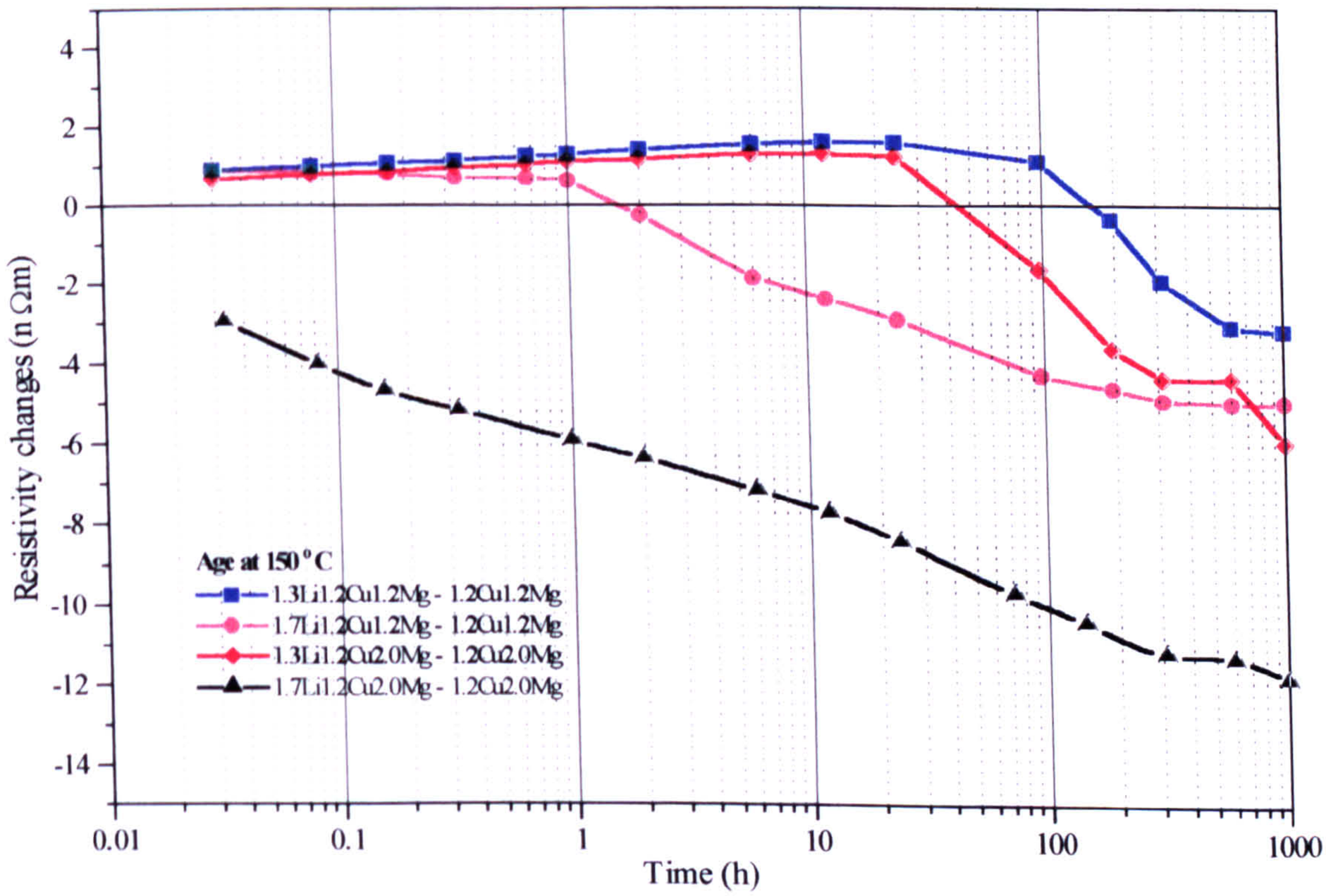

Figure 11.38 (b): Comparative isothermal resistivity plots of 1.2Cu1.2Mg and 1.2Cu2.0Mg alloys with lithium concentrations of 1.3% and 1.7% during ageing at 150°C after the subtraction of the effect of GPB zones.

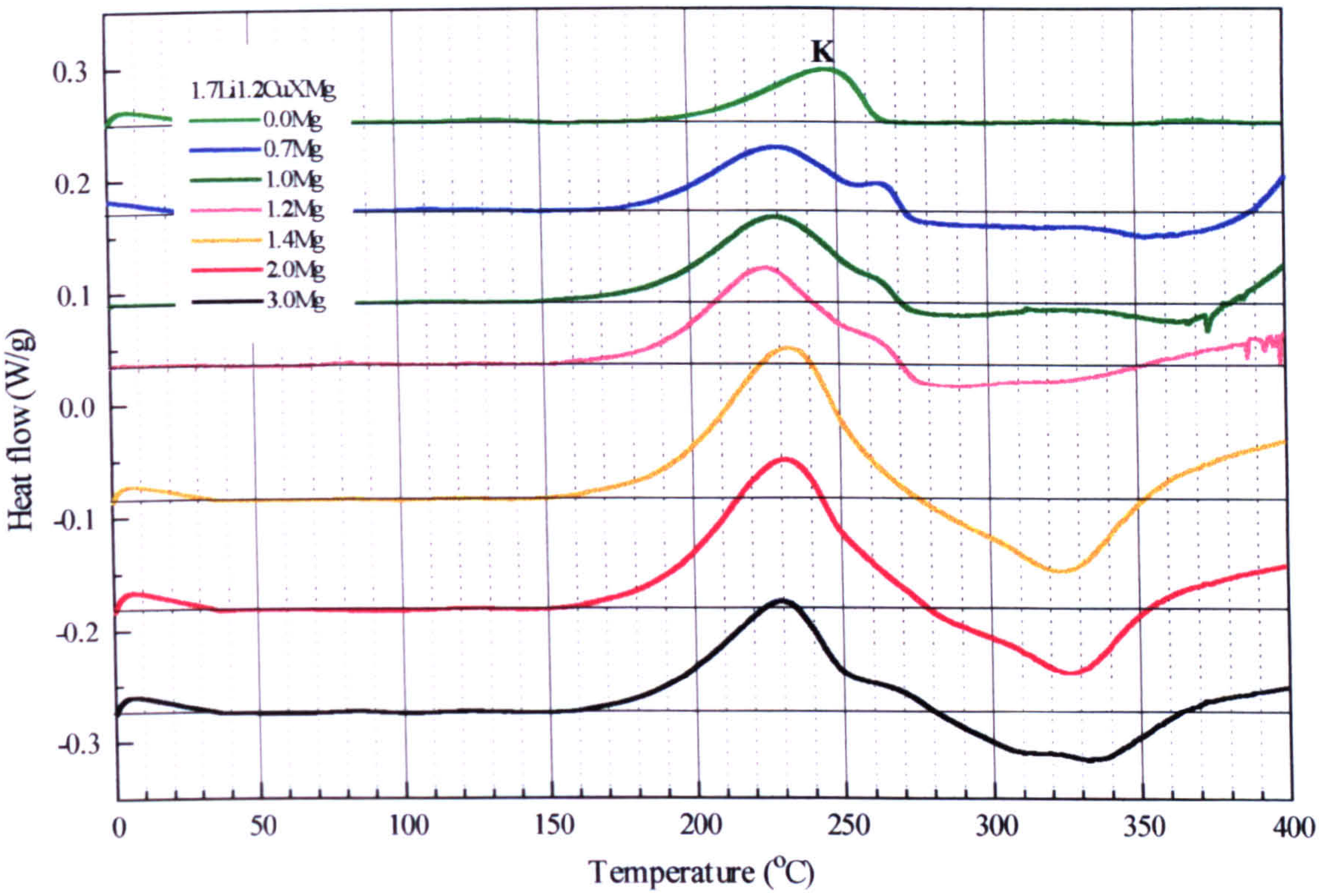

Figure 11.39: Comparative DSC plots of 1.7Li1.2CuXMg alloys after ageing for 24 h at 150°C.

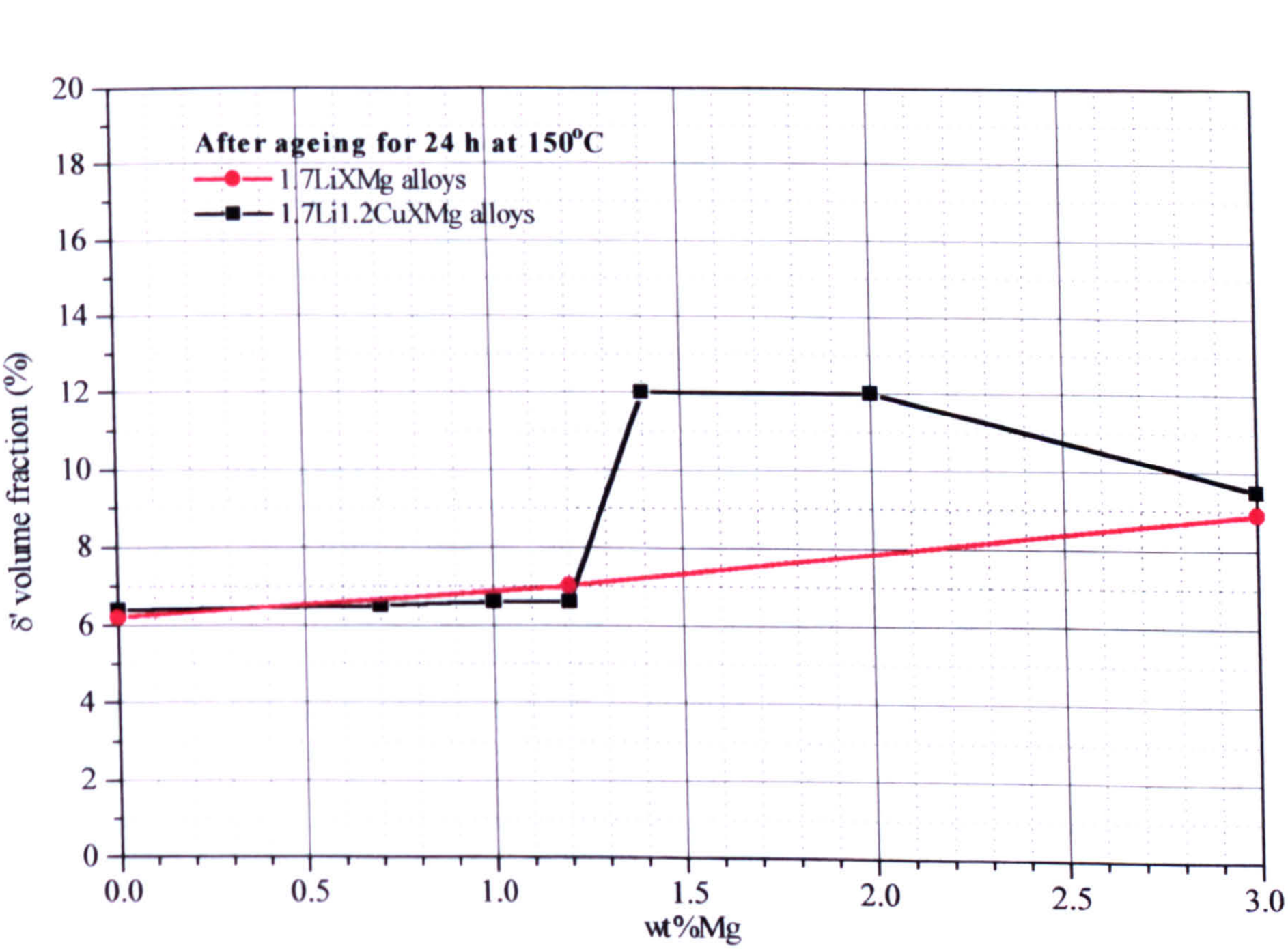

Figure 11.40: δ′ volume fraction produced in 1.7Li1.2CuXMg and 1.7LiXMg alloys after ageing for 24 h at 150°C.

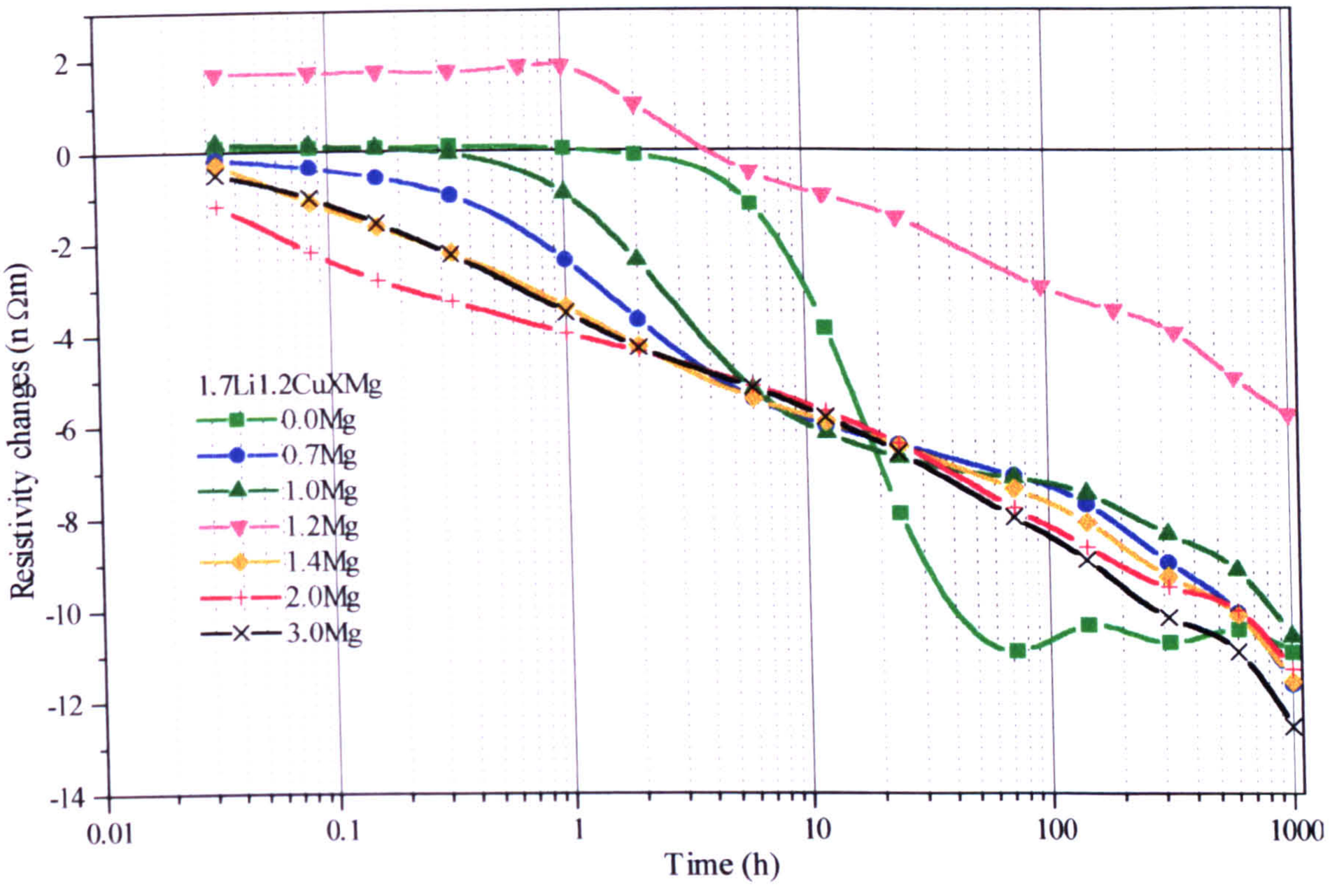

Figure 11.41 (a): Isothermal resistivity changes of 1.7Li1.2CuXMg alloys during ageing at 150°C.

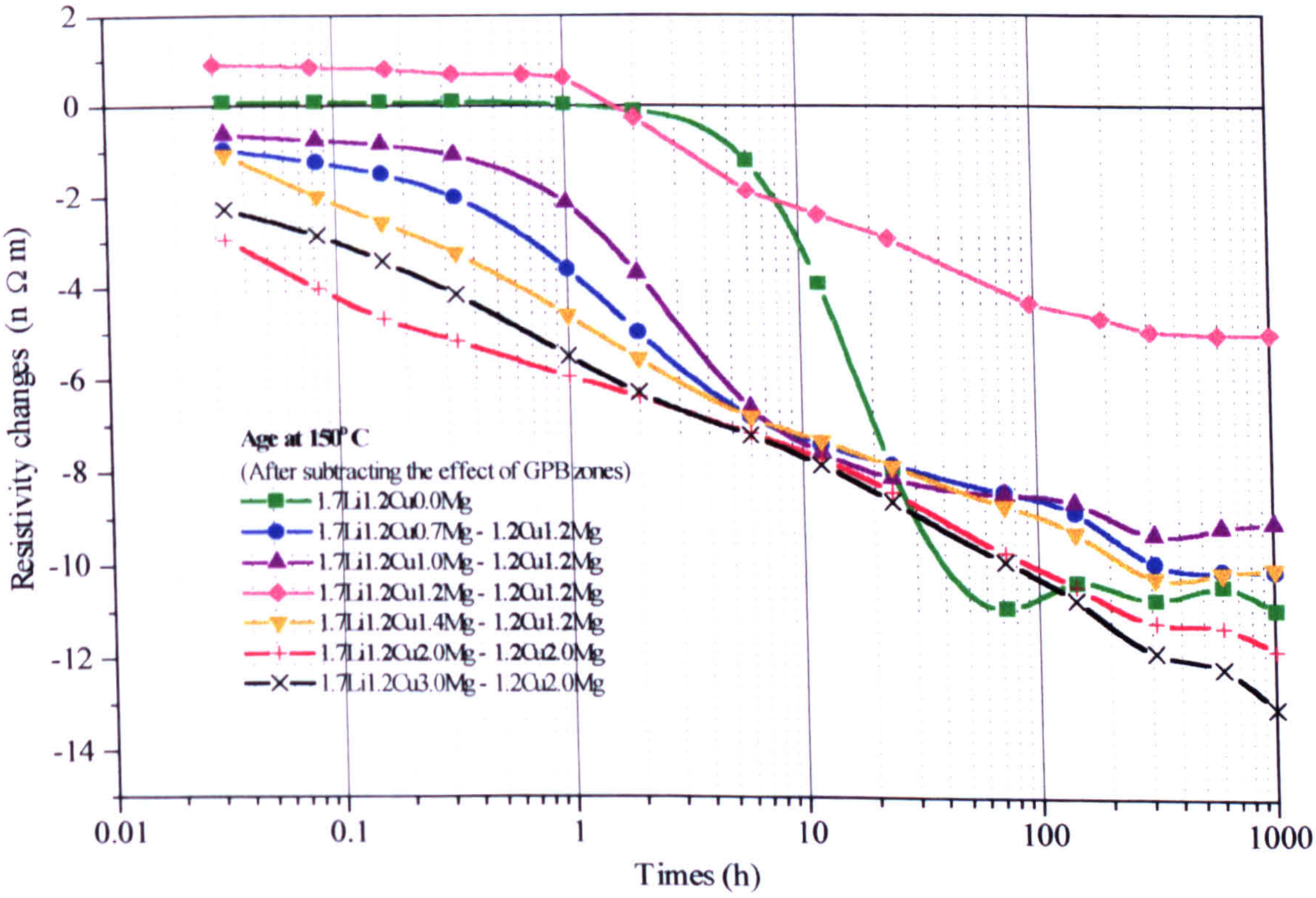

Figure 11.41 (b): Isothermal resistivity changes of 1.7Li1.2CuXMg alloys during ageing at 150 °C after the subtraction of GPB zones.

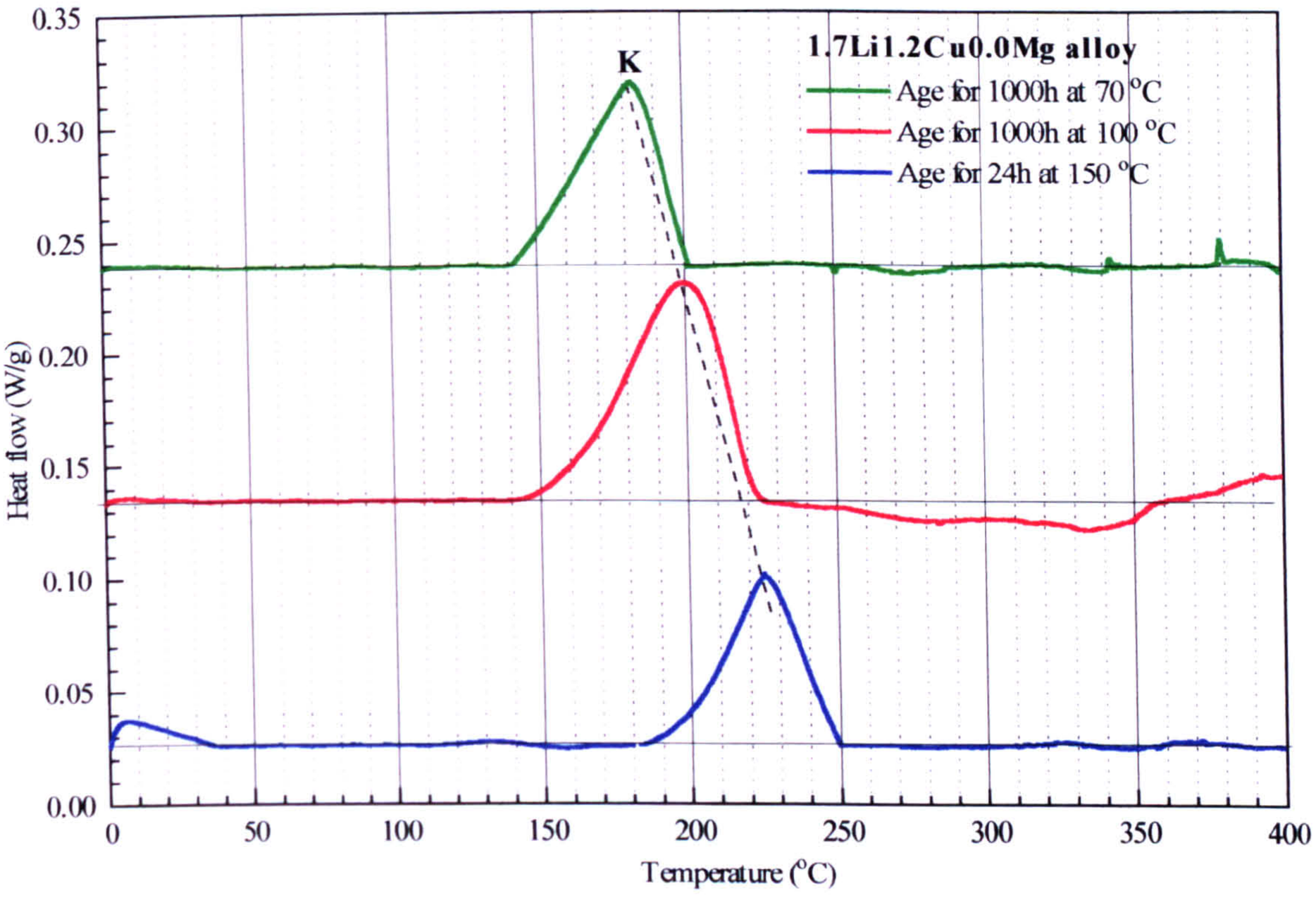

Figure 11.42: Effect of ageing temperature on the DSC thermogram of an 1.7Li1.2Cu0.0Mg alloy.

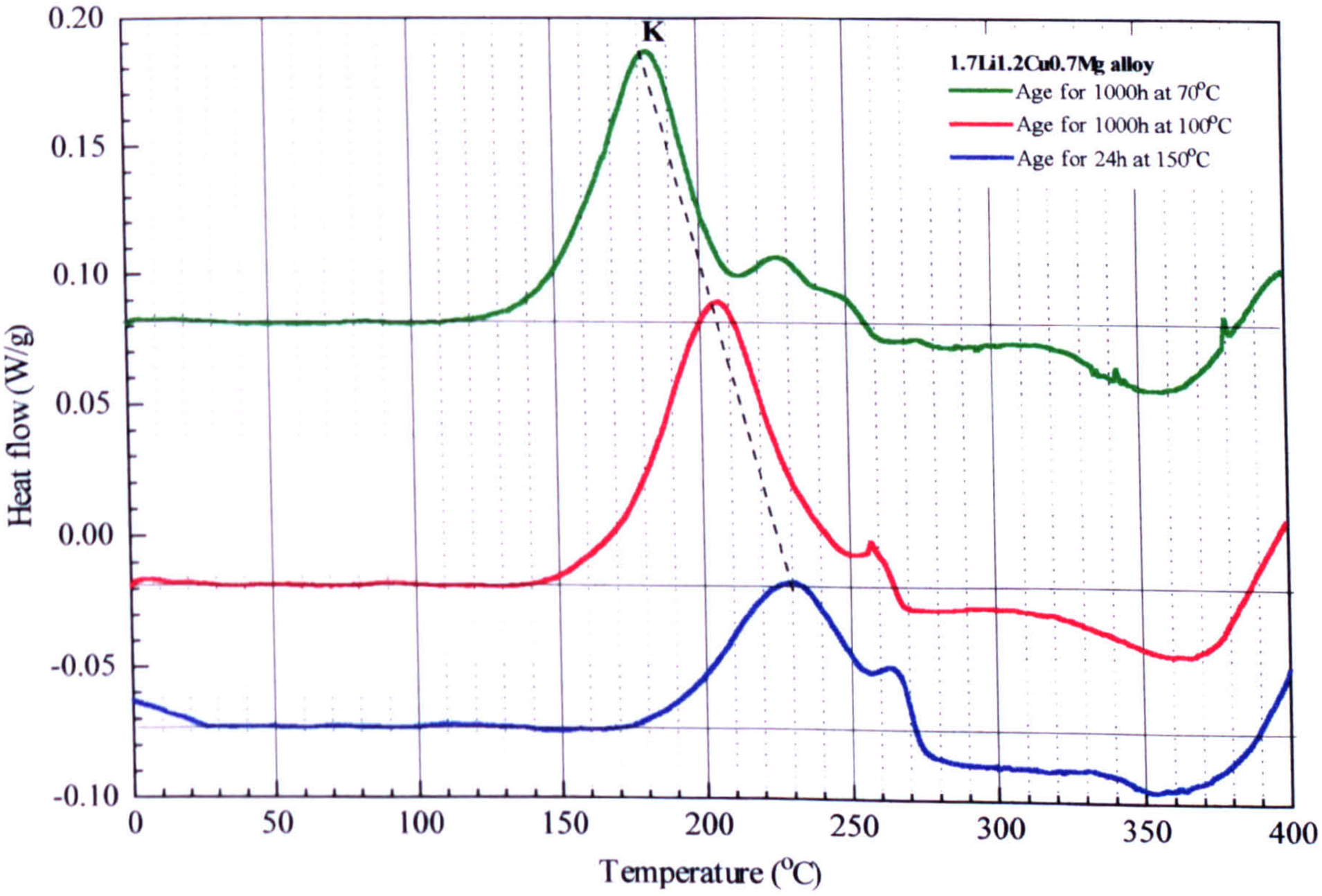

Figure 11.43: Effect of ageing temperature on the DSC thermogram of an 1.7Li1.2Cu0.7Mg alloy.

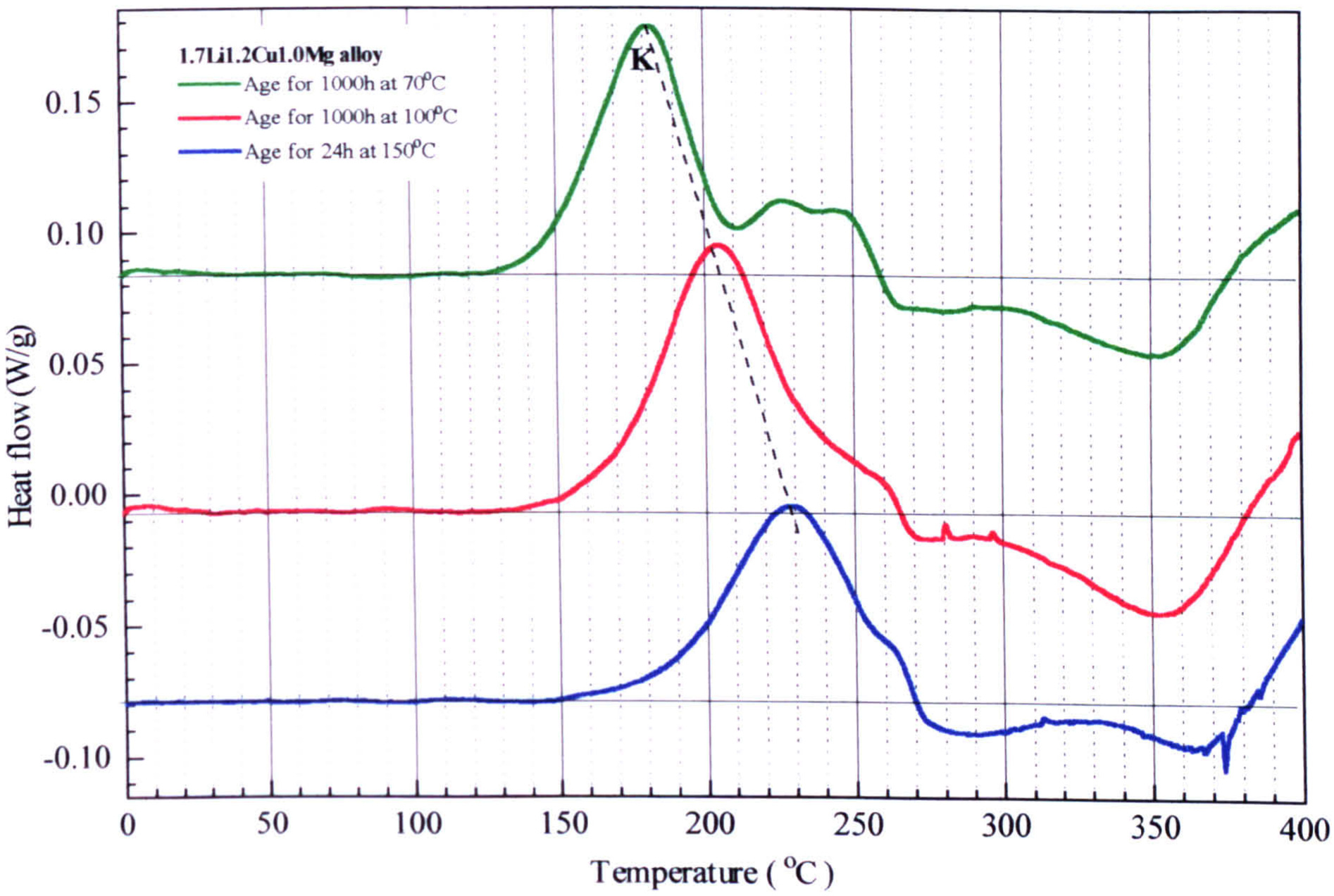

Figure 11.44: Effect of ageing temperature on the DSC thermogram of an 1.7Li1.2Cu1.0Mg alloy.

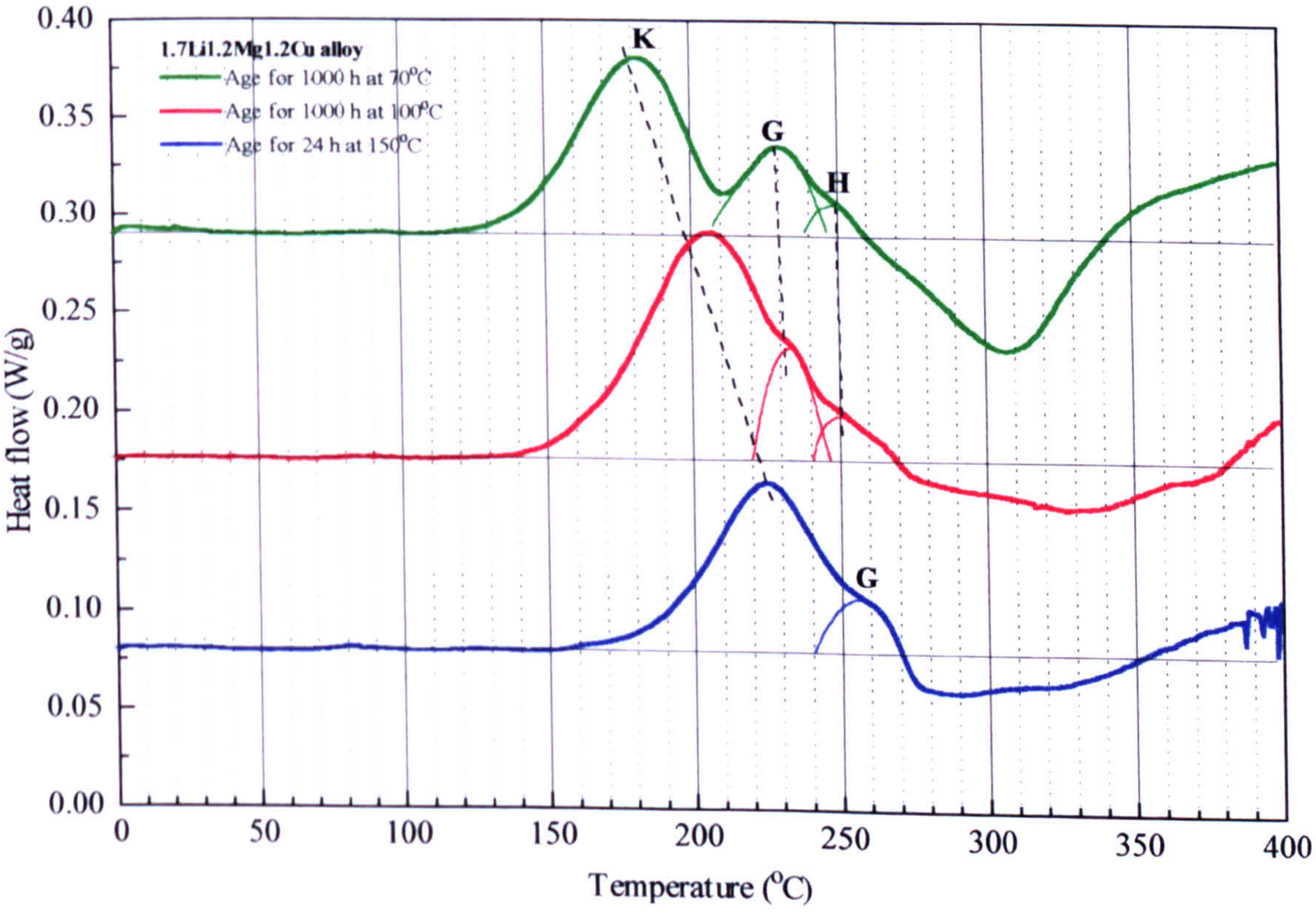

Figure 11.45: Effect of ageing temperature on the DSC thermogram of an 1.7Li1.2Cu1.2Mg alloy.

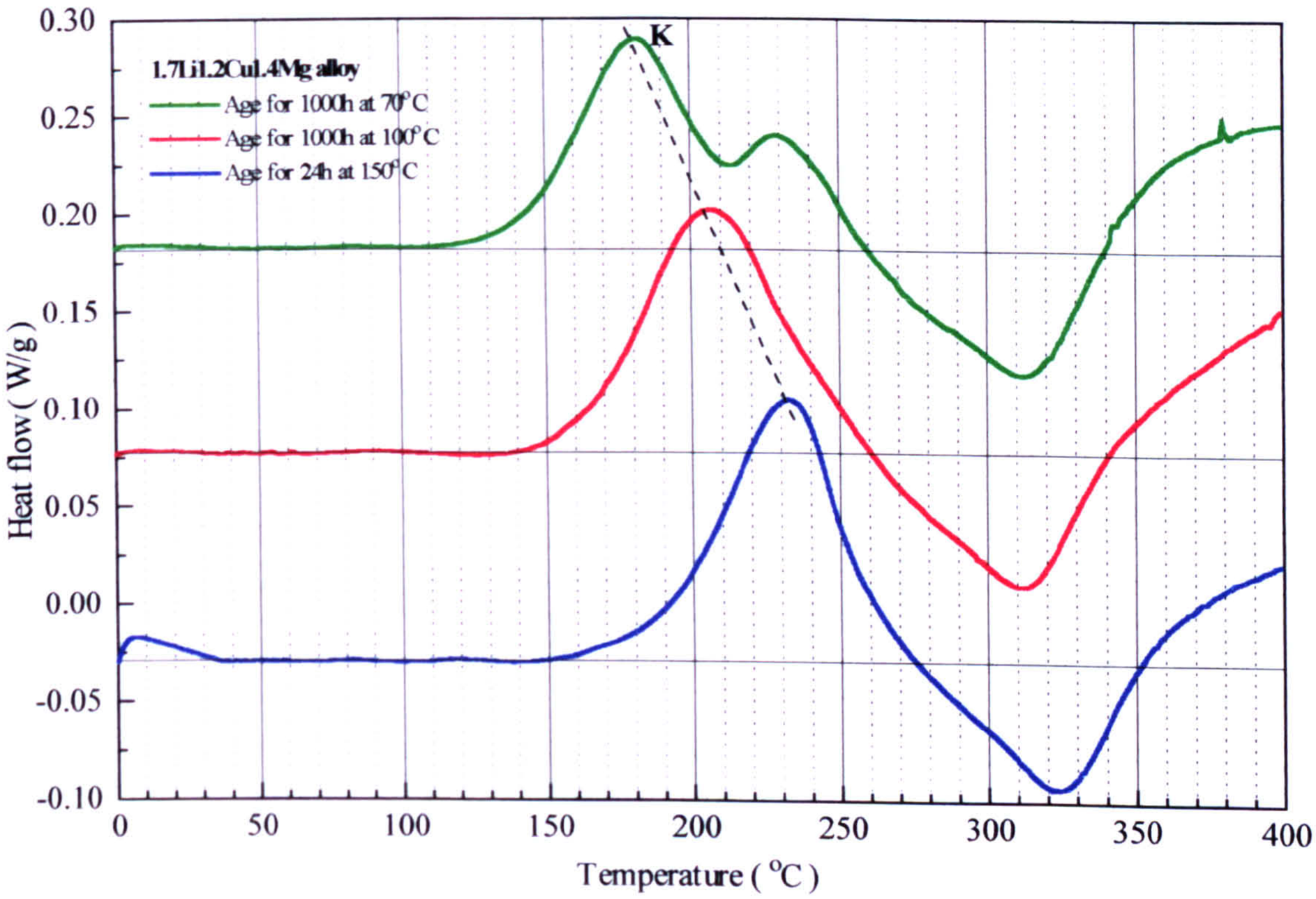

Figure 11.46: Effect of ageing temperature on the DSC thermogram of an 1.7Li1.2Cu1.4Mg alloy.

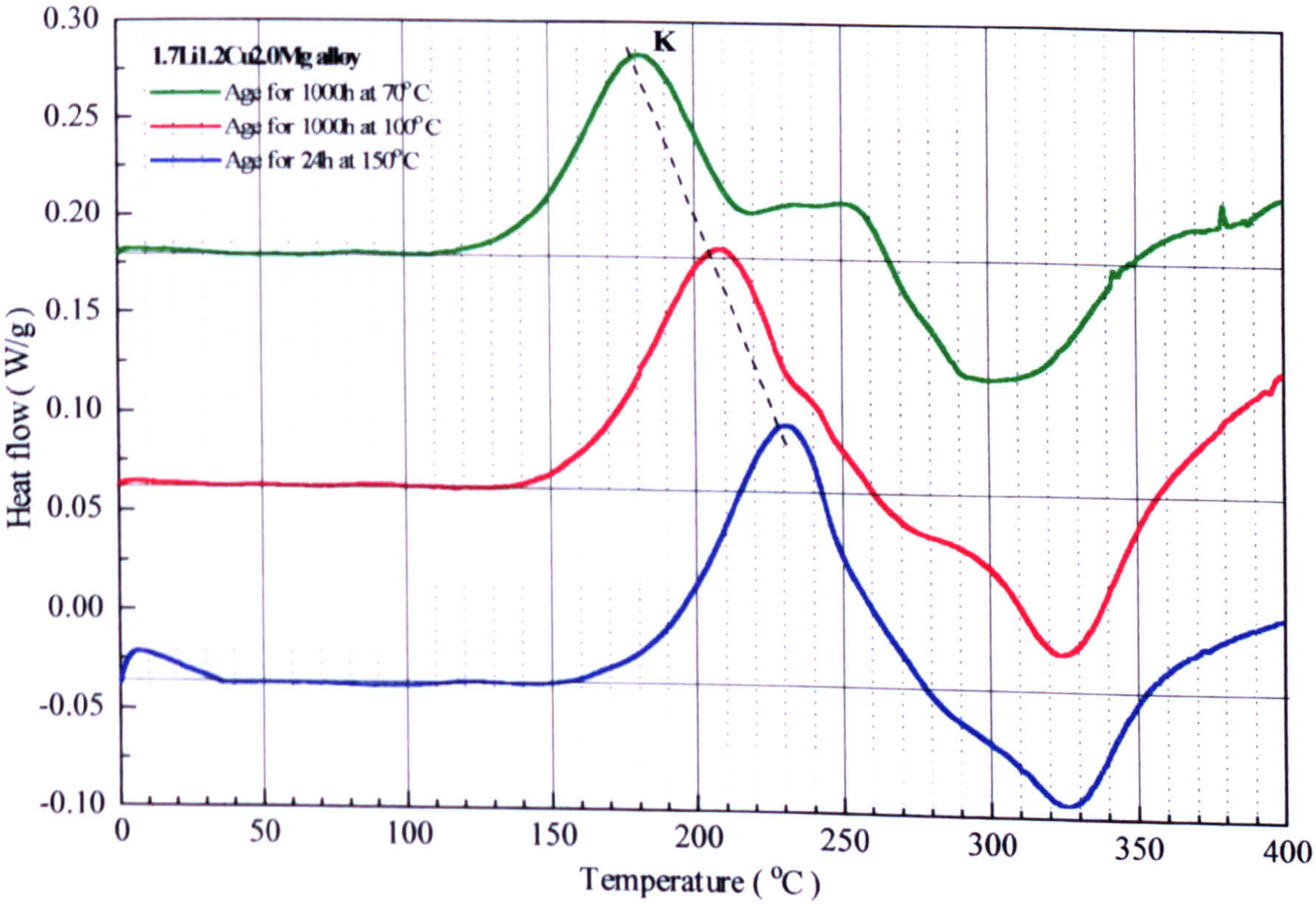

Figure 11.47: Effect of ageing temperature on the DSC thermogram of an 1.7Li1.2Cu2.0Mg alloy.

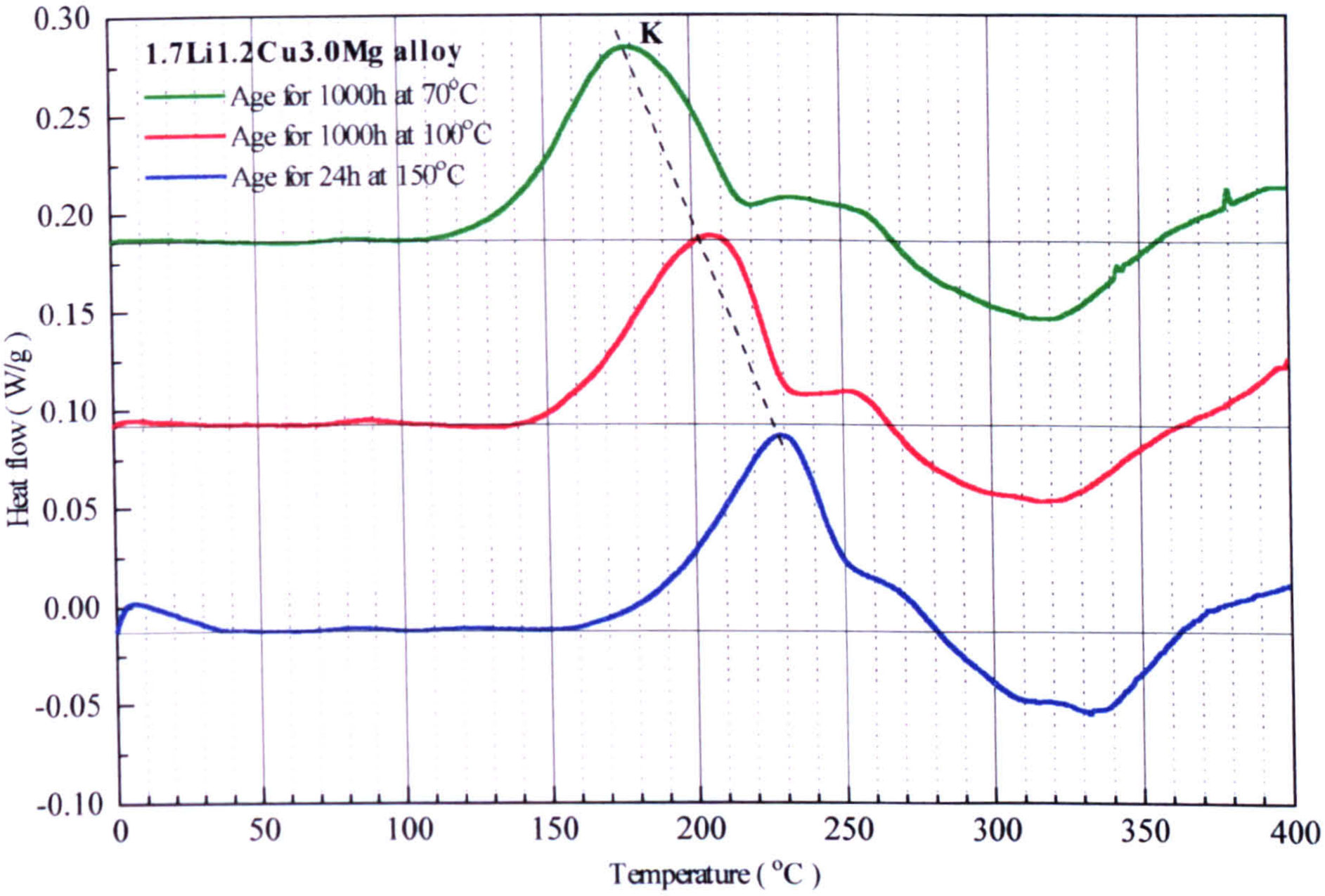

Figure 11.48: Effect of ageing temperature on the DSC thermogram of an 1.7Li1.2Cu3.0Mg alloy.

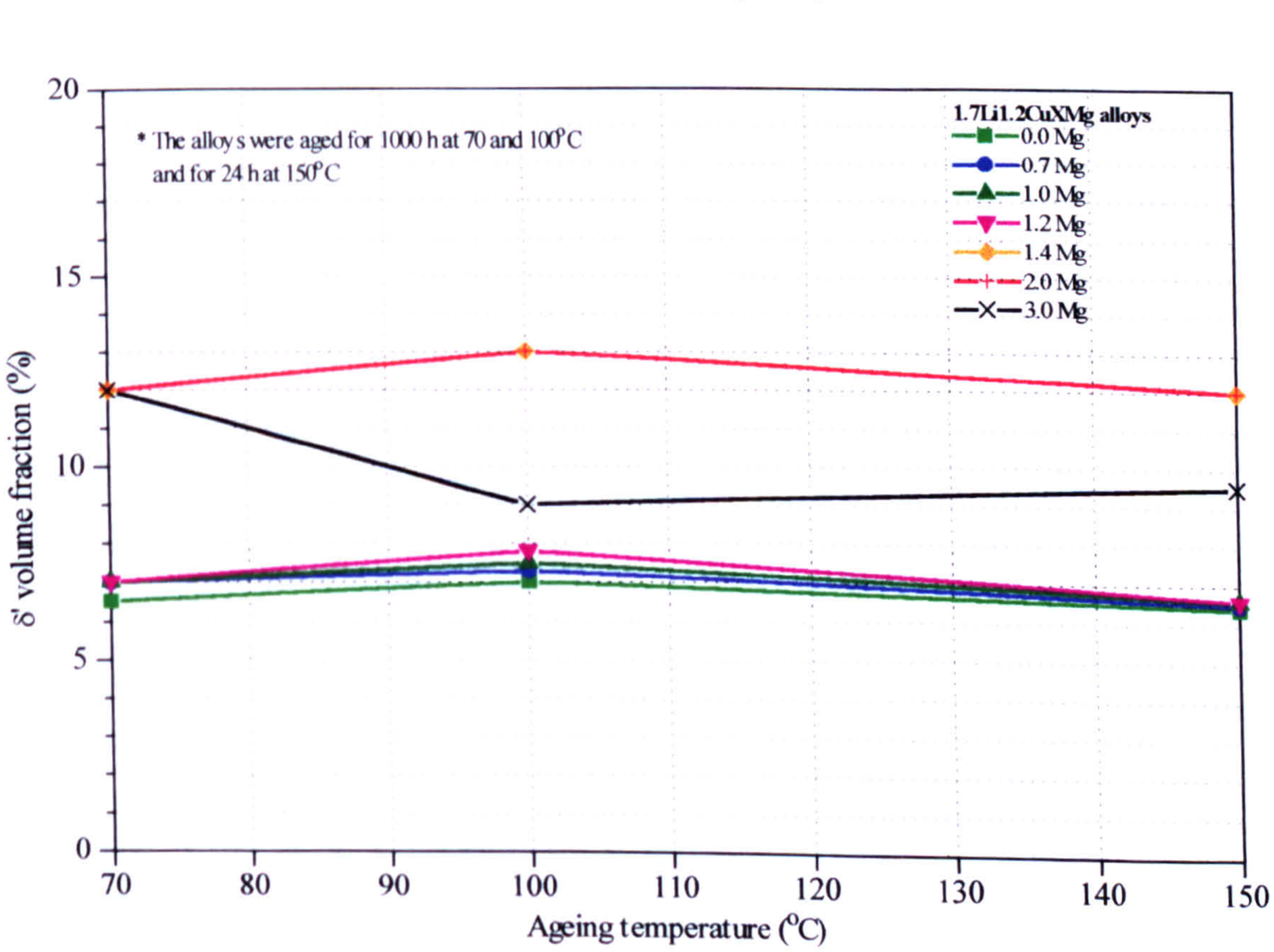

Figure 11.49: Effect of magnesium concentration and ageing temperature on δ′ volume fraction.

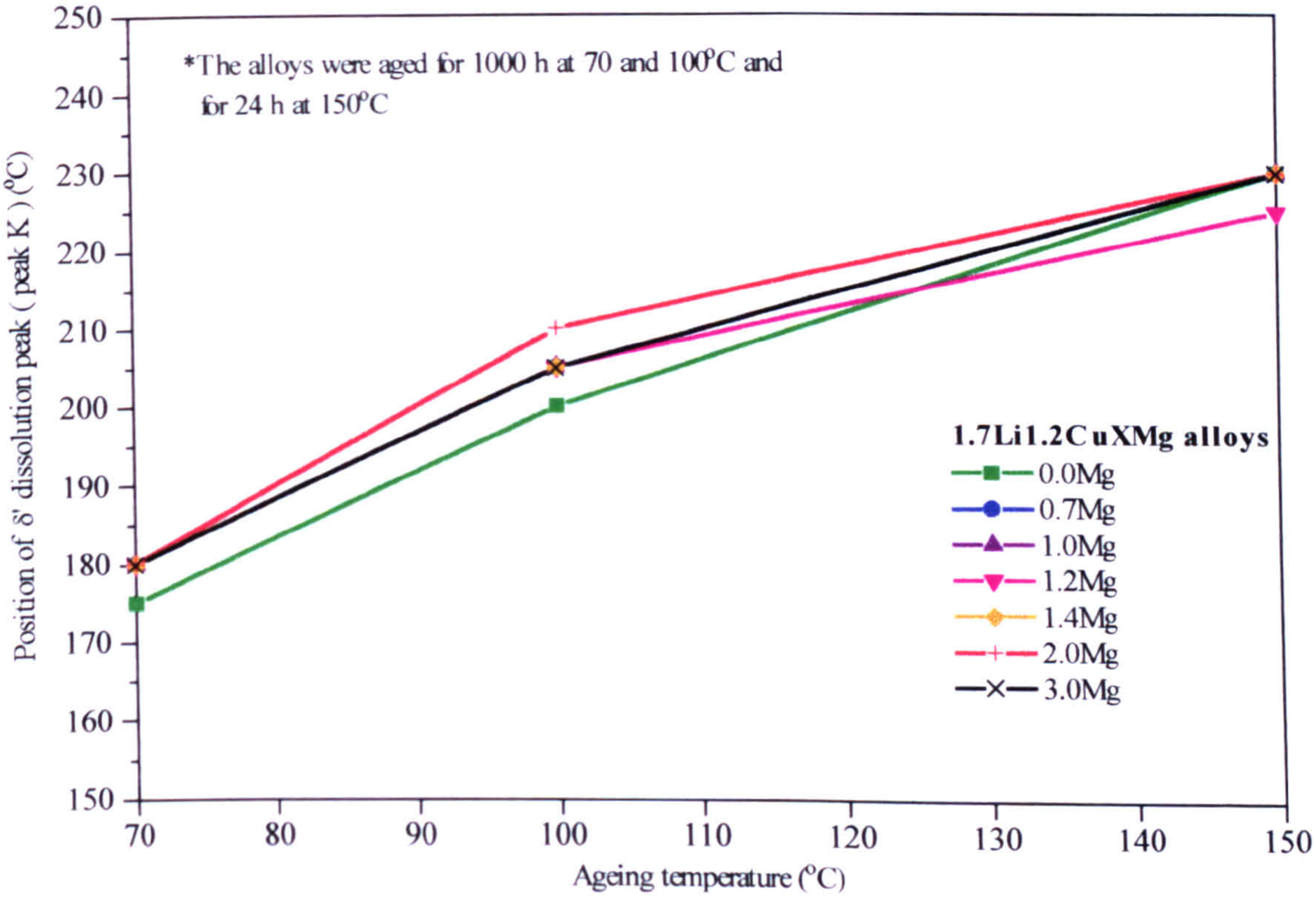

Figure 11.50: Position of the δ′ dissolution peak (peak K).

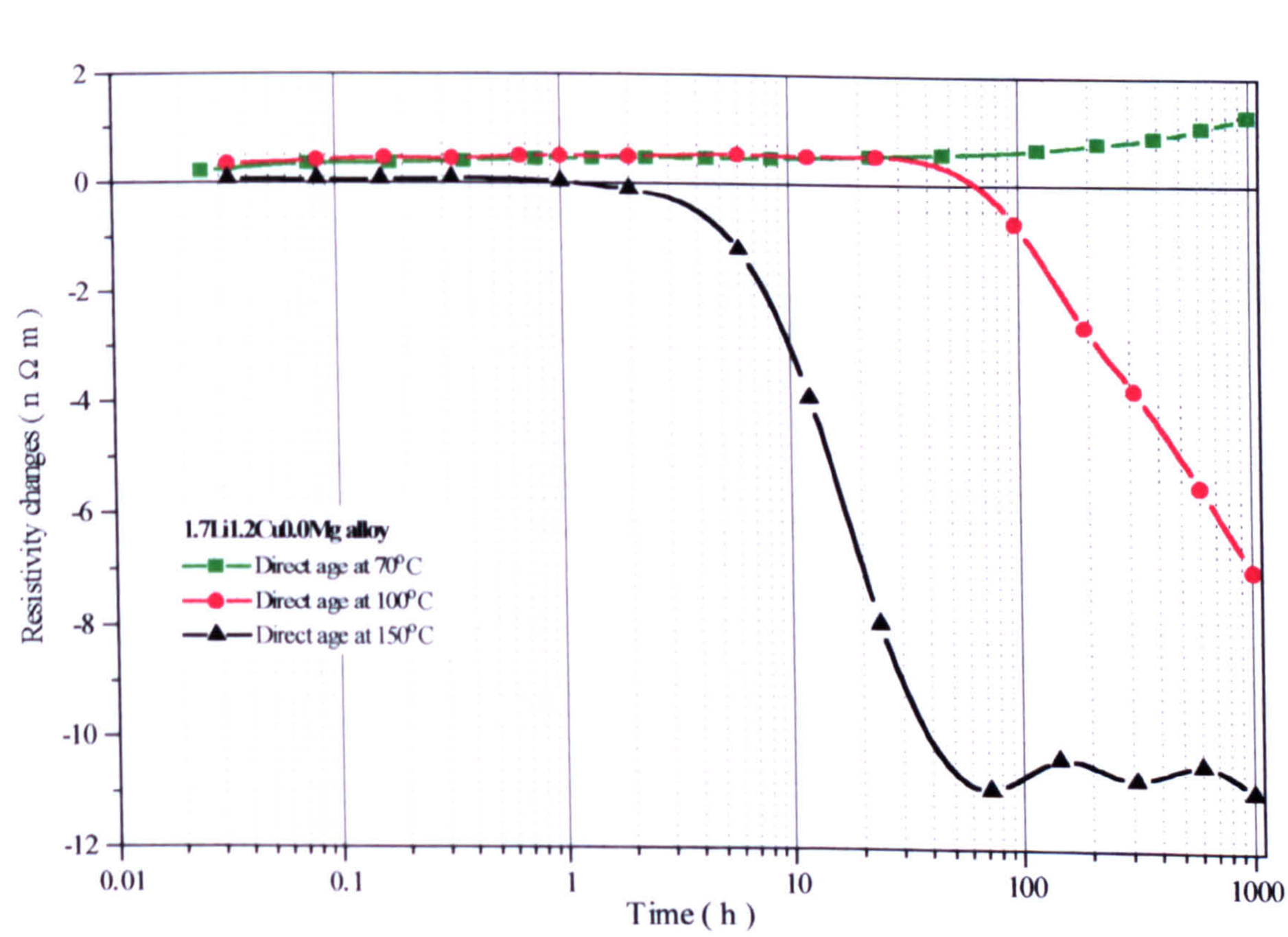

Figure 11.51: Effect of ageing temperature on the resistivity of an 1.7Li1.2Cu0.0Mg alloy.

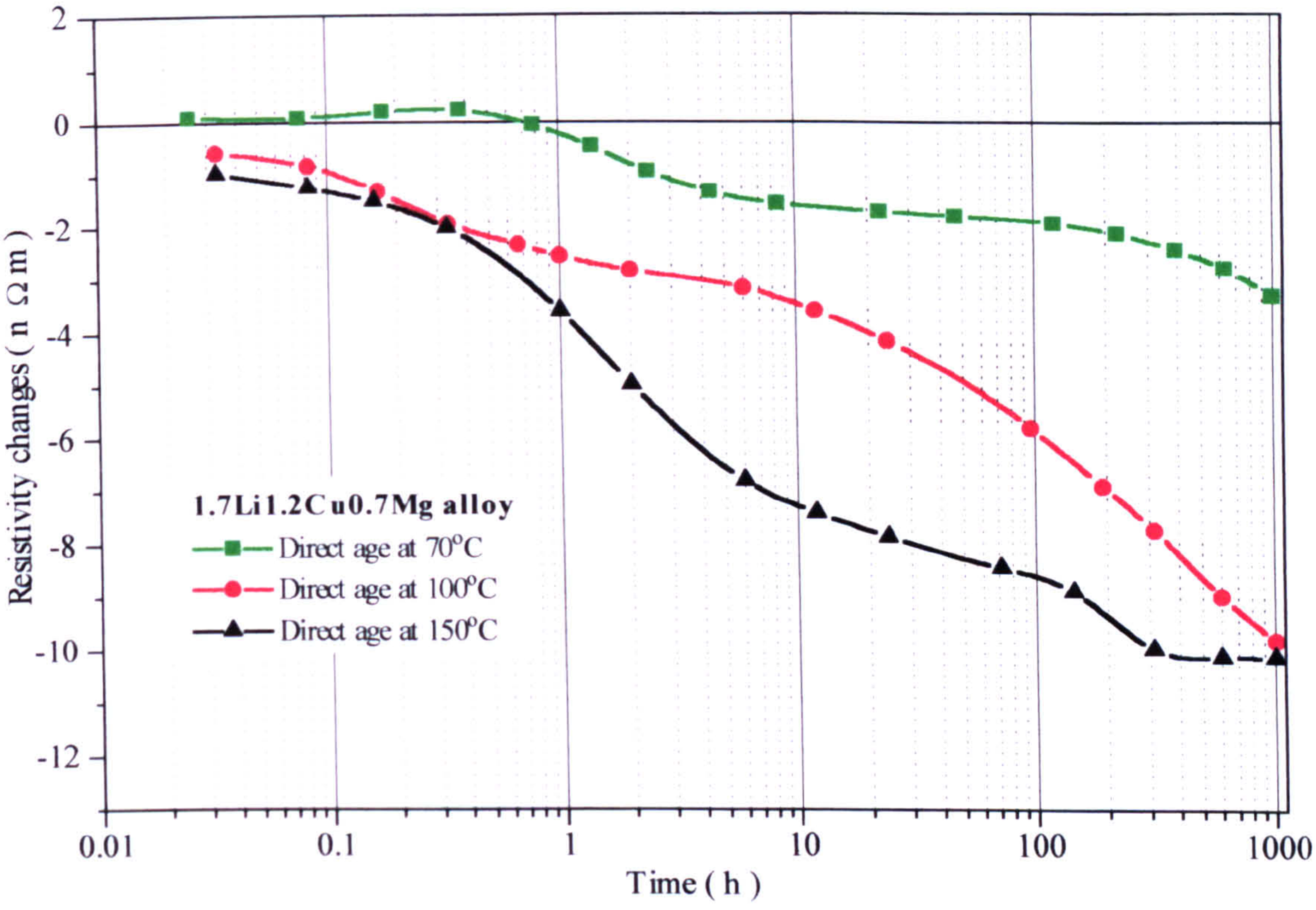

Figure 11.52: Effect of ageing temperature on the resistivity of an 1.7Li1.2Cu0.7Mg alloy.

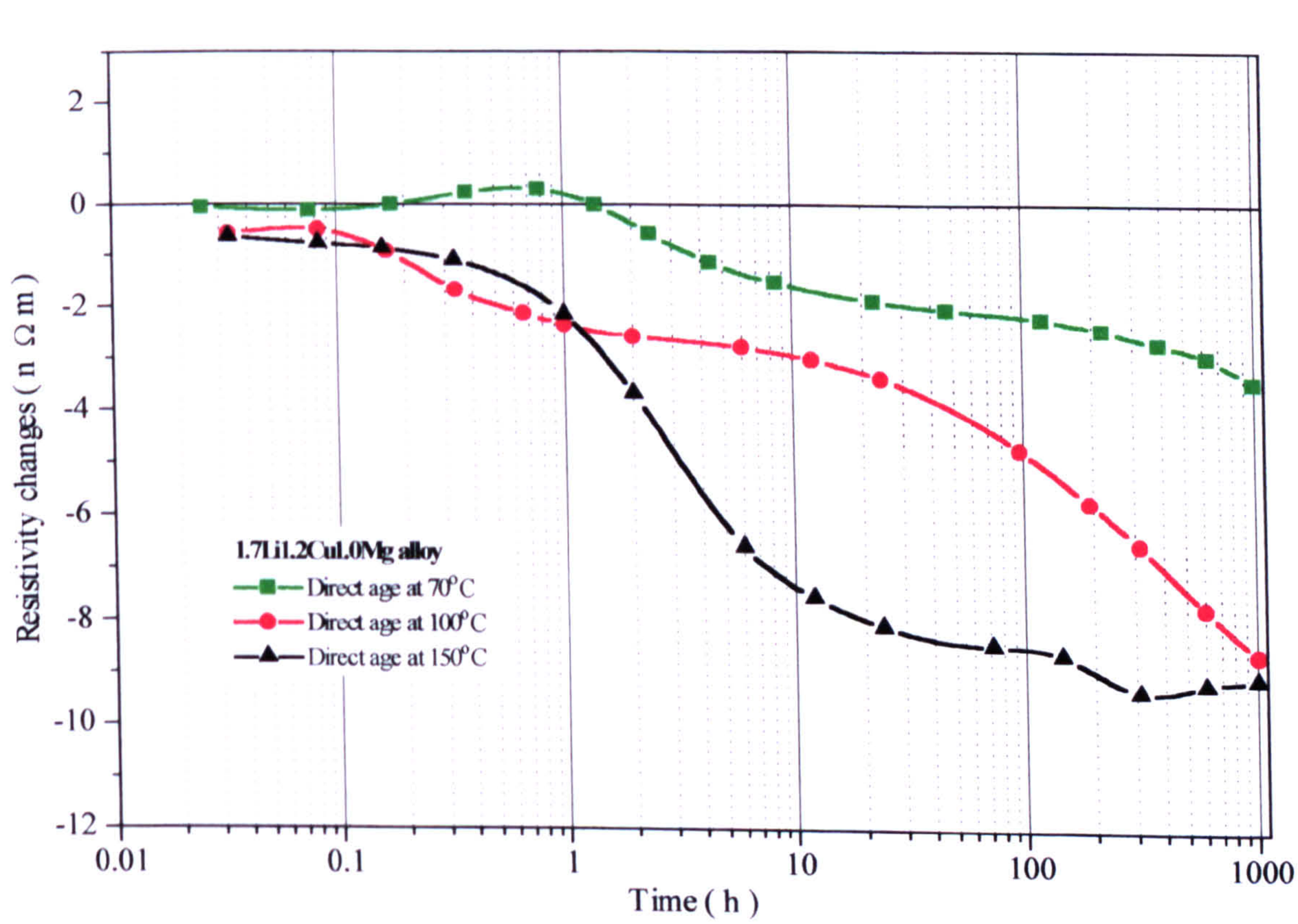

Figure 11.53: Effect of ageing temperature on the resistivity of an 1.7Li1.2Cu1.0Mg alloy.

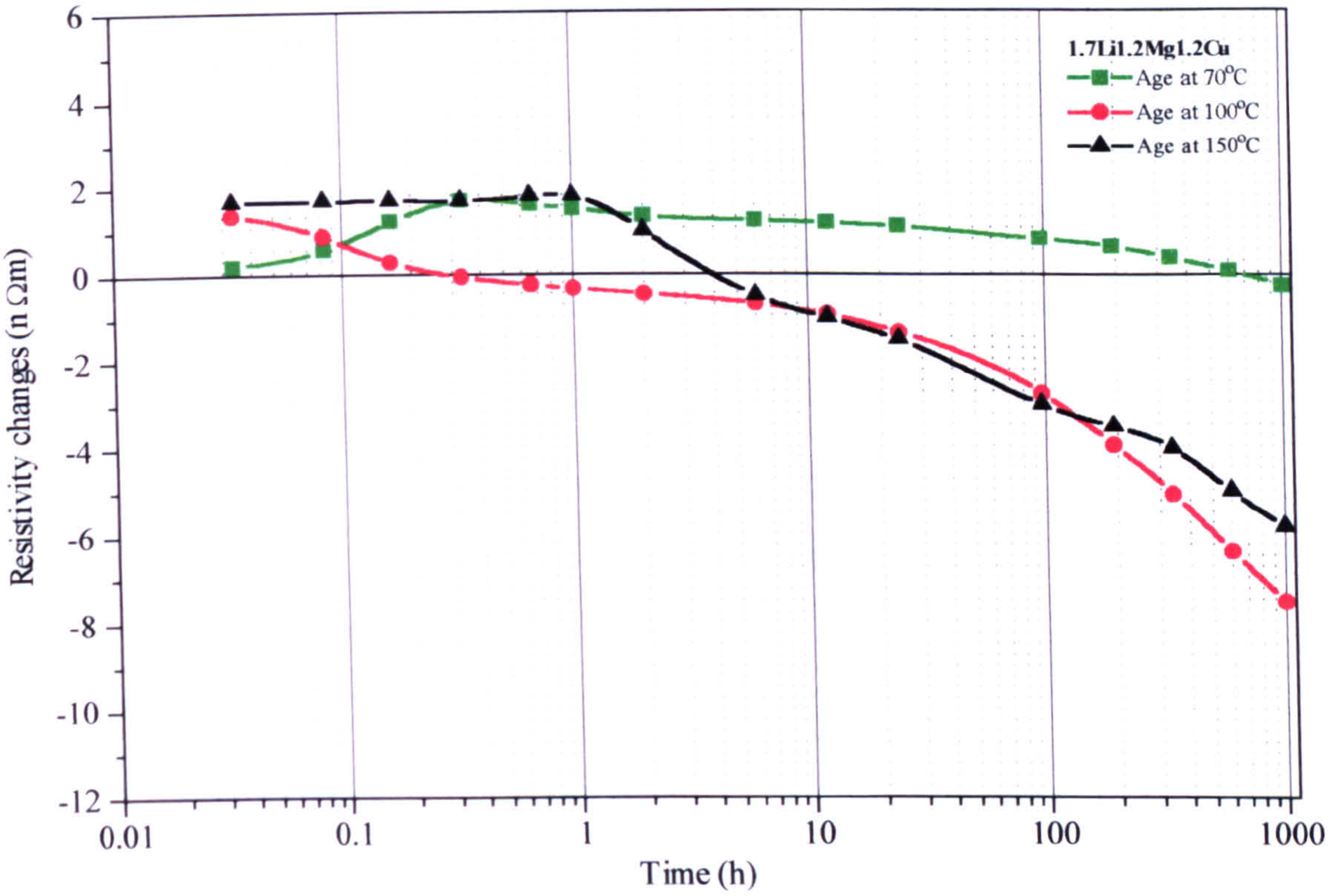

Figure 11.54: Effect of ageing temperature on the resistivity of an 1.7Li1.2Cu1.2Mg alloy.

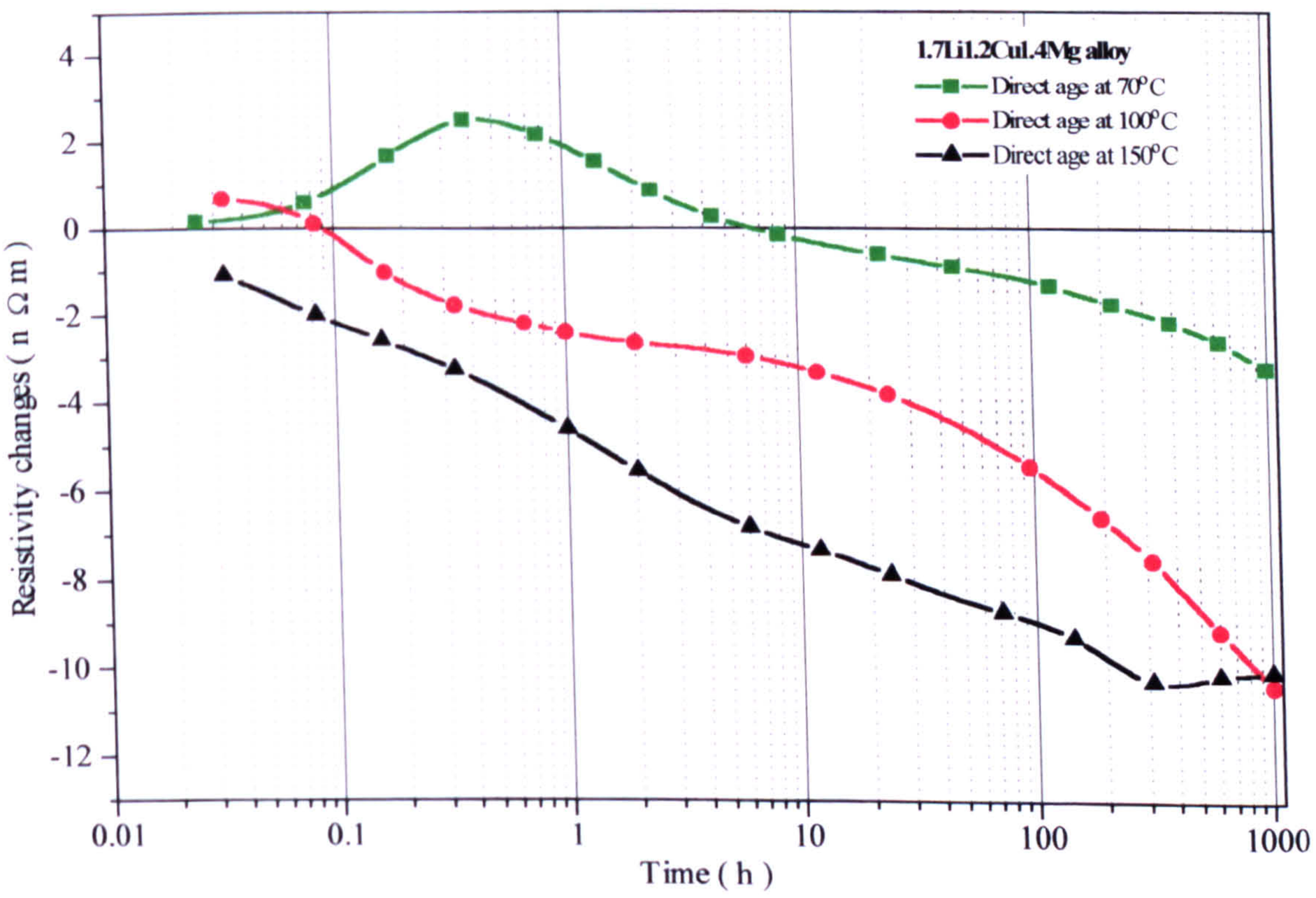

Figure 11.55: Effect of ageing temperature on the resistivity of an 1.7Li1.2Cu1.4Mg alloy.

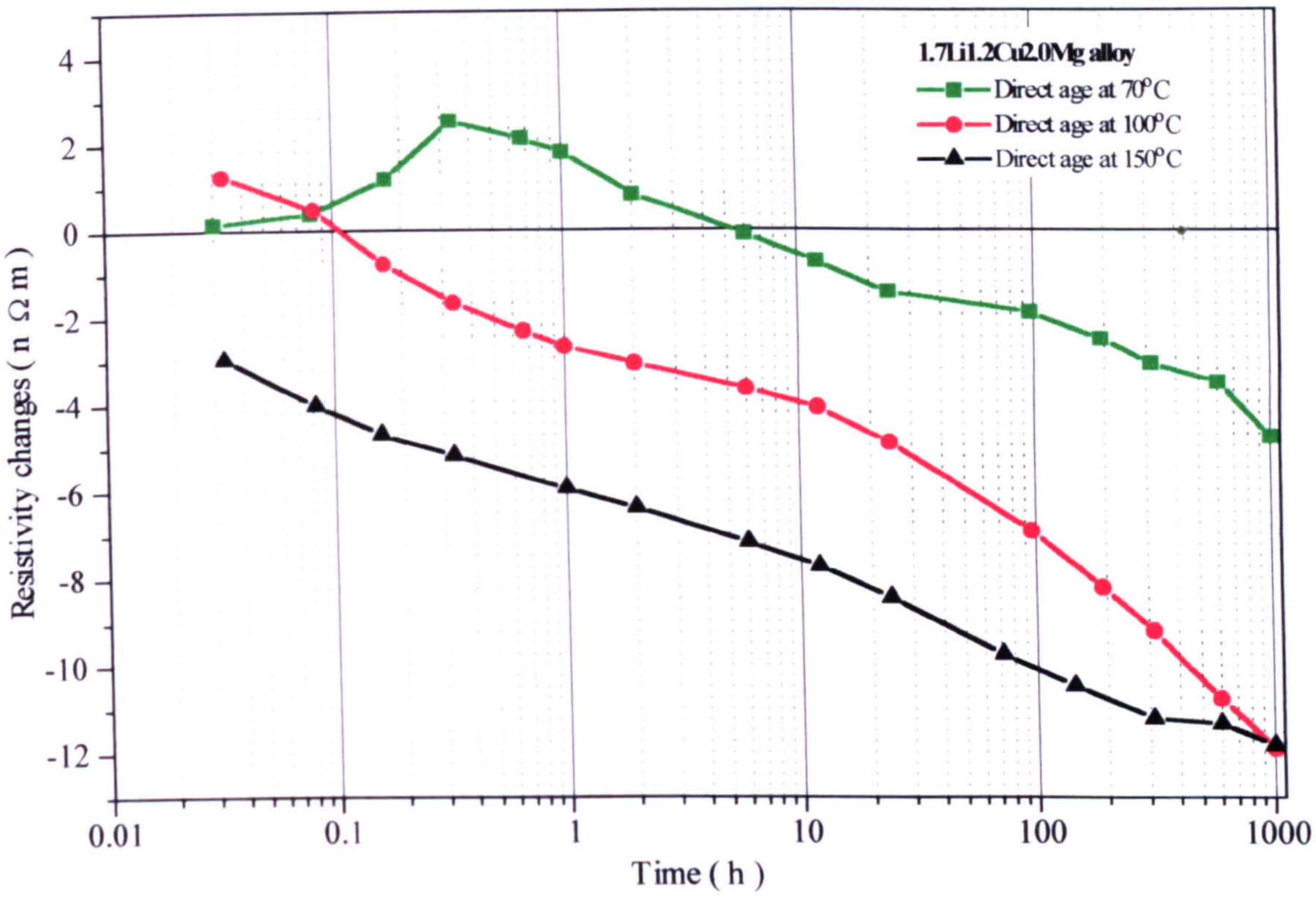

Figure 11.56: Effect of ageing temperature on the resistivity of an 1.7Li1.2Cu2.0Mg alloy.

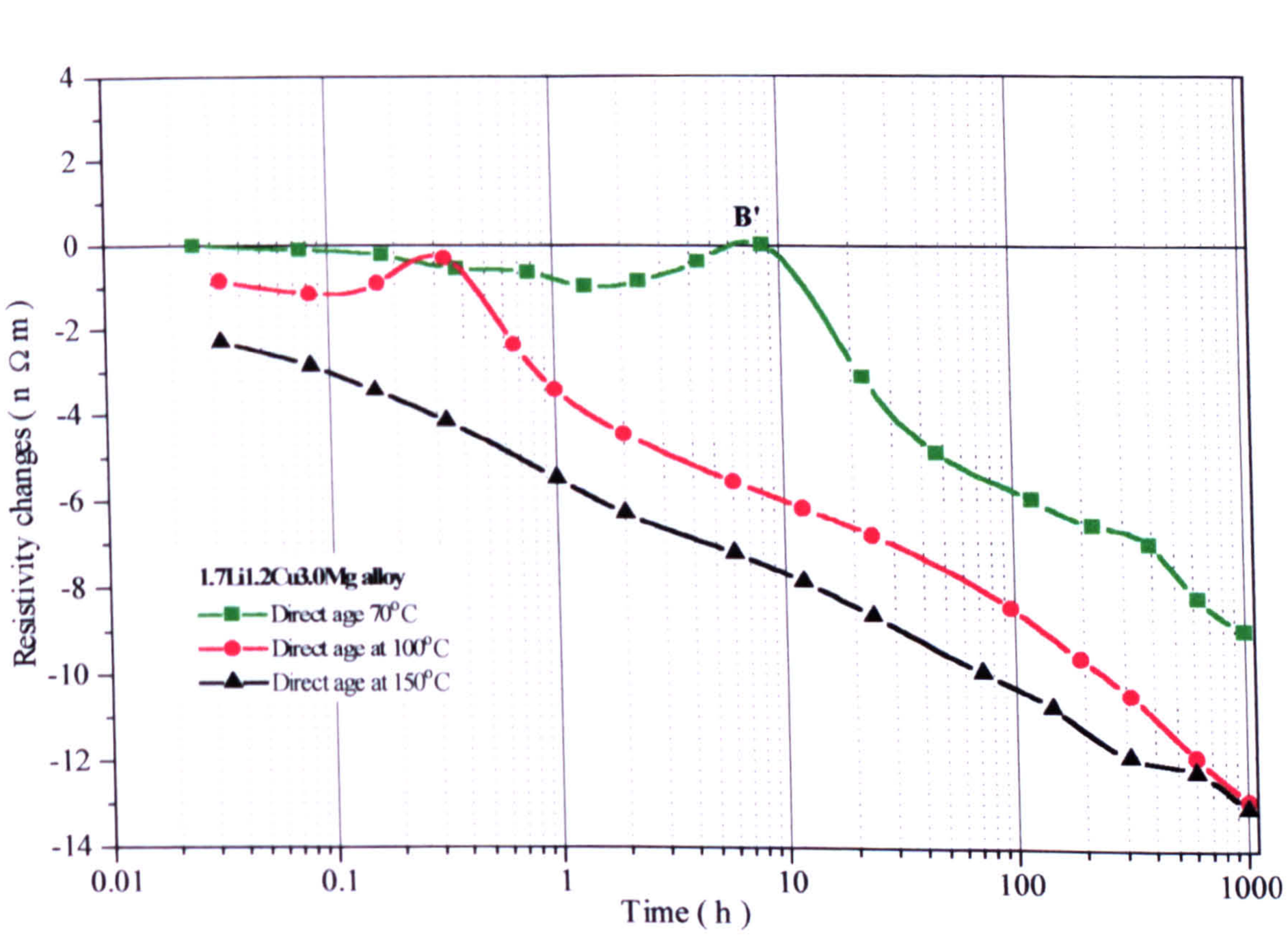

Figure 11.57: Effect of ageing temperature on the resistivity of an 1.7Li1.2Cu3.0Mg alloy.

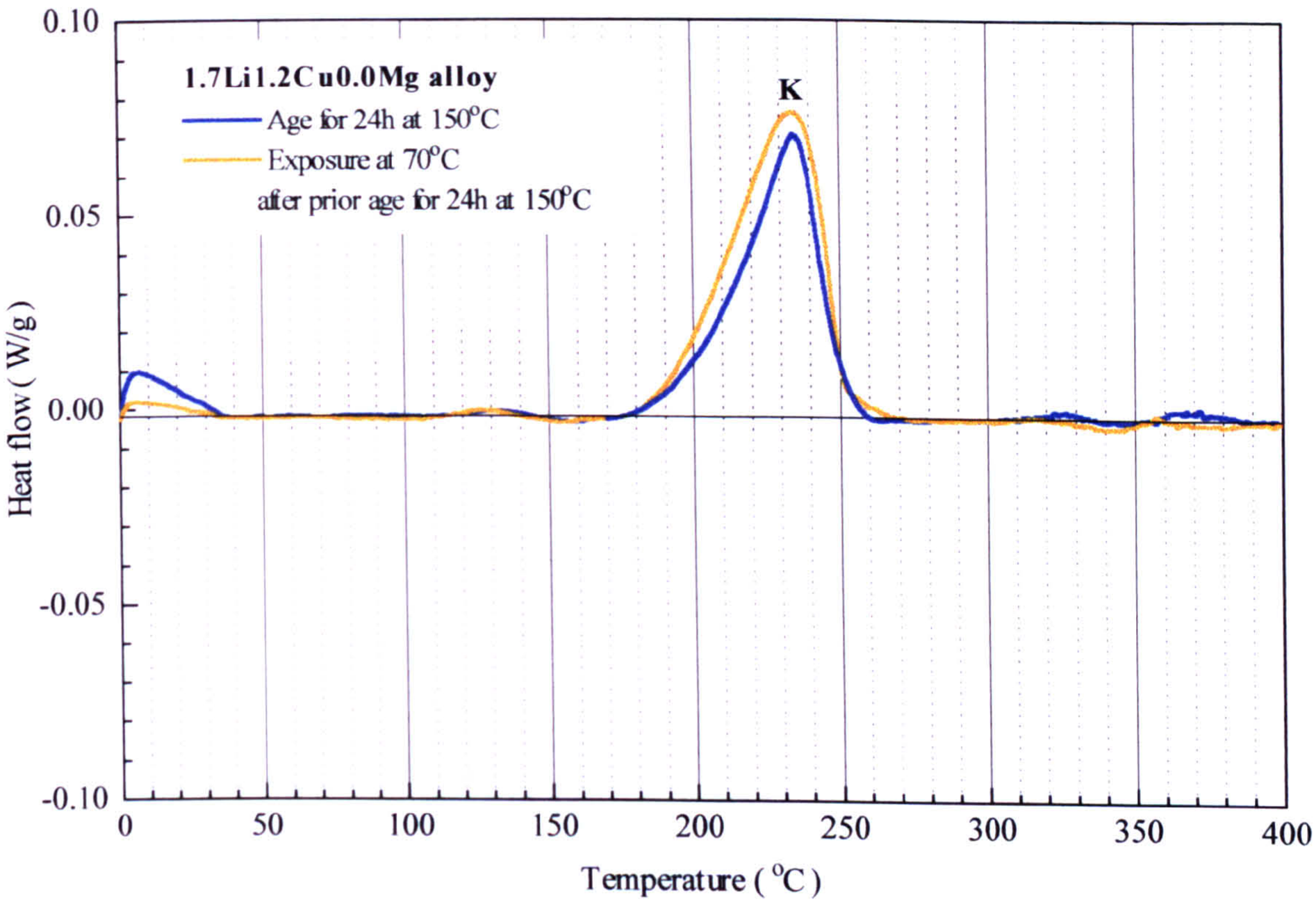

Figure 11.58: Effect of exposure on 1.7Li1.2Cu0.0Mg alloy.

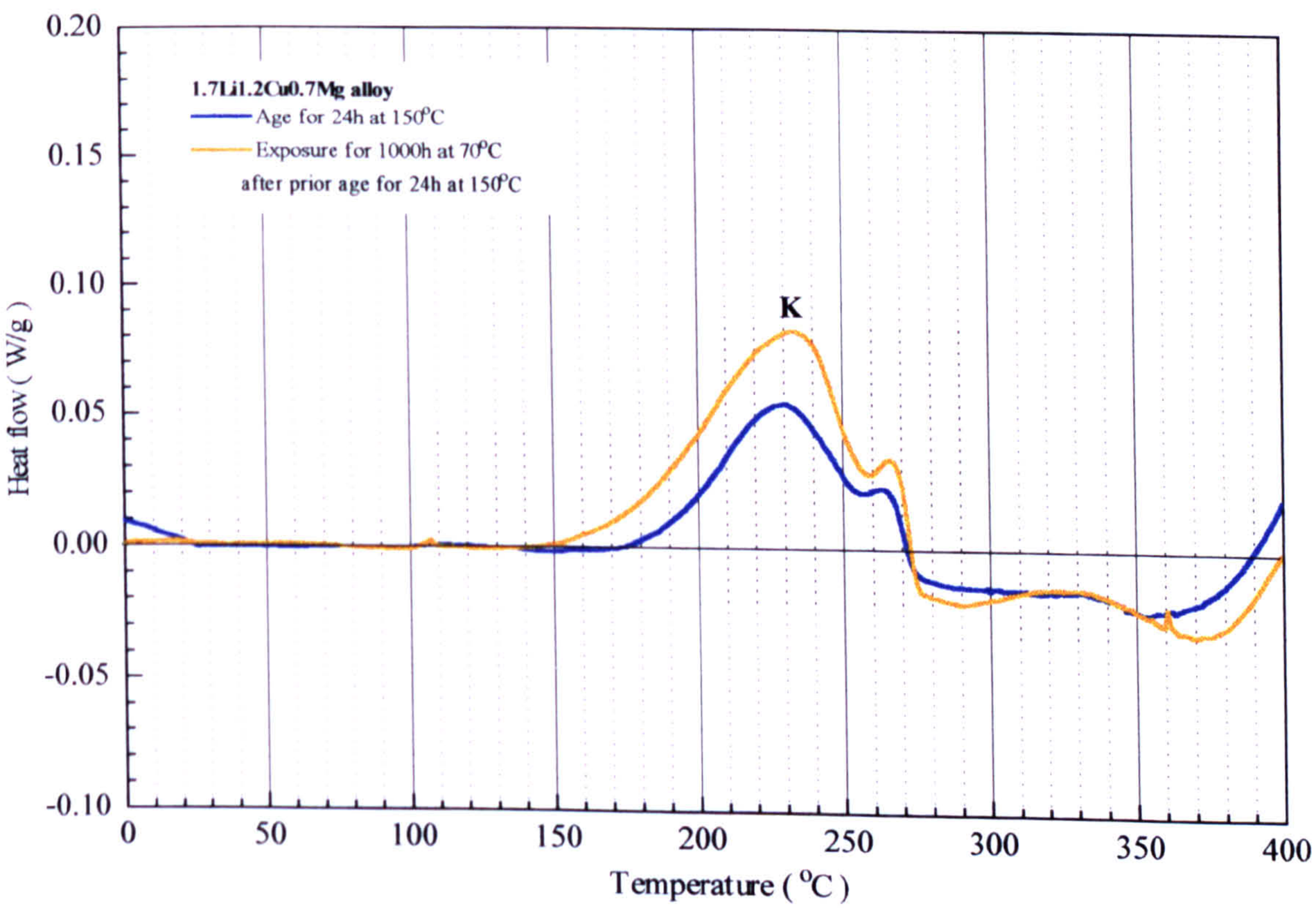

Figure 11.59: Effect of exposure on 1.7Li1.2Cu0.7Mg alloy.

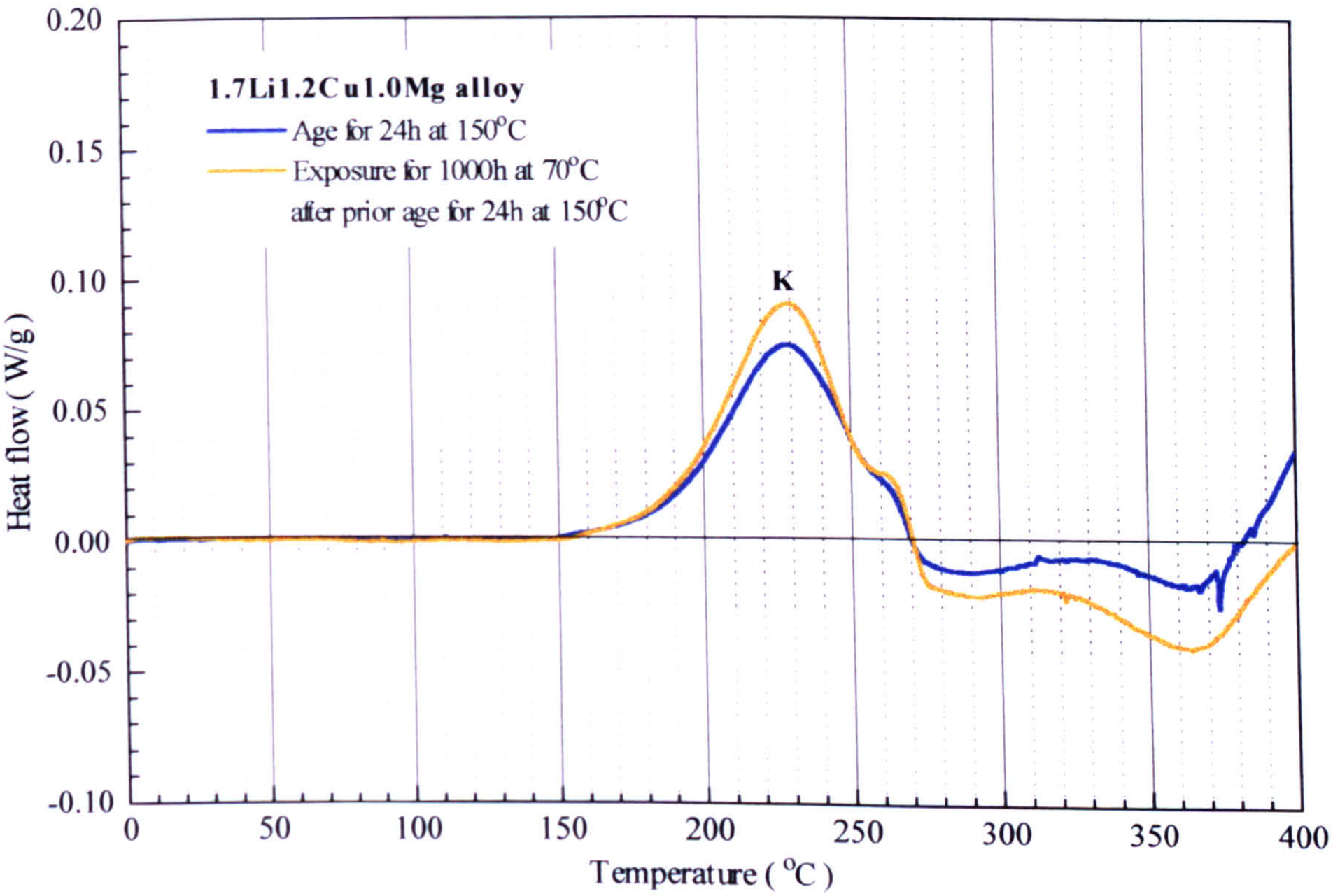

Figure 11.60: Effect of exposure on 1.7Li1.2Cu1.0Mg alloy.

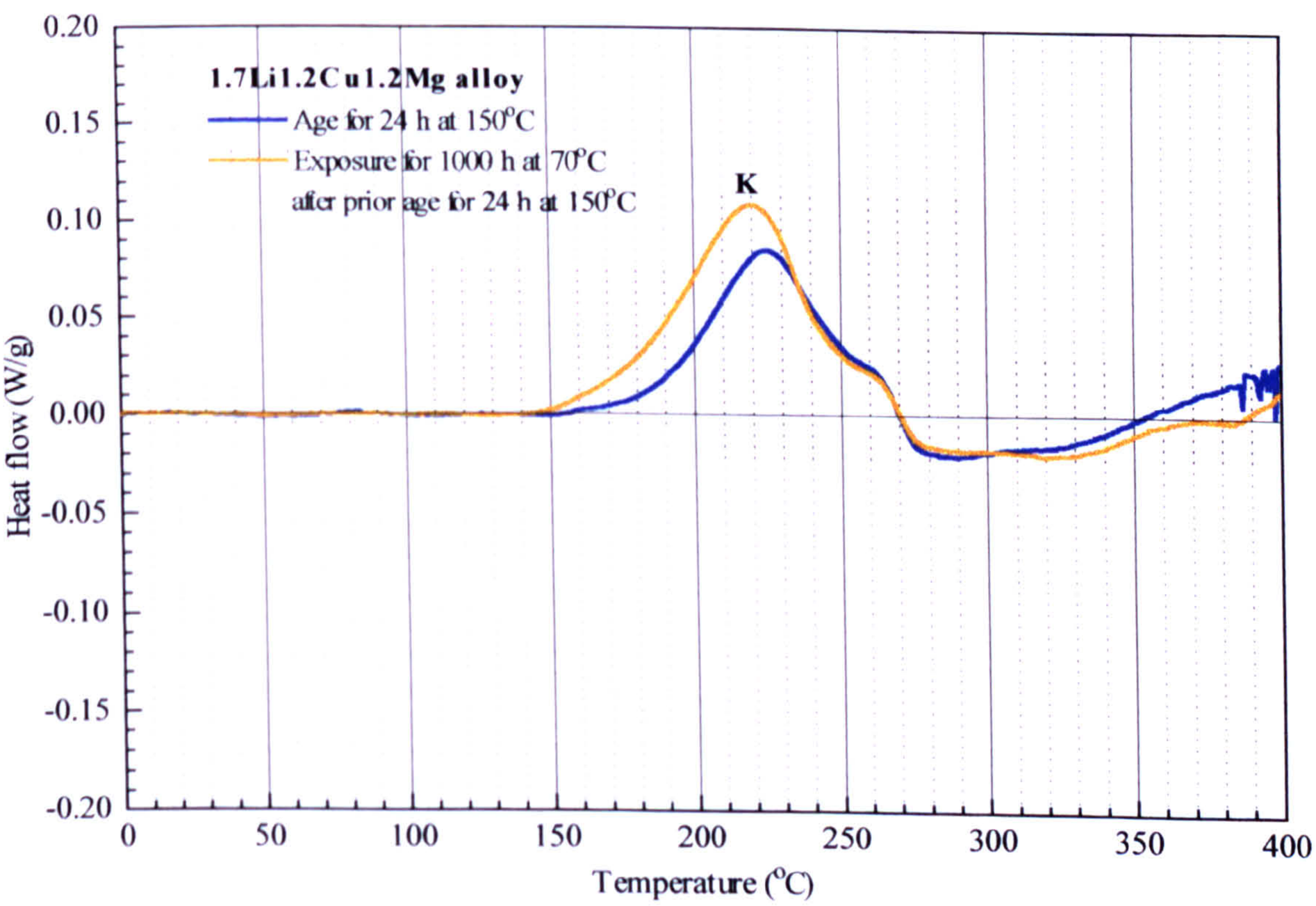

Figure 11.61: Effect of exposure on 1.7Li1.2Cu1.2Mg alloy.

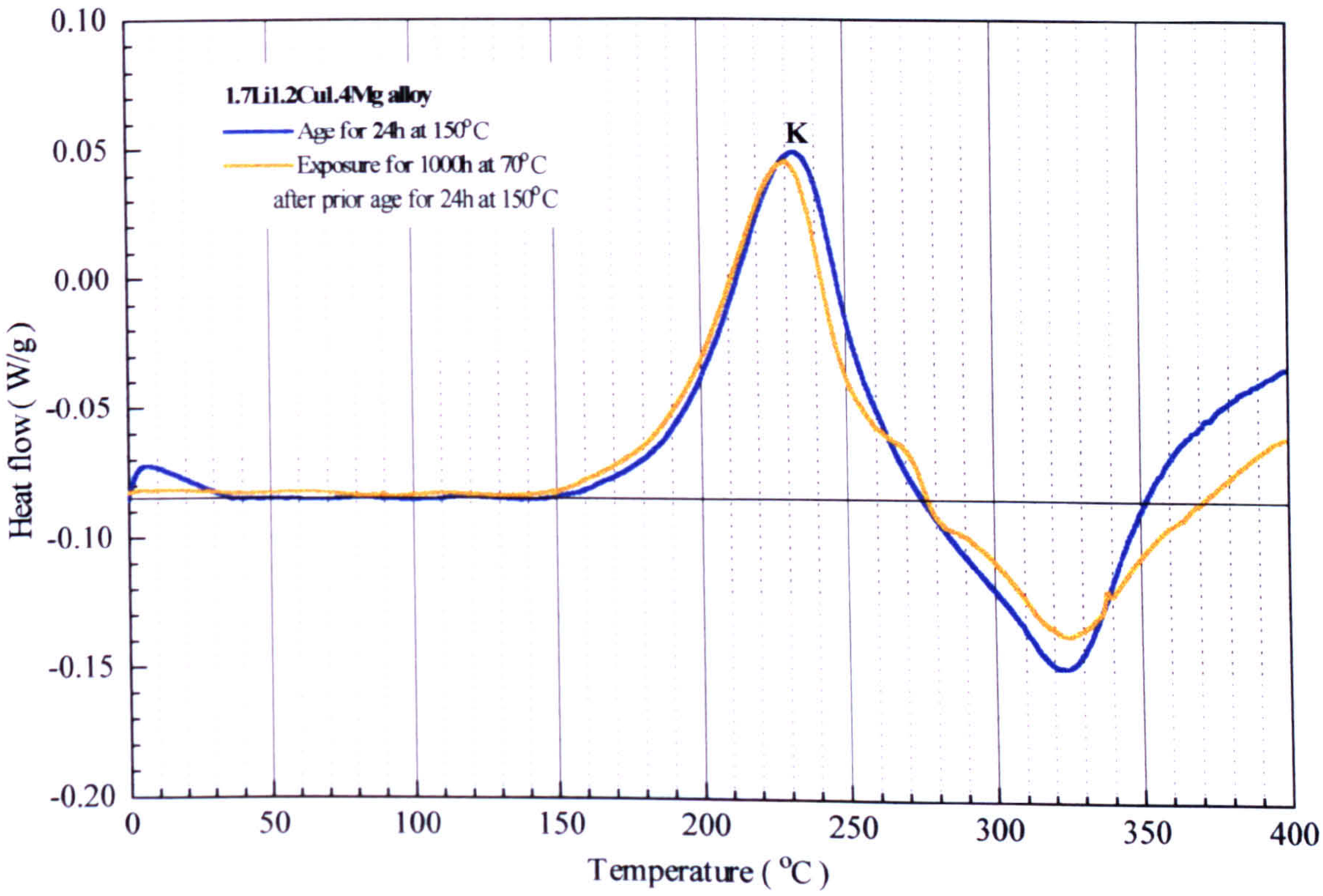

Figure 11.62: Effect of exposure on 1.7Li1.2Cu1.4Mg alloy.

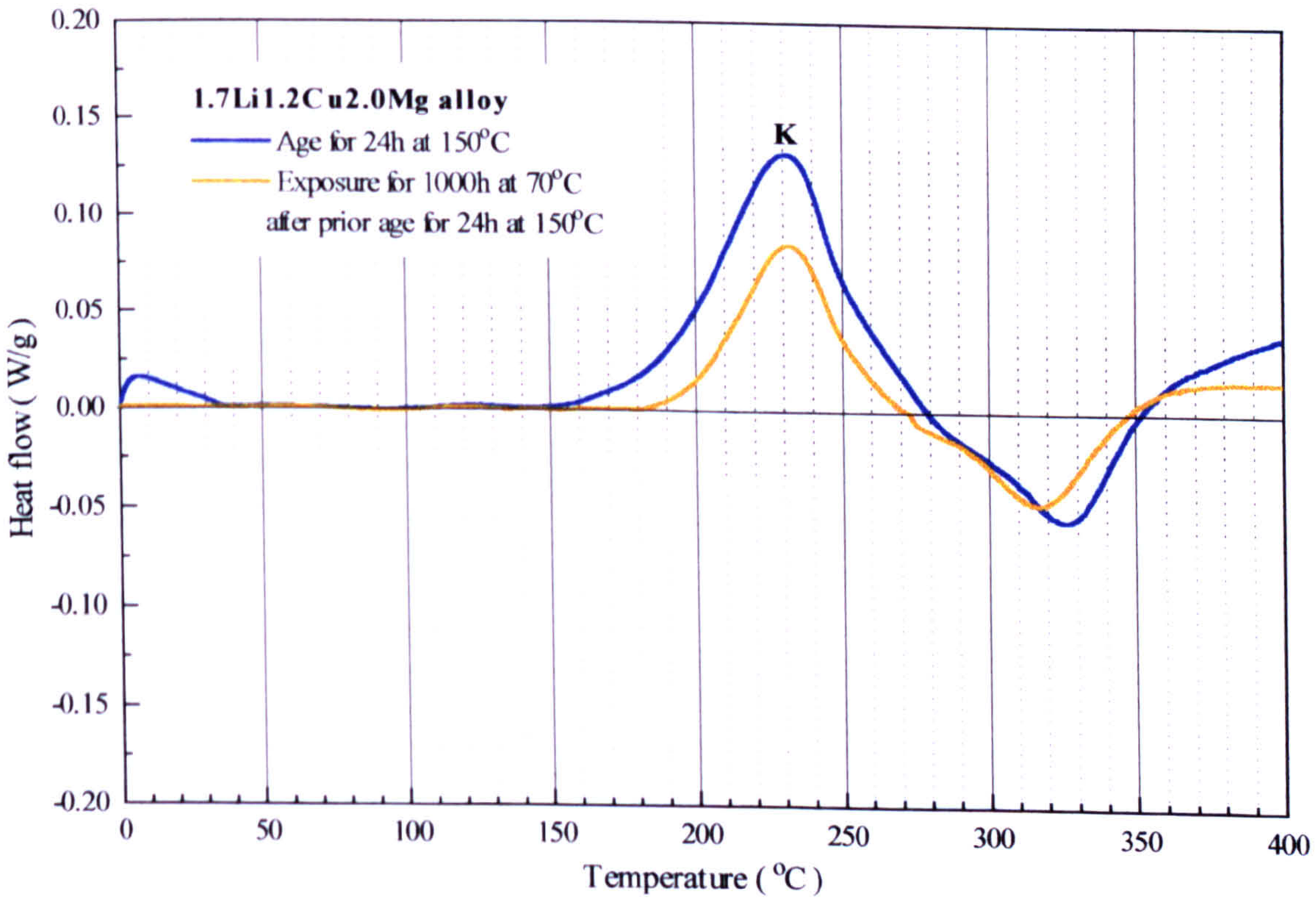

Figure 11.63: Effect of exposure on 1.7Li1.2Cu2.0Mg alloy.

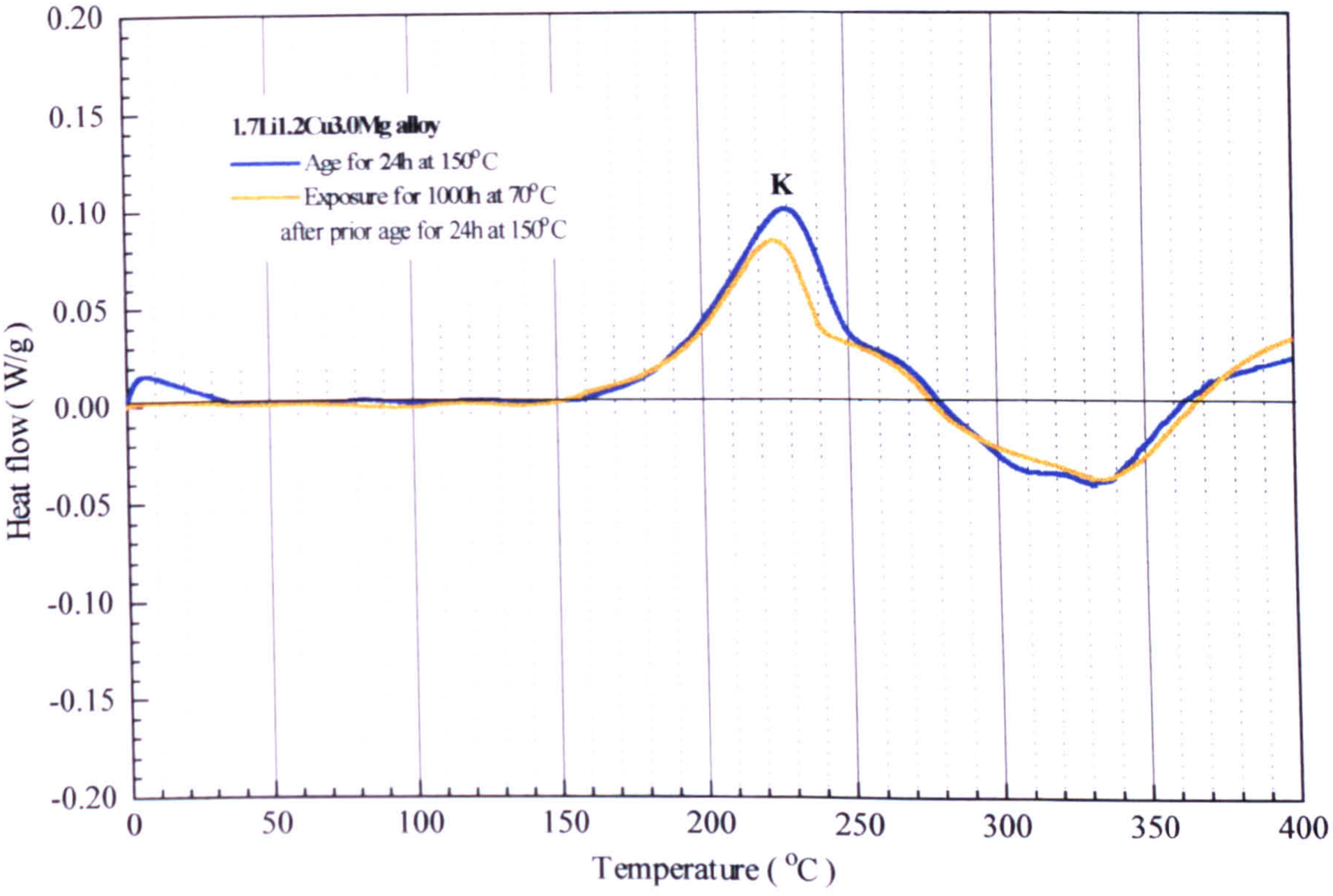

Figure 11.64: Effect of exposure on 1.7Li1.2Cu3.0Mg alloy.

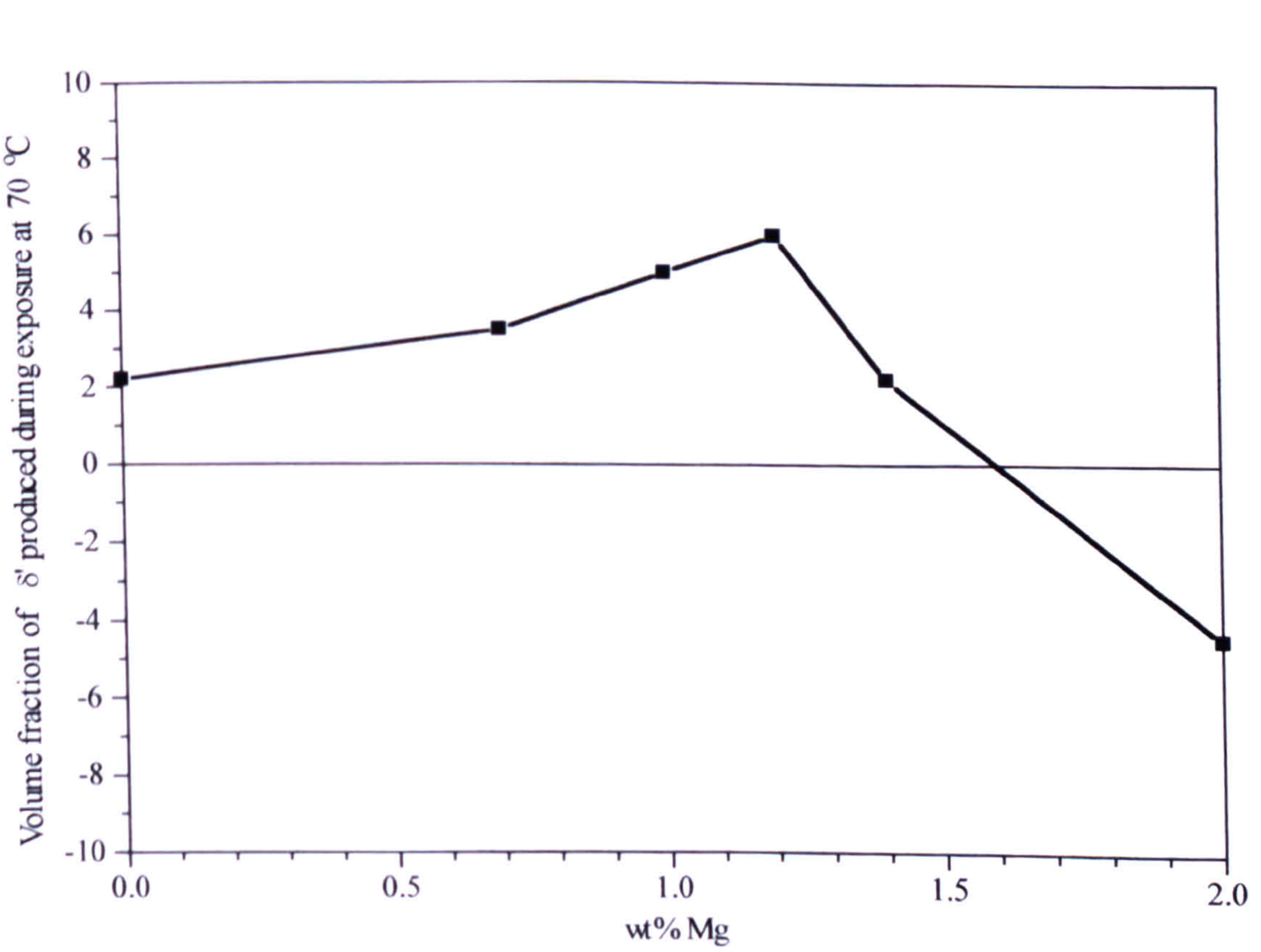

Figure 11.65: Volume fraction of δ′ produced in 1.7Li1.2CuXMg alloys during exposure.

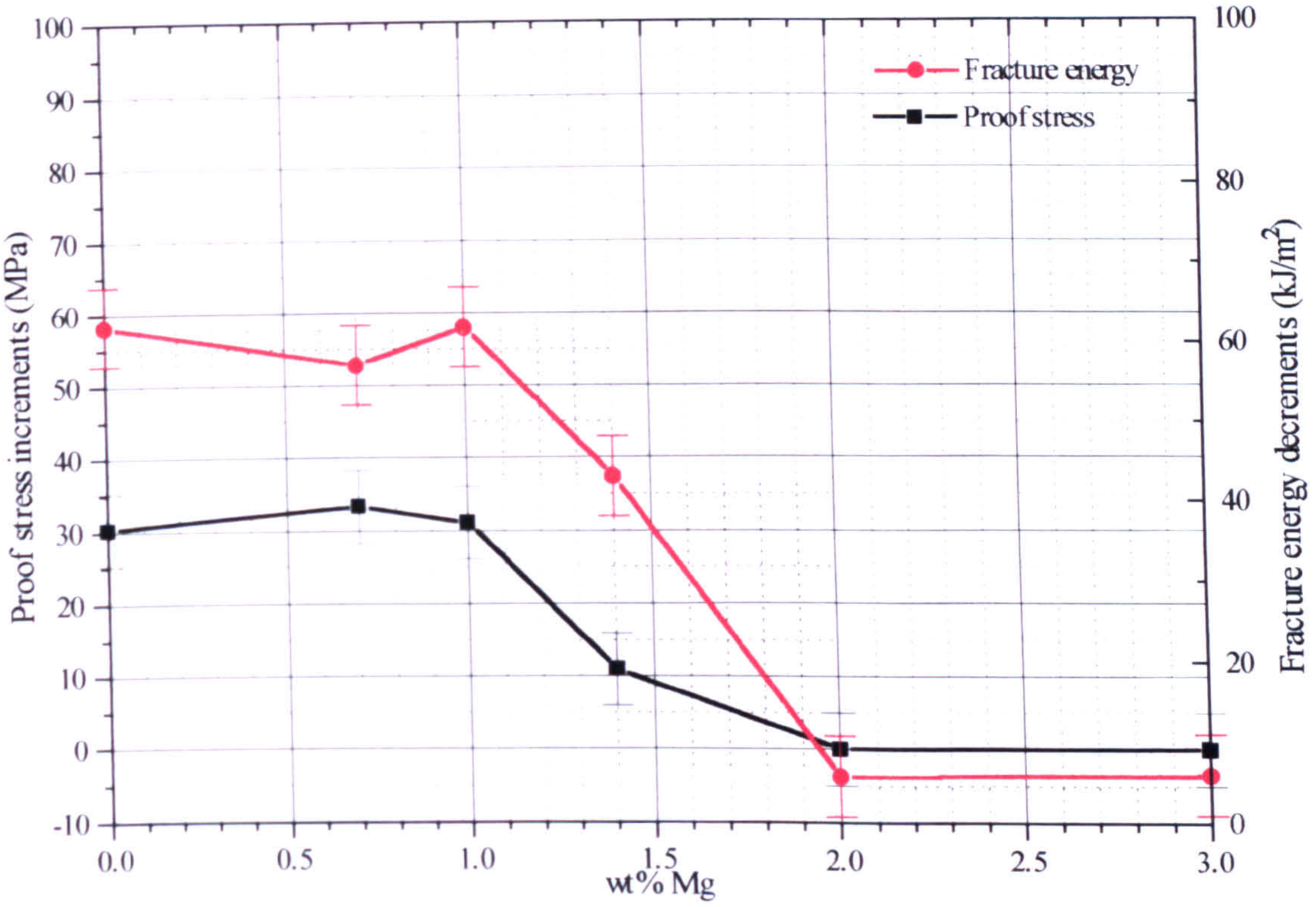

Figure 11.66: Effect of exposure on the mechanical properties of 1.7Li1.2CuXMg alloys.

CHAPTER 12

Effect of copper concentration on the ageing characteristics of Al-Li-Cu-Mg alloys

In the previous chapter, the effect of magnesium on the precipitation characteristics of Al-Li-Cu-Mg alloys was investigated. Magnesium stimulated significantly the precipitation of δ′ over the concentration range 1.4%-2.0%. The analysis of the results showed that this stimulation came about via the formation of Li-Cu-Mg clusters. GPB zones appeared to have only a small effect on δ′. Stimulation of δ′ precipitation by a shift of the α/δ′ solvus line to higher temperatures with increasing magnesium concentration, was of secondary importance.

In the present chapter, the role of copper on the precipitation reactions taking place in 1.7Li1.2MgXCu alloys is investigated. For this, five different alloys with increasing copper additions from 0 to 3.0% were used. The chapter is divided into two main parts:

- Isochronal precipitation characteristics.
- Isothermal precipitation characteristics

12.1 Isochronal precipitation characteristics

The isochronal results to be displayed in this section indicate that increasing copper concentration produces increasing volume fractions of δ′. Taking into consideration the results of chapter 9 where it was shown that copper had no effect on the α/δ′ metastable solvus line, the mechanisms by which the stimulation of δ′ takes place could be one of the following:

- Formation of δ′ on GPB zones. As shown in chapter 10, copper stimulates the formation of GPB zones. If δ′ were to form heterogeneously on GPB zones then stimulation of δ′ will result.
- Formation of Li-Cu-Mg clusters that are capable of nucleating δ′ in a manner similar to that described in the previous chapter. As the concentration of copper increases a larger number of these clusters may form and consequently increase the volume fraction of δ′.

12.1.1 DSC (as-quenched plots)

The DSC comparative plots of the 1.7Li1.2MgXCu alloys are presented in **figure 12.1.** The fast heating rate does not allow sufficient time for δ′ precipitation in 1.7Li1.2Mg0.0-0.6Cu alloys. The high-temperature exothermic peak O at approximately 320°C is due to the precipitation of the equilibrium phase T_2 (**figure 12.2**). Increasing the copper concentration from 0.6% to 1.2% results in the appearance of an exothermal effect (peak I) at approximately 110 °C that is

followed by a broad endotherm that consists of three overlapping peaks, K, G, and H. The DSC plot of the 1.7Li1.2Cu1.2Mg alloy has already been discussed in detail in the last chapter. It was concluded that exothermic peak I is caused by the precipitation of δ′ and GPB zones, whereas endothermic peaks K, G, and H correspond to the dissolution of δ′, GPB zones and S″ respectively. As the copper concentration increases from 1.2% to 2.0% the initial exotherm becomes much broader forming a double exotherm, peaks I′ and I″. Changes are also observed for the broad endotherm (150-270°C) where endothermic peak K has been replaced by two endothermic overlapping peaks, at about 170 and 200°C designated F and L respectively.

In order to assist the identification of the overlapping peaks referred to above, resistivity measurements were made on two low lithium alloys (1.3Li1.2Mg1.2,2.0Cu) (**figure 12.4**). It can be clearly seen that increasing the copper concentration from 1.2 to 2.0% results in the formation of two resistivity peaks (B′ and C′) superimposed on the GPB resistivity peak A′. This must mean that δ′ is being produced by two mechanisms, and it is proposed that these are the formation from Li-Cu-Mg clusters and formation on GPB zones. It is believed that during peak B′, precipitation of δ′ occurs via the formation of Li-Cu-Mg clusters (CLδ′) similar to the processes described for the Al-1.7Li-1.2Cu-XMg alloys, whereas peak C′ corresponds to the nucleation and growth of δ′ on GPB zones (GPδ′). The reason that peak B′ (low temperature peak) was attributed to

CLδ′ and not to GPδ′ is because Li-Cu-Mg clusters can form much easier than GPB zones i.e. no interface has to be created between the clusters and the matrix and therefore there is a lower activation energy barrier for their formation.

As the lithium concentration increases from 1.3% to 1.7%, peak B′ shifts to a lower temperature indicating that growth of CLδ′ to the critical size for electron scattering is faster due to the enhanced kinetics caused by the higher lithium supersaturation.

Finally, comparison of the 1.3,1.7Li1.2Mg1.2,2.0Cu alloys with the Al-1.7Li binary alloy shows that the mechanism of δ′ precipitation in the copper and magnesium containing alloys is quite different from that in the 1.7Li alloy. The increase in resistivity observed in the binary alloy over the range 0-100°C is caused by the formation of ordered domains. A resistivity increase over this temperature range is absent in the copper and magnesium-containing alloys indicating that the nucleation ordering is suppressed and that δ′ precipitation occurs in a different way, i.e. via Li-Cu-Mg clusters and heterogeneous nucleation on GPB zones.

Referring back to the DSC plots in **figure 12.1**, the exothermic peaks I′ and I″ can now be attributed to the precipitation of CLδ′ and GPδ′ respectively. Peaks F and L will then be caused by the dissolution of CLδ′ and GPδ′. As the dissolution of GPδ′ proceeds, the original GPB zone on which the δ′ nucleated is

exposed and thus becomes free to grow producing the overlapping exothermal effect R. This is followed by GPB zone dissolution at about 230°C (peak G). Further DSC heating causes transformation of the larger sized fraction of GPB zones into S″. Finally, dissolution of S″ takes place at approximately 250°C (peak H). DSC heating to even higher temperatures causes a double exothermic peak at 290°C and 320°C, peaks Y and O, that are attributed on the basis of XRD analysis to the precipitation of equilibrium phases S and T_2 respectively.

As the copper concentration rises beyond 2.0% (1.7Li1.2Mg3.0Cu alloy), enlargement of the size of all the DSC peaks is observed. This suggests that further stimulation of δ′ has occurred as a result of the formation of a larger number of Li-Cu-Mg clusters and GPB zones.

By integrating the area of exothermal effect I for 1.7Li1.2Cu1.2Mg alloy and I′+ I″ for 1.7Li1.2Mg2.0,3.0Cu alloys, the enthalpy evolved during δ′ precipitation was measured. Applying equation 8.2, enabled the calculation of δ′ volume fraction that precipitates in each of the 1.7Li1.2MgXCu alloys. These data are plotted as a function of magnesium concentration in **figure 12.3**. It can be seen that for copper concentrations higher than 0.6% the volume fraction of δ′ is increased relative to that in 1.7LiXCu alloys. It can be concluded that the presence of 1.2% magnesium in 1.7LiXCu alloys for copper concentrations higher than 0.6% results in significant stimulation of δ′ through the formation of

Li-Cu-Mg clusters which are capable of rapidly developing into δ′, and GPB zones that act as sites for heterogeneous nucleation of δ′.

12.1.2 Isochronal resistivity

Comparative isochronal resistivity plots of the 1.7Li1.2MgXCu alloys are shown in **figure 12.5**. The 1.7Li1.2Mg0-0.6Cu alloys exhibit very little increase in resistivity suggesting that only very small amounts of δ′ has formed, confirming the DSC results. As the copper increases from 0.6 to 1.2% two resistivity peaks form at 80 and 200°C, peaks B′ and C′, that respectively correspond to the formation of CLδ′ and GPδ′. As the copper concentration increases from 1.2% to 2.0% to 3.0% the height of peak B′ increases without any changes in its position (**figure 12.6**). This suggests that increasing the copper concentration produces a larger number of Li-Cu-Mg clusters that in turn produces a higher number-density of CLδ′ particles.

Peak C′ exhibits similar trends (**figure 12.7**). The height of the peak increases with increasing copper concentration beyond 0.6%. This is attributed to the formation of an increased number of GPB zones that act as precipitation sites for δ′ (GPδ′). The position of peak C′ exhibits a gradual shift to lower temperature as the copper concentration increases indicating that a higher number density of finer GPδ′ particles has been produced.

12.2 Isothermal precipitation characteristics

This section investigates the effect of copper on the isothermal precipitation characteristics of Al-Li-Cu-Mg alloys.

Five different heat treatments have been used:

- Ageing for 1000 h at 70, 100 and 150 °C.
- Ageing for 24 h at 150 °C. This simulates the damage tolerant heat treatment applied to alloys based on the Al-Li system.
- Prior ageing for 24 h at 150 °C following by exposure for 1000 h at 70 °C. This double heat treatment simulates the conditions that a commercial aerospace alloy would encounter whilst in service.

12.2.1 Age at 70°C

12.2.1.1 Investigation of low lithium alloys

DSC and resistivity comparative plots for 0,1.3,1.7Li1.2Mg1.2,2.0Cu alloys are presented in **figures 12.8** and **12.9** respectively. The effects of the additions of 1.3% and 1.7% Li to 1.2Mg1.2Cu alloy have already been discussed in the last chapter and can be summarised as follows:

- Addition of 1.3%Li to a 1.2Mg1.2Cu alloy results in the formation of δ′ during ageing at 70°C (dissolution peak K). This addition of lithium also causes an increase in the size of GPB zones (dissolution peak G) that is attributed to a lower GPB zone nucleation rate. Increasing the lithium

addition from 1.3% to 1.7% (1.7Li1.2Mg1.2Cu alloy) produces a larger volume fraction of finer δ′ (endothermic peak K becomes larger and shifts to a lower temperature) due to the higher driving force for δ′ precipitation.

- Isothermal resistivity plots (**figure 12.9**) show the addition of 1.3%Li to a 1.2Mg1.2Cu alloy (1.3Li1.2Mg1.2Cu alloy) results in a peak after 4 h of ageing due to the precipitation of fine δ′. As the lithium concentration increases from 1.3% to 1.7% (1.7Li1.2Mg1.2Cu alloy) a resistivity peak is attained at earlier times due to the acceleration of δ′ precipitation reaction kinetics.

The situation is not very different for the higher copper alloys (1.3,1.7Li1.2Mg2.0Cu). The addition of 1.3% Li to 1.2Mg2.0Cu alloy results in the development of endothermic peak K that corresponds to the dissolution of δ′. As the lithium concentration increases form 1.3% to 1.7% (1.7Li1.2Mg2.0Cu alloy) enlargement of peak K occurs (**figure 12.8**).

The resistivity plots (**figure 12.9**) show that the addition of 1.3%Li to 1.2Mg2.0Cu alloy causes the development of a resistivity peak after ~2 h of ageing. Longer ageing times (>2 h) result in further growth of δ′ beyond the electron scattering critical size and the resistivity starts decreasing. Increasing the lithium addition from 1.3% to 1.7% (1.7Li1.2Mg2.0Cu alloy) accelerates the kinetics but causes a decrease in the height of the resistivity peak, as was the case for the alloys containing 1.2% copper.

Finally, comparison of the DSC plots of 1.3Li1.2Mg1.2Cu and 1.3Li1.2Mg2.0Cu alloys (**figure 12.8**) indicates that the higher copper alloy (1.3Li1.2Mg2.0Cu) has precipitated a larger volume fraction of finer δ′ (endothermic peak K is larger and exhibits a 5°C-shift to a lower temperature). Furthermore, the isothermal resistivity plots of these two alloys (**figure 12.9**) suggest that as copper concentration increases from 1.2% (1.3Li1.2Mg1.2Cu alloy) to 2.0% (1.3Li1.2Mg2.0Cu alloy) a finer distribution of δ′ is precipitated with enhanced kinetics (a larger resistivity peak is attained at earlier ageing times). This behaviour can be explained by the formation of a larger number of Li-Cu-Mg clusters and GPB zones that assist the nucleation of δ′.

It can therefore be concluded that for ageing Al-Li-Mg-XCu alloys at 70°C:

- The addition of 1.3%Li to 1.2Mg1.2,2.0Cu alloys causes precipitation of δ′ and an increase in the size of GPB zones.
- Increasing lithium concentration from 1.3% to 1.7% causes significant acceleration of the precipitation reaction kinetics of δ′ in the early stages of ageing.

12.2.1.2 Investigation of 1.7Li1.2MgXCu alloys

DSC comparative plots of 1.7Li1.2MgXCu alloys are presented in **figure 12.10.** The DSC plot of 1.7Li1.2Mg alloy exhibits an endothermic peak (peak K) at approximately 175°C caused by the dissolution of δ′. As copper concentration

increases from 0% to 0.6% (1.7Li1.2Mg0.6Cu alloy) three new overlapping thermal events appear at 215°C, 230°C and 245°C, i.e. exotherm R, endotherm G, and endotherm H. Exothermal effect R cannot be clearly seen on the DSC trace but evidence will be presented for its existence later in the chapter; it is associated with the growth of GPB zones during DSC heating. It is postulated that heterogeneous nucleation of δ′ takes place on GPB zones during the age at 70°C. When subsequent dissolution of δ′ takes place during DSC heating, the GPB zones become exposed and grow during the DSC heating giving rise to exothermal effect R. Endothermal effects G and H are then attributed to the dissolution of GPB zones and S″ (the latter being formed during the DSC heating). Finally, the broad high temperature exotherm (290-370°C), with peaks at 310°C and 350°C is due to precipitation of the equilibrium phases T_1 and T_2 respectively (**figure 12.2**)

Increasing the copper concentration from 0.6% to 3.0% (1.7Li1.2Mg1.2,2.0,3.0Cu alloys) results in enlargement of peak K suggesting that stimulation of δ′ precipitation has occurred. Peaks G and H also exhibit an increase in their size which is in agreement with the results of chapter 10 where it was found that copper stimulates the precipitation of GPB zones and in turn the formation of S″. In order to estimate the volume fraction of δ′ precipitated in each alloy, the area under peak K was integrated and equation 8.2 applied. Then, the calculated volume fraction was plotted versus copper concentration (**figure 12.11**). As can be seen, over the concentration range 0-1.2% no stimulation of δ′

precipitation takes place. However, increasing the copper concentration beyond 1.2% does result in an increase in the volume fraction of δ′. Based on the isochronal results of the last section it is postulated that this stimulation of δ′ comes about by nucleation from Li-Cu-Mg clusters and heterogeneous nucleation on GPB zones.

Comparison of the volume fraction plots of 1.7Li1.2MgXCu and 1.7LiXCu alloys in **figure 12.11** indicates that for copper concentrations higher than 1.2% the presence of 1.2% Mg in the 1.7Li1.2MgXCu alloys produces significantly larger volume fractions of δ′ than in magnesium-free, 1.7LiXCu, alloys. Taking into consideration the results of chapter 9 where stimulation of δ′ in 1.7LiXCu alloys was shown to be the result of heterogeneous nucleation on GP_{Cu} zones and surmising that the effect of GPB zones on δ′ precipitation in 1.7Li1.2MgXCu alloys is unlikely to be greater than that of GP_{Cu} zones, it can be concluded that the largest amount of δ′ stimulation in 1.7Li1.2MgXCu alloys aged at 70°C comes about by nucleation from Li-Cu-Mg clusters.

Figure 12.13 shows the isothermal resistivity plots of 1.7Li1.2MgXCu alloys during ageing at 70°C. The isothermal resistivity plot of 1.7Li1.2Mg0.0Cu alloy has already been discussed in detail in chapter 8. The resistivity exhibits a two-stage increase. The initial increase was attributed to the formation of a high density of fine ordered domains and the second increase of resistivity to spinodal

decomposition of the ordered domains. The critical size for electron scattering is reached after 24 h indicating that the kinetics of δ′ precipitation are very slow.

Increasing the copper concentration from 0.0% to 0.6% to 1.2% causes the resistivity peak to be attained in progressively shorter ageing times suggesting that enhancement of the reaction kinetics of δ′ precipitation has occurred. The resistivity peak also exhibits an increase in its magnitude. It is known that for copper concentrations up to 1.2% (1.7Li1.2Mg0-1.2Cu alloys) the copper atoms are consumed in the nucleation and growth of GPB zones and therefore the formation of Li-Cu-Mg clusters is expected to be difficult. Given this, the above enhancement of the reaction kinetics of δ′ precipitation in low copper alloys can be attributed to the formation of a larger number of GPB zones that can accelerate the rate of δ′ nucleation producing a finer dispersion of δ′ particles (GPδ′). However, it should be noted that after 1000 h ageing the effect of the mechanism is smoothed out so that 1.7Li1.2Mg0-0.6-1.2Cu alloys precipitate the same volume fraction of δ′ **(figure 12.11)**.

As the copper concentration increases from 1.2 to 2.0% the magnitude of the resistivity peak exhibits a slight increase and the resistivity peak is shifted to longer age times (~1 h) indicating the precipitation reaction kinetics of δ′ have slowed down. This change in behaviour may be the result of a change in precipitation mechanism, i.e. ≤1.2%Cu the dominant process is GPδ′ and ≥2.0Cu the dominant process is CLδ′. A possible reason for the slowing down of the

kinetics is that before CLδ′ can form, the Li-Cu-Mg clusters have to first develop and this takes a finite time.

Increasing the copper concentration beyond 2% (1.7Li1.2Mg3.0Cu alloy) results in a dramatic increase in resistivity indicating that significant stimulation of δ′ precipitation has happened producing a high number density of very fine δ′ particles.

In order to cast more light onto the effect of GPB zones and Li-Cu-Mg clusters on the nucleation and growth of δ′ during ageing at 70 °C, a 1.7Li1.2Mg3.0Cu alloy was aged for different times and subjected to DSC analysis. The DSC thermograms obtained (**figure 12.12**) were examined in conjunction with the isothermal resistivity plot of the 1.7Li1.2Mg3.0Cu alloy (**figure 12.13**). The DSC plots show that for ageing times up to 6 min (0.1 h) little or no δ′ forms during the age i.e. the size of exothermic peak I equals the total size of endothermal effects F (CLδ′) and L (GPδ′). However, the isothermal resistivity plot shows that a significant increase in resistivity has taken place in the same period of time. This could mean that Li-Cu-Mg clusters are making a positive contribution to resistivity in the early stages of ageing, or alternatively, the nucleation of δ′ in the early stages of ageing can only be detected by the more sensitive resistivity measurements. Ageing for times 20 min-16 h at 70°C cause the alloy to be fully precipitated, i.e. exotherm I disappears. At the same time, two strong endothermic peaks F and L are present corresponding to the dissolution of CLδ′

and GPδ′. As the ageing time increases from 20 min to 16 h the size of endotherm L is approximately constant but endotherm F (CLδ′) both increases in size and is displaced to a higher temperature. This indicated that the dominant event in 1.7Li1.2Mg3.0Cu alloy during the early stages of ageing at 70°C is development of CLδ′. Over this same period (20 min- 2 h) the resistivity passes through its maximum value showing that the CLδ′ has grown through the critical size of 2 nm. A further increase of ageing time to >16 h at 70°C causes overlapping of the endothermal effects F and L, and finally after 100 h they merge into a single endothermic event, peak K.

12.2.2 Age at 100°C

12.2.2.1 Investigation of low lithium alloys

Figure 12.14 exhibits DSC comparative thermograms of 1.3,1.7Li1.2Mg1.2,2.0Cu alloys. The addition of 1.3% Li to 1.2,2.0Cu1.2Mg alloys results in the development of endothermic peak K at about 210°C which is caused by dissolution of δ′. In addition, peak G shifts to a higher temperature suggesting that a coarser distribution of GPB zones has precipitated. This can be explained by lithium causing a decrease in the nucleation rate of GPB zones. Further increase of lithium concentration from 1.3% to 1.7% (1.7Li1.2Mg1.2,2.0Cu alloys) causes stimulation of δ′ precipitation as a consequence of the higher supersaturation of lithium.

The isothermal resistivity plots during ageing at 100°C are presented in **figure 12.15**. The addition of 1.3% lithium to 1.2Mg1.2Cu alloy leads to the formation of a resistivity peak after 2 h that is attributed to the formation of very fine δ′ of size smaller than the critical size for electron scattering. The same addition of lithium to 1.2Mg2.0Cu alloy (1.3Li1.2Mg2.0Cu alloy) also produces a resistivity peak but at earlier times (0.4 h) showing that the reaction kinetics of δ′ are much faster in the 1.3Li1.2Mg2.0Cu alloy compared to 1.3Li1.2Mg1.2Cu alloy. It is believed that the higher copper concentration causes a significant increase in the concentration of GPB zones and Li-Cu-Mg clusters which in turn stimulate the formation of δ′. Higher levels of lithium (1.7Li1.2Mg1.2,2.0Cu alloys) result in an additional shift of the resistivity peak to earlier ageing times showing that further enhancement of δ′ precipitation has occurred due to the increased supersaturation of lithium.

12.2.2.2 Investigation of 1.7Li1.2MgXCu alloys

The DSC comparative plots of 1.7Li1.2MgXCu alloys are given in **figure 12.16**. The 1.7Li1.2Mg0.0Cu alloy exhibits an endothermic peak, peak K, at about 200°C due to the dissolution of δ′. As the copper concentration increases from 0.0% to 0.6%, the endothermic peak K is followed by two small overlapping endothermal effects that are caused by the dissolution of GPB zones and S″. Increasing copper concentration from 0.6% to 3.0% (1.7Li1.2Mg1.2,2.0,3.0Cu alloys) results in enlargement of the endotherm K. By measuring the area of

endotherm K and subtracting the effect of GPB zones and S″, the enthalpy corresponding to the dissolution of δ′ was estimated. Then, by using equation 8.2, the δ′ volume fraction that precipitates in each alloy was calculated. The data obtained are plotted as a function of copper concentration in **figure 12.17.** It can be seen that for copper concentrations up to 1.2% no changes in the volume fraction of δ′ occur in the 1.7Li1.2MgXCu alloys. However, as the copper concentration increases from 1.2% to 3.0% significant stimulation of δ′ precipitation takes place leading to a larger volume fraction of δ′. This can be explained by the formation of a larger number of GPB zones and Li-Cu-Mg clusters that causes significant enhancement in the nucleation rate of δ′. Finally, comparison between the δ′ volume fraction plots of 1.7Li1.2MgXCu and 1.7LiXCu alloys indicates that over the concentration range 0.0-1.2% the presence of 1.2%Mg in 1.7Li1.2MgXCu alloys produces only a small increase in the amount of δ′ precipitated. However, as the copper concentration reaches 3.0% the presence of 1.2%Mg results in significant stimulation of δ′.

The isothermal resistivity plots of 1.7Li1.2MgXCu alloys during ageing at 100°C **(figure 12.18)** exhibit trends very similar to those during ageing at 70°C.

The 1.7Li1.2Mg0.0Cu alloy exhibits an initial increase of resistivity followed by a decrease below the baseline, suggesting nucleation ordering followed by spinodal decomposition. As the copper concentration increases from 0.0 to 1.2% (1.7Li1.2Mg0.6,1.2Cu alloys) the initial resistivity peak becomes larger and is

attained at earlier ageing times. This behaviour suggests that stimulation of δ′ precipitation has taken place together with enhanced kinetics. Knowing that for copper concentrations ≤1.2% the copper atoms are consumed in the nucleation and growth of GPB zones, thus making very difficult the formation of Li-Cu-Mg clusters, the above enhancement of the reaction kinetics of δ′ precipitation is probably caused by a larger number of GPB zones that accelerate the nucleation rate of δ′ producing a finer dispersion of δ′ (GPδ′).

For copper concentration higher than 1.2% (1.7Li1.2Mg2.0-3.0Cu alloys) the resistivity exhibits a significant increase and shifts to longer ageing times. As already discussed in the last section this change of the resistivity behaviour can be attributed to CLδ′ that now is the dominant mechanism for δ′ precipitation.

It can be concluded that during ageing at 100°C the dominant mechanism for δ′ precipitation is GPδ′ for copper concentrations ≤1.2%, whereas for copper concentrations >1.2% the dominant mechanism is CLδ′.

12.2.3 Age at 150°C

12.2.3.1 Investigation of low lithium alloys

DSC comparative plots of 1.3,1.7Li1.2Mg1.2,2.0Cu alloys after ageing for 24 h at 150°C are shown in **figure 12.19**. The addition of 1.3% lithium to 1.2Mg1.2,2.0Cu alloys causes a minimal increase in the area of the endotherm G showing that only a very small amount of δ′ has formed. This is the result of the

very small driving force for δ′ precipitation as the 1.3% Li composition lies very close to the δ′ metastable solvus line. Increasing the lithium concentration to 1.7% causes considerable enlargement of the endotherm (designated K because of the presence of δ′) as a result of the higher supersaturation of lithium.

The isothermal resistivity plots (**figure 12.20**) show some interesting trends:

- In the 1.2Mg1.2Cu alloy the resistivity follows a plateau up to 300 h ageing and this is due to the formation of GPB zones.
- Addition of 1.3Li to the 1.2Mg1.2Cu alloy increases the level of the plateau due to the presence of both fine δ′ and GPB zones. The plateau also ends at an earlier time (80 h) due to the onset of δ′ growth which more than outweighs the positive resistivity contribution from GPB zones.
- Addition of 1.7Li to the 1.2Cu1.2Mg alloy does <u>not</u> increase the level of the plateau observed in the 1.3Li1.2Cu1.2Mg alloy and the plateau ends at a very short ageing time (<0.1 h). This suggests that the increased driving force for δ′ precipitation (due to the higher lithium concentration) causes δ′ to form on GPB zones. If it is assumed that the GPB zones are already at the critical size for electron scattering (reasonable, since the resistivity does not increase beyond the plateau) then the additional shell of δ′ around the GPB zones will cause the resistivity to fall; i.e. the behaviour observed in **figure 12.20**.
- A similar trend is observed in the 0, 1.3, 1.7Li1.2Mg2.0Cu alloys, although here the plateau in the 1.7Li1.2Mg2.0Cu alloy ends at 1 h, i.e. a

larger ageing time that that observed in the 1.7Li1.2Mg1.2Cu alloy (<0.1h).

12.2.3.2 Investigation of 1.7Li1.2MgXCu alloys

The DSC comparative plots of 1.7Li1.2MgXCu alloys are illustrated in **figure 12.21**. As has already been discussed in chapter 8 the endothermic peak K that appears in the DSC plot of 1.7Li1.2Mg0.0Mg alloy is due to the dissolution of δ′. Increasing copper concentration from 0.0% to 3.0% results in an increase in the magnitude of the endotherm. In a way similar to that described in the previous sections the enthalpy associated with the dissolution of δ′ was measured by subtracting the contribution of GPB zones and S″ from the whole endotherm. Then, by applying equation 8.2 the volume fraction of δ′ was calculated and plotted as a function of the copper concentration (**figure 12.22**). It can be seen for copper concentrations up to 1.2% the volume fraction of δ′ in 1.7Li1.2MgXCu alloys does not exhibit any changes. Increasing the copper concentration beyond 1.2% (1.7Li1.2Mg2.0,3.0Cu alloys) produces a moderate increase in the volume fraction of δ′. It is believed that for copper concentrations higher than 1.2% a larger number of GPB zones form that result in a higher rate δ′ nucleation.

The isothermal resistivity plots of the above alloys are given in **figure 12.23**. The 1.7Li1.2Mg0.0,0.6Cu alloys show a well defined incubation period which is

followed by a decrease in resistivity indicating that the mechanism of δ′ precipitation is a nucleation and growth process. The fact that there is no increase in resistivity suggests that the critical size for nucleation is greater than the critical size for electron scattering. Increasing the copper concentration from 0.6 to 3.0% (1.7Li1.2Mg1.2,2.0,3.0Cu alloys) initially causes a resistivity increase that is attributed to the formation of an increasing number-density of GPB zones that can scatter the conduction electrons. The trend in these higher copper alloys is for the resistivity to initially follow a plateau, suggesting that GPB zones have formed early in the ageing cycle. The plateau ends after 1-2 h of ageing, i.e. much earlier than in the Li-free alloys which suggests that δ′ commences to grow on the GPB zones.

12.3 Effect of ageing temperature

In **figures 12.24-12.28** are shown the DSC thermograms of 1.7Li1.2MgXCu alloys after ageing at different temperatures. From these plots the volume fraction of δ′ was calculated and plotted as a function of the ageing temperature for each alloy (**figure 12.29**). It can be seen that for all the alloys the maximum volume fraction of δ′ is formed after ageing for 1000 h at 100°C. Thermodynamically, it would be expected that the amount of δ′ would increase as the ageing temperature decreases from 150°C to 100°C to 70°C. However, the diffusivity becomes lower as the temperature drops, so that the precipitation of δ′ is limited by kinetic considerations. The DSC results also show that for all the

alloys the size of δ′ increases with increasing ageing temperature i.e. the position of endothermic peak K shifts to higher temperatures (**figure 12.30**). This is expected from theory since the smaller undercooling and higher diffusivity at higher ageing temperatures results in a coarser precipitate dispersion.

The isothermal resistivity plots of 1.7Li1.2Mg0-0.6Cu alloys (**figures 12.31,12.32**) show that the increase of ageing temperature not only causes a dramatic decrease in resistivity but also changes the mechanism of δ′ precipitation from nucleation ordering to classical nucleation and growth, i.e. a well defined incubation period is present at an ageing temperature of 150°C.

Increasing the copper concentration to 1.2% (**figure 12.33**) causes the incubation period to be replaced by a resistivity plateau in the early stages of ageing over the period 0-1 h. This plateau is likely to be caused by development of GPB zones. Once formed, δ′ forms on these GPB zones and causes the resistivity to fall after ageing for ~1 h at 150°C. Evidence for this mechanism comes from comparing the resistivity trace of the 1.7Li1.2Mg1.2Cu alloy at 150°C with the trace from the lithium-free alloy (1.2Mg1.2Cu) where the resistivity at 150°C remains at a plateau for 200 h, before decreasing (**figure 12.20**). In this later case, of course, there is no δ′ growing on the GPB zones i.e. the resistivity does not decrease until long ageing times are attained.

The 1.7Li1.2Mg2.0,3.0Cu (**figures 12.34, 12.35**) alloys follow similar trends at

150°C but in these alloys the resistivity changes at 70 and 100°C are also interesting. At 70 and 100°C the resistivity clearly increases during the early stages of ageing suggesting that Li-Cu-Mg clusters are forming and developing into δ′ (i.e. CLδ′). However at 150°C the resistivity follows a plateau and then decreases, indicating that δ′ is growing on GPB zones (i.e. GPδ′). These observations suggest that at high copper supersaturations in Al1.7Li1.2Mg3.0Cu alloys the mechanism of δ′ formation is CLδ′, whereas at low copper supersaturations the mechanism of δ′ formation is GPδ′.

12.4 Exposure at 70°C after prior ageing at 150°C for 24 h

It is well known that Al-Li-Cu-Mg alloys undergo a significant embrittlement when exposed for a long period at 70°C after a prior standard age of 24 h at 150°C. This work examines the effect of copper concentration on the precipitation and embrittlement characteristics of 1.7Li1.2MgXCu alloys during exposure at 70°C.

Figures 12.36-12.40 give the DSC comparative thermograms after ageing for 24 h at 150°C and after subsequently exposing for 1000 h at 70°C for each of the 1.7Li1.2MgXCu alloys. In order to estimate the volume fraction of δ′ formed during exposure, the area of endotherm K developed after ageing 150°C/24h was subtracted from the area of endotherm K after subsequent exposure for 1000 h at 70°C. By using equation 8.2 the δ′ volume fraction forming during exposure was calculated and plotted versus copper concentration (**figure 12.41**). It can be easily seen that as the copper concentration increases from 0% to 1.2% the

volume fraction of δ′ precipitated during exposure at 70°C is increased. However, increasing the copper concentration beyond 1.2% causes the volume fraction of δ′ to start decreasing. Practically no δ′ has precipitated during exposure when the copper concentration reaches 3.0% (1.7Li1.2Mg3.0Cu alloy). Taking into consideration the results of paragraph 12.2.3.2 according to which increasing copper concentration to levels higher than 1.2% caused an increase in the volume fraction of δ′ precipitated after ageing 150°C/24 h, it is postulated that a possible reason for the decrease in δ′ volume fraction during exposure for copper >1.2% is the lower supersaturation of lithium in the matrix after the pre-age at 150°C.

The isothermal resistivity plots (**figure 12.42**) indicate that the largest drop of resistivity is observed for the 1.7Li1.2Mg1.2Cu alloy, which is in good agreement with the DSC results. The question that comes up at this point is why the volume fraction of δ′ precipitated during exposure in 1.7Li1.2Mg0,0.6Cu alloys is not similar to the volume fraction produced in 1.7Li1.2Mg1.2Cu alloy, since it is known (**figure 12.29**) that after ageing 24 h at 150°C the volume fraction of δ′ is similar in all these three alloys. It is surmised that the stimulation of δ′ by Li-Cu-Mg clusters and GPB zones carries on during exposure and that this effect becomes stronger as copper concentration increases from 0 to 1.2%.

The above results on exposure heat treatment have suggested that the maximum amount of δ′ is precipitated during exposure in the 1.7Li1.2Mg1.2Cu alloy. This

alloy should therefore show maximum embrittlement during exposure. This hypothesis is now be tested by measuring the proof stress and fracture energy after exposure of the 1.7Li1.2CuXCu alloys for 1000 h at 70°C.

12.5 Effect of exposure on the mechanical properties of 1.7Li1.2MgXCu alloys

The proof stress and fracture energy changes of the 1.7Li1.2MgXCu alloys after exposure for 1000 h at 70°C are presented in **figure 12.43**. Increasing the copper concentration from 0.0 to 1.2% causes the proof stress to exhibit a significant increase and the fracture energy to decrease. For copper levels higher than 1.2% (1.7Li1.2Mg2.0,3.0Cu alloys) the mechanical behaviour reverses i.e. the proof stress starts decreasing and the alloys exhibit a significantly improved fracture energy. The above are in perfect agreement with the DSC results presented in the last section where it was shown that the 1.7Li1.2Cu1.2Mg alloy produces the largest volume fraction of δ′ during exposure, and therefore this alloy would be expected to show the maximum embrittlement.

Summary

From the above investigation the following points have emerged:

- Isothermal ageing of 1.7Li1.2MgXCu alloys at 70, 100, and 150°C results in the formation of mixtures of δ′ and GPB zones.

- For all the alloys the maximum volume fraction of δ′ is formed at 100°C where there is an optimum combination of thermodynamics and kinetics.
- At low lithium supersaturations the mechanism of δ′ precipitation during isothermal ageing is the growth of δ′ on GPB zones (GPδ′).

  At high lithium supersaturations the mechanism of δ′ precipitation during isothermal ageing is the formation of Li-Cu-Mg clusters which subsequently develop into δ′(CLδ′).
- For alloys with low copper concentrations (0%<Cu≤1.2%)aged at 70°C and 100°C, GPδ′ formation is the dominant process.

  For alloys with high copper concentrations (1.2%<Cu≤3.0%) aged at 70°C and 100°C, CLδ′ formation is the dominant process.
- For alloys with low copper concentrations (Cu≤0.6%) aged at 150°C, classical nucleation and growth of δ′ takes place.

  For alloys with high copper concentrations (Cu>0.6%) aged at 150°C, GPδ′ formation is the dominant process.
- Maximum exposure embrittlement at 70°C is observed to occur in the 1.7Li1.2Mg1.2Cu alloy. Smaller or larger concentrations of copper in the alloy result in less δ′ being formed during exposure and therefore less embrittlement.

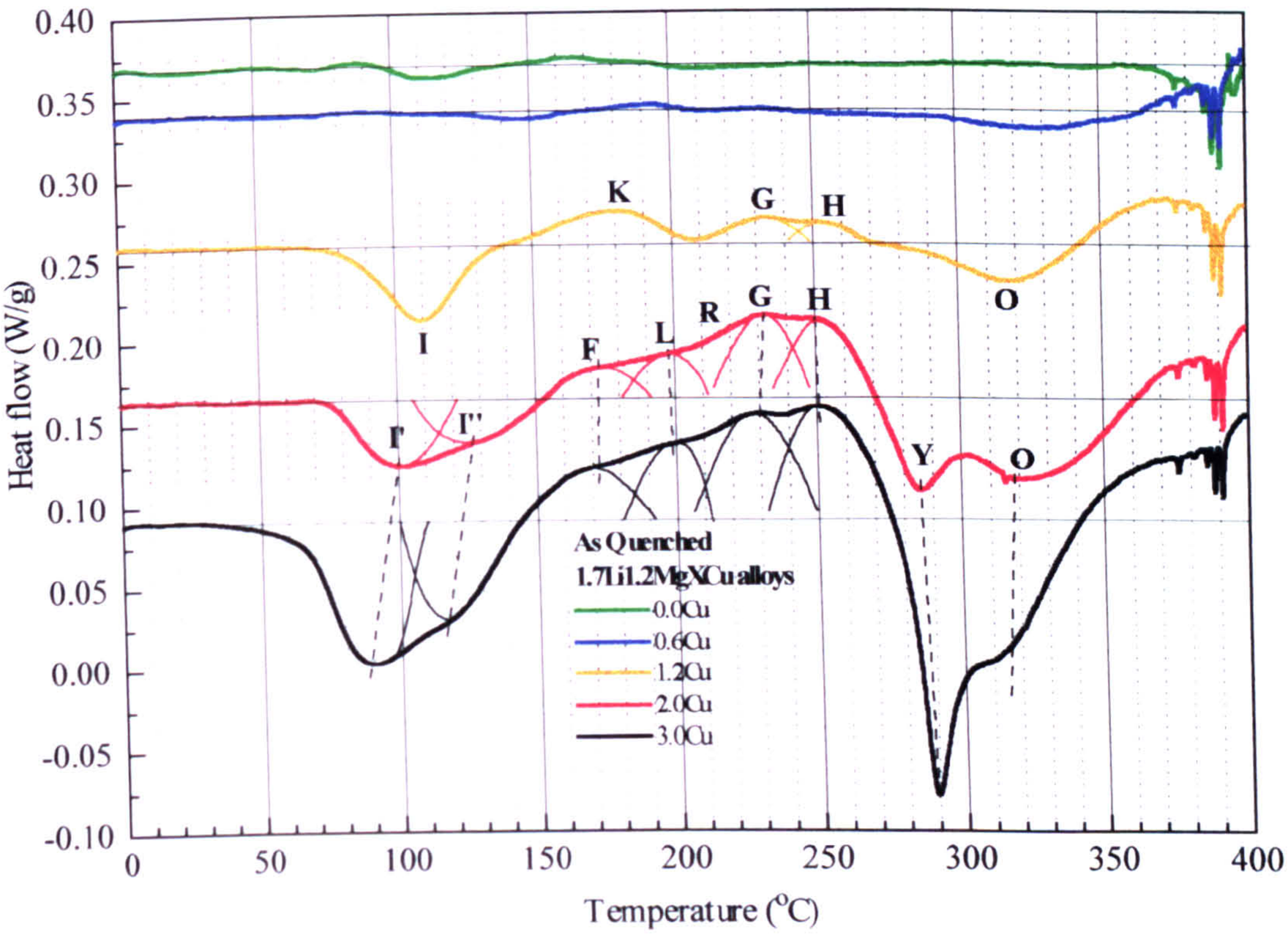

Figure 12.1: Comparative DSC plots of the as-quenched 1.7Li1.2MgXCu alloys.

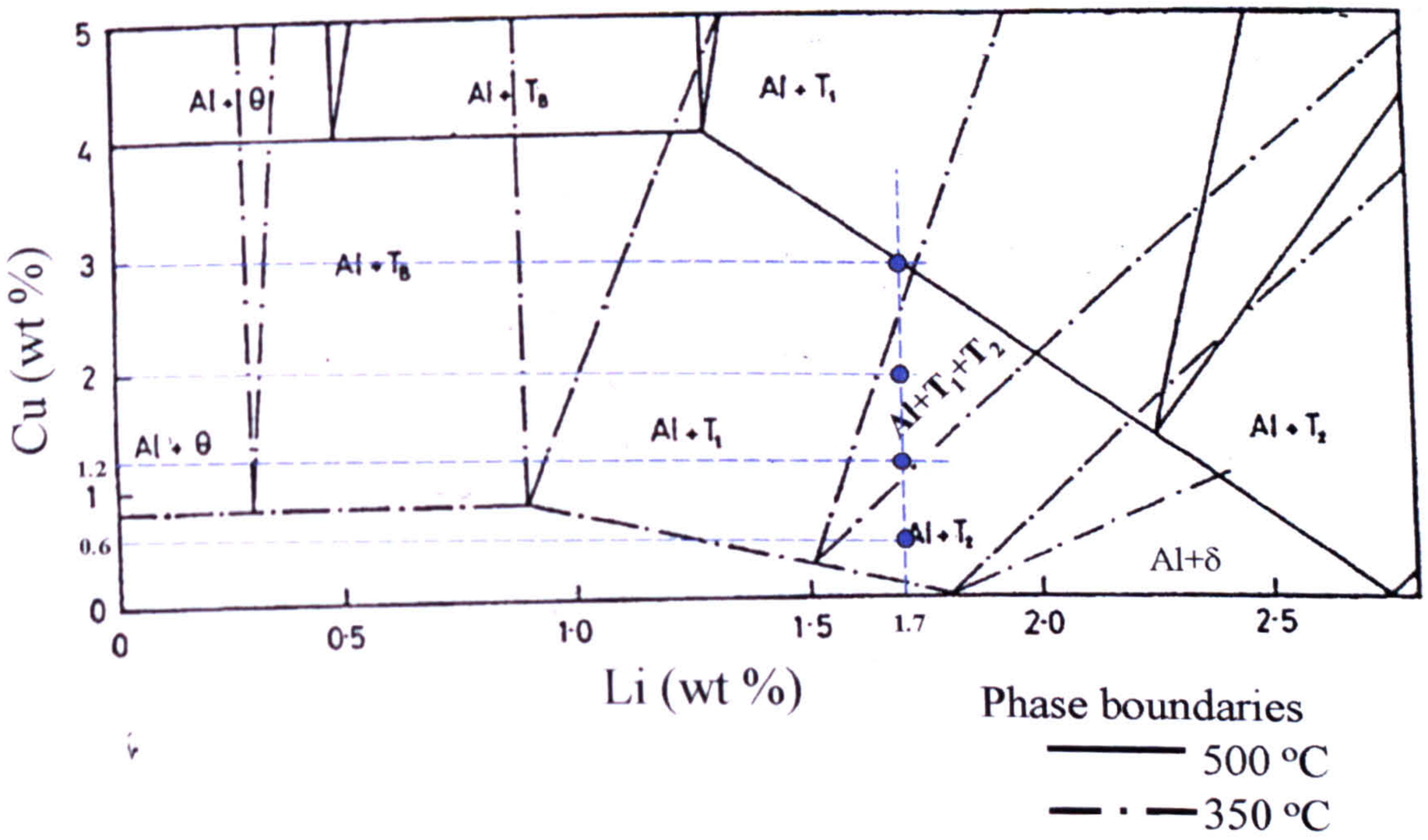

Figure 12.2: Isothermal section of the ternary Al-Li-Cu system at 350°C and 500°C.

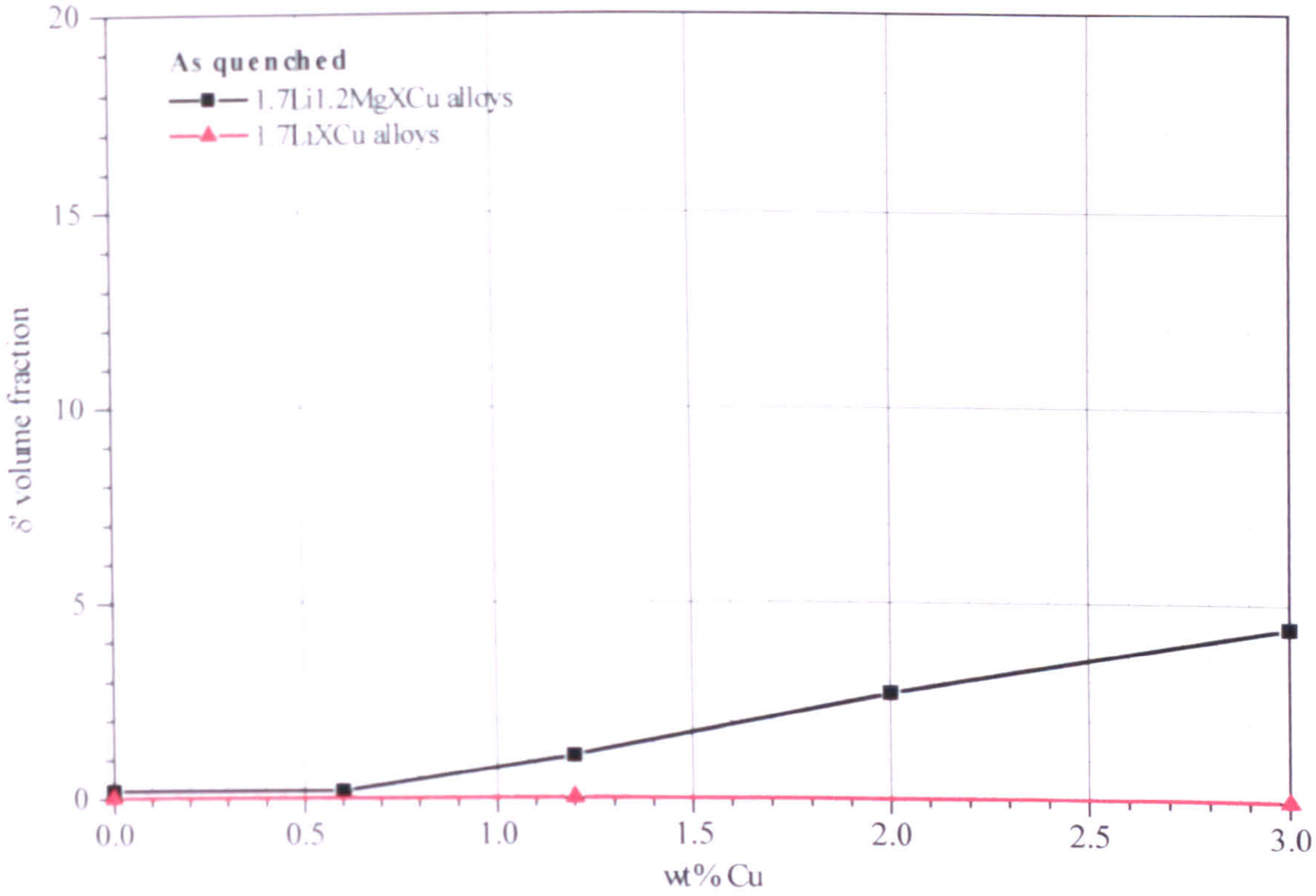

Figure 12.3: Volume fraction of δ′ produced during DSC heating of the as-quenched 1.7Li1.2MgXCu alloys.

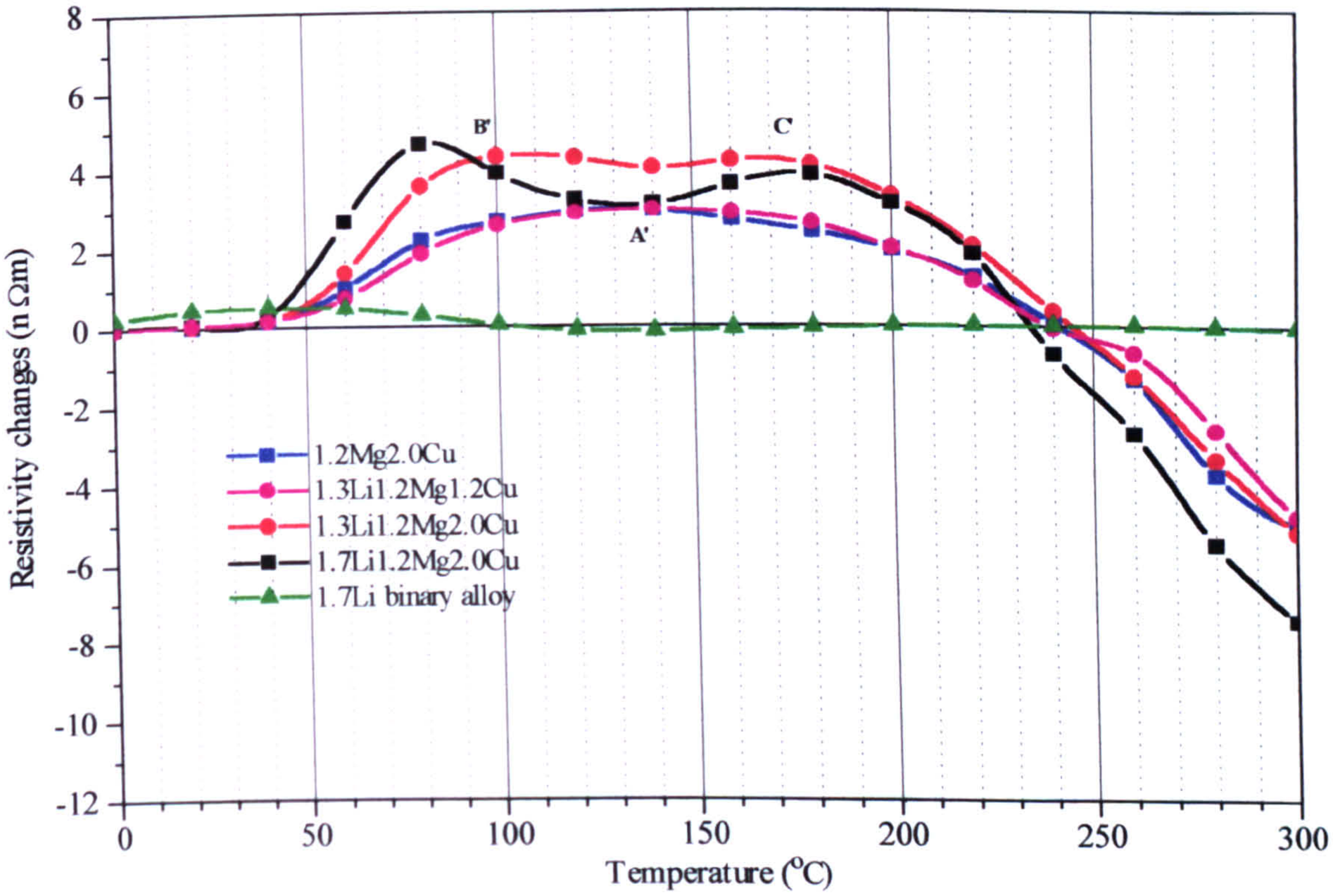

Figure 12.4: Comparative isochronal resistivity plots of 1.7Li binary, 1.2Mg2.0Cu, 1.31.2Mg1.2Cu, 1.3Li1.2Mg2.0Cu, and 1.7Li1.2Mg2.0Cu alloys.

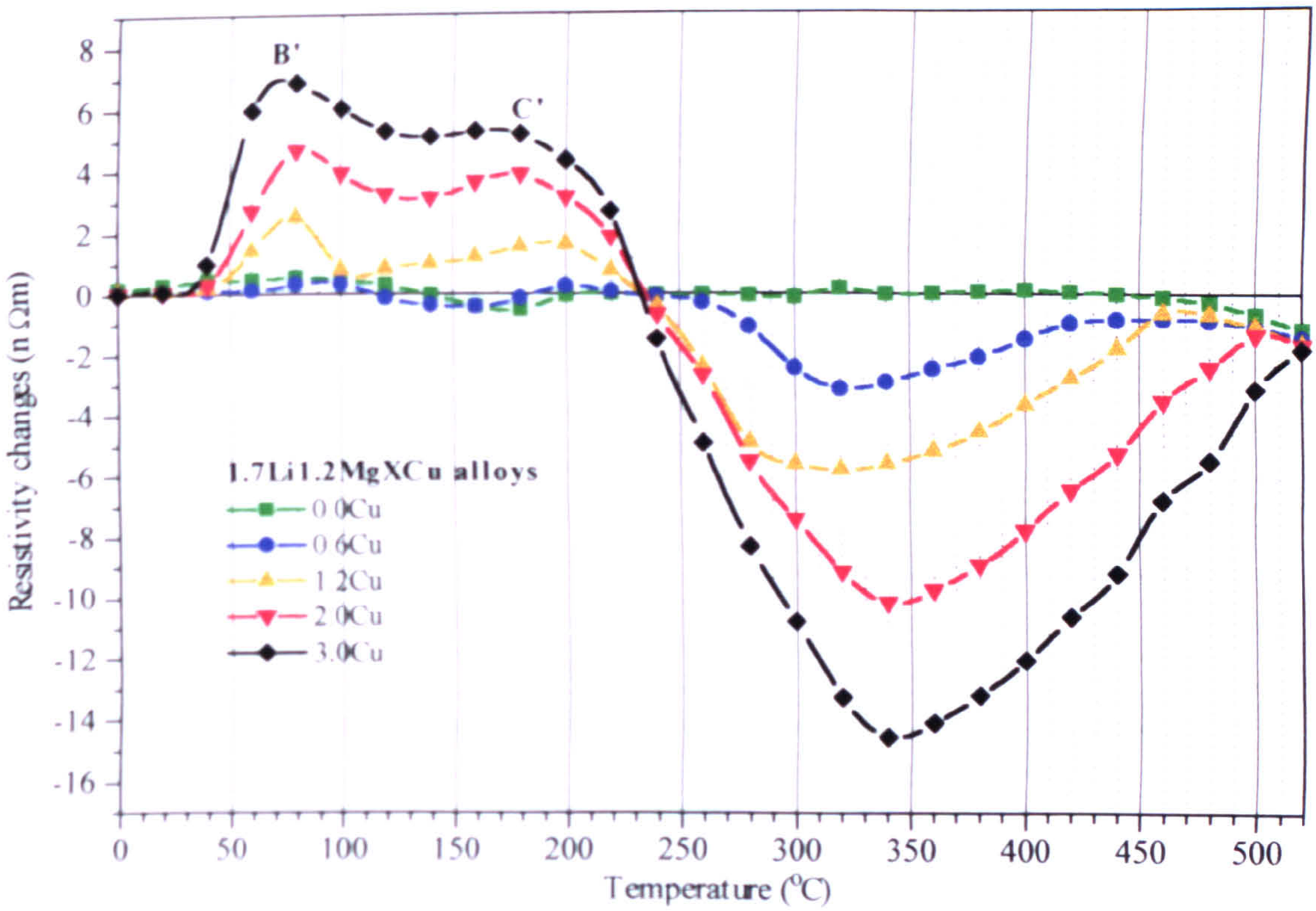

Figure 12.5: Comparative isochronal plots of 1.7Li1.2MgXCu alloys.

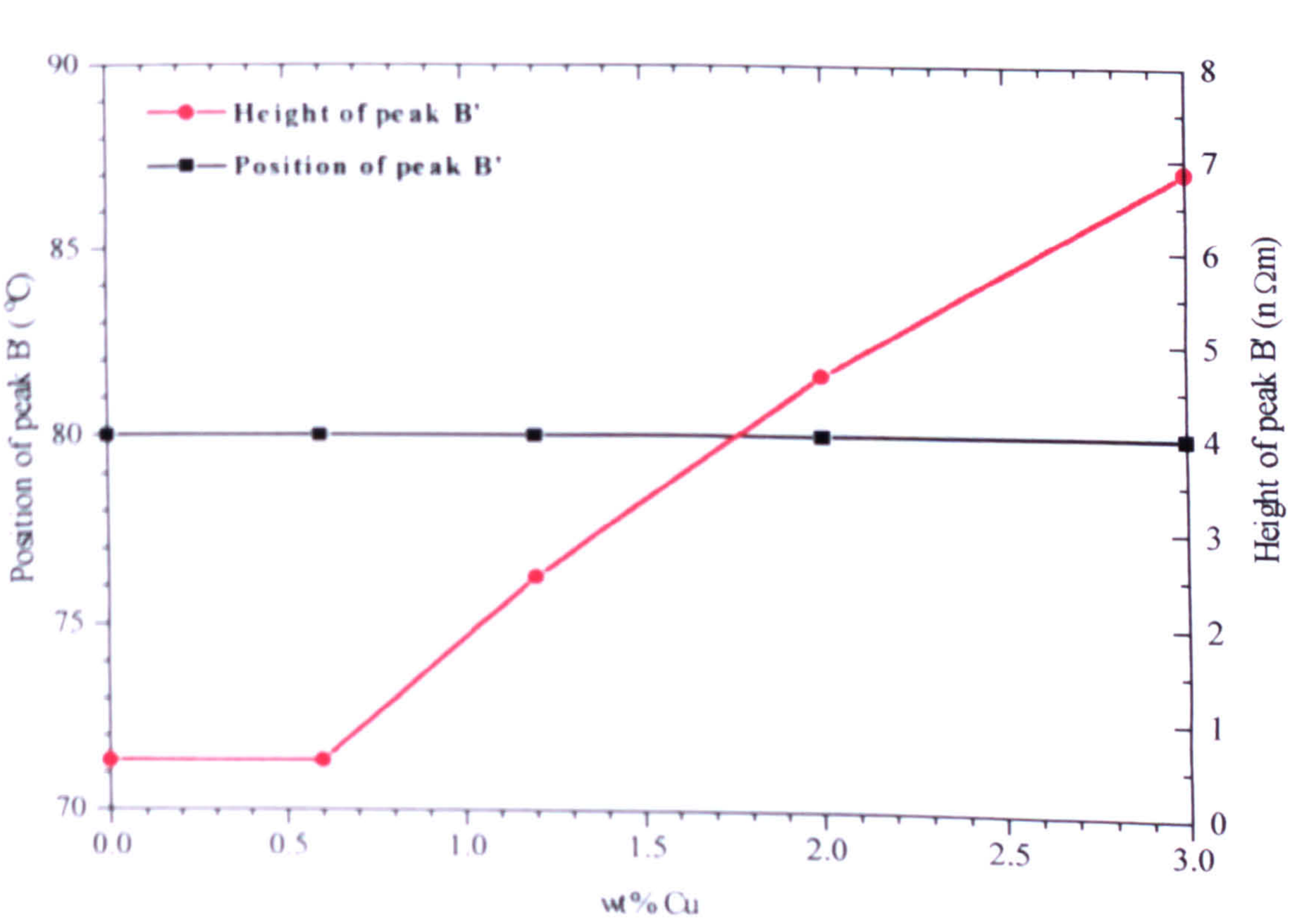

Figure 12.6: Height and position of isochronal resistivity peak B′.

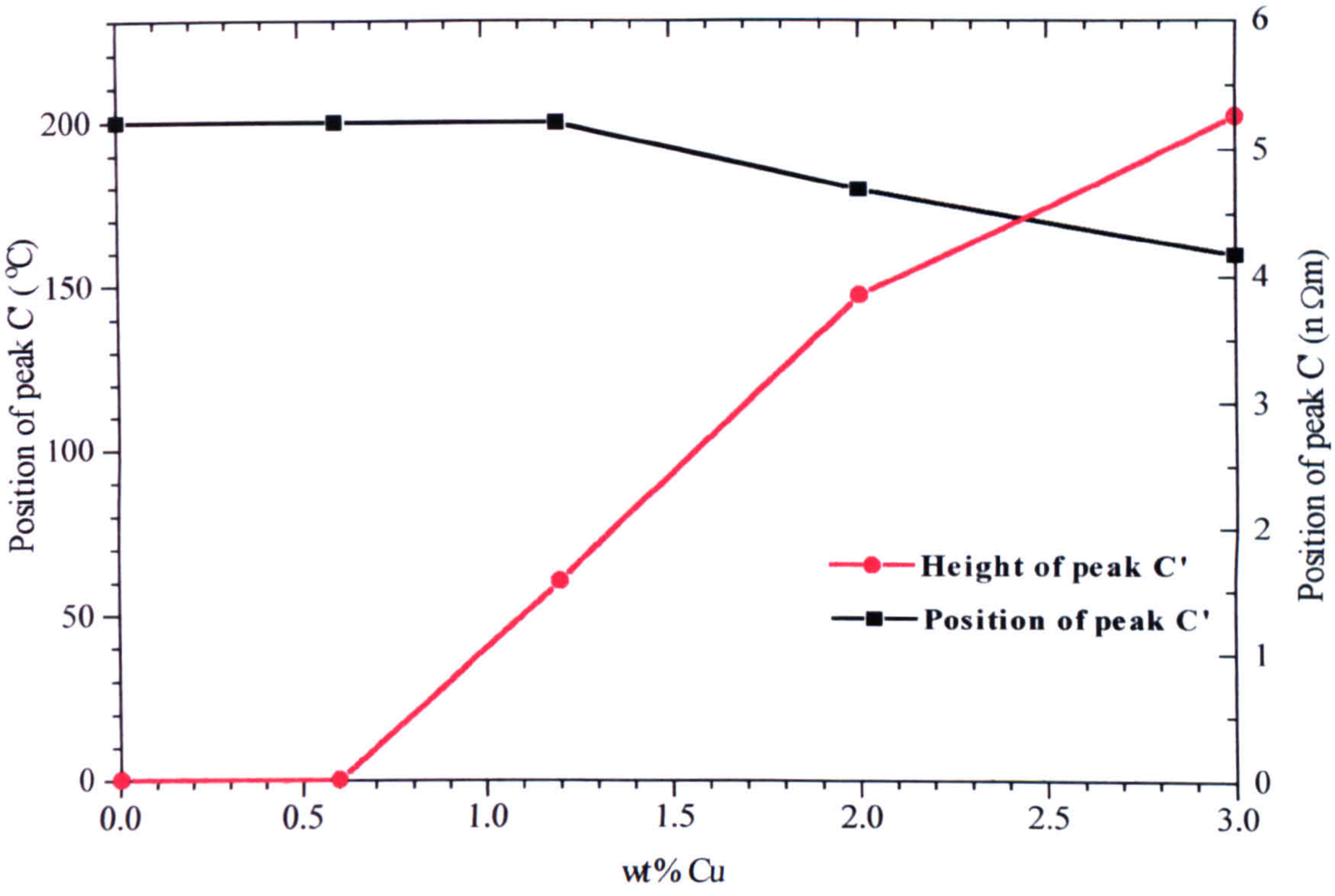

Figure 12.7: Height and position of isochronal resistivity peak C′.

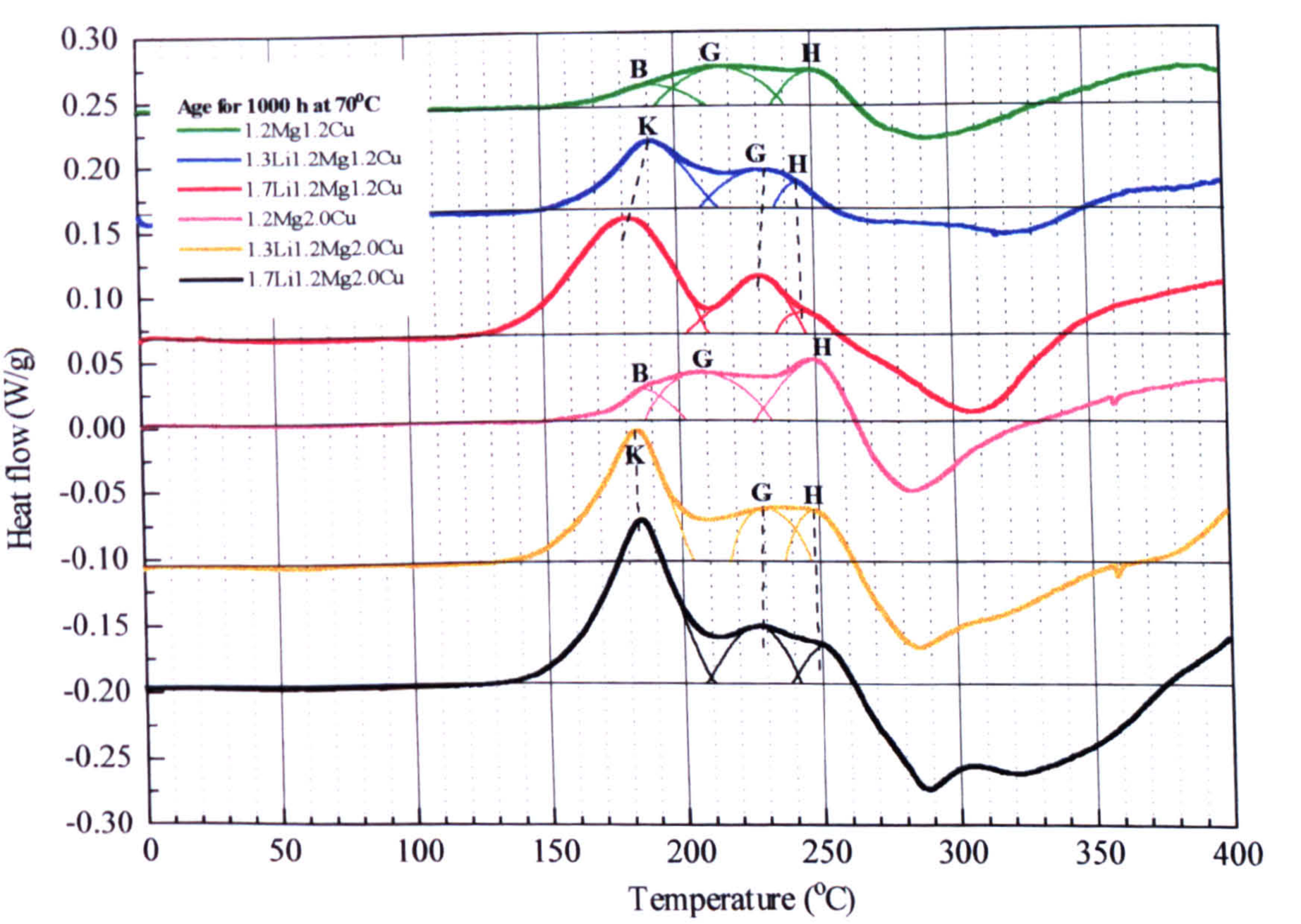

Figure 12.8: Comparative DSC plots of 1.2Mg1.2Cu and 1.2Mg2.0Cu alloys with lithium additions of 1.3% and 1.7% after ageing for 1000 h at 70°C.

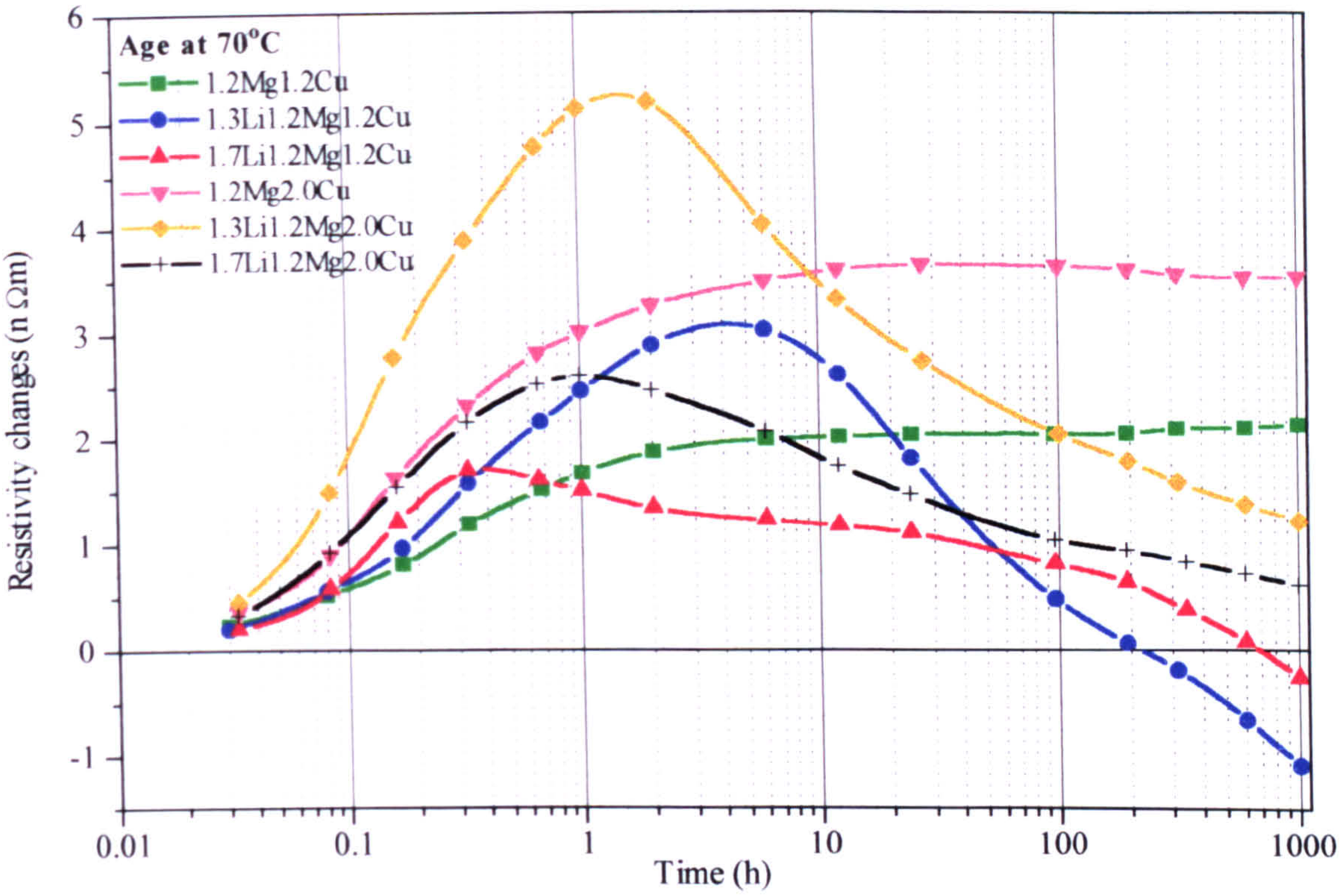

Figure 12.9: Comparative isothermal resistivity plots of 1.2Mg1.2Cu and 1.2Mg2.0Cu alloys with lithium additions of 1.3% and 1.7% during ageing at 70°C.

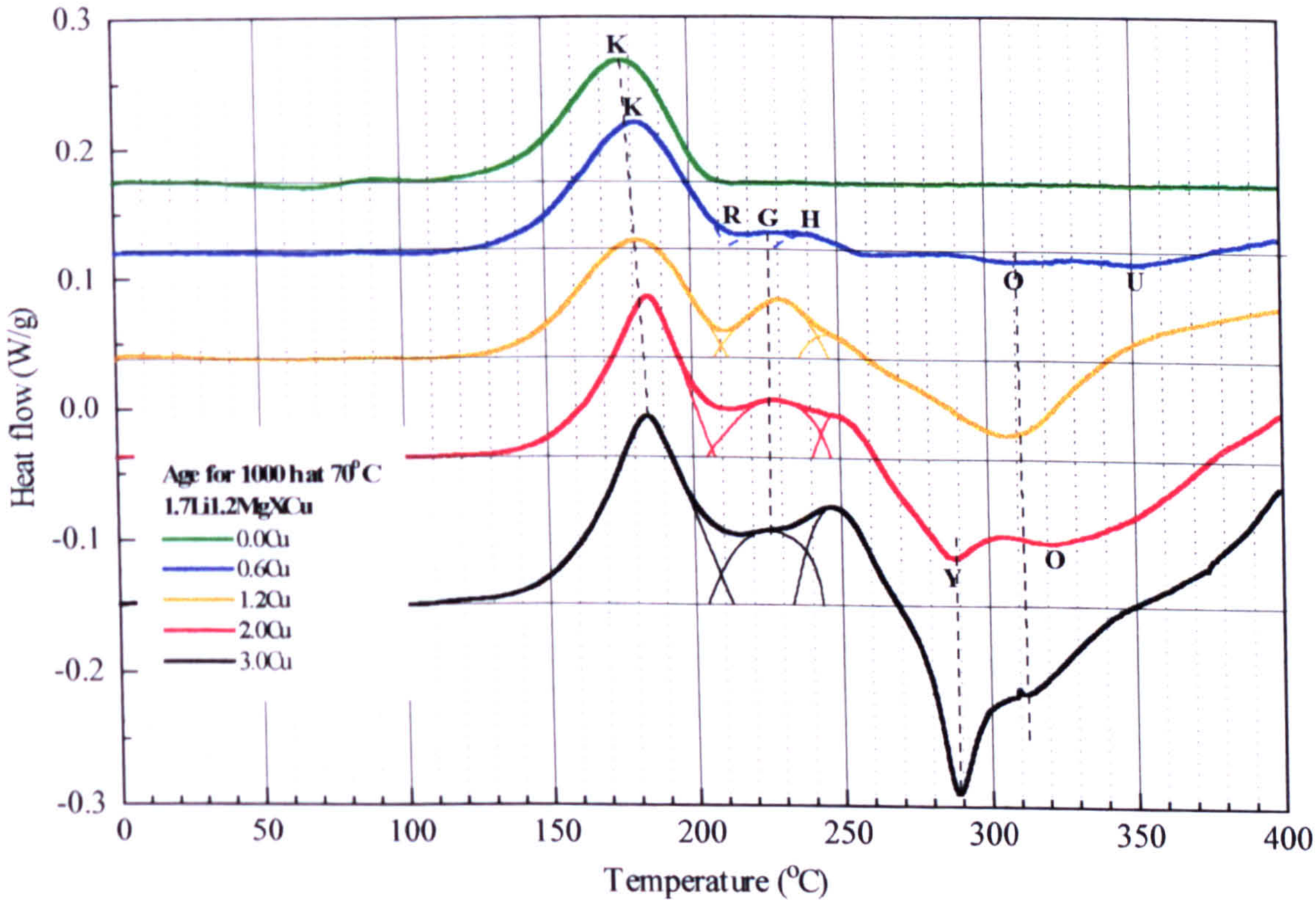

Figure 12.10: Comparative DSC plots of 1.7Li1.2MgXCu alloys after ageing for 1000h at 70°C.

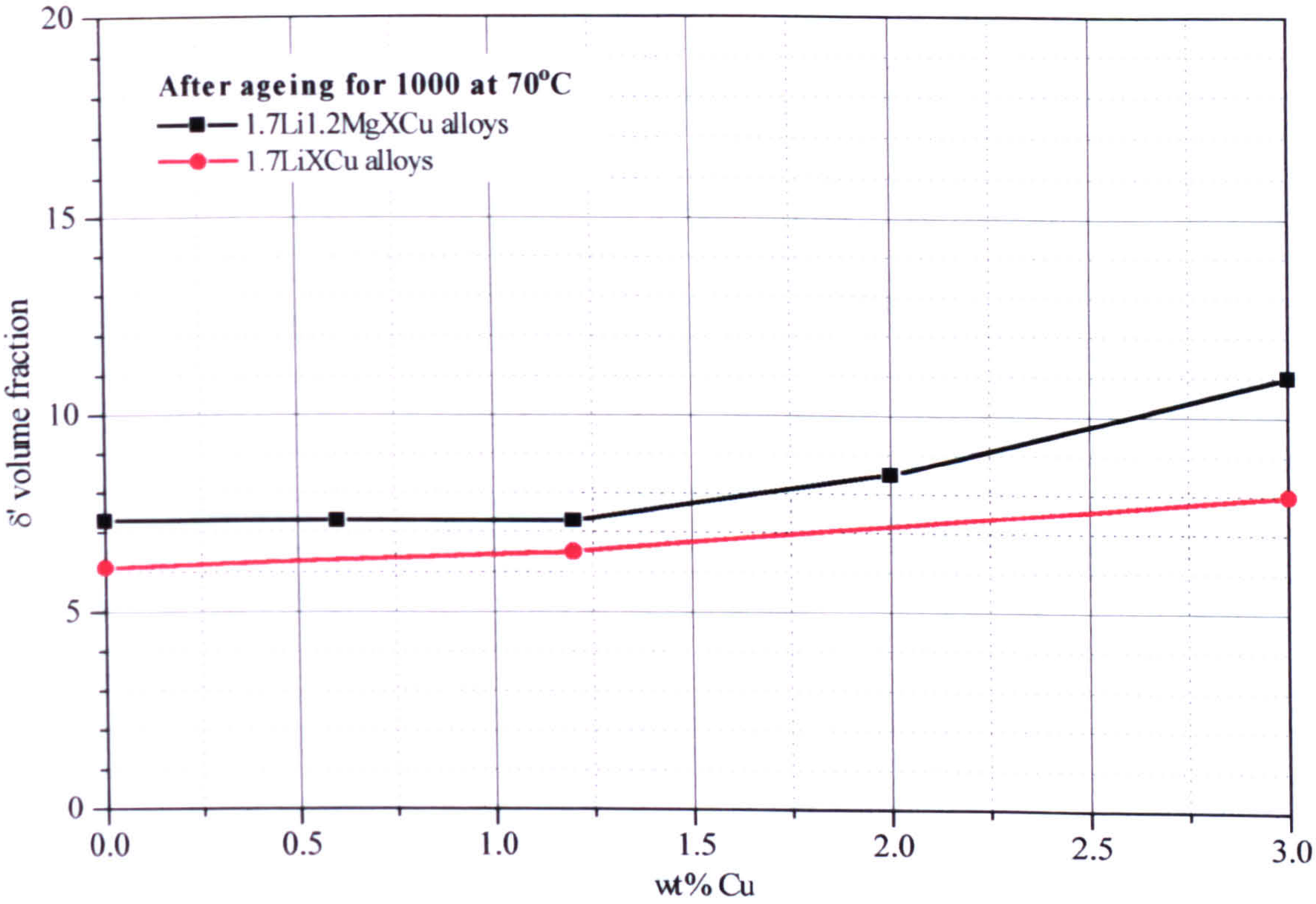

Figure 12.11: δ′ volume fraction produced in 1.7Li1.2MgXCu and 1.7LiXCu alloys after ageing for 1000 h at 70°C.

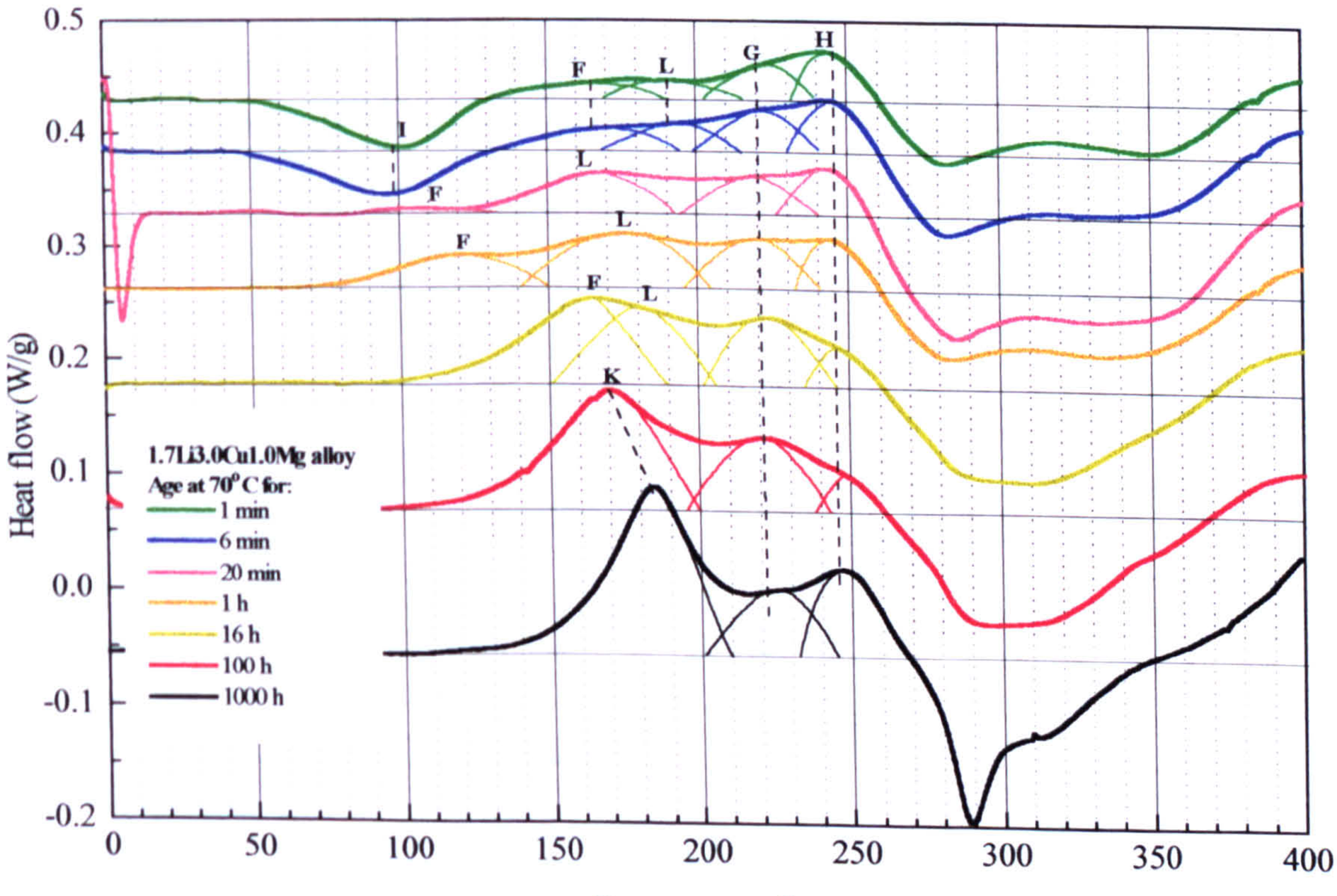

Figure 12.12: DSC plots of a 1.7Li3.0Cu1.0Mg alloy after ageing for different times at 70°C.

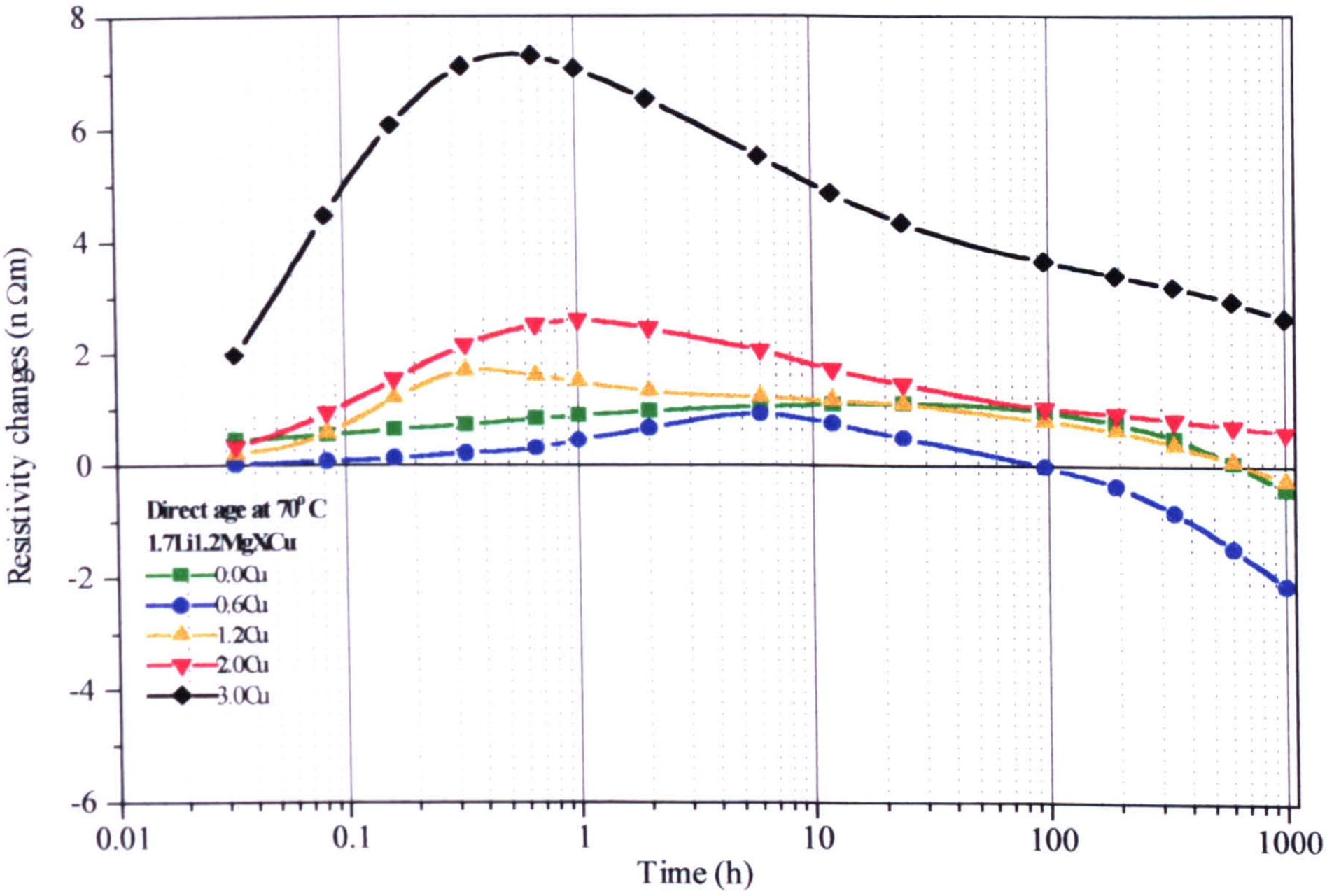

Figure 12.13: Isothermal resistivity changes of 1.7Li1.2Mg XCu alloys during ageing at 70°C.

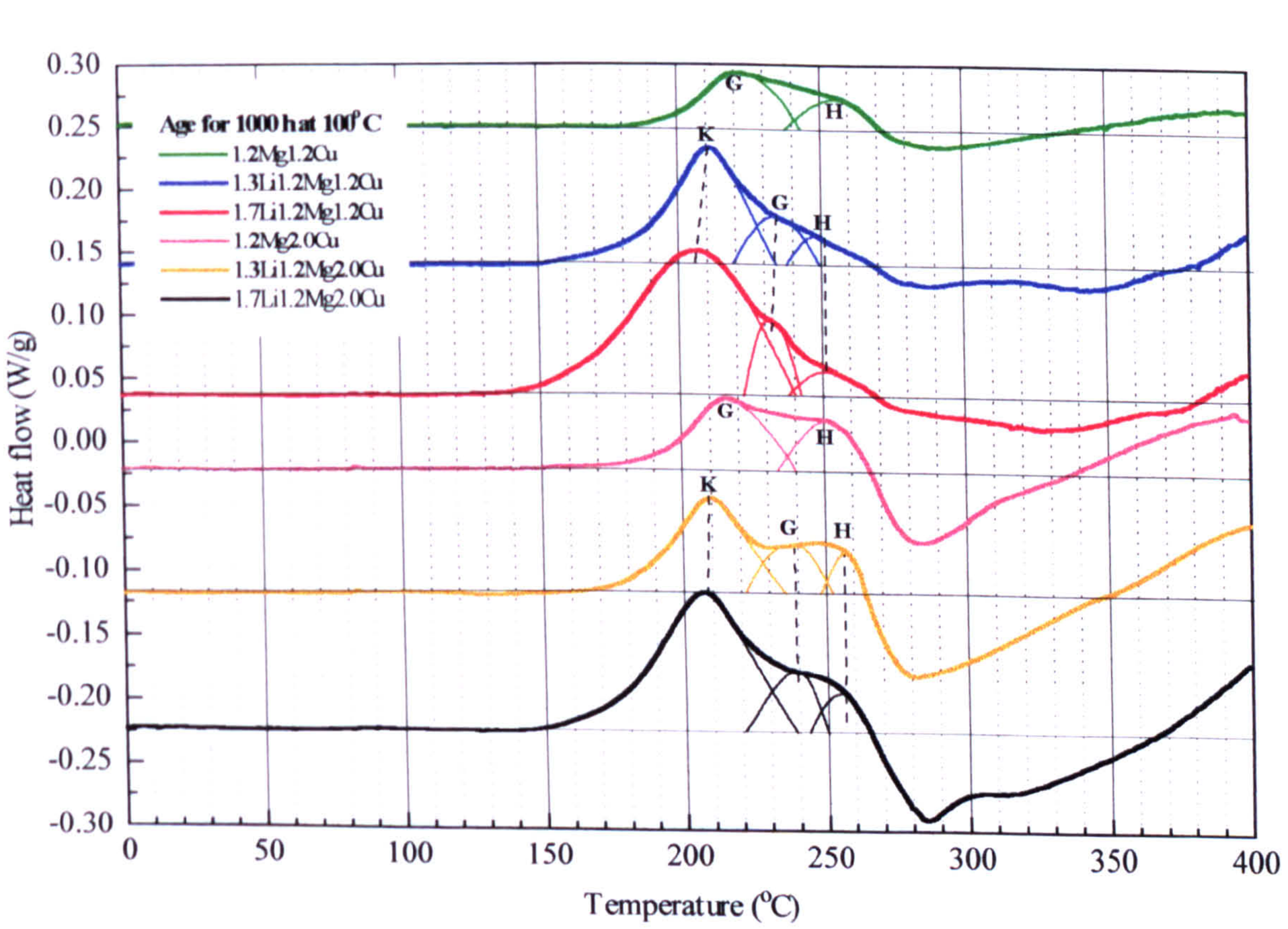

Figure 12.14: Comparative DSC plots of 1.2Mg1.2Cu and 1.2Mg2.0Cu alloys with lithium additions of 1.3 and 1.7% after ageing for 1000 h at 100°C.

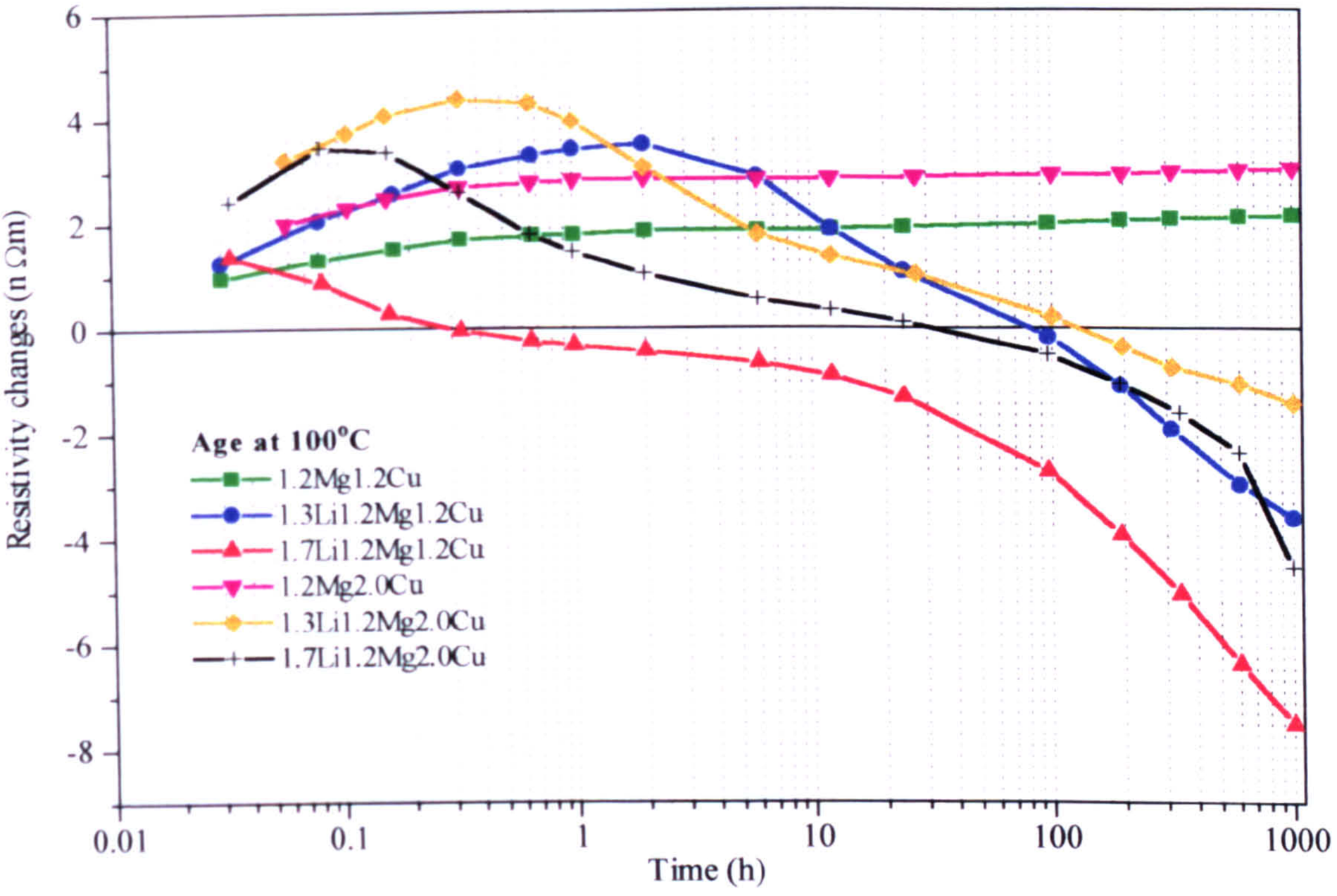

Figure 12.15: Comparative isothermal resistivity plots of 1.2Mg1.2Cu and 1.2Mg2.0Cu alloys with lithium additions of 1.3% and 1.7% during ageing at 100°C.

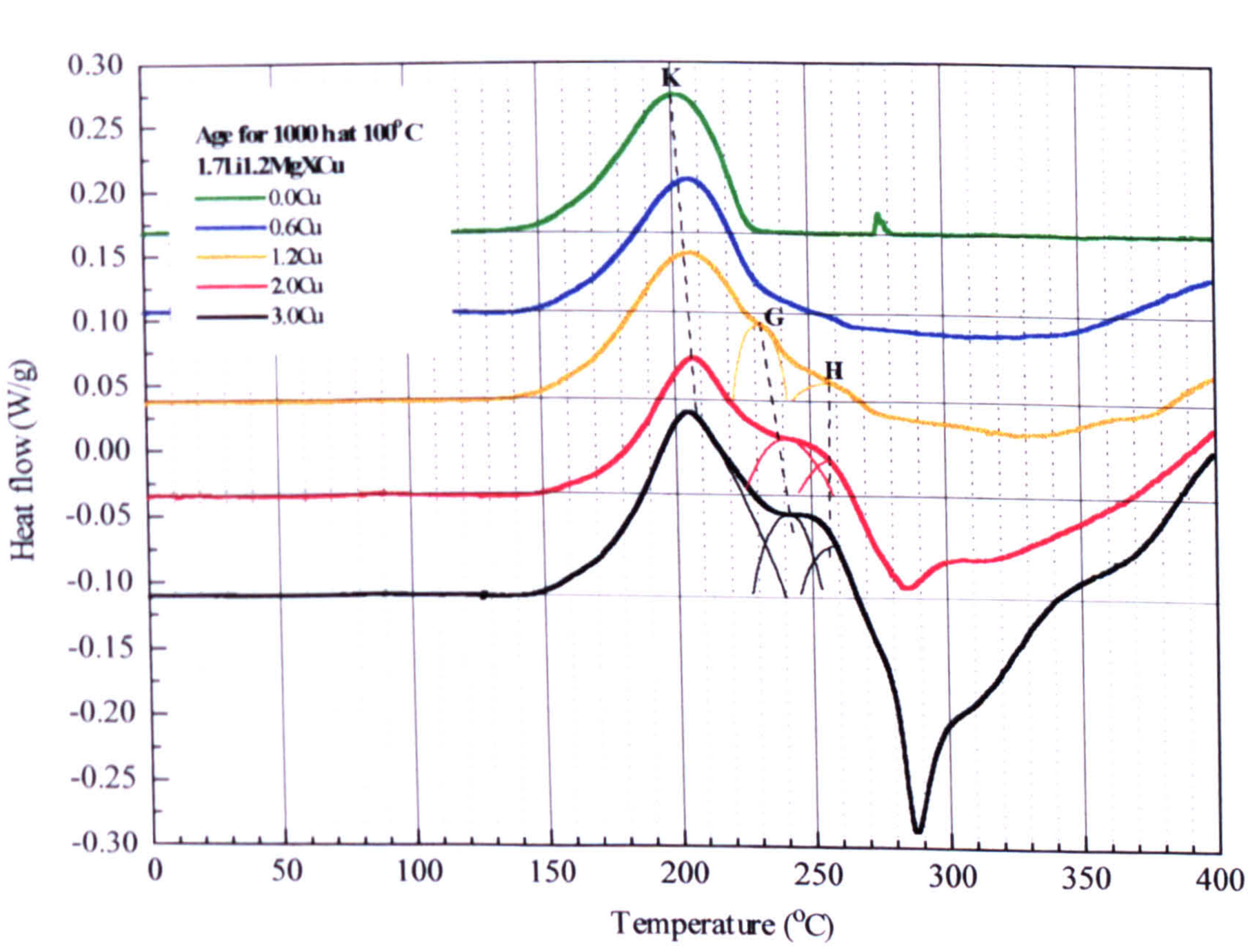

Figure 12.16: DSC comparative plots of 1.7Li1.2MgXCu alloys after ageing for 1000 h at 100°C.

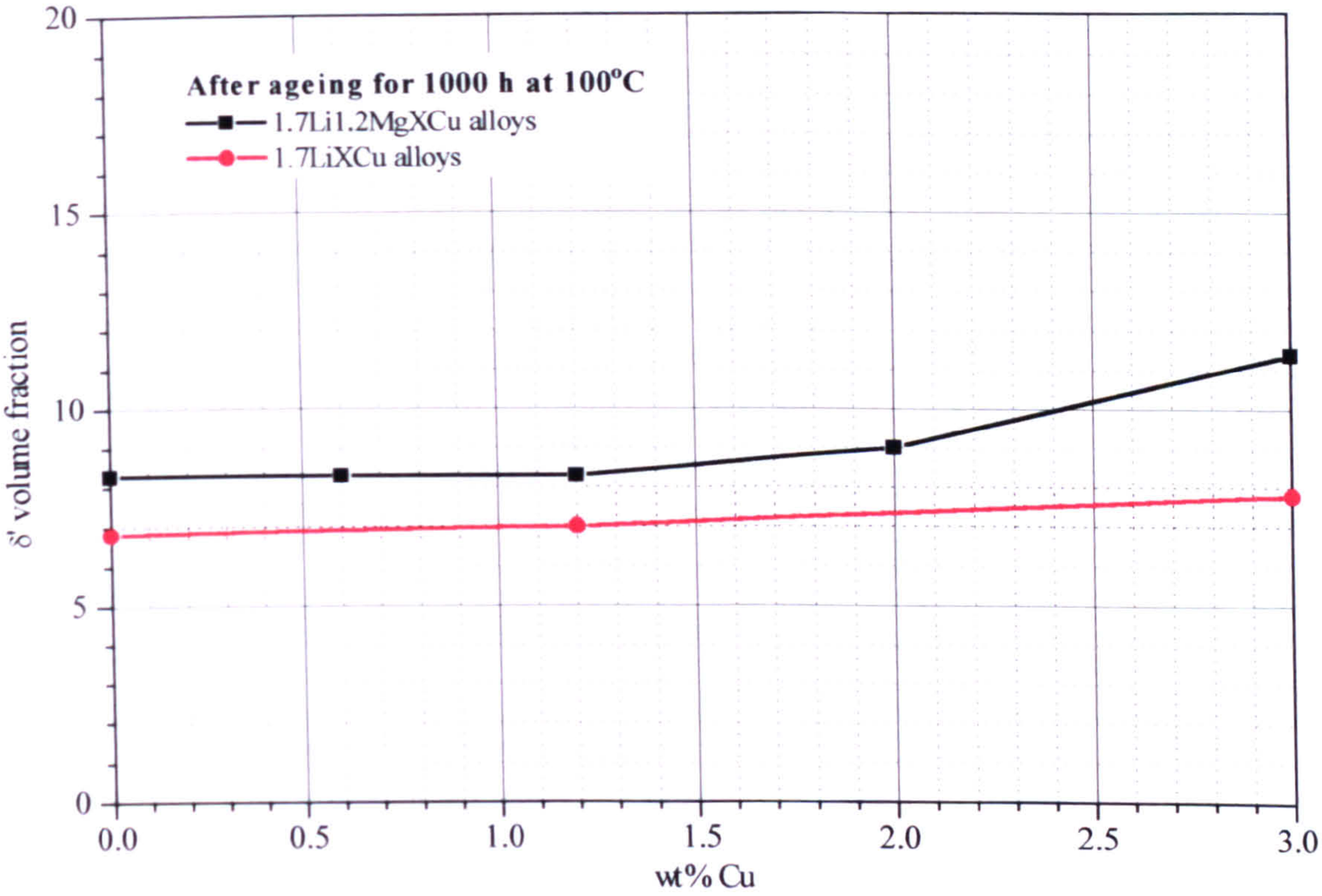

Figure 12.17: δ′ volume fraction produced in 1.7Li1.2MgXCu and 1.7LiXCu alloys after ageing for 1000 h at 100°C.

Figure 12.18: Isothermal resistivity changes of 1.7Li1.2MgXCu alloys during ageing at 100°C.

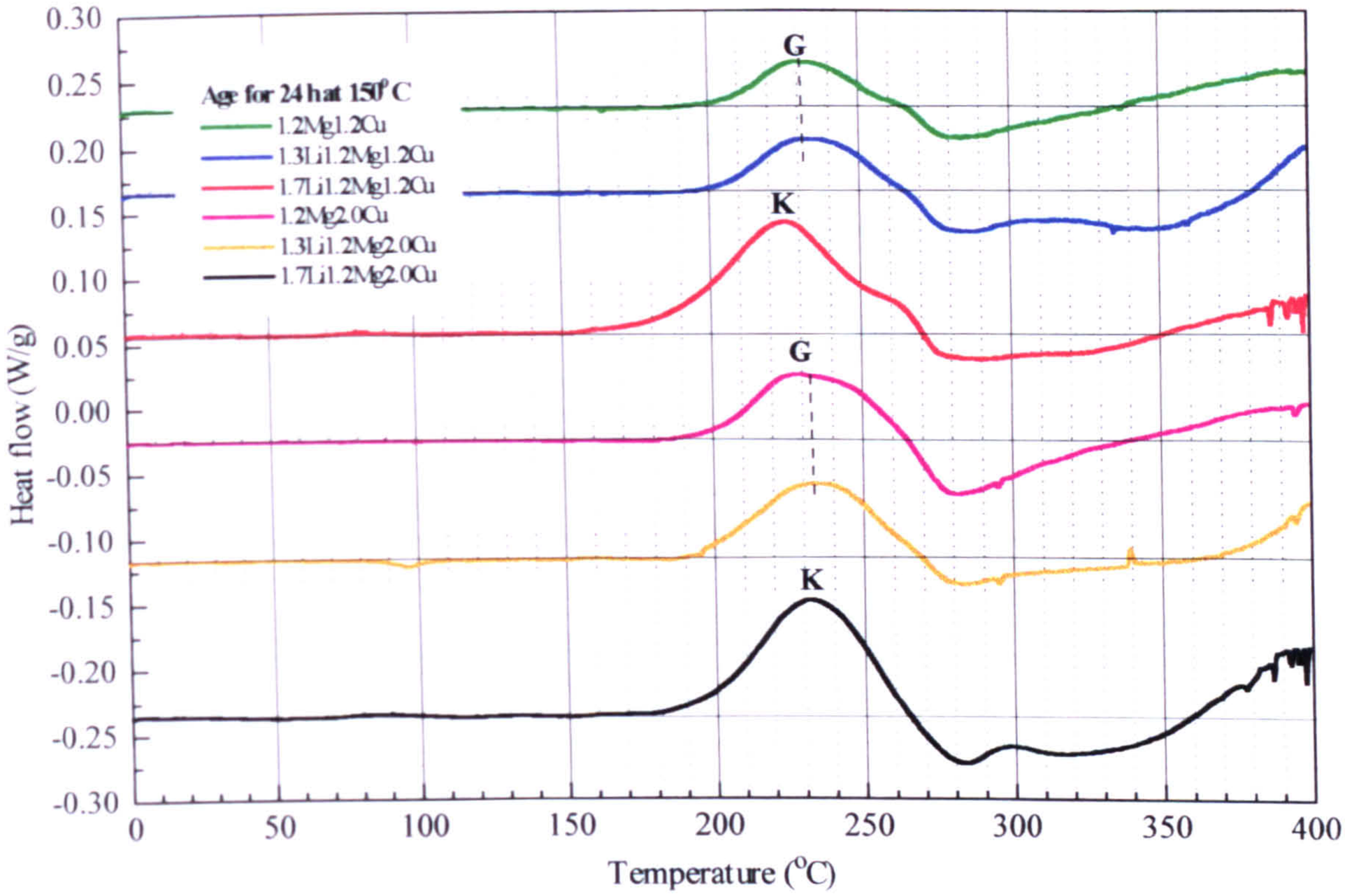

Figure 12.19: DSC comparative plots of 1.2Mg1.2Cu and 1.2Mg2.0Cu alloys with lithium addition of 1.3 and 1.7% after ageing for 24 h at 150°C.

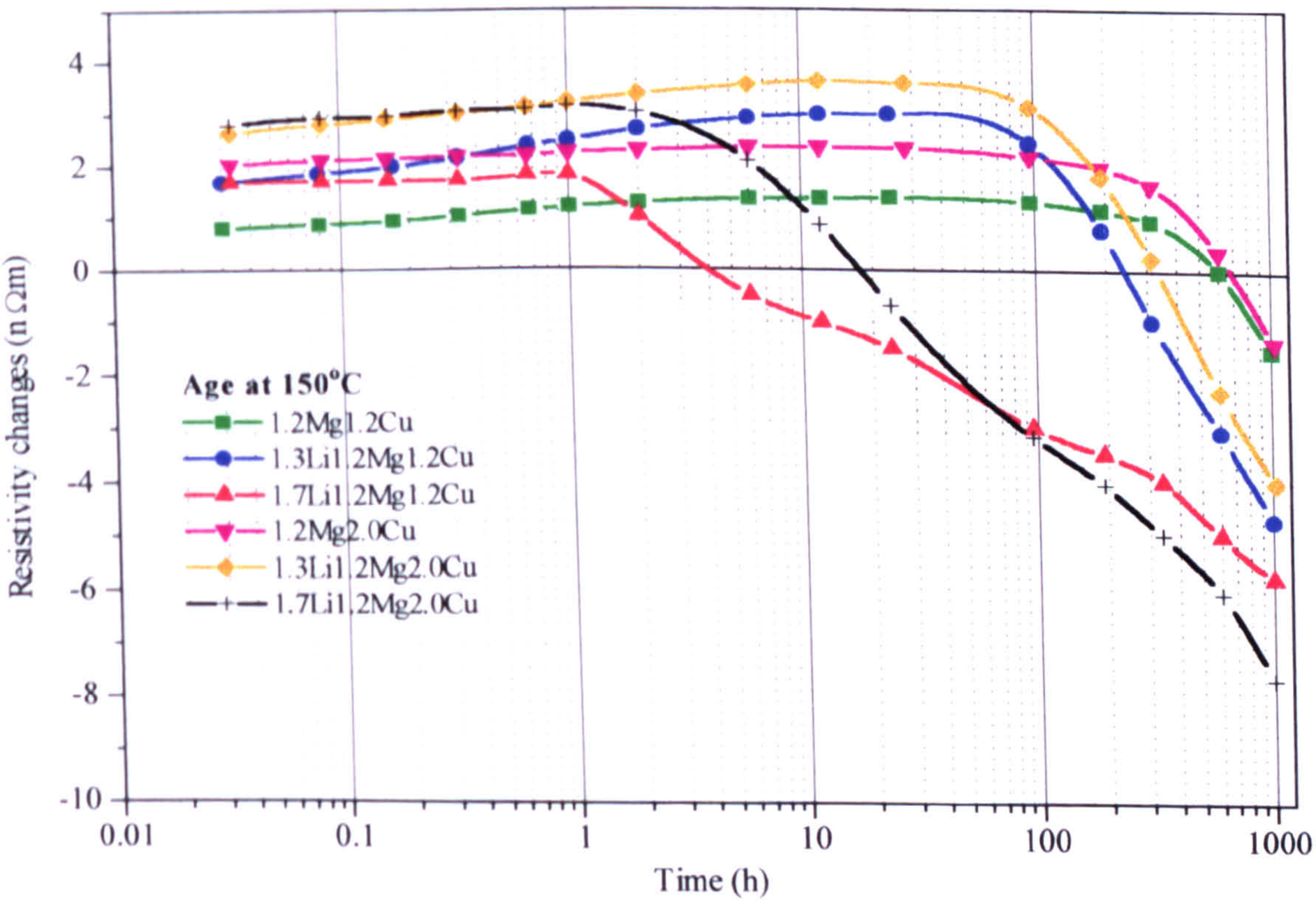

Figure 12.20: Comparative isothermal resistivity plots of 1.2Mg1.2Mg and 1.2Mg2.0Cu alloys with lithium additions of 1.3% and 1.7%.

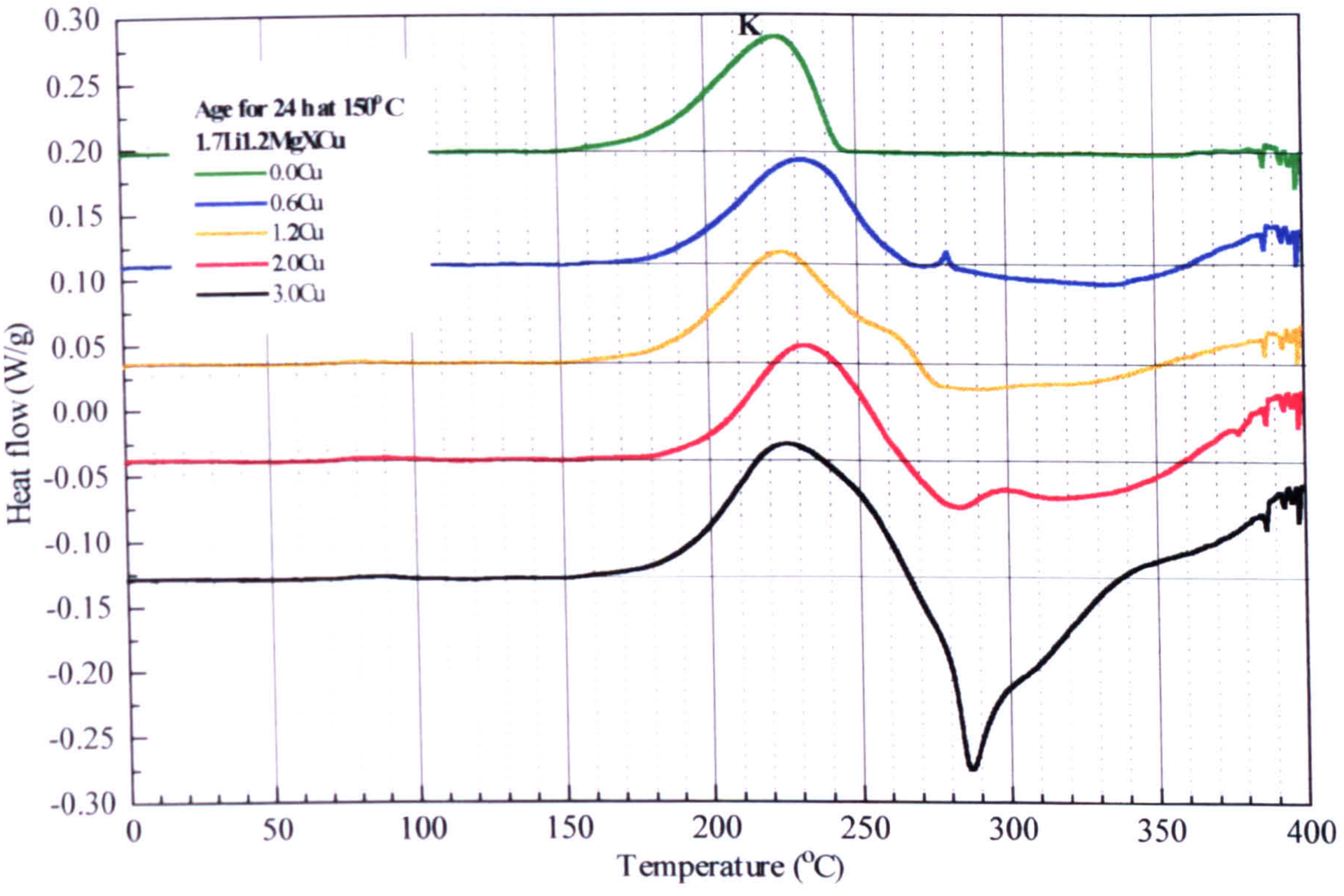

Figure 12.21: Comparative DSC plots of 1.7Li1.2MgXCu alloys after ageing for 24 h at 150°C.

Figure 12.22: δ′ volume fraction produced in 1.7Li1.2MgXCu and 1.7LiXCu alloys after ageing for 24 h at 150°C.

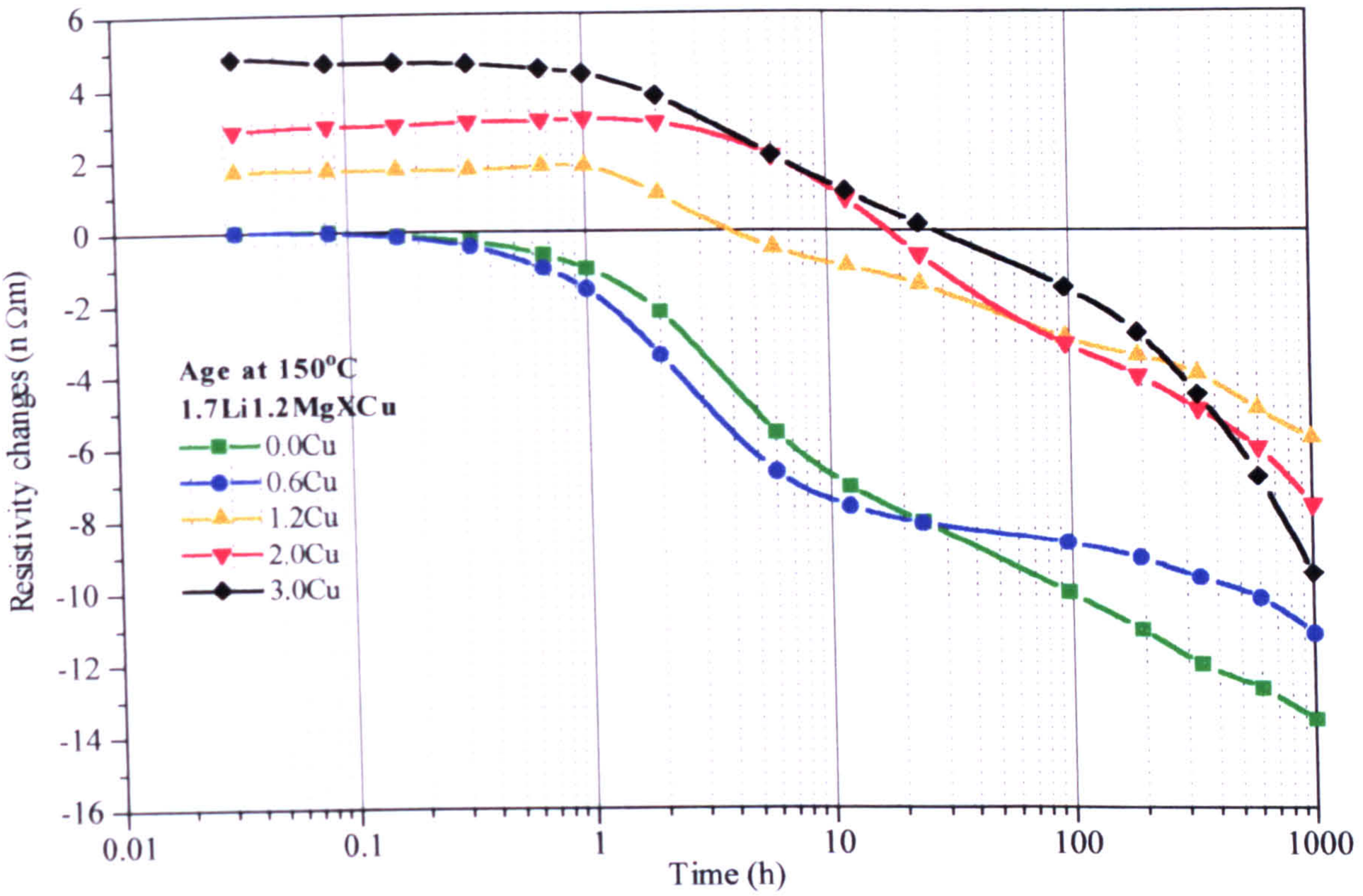

Figure 12.23: Isothermal resistivity changes of 1.7Li1.2MgXCu alloys during ageing at 150°C.

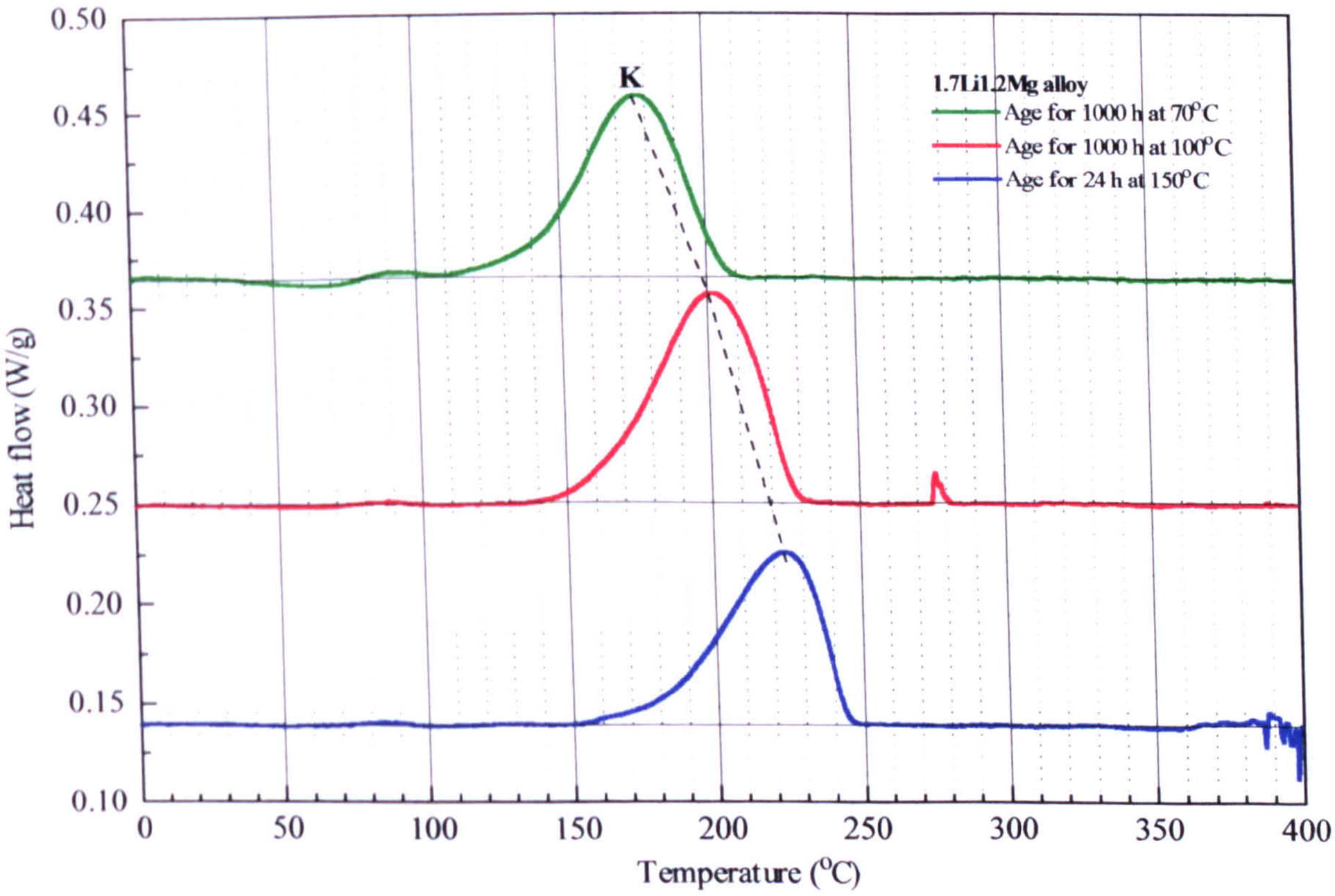

Figure 12.24: Effect of ageing temperature on the DSC thermogram of a 1.7Li1.2Mg0.0Cu alloy.

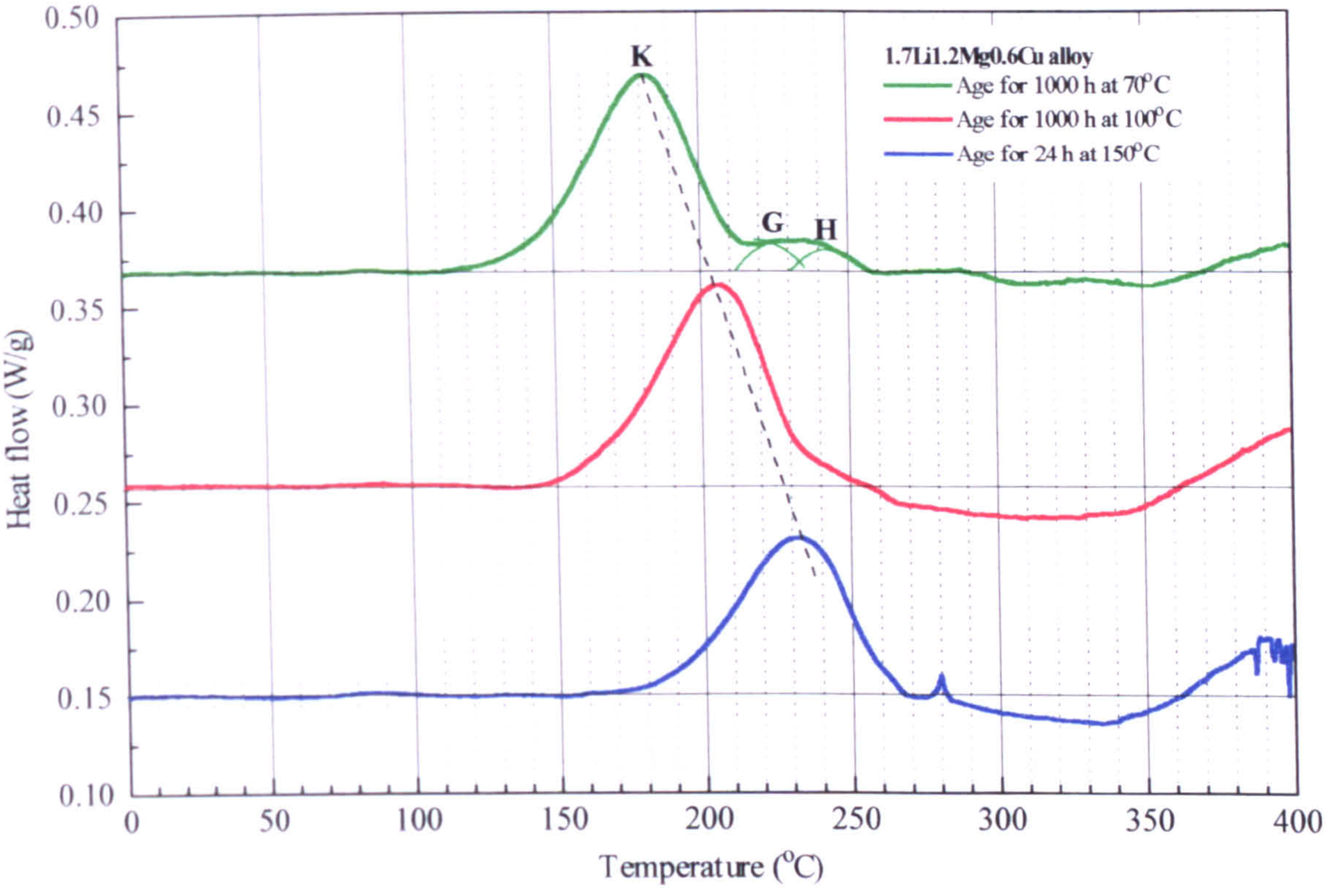

Figure 12.25: Effect of ageing temperature on the DSC thermogram of a 1.7Li1.2Mg0.6Cu alloy.

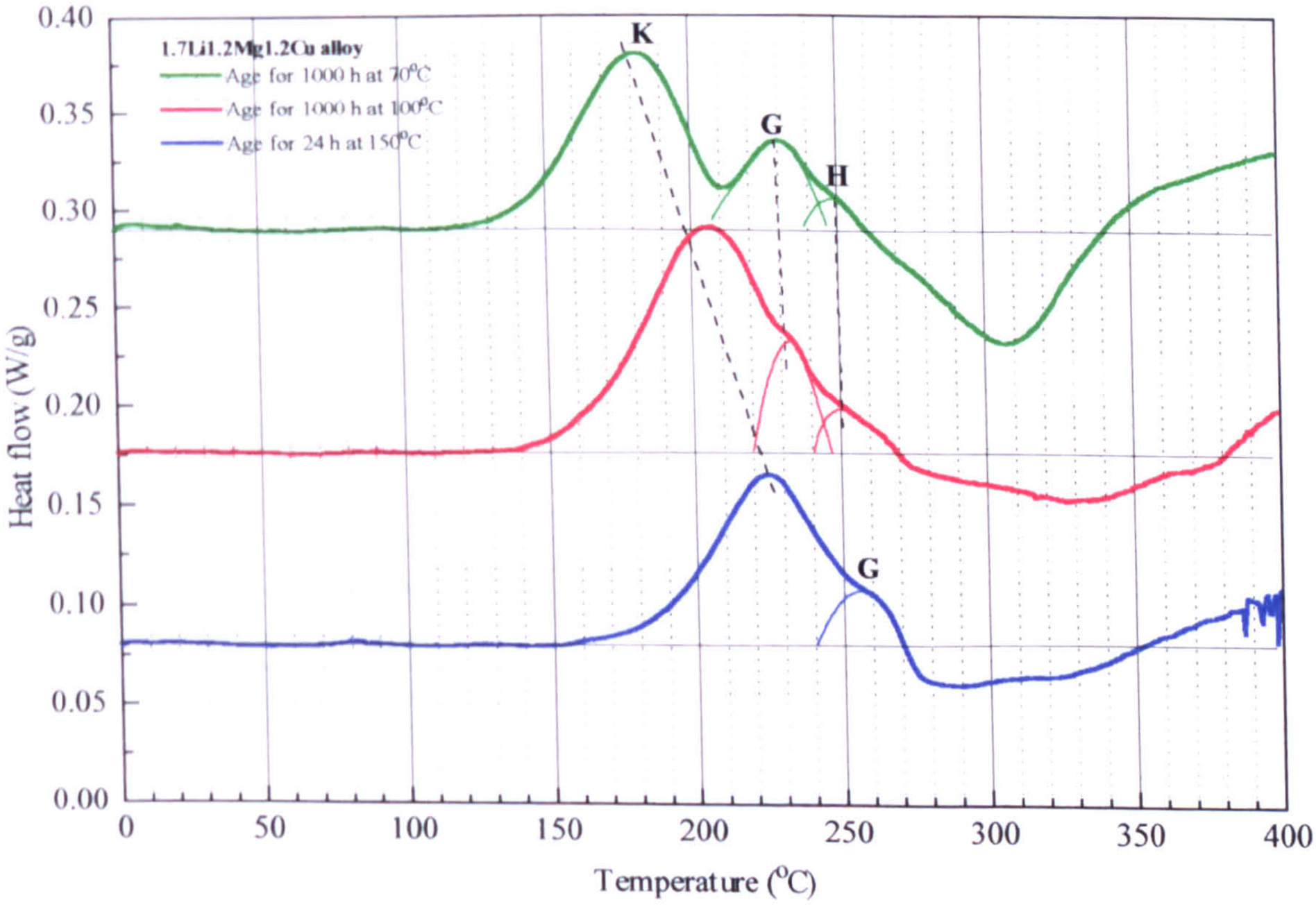

Figure 12.26: Effect of ageing temperature on the DSC thermogram of a 1.7Li1.2Mg1.2Cu alloy.

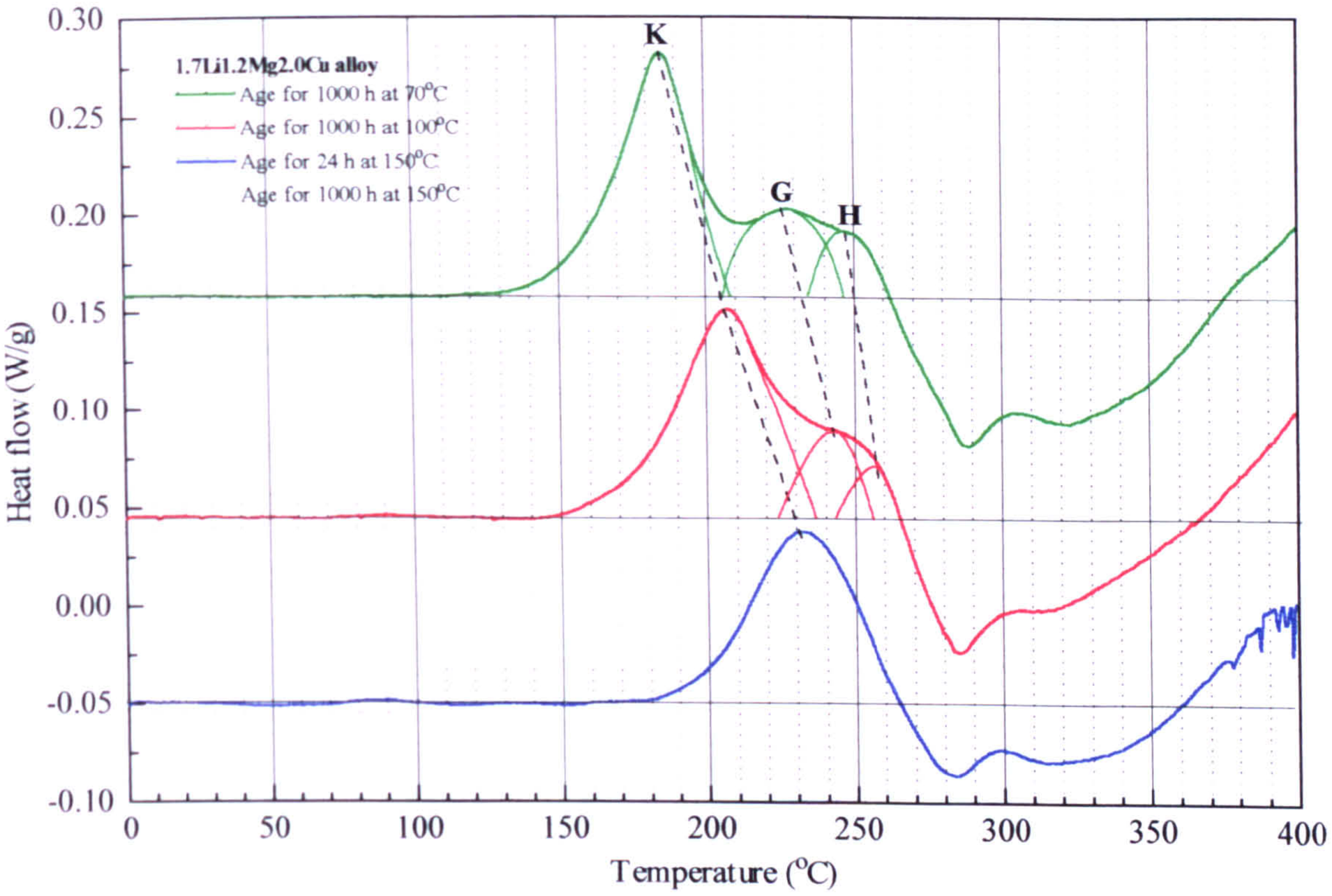

Figure 12.27: Effect of ageing temperature on the DSC thermogram of a 1.7Li1.2Mg2.0Cu alloy.

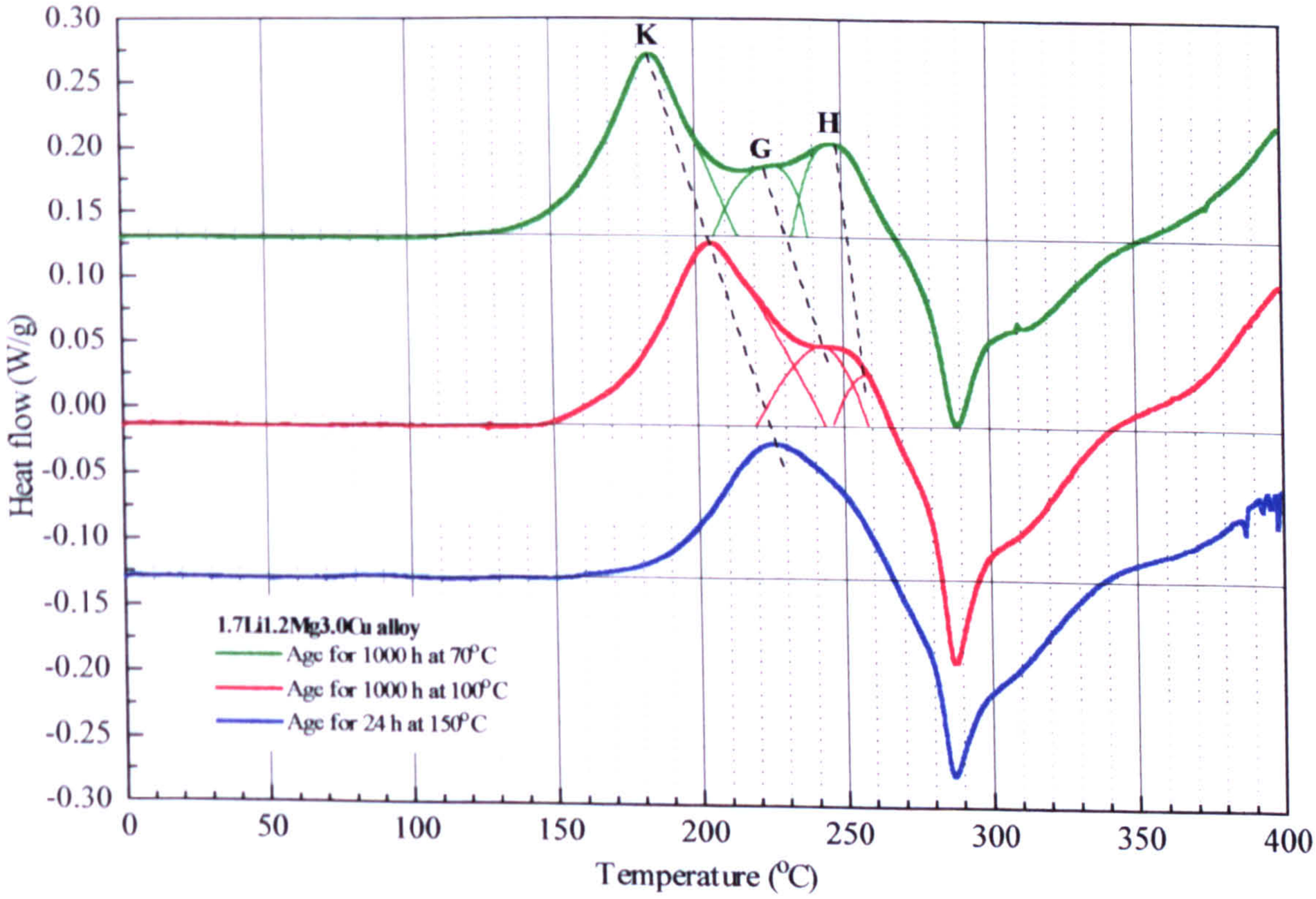

Figure 12.28: Effect of ageing temperature on the DSC thermogram of a 1.7Li1.2Mg3.0Cu alloy.

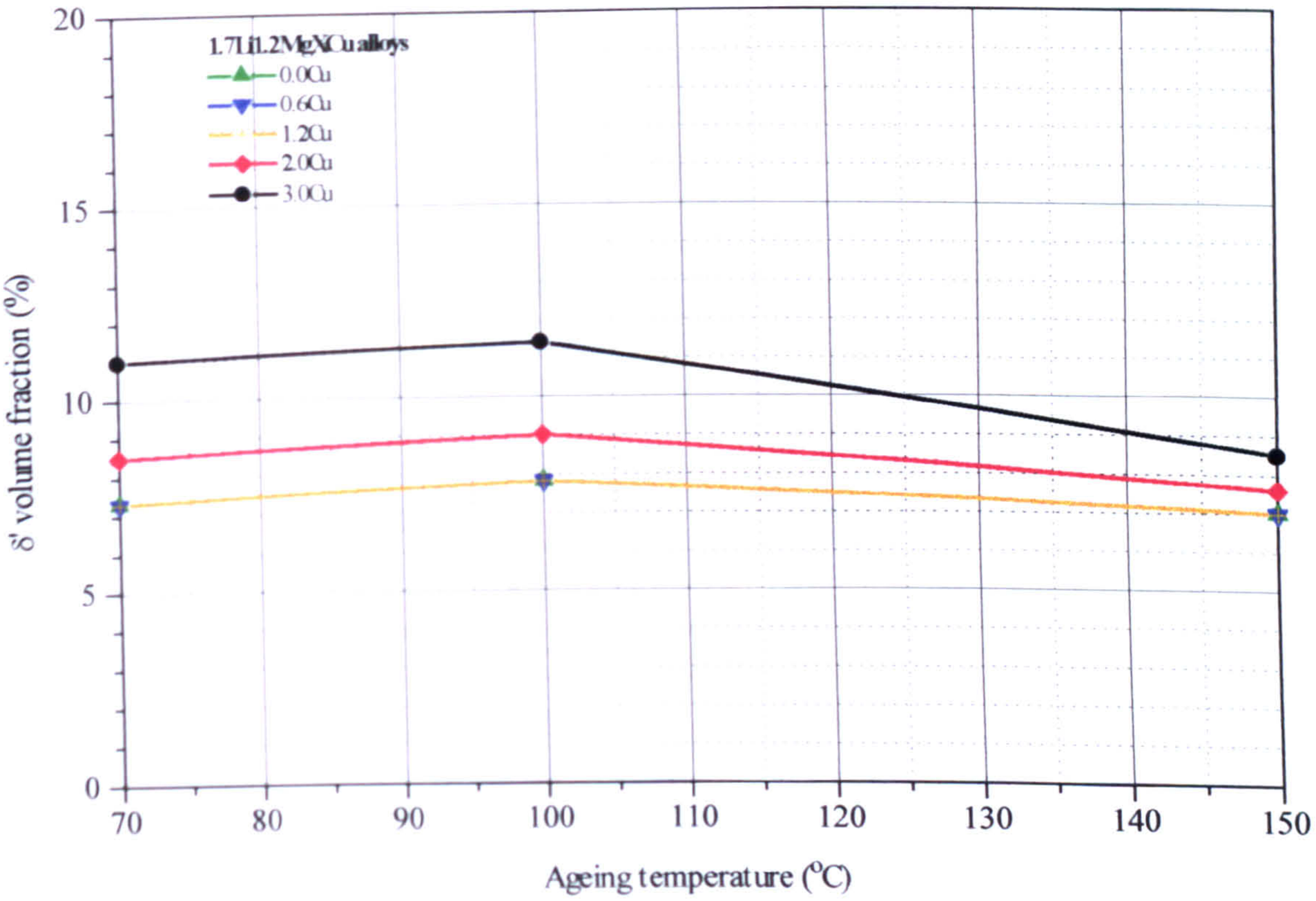

Figure 12.29: Effect of copper concentration and ageing temperaure on the δ′ volume fraction.

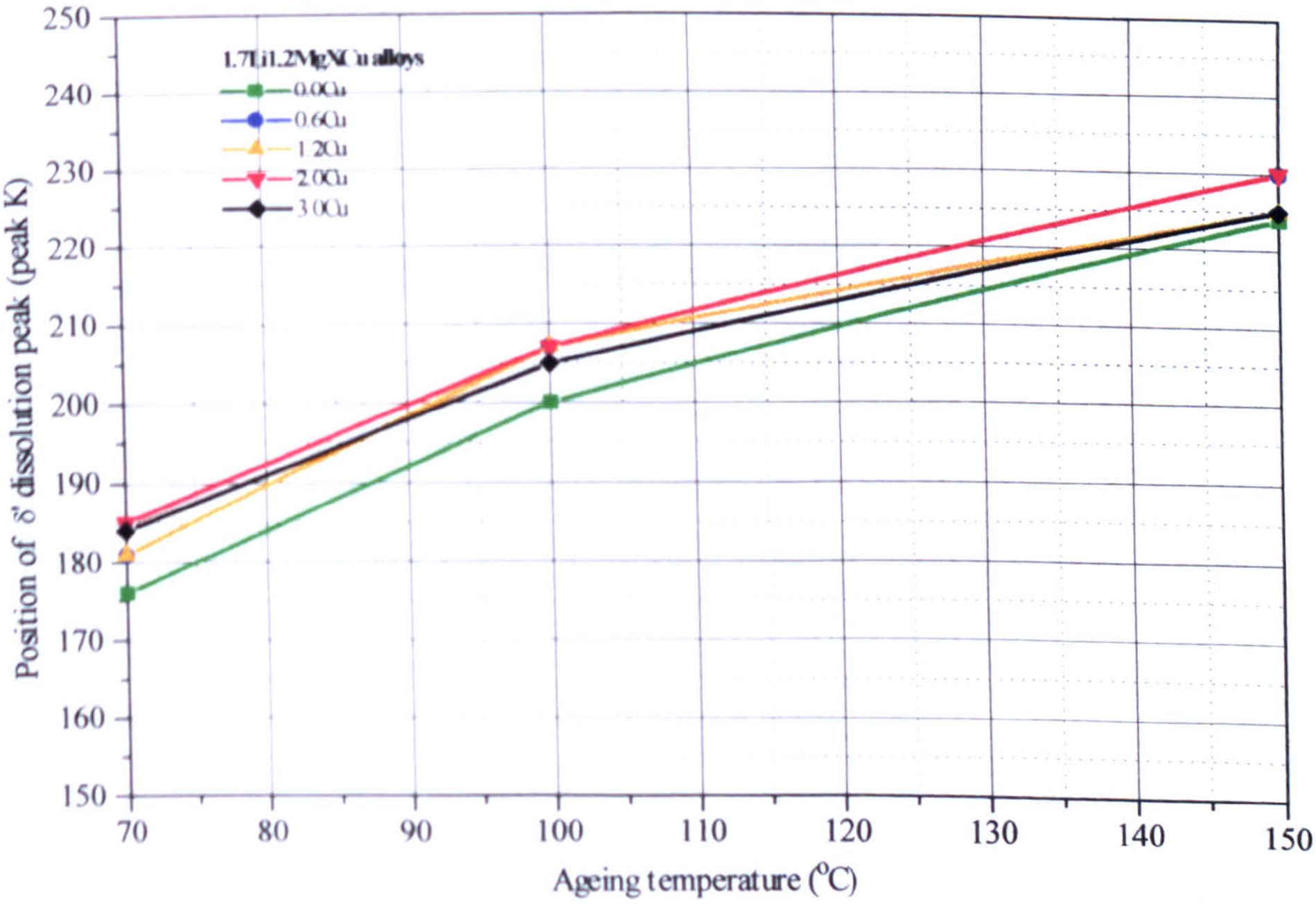

Figure 12.30: Effect of ageing temperature on the position of peak K.

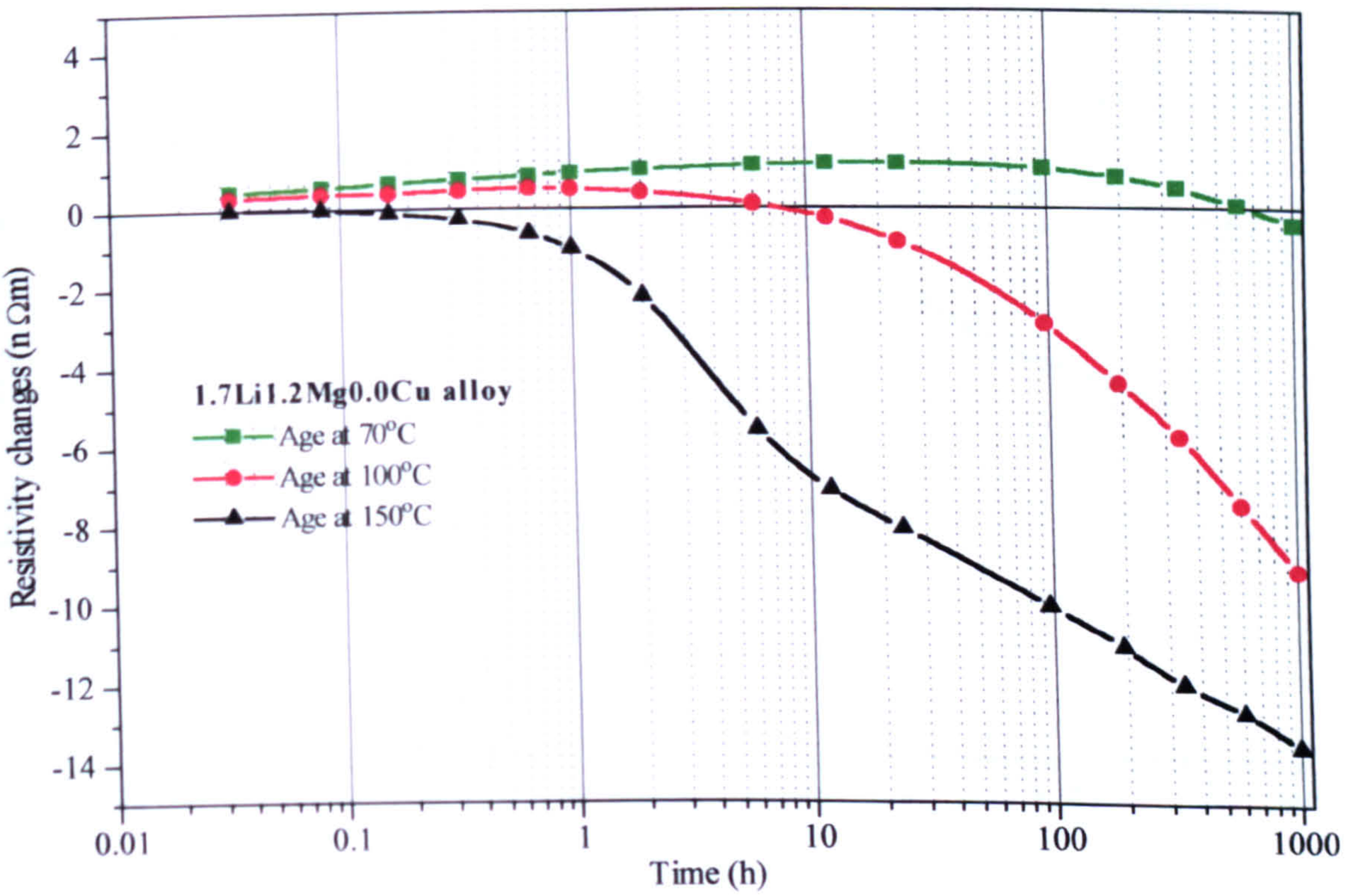

Figure 12.31: Effect of ageing temperature on the isothermal resistivity of a 1.7Li1.2Mg0.0Cu alloy.

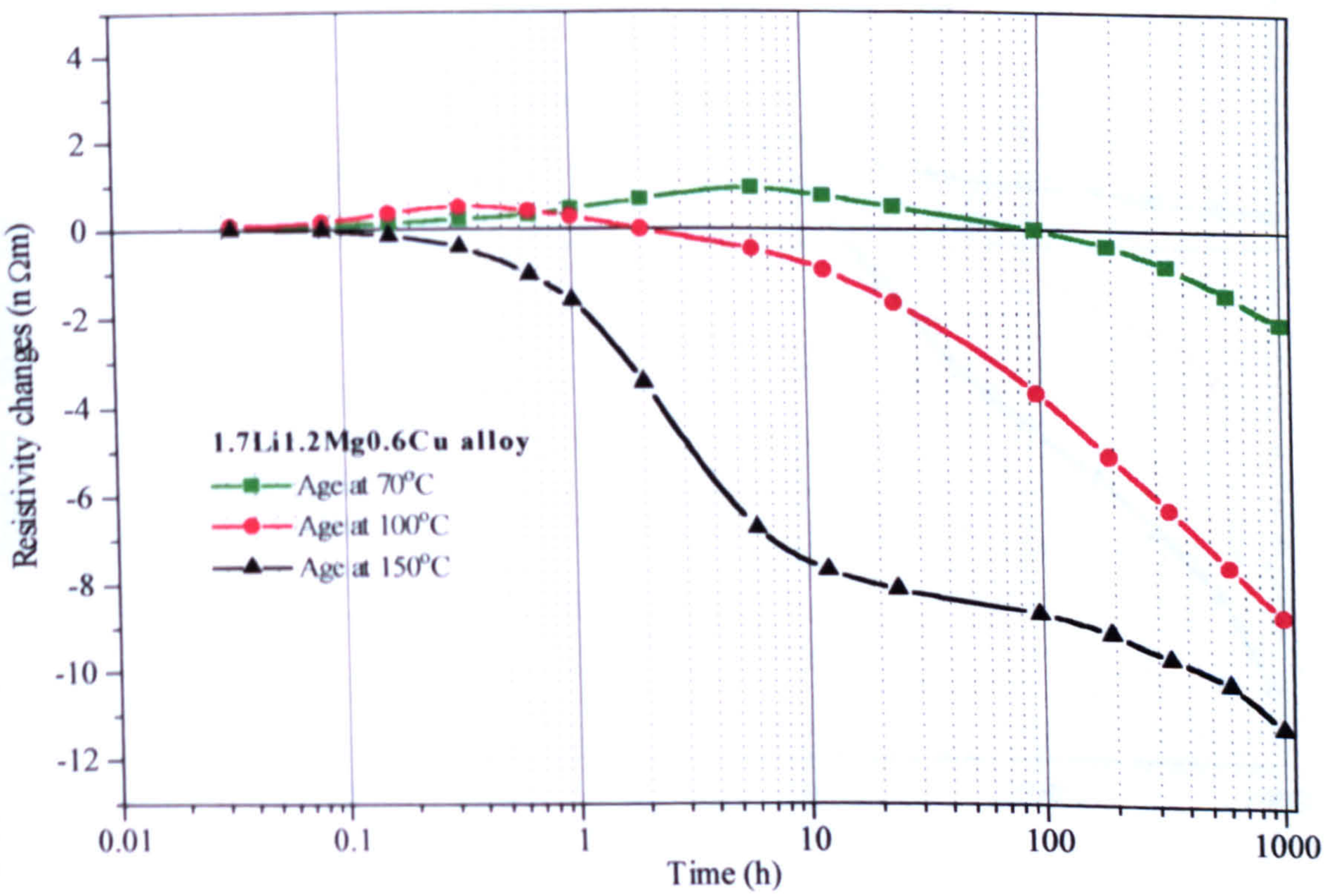

Figure 12.32: Effect of ageing temperature on the isothermal resistivity of a 1.7Li1.2Mg0.6Cu alloy.

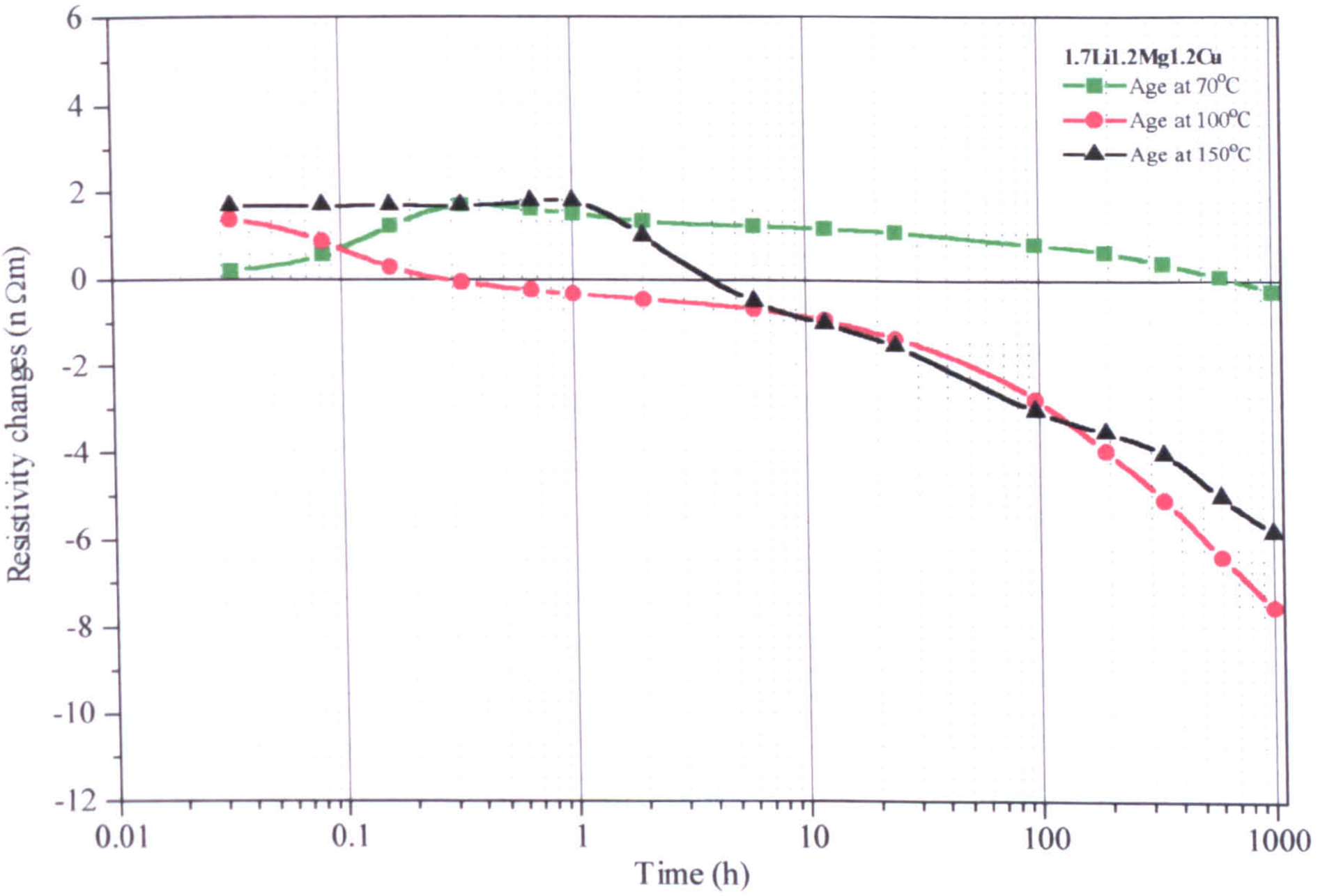

Figure 12.33: Effect of ageing temperature on the isothermal resistivity of a 1.7Li1.2Mg1.2Cu alloy.

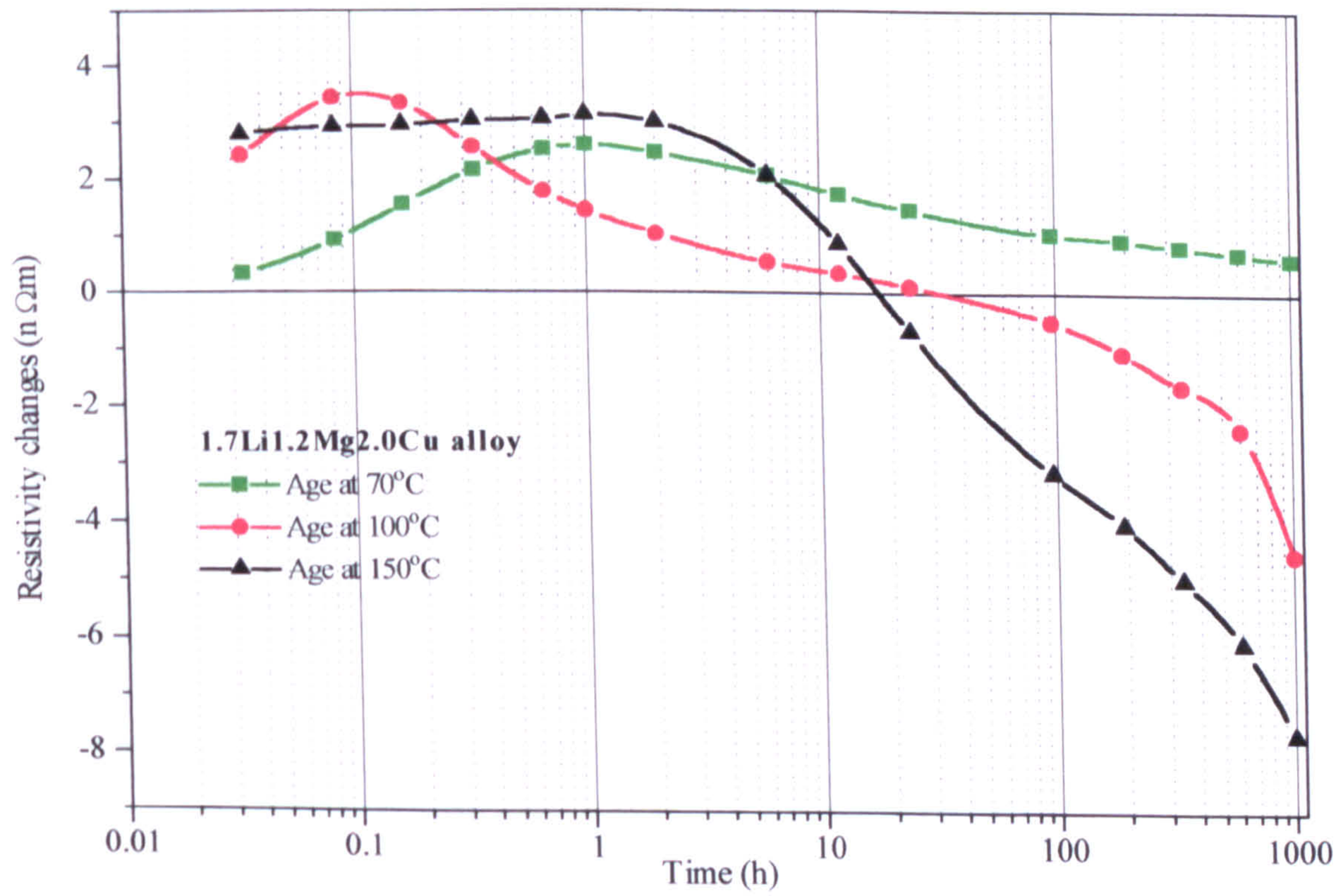

Figure 12.34: Effect of ageing temperature on the isothermal resistivity of a 1.7Li1.2Mg2.0Cu alloy.

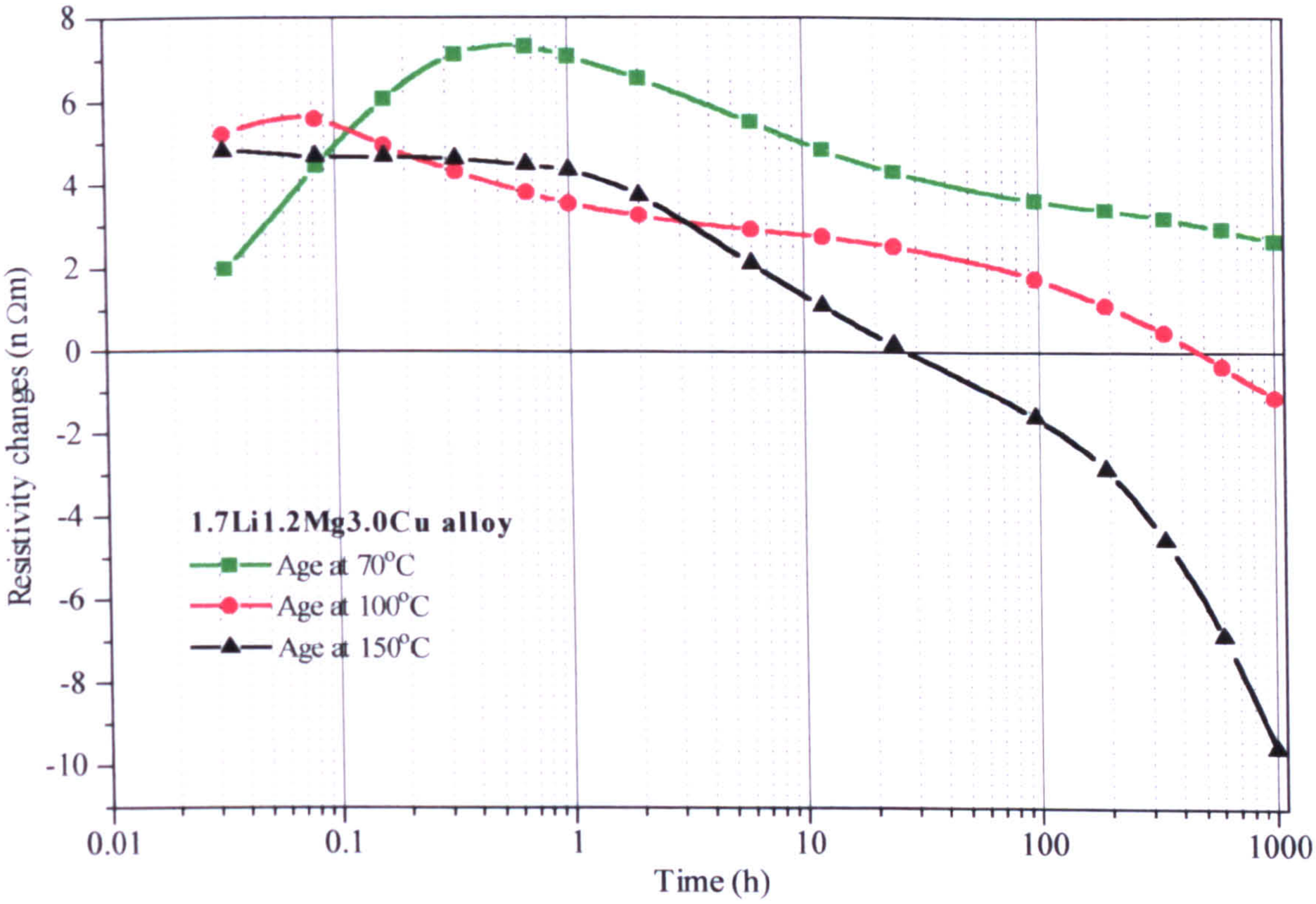

Figure 12.35: Effect of ageing temperature on the isothermal resistivity of a 1.7Li1.2Mg3.0Cu alloy.

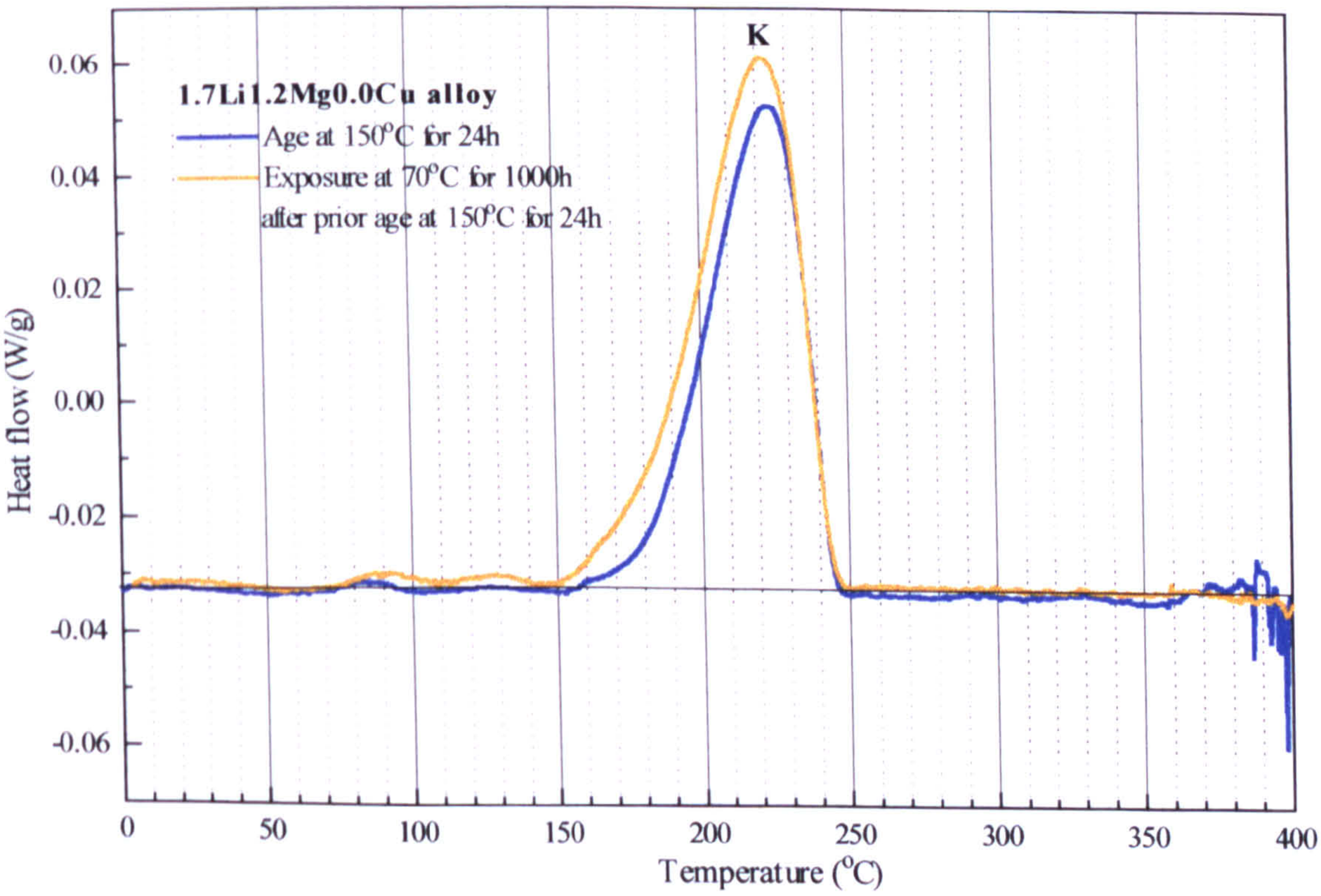

Figure 12.36: Effect of exposure at 70°C on the DSC characteristics of a 1.7Li1.2Mg0.0Cu alloy.

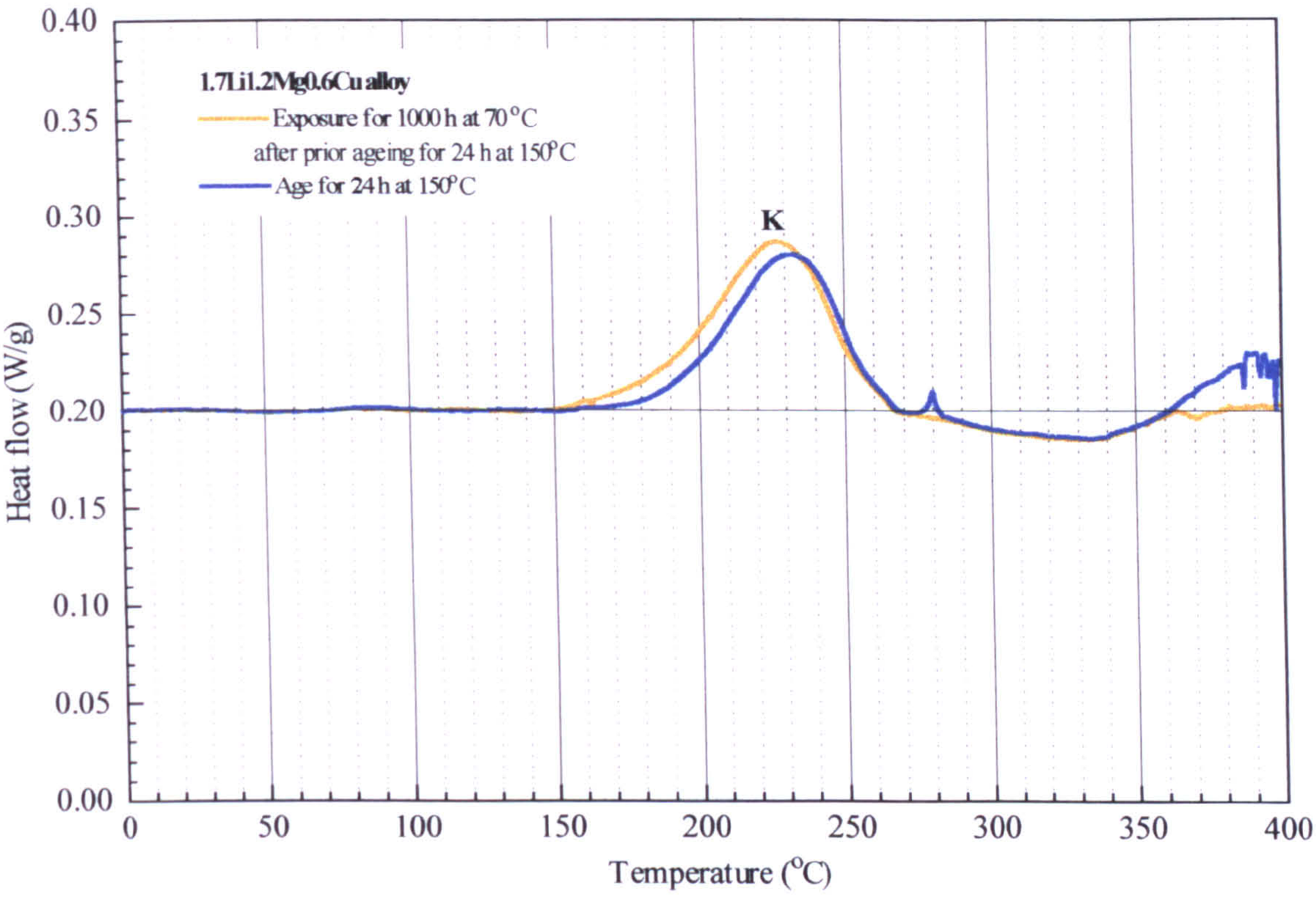

Figure 12.37: Effect of exposure at 70°C on the DSC characteristics of a 1.7Li1.2Mg0.6Cu alloy.

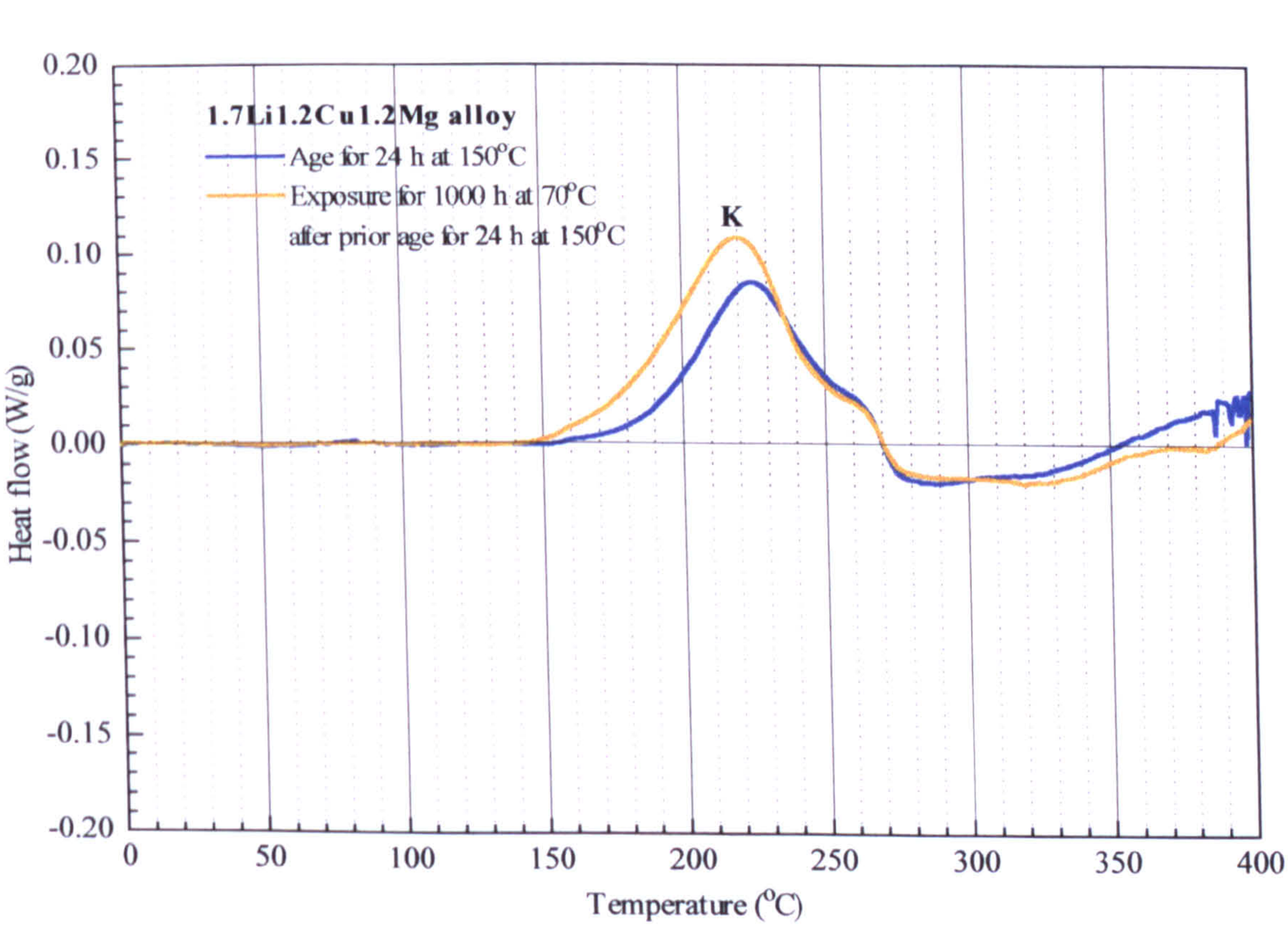

Figure 12.38: Effect of exposure at 70°C on the DSC characteristics of a 1.7Li1.2Mg1.2Cu alloy.

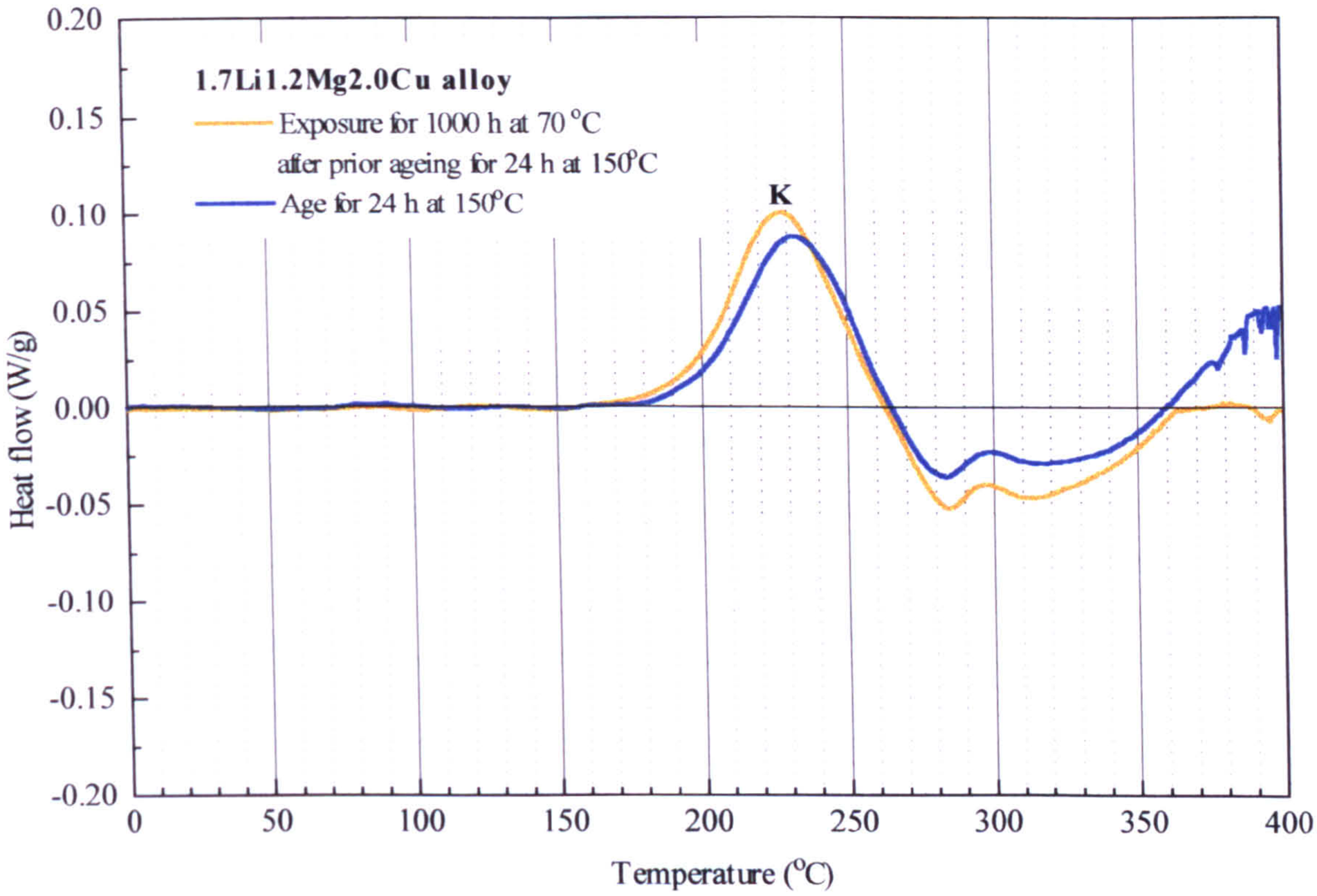

Figure 12.39: Effect of exposure at 70°C on the DSC characteristics of a 1.7Li1.2Mg2.0Cu alloy.

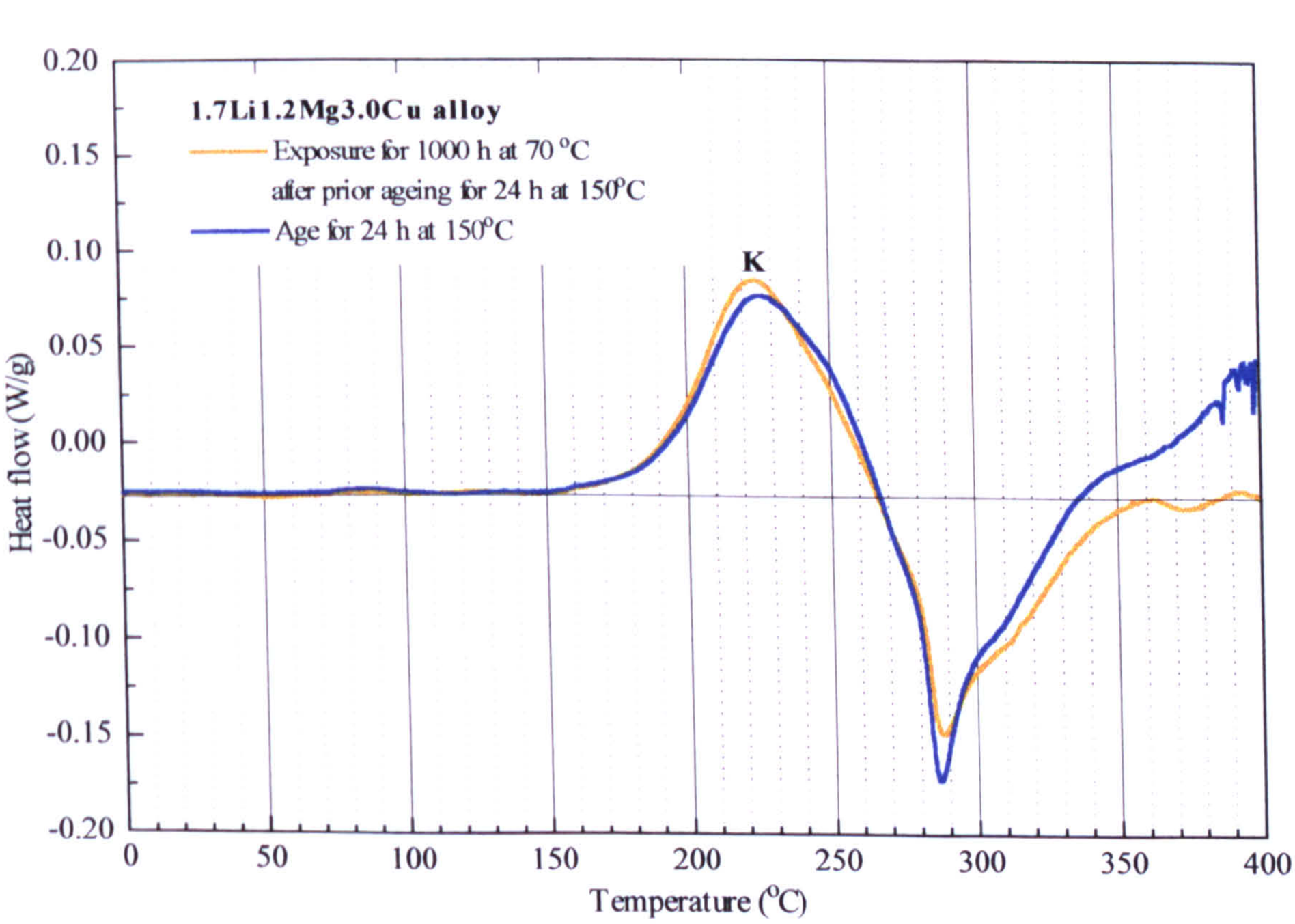

Figure 12.40: Effect of exposure at 70°C on the DSC characteristics of a 1.7Li1.2Mg3.0Cu alloy.

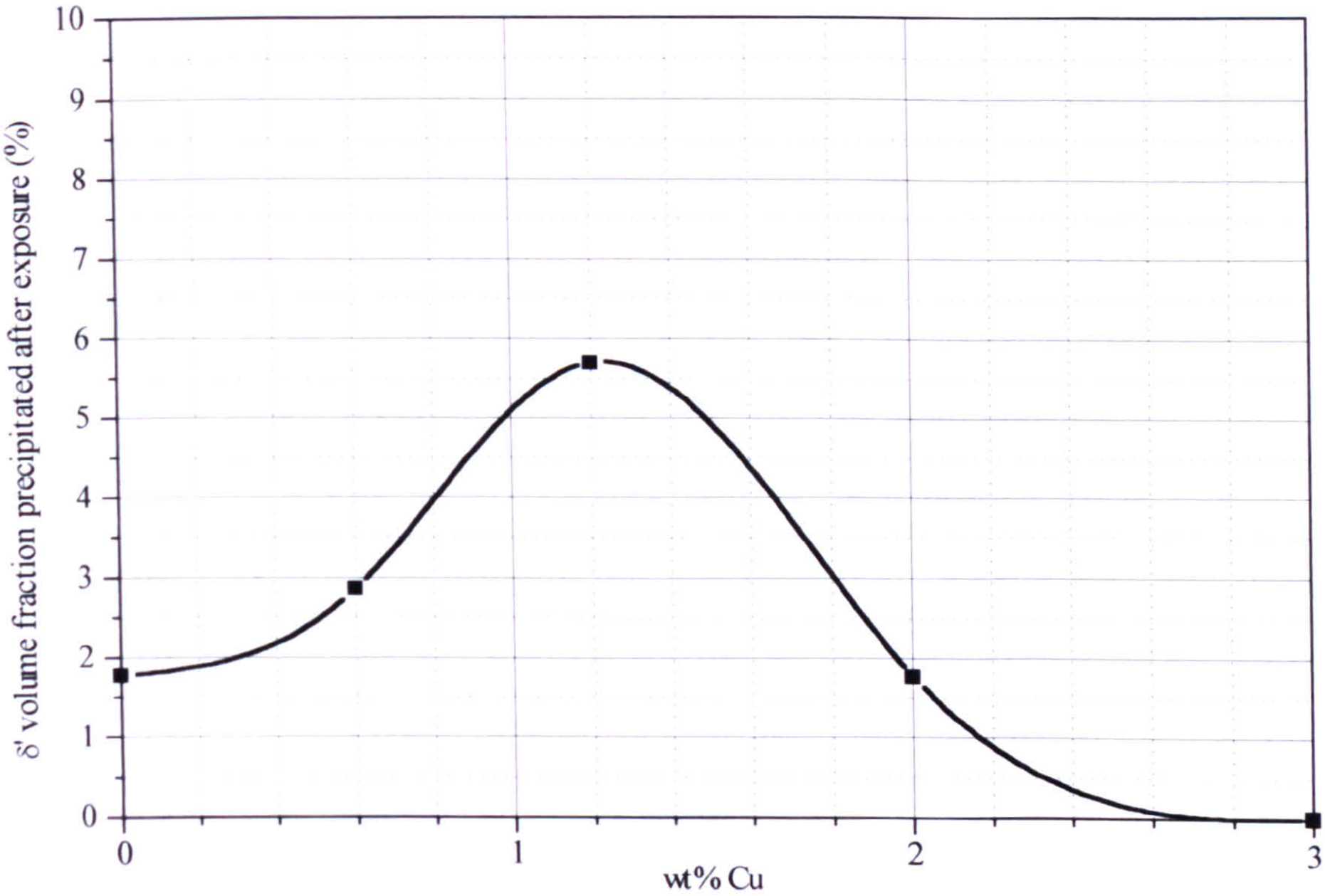

Figure 12.41: δ′ volume fraction precipitated in 1.7Li1.2MgXCu alloys as a result of exposure at 70°C.

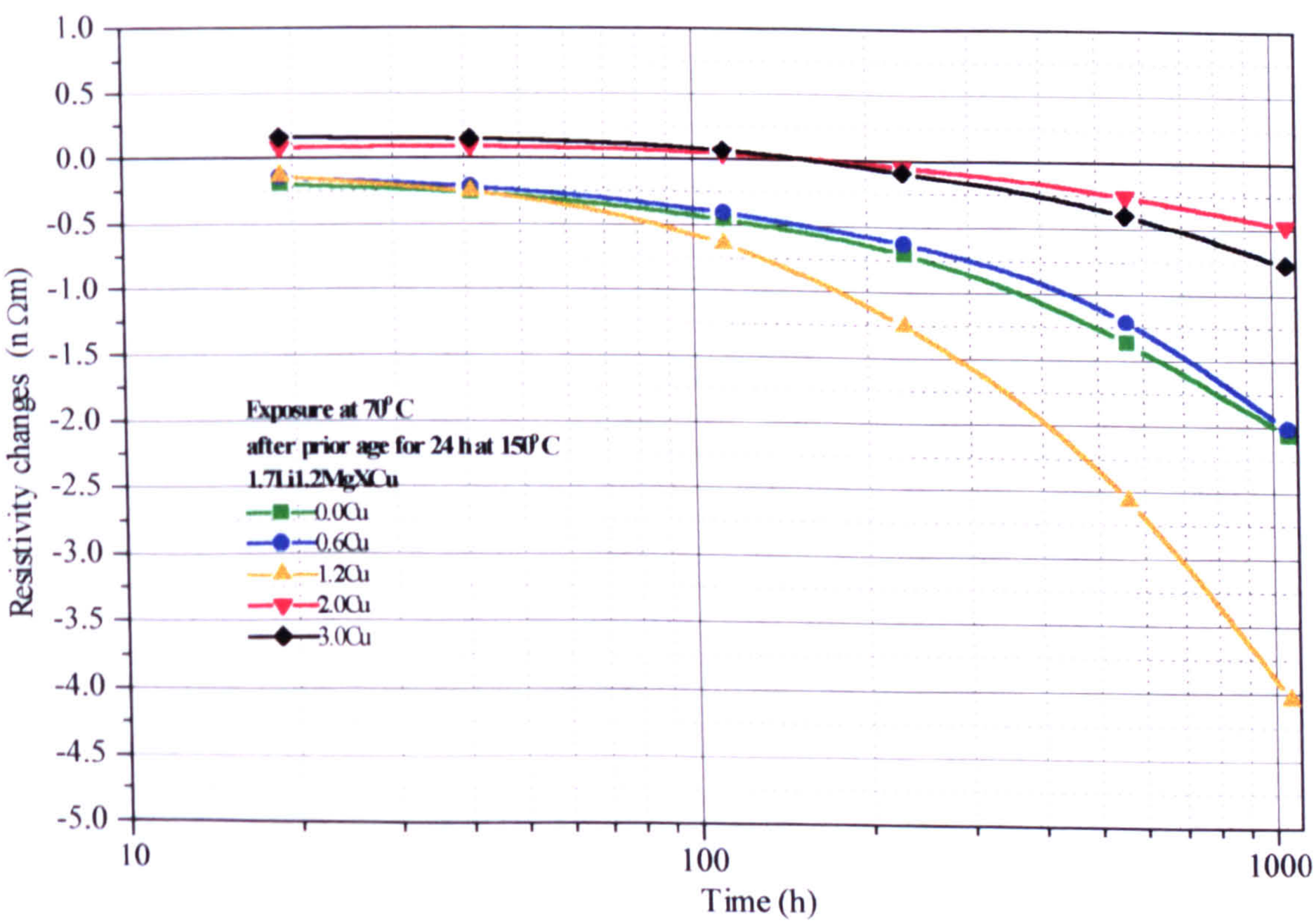

Figure 12.42: Isothermal resistivity changes in 1.7Li1.2MgXCu alloys during exposure at 70°C.

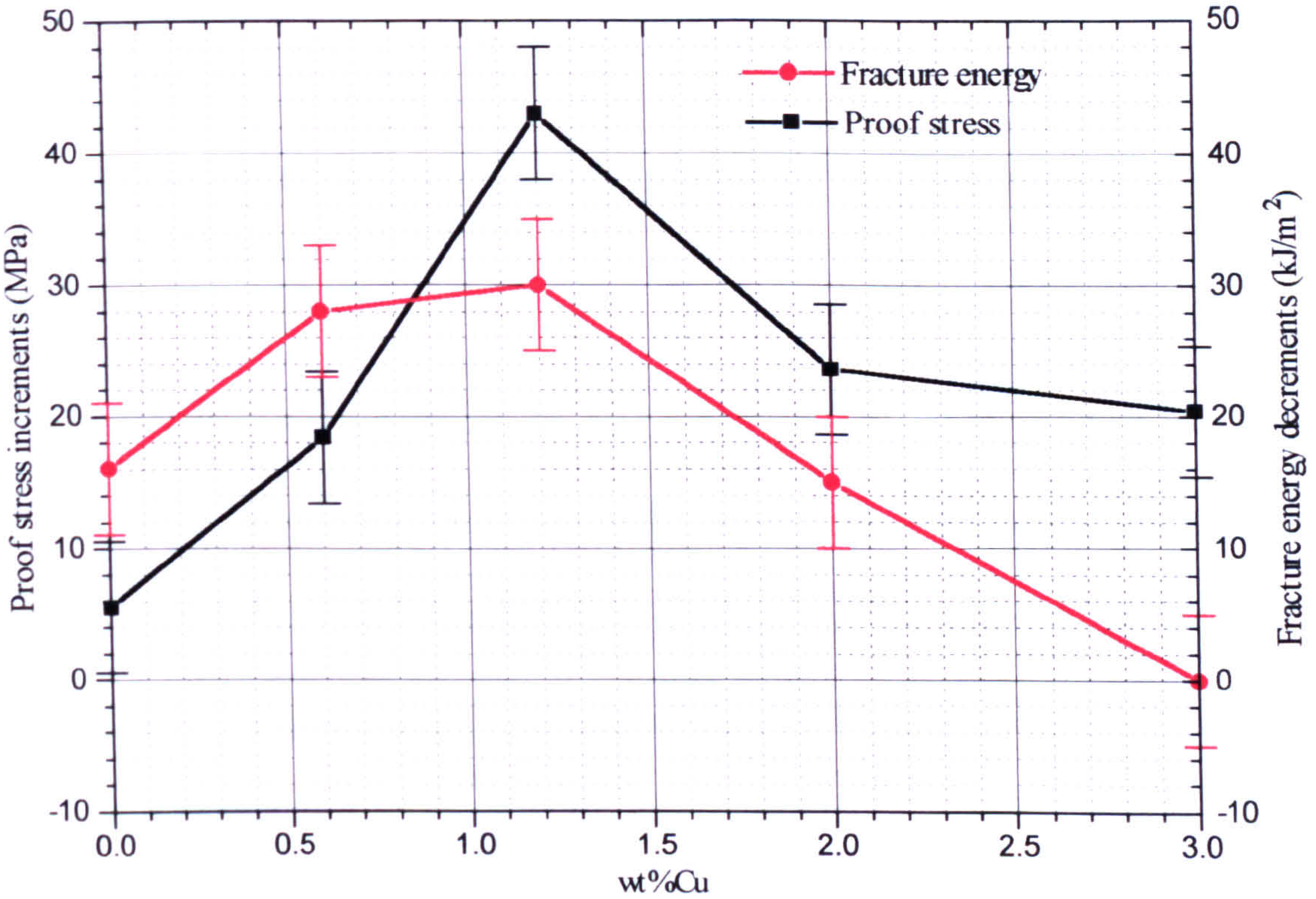

Figure 12.43: Effect of exposure on the mechanical properties of 1.7Li1.2MgXCu alloys.

CHAPTER 13

General Summary and Comparison of the different alloy systems

The precipitation characteristics of Al-Li-XMg, Al-Li-XCu, Al-Li-Cu-XMg and Al-Li-Mg-XCu alloys have been studied in this thesis. The results for each of the alloy systems have been thoroughly discussed in the appropriate chapter and mechanisms of δ′ precipitation proposed for each alloy system. These can be summarised as follows:

- Al-Li-XMg alloys. Increasing magnesium concentration stimulates δ′ precipitation due to an increase in the α/δ′ solvus temperature. It has been shown in the thesis that each 1 wt%Mg increases the solvus temperature by ~7.0°C. At low ageing temperatures (70, 100°C) the mechanism of δ′ precipitation is one of nucleation ordering followed by spinodal decomposition. At high ageing temperatures (150°C) the mechanism of δ′ precipitation is classic nucleation and growth.
- Al-Li-XCu alloys. Increasing copper concentration stimulates δ′ precipitation but this is not the result of an increase in the α/δ′ solvus temperature; the thesis has shown that copper has no effect on the position of the solvus boundary. At low ageing temperatures (70, 100°C) the mechanism of δ′ precipitation is the nucleation on GP_{Cu} zones. At higher

ageing temperatures (150°C) the mechanism is again, classic nucleation and growth.

- Al-Li-Cu-XMg alloys. Stimulation of δ′ again takes but the mechanism of δ′ precipitation in these alloys is quite different from that in Al-Li-XMg alloys. The addition of magnesium, again, produces a shift in the α/δ′ solvus boundary but this is not the prime cause of δ′ stimulation in Al-Li-Cu-XMg alloys. For low magnesium additions (0-1.2%Mg) the stimulation of δ′ is the result of heterogeneous nucleation on GPB zones (in a manner similar to nucleation on GP_{Cu} zones in Al-Li-XCu alloys). At high magnesium concentrations (1.4-3.0%Mg) the enhancement of δ′ precipitation is the result of the formation of Li-Cu-Mg clusters which are capable of rapidly developing into δ′ precipitates (CLδ′). In all Al-Li-Cu-XMg alloys the higher the ageing temperature the greater the tendency for the mechanism to be nucleation on GPB zones (GPδ′).
- Al-Li-Mg-XCu alloys. Stimulation of δ′ again takes place and for alloys of low copper concentration (0-1.2%Cu) aged at 70 and 100°C the mechanism of this stimulation is similar to that in Al-Li-XCu alloys, heterogeneous nucleation on GPB zones (compared to GP_{Cu} in Al-Li-Cu) i.e. GPδ′. In alloys of high copper concentration (≥2.0%Cu) aged at 70 and 100°C the mechanism of δ′ stimulation is similar to that in Al-Li-Cu-XMg alloys, i.e. development of Li-Cu-Mg clusters and their evolution into δ′ (CLδ′). As with Al-Li-Cu-XMg alloys the higher the ageing

temperature the more likely the mechanism of δ′ stimulation is GPδ′ rather than CLδ′.

The question now arises as to which of the various mechanisms in the different alloy systems produces the greatest amount of δ′. To answer this question, the volume fractions of δ′ produced in the four alloy systems (Al-Li-XMg, Al-Li-XCu, Al-Li-Cu-XMg, and Al-Li-Mg-XCu) have been compared for heat treatment conditions of as-quenched, 1000 h at 70°C, 1000 h at 100°C, and 24 h at 150°C in **figures 13.1, 13.2, 13.3** and **13.4**. For all the heat treatments, magnesium and copper concentrations up to 1.2% result in a very close band of δ′ volume fractions suggesting that all the mechanisms that operate in the concentration range 0%<Mg or Cu≤1.2%, i.e. shift of δ′ solvus to higher temperatures (Al-Li-XMg alloys), heterogeneous nucleation on GP_{Cu} zones (Al-Li-XCu alloys), and GPδ′ (Al-Li-Cu-XMg alloys and Al-Li-Mg-XCu alloys), have approximately the same effectiveness.

At concentrations of magnesium and copper >1.2% there are significant differences between the various alloy systems. The least effective δ′ stimulating mechanism in this concentration range is heterogeneous nucleation on GP_{Cu} zones (Al-Li-XCu alloys). The next most effective δ′ stimulation mechanism is shift of the α/δ′ solvus boundary (Al-Li-XMg alloys). The most effective δ′ stimulation comes about in Al-Li-Cu-XMg and Al-Li-Mg-XCu alloys at high magnesium and copper concentrations. Of the two alloy systems the greatest volume fraction of δ′ occurs in Al-Li-Cu-XMg alloys at concentrations of 1.4-

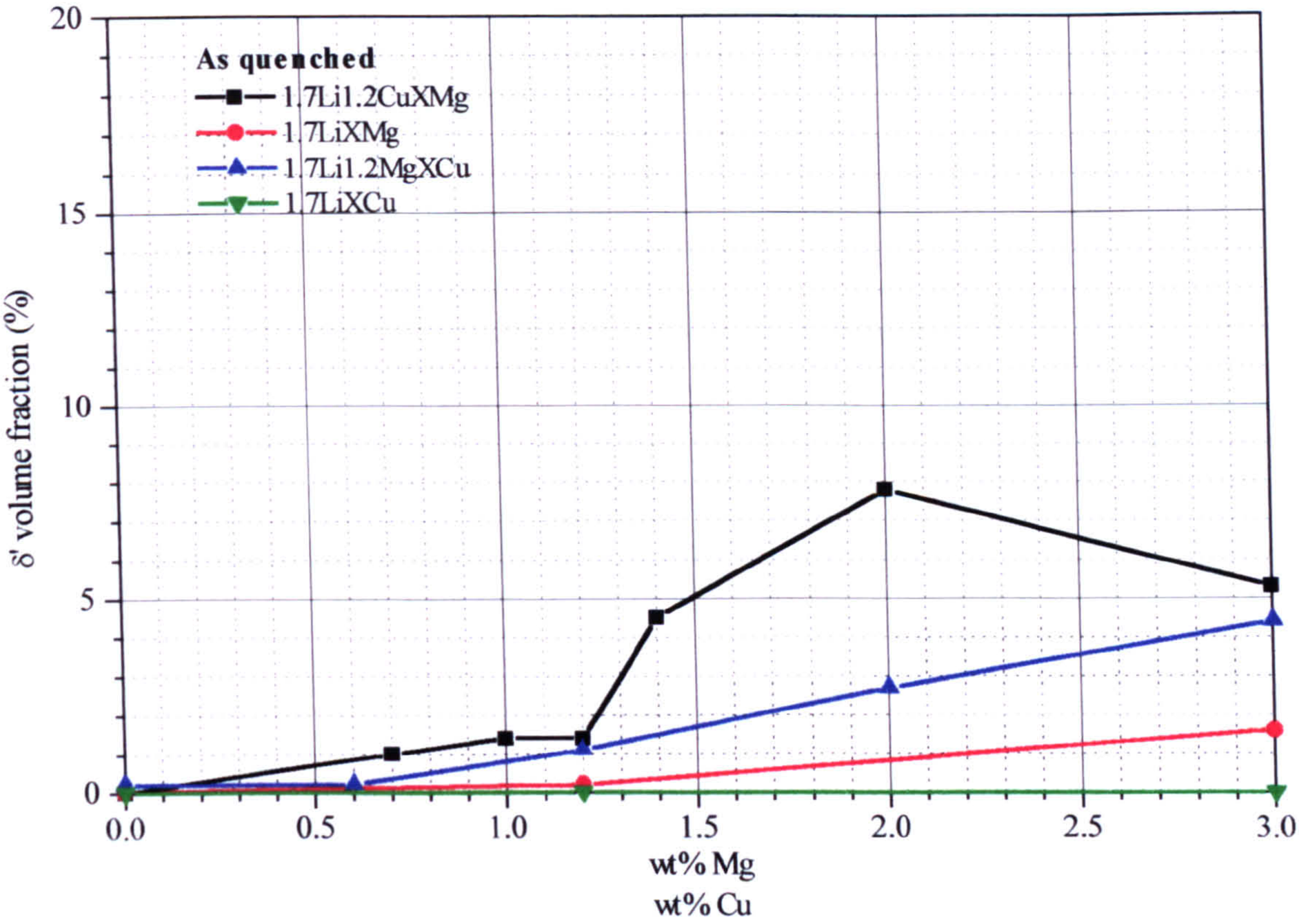

Figure 13.1: δ′ volume fraction precipitated during DSC heating of the as-quenched alloys.

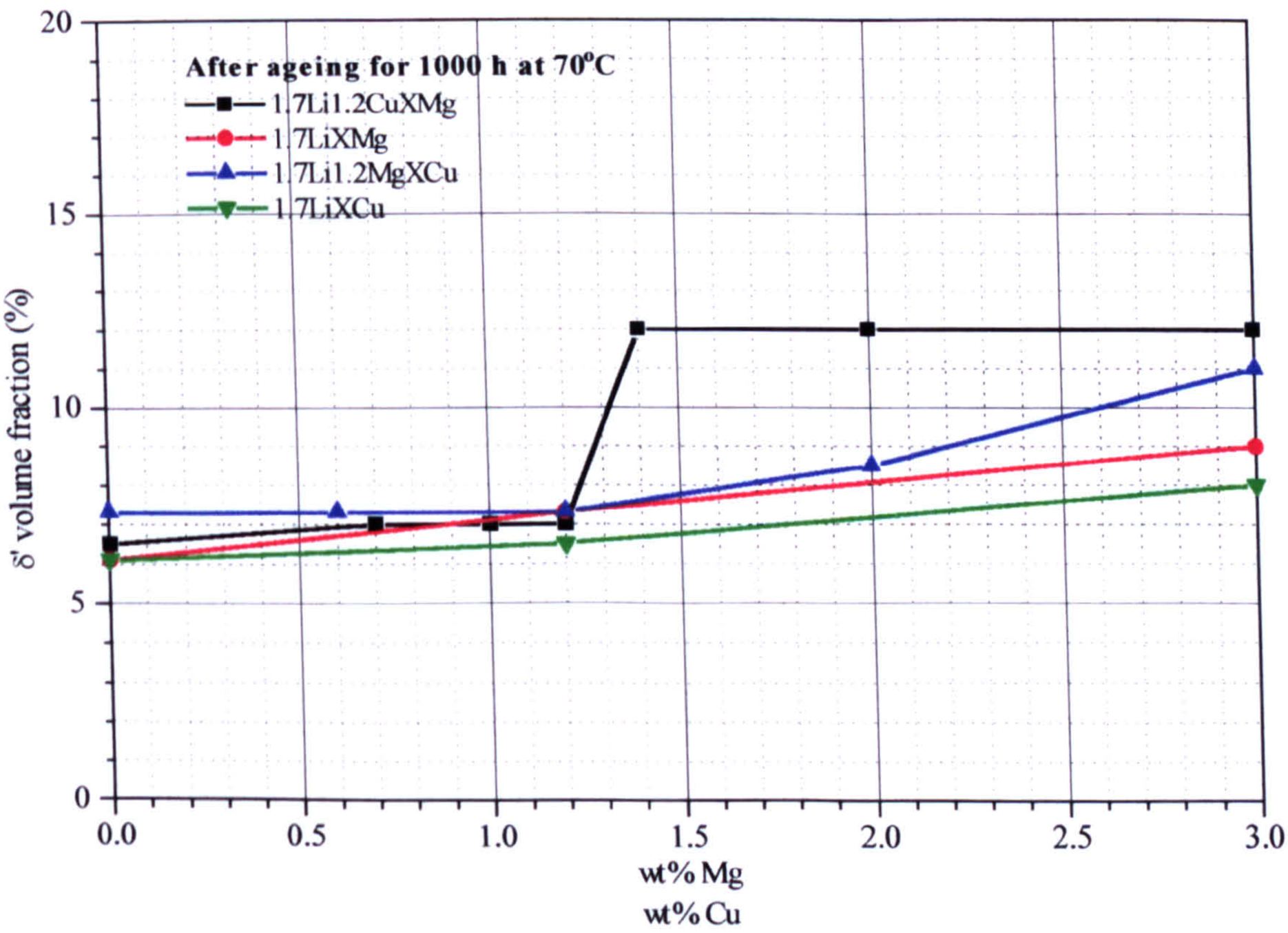

Figure 13.2: δ′ volume fraction precipitated after ageing for 1000 h at 70°C.

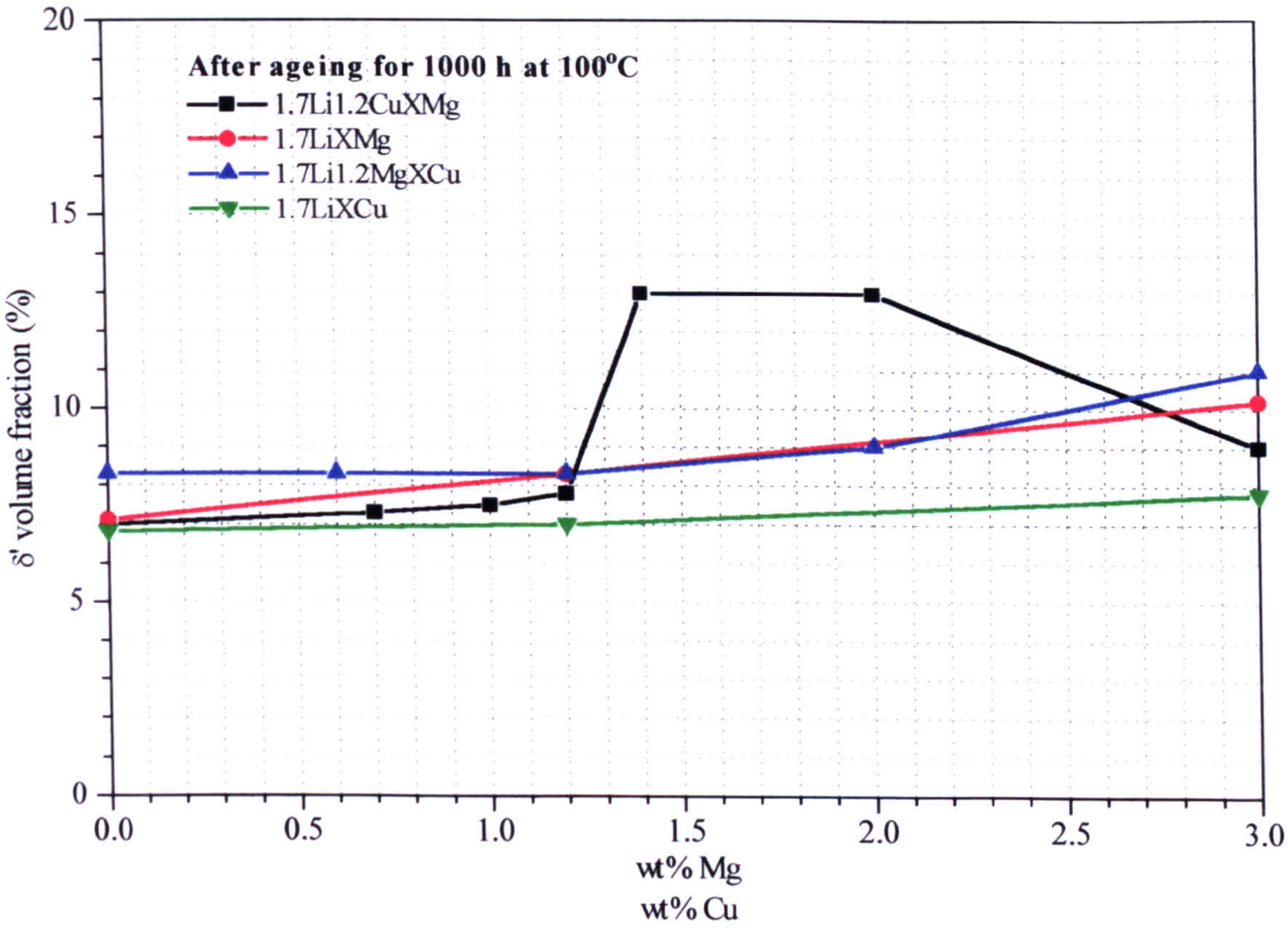

Figure 13.3: δ′ volume fraction precipitated after ageing for 1000 h at 100°C.

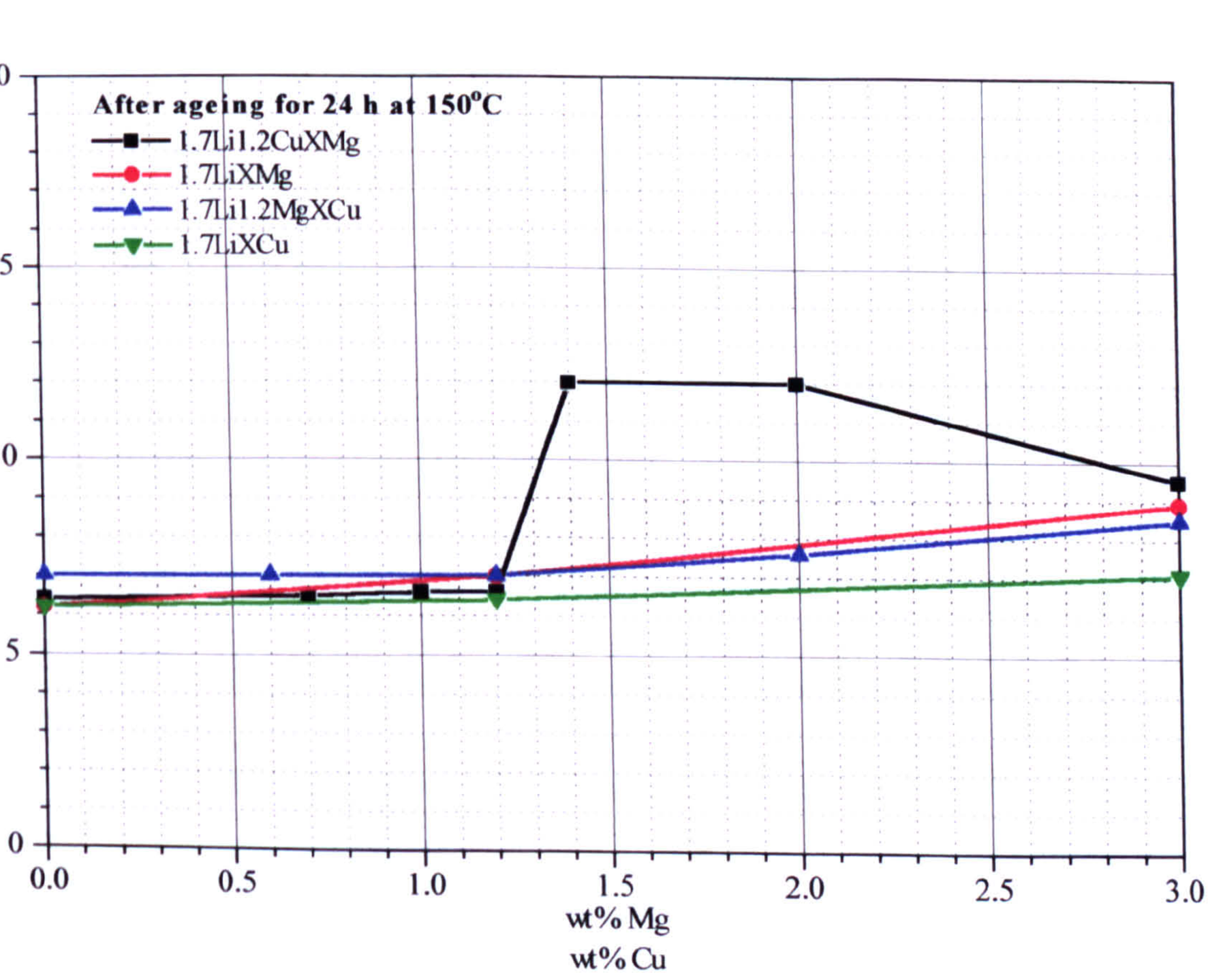

Figure 13.4: δ′ volume fraction precipitated after ageing for 24 h at 150°C.

CHAPTER 14

Conclusions and further work

14.1 Conclusions

Analysis of the results that has been carried out in each of the chapters in the thesis has led to the following conclusions about the effects of copper and magnesium on the precipitation characteristics of Al-Li-Mg, Al-Li-Cu, Al-Cu-Mg and Al-Li-Cu-Mg alloys:

Al-Li-Mg alloys

- Independently of the ageing temperature, increase of the magnesium concentration stimulates the precipitation of δ′ by increasing the α/δ′ solvus temperature by ~7.0°C/wt%Mg.
- The δ′ precipitation process during ageing at 70°C and 100°C is nucleation ordering followed by spinodal decomposition. As the magnesium concentration increases from 0 to 3.0% the spinodal decomposition speeds-up resulting in larger amounts of δ′. Increasing the ageing from 100°C to 150°C causes the mechanism of δ′ formation to change from nucleation ordering/spinodal decomposition to the classical nucleation and growth process.
- The maximum volume fraction of δ′ is produced during ageing at 100°C where there is an optimum combination of driving force and diffusivity.

- For all the alloys studied, the mean size of δ′ particles increases with increasing the ageing temperature.
- A fine dispersion of δ′ is formed during exposure at 70°C. The amount of exposure δ′ increases with increasing concentration of magnesium due to the increase of the α/δ′ solvus temperature. The increased amount of exposure δ′ causes increasing amounts of embrittlement after exposure at 70°C.

Al-Li-Cu alloys

- The addition of copper results in acceleration of the reaction kinetics of δ′ precipitation through the formation of GP_{Cu} zones that act as heterogeneous nucleation centres.
- Copper has no effect on the position of the α/δ′ boundary, hence the equilibrium volume fraction of δ′ precipitated at a given temperature is independent of the copper concentration.
- During ageing at 70°C the volume fraction of δ′ is stimulated with increasing copper concentration. This is due to the fact that even after 1000 h of ageing the equilibrium volume fraction of δ′ is not attained.
- With ageing at 100°C the equilibrium volume fraction of δ′ is reached more rapidly, so that after ageing for 1000 h at 100°C copper has no effect on the volume fraction of δ′.
- With increasing ageing time at 150°C and increasing copper

concentration, there is a significant reduction of δ′ precipitation. This is attributed to the precipitation of large amounts of the equilibrium T_1 and T_2 phases.

- A significant volume fraction of very fine δ′ is formed on GP_{Cu} during exposure at 70°C as the copper concentration increases from 1.2 to 3.0%. This causes a considerable increase in the degree of embrittlement.

Al-Cu-Mg alloys

Effect of copper

- Increasing copper concentration from 1.2 to 3.0% causes stimulation and enhanced kinetics of GPB zone formation during ageing for 1000 h at 70°C and 100°C and 24 h at 150°C. As the ageing conditions increase to 150°C/1000 h, the increase of the copper concentration results in a reduction in the volume fraction of GPB zones due to significant precipitation of S′.
- Copper in the concentration range 1.2-3.0% does not affect the volume fraction of GPB zones formed during exposure at 70°C.

Effect of magnesium

- The as-quenched DSC and isochronal resistivity results showed that magnesium stimulates the clustering of Mg-Cu atoms.
- Magnesium concentration has only a small effect on GPB zone formation at all ageing temperatures i.e. 70, 100, 150°C.

- Magnesium has no effect on the amount of GPB zones formed during exposure at 70°C.

Effect of ageing temperature

- The largest volume fraction of GPB zones is formed during ageing at 100°C.
- Increasing the ageing time at 150°C from 24 h to 1000 h results in an increasing tendency for S″ and S′ precipitation.

Al-Li-Cu-XMg alloys

- In the as-quenched condition, magnesium atoms are behaving as though they were in a simple binary Al-Mg solid solution, i.e. the magnesium atoms do not associate with other solute atoms, i.e. Li, Cu, Zr during or immediately after the quench.
- Isothermal ageing at 70, 100, and 150°C causes significant enhancement of δ′ formation in 1.7Li1.2CuXMg alloys as the magnesium concentration increases beyond 1.2%. It is postulated that the mechanism by which this comes about is the formation of clusters of Li-Cu-Mg atoms that are capable of rapidly developing into δ′ (CLδ′). It is important to note that the clustering process takes place only when the concentration of magnesium is ≥1.2%Mg. It is believed that up to 1.2%Mg the magnesium is consumed in the formation of GPB zones; as the concentration of magnesium increases to levels higher than 1.2% 'free' magnesium is

available in the matrix to gather both copper and lithium thus forming Li-Cu-Mg clusters. This implies that magnesium is the dominating species that controls Li-Cu-Mg cluster formation.

- The kinetics of δ′ precipitation in Al-Li-Cu-Mg alloys is controlled by the presence of excess vacancies that have been quenched-in from the solution treatment temperature.
- At all ageing temperatures (70, 100, 150°C) retardation of δ′ precipitation takes place in the 1.7Li1.2Cu3.0Mg alloy. It is surmised that this due to the formation of a precursor of the equilibrium T_M phase.
- The maximum volume fraction of δ′ forms at 100°C where there is an optimum combination of thermodynamics and kinetics. As the ageing conditions increase from 70°C to 150°C, a coarser dispersion of δ′ forms.
- The volume fraction of δ′ that is precipitated in 1.7Li1.2CuXMg alloys during exposure at 70°C increases with increasing magnesium concentration from 0 to 1.2%. A further increase of magnesium beyond 1.2% results in a reduced volume fraction of δ′ after exposure.
- The 1.7Li1.2Cu1.2Mg alloy exhibits the greatest degree of embrittlement after exposure at 70°C because this alloy precipitates the maximum volume fraction of δ′ during exposure.

Al-Li-Mg-XCu alloys

- The mechanisms by which stimulation of δ′ precipitation takes place in

1.7Li1.2MgXCu alloys with increasing copper concentration are formation of Li-Cu-Mg clusters that can develop into δ′ (CLδ′) and heterogeneous nucleation on GPB zones (GPδ′). The contribution of each mechanism depends on the ageing temperature and the copper concentration.

- During ageing at 70 and 100°C and for low copper concentrations (0%<Cu≤1.2%) the dominant process is GPδ′. For higher copper concentrations (1.2%<Cu≤3.0%) and the same ageing conditions the dominant process is CLδ′.
- Ageing at 150°C results in precipitation of δ′ through classical nucleation and growth for copper concentration up to 0.6%. For copper concentrations in the range 1.2-3.0% the dominant process is GPδ′.
- For all the 1.7Li1.2MgXCu alloys the maximum volume fraction of δ′ occurs at 100°C where there is an optimum combination of diffusivity and δ′ driving force.
- The 1.7Li1.2Mg1.2Cu alloy exhibits the greatest degree of embrittlement after exposure at 70°C as a result of the maximum volume fraction of δ′ that this alloy precipitates during exposure.
- The most effective mechanism for δ′ stimulation in Al-Li-1.2Mg-XCu alloys is the formation of Li-Cu-Mg clusters (CLδ′).

14.2 Future Work

1. More extensive TEM analysis is required on the various alloy systems in order to support/develop the mechanisms of precipitation that have been proposed in the thesis. In particular, high resolution TEM is required to confirm the mechanisms of δ′ precipitation on GPB zones and Li-Cu-Mg clusters.
2. Small angle X-ray and neutron scattering experiments would be extremely beneficial to monitor the size and volume fraction of fine δ′ and GPB zones during the early stages of ageing.
3. DSC analysis, isochronal reversion resistivity measurements and hardness testing are also required after very short ageing times in order to cast more light onto the role of Li-Cu-Mg clusters and GPB zones in the early stages of ageing of Al-Li-Cu-Mg alloys.
4. A series of systematic DSC investigations are required after various ageing times, spanning the range 2 min-1000 h. This will give further information on the development of Li-Cu-Mg clusters, GPB zones, and δ′ during the ageing process.
5. Further investigation into the reasons that cause the decrease in the volume fraction of δ′ during exposure at 70°C in 1.7Li1.2CuXMg and 1.7Li1.2MgXCu alloys when, respectively, the concentration of magnesium and copper is increased beyond 1.2%.

6. DSC analysis and resistivity measurement showed that the 1.7Li1.2Cu3.0Mg alloy exhibits completely different precipitation characteristics compared with the lower magnesium (Mg≤2.0%) 1.7Li1.2CuXMg alloys. It is surmised that in this high magnesium alloy a precursor of T_M phase forms. This needs to be further investigated using DSC, resistivity and in particular TEM analysis.

Acknowledgements

First of all, I would like to express my infinite gratitude to my supervisor Dr. B. Noble not only for his supervision and support from the first to the last minute of this work but also for teaching me how a researcher should think.

I would also like to express my extreme appreciation to Mr K. Dinsdale for all those hours that he spent with me explaining in detail how to operate each machine used for my experiments.

I would like to thank Pr. S. J. Harris for useful discussions and his helpful advice during this work.

N. Bock and J. Armitage are also acknowledged for training me on TEM, XRD and SEM respectively. I would also like to thank J. Thornhill for helping me with the photo-work. In particular I would like to express my appreciation to the staff of the workshop for preparing samples and practical help. Thanks are also due to Dr. A. Spowage for practical help and useful advices.

I would also like to express my appreciation to Pr. C. Panagopoulos for his encouragement before and after I started the present work.

I also want to thank all my colleagues and specially A. Karantzalis for his advices during my first months in England.

Finally, I thank my family for its support and encouragement all these years and the State Scholarships Foundation of Greece for funding me.

References

[1] Kandachar, P.V. Applications for advanced aluminium alloys in aircraft, in 'Advanced materials research and Developments for transport: Light metals', Les Editions de physique, Les Ulis, France, 1986, pp:23-32, R.J.H.Wahnhill, Status and prospects for aluminium-lithium alloys in aircraft structures, Fatigue, Vol.16, No.1, pp.2-20, 1994.

[2] Ekvall.J.C, Rhodes.J.E, Wald.G.G, Methodology for evaluating weight savings from basic material properties, in 'Design of Fatigue and Fracture Resistant Structures', ASTM STP 761, American Society for Testing and Materials, Philadelphia, PA, USA, 1982, pp.328-341, R.J.H.Wahnhill, Status and prospects for aluminium-lithium alloys in aircraft structures, Fatigue, Vol.16, No.1, pp.2-20, 1994.

[3] B.Noble, S.J.Harris and K.Dinsdale: Microstructural stability of binary Al-Li alloys at low temperatures, Acta mater. Vol. 45, No.5, pp 2069-2078, 1997.

[4] A.K.Vasudevan and R.D.Doherty :Aluminum alloys -Contemporary research and applications, Academic press, inc, vol 31, 1989.

[5] R.S.James, Aluminium company of America: Aluminium lithium alloys, Metals Handbook, Vol.2, Properties and selection: Non-ferrous alloys and special purpose materials), tenth edition, pp 178-179, 1990.

[6] C. J. Peel, B. Evans, C. A. Baker, D. A. Bennett, P. J. Gregson, H. M. Flower: The development and application of improved Aluminium –Lithium alloys, Proceedings of the second international Aluminium-Lithium Conference (ed. E. A. Starke Jr and T. H. Sanders Jr), Monterey, California, The metallurgical Society of AIME, pp.363-392, April 12-14, 1983.

[7] J.R. Pickens, Review: Aluminium powder metallurgy technology for high-strength applications, Journal of materials science, Vol.16, pp.1437-1457, 1981.

[8] E.J. Lavernia and N. J. Grant, Review: Aluminium-lithium alloys, Journal of materials science, Vol. 22, p1521, 1987.

[9] Manoj Gupta et al, Spray atomization and deposition of an Al-Cu-Li-Zr alloy, Proceedings of the fifth international aluminium-lithium conference, Williamsburg, Virginia, March 27-31,Vol.1, pp.75-84, 1989.

[10] K.A.Kojima et al, Microstructural characterization and mechanical properties of a spray-cast Al-Li-Cu-Mg-Zr alloy, Proceedings of the fifth international aluminium-lithium conference, Williamsburg, Virginia, March 27-31,Vol.1, pp.85-94, 1989.

[11] Y. C. Zhang et al, Structure and properties of two rapidly solidified Al-Li-Cu-Mg-Zr alloys produced by liquid dynamic compaction, Proceedings of the fifth international aluminium-lithium conference, Williamsburg, Virginia, March 27-31,Vol.1, pp.41-54, 1989.

[12] I.J.Polmear : Recent developments in light alloys, Materials Transactions, JIM, Vol.37, No.1, pp.12-31, 1996.

[13] C.Sigli and J.M.Sanchez, Calculation of phase equilibrium in Al-Li alloys, Acta metall., Vol.34, No.6, pp. 1021-1028, 1986.

[14] A.G. Khachaturyan et al, Theoretical investigation of the precipitation of δ′ in Al-Li, Metallurgical Transactions, Vol.19A, pp. 249-258, February 1988.

[15] J.Lendvai, Precipitation and strengthening in aluminium alloys, Materials Science Forum, vol.217-222, pp.43-56, 1996.

[16] B.Noble and S. E. Bray, On the α(Al)/δ′ (Al_3Li) metastable solvus in Aluminium-Lithium alloys, Acta Metallurgica, Vol., pp.6163-6171, 1998.

[17] B.Noble and G.E.Thompson : Precipitation characteristics of Aluminium-Lithium alloys, Metals Science Journal,Vol.5, pp114-120, 1971.

[18] B.Noble and A.J.Trowsdale : Precipitation in an aluminium-14at% lithium alloy, Philosophical Magazine A,Vol.71, No6, 1345-1362, 1995.

[19] G.Schmitz and P.Haasen : Decomposition of an Al-Li alloy-The early stages observed by HREM, Acta metall.mater, Vol.40, No9, pp.2209-2217, 1992.

[20] S.F.Baumann and D.B.Williams : Experimental observations on the nucleation and growth of δ′ (Al_3Li) in dilute alloys, Metallurgical Transactions A, Vol.16A, pp 1203-1211,1985.

[21] K.Mahalingam, B.P.Gu, G.L.Liedl and T.H.Sanders Jr : Coarsening of δ′ (Al_3Li) precipitates in binary Al-Li alloys, Acta metall., Vol35, No2, pp.483-498, 1987.

[22] S.C.Jha, T.H.Sanders Jr and M.A.Dayananda : Grain boundary precipitate free zones in Al-Li alloys, Acta metall., Vol 35, No.2, pp.473-482, 1987.

[23] H.M.Flower, P.J.Gregson : Solid state phase transformations in aluminium alloys containing lithium, Materials Science and Technology, Vol.3, pp. 81-90, 1987.

[24] B.Noble, S.J.Harris, and K.Dinsdale : Yield characteristics of aluminium-lithium alloys, Metal Science, Vol.16, pp. 425-430, 1982.

[25] B.Noble, S.J.Harris, K.Dinsdale and P.D.Pitcher : Embrittlement in recrystallised and unrecrystallised Al-Li binary alloys, Materials Science Forum, Vols. 217-222 , pp. 1317-1322, 1996.

[26] E.Schürman and I.K.Geissler, "Solid Phase Equilibrium in Mg-Rich Alloys of the Al-Li-Mg system", Giessereiforshung, 32(4), pp.163-174, 1980, N.C.Goel and J. R. Cahoon: The Al-Li-Mg system, Bulletin of alloy phase diagrams, Vol.11, No.6, 1990.

[27] A.J.Trowsdale, B.Noble, S.J.Harris, J.White, and I.G.Palmer : Effect of microstructure on tensile and fracture properties of aluminium alloys with high lithium content, Materials Science and Technology, Vol 11, pp.237-244, 1995.

[28] S.F.Baumann and D.B.Williams: The effect of ternary additions on the δ′/α misfit and δ′ solvus line in Al-Li alloys, Aluminium-lithium alloys II (ed. T.H.Sanders Jr and E.A.Starke Jr), Warrandale, Pa, The Metallurgical Society of AIME, p17, 1984.

[29] M.G.Valentine and T.H.Sanders Jr: The influence of temperature and composition on the distribution of δ′, Aluminium-LithiumV, ed. E.A.Starke Jr and T.H.Sanders Jr, AIME, Warrendale, PA, pp.575-584, 1989.

[30] G. E. Thompson and B. Noble: Resistivity of Al-Li-Cu alloys during T_1 (Al_2CuLi) precipitation, Metal Science Journal, Vol. 7, pp.32-35, 1973.

[31] B.Noble and G.E.Thompson: T_1 (Al_2CuLi) precipitation in Aluminium-Copper-Lithium alloys, Metal Science Journal, vol.6, 1972.

[32] S.Suresh, A.K.Vasudevan, M.Tosten and P.R.Howell : Microscopic and macroscopic aspects of fracture in lithium-containing aluminium alloys, acta metall., Vol 35, No.1, pp.25-46, 1987.

[33] H.K.Hardy and J.M.Silcock:The phase sections at 500°C and 350°C of aluminium rich Aluminium-Copper-Lithium alloys, J.Inst.Met., 84, 423, 1955-1956.

[34] L.F.Mondolfo : Aluminium alloys, Structure and properties, London, Butterworths, 1976.

[35] T.H.Sanders Jr, E.A.Starke Jr : The physical metallurgy of aluminum -lithium alloys-A review, Proceedings of the fifth international aluminum-lithium conference, Williamsburg, Virginia, March 27-31, vol.1, pp.1-37, 1989.

[36] M.J.Starink and P.J.Gregson : Thermodynamics and precipitation in 8090 (Al-Li-Cu-Mg-Zr) alloys studied by DSC and TEM, Materials Science Forum, Vols.217-222, pp.673-678, 1996.

[37] R.E.Crooks, E.A.Kenik, and E.A.Starke : HVEM in situ deformation of Al-Li-X alloys, Scripta Metall., 17, pp.643, 1983.

[38] P.J.Gregson and H.M.Flower : Microstructural control of toughness in aluminium-lithium alloys, Acta metall.,23, pp.527, 1985.

[39] D.L.Gilmore and E.A.Starke Jr : The effects of In, Mg, and impurity trace additions on precipitation, anisotropy, and related properties in an Al-Cu-Li alloy, Materials Science Forum, Vols.217-222, pp.877-882, 1996.

[40] B.Noble, S.J.Harris, K.Dinsdale : Low temperature embrittlement of 8090 in damage tolerant condition aluminium alloys, their physical and mechanical properties, Georgia Inst. of Technology, Atlanta, 460-466, 1994.

[41] B. Noble and S. Bray: Materials Science and Engineering, to be published, 2001

[42] B Noble: Private communication

[43] B. Noble and S. Bray: Coarsening of the δ′ phase in aluminium-lithium alloys, Philosophical Magazine A, Vol.79, No4, pp.859-872, 1999.

[44] S. Bray: Low temperature precipitation in Al-Li alloys, Ph.D. Thesis, The University of Nottingham, October 1997.

[45] S. P. Ringer, G. C. Quan, T. Sakurai: Solute clustering, segregation and microstructure in high strength low alloy Al-Cu-Mg alloys, Materials Science and Engineering, Vol.A250, pp.120-126, 1998

[46] S. P. Ringer, K. Hono, T. Sakurai, I. J. Polmear: Cluster hardening in an aged Al-Cu-Mg alloy, Scripta materiallia, Vol. 36, No. 5, pp. 517-521, 1997.

[47] S. P. Ringer, T. Sakurai, I. J. Polmear: Opigins of hardening in aged Al-Cu-Mg-(Ag) alloys, acta mater., Vol. 45, No. 9, pp. 3731-3744, 1997.

[48] S. P. Ringer, K. Hono, I. J. Polmear, T. Sakurai: Precipitation process during the early stages of ageing in Al-Cu-Mg alloys, Applied Surface Science, Vol. 94/95, pp. 253-260, 1996.

[49] A. M. Zahra, C. Y. Zahra, C. Alfonso, and A. Charaï: Comments on "cluster hardening in an aged Al-Cu-Mg alloy", Scripta Materiallia, Vol. 39, No. 11, pp.

1553-1558, 1998.

[50] S. P. Ringer, S. K. Caraher and I. J. Polmear: Response to comments on cluster hardening in an aged Al-Cu-Mg alloy, Scripta Materiallia, Vol. 36, No. 11, pp. 1559-1567, 1998.

[51] A. Charai, T. Walther, C, Alfonso, A. M. Zahra and C. Y. Zahra: Coexistence of clusters, GPB zones, S''-, S'-, and S-phases in an Al-0.9%Cu-1.4%Mg alloy, acta mater., Vol. 48, pp. 2751-2764, 2000.

[52] E. J. Mittemeijer: Review analysis of the kinetics of phase transformations, Journal of Materials Science, vol.27, pp. 3977-3987, 1992.

[53] J. E. Hatch: Aluminium-Properties and Physical Metallurgy, American Society of Metals, Metals Park, Ohio, pp. 204-205, 1984.